



**HAL**  
open science

# Mécanismes et implications thérapeutiques de l'hypermutation dans les gliomes

Mahdi Touat

► **To cite this version:**

Mahdi Touat. Mécanismes et implications thérapeutiques de l'hypermutation dans les gliomes. Cancer. Université Paris-Saclay, 2020. Français. NNT : 2020UPASL071 . tel-03506253

**HAL Id: tel-03506253**

**<https://theses.hal.science/tel-03506253v1>**

Submitted on 2 Jan 2022

**HAL** is a multi-disciplinary open access archive for the deposit and dissemination of scientific research documents, whether they are published or not. The documents may come from teaching and research institutions in France or abroad, or from public or private research centers.

L'archive ouverte pluridisciplinaire **HAL**, est destinée au dépôt et à la diffusion de documents scientifiques de niveau recherche, publiés ou non, émanant des établissements d'enseignement et de recherche français ou étrangers, des laboratoires publics ou privés.

# Mécanismes et implications thérapeutiques de l'hypermutation dans les gliomes

Thèse de doctorat de l'université Paris-Saclay

École doctorale n° 582, Cancérologie : biologie - médecine - santé (CBMS) Spécialité de  
doctorat : Aspects moléculaires et cellulaires de la biologie  
Unité de recherche : Inserm U 1127, CNRS UMR 7225,  
Institut du Cerveau et de la Moelle épinière, ICM  
Réfèrent : faculté de médecine

Thèse présentée et soutenue à Paris, le 22 décembre 2020, par

**Mahdi TOUAT**

## Composition du Jury

<b>Éric DEUTSCH</b> PU-PH, Université Paris-Saclay	Président & Examineur
<b>Franck BOURDEAUT</b> PH, Université de Paris	Rapporteur & Examineur
<b>Magali SVRCEK</b> PU-PH, Sorbonne Université	Rapporteur & Examinatrice
<b>Alex DUVAL</b> PU-PH, Sorbonne Université	Examineur
<b>Ahmed IDBAIH</b> PU-PH, Sorbonne Université	Directeur de thèse
<b>Keith L. LIGON</b> Ass. Professor, Harvard Medical School	Co-Directeur de thèse
<b>Franck BIELLE</b> MCU-PH, Sorbonne Université	Invité
<b>Marc SANSON</b> PU-PH, Sorbonne Université	Invité



**Titre :** Mécanismes et implications thérapeutiques de l'hypermutation dans les gliomes

**Mots clés :** gliomes, hypermutation, résistance, chimiothérapie, immunothérapie, mismatch repair

**Résumé :** Une élévation majeure de la charge mutationnelle (hypermutation) est observée dans certains gliomes. Néanmoins, les mécanismes de ce phénomène et ses implications thérapeutiques notamment concernant la réponse à la chimiothérapie ou à l'immunothérapie sont encore mal connus. Sur le plan du mécanisme, une association entre hypermutation et mutations des gènes de la voie de réparation des mésappariements de l'ADN (MMR) a été rapportée dans les gliomes, cependant la plupart des mutations MMR observées dans ce contexte n'étaient pas fonctionnellement caractérisées, et leur rôle dans le développement d'hypermutation restait de ce fait incertain. De plus, l'impact de l'hypermutation sur l'immunogénicité des cellules gliales et sur leur sensibilité au blocage des points de contrôles immunitaires (par exemple par traitement anti-PD-1) n'est pas connu. Dans cette étude, nous analysons de manière exhaustive les déterminants cliniques et moléculaires de la charge et des signatures mutationnelles dans 10 294 gliomes, dont 558 (5,4%) tumeurs hypermutées. Nous identifions deux principales voies responsables d'hypermutation dans les gliomes : une voie "de novo" associée à des déficits constitutionnels du système MMR et de la polymérase epsilon (POLE), ainsi qu'une voie "post-traitement", plus fréquente, associée à l'acquisition de déficits MMR et de résistance secondaire dans les gliomes récidivant après chimiothérapie par témozolomide. Expérimentalement, la signature mutationnelle des gliomes hypermutés post-traitement

(signature COSMIC 11) était reproduite par les dommages induits par le témozolomide dans les cellules MMR déficientes. Alors que le déficit MMR s'associe à l'acquisition de résistance au témozolomide, des données cliniques et expérimentales suggèrent que les cellules MMR déficientes conservent une sensibilité à la nitrosouree lomustine. De façon inattendue, les gliomes MMR déficients présentaient des caractéristiques uniques, notamment l'absence d'infiltrats lymphocytaires T marqués, une hétérogénéité intratumorale importante, une survie diminuée ainsi qu'un faible taux de réponse aux traitements anti-PD-1. De plus, alors que l'instabilité des microsatellites n'était pas détectée par des analyses en bulk dans les gliomes MMR déficients, le séquençage du génome entier à l'échelle de la cellule unique de gliome hypermuté post-traitement permettait de démontrer la présence de mutations des microsatellites. Collectivement, ces résultats supportent un modèle dans lequel des spécificités dans le profil mutationnel des gliomes hypermutés pourraient expliquer l'absence de reconnaissance par le système immunitaire ainsi que l'absence de réponse aux traitements par anti-PD-1 dans les gliomes MMR déficients. Nos données suggèrent un changement de pratique selon lequel la recherche d'hypermutation par séquençage tumoral lors de la récurrence après traitement pourrait informer le pronostic et guider la prise en charge thérapeutique des patients.

**Title :** Mechanisms and therapeutic implications of hypermutation in gliomas

**Keywords :** gliomas, hypermutation, resistance, chemotherapy, immunotherapy, mismatch repair

**Abstract :** High tumor mutational burden (hypermutation) is observed in some gliomas; however, the mechanisms by which hypermutation develops and whether it predicts chemotherapy or immunotherapy response are poorly understood. Mechanistically, an association between hypermutation and mutations in the DNA mismatch-repair (MMR) genes has been reported in gliomas, but most MMR mutations observed in this context were not functionally characterized, and their role in causing hypermutation remains unclear. Furthermore, whether hypermutation enhances tumor immunogenicity and renders gliomas responsive to immune checkpoint blockade (e.g. PD-1 blockade) is not known. Here, we comprehensively analyze the clinical and molecular determinants of mutational burden and signatures in 10,294 gliomas, including 558 (5.4%) hypermutated tumors. We delineate two main pathways to hypermutation: a de novo pathway associated with constitutional defects in DNA polymerase and MMR genes, and a more common, post-treatment pathway, associated with acquired resistance driven by MMR defects in chemotherapy-sensitive gliomas recurring after temozolomide. Experimentally, the mutational signature of post-treatment hypermutated gliomas

(COSMIC signature 11) was recapitulated by temozolomide-induced damage in MMR-deficient cells. While MMR deficiency was associated with acquired temozolomide resistance in glioma models, clinical and experimental evidence suggest that MMR-deficient cells retain sensitivity to the chloroethylating nitrosourea lomustine. MMR-deficient gliomas exhibited unique features including the lack of prominent T-cell infiltrates, extensive intratumoral heterogeneity, poor survival and low response rate to PD-1 blockade. Moreover, while microsatellite instability in MMR-deficient gliomas was not detected by bulk analyses, single-cell whole-genome sequencing of post-treatment hypermutated glioma cells demonstrated microsatellite mutations. Collectively, these results support a model where differences in the mutation landscape and antigen clonality of MMR-deficient gliomas relative to other MMR-deficient cancers may explain the lack of both immune recognition and response to PD-1 blockade in gliomas. Our data suggest a change in practice whereby tumor re-sequencing at relapse to identify progression and hypermutation could inform prognosis and guide therapeutic management.

# Remerciements

*Je tiens à exprimer mes sincères remerciements à :*

*Monsieur le Professeur Éric Deutsch, de m'avoir fait l'honneur de présider cette thèse.*

*Monsieur le Professeur Ahmed Idbaih et Monsieur le Professeur Keith Ligon, d'avoir pris le temps de diriger et encadrer cette thèse.*

*Monsieur le Docteur Franck Bourdeaut, Madame la Professeure Magali Svrcek, et Monsieur le Professeur Alex Duval, d'avoir pris le temps de juger ce travail.*

*Monsieur le Docteur Franck Bielle, et Monsieur le Professeur Marc Sanson, pour leur participation à ces travaux.*

*Une partie importante de ces travaux a été réalisée au Dana-Farber Cancer Institute et je tiens à remercier ici très sincèrement mes collègues de Boston pour leur amitié et leurs efforts déterminants dans l'obtention de ces résultats, en particulier Keith Ligon pour son accueil au sein de son laboratoire, ses conseils et ses encouragements.*

*Je tiens à remercier les équipes de recherche du Dana-Farber Cancer Institute, du Brigham and Women's Hospital, du Boston Children's Hospital et du Broad Institute (Ligon Lab, Beroukhim Lab, Bandopadhyay Lab, Meyerson Lab, Park Lab, Harvard Medical School, Boston), de l'Institut du Cerveau (Equipe génétique et développement des tumeurs cerebrales, INSERM, CNRS, APHP et Sorbonne Université, Paris), du Centre de Recherche Saint Antoine (Equipe Instabilité des microsatellites et cancers, INSERM, APHP et Sorbonne Université, Paris) et de Gustave Roussy (DITEP, Université Paris Saclay, Villejuif) pour leur participation à ces travaux de recherche, en particulier Rameen Beroukhim, Pratiti Bandopadhyay, Franck Bielle, Khê Hoang-Xuan, Ahmed Idbaih, Marc Sanson, Alex Duval, Aurélien Marabelle, Yvonne Li, Liam Spurr, Kristine Pelton, Jack Geduldig, Adam Boynton, Sangita Pal, et Craig Bohrsen. Je tiens à remercier également les équipes médicales, paramédicales et de recherche des départements de neuro-oncologie, neurochirurgie, radiothérapie et de neuropathologie de ces hôpitaux pour leur participation au suivi des patients et à la collecte de données cliniques indispensables à ces recherches.*

*Enfin, je tiens à remercier mes amis et ma famille pour leur soutien et leurs encouragements quotidiens.*

**Université Paris-Saclay**

Espace Technologique / Immeuble Discovery  
Route de l'Orme aux Merisiers RD 128 / 91190 Saint-Aubin, France

# Acknowledgements

*I would like to express my sincere thanks to:*

*Professor Éric Deutsch, for doing me the honor of chairing this thesis defense.*

*Professor Ahmed Idbaih and Professor Keith Ligon, for taking the time to supervise my PhD thesis.*

*Doctor Franck Bourdeaut, Professor Magali Svreck, and Professor Alex Duval, for taking the time to evaluate this thesis.*

*Dr. Franck Bielle, and Professor Marc Sanson, for their participation to this work.*

*An important part of this thesis was carried out at the Dana-Farber Cancer Institute and I would like to thank very sincerely my colleagues in Boston for their energy, great spirit and decisive efforts in obtaining these results, in particular Keith Ligon for his friendship, advices and continuous support.*

*I would like to thank the research teams of the Dana-Farber Cancer Institute, Brigham and Women's Hospital, Boston Children's Hospital and Broad Institute (Ligon Lab, Beroukhim Lab, Bandopadhyay Lab, Meyerson Lab, Park Lab, Harvard Medical School, Boston), of the Paris Brain Institute (Genetics and development of brain tumors team, INSERM, CNRS, APHP and Sorbonne University, Paris), of the Saint Antoine Research Center (Team of microsatellites instability and cancers, INSERM, APHP and Sorbonne University, Paris) and Gustave Roussy (DITEP, Université Paris Saclay, Villejuif) for their participation in this research work, in particular Rameen Beroukhim, Pratiti Bandopadhyay, Franck Bielle, Khê Hoang-Xuan, Ahmed Idbaih, Marc Sanson, Alex Duval, Aurélien Marabelle, Yvonne Li, Liam Spurr, Kristine Pelton, Jack Geduldig, Adam Boynton, Sangita Pal, and Craig Bohrsen. I would also like to thank the medical, paramedical and research teams of the neuro-oncology, neurosurgery, radiation therapy and neuropathology departments of these hospitals for their participation in the follow-up of patients and in the collection of clinical data essential for this research.*

*Finally, I want to thank my friends and family for their daily encouragement and support.*

## Table des matières

<b>Liste des abréviations / List of abbreviations.....</b>	<b>8</b>
<b>Table des illustrations et tables .....</b>	<b>11</b>
<b>List of illustrations and tables.....</b>	<b>13</b>
<b>Introduction .....</b>	<b>15</b>
I. Contexte des travaux .....	15
II. Tumeurs neuroépithéliales : définition et traitements .....	17
A. Classification et données épidémiologiques .....	17
B. Diagnostic des gliomes : sous-types moléculaires, aspects pronostiques .....	20
C. Traitements des gliomes : place des agents alkylants .....	23
D. Mécanismes d'action des agents alkylants.....	24
E. Résistance au témozolomide : rôles de la MGMT et du système MMR, phénotype « hypermutant » .....	27
III. Hypermutation dans les gliomes .....	32
A. Etude de la charge et de la signature mutationnelles dans les cancers, potentiel rôle prédictif dans la prédiction de la réponse à l'immunothérapie .....	32
B. Hypermutation dans les gliomes .....	36
IV. Hypothèses et objectifs .....	45
<b>Introduction .....</b>	<b>47</b>
I. Study context.....	47
II. Neuroepithelial tumors: definition and treatments.....	49
A. Classification and epidemiological data .....	49
B. Diagnosis: molecular subtypes, prognostic factors .....	52
C. Treatments: role of alkylating agents.....	55
D. Mechanism of action of alkylating agents.....	57
E. Temozolomide resistance: involvement of MGMT and MMR system, « hypermutator » phenotype .....	60
III. Hypermutation in gliomas .....	65
A. Study of the mutational load and signature in cancers, potential role in the prediction of the response to immunotherapy .....	65
B. Hypermutation in gliomas.....	68
IV. Hypothesis and objectives .....	78

<b>Article</b> .....	<b>80</b>
<b>Discussion</b> .....	<b>118</b>
<b>Discussion</b> .....	<b>121</b>
<b>Annexe / Annex</b> .....	<b>124</b>
V. Autres contributions à des articles publiés sur la thématique pendant la Thèse de Sciences / Other contributions to articles published on the theme during the Thesis .....	124
Article sur la déficience MMR et la réponse à l'immunothérapie dans un autre sous-type de tumeur cérébrale primitive, les méningiomes / Article on MMR deficiency and response to immunotherapy in another subtype of primary brain tumor, meningiomas.....	124
VI. Autres articles publiés pendant la Thèse de Sciences / Other articles published during the Science Thesis .....	137
A. Revue sur le développement de thérapies ciblées dans les gliomes malins / Review on the development of targeted therapies in gliomas .....	137
B. Article sur le ciblage des mutation BRAF par vemurafenib dans les gliomes malins / Article on the targeting of BRAF mutations with vemurafenib .....	154
C. Article sur le ciblage de fusion ATG7-RAF1 par cobimetinib dans un gliome malin / Article on the taregting of an ATG7-RAF1 fusion with cobimetinib.....	165
D. Article sur le ciblage d'altérations moléculaires de la voie PI3K par buparlisib dans les gliomes malins / Article on the targeting of PI3K aberrations with buparlisib .....	173
E. Article sur le ciblage de mutations IDH1 par ivosidenib dans les gliomes malins / Article on the targeting of IDH1 mutations with ivosidenib .....	194
<b>Conclusions</b> .....	<b>206</b>
<b>Conclusions</b> .....	<b>208</b>
<b>Références</b> .....	<b>210</b>

## LISTE DES ABBREVIATIONS / LIST OF ABBREVIATIONS

- ALKBH2** : alkB homolog 2, alpha-ketoglutarate dependent dioxygenase
- ALKBH3** : alkB homolog 3, alpha-ketoglutarate dependent dioxygenase
- APC** : APC regulator of WNT signaling pathway
- APEX1** : apurinic/aprimidinic endodeoxyribonuclease 1
- APOBEC** : Apolipoprotéins B mRNA editing enzyme, catalytic polypeptide-like
- ATG7** : autophagy related 7
- ATRX** : ATRX chromatin remodeler
- BER** : base excision repair
- BRAF** : B-Raf proto-oncogene, serine/threonine kinase
- CIC** : capicua transcriptional repressor
- CDKN2A** : cyclin dependent kinase inhibitor 2A
- CMMRD** : constitutional mismatch repair deficiency
- DSB** : double-strand breaks
- EGFR** : epidermal growth factor receptor
- EXO** : site actif de l'exonucléase
- FANCM** : FA complementation group M
- FUBP1** : far upstream element binding protein 1
- H3F3A** : H3.3 histone A
- ICI** : inhibiteurs de checkpoints immunitaires
- IDH1** : isocitrate déshydrogénase 1
- IDH2** : isocitrate déshydrogénase 2
- Indels** : petites insertions et délétions
- KU70** : X-ray repair cross complementing 6
- KU80** : X-ray repair cross complementing 5
- Mb** : Mégabases
- MGMT** : O-6-methylguanine-DNA methyltransferase
- MMR** : mismatch repair
- MLH1** : mutL homolog 1

**MLH3** : mutL homolog 3

**MPG** : N-methylpurine DNA glycosylase

**MSH2** : mutS homolog 2

**MSH3** : mutS homolog 3

**MSH6** : mutS homolog 6

**MSI** : instabilité des microsatellites

**MTIC** : méthyltriazenoimidazole-4-carboxamide

**MYC** : MYC proto-oncogene, bHLH transcription factor

**NF1** : neurofibromin 1

**NF2** : neurofibromin 2

**NER** : nucleotide excision repair

**OGG1** : 8-oxoguanine DNA glycosylase

**PARP** : poly(ADP-ribose) polymerases

**PHLDB1** : pleckstrin homology like domain family B member 1

**PI3K** : phosphatidylinositol 3-kinase

**PMS2** : PMS1 homolog 2, mismatch repair system component

**POL** : site actif de la polymérase

**POLB** : DNA polymerase beta

**POLE** : DNA polymerase epsilon, catalytic subunit

**POLD1** : DNA polymerase delta 1, catalytic subunit

**PTCH1** : patched 1

**PTEN** : phosphatase and tensin homolog

**NGS** : next generation sequencing

**OMS** : organisation mondiale de la sante

**PCR** : polymerase chain reaction

**RAF1** : Raf-1 proto-oncogene, serine/threonine kinase

**RELA** : RELA proto-oncogene, NF-kB subunit

**SMARCB1** : SWI/SNF related, matrix associated, actin dependent regulator of chromatin, subfamily b, member 1

**SNC** : système nerveux central

**SNV** : single nucleotide variant

**SSB** : single-strand breaks

**STMN3** : stathmin 3

**TCGA** : The Cancer Genome Atlas

**TERT** : telomerase reverse transcriptase

**Université Paris-Saclay**

Espace Technologique / Immeuble Discovery

Route de l'Orme aux Merisiers RD 128 / 91190 Saint-Aubin, France

**TP53** : tumor protein p53

**TSC1** : TSC complex subunit 1

**TSC2** : TSC complex subunit 2

**VHL** : von Hippel-Lindau tumor suppressor

**XRCC1** : X-ray repair cross complementing 1

## TABLE DES ILLUSTRATIONS ET TABLES

### Tables :

**Table 1.** Classification simplifiée des tumeurs neuroépithéliales selon l'OMS 2016.

**Table 2.** Syndromes de prédisposition génétique au cancer associés au risque de tumeur neuroépithéliale.

### Figures :

**Figure 1.** Distribution des tumeurs primitives du SNC aux Etats-Unis sur la période 2012-2016 (d'après Ostrom et al.<sup>2</sup>).

**Figure 2.** Tumeur fronto-pariétale gauche correspondant à un gliome de haut grade chez un patient âgé de 64 ans.

**Figure 3.** Principaux sous-types de gliomes diffus et stratégie diagnostique en fonction des statuts *IDH1/2* et *1p/19q*.

**Figure 4.** Courbes de survie associées aux sous-types moléculaires des gliomes diffus inclus dans le TCGA (d'après Brat et al.<sup>7</sup>).

**Figure 5.** Principaux types d'agents alkylants utilisés pour le traitement des gliomes malins (a) et leurs effets biologiques sur l'ADN (b) (d'après Fu et al.<sup>53</sup> [a-b] et Preston et al.<sup>62</sup> [c]).

**Figure 6.** Représentation schématique des principaux dommages ADN causés par les agents alkylants utilisés dans les gliomes et leurs mécanismes de réparation associés (d'après Fu et al.<sup>53</sup>).

**Figure 7.** Mécanisme de cytotoxicité du témozolomide et réparation médiée par la MGMT (d'après Wick et al.<sup>86</sup>).

**Figure 8.** Représentation schématique de la réparation des erreurs d'incorporation de l'ADN polymérase par les systèmes de « proofreading » et MMR (d'après Preston et al.<sup>62</sup> [a] et Jiricny<sup>81</sup> [b]).

**Figure 9.** Modèle suggérant un lien mécanistique entre déficits MGMT et du système MMR, résistance témozolomide et phénotype hypermutant dans les gliomes malins (d'après Allan et al.<sup>26</sup>).

**Figure 10.** Processus mutationnels exogènes et endogènes contribuant à l'accumulation de mutations somatiques dans les tumeurs humaines et technique d'analyse des mutations ponctuelles (SNV, *single nucleotide variants*).

**Figure 11.** Analyse de la charge mutationnelle dans les tumeurs du TCGA (a) et réponse aux immunothérapies par inhibiteurs de checkpoints immunitaires dans des cancers avec charge mutationnelle élevée (b, mélanome) ou faible (c, glioblastomes) (d'après Alexandrov et al.<sup>2</sup> [a], Larkin et al.<sup>115</sup> et Reardon et al.<sup>116</sup>).

**Figure 12.** Réponse aux traitements par ICI dans des tumeurs MMR-déficientes (gauche, gliomes ; droite, pan-cancer) (d'après Bouffet et al.<sup>117</sup> [a] et Le et al.<sup>124</sup>).

**Figure 13.** Signatures mutationnelles retrouvées dans les gliomes avec charge mutationnelle faible (en bleu) ou avec hypermutation *de novo* (vert) ou post-traitement (rouge) (d'après Alexandrov et al.<sup>103</sup>).

**Figure 14.** Fréquence des mutations des principaux gènes du MMR dans des gliomes malins séquencés lors du diagnostic initial (données TCGA<sup>6,7</sup>).

**Figure 15.** Etablissement d'une lignée de gliome malin dérivée d'une patiente avec mutation germinale *MSH2*.

**Figure 16.** Evolution clonale temporelle et spatiale chez des patients atteints de gliome diffus avec mutation *IDH1/2* (d'après Johnson et al.<sup>90</sup>).

**Figure 17.** Acquisition d'hypermutation avec signature mutationnelle 11 lors de la récurrence après témozolomide dans un astrocytome anaplasique avec mutation *IDH1*.

**Figure 18.** Analyses des anomalies de nombre de copies (partie haute) et de la clonalité des mutations somatiques (bas) dans 3 paires de gliomes pré- et post-témozolomide analysées par séquençage de l'exome (d'après Bai et al.<sup>149</sup>).

**Figure 19.** Synthèse des études de paires de gliomes malins pré- et post-traitement montrant l'association du phénomène d'hypermutation avec les antécédents d'exposition aux agents alkylants et la présence de mutation *IDH1/2* et/ou de méthylation du promoteur *MGMT* (d'après TCGA<sup>109</sup>, Bai et al.<sup>149</sup>, Wang et al.<sup>94</sup>, Kim et al.<sup>93</sup>, Kim et al.<sup>92</sup>, et Johnson et al.<sup>90</sup>).

**Figure 20.** Arbres phylogénétiques représentant la composition clonale des tumeurs du TCGA (d'après McGranahan et al.<sup>152</sup>).

**Figure 21.** Analyse pan-cancer des sous-types immunitaires dans les tumeurs TCGA (d'après Thorsson et al.<sup>153</sup>).

## LIST OF ILLUSTRATIONS AND TABLES

### Tables :

**Table 1.** Simplified classification of neuroepithelial tumors according to WHO 2016.

**Table 2.** Cancer predisposition syndromes associated with the risk of neuroepithelial tumor.

### Figures :

**Figure 1.** Distribution of primary CNS tumors in the United States over the period 2010-2014 (from Ostrom et al. 2).

**Figure 2.** Left fronto-parietal tumor corresponding to a high-grade glioma in a 64-year-old patient.

**Figure 3.** Main subtypes of diffuse glioma and diagnostic strategy according to the determination of IDH1/2 and 1p/19q statuses.

**Figure 4.** Survival associated with the molecular subtypes of diffuse gliomas included in the TCGA (from Brat et al. 7).

**Figure 5.** Main types of alkylating agents used for the treatment of malignant gliomas (a) and their biological effects on DNA (b) (after Fu et al. 53 [a-b] and Preston et al. 62 [c]).

**Figure 6.** Schematic representation of the main DNA damage caused by alkylating agents used in gliomas and their associated repair mechanisms (from Fu et al. 53).

**Figure 7.** Mechanism of temozolomide cytotoxicity and MGMT mediated repair (from Wick et al. 86).

**Figure 8.** Schematic representation of the repair of DNA polymerase incorporation errors by "proofreading" and MMR systems (from Preston et al. 62 [a] and Jiricny 81 [b]).

**Figure 9.** Model suggesting a mechanistic link between MGMT and MMR system deficits, temozolomide resistance and hypermutant phenotype in malignant gliomas (from Allan et al. 26).

**Figure 10.** Exogenous and endogenous mutational processes contributing to the accumulation of somatic mutations in human tumors and point mutation (SNV) analysis method.

**Figure 11.** Analysis of the mutational load in TCGA tumors (a) and response to ICI in cancers with high (b, melanoma) or low (c, glioblastoma) mutational load (from Alexandrov et al. <sup>103</sup> [a], Larkin et al. <sup>115</sup> [b] and Reardon et al. <sup>116</sup> [c]).

**Figure 12.** Response to ICI treatments in MMR-deficient tumors (left, gliomas; right, pan-cancer) (from Bouffet et al. <sup>117</sup> [a] and Le et al. <sup>124</sup>).

**Figure 13.** Mutational signatures found in gliomas with low mutational burden (blue) or with de novo (green) or post-treatment hypermutation (red) (from Alexandrov et al. <sup>103</sup>).

**Figure 14.** Frequency of mutations in the main MMR genes in malignant gliomas sequenced at initial diagnosis (TCGA data <sup>6,7</sup>).

**Figure 15.** Establishment of a malignant glioma PDCL derived from a patient with MSH2 germline mutation.

**Figure 16.** Temporal and spatial clonal evolution in patients with diffuse glioma with IDH1/2 mutation (from Johnson et al. <sup>90</sup>).

**Figure 17.** Acquisition of hypermutation with mutational signature 11 during recurrence after temozolomide in an anaplastic astrocytoma with *IDH1* mutation.

**Figure 18.** Analysis of copy number abnormalities (upper part) and clonality of somatic mutations (lower) in 3 pairs of pre- and post-temozolomide gliomas analyzed by exome sequencing (from Bai et al. <sup>149</sup>).

**Figure 19.** Summary of pre- and post-treatment malignant glioma pair studies showing the association of = hypermutation with history of exposure to alkylating agents and the presence of *IDH1/2* mutation and/or *MGMT* promoter methylation (from TCGA <sup>109</sup>, Bai et al. <sup>149</sup>, Wang et al. <sup>94</sup>, Kim et al. <sup>93</sup>, Kim et al. <sup>92</sup>, and Johnson et al. <sup>90</sup>).

**Figure 20.** Phylogenetic trees representing the clonal composition of TCGA tumors (from McGranahan et al. <sup>152</sup>).

**Figure 21.** Pan-cancer analysis of immune subtypes in TCGA tumors (from Thorsson et al. <sup>153</sup>).

# INTRODUCTION

## I. Contexte des travaux

Les tumeurs primitives du système nerveux central (SNC) forment un ensemble hétérogène de pathologies bénignes ou malignes touchant l'enfant et l'adulte. Selon la classification de l'Organisation mondiale de la santé (OMS) de 2016, on distingue cinq principaux types de tumeurs primitives du SNC : les tumeurs des méninges, les tumeurs neuroépithéliales, les tumeurs germinales, les tumeurs de la région sellaire et les tumeurs hématopoïétiques <sup>1</sup>. Ces cinq types sont eux-mêmes subdivisés en plusieurs sous-types histologiques formant au total plus de 150 pathologies aux caractéristiques biologiques et cliniques hautement hétérogènes. Les gliomes malins constituent la majorité des tumeurs neuroépithéliales et plus de 80% des tumeurs primitives malignes du SNC <sup>2</sup>. Bien qu'appartenant au groupe des cancers rares (incidence annuelle inférieure à 6/100 000 personnes), les gliomes malins représentent un enjeu particulier de santé publique en raison de la morbidité associée à leur développement dans le SNC, de la complexité de leur diagnostic et de leur suivi, et de leur caractère le plus souvent incurable. La prise en charge des patients atteints de gliome malin est très hétérogène, allant de la simple surveillance pour certaines tumeurs peu évolutives (grade I selon l'OMS) à des traitements lourds combinant chirurgie d'exérèse, radiothérapie et chimiothérapie pour les tumeurs les plus agressives (grade IV selon l'OMS). Pour ces dernières, les progrès thérapeutiques au cours des 15 dernières années demeurent très modestes (survie globale médiane de 18 mois environ). De plus, même les tumeurs initialement moins agressives (grades II et III selon l'OMS) finissent le plus souvent par évoluer vers un stade réfractaire au traitement et sont responsables du décès chez la majorité des patients. Une meilleure caractérisation des mécanismes de résistance aux traitements est donc indispensable pour améliorer la survie des patients atteints de gliome malin.

Les progrès accomplis dans la compréhension de la biologie des gliomes ont permis la mise en évidence d'altérations moléculaires de l'ADN constituant des outils précieux pour la clinique <sup>3-18</sup>. Ces

« biomarqueurs moléculaires » ont des applications pour le diagnostic (définition de sous-types) mais aussi pour la prédiction du pronostic et de la réponse aux traitements. Dans les gliomes malins, on peut citer les mutations des gènes *IDH1* et *IDH2* (ci-après mutations *IDH1/2*) et la co-délétion des bras chromosomiques 1p et 19q (co-délétion 1p/19q). Ces altérations moléculaires fondatrices (*drivers*), associées au développement des astrocytomes diffus et des oligodendrogliomes, sont aujourd'hui des outils indispensables au diagnostic ainsi qu'à la stratification des traitements. Au total, l'avènement des biomarqueurs moléculaires représente un changement de paradigme pour la prise en charge des patients atteints de gliomes malins, dont le diagnostic avant l'OMS 2016 reposait essentiellement sur l'analyse histologique des tumeurs au microscope. Avec la diminution des coûts associés au séquençage à haut débit et le développement de panels ciblant des gènes et altérations moléculaires d'intérêt disponibles en clinique, le séquençage des gliomes malins tend à devenir une pratique courante dès le diagnostic initial, et nous sommes ainsi amenés à obtenir en clinique une caractérisation moléculaire de plus en plus exhaustive.

Dans ces travaux, nous avons cherché à identifier des applications du séquençage tumoral au-delà de l'identification de sous-types moléculaires tels que définis par l'OMS 2016. Dans l'*Article 1*<sup>19</sup>, l'objectif était de mieux comprendre un phénomène nommé « hypermutation », c'est à dire une élévation très importante de la charge mutationnelle observée dans certains gliomes malins, et son rôle dans la prédiction de la réponse à la chimiothérapie et à l'immunothérapie. Nous nous sommes en particulier focalisés sur des anomalies du système de réparation des mésappariements de l'ADN (système MMR pour *Mismatch Repair* en anglais), caractérisées également dans des tumeurs méningées (*Article 2*, Annexe)<sup>20</sup>. Dans les *Articles 3-7* (Annexe)<sup>21-25</sup>, nous rapportons le développement de nouvelles thérapies ciblées visant des sous-types rares associés à des drivers moléculaires spécifiques (*i.e.* gliomes avec mutations activatrices *BRAF*, gliomes avec mutations *IDH1/2*, gliomes avec altérations de la voie PI3K, gliomes avec gène de fusion *ATG7-RAF1*). Collectivement ces travaux mettent en évidence des modifications génétiques associées à une résistance ou une réponse aux traitements dans certains gliomes et contribuent à mieux comprendre l'efficacité encore limitée de l'immunothérapie dans ces tumeurs.

## II. Tumeurs neuroépithéliales : définition et traitements

### A. Classification et données épidémiologiques

Les tumeurs primitives du SNC constituent un ensemble hétérogène de pathologies bénignes ou malignes touchant l'enfant et l'adulte. Elles se développent à partir des cellules spécialisées formant les tissus du SNC (parenchyme cérébral, médullaire, épendymaire et hypophysaire, vaisseaux et méninges). On les oppose aux tumeurs secondaires (c'est à dire les métastases) qui se développent initialement à partir d'un autre organe. La classification de référence permettant le diagnostic des tumeurs du SNC est celle de l'OMS <sup>1</sup>. Elle intègre depuis 2016 des données de biologie moléculaire permettant un diagnostic dit « intégré », c'est à dire basé sur l'analyse conjointe de l'histologie et l'identification d'altérations génétiques associées à des sous-types histo-moléculaires. Certaines tumeurs du SNC sont en effet caractérisées par des voies d'oncogenèse spécifiques définies par l'acquisition d'altérations génétiques comme les mutations *IDH1/2* et la co-délétion 1p/19q. Outre ces anomalies moléculaires, la classification OMS est basée sur la localisation, le degré de différenciation, et le phénotype des cellules formant la tumeur. On distingue ainsi cinq principaux types de tumeurs primitives du SNC : les tumeurs des méninges, les tumeurs neuroépithéliales, les tumeurs germinales, les tumeurs de la région sellaie et les tumeurs hématopoïétiques <sup>1</sup>. Les tumeurs neuroépithéliales, représentant plus de 80% des tumeurs primitives malignes du SNC <sup>2</sup> (Figure 1), font l'objet de ce travail de thèse.

Les tumeurs neuroépithéliales ont pour origine soit les neurones, soit les cellules formant l'environnement des neurones (cellules gliales) ou leurs précurseurs. La classification de l'OMS 2016 distingue huit principales catégories de tumeurs neuroépithéliales, en grande majorité représentées par les gliomes malins (groupe des « Tumeurs gliales astrocytaires et oligodendrogiales ») (Table 1). En plus de la détermination du sous-type, le diagnostic histologique des tumeurs neuroépithéliales permet de d'attribuer à ces tumeurs un grade de malignité pouvant aller de I (tumeurs potentiellement curables en cas de résection complète comme les astrocytomes pilocytiques), au grade IV (tumeurs les plus agressives, principalement représentées par les glioblastomes). Ce grade est fonction de la présence de caractéristiques histologiques associées à un risque de récurrence après exérèse chirurgicale : densité cellulaire et activité mitotique, atypies cytonucléaires, prolifération endothéliocapillaire et nécrose <sup>1</sup>. Il reflète ainsi l'agressivité des tumeurs et permet d'orienter la stratégie thérapeutique.

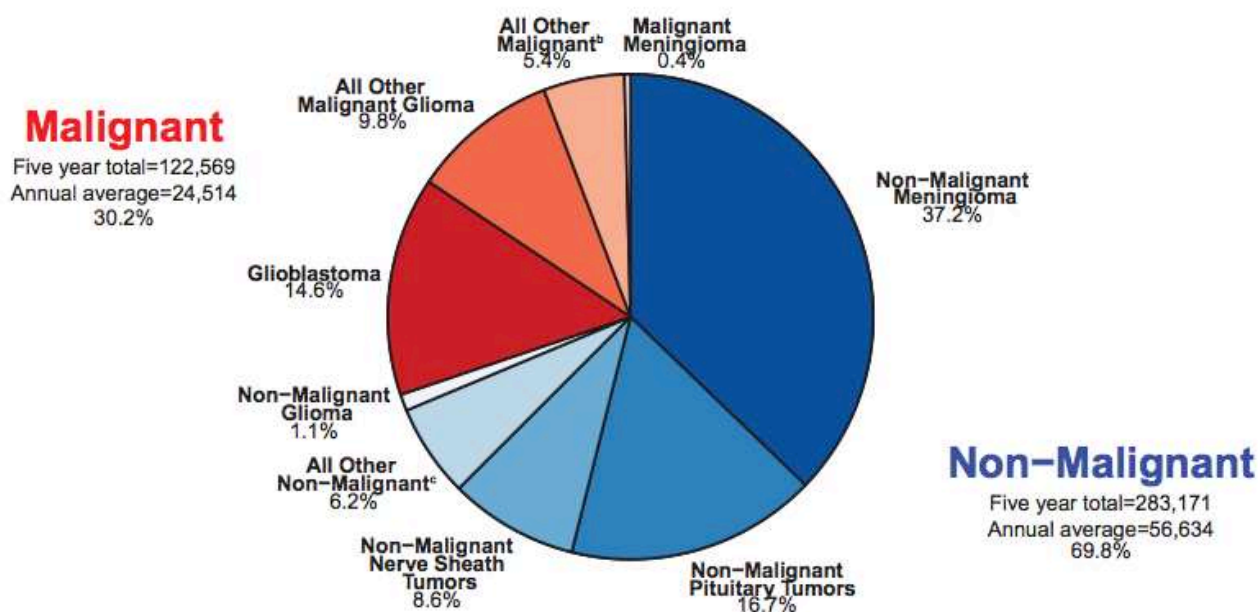


Figure 1. Distribution des tumeurs primitives du SNC aux Etats-Unis sur la période 2012-2016 (d'après Ostrom et al. <sup>2</sup>).

Les tumeurs neuroépithéliales appartiennent au groupe des cancers rares (incidence annuelle inférieure à 6/100 000 personnes) <sup>2</sup>. Fréquentes chez l'enfant (1<sup>er</sup> cancer solide, 2<sup>ème</sup> cancer le plus fréquent après les hémopathies), les tumeurs neuroépithéliales malignes présentent ensuite une incidence faible jusqu'à l'âge de 40 ans. Au-delà, le taux d'incidence progresse pour atteindre un pic entre 80 et 84 ans de 35/100 000 personnes environ. Les courbes de mortalité suivent des tendances comparables à celles décrites pour l'incidence. Le sous-type le plus fréquent (55% des tumeurs neuroépithéliales) – et également le plus agressif – est le glioblastome dont l'incidence dans les pays industrialisés est estimée à 3.2/100 000 personnes <sup>2</sup>. Entre 1990 et 2018, le nombre annuel de nouveaux cas de tumeurs neuroépithéliales a presque doublé, avec un léger ralentissement de l'augmentation de l'incidence observé à partir de 2010. Cette hausse semble attribuable pour moitié à une augmentation du risque et pour moitié au vieillissement de la population.

**Table 1. Classification simplifiée des tumeurs neuroépithéliales selon l’OMS 2016.**

<b>Histologie (altérations moléculaires associées)</b>	<b>Grade OMS</b>
<b><i>Tumeurs gliales diffuses astrocytaires et oligodendrogiales</i></b>	
Astrocytome diffus ( <i>IDH1/2</i> -muté ou -sauvage ou NOS)	Grade II
Astrocytome anaplasique ( <i>IDH1/2</i> -muté ou -sauvage ou NOS)	Grade III ou IV
Glioblastome ( <i>IDH1/2</i> -sauvage ou NOS)	Grade IV
Oligodendrogliome ( <i>IDH1/2</i> -muté et codéléte 1p19q)	Grade II
Oligodendrogliome anaplasique ( <i>IDH1/2</i> -muté et codéléte 1p19q)	Grade III
Gliome diffus de la ligne médiane ( <i>H3F3A</i> -muté)	Grade IV
<b><i>Autres tumeurs astrocytaires et gliales</i></b>	
Astrocytome pilocytique	Grade I
Gliome choroïde du 3 <sup>ème</sup> ventricule	Grade II
Xanthoastrocytome pléomorphe	Grade II
Xanthoastrocytome pléomorphe anaplasique	Grade III
Astroblastome	Non défini
<b><i>Tumeurs épendymaires</i></b>	
Ependymome myxopapillaire	Grade I
Ependymome (avec ou sans fusion <i>RELA</i> )	Grade II
Ependymome anaplasique	Grade III
<b><i>Tumeurs des plexus choroïdes</i></b>	
Papillome des plexus choroïdes	Grade I
Carcinome des plexus choroïdes	Grade III
<b><i>Tumeurs neuronales et glioneuronales</i></b>	
Tumeur dysembryoplasique neuroépithéliale	Grade I
Gangliogliome	Grade I
Gangliogliome anaplasique	Grade III
Gangliocytome dysplasique du cervelet	Grade I
Tumeur glioneuronale papillaire	Grade I
<b>Tumeur glioneuronale formant des rosettes du quatrième ventricule</b>	Grade I
<b><i>Tumeurs de la région pinéale</i></b>	
Tumeur papillaire de la région pinéale	Grade II ou III
Pinéaloblastome	Grade IV
<b><i>Tumeurs embryonnaires</i></b>	
Médulloblastome	Grade IV
Tumeur embryonnaire avec rosettes pluristratifiées	Grade IV
Tumeurs rhabdoïdes/tératoïdes atypiques (avec perte <i>SMARCB1</i> )	Grade IV

\*NOS : *not otherwise specified*, tumeurs pour lesquelles le statut moléculaire n'a pas été déterminé avec certitude (absence de génotypage ou génotypage incomplet).

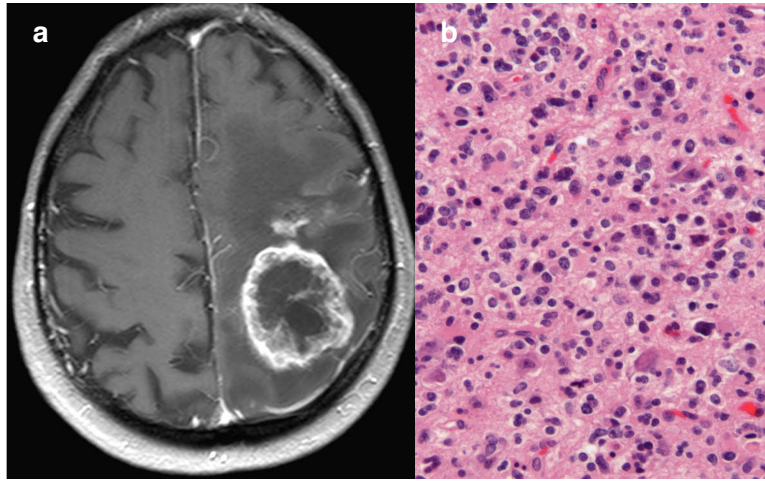
En dehors de cas minoritaires (moins de 5% au total) survenant dans des contextes d'exposition aux rayonnements ionisants (par exemple, antécédent de radiothérapie cérébrale) ou de syndrome de prédisposition génétique au cancer (Table 2), les tumeurs neuroépithéliales sont des tumeurs sporadiques à génétique complexe et ne disposent à ce jour d'aucun facteur étiologique reconnu. Des études d'association pangénomique (*Genome-Wide Association Study*, GWAS) ont néanmoins permis l'identification récente de plusieurs polymorphismes associés au risque de développement de gliome malin (notamment les loci 5p15.33, 7p11.2, 8q24.21, 9p21.3, 11q23.3, 17p13.1, et 20q13.33 à proximité des gènes *TERT*, *EGFR*, *MYC*, *CDKN2A*, *PHLDB1*, *TP53* et *STMN3*)<sup>26,27</sup>. Une meilleure caractérisation de la base fonctionnelle de ces polymorphismes pourrait permettre une meilleure compréhension des mécanismes contribuant au développement des gliomes malins.

**Table 2. Syndromes de prédisposition génétique au cancer associés au risque de tumeur neuroépithéliale.**

Syndrome de prédisposition génétiques au cancer	Gene(s) implique(s)
Syndrome de Lynch	<i>MLH1, MSH2, MSH6, PMS2</i>
<b>Syndrome de déficience constitutionnelle des gènes MMR (CMMRD)</b>	<i>MLH1, MSH2, MSH6, PMS2</i>
<b>Syndrome de von Hippel-Lindau</b>	<i>VHL</i>
Syndrome de Turcot A	<i>APC</i>
Syndrome astrocytome-mélanome	<i>CDKN2A</i>
Syndrome de Gorlin	<i>PTCH1</i>
Sclérose tubéreuse de Bourneville	<i>TSC1, TSC2</i>
Syndrome de Cowden	<i>PTEN</i>
Syndrome de Li-Fraumeni	<i>TP53</i>
Neurofibromatose de type 1	<i>NF1</i>
Neurofibromatose de type 2	<i>NF2</i>
<b>Syndrome de prédisposition aux tumeurs rhabdoïdes</b>	<i>SMARCB1</i>
<b>Syndromes associés aux mutations constitutionnelles POLE et POLD1</b>	<i>POLE, POLD1</i>

## B. Diagnostic des gliomes : sous-types moléculaires, aspects pronostiques

Les tumeurs du SNC peuvent se révéler par des symptômes et manifestations cliniques très variables d'un patient à l'autre, dépendant principalement du volume et de la vitesse de croissance des lésions ainsi que de leur localisation dans le SNC<sup>28-30</sup>. Les principaux modes de révélation sont



les crises d'épilepsie, les déficits neurologiques focaux, les troubles cognitifs ou du comportement, et/ou le syndrome d'hypertension intracrânienne (Figure 2).

**Figure 2. Tumeur fronto-pariétale gauche correspondant à un gliome de haut grade chez un patient âgé de 64 ans.** (a) IRM cérébrale en séquence axiale T1 après injection de produit de contraste. (b) Coupe histologique après coloration à l'hématoxyline et à l'éosine.

L'imagerie et notamment l'imagerie par résonance magnétique nucléaire (IRM) sont indispensables pour le diagnostic et le suivi des patients <sup>28-30</sup>. Le diagnostic définitif requiert néanmoins l'analyse anatomopathologique du tissu tumoral obtenu après résection tumorale (partielle ou complète) lorsque la tumeur est opérable, ou bien par biopsie. Outre l'effet thérapeutique en cas de résection, ceci permet l'obtention de matériel tumoral à visée diagnostique et éventuellement de recherche. Sur le plan anatomopathologique, l'approche diagnostique repose sur la combinaison d'analyses histologiques et moléculaires permettant le classement des gliomes malins dans quatre catégories principales : les oligodendrogliomes (avec mutation *IDH1/2* et co-délétion 1p/19q), les astrocytomes diffus (avec mutation *IDH1/2*, sans co-délétion 1p/19q), les glioblastomes (sans mutation *IDH1/2* ni co-délétion 1p/19q), et les autres sous-types plus rares de gliomes <sup>1</sup>. Ces techniques peuvent être combinées selon des algorithmes associant plusieurs analyses séquentielles permettant d'aboutir au diagnostic (Figure 3) :

- immunohistochimie, par exemple pour la mutation *IDH1* majoritaire (R132H) <sup>31</sup>;
- recherche de mutations hotspots par PCR puis séquençage Sanger ou pyroséquencage <sup>32,33</sup>;
- analyse en *next generation sequencing* (NGS) de panels de gènes associés au cancer permettant la recherche simultanée de nombreuses anomalies moléculaires récurrentes (mutations hotspots, autres mutations, anomalies du nombre de copies, fusions) <sup>34-38</sup>;
- utilisation de techniques émergentes comme l'analyse du méthylome <sup>39</sup>, de l'exome ou du génome complet <sup>40</sup>, ou encore du transcriptome tumoral <sup>41</sup>.

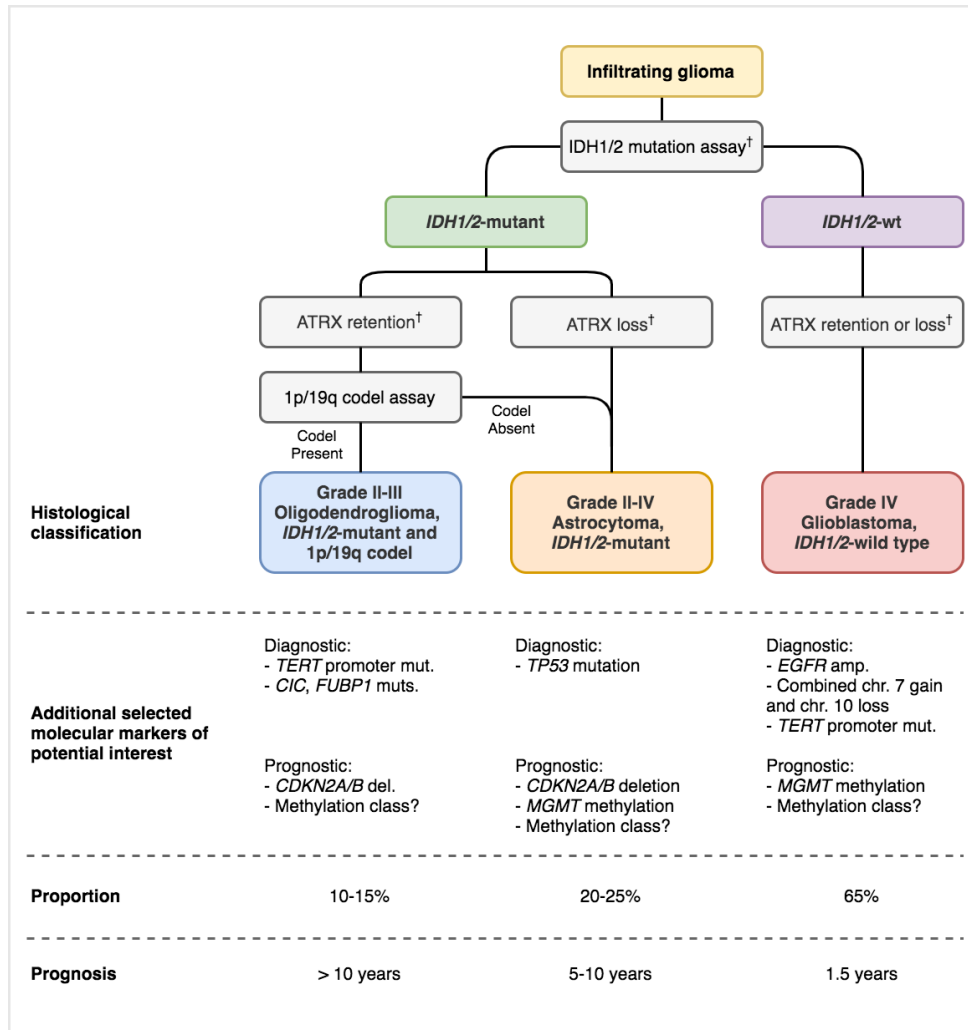


**Figure 3. Principaux sous-types de gliomes diffus et stratégie diagnostique en fonction des statuts *IDH1/2* et *1p/19q*.** †Statut obtenu par immunohistochimie ou séquençage.

Le pronostic des gliomes malins est très hétérogène selon les différents sous-types (Figure 4), et varie également de façon considérable au sein d'un même sous-type histologique. Cette variabilité est influencée par le terrain (*e.g.* âge, état général), par l'étendue de l'exérèse chirurgicale, et par une importante hétérogénéité inter-tumorale en termes de sensibilité intrinsèque aux traitements adjuvants par radiothérapie et chimiothérapie. Outre les mutations *IDH1/2* et la co-délétion *1p/19q*, toutes deux associées à une meilleure réponse aux traitements médicaux<sup>42-45</sup>, la méthylation du promoteur du gène *MGMT* codant l'enzyme de réparation de l'ADN O6-méthylguanine-ADN-méthyltransférase (*MGMT*) est associée à une meilleure réponse à la chimiothérapie par agents alkylants (voir section suivante)<sup>46</sup>. Ces biomarqueurs permettent une prédiction – imparfaite – du pronostic et une aide à la décision thérapeutique dans les gliomes les plus fréquents. Dans les tumeurs plus rares, certains biomarqueurs moléculaires sont explorés mais les effectifs limités et l'hétérogénéité des modalités thérapeutiques sont des obstacles pour la validation de leur pertinence en clinique.

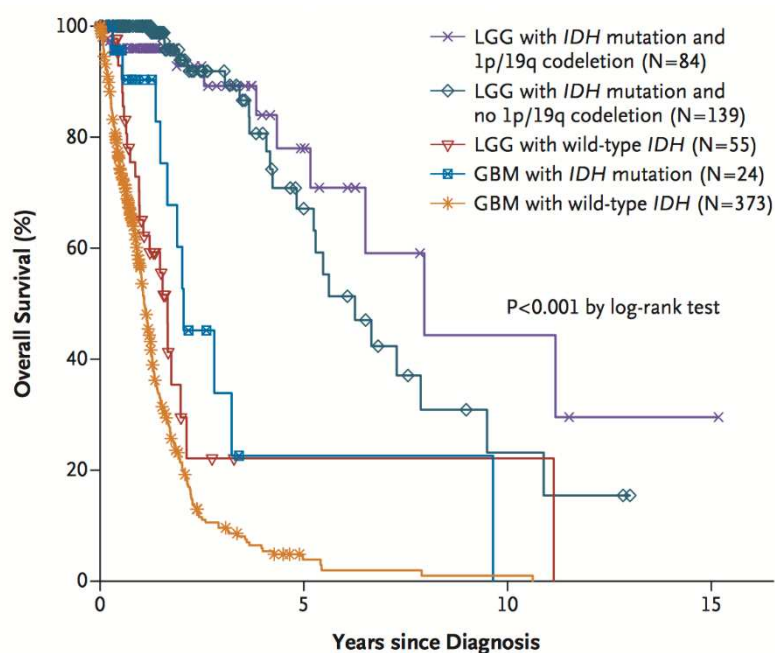


**Figure 4. Courbes de survie associées aux sous-types moléculaires des gliomes diffus inclus dans le TCGA (d'après Brat et al.<sup>7</sup>).** Abréviations : *IDH* (gènes *IDH1/2*) LGG, lower grade glioma (gliomes de grade II et III) ; GBM, glioblastoma (glioblastome).

### C. Traitements des gliomes : place des agents alkylants

Le traitement standard des gliomes malins repose sur le trépied chirurgie, radiothérapie et chimiothérapie<sup>28-30</sup>. La première étape du traitement repose le plus souvent sur la chirurgie, qui lorsqu'elle est réalisable est proposée soit dès le diagnostic initial dans les gliomes de haut grade, ou bien après une période d'observation initiale dans les gliomes diffus de grade II. Malgré l'absence d'essais randomisés, plusieurs séries chirurgicales ont montré un impact significatif de la résection complète ou subtotale sur la survie globale<sup>47-50</sup>. Néanmoins, la localisation dans le cerveau et le caractère infiltrant des gliomes rendent difficile l'exérèse chirurgicale complète. Selon la localisation de la tumeur, l'utilisation de la chirurgie éveillée et des techniques de cartographie fonctionnelle permet d'optimiser l'étendue de l'exérèse, d'augmenter le pourcentage de patients pouvant bénéficier d'une résection en régions fonctionnelles, et de diminuer le risque de déficits neurologiques postopératoires. Outre le bénéfice potentiel en survie globale, l'exérèse chirurgicale permet une amélioration souvent rapide certains symptômes comme l'hypertension intracrânienne ou l'épilepsie.

La radiothérapie est délivrée à des doses (54-60 Gy) et fractions (15-30 séances) variables selon le diagnostic histologique (notamment grade et voie moléculaire) et le terrain (notamment âge et état

général). Sauf dans certains rares cas où les protons peuvent être indiqués, des techniques classiques par faisceaux de photons sont généralement utilisées. L'irradiation vise le volume tumoral auquel des marges sont ajoutées afin de cibler d'éventuelles zones d'infiltration tumorale. Ce traitement exerce des effets anti-tumoraux sur les cellules gliales, notamment via l'induction de cassures de l'ADN et d'espèces réactives de l'oxygène, et permet souvent de diminuer les crises d'épilepsie. Dans les gliomes de grade III ou IV, l'irradiation est généralement proposée dès le diagnostic initial après la chirurgie ou la biopsie. Dans les gliomes diffus de grade II, le *timing* optimal de l'irradiation cérébrale n'est pas bien codifié. La radiothérapie précoce permet en effet d'allonger la survie sans progression mais pas la survie globale <sup>51</sup>, et augmente probablement le risque de troubles cognitifs au long terme. Des stratégies visant à différer le traitement par radiothérapie sont actuellement en cours d'évaluation dans les sous-types les plus chimiosensibles comme les oligodendrogliomes.

La chimiothérapie des gliomes malins repose sur des schémas à base d'agents alkylants qui exercent des effets anti-tumoraux sur les cellules gliales et présentent pour certains l'avantage d'une bonne pénétration de la barrière hémato-encéphalique (Figure 5a). Le concept de chimiothérapie par agents alkylants est né de l'observation par Edward Krumbhaar en 1919 que les soldats canadiens victimes d'exposition au gaz moutarde souffraient d'atteintes respiratoires et d'aplasie lymphoïde <sup>52</sup>. On distingue aujourd'hui 7 grandes familles d'agents alkylants dits « classiques » parmi lesquels des molécules des familles des nitrosourées (*e.g.* carmustine, lomustine) et des triazènes hydrazines (témozolomide, procarbazine) sont les plus fréquemment utilisés dans le traitement des gliomes <sup>53</sup>. Ces traitements sont délivrés selon 3 principaux protocoles : polychimiothérapie par PCV (procarbazine et lomustine associés à un alcaloïde extrait de la pervenche, la vincristine) ou monothérapie par témozolomide ou lomustine. Ces protocoles en association avec la radiothérapie ont démontré des bénéfices en survie allant de 2.5 mois avec le témozolomide dans le glioblastome à 5.5 ans avec le protocole PCV dans les gliomes de grade II <sup>42-45,54-59</sup>. Cependant, malgré l'efficacité de ces agents, les gliomes malins développent quasi systématiquement des mécanismes de résistance conduisant à la rechute. Identifier, comprendre et contourner ces mécanismes de résistance est un objectif majeur de la recherche préclinique et clinique en cours.

## D. Mécanismes d'action des agents alkylants

Parmi les agents alkylants utilisés dans les gliomes, les 2 molécules considérées comme les plus efficaces sont le témozolomide et la lomustine (cis-chloroethylnitrosourea [CCNU] ou encore son analogue la carmustine, bis-chloroethylnitrosourea [BCNU]) (Figure 5a). Le témozolomide est un

agent alkylant de la famille des triazènes hydrazines. Il s'agit d'une pro-drogue activée à pH physiologique via une hydrolyse enzyme-indépendante suivie d'une décarboxylation formant le 5-méthyltriazenoimidazole-4-carboxamide (MTIC) puis le 5-aminoimidazole-4-carboxamide et enfin son espèce réactive, l'ion methyldiazonium qui méthyle l'ADN <sup>60</sup>. La lomustine (cis-chloroethylnitrosourea, CCNU) et la carmustine (bis-chloroethylnitrosourea, BCNU) sont des chloroéthylnitrosourées métabolisées en 2 composés actifs : le diazohydroxyde responsable de chloroéthylation de l'ADN, et l'isocyanate responsable de carbamoylation des protéines <sup>61</sup>.

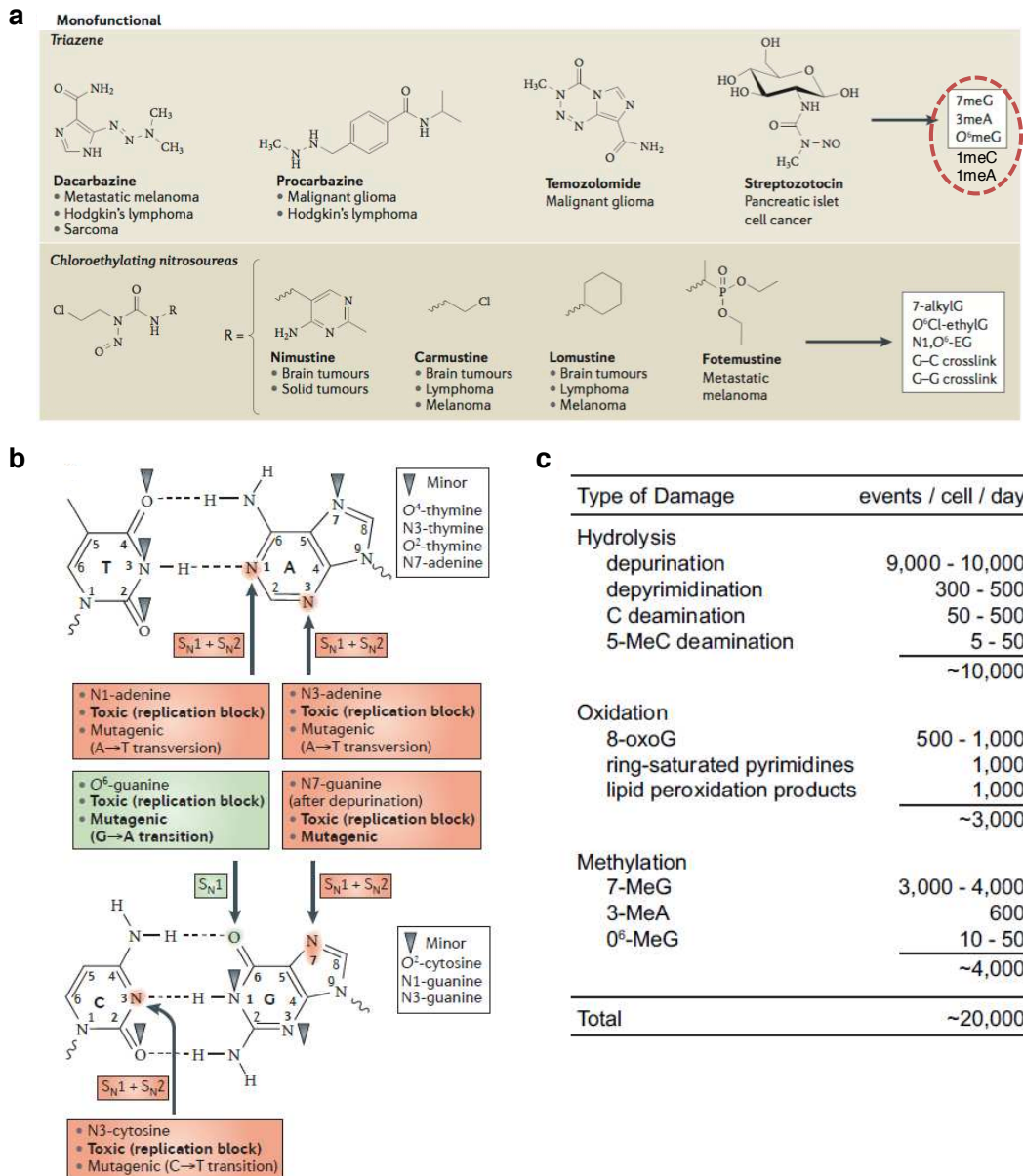


**Figure 5. Principaux types d'agents alkylants utilisés pour le traitement des gliomes malins (a) et leurs effets biologiques sur l'ADN (b) (d'après Fu et al. <sup>53</sup> [a-b] et Preston et al. <sup>62</sup> [c]). Certaines lésions induites par les agents alkylants se produisent spontanément en conditions physiologiques (c).**

Sur le plan biologique, les agents alkylants sont des composés organiques électrophiles capables de réagir avec des radicaux nucléophiles (e.g. -SH, -OH, -COOH ou -NH<sub>2</sub>) que l'on retrouve dans les protéines et les acides nucléiques<sup>53,62</sup>. Au niveau de l'ADN, ces interactions aboutissent à la formation de différents types d'adduits liés de façon covalente sur des sites préférentiels, principalement au niveau des bases puriques (N1-adenine, N3-adenine, N7-guanine, O6-guanine, etc.) (Figure 5b). L'azote N7 de la guanine est la cible principale des dommages d'alkylation sur l'ADN (60 à 80% de l'ensemble des adduits)<sup>53</sup>. Selon les types d'adduits qu'ils produisent, les agents alkylants sont dits mono- (adduit sur un nucléotide) ou bi-fonctionnels (adduit reliant deux nucléotides adjacents pour former des ponts inter- ou intra-brins). Ces adduits modifient la structure de la double hélice, empêchent la réplication et la transcription (notamment adduits inter- ou intra-brin), et induisent des cassures simple- ou double-brin de l'ADN. Ceci conduit à la mise en jeu de systèmes de réparations et éventuellement à l'apoptose de la cellule lésée en cas de dommage irréversible. De façon importante, certaines lésions de l'ADN causées par les agents alkylants (e.g. N7-méthylguanine, N7-méthyladénine, O6-méthylguanine) sont également fréquemment formées en conditions physiologiques (Figure 5c) ; les cellules disposent donc de mécanismes permettant de réparer ces lésions.

Sur le plan de la thérapeutique anti-tumorale, de nombreux phénomènes de résistance limitent l'efficacité des agents alkylants, parmi lesquels on peut citer :

- Une faible concentration de drogue par une augmentation de l'efflux ou une diminution de son entrée dans les cellules<sup>63,64</sup>;
- L'inactivation de la drogue par des mécanismes de détoxification, comme l'interaction avec le glutathion<sup>65-67</sup>;
- L'augmentation de la réparation de l'ADN, notamment via l'activité des déméthylases ALKBH2-3 et MGMT, et des systèmes BER et NER (*Base Excision Repair* et *Nucleotide Excision Repair*)<sup>46,53,68-72</sup>;
- L'inactivation du système de réparation MMR<sup>73-78</sup>;
- L'expression de protéines impliquées dans la signalisation anti-apoptotique comme Bcl-2 et Bcl-xL<sup>79</sup>.

Les mécanismes de résistance en lien avec la réparation de l'ADN sont de loin les mieux caractérisés (Figure 6). Certains de ces mécanismes sont redondants et leur mise en jeu dépend ainsi de leur disponibilité à proximité des lésions de l'ADN. Parmi ces différentes protéines et mécanismes, l'expression de la protéine MGMT et des protéines du MMR ont été associées à des mécanismes de résistance au témozolomide et à l'acquisition d'un phénotype dit « hypermutant » sous traitement.

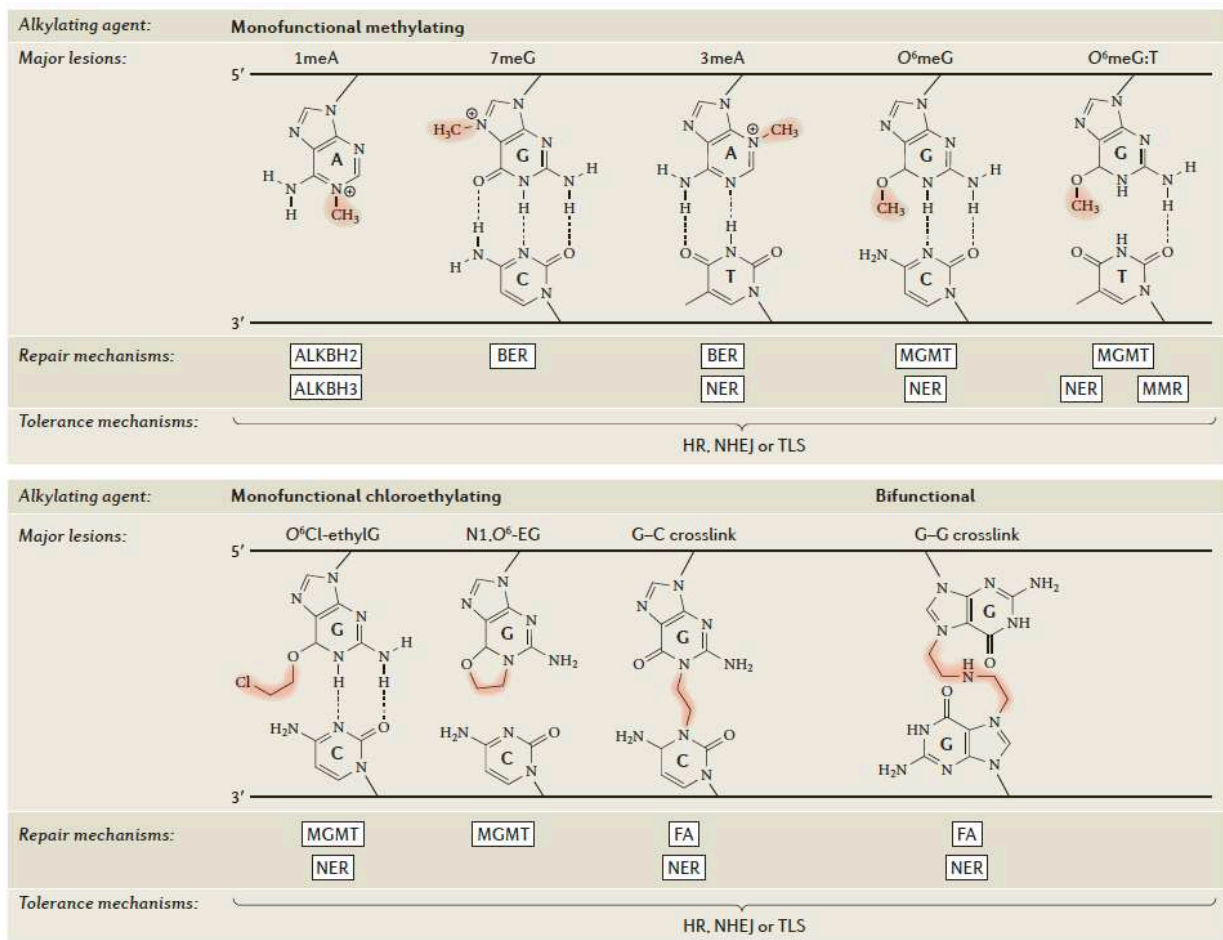


**Figure 6. Représentation schématique des principaux dommages ADN causés par les agents alkylants utilisés dans les gliomes et leurs mécanismes de réparation associés (d'après Fu et al.<sup>53</sup>).** Partie supérieure : lésions induites par le témozolomide. Partie inférieure : lésions induites par les chloroéthylnitrosourées.

## E. Résistance au témozolomide : rôles de la MGMT et du système MMR, phénotype « hypermutant »

Le témozolomide est l'agent actuellement le plus fréquemment utilisé pour le traitement des gliomes malins. L'efficacité du témozolomide résulte principalement de la formation d'adduits O6-méthylguanane (O6-meG) au niveau de l'ADN<sup>80</sup>. En conditions physiologiques, les adduits O6-meG sont nettement moins fréquents que les autres types de lésions plus fréquemment induites par le témozolomide comme la N7-méthylguanane (rapport 1:100 environ)<sup>62</sup>. Ceci explique en partie le rôle important des lésions O6-meG dans la cytotoxicité des alkylants. La protéine MGMT permet la réparation directe des lésions O6-meG, de même que les adduits O6-chloroéthylguanane formés par les chloroéthylnitrosourées. Au cours de cette réparation, la MGMT séquestre le groupe méthyle de

l'O6-meG par transfert covalent, rétablissant ainsi la guanine à son état normal. Cette réaction aboutit néanmoins à une inactivation irréversible de la protéine après ubiquitination (Figure 7). La MGMT n'est donc pas stricto sensu une enzyme, puisqu'elle n'est capable d'effectuer qu'un seul cycle de réparation (enzyme suicide). Etant donné cette particularité, l'expression de la MGMT a été proposée comme l'une des principales causes de résistance au témozolomide. La méthylation du promoteur de *MGMT*, qui conduit à un *silencing* épigénétique de son expression, est en effet associée à une sensibilité accrue aux traitements par témozolomide et chloroéthylnitrosourées et à un meilleur pronostic chez les patients atteints de gliome malin <sup>46,69,72</sup>.

En l'absence de MGMT (par exemple en cas de méthylation du promoteur ou de dégradation du pool de protéines disponibles), une thymine est incorporée face au résidu O6-meG – reconnu comme une adénine – lors de la réplication de l'ADN par les polymérases, créant à ce niveau un mésappariement O6-meG:T. Ce mésappariement est reconnu par les protéines du système MMR, un complexe multiprotéique (protéines MSH2, MSH6, MLH1 et PMS2 notamment) permettant de reconnaître et de réparer les mésappariements de l'ADN et erreurs de réplication par glissement (*slippage*) de la polymérase lors de la réplication de l'ADN <sup>81,82</sup> (Figure 8). Selon le modèle dit de « cycles futiles » (*futile cycling*), l'alternance successive d'excisions de thymine mésappariée par le système MMR puis de resynthèses d'une thymine face au résidu O6-meG non réparé par les polymérases aboutit à la mise en tension de la double-hélice et à la formation de cassures double-brin de l'ADN, hautement toxiques et aboutissant éventuellement à l'activation de programmes apoptotiques <sup>75,83</sup> (Figure 7). Ainsi, selon ce modèle, la toxicité de l'O6-meG dépend indirectement de l'intégrité du système MMR <sup>84,85</sup>. Cette hypothèse a été confortée par l'observation dans des modèles déficients en MMR (*e.g.* lignées cellulaires de cancer du côlon avec mutations dans les gènes codant pour les protéines MMR) de résistance majeure aux agents alkylants tels que le témozolomide <sup>73-78</sup>. De façon importante, dans d'autres cancers, la déficience MMR s'associe à des phénomènes d'hypermutabilité et d'accumulation de petites insertions et délétions (indels) au niveau de courtes séquences répétées dans le génome, un phénotype appelé instabilité des microsatellites (MSI) (Figure 8).

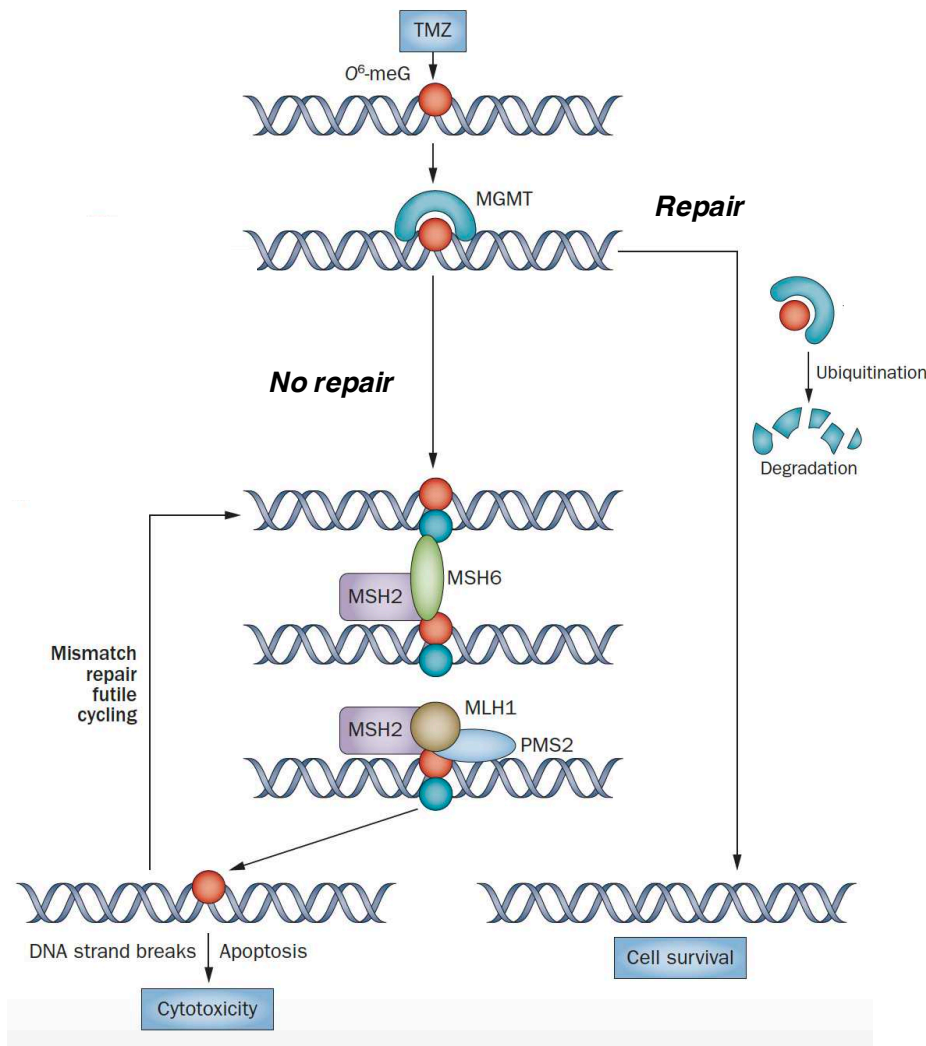


**Figure 7. Mécanisme de cytotoxicité du témozolomide et réparation médiée par la MGMT (d'après Wick et al.<sup>86</sup>).** En l'absence de réparation des adduits O<sup>6</sup>-meG par la MGMT, la cytotoxicité de ces lésions dépend indirectement de l'intégrité du système MMR.

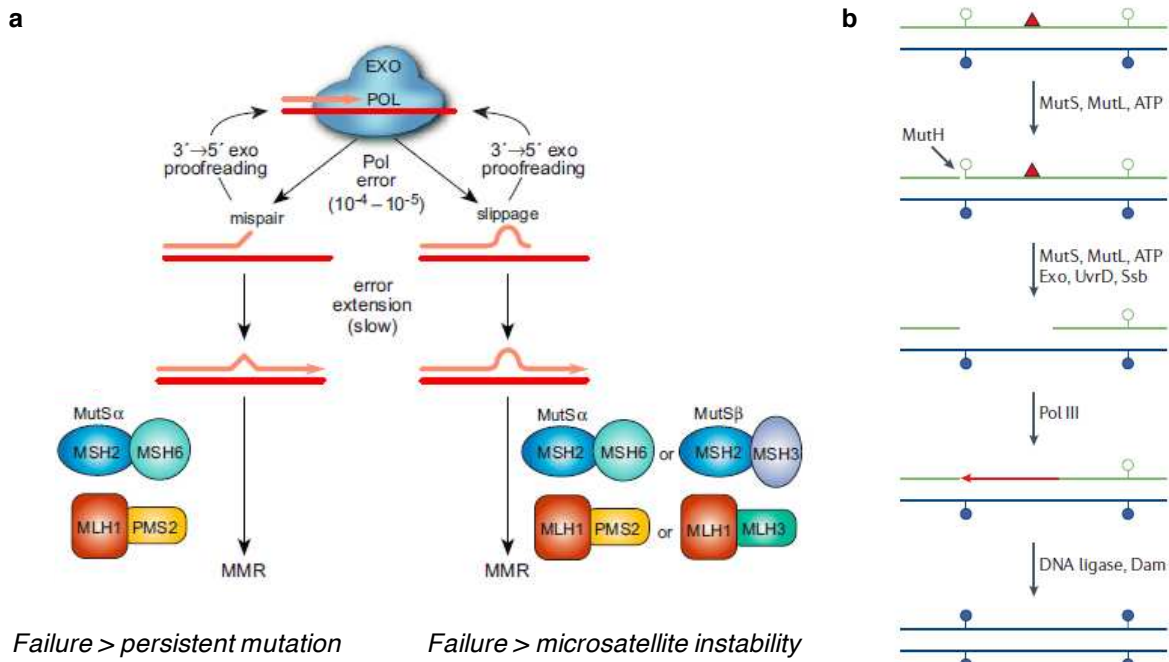


**Figure 8. Représentation schématique de la réparation des erreurs d'incorporation de l'ADN polymérase par les systèmes de *proofreading* et MMR (d'après Preston et al.<sup>62</sup> [a] et Jiricny<sup>81</sup>[b]).** a) Pendant la synthèse de l'ADN, de rares erreurs des polymérase (mésappariements de bases à gauche ou glissement de la matrice à droite) empêchent l'extension de l'amorce et déclenchent le transfert du brin d'ADN en croissance du site actif de la polymérase (POL) vers le site actif de l'exonucléase (EXO) où l'erreur est éventuellement excisée. Les erreurs qui échappent au système de *proofreading* de la polymérase sont corrigées, au moins en partie, par deux voies partiellement redondantes du système MMR. Les protéines MSH2 et MLH1 sont indispensables au fonctionnement de ce système. Les protéines MSH6 et PMS2 ont des protéines *back-ups* permettant la formation de complexes MutS et MutL alternatifs (hétéroduplexes MSH2:MSH3 et MLH1:MLH3), notamment pour la réparation des erreurs de glissement de la matrice (*slippage*). En l'absence de réparation, les mésappariements de bases aboutissent à la transmission d'une mutation ou d'une insertion/délétion dans une des cellules filles. L'accumulation de ces erreurs est à l'origine d'un phénotype hypermutant avec signature mutationnelle spécifique (en lien avec les mutations) plus ou moins associé à un phénotype d'instabilité des microsatellites (en lien avec les insertions/délétions) qui correspond à la présence dans différentes cellules de fragments de tailles différents au niveau des séquences microsatellites. MutS reconnaît les dommages à l'ADN et signale également l'apoptose. b) Modèle représentant l'excision/resynthèse de mésappariement de l'ADN (triangle rouge) par le système MMR et la polymérase chez *Escherichia coli*. L'ADN nouvellement synthétisé (vert) est reconnu par le système MMR car non méthylé (cercles vides).

Alors que les anomalies du système MMR sont extrêmement rares dans les gliomes malins nouvellement diagnostiqués, des mutations MMR – souvent non caractérisées sur le plan fonctionnel – ont été observées chez 5 à 30% des patients atteints de gliome malin en récurrence après exposition à des agents alkylants<sup>4,87-96</sup>. De plus, certaines de ces études ont pu comparer les profils moléculaires de paires de gliomes pré- et post-traitement et ont montré qu'un sous-groupe de tumeurs développait un phénotype « hypermutant » caractérisé par l'accumulation de centaines de mutations, après traitement par témozolomide notamment. Collectivement, ces observations, ainsi que les données indiquant une résistance aux agents alkylants dans les modèles MMR-déficents<sup>73-78,97-101</sup>, ont suggéré un lien mécanistique entre déficits MGMT et du système MMR, résistance au témozolomide et phénotype hypermutant dans les gliomes malins<sup>102</sup> (Figure 9). Néanmoins, ce lien n'a jamais été démontré dans des modèles isogéniques de gliomes, et les gliomes hypermutants présentent des caractéristiques inhabituelles – notamment une signature mutationnelle unique et l'absence de phénotype MSI (voir section suivante) – ne permettant pas de les relier formellement au groupe des cancers avec anomalies du système MMR. Ceci nous a conduit à étudier plus en profondeur les caractéristiques cliniques et moléculaires des gliomes hypermutants.

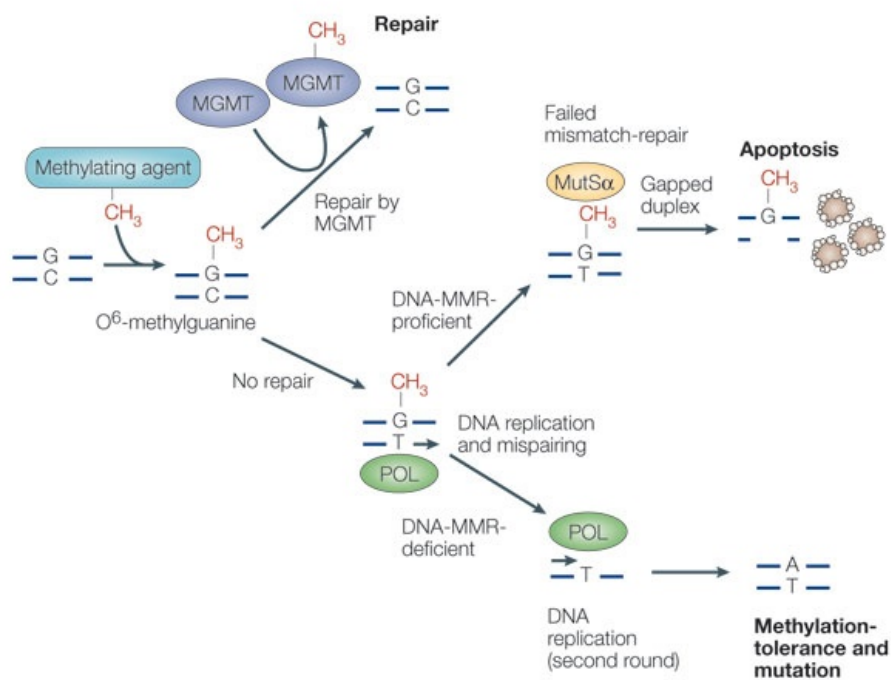


**Figure 9. Modèle suggérant un lien mécanistique entre déficits MGMT et du système MMR, résistance témozolomide et phénotype hypermutant dans les gliomes malins (d'après Allan et al<sup>26</sup>).**

### **III. Hypermutation dans les gliomes**

#### **A. Etude de la charge et de la signature mutationnelles dans les cancers, potentiel rôle prédictif dans la prédiction de la réponse à l'immunothérapie**

Les mutations somatiques retrouvées dans les cancers sont causées par des processus mutationnels d'origine exogène et endogène qui opèrent au cours du développement de la cellule œuf à la cellule tumorale <sup>103-108</sup>. Chaque processus mutationnel peut impliquer des composantes de dommages ou modifications de l'ADN, d'anomalie de réplication ou de réparation de l'ADN et génère une signature mutationnelle caractéristique qui peut comprendre des substitutions de bases (Figure 10), des indels, des réarrangements chromosomiques et des anomalies du nombre de copies génomiques. Parfois, plusieurs processus mutationnels opèrent simultanément, et le profil mutationnel de la tumeur incorpore différentes signatures mutationnelles superposées. En conséquence, la caractérisation systématique des profils mutationnels d'échantillons tumoraux offre le potentiel de révéler les processus normaux et pathologiques contribuant à l'accumulation de mutations et donc au développement des cancers (Figure 10). Avec l'avènement des techniques de séquençage à haut débit et l'analyse génomique de larges cohortes de tumeurs humaines par des consortiums internationaux <sup>109</sup>, des techniques mathématiques ont été développées afin de permettre l'analyse systématique de signatures mutationnelles à partir de catalogues de mutations somatiques, et ainsi d'estimer le nombre de mutations attribuables à chaque signature mutationnelle dans des échantillons individuels <sup>103,105,110-112</sup>. De façon importante, ces méthodes, initialement développées à partir de données de séquençage d'exomes ou génomes tumoraux, ont récemment été appliquées avec succès à l'analyse d'échantillons séquencés par panels NGS de 1-2 Mégabases (Mb), notamment en présence d'hypermutation <sup>38,113,114</sup>. Ceci les rend potentiellement applicables aux données de séquençage obtenues dans le cadre de la pratique clinique courante, par exemple pour la détermination des sous-types moléculaires des gliomes.

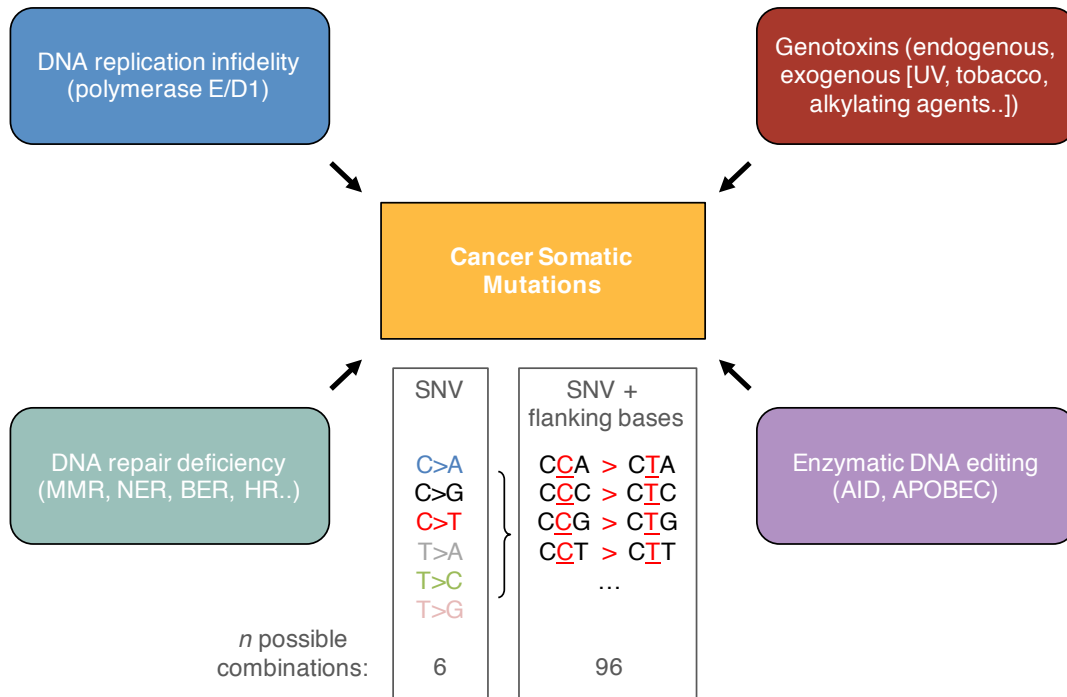


**Figure 10. Processus mutationnels exogènes et endogènes contribuant à l'accumulation de mutations somatiques dans les tumeurs humaines et technique d'analyse des mutations ponctuelles (SNV, *single nucleotide variants*).** S'il existe de très nombreux processus mutationnels fruits de diverses combinaisons de dommages et de capacités de réparation de l'ADN, le nombre de mutations ponctuelles différentes se limite à 6 lorsque seul le nucléotide mutant est pris en compte. Cette limite est contournée par l'inclusion lors de l'analyse du contexte trinuécléotidique de chaque variant, permettant d'augmenter le nombre de combinaisons possibles à 96, et d'augmenter la spécificité de l'analyse des processus mutationnels opérationnels.

Outre la caractérisation des processus mutationnels, ces progrès ont permis d'estimer de façon précise le nombre de mutations somatiques dans chaque échantillon tumoral par le calcul de la charge mutationnelle (nombre de mutations somatiques par Mb). Même s'il n'existe actuellement pas de méthode référence pour le calcul de la charge mutationnelle ni de seuil permettant de définir l'hypermutation (dans les travaux reposant sur des exomes, ce seuil est habituellement fixé à 10 mutations par Mb), l'analyse de grands nombres d'échantillons a permis d'identifier des tumeurs se distinguant des autres du fait de la présence d'une charge mutationnelle particulièrement élevée ; ces échantillons sont dits hypermutants. La charge mutationnelle est influencée par le type de tumeur (notamment le nombre de réplifications cellulaires nécessaires au processus de transformation) et les processus mutationnels opérants. Tous types de cancers confondus, ces facteurs ne contribuent qu'à des variations modestes de la charge mutationnelle et la majorité des cancers – notamment les gliomes – ont un nombre relativement faible de mutations somatiques (Figure 11a). Certains cancers comme le cancer colorectal, le mélanome ou le cancer pulmonaire sont au contraire fréquemment associés à un phénotype hypermutant <sup>103</sup>. L'hypermutation peut être causée par des facteurs environnementaux

(e.g. exposition aux UV ou aux cancérogènes du tabac), par une dérégulation des enzymes de la famille des cytidine désaminases APOBEC, ou encore par des anomalies de réplication (mutations des principales polymérases Pol $\epsilon$  et Pol $\delta$ 1) ou de réparation de l'ADN (déficit du système MMR notamment) <sup>103,105,113</sup>.

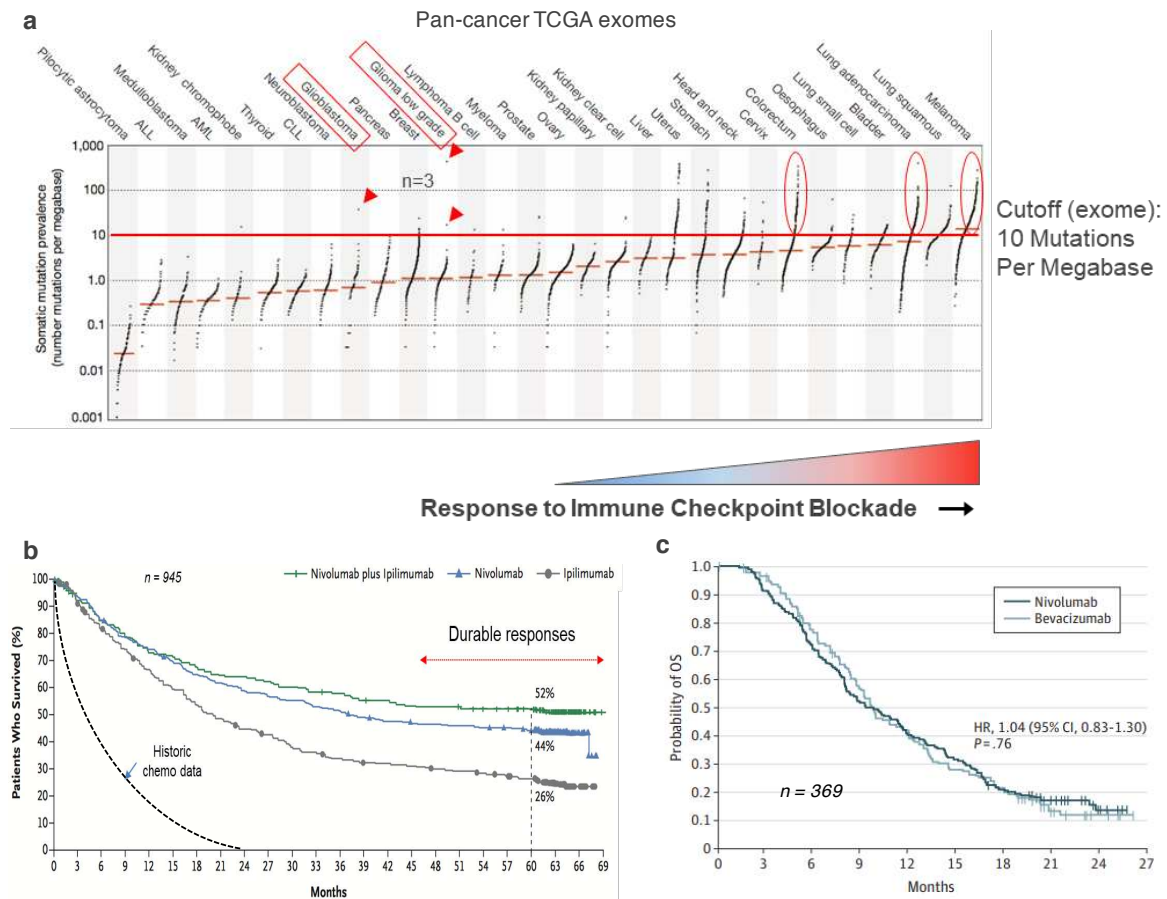


**Figure 11.** Analyse de la charge mutationnelle dans les tumeurs du TCGA (a) et réponse aux immunothérapies par inhibiteurs de checkpoints immunitaires dans des cancers avec charge mutationnelle élevée (b, mélanomes) ou faible (c, glioblastomes) (d'après Alexandrov et al. <sup>2</sup> [a], Larkin et al. <sup>115</sup> et Reardon et al. <sup>116</sup>).

Alors que les travaux sur les processus mutationnels se focalisaient initialement sur la meilleure compréhension des facteurs participant aux processus d'oncogenèse et visant à prédire la trajectoire évolutive des cancers et l'accumulation de mutations supplémentaires, des données récentes indiquent que l'hypermutation pourrait représenter un facteur prédictif de réponse aux traitements par inhibiteurs de checkpoints immunitaires (ICI) chez les patients atteints de cancer <sup>117-130</sup>. Les ICI (e.g. anticorps monoclonaux anti-PD-1, PD-L1, CTLA-4) sont des traitements dirigés contre des récepteurs membranaires (points de contrôle du système immunitaire) essentiels dans le processus d'activation des cellules immunitaires. Les ICI ont pour objectif principal de lever l'inhibition de la

réponse immunitaire anti-tumorale effectrice (e.g. par les lymphocytes cytotoxiques) induite par l'expression de points de contrôle du système immunitaire les cellules tumorales. Ces traitements ont démontré une efficacité impressionnante dans plusieurs types tumoraux, notamment certains cancers avec déficience MMR (e.g. cancers colorectaux et de l'endomètre)<sup>123,124,130,131</sup> et d'autres cancers hypermutants (e.g. mélanome et cancer du poumon)<sup>115,118-120,125,128</sup> (Figures 11b, 12). Les facteurs pouvant expliquer cette association sont nombreux. Parmi ceux-ci, il a été démontré que les cancers hypermutants présentent une augmentation significative de leur charge en néoantigènes, ce qui les rend plus susceptibles à une reconnaissance par les cellules effectrices du système immunitaire<sup>119,122,132</sup>. A l'inverse, Dans les cancers avec charge mutationnelle habituellement faible comme les gliomes malins, les traitements par ICI ont montré des résultats très modestes (Figure 11c)<sup>116</sup>. De façon importante, plusieurs observations cliniques récentes ont rapporté une efficacité significative des traitements par ICI chez des patients atteints de gliome malin avec phénotype hypermutant<sup>117,126,127</sup> (Figure 12). Néanmoins, ces observations se limitaient à de rares cas survenant dans des contextes relativement uniques (e.g. syndrome de déficience constitutionnelle des gènes MMR). Leur applicabilité dans d'autres contextes moins rares reste ainsi à déterminer.

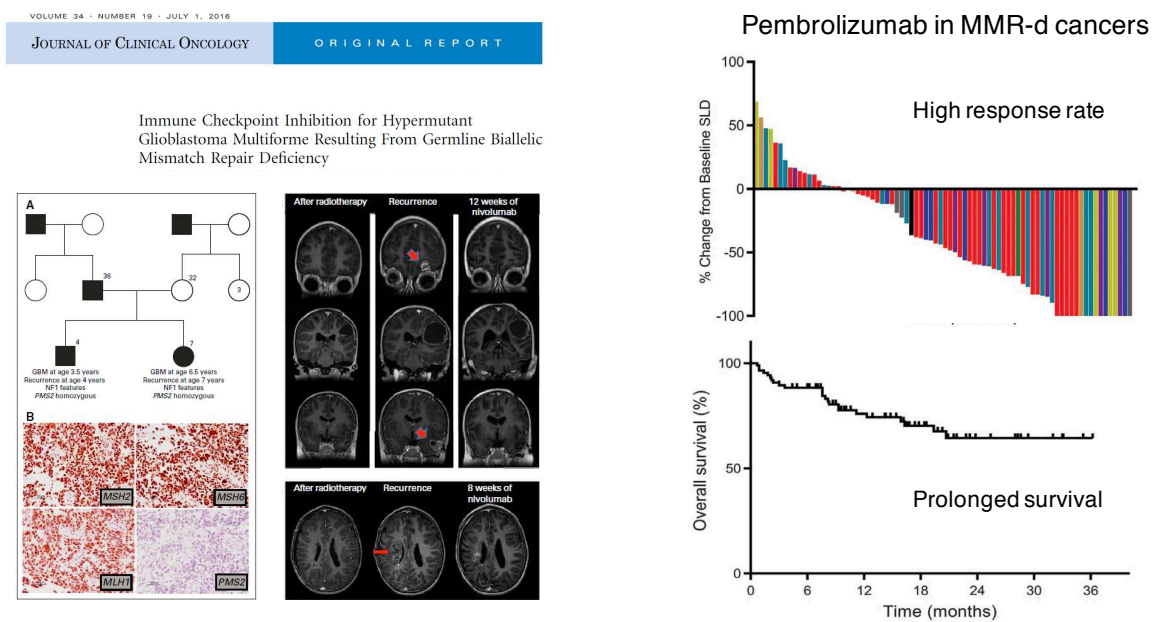


**Figure 12. Réponse aux traitements par ICI dans des tumeurs MMR-déficientes (gauche, gliomes ; droite, pan-cancer) (d'après Bouffet et al.<sup>117</sup> [a] et Le et al.<sup>124</sup>).**

Ainsi, nous disposons désormais de méthodes permettant d'établir une cartographie détaillée de la charge et des signatures mutationnelles retrouvées dans de larges cohortes de tumeurs séquencées, avec le potentiel de mieux prédire la réponse aux traitements par ICI. Nous nous sommes donc intéressés à la question des mécanismes responsables d'hypermutation dans les gliomes et à leur réponse éventuelle aux ICI.

## B. Hypermutation dans les gliomes

L'hypermutation dans les gliomes survient dans deux contextes très différents. Dans un premier cadre (hypermutation *de novo*), elle est retrouvée dès le diagnostic initial, suggérant la mise en jeu dans ces tumeurs de processus d'oncogenèse associés à l'hypermutation. Ces tumeurs se développent en effet le plus souvent chez des patients avec syndrome de prédisposition génétique au cancer associés à des anomalies constitutionnelles des systèmes de réplication de l'ADN (mutations des polymérase Pol $\epsilon$  et Pol $\delta$ 1) ou du système MMR<sup>113,133-139</sup>. Dans un second cadre (hypermutation « post-traitement »), l'hypermutation est absente lors du diagnostic initial mais retrouvée lors de la récurrence après traitement notamment par agents alkylants<sup>4,87-96</sup>, suggérant que l'hypermutation est soit la conséquence directe du traitement, soit elle s'associe à des mécanismes de résistance au traitement. L'analyse des signatures mutationnelles telles que décrites précédemment confirme que ces deux cadres (hypermutation *de novo* et post-traitement) sont différents sur le plan mécanistique (Figure 13). En effet, on retrouve le plus souvent dans les gliomes avec hypermutation *de novo* des signatures mutationnelles associées aux déficiences MMR (*e.g.* signatures COSMIC 6, 15 ou 20) ou des polymérase Pol $\epsilon$  et Pol $\delta$ 1 (signature COSMIC 10), alors que les gliomes avec hypermutation post-traitement présentent une signature mutationnelle formée par une très grande majorité de transitions C>T au niveau de régions CpC et CpT, la signature 11<sup>103</sup>. Bien que l'étiologie de la signature 11 reste inconnue, elle se rapproche de signatures observées dans des modèles *in vitro* exposés aux agents alkylants<sup>140</sup>.

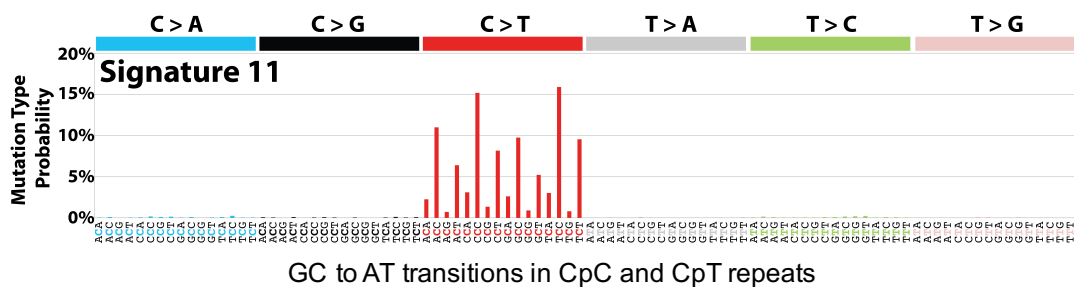
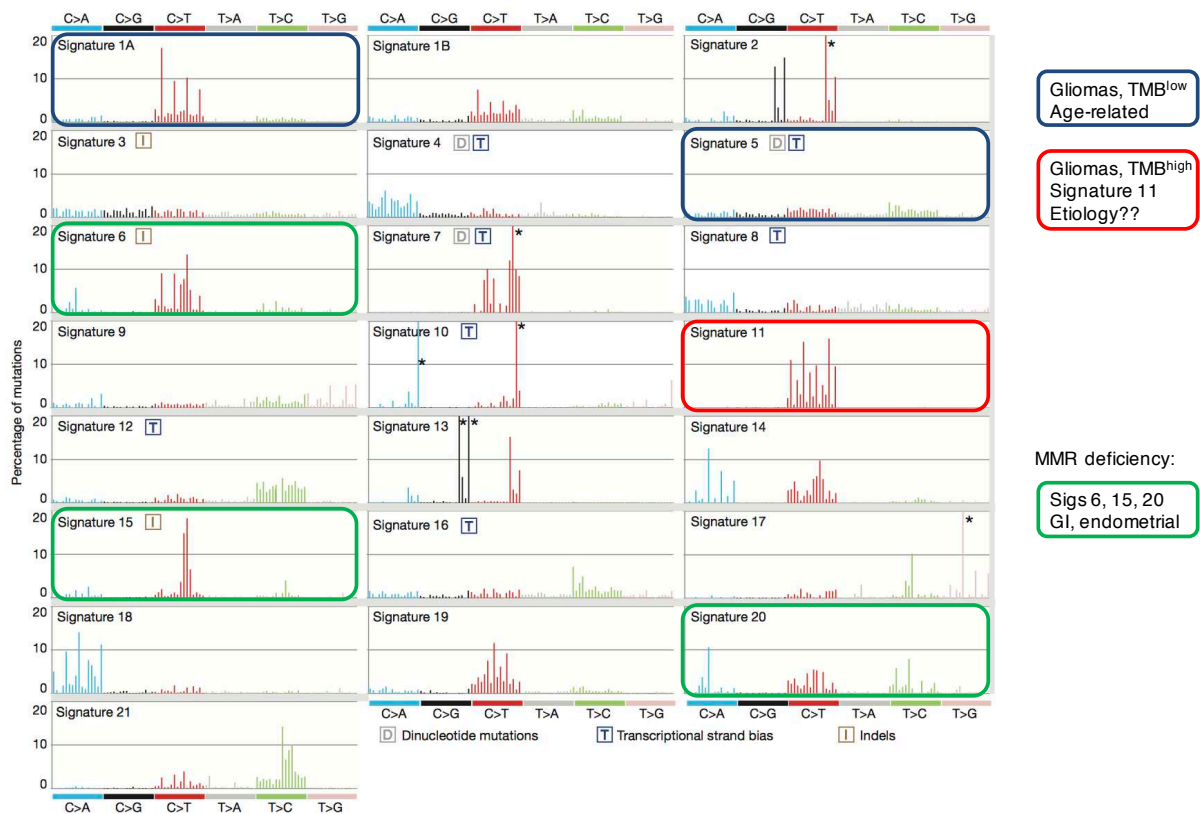


**Figure 13. Signatures mutationnelles retrouvées dans les gliomes avec charge mutationnelle faible (en bleu) ou avec hypermutation *de novo* (vert) ou post-traitement (rouge) (d'après Alexandrov et al.<sup>103</sup>). Le spectre mutationnel de la signature 11 est représenté en bas.**

### 1. Hypermutation dans les gliomes lors du diagnostic initial

Cette catégorie regroupe quatre principaux cadres, tous rares ou exceptionnels :

- Syndrome de prédisposition génétique au cancer causés par une déficience mono-allélique du système MMR<sup>113,135,139,141</sup>;
- Syndrome de prédisposition génétique au cancer causés par une déficience bi-allélique du système MMR<sup>113,134,136-138,142</sup>;
- Syndrome de prédisposition génétique au cancer causés par des mutations constitutionnelles des polymérase Polε et Polδ1<sup>113,143</sup>;

**Université Paris-Saclay**

Espace Technologique / Immeuble Discovery

Route de l'Orme aux Merisiers RD 128 / 91190 Saint-Aubin, France

- Anomalies somatiques du système MMR ou des polymérase Polε et Polδ<sup>126,127,144</sup>.

### a) Déficiences du système MMR

Les gliomes malins associés à des déficits constitutionnels ou somatiques du système MMR sont très rares : ils représentent moins de 1% des gliomes diffus dans le TCGA (Figure 14)<sup>6,7</sup>.

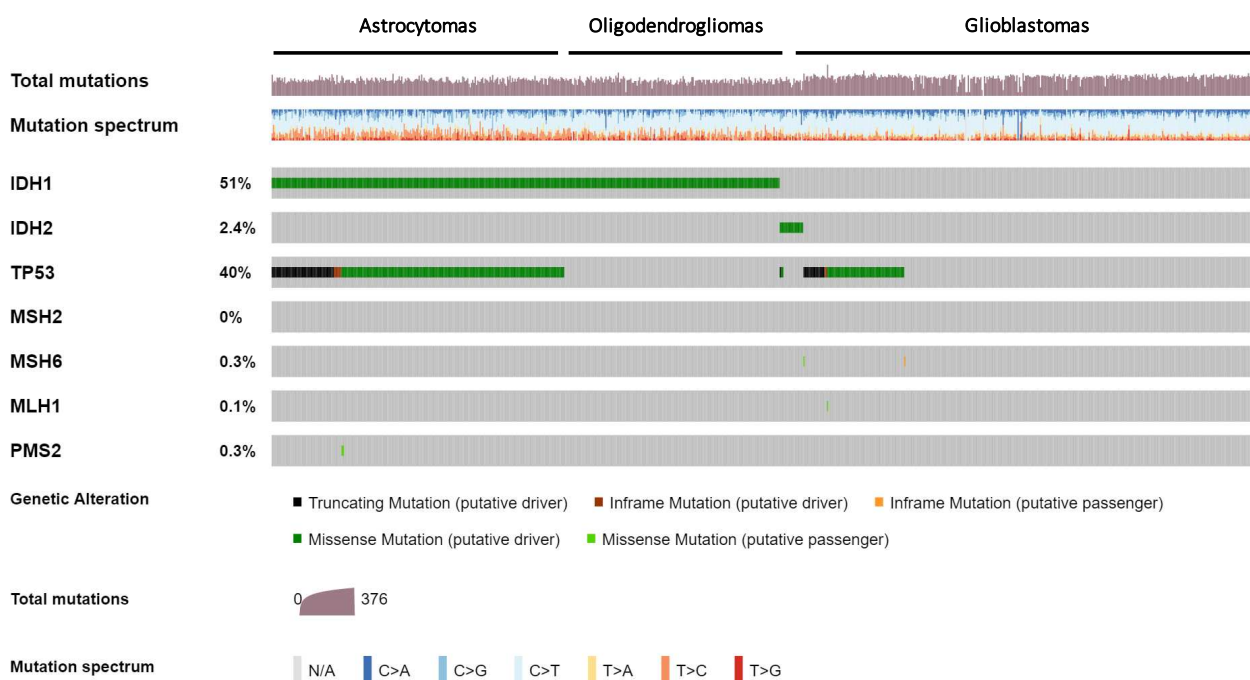


**Figure 14. Fréquence des mutations des principaux gènes du MMR dans des gliomes malins séquencés lors du diagnostic initial (données TCGA<sup>6,7</sup>).**

Des déficits constitutionnels du système MMR sont retrouvés dans deux syndromes de prédisposition au cancer : le syndrome de Lynch – le syndrome de prédisposition génétique au cancer le plus fréquent (1/800-1/1000 dans la population générale) – et le déficit constitutionnel bi-allélique de réparation des mésappariements (CMMRD), beaucoup plus rare. Ces syndromes sont causés par des mutations mono- ou bi-alléliques germinales des gènes MMR (*MSH2*, *MSH6*, *MLH1*, *PMS2*) ou plus rarement par mutation du gène *EPCAM* responsable d'une inactivation épigénétique de *MSH2*. Dans le syndrome de Lynch, l'inactivation somatique du second allèle sauvage par mutation ou perte d'hétérozygotie entraîne une perte de la fonction du MMR<sup>145</sup>. Les patients atteints de syndrome de Lynch développent le plus souvent des carcinomes (*e.g.* cancer colorectal, de l'endomètre, urothélial, gastrique, pancréatique et de l'intestin grêle). La raison pour laquelle certains patients développent des gliomes malins plutôt que des carcinomes est inconnue<sup>113,135,139,141,146</sup>. A l'inverse, les patients atteints de CMMRD développent le plus souvent des hémopathies malignes, des carcinomes

colorectaux et des gliomes malins dans l'enfance ou l'adolescence<sup>113,134,136-138,142</sup>. Les patients atteints de syndrome de Lynch ou de CMMRD développant des gliomes malins ont un pronostic sombre.

Sur le plan moléculaire, bien que l'ensemble des gliomes associés au CMMRD soient hypermutants, on ne sait pas si la même chose est vraie dans le syndrome de Lynch. Sur le plan du diagnostic, les gliomes avec déficience MMR semblent présenter des différences importantes avec d'autres cancers avec déficience MMR comme les cancers colorectaux. Des données issues de patients avec syndrome de Lynch ou CMMRD suggèrent en effet que le phénotype MSI – marqueur diagnostique utilisé en pratique clinique courante et fortement corrélé à la déficience MMR dans les cancers colorectaux<sup>147,148</sup> – pourrait être absent dans les gliomes malins<sup>133,134,136,137</sup>. Les mécanismes sous-tendant ces différences ne sont pas connus. En pratique clinique, cette particularité peut rendre difficile le diagnostic de déficience MMR chez un patient atteint de gliome. Etant donné la fréquence des mutations *MSH6* et *PMS2* et les difficultés d'interprétation de la technique dans les gliomes, il est préférable d'utiliser l'immunohistochimie des quatre protéines MMR (*MSH2*, *MSH6*, *MLH1*, *PMS2*), si possible en association à un séquençage des gènes MMR plus ou moins associé à une étude de la charge et des signatures mutationnelles. L'application de ces techniques a permis l'établissement récent au laboratoire de lignées de gliomes dérivées de patients atteints de syndrome de Lynch (Figure 15).

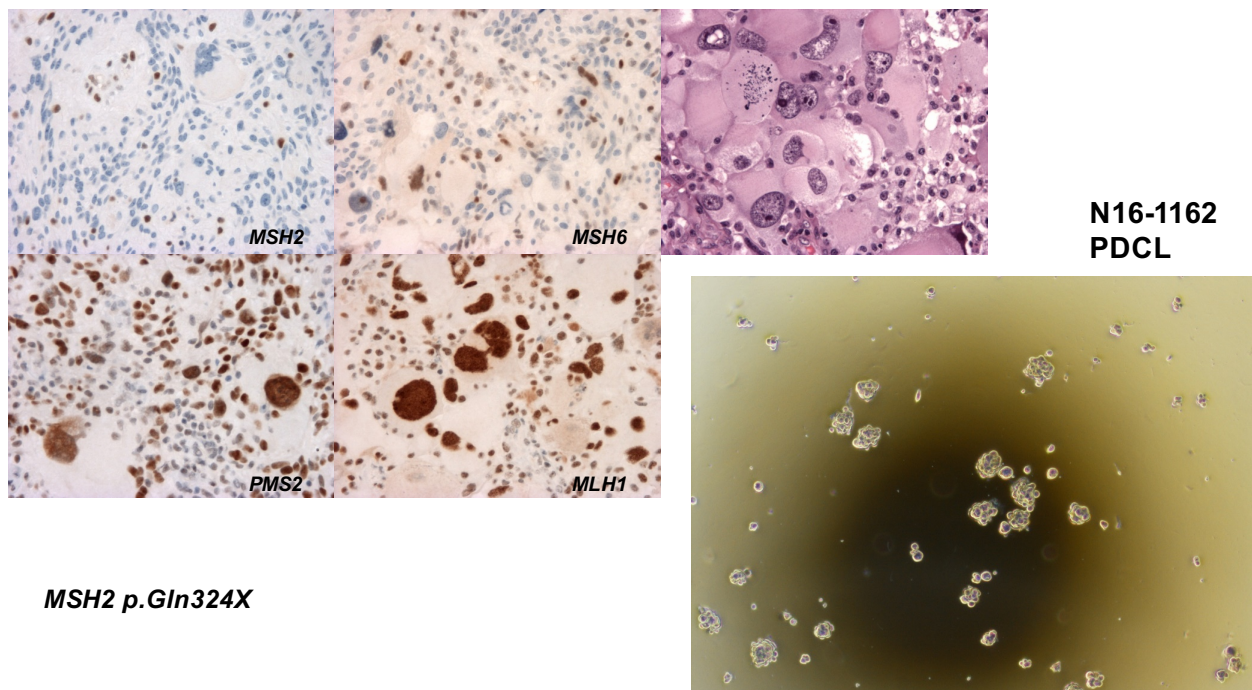


**Figure 15. Etablissement d'une lignée de gliome malin dérivée d'une patiente avec mutation germinale *MSH2*.** Haut, gauche : immunohistochimie des principales protéines MMR (*MSH2*, *MSH6*, *MLH1*, *PMS2*) et

**Université Paris-Saclay**

Espace Technologique / Immeuble Discovery

Route de l'Orme aux Merisiers RD 128 / 91190 Saint-Aubin, France

coloration à l'hématoxyline et à l'éosine sur la tumeur de la patiente. Bas, droite : gliomasphères dérivées de la tumeur en culture *in vitro*. La présence de la mutation tronquante de *MSH2* et d'un phénotype hypermutant avec signature mutationnelle MMR a été confirmée dans la tumeur et la lignée.

## b) Déficiences des polymérases Polε et Polδ1

Les gènes *POLE* et *POLD1* codent pour les principales ADN polymérases Polε et Polδ1 qui ont un rôle dans la fidélité de réplication de l'ADN (fonction *proofreading*) et interviennent dans divers mécanismes de réparation de l'ADN (*e.g.* BER, NER et MMR). Les mutations constitutionnelles des gènes *POLE* et *POLD1* sont principalement retrouvées dans des familles atteintes de cancers colorectaux ou de polypes coliques adénomateux multiples. Ces mutations sont situées dans le domaine exonucléase des gènes. Dans des cas exceptionnels, de telles mutations ont également été rapportées chez des patients atteints de gliomes malins<sup>113,143</sup>. Des mutations somatiques domaines exonucléase des gènes *POLE* et *POLD1* sont également observées chez des patients atteints de gliomes malins, notamment en tant qu'évènements secondaires chez des patients avec déficience bi-allélique du système MMR<sup>113,135,144</sup>. Sur le plan moléculaire, on retrouve souvent dans les gliomes malins avec déficience Polε ou Polδ1 un phénotype dit « ultra-hypermutant » – c'est à dire avec une charge mutationnelle dépassant 100 mutations par Mb – associé à une signature mutationnelle 10. Des cas de réponse aux traitements par ICI ont été rapportés chez des patients atteints de gliomes malins avec déficience Polε<sup>117,126,127</sup>.

## 2. Hypermutation dans les gliomes lors de la récurrence après traitement

Il s'agit du cas le plus fréquemment rapporté dans la littérature avec des premières observations remontant à 2006 chez des patients traités par témozolomide<sup>4,87-96</sup>. Chez ces patients, alors que la tumeur initiale ne présentait pas d'hypermutation, on retrouvait sur des prélèvements tumoraux réalisés après traitement par témozolomide une élévation significative de la charge mutationnelle. Outre la présence d'hypermutation, on notait dans ces tumeurs récidivantes la présence fréquente de mutations touchant les gènes du MMR<sup>4,87-89</sup>. Il est important de noter ici que la majorité de ces mutations des gènes MMR étaient des mutations faux-sens non caractérisées sur le plan fonctionnel. Ceci rendait difficile la détermination de leur caractère *driver* (*i.e.* responsable du phénotype hypermutant) ou bien *passenger* (*i.e.* associé au phénomène d'hypermutation). En effet, en présence

de processus d'hypermutation, la probabilité de retrouver au moins une mutation faux-sens sur un des gènes MMR est très élevée et directement corrélée à l'élévation de la charge mutationnelle.

Avec l'apport des données issues de séquençage de l'exome et l'analyse d'un plus grand nombre de paires de tumeurs (Figure 16) <sup>90-96</sup>, les caractéristiques moléculaires des gliomes avec hypermutation post-traitement ont pu être précisées :

- i) Elévation claire de la charge mutationnelle somatique après traitement (Figure 16) ;
- ii) Présence d'une signature mutationnelle très spécifique (signature 11), se rapprochant de signatures observées dans des modèles *in vitro* exposés aux agents alkylants <sup>140</sup>, formée par une très grande majorité de transitions C>T au niveau de régions CpC et CpT (Figures 13 et 17) ;
- iii) Présence fréquente de variants de signification indéterminée des gènes MMR dans les tumeurs récidives, non retrouvés dans les prélèvements initiaux (Figure 18) ;
- iv) Association claire du phénomène d'hypermutation post-traitement avec une exposition aux agents alkylants avant la récurrence (97% des récurrences hypermutantes) (Figure 19) ;
- v) Association avec des biomarqueurs moléculaires eux-mêmes associées à une plus grande sensibilité à la chimiothérapie par agents alkylants, comme les mutations *IDH1/2* (55% des récurrences hypermutantes vs 22% des récurrences non hypermutantes) et la méthylation du promoteur *MGMT* (94% vs 30%) (Figure 19).

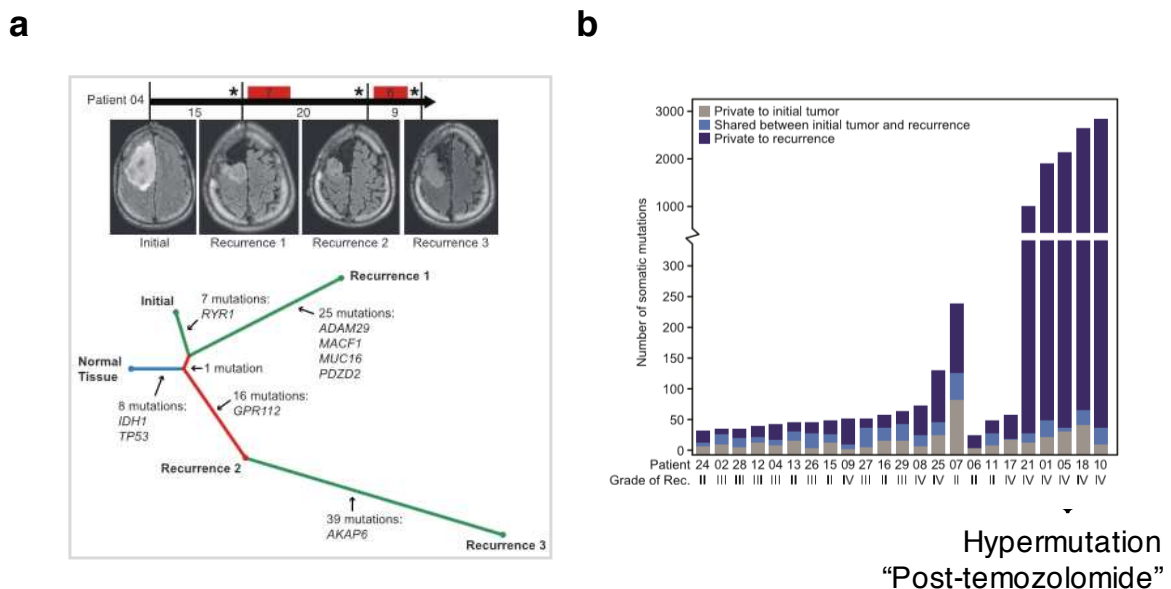


**Figure 16. Evolution clonale temporelle et spatiale chez des patients atteints de gliome diffus avec mutation *IDH1/2* (d'après Johnson et al.<sup>90</sup>).** a) Etablissement d'un arbre phylogénétique clonale à partir de données de séquençage d'exome dans des gliomes malins prélevés au diagnostic initial puis lors de la récurrence après traitement (paires). b) Histogrammes montrant le nombre de mutations somatiques dans 15 paires, dont huit paires pré- et post-témozolomide (extrémité droite). Les mutations représentées en gris sont retrouvées

dans l'échantillon initial uniquement ; les mutations représentées en bleu foncé sont retrouvées dans l'échantillon récidive uniquement ; les mutations représentées en bleu clair sont communes aux deux échantillons. On observe une élévation majeure de la charge mutationnelle dans 5/8 tumeurs récidive post-témzolomide.

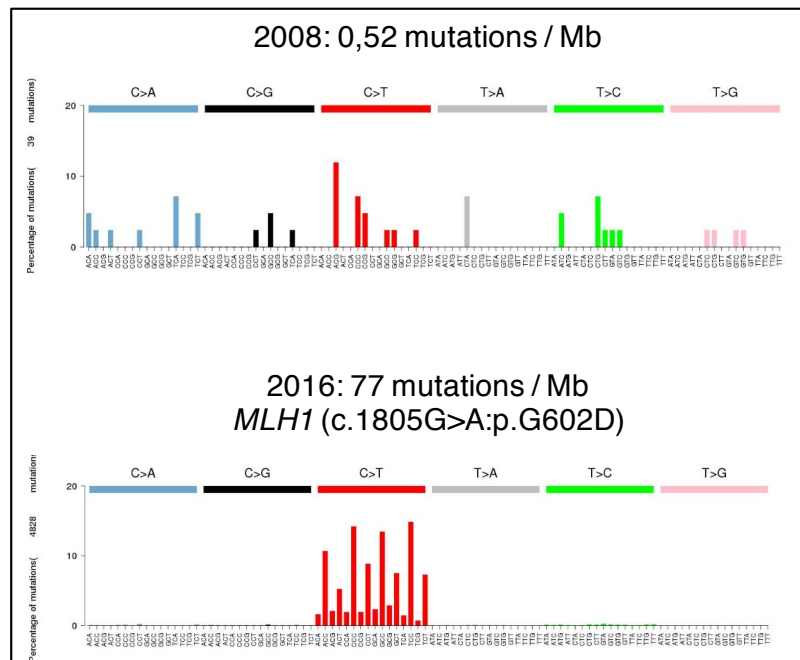


**Figure 17. Acquisition d'hypermutation avec signature mutationnelle 11 lors de la récidive après témzolomide dans un astrocytome anaplasique avec mutation *IDH1*. Données issues de séquençage de l'exome (tumeurs initiale, récidive et contrôle constitutionnel).**

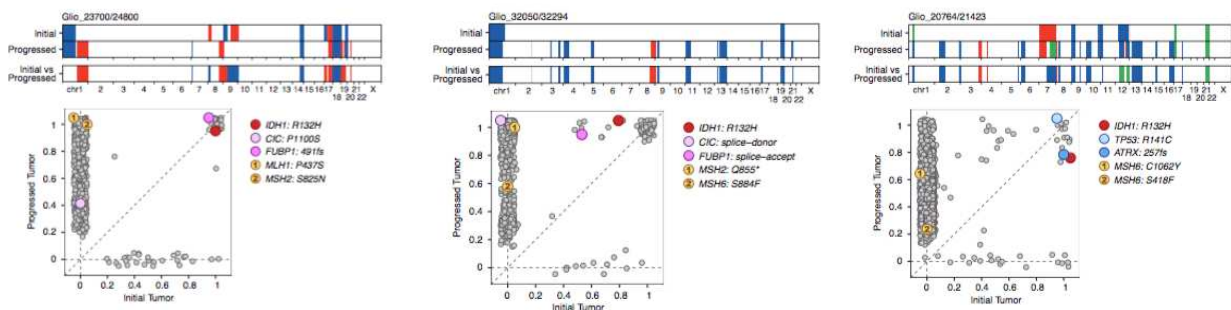


**Figure 18. Analyses des anomalies de nombre de copies (partie haute) et de la clonalité des mutations somatiques (bas) dans 3 paires de gliomes pré- et post-témzolomide analysées par séquençage de l'exome (d'après Bai et al.<sup>149</sup>). Chaque mutation (cercle) est représentée selon sa clonalité dans l'échantillon initial (allant de 0 [0% des cellules tumorales] à 1 [100% des cellules tumorales] sur l'axe des abscisses) et**

**Université Paris-Saclay**

Espace Technologique / Immeuble Discovery

Route de l'Orme aux Merisiers RD 128 / 91190 Saint-Aubin, France

récidive (idem sur l'axe des ordonnées). Les mutations des gènes MMR sont représentées par des cercles jaunes.

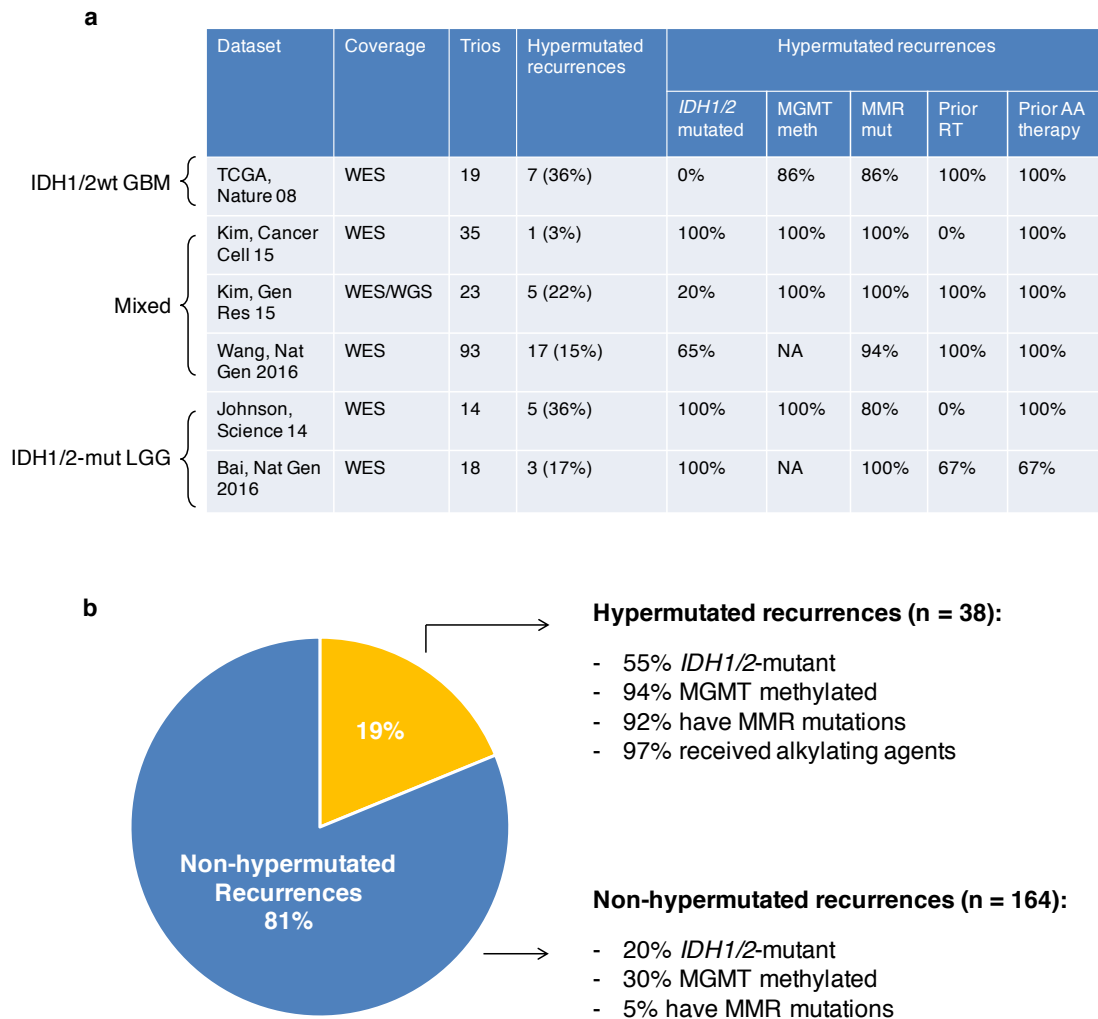


**Figure 19. Synthèse des études de paires de gliomes malins pré- et post-traitement montrant l'association du phénomène d'hypermutation avec les antécédents d'exposition aux agents alkylants et la présence de mutation *IDH1/2* et/ou de méthylation du promoteur *MGMT* (d'après TCGA<sup>109</sup>, Bai et al.<sup>149</sup>, Wang et al.<sup>94</sup>, Kim et al.<sup>93</sup>, Kim et al.<sup>92</sup>, et Johnson et al.<sup>90</sup>).** Les « trios » désignent des échantillons pour lesquels les données de séquençage d'exome ou de génome sont disponibles pour les tumeurs initiale, récidive et le contrôle constitutionnel.

Ces observations suggèrent l'existence d'un lien mécanistique entre acquisition de résistance à la chimiothérapie, apparition d'un phénotype hypermutant et présence de mutations dans les gènes MMR dans les gliomes malins traités par témozolomide. Cependant, plusieurs points remettent en question ce lien potentiel. D'une part la signature mutationnelle des gliomes avec hypermutation post-traitement (signature 11, parfois dénommée signature « témozolomide ») est unique et se distingue notamment des signatures mutationnelles observées dans les cancers MMR-déficients (signatures 6,

15 ou 20) <sup>103</sup>. Certains auteurs ont émis l'hypothèse que la signature 11 pourrait être la conséquence directe de l'exposition au témozolomide <sup>90</sup>. Néanmoins, cette signature mutationnelle n'est pas retrouvée dans la majorité des gliomes malins traités par témozolomide (Figure 19) <sup>92-95</sup>. A titre de comparaison, dans les mélanomes ou les cancers pulmonaires, l'exposition aux UV ou aux carcinogènes du tabac se traduit par la détection de signatures mutationnelles spécifiques associées (signatures mutationnelles 4 et 7 respectivement) dans la vaste majorité des échantillons exposés à ces mutagènes <sup>103</sup>. Ceci suggère que la seule exposition au témozolomide n'est pas suffisante pour causer le développement d'une hypermutation avec signature 11. D'autre part, malgré que le fait les déficits MMR sont fortement suspectés de contribuer à l'acquisition d'hypermutation et de résistance au témozolomide, les gliomes avec hypermutation post-traitement présentent des caractéristiques uniques les distinguant des autres cancers MMR-déficients, notamment l'absence de phénotype MSI. Ceci a conduit d'autres auteurs à remettre en cause ce lien mécanistique initialement suspecté <sup>150,151</sup>.

## IV. Hypothèses et objectifs

Collectivement, les données de la littérature convergent vers l'existence d'un lien mécanistique entre hypermutation post-traitement, déficit du système MMR, et résistance au témozolomide dans les gliomes malins<sup>73-78,97-101</sup>. Si des avancées significatives ont été accomplies dans ce domaine, le mécanisme précis sous-tendant un tel lien reste indéterminé et plusieurs questions importantes pouvant contribuer à améliorer la prise en charge des patients restent à résoudre :

1) Existe-t-il une association entre hypermutation (*de novo* et post-traitement) et certaines caractéristiques clinico-moléculaires (e.g. sous-type moléculaire, méthylation promoteur *MGMT*, pattern de traitement) dans les gliomes malins ? Ceci permettrait de mieux prédire et éventuellement prévenir le risque d'émergence d'un tel phénomène dans certaines tumeurs à plus haut risque. De même, l'impact pronostique – positif ou négatif – de l'hypermutation dans ces tumeurs n'a jamais été étudié. Répondre à ces questions nécessite l'analyse d'un grand échantillon de tumeurs annotées sur le plan clinique, or les précédentes études ne disposaient que d'un nombre d'échantillons très limité (au maximum 17 tumeurs hypermutées)<sup>90-96</sup>.

2) La déficience MMR est-elle suffisante pour produire une résistance au témozolomide ou bien d'autres facteurs sont-ils nécessaires<sup>73-78,97-101</sup> ? Produit-elle de façon équivalente une résistance aux autres agents alkylants comme le CCNU ? Ceci nécessite l'étude systématique de la réponse aux agents alkylants dans un large échantillon de lignées cellulaires (PDCL) et de xénogreffes (PDX) dérivées de patient et reflétant la biologie de ces tumeurs, y compris ces modèles isogéniques de gliomes avec déficience MMR.

3) Quel mécanisme sous-tend le développement d'hypermutation post-traitement avec signature 11 ? Cette signature est le plus fréquemment retrouvée dans des gliomes avec mutations MMR, mais elle diffère des autres signatures associées à la déficience MMR et chacune sont retrouvées dans des groupes distincts de gliomes. Les mutations MMR des gliomes avec hypermutation post-traitement pourraient être de simples événements *passenger* directement créés par le témozolomide et l'élévation de la charge mutationnelle, ou bien être responsables de la signature 11 et de l'acquisition de résistance au témozolomide.

4) L'hypermutation s'associe-t-elle à une meilleure réponse aux traitements par ICI comme dans d'autres types de cancer <sup>117-130</sup> ? Bien que les gliomes soient associés à un microenvironnement hautement immunosuppresseur, des travaux récents suggèrent que les gliomes hypermutés pourrait bénéficier des ICI <sup>117,126,127</sup>. Ces observations proviennent néanmoins de contextes relativement uniques (*e.g.* CMMRD) et leur applicabilité dans d'autres contextes reste à déterminer.

Afin de répondre à ces questions, nous avons caractérisé la charge et les signatures mutationnelles dans un très large échantillon de gliomes séquencés par panels NGS (10.294 tumeurs dont 558 hypermutantes) et étudié les associations entre hypermutation et caractéristiques clinico-moléculaires dans cette cohorte. Nous avons étudié le lien mécanistique entre hypermutation avec signature 11, déficit du système MMR, et résistance aux agents alkylants dans des modèles de gliomes malins. Enfin, nous avons étudié l'impact de l'hypermutation sur le pronostic des patients atteints de gliome et sur leur réponse aux traitements par ICI.

# INTRODUCTION

## I. Study context

Primary central nervous system (CNS) tumors form a heterogeneous set of benign or malignant pathologies affecting children and adults. According to the 2016 World Health Organization (WHO) classification, there are five main types of primary CNS tumors: tumors of the meninges, neuroepithelial tumors, germ cell tumors, tumors of the sellar region and hematopoietic tumors <sup>1</sup>. These five types are themselves subdivided into several histological subtypes forming a total of more than 150 distinct tumor types with highly heterogeneous biological and clinical characteristics. Malignant gliomas constitute the majority of neuroepithelial tumors and more than 80% of primary malignant CNS tumors <sup>2</sup>. While belonging to the group of rare cancers (annual incidence of less than 6/100.000 people), malignant gliomas represent a particular public health issue due to the morbidity associated with their development in the CNS, the complexity of their diagnosis and monitoring, and their incurable nature. The management of patients with malignant glioma is very heterogeneous, ranging from simple monitoring for certain tumors do not significantly progress (grade I according to the WHO) to heavy treatments combining surgery, radiotherapy and chemotherapy for the most aggressive tumors (grade IV according to the WHO). For the latter, therapeutic progress over the past 15 years remains very modest (median survival of around 18 months). In addition, even initially less aggressive tumors (grades II and III according to WHO) most often end up progressing to a treatment refractory stage and are responsible for death in the majority of patients. A better characterization of the mechanisms of resistance to treatments is therefore essential to improve the survival of patients with malignant glioma.

Advances in the understanding of the biology of gliomas have led to the identification of molecular alterations in DNA representing valuable tools for the clinic <sup>3-18</sup>. These “molecular biomarkers” have applications for diagnosis (subtype definition) as well as for the prediction of prognosis and response to treatments. In malignant gliomas, mention may be made of mutations in

the *IDH1* and *IDH2* genes (hereinafter *IDH1/2* mutations) and co-deletion of the 1p and 19q chromosomal arms (1p/19q co-deletion). These founding molecular alterations (“drivers”), associated with the development of diffuse astrocytomas and oligodendrogliomas, are today essential tools for diagnosis and for the stratification of treatments. The advent of molecular biomarkers represents a paradigm shift for the management of patients with malignant gliomas, whose diagnosis before WHO 2016 was essentially based on the histological analysis of tumors under a microscope. With the decrease in costs associated with high throughput sequencing and the development of panels encompassing genes and molecular alterations of interest available in the clinic, sequencing of malignant gliomas tends to become common practice from the initial diagnosis, and we are thus led to obtain an increasingly exhaustive molecular characterization in the clinic.

In this work, we sought to identify applications of tumor sequencing beyond the identification of molecular subtypes as defined by WHO 2016. In *Article 1*<sup>19</sup>, our objective was to better understand a phenomenon called "hypermutation", ie a significant increase in the mutational load observed in certain malignant gliomas, and its role in the prediction of the response to chemotherapy and immunotherapy. We focused in particular on abnormalities of the DNA mismatch repair system (MMR), also characterized in meningeal tumors (*Article 2, Annex*)<sup>20</sup>. In *Articles 3- 7 (Annex)*<sup>21-25</sup>, we report the development of new targeted therapies targeting rare subtypes associated with specific molecular drivers (ie gliomas with activating *BRAF* mutations, gliomas with *IDH1/2* mutations, gliomas with alterations of the PI3K pathway , gliomas with *ATG7-RAF1* fusion). Collectively, this work uncovers novel genetic modifications associated with resistance or response to treatments in certain gliomas and contributes to a better understanding of the still limited efficacy of immunotherapy in these tumors.

## II. Neuroepithelial tumors: definition and treatments

### A. Classification and epidemiological data

Primary CNS tumors constitute a heterogeneous set of benign or malignant pathologies affecting children and adults. They develop from specialized cells that form the tissues of the CNS (brain, medullary, ependymal and pituitary parenchyma, vessels and meninges). They are opposed to secondary tumors (that is, metastases) that initially develop from another organ. The reference classification for diagnosing CNS tumors is that of the WHO <sup>1</sup>. Since 2016, it includes molecular biology data enabling a so-called “integrated” diagnosis, ie a diagnosis based on the joint analysis of the histology and identification of genetic alterations associated with histomolecular subtypes. Some CNS tumors are indeed driven by specific biologic pathways defined by the acquisition of genetic alterations such as *IDH1/2* mutations and the 1p/19q co-deletion. In addition to these molecular abnormalities, the diagnosis is based on the location, degree of differentiation, and phenotype of the cells forming the tumor. In all, there are five main types of primary CNS tumors: tumors of the meninges, neuroepithelial tumors, germinal tumors, tumors of the sellar region and hematopoietic tumors <sup>1</sup>. Neuroepithelial tumors, representing more than 80% of primary malignant tumors CNS <sup>2</sup> (Figure 1), are the subject of this thesis.

Neuroepithelial tumors originate either in neurons or in cells that form the environment of neurons (glial cells) or their precursors. The WHO 2016 classification distinguishes eight main categories of neuroepithelial tumors, the vast majority of which are malignant gliomas (group of "Astrocytic and oligodendroglial glial tumors") (Table 1). In addition to the determination of the subtype, the histological diagnosis of neuroepithelial tumors makes it possible to assign these tumors a grade of malignancy ranging from grade I (tumors potentially curable in the event of complete resection such as pilocytic astrocytomas), to grade IV (the most aggressive tumors, mainly represented by glioblastomas). This grade depends on the presence of histological characteristics associated with a risk of recurrence after surgical excision: cell density and mitotic activity, cytonuclear atypia, endotheliocapillary proliferation and necrosis <sup>1</sup>. It thus reflects the aggressiveness of the tumors and guides the therapeutic strategy.

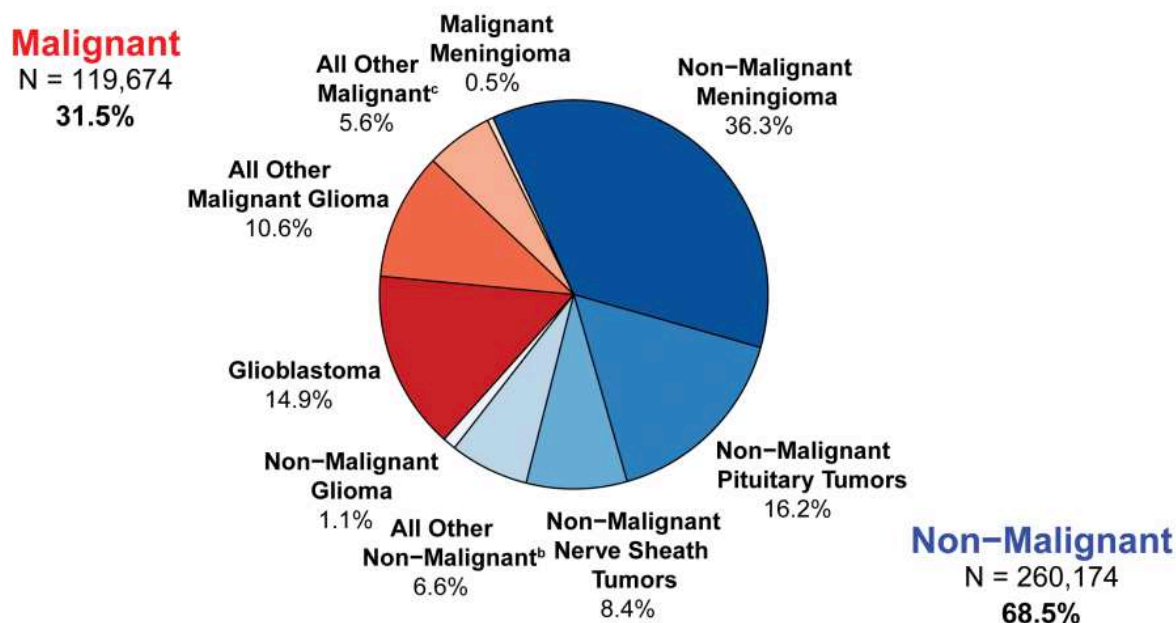


Figure 1. Distribution of primary CNS tumors in the United States over the period 2010-2014 (from Ostrom et al. <sup>2</sup>).

Neuroepithelial tumors belong to the group of rare cancers (annual incidence of less than 6/100 000 people) <sup>2</sup>. Frequent in children (2nd most common cancer after hematologic malignancies), malignant neuroepithelial tumors then have a low incidence up to the age of 40. Beyond that, the incidence rate increases to reach a peak between 80 and 84 years of age of approximately 35/100.000 people. The mortality curves follow trends comparable to those described for incidence. The most common subtype (55% of neuroepithelial tumors) - and also the most aggressive - is glioblastoma, the incidence of which in industrialized countries is estimated at 3.2 / 100.000 people <sup>2</sup>. Between 1990 and 2018, the annual number new cases of neuroepithelial tumors almost doubled, with a slight slowdown in the increase in incidence observed from 2010. This increase seems to be attributable half to an increased risk and half to the aging of the population.

**Table 1. Simplified classification of neuroepithelial tumors according to WHO 2016.**

<b>Histologie (altérations moléculaires associées)</b>	<b>Grade OMS</b>
<b><i>Tumeurs gliales astrocytaires et oligodendrogiales</i></b>	
Astrocytome diffus ( <i>IDH1/2</i> -muté ou -sauvage ou NOS)	Grade II
Astrocytome anaplasique ( <i>IDH1/2</i> -muté ou -sauvage ou NOS)	Grade III
Glioblastome ( <i>IDH1/2</i> -muté ou -sauvage ou NOS)	Grade IV
Oligodendrogliome ( <i>IDH1/2</i> -muté et codéléte 1p19q)	Grade II
Oligodendrogliome anaplasique ( <i>IDH1/2</i> -muté et codéléte 1p19q)	Grade III
Gliome infiltrant du tronc cérébral ( <i>H3F3A</i> -muté)	Grade IV
<b><i>Autres tumeurs astrocytaires et gliales</i></b>	
Astrocytome pilocytique	Grade I
Gliome choroïde du 3 <sup>ème</sup> ventricule	Grade II
Xanthoastrocytome pléomorphe	Grade II
Xanthoastrocytome pléomorphe anaplasique	Grade III
Astroblastome	Non défini
<b><i>Tumeurs épendymaires</i></b>	
Ependymome myxopapillaire	Grade I
Ependymome (avec ou sans fusion <i>RELA</i> )	Grade II
Ependymome anaplasique	Grade III
<b><i>Tumeurs des plexus choroïdes</i></b>	
Papillome du plexus choroïde	Grade I
Carcinome du plexus choroïde	Grade III
<b><i>Tumeurs neuronales et glioneuronales</i></b>	
Tumeur dysembryoplasique neuroépithéliale	Grade I
Gangliogliome	Grade I
Gangliogliome anaplasique	Grade III
Gangliocytome dysplasique du cervelet	Grade I
Tumeur glioneuronale papillaire	Grade I
Tumeur glioneuronale formant des rosettes du quatrième ventricule	Grade I
<b><i>Tumeurs de la région pinéale</i></b>	
Tumeur papillaire de la région pinéale	Grade II ou III
Pinéaloblastome	Grade IV
<b><i>Tumeurs embryonnaires</i></b>	
Médulloblastome	Grade IV
Tumeur embryonnaire avec rosettes pluristratifiées	Grade IV
Tumeurs rhabdoïdes/tératoïdes atypiques (avec perte <i>SMARCB1</i> )	Grade IV

\*NOS : « not otherwise specified », tumors for which the molecular status has not been determined with certainty (lack of genotyping or incomplete genotyping).

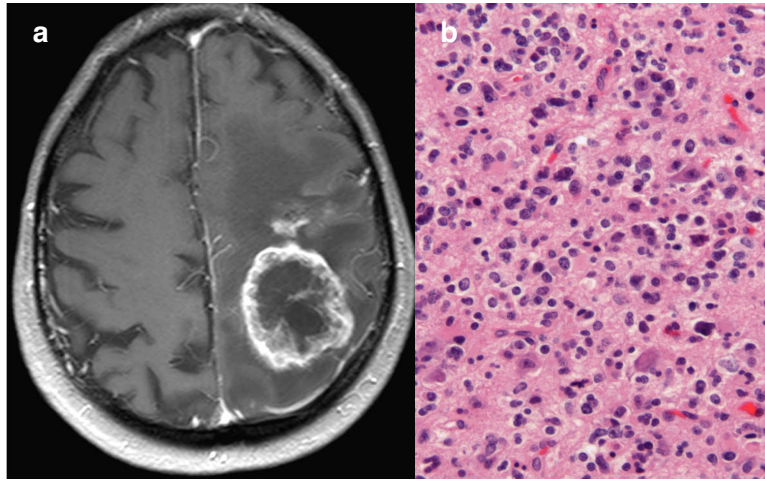
Apart from rare cases (less than 5% in total) occurring in contexts of exposure to ionizing radiation (for instance, history of brain radiotherapy) or cancer predisposition syndromes (Table 2), neuroepithelial tumors are sporadic tumors with complex genetics and to date have no recognized etiological factor. Genome-wide association studies (GWAS) have nevertheless enabled the recent identification of several polymorphisms associated with the risk of developing malignant glioma (in particular the 5p15.33, 7p11.2, 8q24 loci .21, 9p21.3, 11q23.3, 17p13.1, and 20q13.33 near the *TERT*, *EGFR*, *MYC*, *CDKN2A*, *PHLDB1*, *TP53* and *STMN3* genes) <sup>26,27</sup>. A better characterization of the functional basis of these polymorphisms could provide a better understanding of the mechanisms contributing to the development of malignant gliomas.

**Table 2. Cancer predisposition syndromes associated with the risk of neuroepithelial tumor.**

Syndrome de prédisposition génétiques au cancer	Gene(s) implique(s)
Syndrome de Lynch	<i>MLH1, MSH2, MSH6, PMS2</i>
Syndrome de déficience constitutionnelle des gènes MMR (CMMRD)	<i>MLH1, MSH2, MSH6, PMS2</i>
Syndrome de von Hippel-Lindau	<i>VHL</i>
Syndrome de Turcot A	<i>APC</i>
Syndrome astrocytome-mélanome	<i>CDKN2A</i>
Syndrome de Gorlin	<i>PTCH1</i>
Sclérose tubéreuse de Bourneville	<i>TSC1, TSC2</i>
Syndrome de Cowden	<i>PTEN</i>
Syndrome de Li-Fraumeni	<i>TP53</i>
Neurofibromatose de type 1	<i>NF1</i>
Neurofibromatose de type 2	<i>NF2</i>
Syndrome de prédisposition aux tumeurs rhabdoïdes	<i>SMARCB1</i>
Syndromes associés aux mutations constitutionnelles POLE et POLD1	<i>POLE, POLD1</i>

## B. Diagnosis: molecular subtypes, prognostic factors

CNS tumors can present with widely varying symptoms and clinical manifestations from patient to patient, depending primarily on the size and rate of lesion growth and their location in the

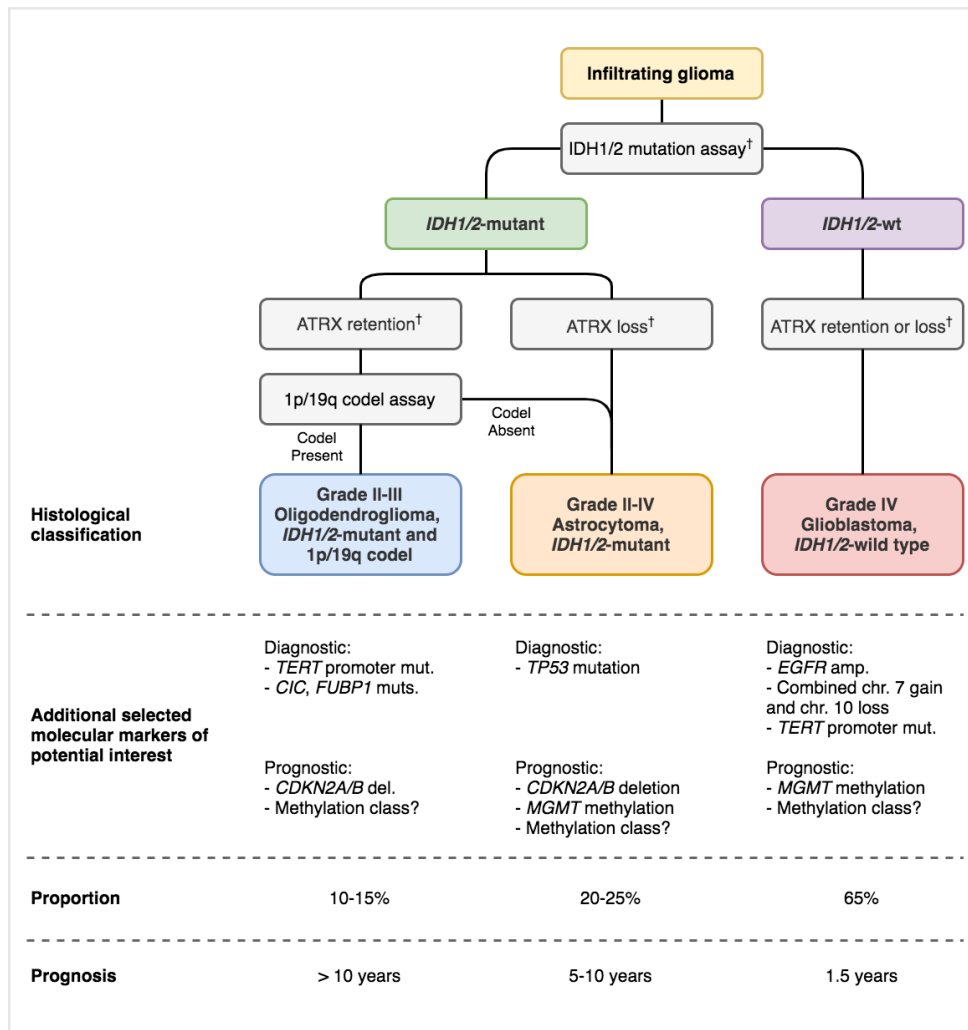


CNS<sup>28-30</sup>. The main modes of disclosure are epileptic seizures, focal neurological deficits and/or cognitive or behavioral disorders, and intracranial hypertension syndrome (Figure 2).

**Figure 2. Left fronto-parietal tumor corresponding to a high-grade glioma in a 64-year-old patient. (a)** Cerebral MRI in axial T1 sequence after injection of contrast product. (b) Histological section after staining with hematoxylin and eosin

Imaging and in particular nuclear magnetic resonance imaging (MRI) are key for the diagnosis and follow-up of patients<sup>28-30</sup>. The definitive diagnosis nevertheless requires the pathological analysis of the tumor tissue obtained after tumor resection (partial or complete) when the tumor is operable, otherwise by biopsy. In addition to the therapeutic effect in the event of resection, the surgery provides tumor material for diagnostic, and possibly research purposes. The diagnostic approach is based on the combination of histological and molecular analyzes allowing the classification of malignant gliomas in four main categories: oligodendrogliomas (with both an *IDH1/2* mutation and 1p/19q co-deletion), diffuse astrocytomas (with an *IDH1/2* mutation, without 1p/19q co-deletion), glioblastomas (without *IDH1/2* mutation or 1p/19q co-deletion), and other rarer subtypes of glioma<sup>1</sup>. These techniques can be combined according to algorithms combining several sequential analyzes enabling to obtain a final diagnosis (Figure 3):

- immunohistochemistry, for instance for the dominant IDH1 mutation (R132H)<sup>31</sup>;
- search for hotspot mutations by PCR then Sanger sequencing or pyrosequencing<sup>32,33</sup>;
- next generation sequencing (NGS) analysis of panels of genes associated with cancer allowing the simultaneous search for numerous recurrent molecular abnormalities (hotspot mutations, other mutations, copy number anomalies, fusions)<sup>34-38</sup>;



- use of emerging techniques such as the analysis of the methylome<sup>39</sup>, exome or genome sequencing<sup>40</sup>, transcriptome<sup>41</sup>.

**Figure 3. Main subtypes of diffuse glioma and diagnostic strategy according to the determination of *IDH1/2* and 1p/19q statuses.** † Status obtained by immunohistochemistry or sequencing.

The prognosis of malignant gliomas is very heterogeneous depending on the different subtypes (Figure 4), and also varies considerably within the same histological subtype. This variability is influenced by patient-related factors (e.g. age, general condition), the extent of surgical excision, as well as intrinsic sensitivity to adjuvant treatments by radiotherapy and chemotherapy. In addition to *IDH1/2* mutations and the 1p/19q co-deletion, both associated with a better response to adjuvant treatments<sup>42-45</sup>, the methylation of the promoter of the DNA repair enzyme O6-methylguanine-DNA-methyltransferase (*MGMT*) has been associated with a better response to chemotherapy with alkylating agents (see next section)<sup>46</sup>. These biomarkers enable an - imperfect - prediction of the prognosis and an aid in the therapeutic decision in the most frequent gliomas. In the rarer tumors, certain molecular biomarkers are explored but the limited numbers and the heterogeneity of the therapeutic modalities are obstacles for the validation of their clinical relevance.

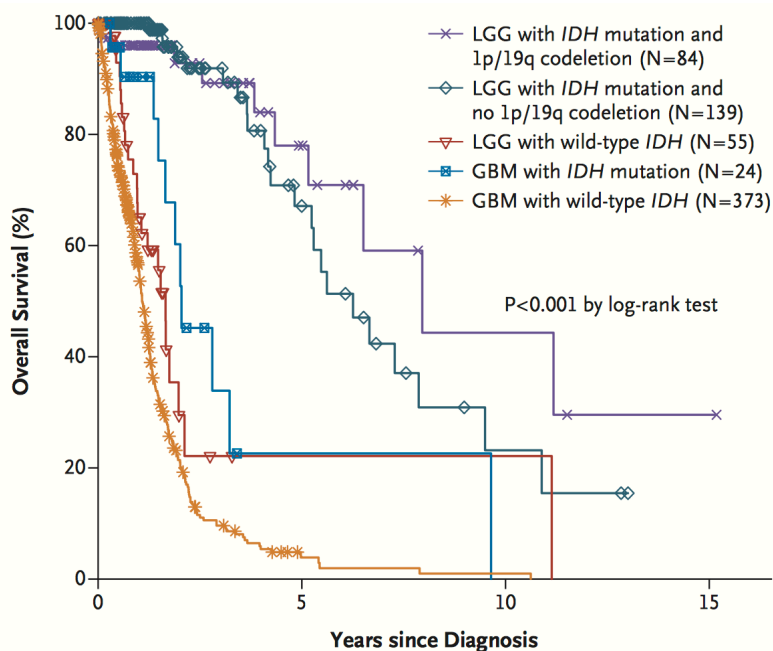


**Figure 4. Survival associated with the molecular subtypes of diffuse gliomas included in the TCGA (from Brat et al. <sup>7</sup>). Abbreviations: IDH (IDH1/2 genes) LGG, lower grade glioma (grade II and III gliomas); GBM, glioblastoma (glioblastoma).**

### C. Treatments: role of alkylating agents

The standard treatment for malignant gliomas includes surgery, radiotherapy and chemotherapy <sup>28-30</sup>. The first step of the treatment is most often surgery, which when possible is offered either upon initial diagnosis in high-grade gliomas, or after an initial observation period in grade II diffuse gliomas. Despite the absence of randomized trials, several surgical series have shown a significant impact of complete or subtotal resection on overall survival <sup>47-50</sup>. However, the location in the brain and the invasive nature of gliomas make complete surgical removal often difficult. Depending on the location of the tumor, the use of awake surgery and functional mapping techniques can optimize the extent of resection, increase the percentage of patients who can benefit from resection in functional regions, and reduce the risk of postoperative neurological deficits. In addition to the potential overall survival benefit, surgical excision often results in rapid improvement in certain symptoms such as intracranial hypertension or epilepsy.

**Université Paris-Saclay**

Espace Technologique / Immeuble Discovery  
Route de l'Orme aux Merisiers RD 128 / 91190 Saint-Aubin, France

Radiation therapy is delivered at doses (54-60 Gy) and fractions (15-30 sessions) which vary according to the histological diagnosis (in particular grade and molecular subtype) and the patient (in particular age and general condition). Except in some rare instances where protons can be indicated, conventional electron beam techniques are generally used. The radiation therapy targets the tumor volume to which margins are added in order to target possible areas of tumor infiltration. This treatment exerts antitumor effects on glial cells, in particular by inducing DNA breaks and reactive oxygen species, and often reduces epileptic seizures. In grade III or IV gliomas, radiation therapy is usually offered upon initial diagnosis after surgery or biopsy. In grade II diffuse gliomas, the optimal timing of brain radiation therapy is not well codified. Early radiation therapy prolongs progression-free survival but not overall survival<sup>51</sup>, and likely increases the risk of cognitive disorders in the long term. Strategies aiming at postponing radiotherapy treatment are currently being evaluated in the most chemosensitive subtypes such as oligodendrogliomas.

The chemotherapy of malignant gliomas consists of regimens based on alkylating agents which exert anti-tumor effects on the glial cells and have the advantage of having good blood-brain barrier penetration (Figure 5a). The concept of chemotherapy with alkylating agents arose from the observation by Edward Krumbhaar in 1919 that Canadian soldiers who had been exposed to mustard gas suffered from respiratory distress and lymphoid aplasia<sup>52</sup>. Today, there are 7 major families of 'classic' alkylating agents among which molecules of the nitrosourea (carmustine, lomustine) and triazene hydrazines families (temozolomide, procarbazine) are the most frequently used in the treatment of gliomas<sup>53</sup>. These treatments are delivered according to 3 main protocols: polychemotherapy with PCV (procarbazine and lomustine combined with the vinca alkaloid vincristine) or monotherapy with temozolomide or lomustine. These protocols in combination with radiotherapy have demonstrated survival benefits ranging from 2.5 months with temozolomide in glioblastoma to 5.5 years with the PCV protocol in grade II gliomas<sup>42-45,54-59</sup>. However, despite their efficacy of these agents, malignant gliomas almost systematically develop resistance mechanisms leading to relapse. Identifying, understanding and circumventing these resistance mechanisms is a major objective of the ongoing preclinical and clinical research.

## D. Mechanism of action of alkylating agents

Among the alkylating agents used in gliomas, the 2 molecules considered to be the most effective are temozolomide and lomustine (cis-chloroethylnitrosourea [CCNU] or its analogue carmustine, bis-chloroethylnitrosourea [BCNU]) (Figure 5a). Temozolomide is an alkylating agent from the triazene hydrazine family. It is a prodrug activated at physiological pH via enzyme-independent hydrolysis followed by decarboxylation forming 5-methyltriazenoimidazole-4-carboxamide (MTIC) then 5-aminoimidazole-4-carboxamide and finally its species reactive, the methyldiazonium ion which methylates DNA<sup>60</sup>. Lomustine (cis-chloroethylnitrosourea, CCNU) and carmustine (bis-chloroethylnitrosourea, BCNU) are chloroethylnitrosoureas metabolized into 2 active compounds: diazohydroxide responsible for chloroethylation of DNA, and isocyanate responsible for protein carbamylation<sup>61</sup>.

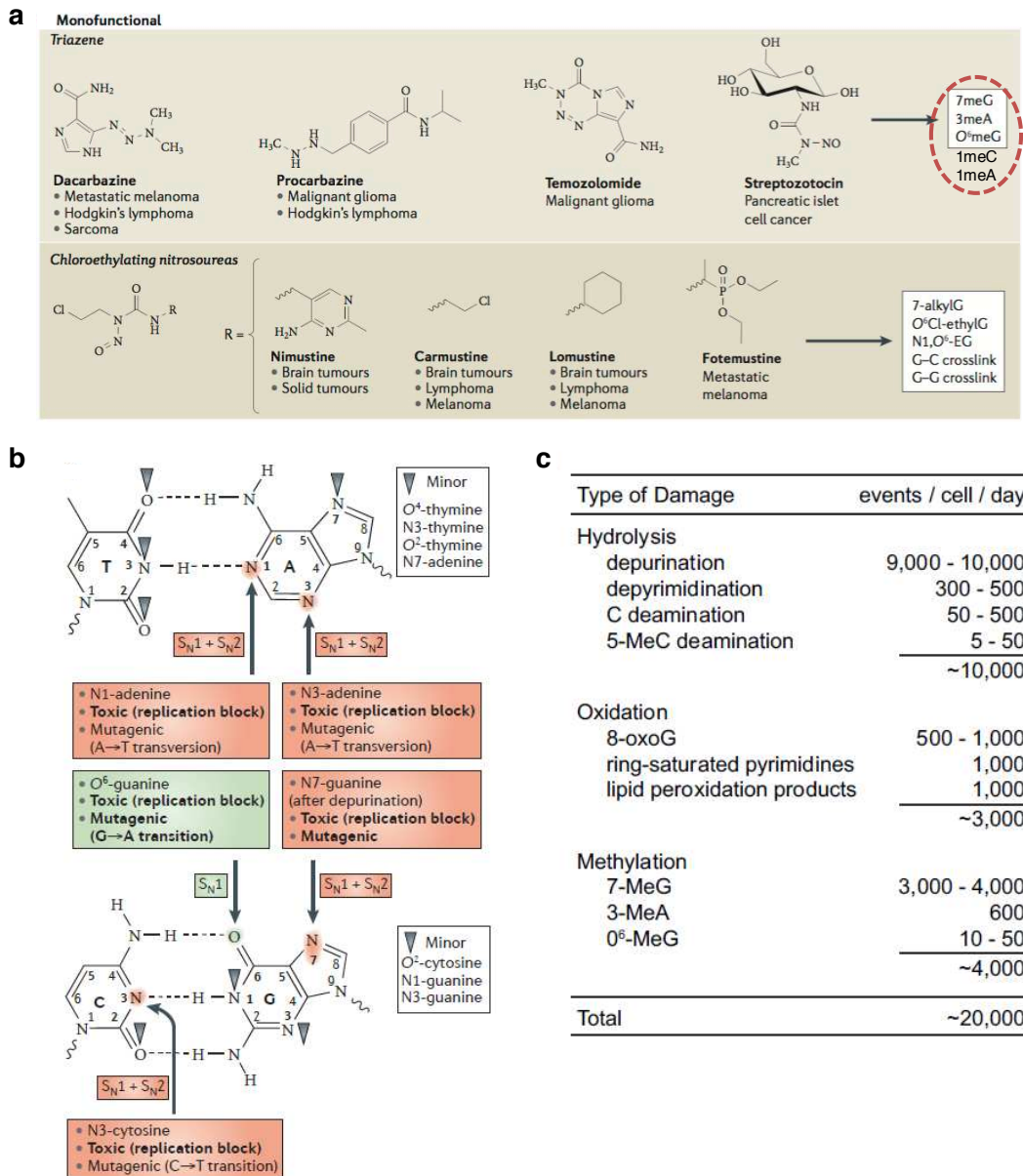


**Figure 5. Main types of alkylating agents used for the treatment of malignant gliomas (a) and their biological effects on DNA (b) (after Fu et al. <sup>53</sup> [a-b] and Preston et al. <sup>62</sup> [c]). Note that some lesions induced by alkylating agents occur spontaneously under physiological conditions (c).**

Biologically, alkylating agents are electrophilic organic compounds capable of reacting with nucleophilic radicals (e.g. -SH, -OH, -COOH or -NH<sub>2</sub>) found in proteins and nucleic acids <sup>53,62</sup>. At the DNA level, these interactions result in the formation of different types of adducts covalently linked to the DNA on preferential sites, mainly on purine bases (N1-adenine, N3-adenine, N7-guanine, O6-guanine, etc.) (Figure 5b). The N7 nitrogen of guanine is the main target of DNA alkylation damage (60 to 80% of all adducts) <sup>53</sup>. Depending on the types of adducts they produce, alkylating agents are

said to be mono- (single nucleotide adduct) or bi-functional (adduct connecting two adjacent nucleotides to form inter- or intra-strand bridges). These adducts modify the structure of the double helix, prevent DNA replication and transcription (especially inter- or intra-strand adducts), and induce single- or double-strand breaks in DNA. This leads to the activation of repair systems and possibly to apoptosis of the damaged cell in the event of irreversible damage. Importantly, some DNA damage caused by alkylating agents (e.g. N7-methylguanine, N7-methyladenine, O6-methylguanine) are also frequently formed under physiological conditions (Figure 5c); cells therefore have intrinsic mechanisms to repair these lesions.

In terms of antitumor therapy, many resistance phenomena limit the effectiveness of alkylating agents, among which we can mention:

- A low drug concentration due to an increase in efflux or a decrease in its entry into cells <sup>63,64</sup>;
- Inactivation of the drug by detoxification mechanisms, such as the interaction with glutathione <sup>65-67</sup>;
- Increase in the activity of DNA repair, in particular of the demethylases ALKBH2-3 and MGMT, and the BER and NER systems (Base Excision Repair and Nucleotide Excision Repair respectively) <sup>46,53,68-72</sup>;
- Inactivation of the MMR system <sup>73-78</sup>;
- The expression of proteins involved in anti-apoptotic signaling such as Bcl-2 and Bcl-xL <sup>79</sup>.

The resistance mechanisms associated with DNA repair are by far the best characterized (Figure 6). Some of these mechanisms are redundant and their involvement thereby depends on their availability near DNA lesions. Among these various proteins and mechanisms, the expression of the MGMT protein and of the MMR proteins have been associated with mechanisms of resistance to temozolomide and with the acquisition of a so-called “hypermutant” phenotype under treatment.

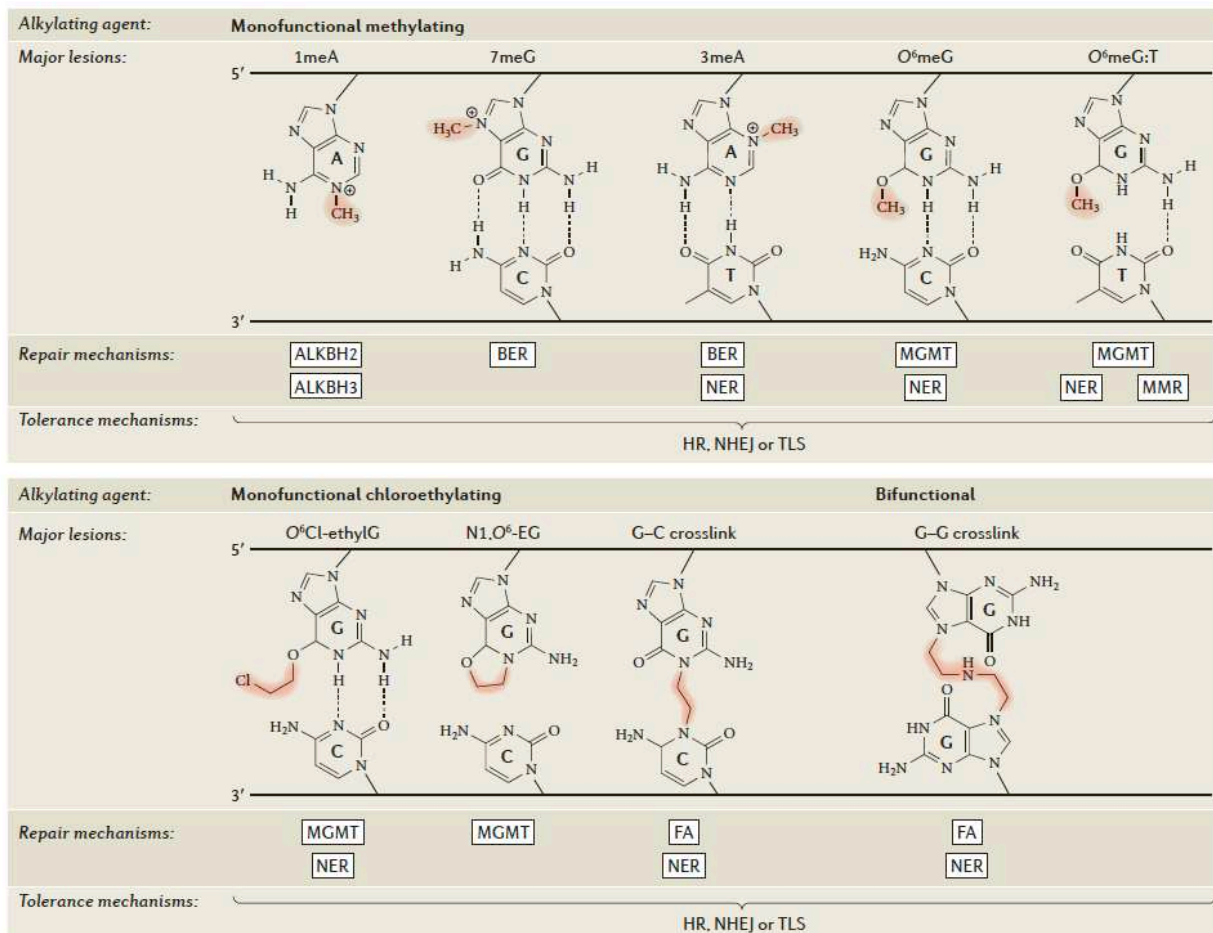


Figure 6. Schematic representation of the main DNA damage caused by alkylating agents used in gliomas and their associated repair mechanisms (from Fu et al. <sup>53</sup>). Upper part: lesions induced by temozolomide. Lower part: lesions induced by chloroethylnitrosoureas.

### E. Temozolomide resistance: involvement of MGMT and MMR system, « hypermutator » phenotype

Temozolomide is currently the most frequently used agent for the treatment of malignant gliomas. The efficacy of temozolomide is thought to result mainly from the formation of O6-methylguanine (O6-meG) adducts at the DNA level <sup>80</sup>. Under physiological conditions, O6-meG adducts are much less frequent than other types of lesions more frequently induced by temozolomide such as N7-methylguanine (approximately 1: 100 ratio) <sup>62</sup>. This partly explains the important role of O6-meG lesions in the cytotoxicity of alkylating agents. The MGMT protein allows direct repair of O6-meG lesions, as do the O6-chloroethylguanine adducts formed by chloroethylnitrosoureas. During this repair, MGMT sequesters the methyl group of O6-meG by covalent transfer, thus

Université Paris-Saclay

Espace Technologique / Immeuble Discovery

Route de l'Orme aux Merisiers RD 128 / 91190 Saint-Aubin, France

restoring guanine to its normal state. This reaction nevertheless leads to irreversible inactivation of the protein after ubiquitination (Figure 7). MGMT is therefore not strictly speaking an enzyme, since it is only capable of carrying out one repair cycle (suicide enzyme). Given this peculiarity, the expression of MGMT has been proposed as one of the main causes of resistance to temozolomide. *MGMT* promoter methylation, which leads to epigenetic silencing of its expression, is indeed associated with increased sensitivity to temozolomide and chloroethylnitrosoureas and a better prognosis in patients with malignant glioma<sup>46,69,72</sup>.

In the absence of MGMT (for example in the event of silencing by promoter methylation or degradation of the pool of available proteins), a thymine is incorporated in front of the O6-meG residue - recognized as an adenine - during DNA replication by polymerases, creating at this level an O6-meG:T mismatch. This mismatch is recognized by the proteins of the MMR system, a multiprotein complex (MSH2, MSH6, MLH1 and PMS2 proteins in particular) which recognizes and repairs DNA mismatches and replication errors by slippage of the polymerase during of DNA replication<sup>81,82</sup> (Figure 8). According to the so-called “futile cycling” model, successive excisions by the MMR system of mismatched thymine and then resyntheses by the polymerases of a thymine in front of the O6-meG residue not repaired results in tensioning of the double helix and the formation of double-stranded DNA breaks, which are highly toxic and eventually lead to the activation of apoptotic programs<sup>75,83</sup> (Figure 7). Thus, according to this model, the toxicity of O6-meG requires a functional MMR system<sup>84,85</sup>. This hypothesis was supported by the observation in MMR-deficient models (e.g. colon cancer cell lines with mutations in the genes encoding MMR proteins) of major resistance to alkylating agents such as temozolomide<sup>73-78</sup>. Importantly, in other cancers, MMR deficiency is associated hypermutability and accumulation of small insertions and deletions (indels) at short repeated sequences in the genome, a phenotype called microsatellite instability (MSI) (Figure 8).

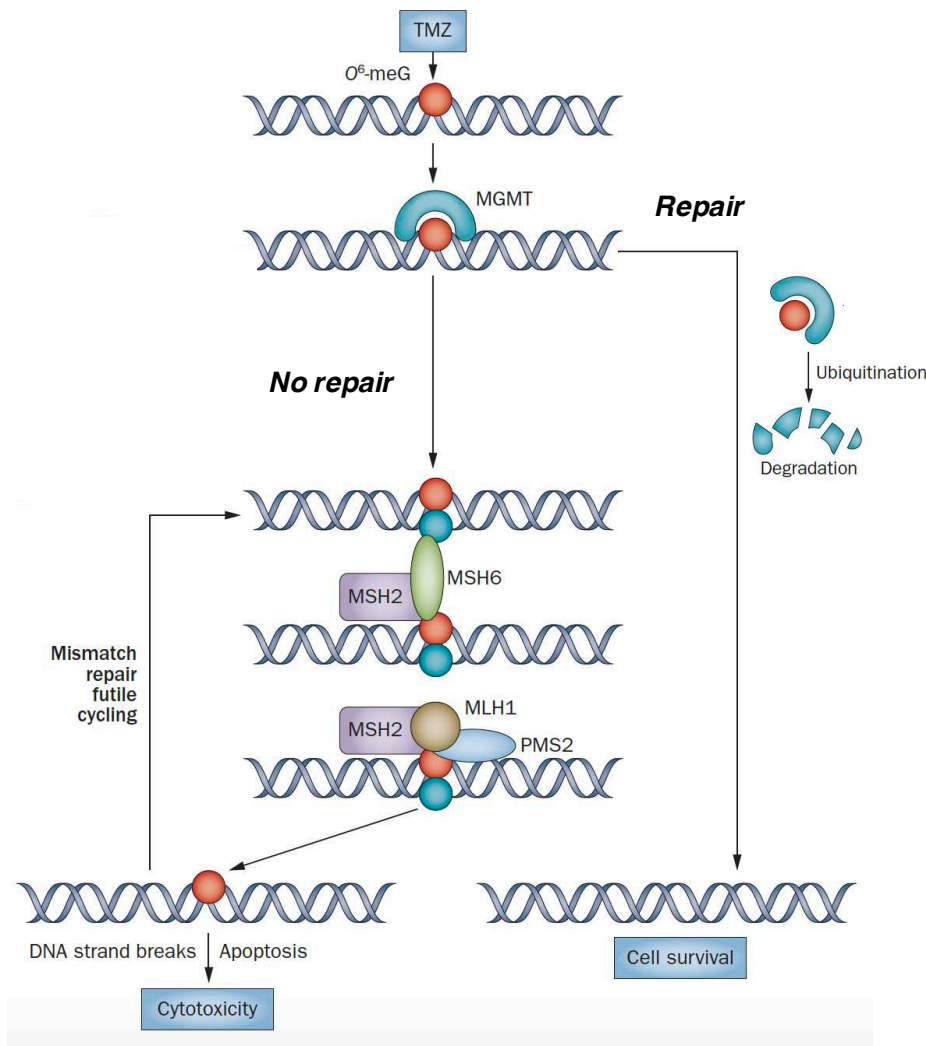


**Figure 7. Mechanism of temozolomide cytotoxicity and MGMT mediated repair (from Wick et al. <sup>86</sup>).** In the absence of repair of O<sup>6</sup>-meG adducts by MGMT, the cytotoxicity of O<sup>6</sup>-meG lesions indirectly requires a functional MMR system.

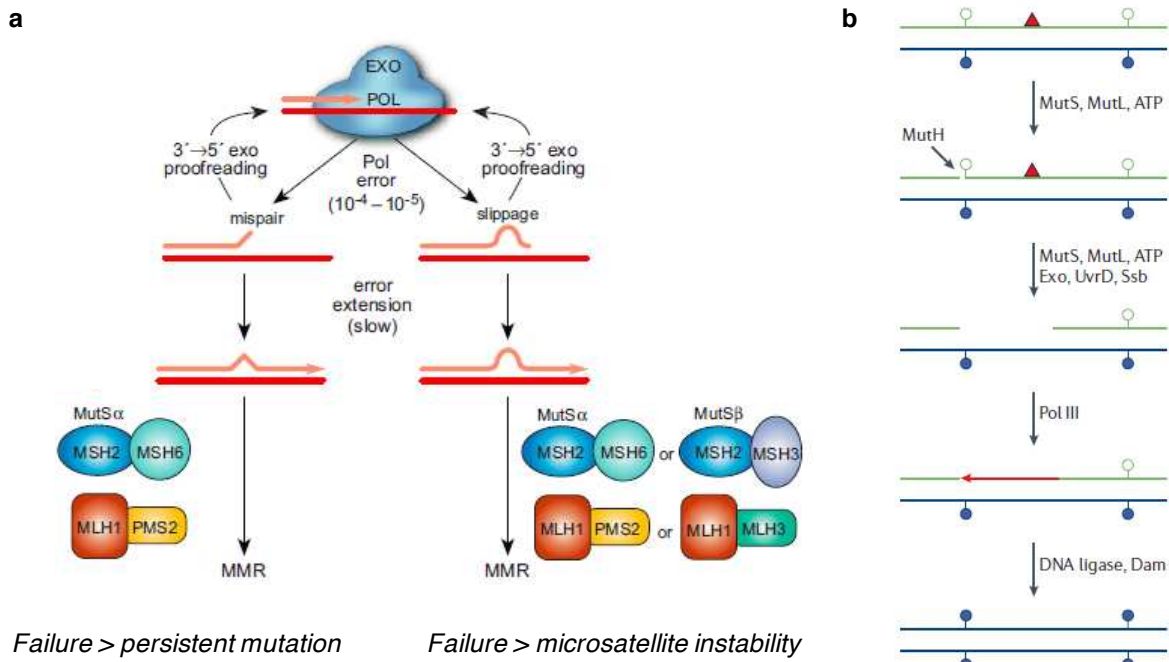


**Figure 8. Schematic representation of the repair of DNA polymerase incorporation errors by "proofreading" and MMR systems (from Preston et al.<sup>62</sup> [a] and Jiricny<sup>81</sup> [b]).** a) During DNA synthesis, rare polymerase errors (base mismatches to the left or template slip to the right) prevent primer extension and trigger transfer of the growing DNA strand from the site active polymerase (POL) to the active exonuclease site (EXO) where the error is possibly excised. The errors which escape the system of "proofreading" of the polymerase are corrected, at least in part, by two partially redundant pathways of the MMR system. The MSH2 and MLH1 proteins are essential for the MMR pathway functions. The MSH6 and PMS2 proteins have "back-ups" proteins enabling the formation of alternative MutS and MutL complexes (MSH2: MSH3 and MLH1: MLH3 heteroduplexes), in particular for the repair of matrix sliding errors ("slippage"). In the absence of repair, base mismatches result in the transmission of a mutation or insertion/deletion in one of the daughter cells. The accumulation of these errors is responsible for an hypermutant phenotype with specific mutational signature (linked to mutations) more or less associated with microsatellite instability (related to insertions/deletions) which corresponds the presence in different cells of fragments of different sizes at the level of microsatellite repeats. MutS recognizes DNA damage and also signals apoptosis. b) Model representing the excision/resynthesis of DNA mismatch (red triangle) by the MMR system and the polymerase in Escherichia coli. The newly synthesized DNA (green) is recognized by the MMR system because it is not methylated (open circles).

While abnormalities of the MMR system are extremely rare in newly diagnosed gliomas, MMR mutations - often not functionally characterized - have been observed in 5 to 30% of patients with recurrent malignant glioma after alkylating agent<sup>4, 87-96</sup>. In addition, some of these studies were able to compare the molecular profiles of pre- and post-treatment glioma pairs and showed that a subgroup of tumors developed a “hypermutant” phenotype characterized by the accumulation of hundreds of mutations, after treatment with temozolomide in particular. Collectively, these observations, along with data indicating resistance to alkylating agents in MMR-deficient models<sup>73-78,97-101</sup>, suggested a mechanistic link between MGMT and MMR deficits, resistance to temozolomide, and hypermutant phenotype in malignant gliomas<sup>102</sup> (Figure 9). However, this link has never been demonstrated in isogenic models of gliomas, and hypermutant gliomas exhibit unusual characteristics - notably a unique mutational signature and the absence of an MSI phenotype (see next section) - which do not enable them to be linked to the group of cancers with abnormalities of the MMR system. This led us to further study the clinical and molecular characteristics of hypermutant gliomas.

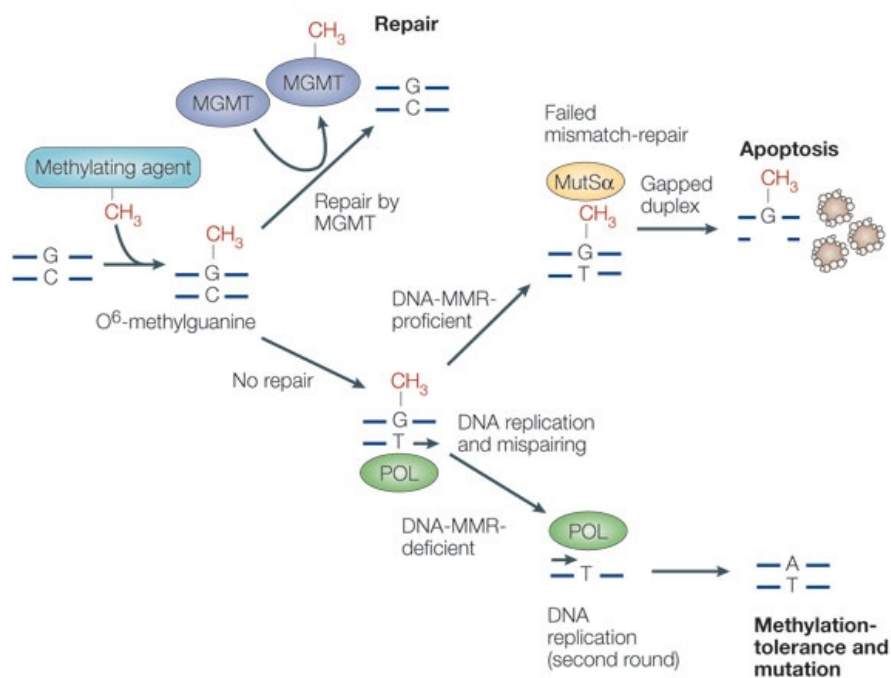


**Figure 9. Model suggesting a mechanistic link between MGMT and MMR system deficits, temozolomide resistance and hypermutant phenotype in malignant gliomas (from Allan et al.<sup>26</sup>).**

### **III. Hypermutation in gliomas**

#### **A. Study of the mutational load and signature in cancers, potential role in the prediction of the response to immunotherapy**

Somatic mutations found in cancers are caused by mutational processes of exogenous and endogenous origin which operate during development from the egg cell to the tumor cell<sup>103-108</sup>. Each mutational process can involve components of DNA damage or modification, abnormal DNA replication or repair and generates a characteristic mutational signature, which can include base substitutions (Figure 10), indels, chromosome rearrangements and copy number abnormalities. Sometimes several mutational processes operate simultaneously, and the tumor mutational profile therefore incorporates different overlapping mutational signatures. Accordingly, the systematic characterization of mutational profiles of tumor samples provides the potential to uncover the normal and pathological processes contributing to the accumulation of mutations and therefore the development of cancers (Figure 10). With the advent of high throughput sequencing techniques and the genomic analysis of large cohorts of human tumors by international consortia<sup>109</sup>, mathematical techniques have been developed to enable systematic analysis of mutational signatures from catalogs of somatic mutations, and thereby estimate the number of mutations attributable to each mutational signature in individual samples<sup>103,105,110-112</sup>. Importantly, these methods, initially developed from sequencing data of tumor exomes or genomes, have recently been successfully applied to the analysis of samples sequenced by NGS panels of 1-2 Megabases (Mb), in particular in the presence of hypermutation<sup>38,113,114</sup>. This makes them potentially applicable to sequencing data obtained in the context of current clinical practice, for example for the determination of molecular subtypes of gliomas.

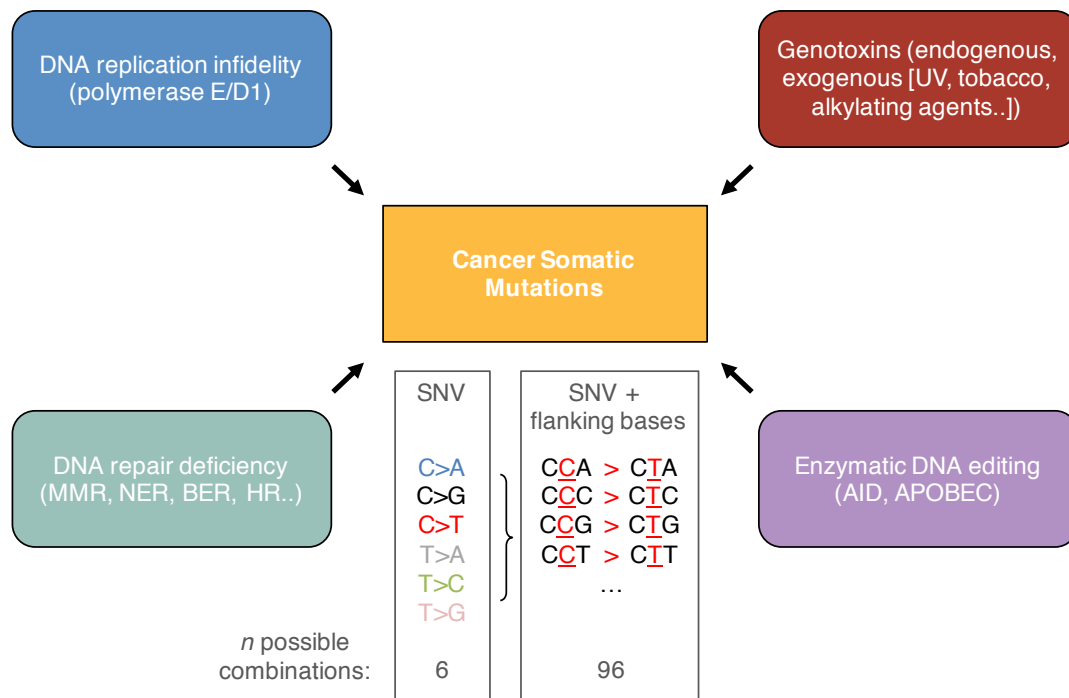


**Figure 10. Exogenous and endogenous mutational processes contributing to the accumulation of somatic mutations in human tumors and point mutation (SNV) analysis method.** While there are many mutational processes resulting from various combinations of damage and DNA repair capacities, the number of different point mutations is limited to 6 when only the mutant nucleotide is taken into account. This limit is circumvented by the inclusion of the trinucleotide context of each variant during the analysis, enabling to increase the number of possible combinations to 96, and to increase the specificity of the analysis.

In addition to the characterization of mutational processes, these advances enabled to accurately estimate the number of somatic mutations in each tumor sample by calculating the mutational load (number of somatic mutations per Mb). Even if there is currently no reference method for calculating the mutational load nor a threshold for defining hypermutation (in studies based on exomes, this threshold is usually set at 10 mutations per Mb), analysis of large numbers of samples allowed to identify tumors differing from others due to the presence of a particularly high mutational load, hypermutant samples. The mutational load is influenced by the tumor type (for instance the number of cell replications required for the transformation process) and the mutational processes involved. All types of cancer combined, these factors only contribute to modest variations in the mutational load and the majority of cancers - especially gliomas - have a relatively low number of somatic mutations (Figure 11a). In contrast, some cancers such as colorectal cancer, melanoma or lung cancer are frequently associated with a hypermutant phenotype<sup>103</sup>. Hypermutation can be caused by environmental factors (eg exposure to UV rays or to tobacco carcinogens), deregulation of enzymes of the APOBEC cytidine deaminase family, or defects in DNA replication (mutations in Pol $\epsilon$  and Pol $\delta$ 1 polymerases) or repair (MMR system deficiency)<sup>103,105,113</sup>.

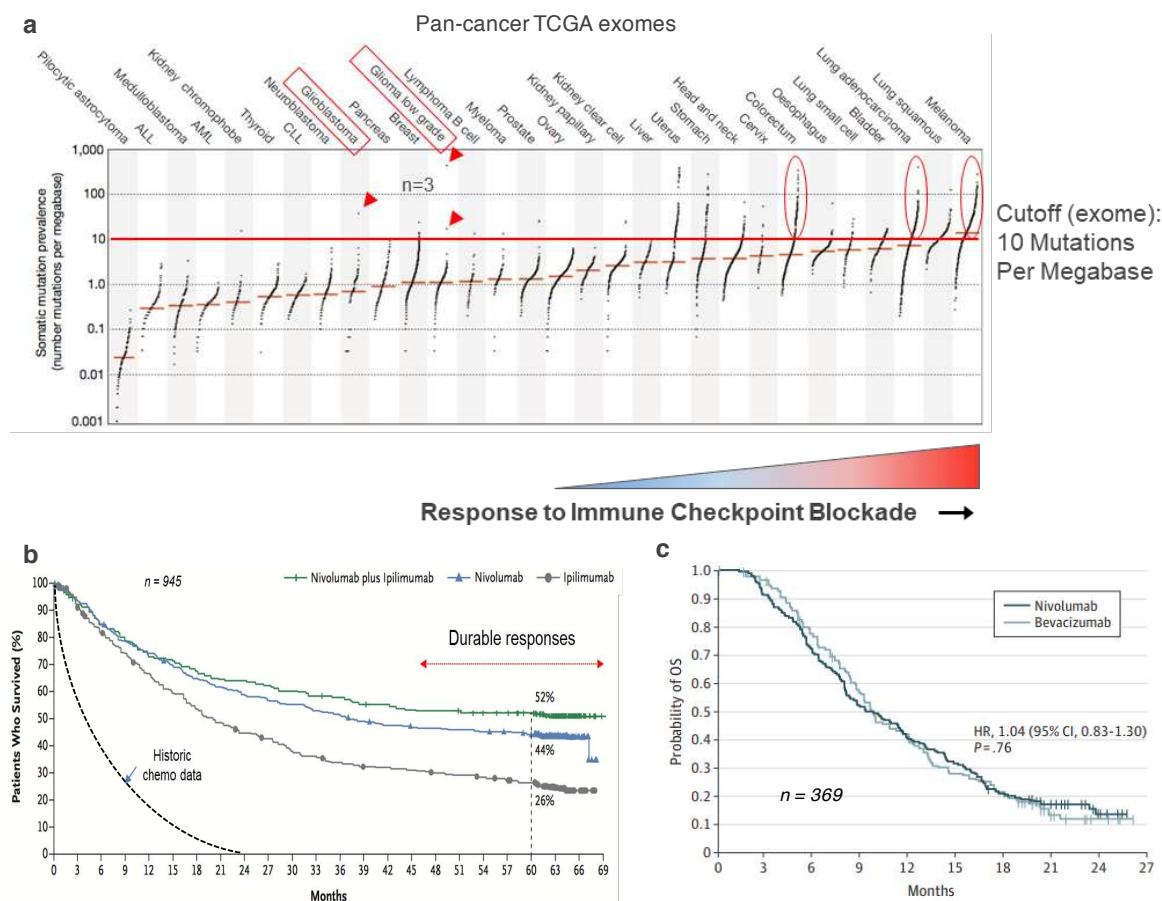


**Figure 11. Analysis of the mutational load in TCGA tumors (a) and response to ICI in cancers with high (b, melanoma) or low (c, glioblastoma) mutational load (from Alexandrov et al. <sup>103</sup> [a], Larkin et al. <sup>115</sup> [b] and Reardon et al. <sup>116</sup> [c]).**

While work on mutational processes initially focused on better understanding the factors involved in oncogenesis processes and aimed at predicting the evolutionary trajectory of cancers, recent data indicate that hypermutation could represent a predictor of response to immune checkpoint inhibitor (ICI) therapy in cancer patients <sup>117-130</sup>. ICIs (e.g. anti-PD-1, PD-L1, CTLA-4 monoclonal antibodies) are treatments directed against membrane receptors essential in the activation of immune cells. The aim of ICIs is to release the inhibition of the effector antitumor immune response (e.g. cytotoxic lymphocytes) induced by the expression of immune system checkpoints in tumor cells. These treatments have demonstrated impressive efficacy in several tumor types, in particular some cancers with MMR deficiency (eg colorectal and endometrial cancers) <sup>123,124,130,131</sup> and other hypermutant cancers (eg melanoma and lung cancer) <sup>115,118-120,125,128</sup> (Figures 11b, 12). There are many factors that can explain this association. Among these, hypermutant cancers have been shown to exhibit a significant increase in their neoantigen load, which makes them more susceptible to

recognition by effector cells of the immune system<sup>119,122,132</sup>. Conversely, in cancers with a usually low mutational load such as malignant gliomas, treatments with ICI have shown very modest results (Figure 11c)<sup>116</sup>. Importantly, several recent clinical observations have reported a significant efficacy of treatments with ICI in patients with malignant glioma with hypermutant phenotype<sup>117,126,127</sup> (Figure 12). However, these observations were limited to rare cases occurring in relatively unique settings (e.g. MMR constitutional deficiency syndrome). Their applicability in other less rare contexts thus remains to be determined.

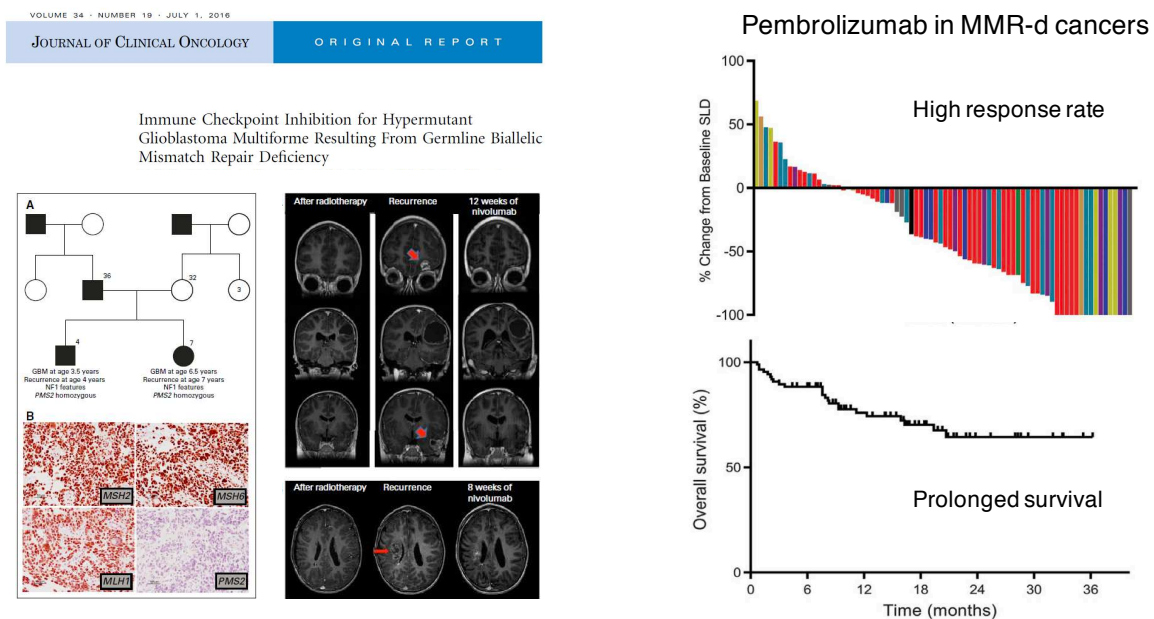


**Figure 12. Response to ICI treatments in MMR-deficient tumors (left, gliomas; right, pan-cancer) (from Bouffet et al.<sup>117</sup> [a] and Le et al.<sup>124</sup>).**

In all, we now have methods for establishing a detailed mapping of the burden and mutational signatures found in large cohorts of sequenced tumors, with the potential to better predict the response to ICI treatments. We therefore focused on the question of the mechanisms responsible for hypermutation in gliomas and their possible response to ICIs.

## B. Hypermutation in gliomas

Hypermutation in gliomas occurs in two very different contexts. In a first setting (“de novo” hypermutation), it is found from the initial diagnosis, suggesting the involvement of oncogenesis

processes associated with hypermutation in these tumors. These tumors indeed most often develop in patients with cancer predisposition syndrome associated with constitutional abnormalities of the DNA replication (Polε and Polδ1 polymerase mutations) or MMR systems<sup>113,133-139</sup>. In a second setting (“post-treatment” hypermutation), hypermutation is absent during the initial diagnosis but found during recurrence after treatment with alkylating agents<sup>4,87-96</sup>, suggesting that the hypermutation is either a direct consequence treatment or associated with mechanisms of resistance to treatment. Analysis of mutational signatures as described above confirms that these two pathways (de novo hypermutation and post-processing) are mechanistically different (Figure 13). Mutational signatures associated with MMR deficiencies (eg COSMIC 6, 15 or 20 signatures) or Polε and Polδ1 polymerases (COSMIC 10 signature) are most often found in gliomas with de novo hypermutation, while gliomas with post-treatment hypermutation have a mutational signature formed by a large majority of C> T transitions at CpC and CpT regions (signature 11)<sup>103</sup>. Although the etiology of the signature 11 remains unknown, it is similar to signatures observed in in vitro models exposed to alkylating agents<sup>140</sup>.

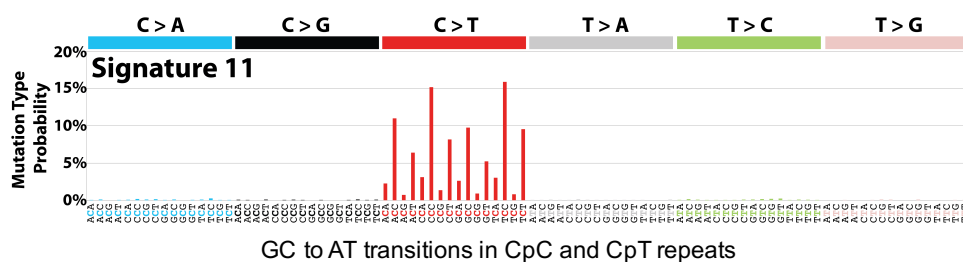


**Figure 13. Mutational signatures found in gliomas with low mutational burden (blue) or with de novo (green) or post-treatment hypermutation (red) (from Alexandrov et al. <sup>103</sup>). The mutational spectrum of signature 11 is shown below.**

### 1. Hypermutation in newly-diagnosed gliomas

This category includes four main situations, all rare or exceptional:

- Syndrome of genetic predisposition to cancer caused by mono-allelic deficiency of the MMR system <sup>113,135,139,141</sup>;
- Syndrome of genetic predisposition to cancer caused by bi-allelic MMR deficiency (CMMRD) <sup>113,134,136-138,142</sup>;
- Syndrome of genetic predisposition to cancer caused by constitutional mutations of Polε and Polδ1 polymerases <sup>113,143</sup>;
- Somatic abnormalities of the MMR system or Polε and Polδ1 polymerases <sup>126,127,144</sup>.

#### a) MMR deficiency

Malignant gliomas associated with constitutional or somatic deficits of the MMR system are very rare: they represent less than 1% of diffuse gliomas in the TCGA (Figure 14) <sup>6,7</sup>.

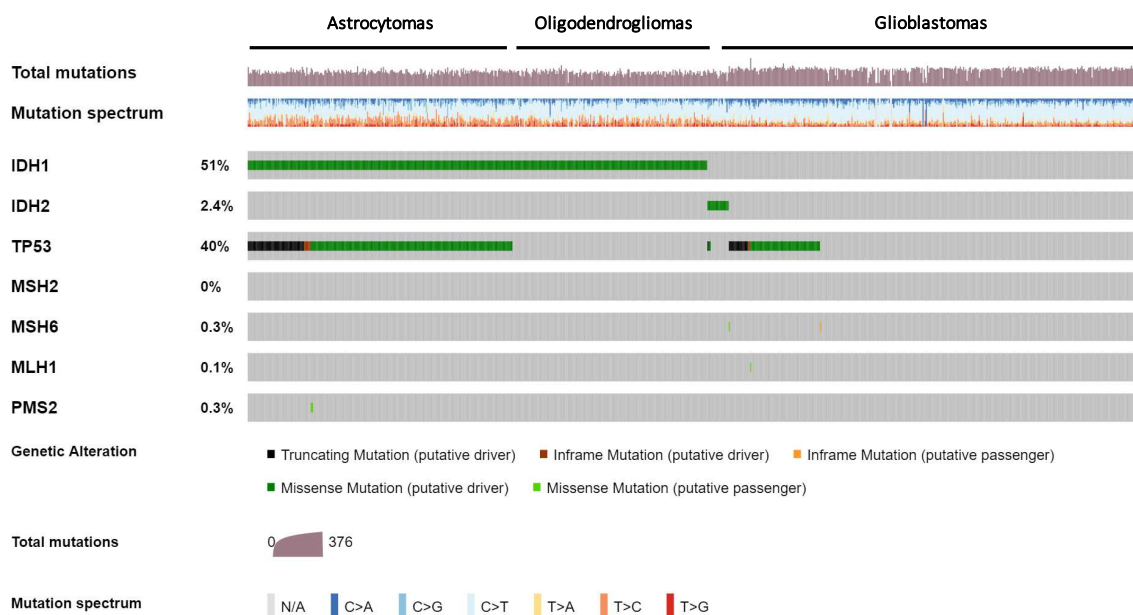


**Figure 14. Frequency of mutations in the main MMR genes in malignant gliomas sequenced at initial diagnosis (TCGA data <sup>6,7</sup>).**

Constitutional defects of the MMR system are found in two cancer predisposition syndromes: Lynch syndrome - the most common cancer predisposition syndrome (1/800 to 1/1000 in the general

population) - and CMMRD, much rarer. These syndromes are caused by germline mono- or bi-allelic mutations of the MMR genes (*MSH2*, *MSH6*, *MLH1*, *PMS2*) or more rarely mutation of the *EPCAM* resulting in epigenetic inactivation of *MSH2*. In Lynch syndrome, the somatic inactivation of the second wild-type allele by mutation or loss of heterozygosity results in a loss of MMR function<sup>145</sup>. Patients with Lynch syndrome most often develop carcinomas (eg colorectal cancer, endometrium, urothelial, gastric, pancreatic and small intestine). The reason why some Lynch syndrome patients develop malignant gliomas rather than carcinomas is unknown<sup>113,135,139,141,146</sup>. Conversely, patients with CMMRD most often develop hematologic malignancies, colorectal carcinomas and malignant gliomas in the childhood or adolescence<sup>113,134,136-138,142</sup>. Patients with Lynch syndrome or CMMRD developing malignant gliomas have a poor prognosis.

Molecularly, although all gliomas associated with CMMRD are hypermutated, it is not known if the same is true in Lynch syndrome. MMR-deficient gliomas differ significantly from other MMR-deficient cancers such as colorectal cancers. Data from Lynch syndrome or CMMRD patients indeed suggest MSI - a diagnostic marker used in current clinical practice and strongly correlated with MMR deficiency in colorectal cancers<sup>147,148</sup> - is absent in malignant gliomas<sup>133,134,136,137</sup>. The mechanisms underlying these differences are not known. In clinical practice, this feature makes it difficult to diagnose MMR deficiency in a patient with glioma. Given the frequency of *MSH6* and *PMS2* mutations and the difficulties in interpreting the technique in gliomas, it is preferable to use the immunohistochemistry of the four MMR proteins (*MSH2*, *MSH6*, *MLH1*, *PMS2*), if possible in combination with a sequencing of the MMR genes more or less associated with a study of the mutational burden and signature. These techniques gave enabled the recent establishment in the laboratory of glioma lines derived from patients with Lynch syndrome (Figure 15).

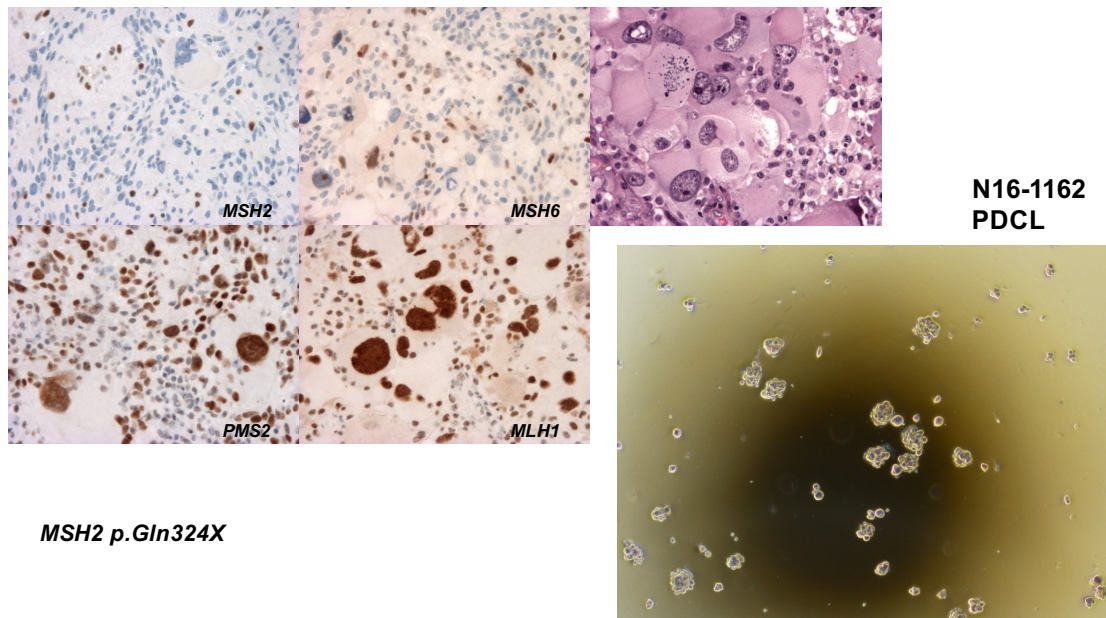


**Figure 15. Establishment of a malignant glioma PDCL derived from a patient with *MSH2* germline mutation.** Top, left: immunohistochemistry of the main MMR proteins (*MSH2*, *MSH6*, *MLH1*, *PMS2*) and staining with hematoxylin and eosin on the patient's tumor. Bottom, right: tumor-derived gliomaspheres in in vitro culture. The presence of an *MSH2* truncating mutation and hypermutant phenotype with MMR mutational signature was confirmed in both the tumor and PDCL.

### b) *Polε* and *Polδ1* deficiencies

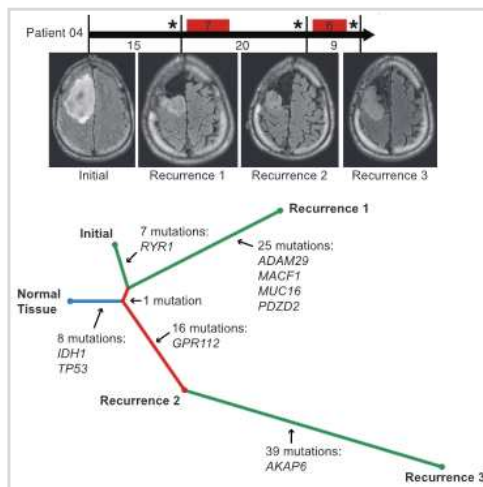
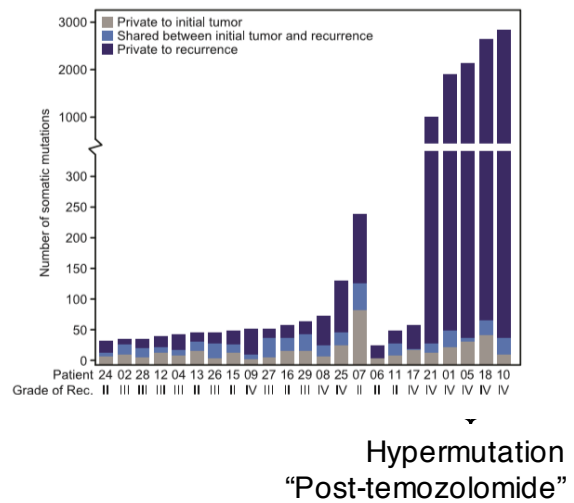
The *POLE* and *POLD1* genes code for the main DNA polymerases *Polε* and *Polδ1* which have a role in the fidelity of DNA replication (“proofreading” function) and are involved in various DNA repair mechanisms (eg BER, NER and MMR). Constitutional mutations in the *POLE* and *POLD1* genes are mainly found in families with colorectal cancers or multiple adenomatous colonic polyps. These mutations are located in the exonuclease domain of genes. In exceptional cases, such mutations have also been reported in patients with malignant gliomas<sup>113,143</sup>. Somatic exonuclease domain mutations of the *POLE* and *POLD1* genes are also observed in patients with malignant gliomas, in particular as secondary events in patients with bi-allelic deficiency of the MMR system<sup>113,135,144</sup>. On the molecular level, we often find in malignant gliomas with *Polε* or *Polδ1* deficiency a so-called “ultra-hypermutant” phenotype, which corresponds to a mutational load exceeding 100 mutations per Mb, often associated with a mutational signature 10. Response to ICI has been reported in patients with malignant glioma with *Polε* deficiency<sup>117,126,127</sup>.

## 2. Hypermutation in recurrent gliomas

This is the most frequently reported case in the literature with the first observations dating back to 2006 in patients treated with temozolomide<sup>4,87-96</sup>. In these patients, while the initial tumor did not exhibit hypermutation, tumor samples taken after treatment with temozolomide were found to show a significant increase in the mutational load. In addition, these recurrent tumors frequently harbored mutations affecting the genes of MMR<sup>4,87-89</sup>. It is important to note here that the majority of these MMR gene mutations were missense mutations of unknown functional significance. This made it difficult to determine their “driver” (i.e. responsible for the hypermutant phenotype) or “passenger” (i.e. associated with the phenomenon of hypermutation) character. In the presence of hypermutation, the probability of finding at least one missense mutation in one of the MMR genes is high and directly correlated with the increase in the mutational load.

With the accumulation of data from exome sequencing and the analysis of a larger number of tumor pairs (Figure 16)<sup>90-96</sup>, the molecular characteristics of gliomas with post-treatment hypermutation have been somewhat clarified:

- i) Clear increase in somatic mutational load after treatment (Figure 16);
- ii) Presence of a very specific mutational signature (signature 11), similar to signatures observed in in vitro models exposed to alkylating agents<sup>140</sup>, formed by a large majority of C> T transitions at CpC and CpT repeats (Figures 13 and 17);
- iii) Frequent presence of variants of unknown significance in MMR genes, not found in the initial samples (Figure 18);
- iv) Clear association of post-treatment hypermutation with exposure to alkylating agents before relapse (97% of hypermutant relapses) (Figure 19);
- v) Association with molecular biomarkers themselves associated with greater sensitivity to chemotherapy with alkylating agents, such as *IDH1/2* mutations (55% of hypermutant recurrences vs 22% of non-hypermutant recurrences) and *MGMT* promoter methylation (94% vs 30%) (Figure 19).

**a****b**

**Figure 16. Temporal and spatial clonal evolution in patients with diffuse glioma with *IDH1/2* mutation (from Johnson et al. <sup>90</sup>).** a) Establishment of a clonal phylogenetic tree from exome sequencing data in malignant gliomas taken at initial diagnosis and then during recurrence after treatment (pairs). b) Histograms showing the number of somatic mutations in 15 pairs, including eight pre- and post-temozolomide pairs (right end). The mutations represented in gray are found in the initial sample only; the mutations represented in dark blue are found in the recurrence sample only; the mutations shown in light blue are common to both samples. A major elevation of the mutational load was observed in 5/8 post-temozolomide recurrent tumors.

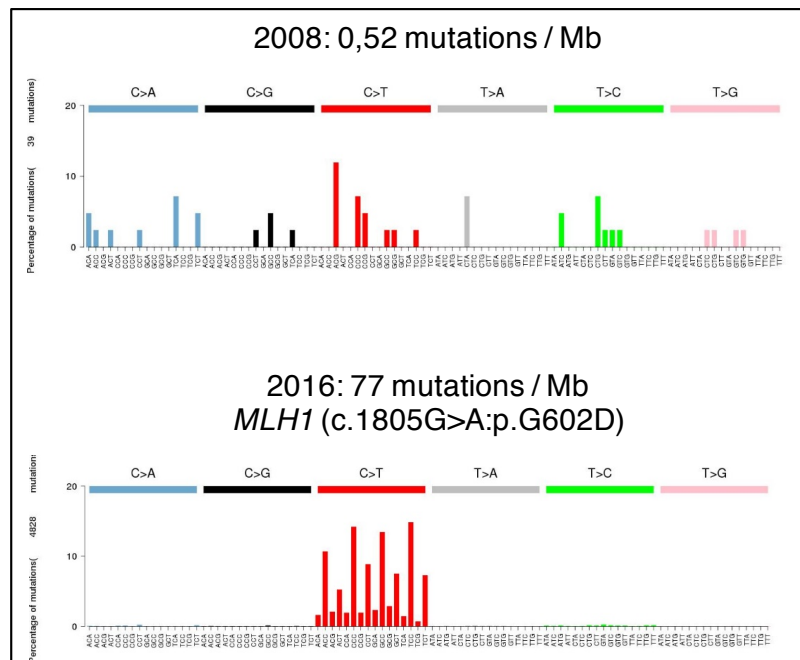


**Figure 17.** Acquisition of hypermutation with mutational signature 11 during recurrence after temozolomide in an anaplastic astrocytoma with *IDH1* mutation. Data from exome sequencing (initial tumors, recurrence and constitutional control).

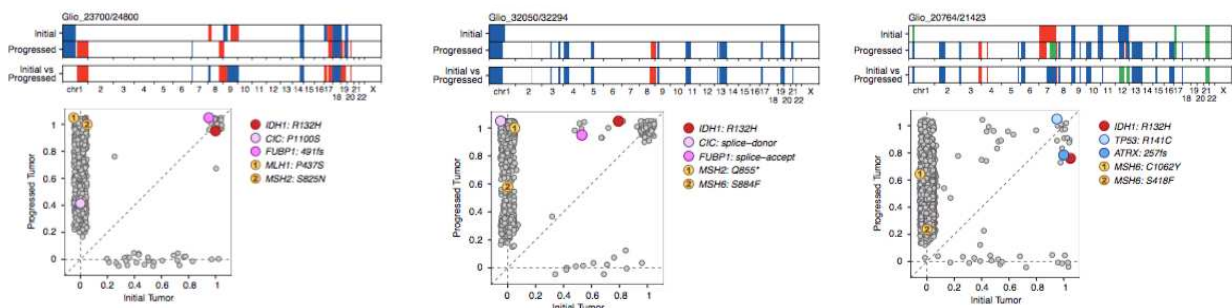


**Figure 18.** Analysis of copy number abnormalities (upper part) and clonality of somatic mutations (lower) in 3 pairs of pre- and post-temozolomide gliomas analyzed by exome sequencing (from Bai et al. <sup>149</sup>). Each mutation (circle) is represented according to its clonality in the initial sample (ranging from 0 [0% of tumor cells] to 1 [100% of tumor cells] on the x-axis) and recurrence (ditto on the axis ordinates). Mutations in the MMR genes are represented by yellow circles.

**a**

	Dataset	Coverage	Trios	Hypermuted recurrences	Hypermuted recurrences				
					<i>IDH1/2</i> mutated	MGMT meth	MMR mut	Prior RT	Prior AA therapy
IDH1/2wt GBM	TCGA, Nature 08	WES	19	7 (36%)	0%	86%	86%	100%	100%
	Kim, Cancer Cell 15	WES	35	1 (3%)	100%	100%	100%	0%	100%
Mixed	Kim, Gen Res 15	WES/WGS	23	5 (22%)	20%	100%	100%	100%	100%
	Wang, Nat Gen 2016	WES	93	17 (15%)	65%	NA	94%	100%	100%
IDH1/2-mut LGG	Johnson, Science 14	WES	14	5 (36%)	100%	100%	80%	0%	100%
	Bai, Nat Gen 2016	WES	18	3 (17%)	100%	NA	100%	67%	67%

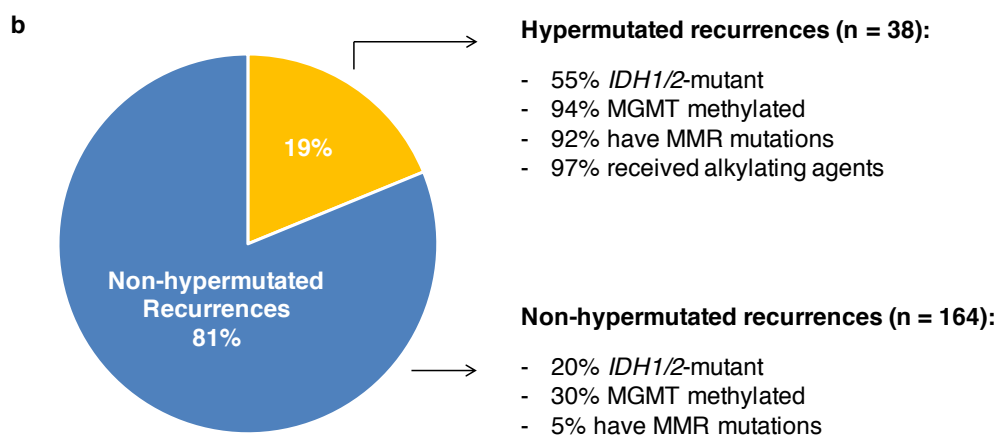


**Figure 19. Summary of pre- and post-treatment malignant glioma pair studies showing the association of = hypermutation with history of exposure to alkylating agents and the presence of *IDH1/2* mutation and/or *MGMT* promoter methylation (from TCGA<sup>109</sup>, Bai et al.<sup>149</sup>, Wang et al.<sup>94</sup>, Kim et al.<sup>93</sup>, Kim et al.<sup>92</sup>, and Johnson et al.<sup>90</sup>). “Trios” refer to samples for which exome or genome sequencing data is available for initial, recurrent, and constitutional control tumors.**

These observations suggest the existence of a mechanistic link between the acquisition of resistance to chemotherapy, the development of hypermutation and the presence of mutations in the MMR genes in malignant gliomas treated with temozolomide. However, several points call into question this potential link. On one hand, the mutational signature of gliomas with post-treatment hypermutation (signature 11, sometimes called the “temozolomide” signature) is unique and differs from the mutational signatures observed in MMR-deficient cancers (signatures 6, 15 or 20)<sup>103</sup>. Some authors have therefore hypothesized that signature 11 could be the direct consequence of exposure to temozolomide<sup>90</sup>. However, this mutational signature is not found in the majority of malignant

gliomas treated with temozolomide (Figure 19) <sup>92- 95</sup>. In contrast, in melanoma or lung cancer, exposure to UV rays or tobacco carcinogens results in the detection of associated specific mutational signatures (mutational signatures 4 and 7 respectively) in the vast majority of samples exposed to these mutagens <sup>103</sup>. This suggests that exposure to temozolomide alone is not sufficient to cause the development of signature 11. On the other hand, despite the fact that MMR deficits are strongly suspected of contributing to the development of hypermutation and temozolomide resistance, gliomas with post-treatment hypermutation exhibit unique characteristics that distinguish them from other MMR-deficient cancers, notably the absence of the MSI phenotype. This has led other authors to question this mechanistic link initially suspected <sup>150,151</sup>.

## IV. Hypothesis and objectives

Collectively, the data in the literature converge towards the existence of a mechanistic link between post-treatment hypermutation, MMR deficits, and temozolomide resistance in malignant gliomas<sup>73-78,97-101</sup>. While significant progress has been made in this field, the precise mechanism underlying such a link remains undetermined and several important questions that may help improve patient care remains unsolved:

1) Is there an association between hypermutation (de novo and post-treatment) and clinical-molecular characteristics (e.g. molecular subtype, *MGMT* promoter methylation, treatment pattern) in malignant gliomas? This would make it possible to better predict and possibly prevent the risk for the emergence of such a phenomenon in tumors at higher risk. Likewise, the prognostic impact - positive or negative - of hypermutation in these tumors has never been studied. Answering these questions requires the analysis of a large sample of clinically annotated tumors, yet previous studies only had very limited samples (a maximum of 17 hypermutated tumors)<sup>90-96</sup>.

2) Is MMR deficiency sufficient to produce temozolomide resistance or are other factors necessary<sup>73-78,97-101</sup>? Does it produce equivalent resistance to other alkylating agents such as CCNU? This requires the systematic study of the response to alkylating agents in a large sample of cell lines (PDCL) and xenografts (PDX) derived from patient and reflecting the biology of these tumors, including these isogenic models of gliomas with MMR deficiency.

3) What mechanism underlies the development of post-treatment hypermutation with signature 11? This signature is most frequently found in gliomas with MMR mutations, but it differs from other signatures associated with MMR deficiency and each is found in distinct groups of gliomas. MMR mutations in post-treatment hypermutation gliomas could be simple “passenger” events directly created by temozolomide and the elevation of the mutational load, or responsible for the signature 11 and the acquisition of temozolomide resistance.

4) Is hypermutation associated with better response to ICI treatments as in other types of cancer<sup>117-130</sup>? Although gliomas are associated with a highly immunosuppressive microenvironment, recent work suggests that hypermutated gliomas may benefit from ICI<sup>117,126,127</sup>. These observations

nonetheless come from relatively unique contexts (e.g. CMMRD) and their applicability in other contexts remains to be determined.

In order to address these questions, we characterized the burden and mutational signatures of a very large sample of gliomas sequenced by NGS panels (10,294 tumors including 558 hypermutant gliomas) and studied the associations between hypermutation and clinical-molecular characteristics in this cohort. We studied the mechanistic link between hypermutation with signature 11, MMR defects, and resistance to alkylating agents in models of malignant gliomas. Finally, we studied the impact of hypermutation on the prognosis of patients with glioma and their response to ICI.

# ARTICLE

# Mechanisms and therapeutic implications of hypermutation in gliomas

<https://doi.org/10.1038/s41586-020-2209-9>

Received: 22 July 2019

Accepted: 4 March 2020

Published online: 15 April 2020

 Check for updates

Mehdi Touat<sup>1,2,3,34</sup>, Yvonne Y. Li<sup>2,4,34</sup>, Adam N. Boynton<sup>2,5</sup>, Liam F. Spurr<sup>2,4</sup>, J. Bryan Iorgulescu<sup>4,6</sup>, Craig L. Bohrsen<sup>7,8</sup>, Isidro Cortes-Ciriano<sup>9</sup>, Cristina Birzu<sup>3</sup>, Jack E. Geduldig<sup>1</sup>, Kristine Pelton<sup>1</sup>, Mary Jane Lim-Fat<sup>4,10</sup>, Sangita Pal<sup>2,4</sup>, Ruben Ferrer-Luna<sup>2,4,11</sup>, Shakti H. Ramkissoon<sup>11,12</sup>, Frank Dubois<sup>2,4</sup>, Charlotte Bellamy<sup>1</sup>, Naomi Currimjee<sup>4</sup>, Juliana Bonardi<sup>1</sup>, Kenin Qian<sup>5</sup>, Patricia Ho<sup>5</sup>, Seth Malinowski<sup>1</sup>, Leon Taquet<sup>1</sup>, Robert E. Jones<sup>1</sup>, Aniket Shetty<sup>13</sup>, Kin-Hoe Chow<sup>13</sup>, Radwa Sharaf<sup>11</sup>, Dean Pavlick<sup>11</sup>, Lee A. Albacker<sup>11</sup>, Nadia Younan<sup>3</sup>, Capucine Baldini<sup>14</sup>, Maïté Verreault<sup>15</sup>, Marine Giry<sup>15</sup>, Erell Guillem<sup>16</sup>, Samy Ammari<sup>17,18</sup>, Frédéric Beuvon<sup>19</sup>, Karima Mokhtari<sup>20</sup>, Agusti Alentorn<sup>3</sup>, Caroline Dehais<sup>3</sup>, Caroline Houillier<sup>3</sup>, Florence Laigle-Donadey<sup>3</sup>, Dimitri Psimaras<sup>3</sup>, Eudocia Q. Lee<sup>4,10</sup>, Lakshmi Nayak<sup>4,10</sup>, J. Ricardo McFaline-Figueroa<sup>4,10</sup>, Alexandre Carpentier<sup>21</sup>, Philippe Cornu<sup>21</sup>, Laurent Capelle<sup>21</sup>, Bertrand Mathon<sup>21</sup>, Jill S. Barnholtz-Sloan<sup>22</sup>, Arnab Chakravarti<sup>23</sup>, Wenya Linda Bi<sup>24</sup>, E. Antonio Chiocca<sup>24</sup>, Katie Pricola Fehnel<sup>25</sup>, Sanda Alexandrescu<sup>26</sup>, Susan N. Chi<sup>5,27</sup>, Daphne Haas-Kogan<sup>28</sup>, Tracy T. Batchelor<sup>4,10</sup>, Garrett M. Frampton<sup>11</sup>, Brian M. Alexander<sup>11,28</sup>, Raymond Y. Huang<sup>29</sup>, Azra H. Ligon<sup>6</sup>, Florence Coulet<sup>16</sup>, Jean-Yves Delattre<sup>3,30</sup>, Khê Hoang-Xuan<sup>3</sup>, David M. Meredith<sup>1,6</sup>, Sandro Santagata<sup>1,6,31,32</sup>, Alex Duval<sup>33</sup>, Marc Sanson<sup>3,30</sup>, Andrew D. Cherniack<sup>2,4</sup>, Patrick Y. Wen<sup>4,10</sup>, David A. Reardon<sup>4</sup>, Aurélien Marabelle<sup>14</sup>, Peter J. Park<sup>7</sup>, Ahmed Idbaih<sup>3</sup>, Rameen Beroukhi<sup>2,4,10,35,35</sup>, Pratiti Bandopadhyay<sup>2,5,27,35</sup>, Franck Bielle<sup>20,35</sup> & Keith L. Ligon<sup>1,2,6,13,26,35</sup>

A high tumour mutational burden (hypermutation) is observed in some gliomas<sup>1–5</sup>; however, the mechanisms by which hypermutation develops and whether it predicts the response to immunotherapy are poorly understood. Here we comprehensively analyse the molecular determinants of mutational burden and signatures in 10,294 gliomas. We delineate two main pathways to hypermutation: a de novo pathway associated with constitutional defects in DNA polymerase and mismatch repair (MMR) genes, and a more common post-treatment pathway, associated with acquired resistance driven by MMR defects in chemotherapy-sensitive gliomas that recur after treatment with the chemotherapy drug temozolomide. Experimentally, the mutational signature of post-treatment hypermutated gliomas was recapitulated by temozolomide-induced damage in cells with MMR deficiency. MMR-deficient gliomas were characterized by a lack of prominent T cell infiltrates, extensive intratumoral heterogeneity, poor patient survival and a low rate of response to PD-1 blockade. Moreover, although bulk analyses did not detect microsatellite instability in MMR-deficient gliomas, single-cell whole-genome sequencing analysis of post-treatment hypermutated glioma cells identified microsatellite mutations. These results show that chemotherapy can drive the acquisition of hypermutated populations without promoting a response to PD-1 blockade and supports the diagnostic use of mutational burden and signatures in cancer.

Identifying genomic markers of response to immune checkpoint blockade (for example, PD-1 blockade) may benefit cancer patients by providing predictive biomarkers for patient stratification and identifying resistance mechanisms for therapeutic targeting. Gliomas typically have a low tumour mutational burden (TMB) and a highly immunosuppressive microenvironment—two features associated with immunotherapy resistance. Nevertheless, recent work has suggested that a subset of patients with high-TMB (hypermutated) gliomas might benefit from PD-1 blockade<sup>6</sup>. Although consistent with

data from other cancers<sup>7–9</sup>, these initial observations were derived from unique disease contexts such as constitutional DNA mismatch-repair (MMR) deficiency syndrome<sup>6</sup>. Therefore, the extent to which glioma patients at large will benefit from this approach is unknown. While large amounts of genomic data on gliomas exist<sup>2,4,5,10,11,12</sup>, our understanding of the clinical landscape of hypermutation and the mechanisms that underlie its development remain unclear. Hypermutation is rare in newly-diagnosed gliomas (de novo hypermutation), but common in tumours that have recurred after the use of alkylating

A list of affiliations appears at the end of the paper.

agents (post-treatment hypermutation)<sup>4,5,10,11</sup>. Given that gliomas exhibit substantial inter-patient and intra-tumoral genomic variation<sup>10,11,12</sup>, it remains to be determined whether molecular biomarkers (for example, *IDH1* or *IDH2* (hereafter *IDH1/2*) mutations) reliably predict the development of hypermutation or response to immunotherapy.

An association between hypermutation and MMR mutations has been observed in gliomas<sup>1-4,13</sup>, but most of the reported MMR mutations were not functionally characterized, and their role in causing hypermutation is unclear. Other studies have suggested that alkylating agents such as temozolomide are the direct cause of hypermutation<sup>3</sup>. This was supported by the discovery of a mutational signature (single base substitution (SBS) signature 11) characterized by the accumulation of G:C>A:T transitions at non-CpG sites in hypermutated gliomas after exposure to alkylating agents<sup>14</sup>. However, the fact that hypermutation is undetectable in most gliomas that recur after temozolomide treatment challenges this notion<sup>4,5</sup>. Furthermore, it remains unclear whether this mutational pattern enhances tumour immunogenicity and renders gliomas responsive to PD-1 blockade. Not all hypermutated cancers respond to such treatments<sup>7-9</sup>; a more accurate characterization of the phenotypic and molecular features of hypermutated gliomas therefore would help clinicians to manage such patients more effectively.

### Mutational burden and signatures in gliomas

Previous studies included too few hypermutated gliomas to characterize the landscape of hypermutation in gliomas<sup>1-5</sup>. We therefore created a cohort of sufficient scale ( $n = 10,294$ ) and subtype diversity by leveraging large datasets generated from clinical sequencing panels (DFCI-Profile, MSKCC-IMPACT and FMI)<sup>15-17</sup>. All samples from patients with a histopathological diagnosis of glioma were included and classified into molecular subgroups according to histopathology, mutational status of *IDH1/2*, and whole-arm co-deletion of chromosomes 1p and 19q (1p/19q co-deletion) (Extended Data Fig. 1, Supplementary Tables 1, 2). We quantified the TMB of all samples (median 2.6 mutations (mut.) per Mb (range 0.0–781.3)), established thresholds for hypermutation by examining the distribution of TMB (Extended Data Fig. 2)<sup>17,18</sup>, and identified 558 (5.4%) hypermutated gliomas (median TMB 50.8 mut. per Mb (8.8–781.3)) for further analysis.

Using samples with detailed clinical annotation (DFCI-Profile), we found that the prevalence of hypermutation varied between and within subgroups (Fig. 1a, b, Extended Data Fig. 3a, b, Supplementary Table 3). Hypermutation was detected almost exclusively in diffuse gliomas (99.1% of hypermutated samples) with high-grade histology (95.6%) and was more prevalent in recurrent tumours (16.6% versus 2.0% in newly diagnosed tumours; Fisher's exact test,  $P < 10^{-15}$ ) (Fig. 1b). In samples of recurrent tumours, hypermutation was associated with markers of response to alkylating agents, including *IDH1/2* mutation (hypermutation in 1.4% of newly diagnosed versus 25.4% of post-treatment *IDH1/2*-mutant tumours, Fisher's exact test,  $P = 2.0 \times 10^{-13}$ ), 1p/19q co-deletion (0.0% versus 33.8%,  $P = 7.3 \times 10^{-11}$ ), and *MGMT* promoter methylation (2.4% versus 24.2%,  $P = 9.0 \times 10^{-12}$ ). The effect of *IDH1/2* mutation was confirmed only in *MGMT*-methylated tumours (Extended Data Fig. 3c). These findings suggest that selective pressure from therapy may elicit progression towards hypermutation.

The standard treatment for gliomas includes surgery, radiation and chemotherapy with alkylating agents<sup>19,20</sup>. To assess the role of each of these in the development of hypermutation, we analysed associations between TMB and detailed patterns of treatment in 356 recurrent gliomas. Hypermutation was associated with prior treatment with temozolomide (Fisher's exact test,  $P < 10^{-15}$ ) in a dose-dependent manner (Fig. 1b, Extended Data Fig. 3d, e), but not with radiation ( $P = 0.88$ ) or nitrosoureas ( $P = 0.78$ ). Among recurrent tumours from patients who had received only one adjuvant treatment modality, TMB was increased only in temozolomide-treated samples (median 16.32 (interquartile range (IQR) 6.95–70.32) versus 6.08 (3.80–7.97) with surgery

only,  $P = 4.0 \times 10^{-7}$ ; Extended Data Fig. 3f). Of note, the prevalence of hypermutation in post-temozolomide samples correlated with the chemosensitivity of the primary, molecularly defined tumour type (1p/19q co-deleted oligodendrogliomas (59.5%) > *IDH1/2*-mutant astrocytomas (30.2%) > *MGMT*-methylated *IDH1/2* wild-type glioblastomas (23.1%) > *MGMT*-unmethylated *IDH1/2* wild-type glioblastomas (5.6%);  $P = 3.8 \times 10^{-7}$ ; Fig. 1b). We observed a similar pattern in the FMI validation dataset (Extended Data Fig. 3g-i).

The systematic analysis of somatic mutation patterns by genome sequencing has identified a variety of mutation signatures in human cancer which are driven by known and unknown DNA damage and repair processes<sup>14</sup>. We examined the contributions of 30 previously reported signatures (COSMIC signatures v2) within our cohort to investigate the biological processes that cause hypermutation in gliomas. We first validated that mutational signatures can be predicted using large targeted panel sequencing in hypermutated samples (Extended Data Figs. 4, 5a–c). The majority of de novo hypermutated gliomas harboured mutational signatures associated with defects in the MMR pathway (COSMIC signatures 6, 15, 26 and 14) or the DNA polymerase POLE (10 and 14)<sup>14</sup> (69% and 35% of samples, respectively; Extended Data Fig. 5d, e), implying that constitutional deficiency in MMR or POLE was likely to be the underlying genetic cause of hypermutation. By contrast, 98% of post-treatment hypermutated gliomas showed a mutational signature that has been previously associated with temozolomide exposure (signature 11). We also identified two distinct mutational signatures that were highly correlated with mutational signature 11 (Extended Data Fig. 5b, c) including a previously undescribed signature (S2) associated with 1p/19q co-deletion and lack of prior radiation therapy. Finally, half of the samples with a dominant signature 11 showed a co-existing minor MMR- or POLE-deficiency signature component (Extended Data Fig. 5e), suggesting that defective DNA repair and mutagen exposure cooperate to drive hypermutation in recurrent gliomas.

### Molecular drivers of hypermutation

Only a subset of temozolomide-treated samples (58 of 225, 25.8%) showed evidence of hypermutation, suggesting that additional factors are required for its development. Although MMR defects have been consistently observed in hypermutated gliomas<sup>1-4,13</sup>, their co-occurrence with high TMB did not enable prior studies to determine the degree to which MMR mutations represent passenger versus hypermutation-causing driver events. We systematically characterized mutations and copy number variants (CNVs; Supplementary Figs. 1, 2) to identify hypermutation drivers using an unbiased approach that controlled for the increased incidence of passenger mutations associated with hypermutation<sup>21</sup>. In the merged DFCI-Profile/MSKCC-IMPACT dataset, 36 genes were significantly enriched ( $q$  value  $< 0.01$ ) in hypermutated tumours (Fig. 2a). Collectively, MMR mutations stood out among the most enriched (91.2% versus 4.9% in non-hypermutated samples,  $q < 1.6 \times 10^{-15}$ ), and mutations in *MSH6* showed the highest enrichment (43.0% versus 1.2%,  $q = 3.3 \times 10^{-7}$ ) (Extended Data Figs. 3j–l, 6a, b). MMR-variant allele frequencies (VAFs) and cancer cell fractions (CCFs) in gliomas were most similar to those in MMR-deficient colorectal (CRC) or endometrial cancers and were higher than in MMR-proficient hypermutated cancers (Extended Data Fig. 6c, d). Some MMR variants in post-treatment hypermutated samples matched the canonical signature 11 sequence context (Extended Data Fig. 5f), suggesting that a subset of these variants are likely to have been caused by temozolomide treatment.

As most MMR variants lacked functional annotation, we next integrated sequencing data with immunohistochemistry for protein loss (Extended Data Fig. 6e). Overall, results from both assays were concordant, consistent with MMR mutations leading to loss of function. In rare samples that lacked MMR variants, signature analysis and MMR immunohistochemistry revealed evidence for MMR deficiency,

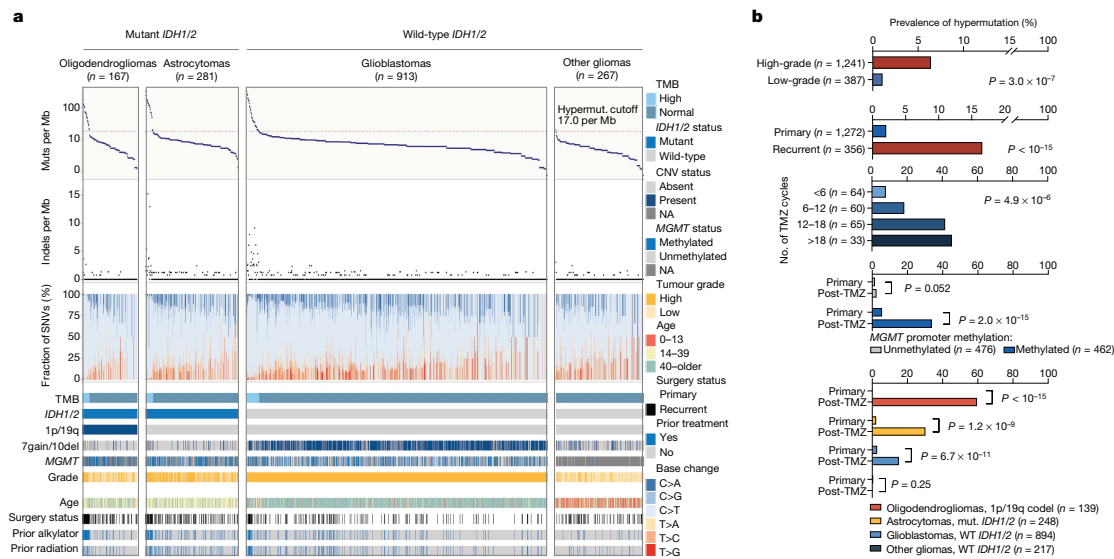


**Fig. 1 | TMB and mutational signature analysis reveals clinically distinct subgroups of hypermutated gliomas.** **a**, Integrated analysis of the DFCI-Profile dataset ( $n = 1,628$  gliomas) depicting TMB, indels at homopolymer regions, and the single nucleotide variant (SNV) mutation spectrum in each tumour according to molecular status of *IDH1/2*, 1p/19q co-deletion, chromosome 7 gain and/or chromosome 10 deletion (7gain/10del), *MGMT*

promoter methylation, histological grade, age at initial diagnosis, and prior treatment. Red line denotes high TMB ( $\geq 17.0$  mut. per Mb). **b**, Prevalence of hypermutation in the DFCI-Profile dataset. Chi-squared test and two-sided Fisher's exact test. NA, not available; TMZ, temozolomide; WT, wild-type; mut, mutant; codel, co-deleted.

suggesting that these samples harboured underlying MMR defects that could not be identified by sequencing (for example, promoter methylation). We identified several MMR mutational hotspots (Extended Data Fig. 6f, Supplementary Table 4), including a recurrent *MSH6* mutation (p.T1219I, in 7.4% of hypermutated tumours) that has been previously identified in Lynch syndrome and shown to exert a dominant-negative effect without affecting protein expression<sup>22,23</sup> (Extended Data Fig. 6g, h).

Immunohistochemistry on an independent cohort of 213 recurrent post-alkylator gliomas further validated these findings (Supplementary Table 2). MMR protein expression was lost in 22 post-treatment samples, and this loss was associated with *IDH1/2* mutations (20% mutant versus 2% wild-type; Fisher's exact test,  $P = 8.0 \times 10^{-6}$ ) (Extended Data Fig. 7a, b). Sequencing of samples with MMR protein loss confirmed hypermutation, with MMR mutations in 18 of 19 (94.7%) of these samples. Subclonal loss of MMR proteins (that is, protein retained in more than 20% of tumour cells) was more common in post-treatment than de novo hypermutated gliomas (12 of 46 (26.1%) versus 0 of 16 (0.0%),  $P = 0.03$ ) (Extended Data Fig. 7c–f).

We next assessed the relationship between MMR deficiency and acquired chemotherapy resistance. Because hypermutation and MMR defects were almost exclusively seen after temozolomide treatment, we hypothesized that nitrosoureas and temozolomide might not show complete cross-resistance. Analysis of temozolomide sensitivity in 30 cell lines derived from patients with glioma (patient-derived cell lines, PDCLs), including four derived from MMR-deficient gliomas (Extended Data Fig. 8a–c), showed that all native MMR-deficient PDCLs had striking temozolomide resistance compared to MMR-proficient PDCLs (6.46- and 1.35-fold increase in median area under the curve (AUC) versus MMR-proficient–*MGMT*-deficient and MMR-proficient–*MGMT*-proficient PDCLs, respectively) (Fig. 2b, Extended Data Fig. 8d–f). We next treated native and engineered isogenic MMR-knockout

glioma models with temozolomide or the nitrosourea lomustine (CCNU), a chloroethylating alkylating agent that generates DNA interstrand crosslinks and double-strand breaks (Fig. 2c, Extended Data Fig. 8g–i). All MMR-deficient models were resistant to temozolomide and sensitive to CCNU, consistent with the lack of hypermutation in samples from nitrosourea-treated patients<sup>24</sup> (Extended Data Fig. 3f).

### Mismatch repair deficiency and signature 11

Our analyses indicated that MMR deficiency together with temozolomide exposure might cause signature 11, as opposed to it being a 'pure' temozolomide signature. To test this idea, we exposed isogenic models of MMR deficiency to temozolomide (Extended Data Fig. 9a, b). After treatment with temozolomide, MMR-deficient PDCLs developed hypermutation with signature 11, whereas MMR-proficient controls (expressing sgGFP) did not (Fig. 2d). We then chronically treated temozolomide-sensitive glioblastoma xenografts (PDXs) with temozolomide until resistance was acquired (Fig. 2e, Extended Data Fig. 9c, d). These tumours developed hypermutation with signature 11 (Fig. 2f, Extended Data Fig. 9e) and shared four unique variants; the dominant-negative *MSH6* hotspot mutation (p.T1219I) and three non-coding variants (Fig. 2g), consistent with the theory that the *MSH6* mutation drives both hypermutation and acquired temozolomide resistance (Extended Data Fig. 9f).

Collectively, these findings show that temozolomide exerts a previously underappreciated selective pressure in favour of MMR-deficient cells, which are resistant to temozolomide. Exposing MMR-deficient cells to temozolomide induces hypermutation with signature 11 by causing DNA damage in the absence of functional MMR. Therefore, hypermutation with signature 11 represents a potential biomarker for MMR deficiency and temozolomide resistance in gliomas (Extended Data Fig. 9g).

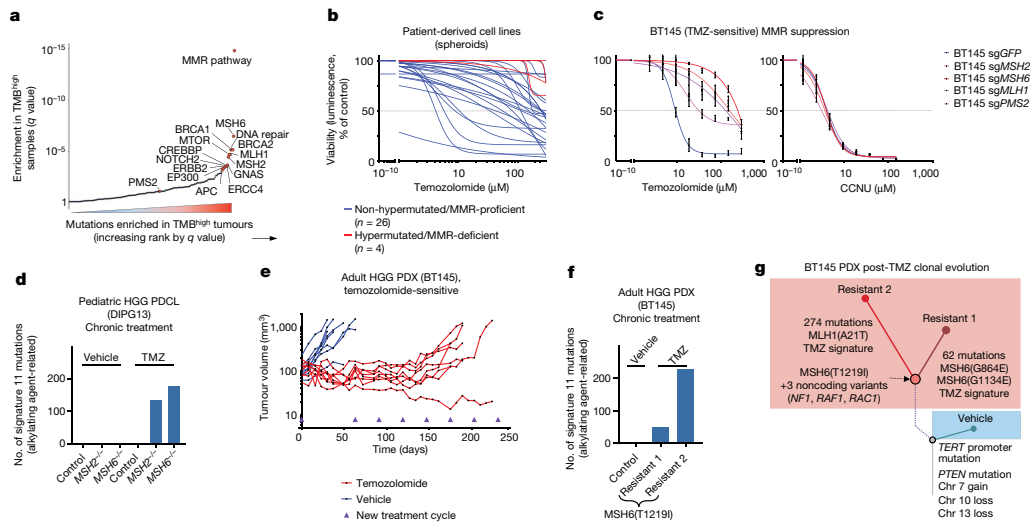


**Fig. 2 | MMR deficiency drives hypermutation and chemotherapy resistance in gliomas.** **a**, Mutated genes and pathways enriched in hypermutated gliomas in the merged DFCI-Profile/MSKCC-IMPACT dataset ( $n = 2,173$ ) using a permutation test to control for random mutation rate in the setting of hypermutability. **b**, Response to temozolomide across a panel ( $n = 30$ ) of native spheroid glioma PDCLs (blue, MMR-proficient; red, MMR-deficient). Dose-response curves were calculated using mean surviving fractions from three independent assays. **c**, Response to temozolomide and CCNU in the glioblastoma PDCL BT145 following knockout of *MSH2*, *MSH6*, *MLH1* or *PMS2* by CRISPR-Cas9. Dose-response curves were calculated using mean surviving fractions from three independent assays (mean  $\pm$  s.e.m.). **d**, Number of signature 11 variants after chronic temozolomide treatment of the PDCL DIPG13 with *MSH2* or *MSH6* knockout by CRISPR-Cas9. Mutational signatures could not be called in

the vehicle-treated samples (too few variants). **e**, Tumour volume ( $n = 8$  mice per group) during treatment with vehicle (blue) or temozolomide (red) in BT145 patient-derived xenografts (PDXs). **f**, Number of signature 11 variants found after chronic temozolomide exposure in BT145 PDXs. Mutational signatures could not be called in the vehicle-treated tumours (too few variants). **g**, Schematic representation of BT145 PDXs clonal evolution under temozolomide exposure. Two independent secondary resistant tumours (Resistant 1 and 2) and one vehicle-treated tumour are represented. Resistant tumours had four private variants that were not detected in the vehicle-treated tumour: an *MSH6*(T1219I) mutation (VAF 0.27 and 0.37 for resistant 1 and 2, respectively), and three non-coding variants of *NFI* (VAF 1.0 and 0.99), *RAC1* (VAF 0.86 and 0.86) and *RAF1* (0.44 and 0.56). HGG, high-grade glioma; Chr, chromosome.

**Characteristics of MMR-deficient gliomas**

MMR deficiency recently emerged as an indicator of response to PD-1 blockade in patients with cancer<sup>8,25</sup>, leading to the first tissue-agnostic cancer-drug approval by the US Food and Drug Administration for use of the PD-1 blocker pembrolizumab in patients with MMR-deficient cancers. However, in CRCs and some other cancers, MMR inactivation occurs early in tumour progression, whereas in post-treatment gliomas it arises late. Gliomas might therefore differ from other cancers on which the approval was based and these differences might influence immune recognition of tumours and the response to immunotherapy. To test this hypothesis, we first assessed the outcome of hypermutated gliomas. In CRC, MMR deficiency is associated with improved outcomes. By contrast, among patients with recurrent glioma, we observed worse survival in both hypermutated high-grade 1p/19q co-deleted oligodendrogliomas (median overall survival (OS) 96.5 months (95% confidence interval (CI) 20.8–NA (not applicable)) versus 137.2 months (95% CI 41.8–NA) in non-hypermutated tumours,  $P = 0.0009$ , two-sided log-rank test) and *IDH1/2*-mutant astrocytomas (median OS 15.7 months (95% CI 12.9–18.3) versus 21.5 months (95% CI 19.2–29.8),  $P = 0.0015$ ) (Fig. 3a, Extended Data Fig. 10a–c). We observed a similar trend in *IDH1/2* wild-type glioblastomas ( $P = 0.0809$ ). The finding of poor survival in recurrent hypermutated gliomas remained significant in multivariable analysis (hazard ratio 2.16 (95% CI 1.38–3.38),  $P = 0.0008$ ; Supplementary Table 5).

The current hypothesis behind the response of MMR-deficient CRCs to PD-1 blockade is based on their increased neoantigen burden and immune infiltration. We therefore assessed the association between

MMR deficiency and T-cell infiltration in gliomas ( $n = 43$ ) and CRCs ( $n = 19$ ). As expected, MMR-deficient CRCs exhibited significantly more infiltrating T-cells than their MMR-proficient counterparts (Fig. 3b). By contrast, both MMR-deficient and MMR-proficient glioma samples lacked significant T-cell infiltrates (Fig. 3c).

We next assessed whether the neoantigen burden was lower in MMR-deficient gliomas than in other hypermutated cancers using samples from the GENIE and TCGA datasets ( $n = 1,748$  and 699 hypermutated cancers, respectively). As neoantigen prediction was not feasible using panel sequencing data, we used the nonsynonymous mutational burden as a surrogate measure. This showed that both de novo and post-treatment MMR-deficient gliomas had an increase in their nonsynonymous mutational burden, when compared to non-hypermutated gliomas, and the glioma nonsynonymous mutational burden was similar to other hypermutated cancers (Fig. 3d, Extended Data Fig. 11a, b, Supplementary Table 6). This finding suggested that the total number of neoantigens is unlikely to explain the differences in immune response between gliomas and other hypermutated cancers.

Recent data suggest that, among mutations associated with MMR deficiency, small insertions and deletions (indels) at homopolymers (microsatellites)—which accumulate in MMR-deficient cells and can cause frameshift mutations—are crucial for producing ‘high-quality’ neoantigens that are recognized by immune cells<sup>26,28</sup>. Unexpectedly, although the high TMB was associated with an increased homopolymer indel burden in MMR-deficient CRCs, this association was not found in MMR-deficient gliomas (de novo hypermutated gliomas showed a modest increase; Fig. 3d, Extended Data Fig. 11c). This was validated using testing for microsatellite instability (MSI), a clinical biomarker for MMR

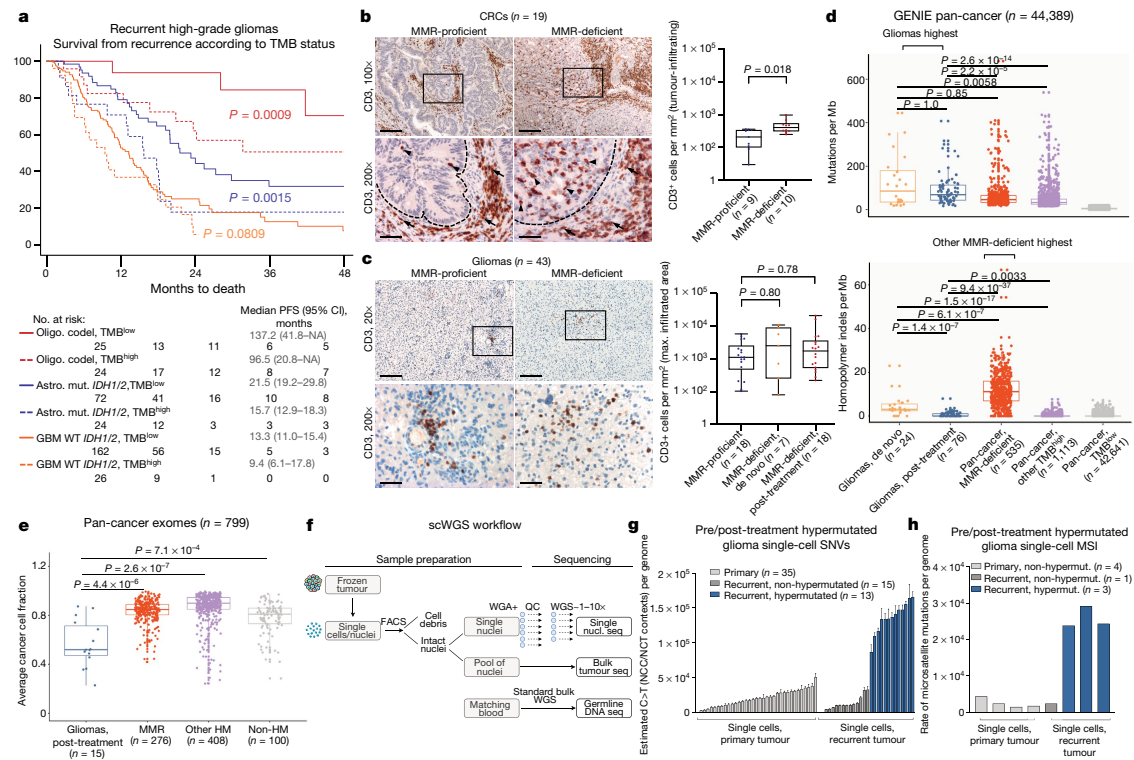


**Fig. 3 | Hypermutated and MMR-deficient gliomas harbour unique phenotypic and molecular characteristics including poor outcome and lack of MSI in bulk sequencing.** **a**, Survival of patients with recurrent high-grade glioma from the time of sample collection according to histomolecular group and TMB status ( $n = 333$  recurrent samples; 238 from DFCI-Profile, 95 from MSKCC-IMPACT). Two-sided log-rank test. **b**, Quantification of tumour-infiltrating CD3-positive T-cells in CRC samples ( $n = 19$ ). Left, representative low- and high-magnification images of CD3 immunolabelling (brown); intraepithelial lymphocytes, black arrowheads; stromal lymphocytes, black arrows) and nuclear counterstaining (blue). Dashed lines, border between tumour and stroma. Only intraepithelial lymphocytes were quantified. Scale bars: 100  $\mu\text{m}$  (100 $\times$ ), 50  $\mu\text{m}$  (200 $\times$ ). Right: boxes, quartiles; centre lines, median ratio for each group; whiskers, absolute range. Two-sided Wilcoxon rank-sum test. **c**, Quantification of tumour-infiltrating CD3-positive T-cells in gliomas according to their MMR status ( $n = 43$ ). For each group, three areas with the maximal CD3 infiltration were selected for quantification (representative images, left). Scale bars: 500  $\mu\text{m}$  (20 $\times$ ), 50  $\mu\text{m}$  (200 $\times$ ). Right: boxes, quartiles; centre lines, median ratio for each group; whiskers, absolute range. Kruskal–Wallis test and Dunn’s multiple comparison test. **d**, TMB (top) and homopolymer indel burden

(bottom) in hypermutated gliomas compared with other hypermutated cancers from the GENIE dataset. Tukey’s boxplots are shown. Two-sided Wilcoxon rank-sum test with Bonferroni correction. **e**, Pan-cancer analysis of cancer cell fractions in hypermutated gliomas (post-treatment) compared with other hypermutated cancers from the TCGA and ref. <sup>4</sup> exome datasets ( $n = 798$ ). One hundred non-hypermutated samples from the TCGA were randomly selected as controls. Boxes, quartiles; centre lines, median ratio for each group; whiskers, absolute range excluding outliers. Two-sided Wilcoxon rank-sum test with Bonferroni correction. **f**, Workflow for scWGS and bulk tumour DNA sequencing. **g**, Single-cell sequencing estimate of the number of G:C>A:T transitions at NCC and NCT trinucleotide contexts in 63 cells from a glioblastoma patient with post-temozolomide hypermutation using 1 $\times$  scWGS sequencing. Error bars show 95% CI. The absolute computed purity was 0.66 for the primary tumour sample and 0.47 for the recurrent tumour sample in the bulk sequencing. **h**, Single-cell sequencing estimate of microsatellite mutation rate in eight cells from a patient with glioblastoma with post-temozolomide hypermutation. Eight cells were analysed for the presence of MSI using 10 $\times$  scWGS sequencing. WGA, whole genome amplification; QC, quality control; nucl, nuclei; seq, sequencing.

deficiency. Whereas MSI was identified in all MMR-deficient CRCs, all tested gliomas with MMR protein loss ( $n = 15$ ) were microsatellite-stable (MSS) (Extended Data Figs. 7d–f, 11d).

We hypothesized that, in hypermutated gliomas, more of the homopolymer indels are subclonal and below the detection limits of bulk sequencing, relative to other MMR-deficient cancers. Indeed, analysis of CCFs indicated that hypermutated gliomas contained a greater burden of subclonal variants than did other hypermutated cancers (Fig. 3e, Extended Data Fig. 11e–h). We therefore performed single-cell whole-genome DNA sequencing (scWGS) of 28 cells from a hypermutated, post-temozolomide glioblastoma with an MSH6(T1219I)

mutation, and compared these to 35 non-hypermutated cells from the matched pre-treatment sample (Fig. 3f, Extended Data Fig. 11i–k). In the post-temozolomide sample, 13 of 28 cells (46.4%) were hypermutated with signature 11 (Fig. 3g, Extended Data Fig. 11l). Strikingly, whereas this tumour harboured only a minor increase in its homopolymer indel burden at the bulk level (0.49 versus 0.0 per Mb), the scWGS analysis showed a ninefold increase in microsatellite mutations in all hypermutated cells (Fig. 3h). This suggested that glioma cells with an MSH6(T1219I) variant harbour a subtle MSI phenotype that is not revealed by standard bulk sequencing or clinical MSI assays (Extended Data Fig. 11m).

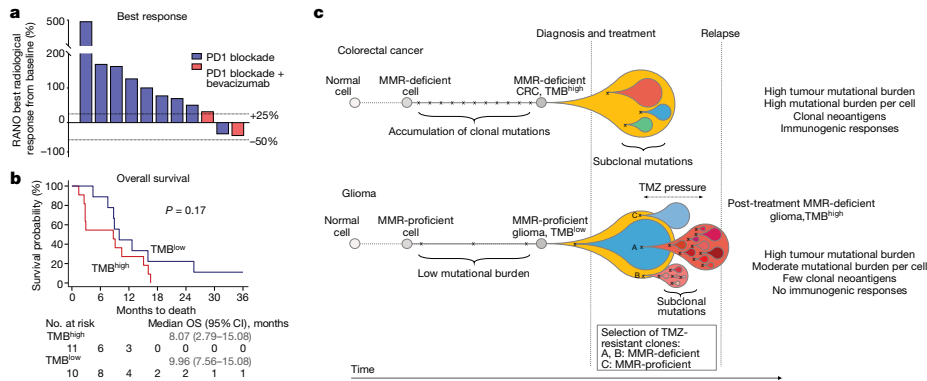


**Fig. 4 | Treatment of hypermutated gliomas with PD-1 blockade.** **a, b**, Best radiological response (**a**, measured as the best change in the sum of the products of perpendicular diameters of target lesions), and overall survival (**b**) of 11 patients with hypermutated and MMR-deficient gliomas who were treated with PD-1 blockade. A cohort of patients with non-hypermutated gliomas who were treated with PD-1 blockade is depicted as control ( $n = 10$ , best matches according to diagnosis, primary versus recurrent status, and prior treatments). Two-sided log-rank test. **c**, Proposed model explaining differential response to PD-1 blockade in MMR-deficient CRCs and gliomas. In CRCs (top), MMR deficiency is acquired early in pre-cancerous cells, creating mutations and indels at homopolymer regions. Over time, clonal neoantigens of both types emerge and

strong immune infiltrates are seen at diagnosis. Treatment with anti-PD-1 results in expansion of T cells that recognize these clonal neoantigens and substantial antitumour responses. In gliomas (bottom), few mutations are acquired early during tumorigenesis in the majority of tumours. Temozolomide drives the expansion of cells with MMR deficiency and late accumulation of random temozolomide-induced mutations. Ineffective antitumour responses may result from poor neoantigen quality (high burden of missense mutations versus frameshift-producing indels) and high subclonality associated with an immunosuppressive microenvironment. In some tumours, MMR-proficient subclones that have acquired therapy resistance through other pathways can co-exist with MMR-deficient subclones, giving rise to a mixed phenotype.

**PD-1 blockade in MMR-deficient gliomas**

As hypermutation in gliomas that acquire MMR deficiency tends to be subclonal and does not generate optimal antitumour T-cell responses, we hypothesized that these tumours might not have high response rates to PD-1 blockade. We performed a retrospective institutional review of patients treated with PD-1 pathway blockade for which the TMB at treatment initiation was available ( $n = 210$ ). This identified 11 patients with MMR-deficient glioma (5 de novo, 6 post-treatment) who were treated with PD-1 blockade for a median of 42 days (range 13–145; Supplementary Table 7). Nine (81.8%) had disease progression as their best response (Fig. 4a), and the median progression-free survival (PFS) and OS were 1.38 months (95% CI 0.95–2.69) and 8.7 months (95% CI 2.79–15.08), which were not significantly different from the data for matched patients with non-hypermutated glioma (PFS 1.87 months (95% CI 1.28–2.92), OS 9.96 months (95% CI 7.56–15.08); Fig. 4b, Extended Data Fig. 10d).

Because our prior analyses indicated that patients with hypermutated gliomas might have reduced survival, we used a second set of historical controls to compare the outcome of hypermutated gliomas treated with PD-1 blockade versus other systemic agents (Supplementary Table 7). Unexpectedly, we observed a longer median OS for patients treated with other systemic agents when compared to those treated with PD-1 blockade (16.10 months (95% CI 3.98–22.21) versus 8.07 (95% CI 2.79–15.08.21);  $P = 0.02$ , two-sided log-rank test; Extended Data Fig. 10e, f, Supplementary Table 8). In one patient with hypermutated glioma that showed rapid imaging changes, histopathologic analysis of samples taken before and after treatment with PD-1 blockade showed highly proliferative tumour in both samples, with no significant evidence of pathologic response or increase in immune infiltrates after PD-1 blockade (Extended Data Fig. 10g).

**DISCUSSION**

Collectively, these results support a model in which differences in the mutation landscape and antigen clonality of hypermutated gliomas relative to other hypermutated cancers markedly affect the

response to immunotherapy (Fig. 4c) and may explain the lack of both recognition of MMR-deficient glioma cells by the host immune system and response to PD-1 blockade, compared to other MMR-deficient cancers<sup>8,25</sup>. A key difference is that MMR-deficient gliomas lack detectable MSI by standard assays, similar to data from patients with constitutional MMR deficiency syndromes<sup>30</sup>. Our scWGS analyses suggest that this discordance might be due to intratumour heterogeneity and a lack of sufficient evolutionary time to select clonal MSI populations. Mechanistically, selective pressure exerted by temozolomide drives the late evolution of MMR-deficient subclones, which further accumulate temozolomide-induced mutations in individual cells. In line with previous data, therapy-induced single nucleotide variant mutations might not elicit effective antitumour responses, possibly because of the quality (missense mutations versus frameshift-producing indels) or subclonal nature of their associated neoantigens<sup>8,27–29</sup>. However, future evaluation of longer treatment exposure or combinatorial strategies is warranted to determine whether checkpoint blockade can be effective in this or other selected populations (for example, individuals with newly diagnosed MMR- or POLE-deficient gliomas)<sup>6</sup>.

We have presented evidence that recurrent defects in the MMR pathway drive hypermutation and acquired temozolomide resistance in chemotherapy-sensitive gliomas. Although it is difficult to determine the origin of MMR deficiency by sequence context alone in individual post-treatment samples, our data suggests that some MMR variants are likely to be caused by temozolomide. However, as acquired MMR deficiency occurs in the most temozolomide-sensitive tumours, it is not clear whether the acquired MMR deficiency outweighs the positive effects of temozolomide in gliomas. Our finding that MMR-deficient cells retain sensitivity to CCNU supports the hypothesis that hypermutation reduces cellular fitness and tolerance to DNA-damaging agents other than temozolomide. These alternatives are of interest in light of recent evidence showing that the addition of CCNU to chemoradiation improves the outcome of patients with *MGMT*-methylated glioblastomas<sup>31</sup>. Future studies are warranted to address the possibility that upfront temozolomide with CCNU may attenuate the process of post-treatment hypermutation. Furthermore, mechanisms of

resistance to temozolomide that are not associated with hypermutation will need to be addressed.

Finally, our data indicate that the absence of an immune response in gliomas is likely to result from several aspects of immunosuppression in the brain that require further characterization. Approaches that increase infiltration by cytotoxic lymphocytes into the glioma microenvironment will probably be required to improve immunotherapy response. Our data also suggest a change in practice whereby repeated biopsies and sequencing to identify progression and hypermutation could inform prognosis and guide therapeutic management.

### Online content

Any methods, additional references, Nature Research reporting summaries, source data, extended data, supplementary information, acknowledgements, peer review information; details of author contributions and competing interests; and statements of data and code availability are available at <https://doi.org/10.1038/s41586-020-2209-9>.

1. Hunter, C. et al. A hypermutation phenotype and somatic MSH6 mutations in recurrent human malignant gliomas after alkylator chemotherapy. *Cancer Res.* **66**, 3987–3991 (2006).
2. Cancer Genome Atlas Research Network. Comprehensive genomic characterization defines human glioblastoma genes and core pathways. *Nature* **455**, 1061–1068 (2008).
3. Johnson, B. E. et al. Mutational analysis reveals the origin and therapy-driven evolution of recurrent glioma. *Science* **343**, 189–193 (2014).
4. Wang, J. et al. Clonal evolution of glioblastoma under therapy. *Nat. Genet.* **48**, 768–776 (2016).
5. Barthel, F. P. et al. Longitudinal molecular trajectories of diffuse glioma in adults. *Nature* **576**, 112–120 (2019).
6. Bouffet, E. et al. Immune checkpoint inhibition for hypermutant glioblastoma multiforme resulting from germline biallelic mismatch repair deficiency. *J. Clin. Oncol.* **34**, 2206–2211 (2016).
7. Rizvi, N. A. et al. Mutational landscape determines sensitivity to PD-1 blockade in non-small cell lung cancer. *Science* **348**, 124–128 (2015).
8. Le, D. T. et al. PD-1 blockade in tumors with mismatch-repair deficiency. *N. Engl. J. Med.* **372**, 2509–2520 (2015).
9. McGranahan, N. et al. Clonal neoantigens elicit T cell immunoreactivity and sensitivity to immune checkpoint blockade. *Science* **351**, 1463–1469 (2016).
10. Brennan, C. W. et al. The somatic genomic landscape of glioblastoma. *Cell* **155**, 462–477 (2013).
11. Brat, D. J. et al. Comprehensive, integrative genomic analysis of diffuse lower-grade gliomas. *N. Engl. J. Med.* **372**, 2481–2498 (2015).
12. Louis, D. N. et al. World Health Organization Histological Classification of Tumours of the Central Nervous System (ed. 2) (International Agency for Research on Cancer, 2016).
13. Cahill, D. P. et al. Loss of the mismatch repair protein MSH6 in human glioblastomas is associated with tumor progression during temozolomide treatment. *Clin. Cancer Res.* **13**, 2038–2045 (2007).
14. Alexandrov, L. B. et al. Signatures of mutational processes in human cancer. *Nature* **500**, 415–421 (2013).
15. Frampton, G. M. et al. Development and validation of a clinical cancer genomic profiling test based on massively parallel DNA sequencing. *Nat. Biotechnol.* **31**, 1023–1031 (2013).
16. Sholl, L. M. et al. Institutional implementation of clinical tumor profiling on an unselected cancer population. *JCI Insight* **1**, e87062 (2016).
17. Zehir, A. et al. Mutational landscape of metastatic cancer revealed from prospective clinical sequencing of 10,000 patients. *Nat. Med.* **23**, 703–713 (2017).
18. Campbell, B. B. et al. Comprehensive analysis of hypermutation in human cancer. *Cell* **171**, 1042–1056.e10 (2017).
19. Stupp, R. et al. Radiotherapy plus concomitant and adjuvant temozolomide for glioblastoma. *N. Engl. J. Med.* **352**, 987–996 (2005).
20. van den Bent, M. J. et al. Adjuvant procarbazine, lomustine, and vincristine chemotherapy in newly diagnosed anaplastic oligodendroglioma: long-term follow-up of EORTC brain tumor group study 26951. *J. Clin. Oncol.* **31**, 344–350 (2013).
21. Kim, J. et al. Somatic ERCC2 mutations are associated with a distinct genomic signature in urothelial tumors. *Nat. Genet.* **48**, 600–606 (2016).
22. Berends, M. J. et al. Molecular and clinical characteristics of MSH6 variants: an analysis of 25 index carriers of a germline variant. *Am. J. Hum. Genet.* **70**, 26–37 (2002).
23. Yang, G. et al. Dominant effects of an Msh6 missense mutation on DNA repair and cancer susceptibility. *Cancer Cell* **6**, 139–150 (2004).
24. Ollier, E. et al. Analysis of temozolomide resistance in low-grade gliomas using a mechanistic mathematical model. *Fundam. Clin. Pharmacol.* **31**, 347–358 (2017).

25. Marabelle, A. et al. Efficacy of pembrolizumab in patients with noncolorectal high microsatellite instability/mismatch repair-deficient cancer: results from the phase II KEYNOTE-158 study. *J. Clin. Oncol.* **38**, 1–10 (2020).
26. Germano, G. et al. Inactivation of DNA repair triggers neoantigen generation and impairs tumour growth. *Nature* **552**, 116–120 (2017).
27. Mandal, R. et al. Genetic diversity of tumors with mismatch repair deficiency influences anti-PD-1 immunotherapy response. *Science* **364**, 485–491 (2019).
28. Rosenthal, R. et al. Neoantigen-directed immune escape in lung cancer evolution. *Nature* **567**, 479–485 (2019).
29. Gejman, R. S. et al. Rejection of immunogenic tumor clones is limited by clonal fraction. *eLife* **7**, e41090 (2018).
30. Gylling, A. H. et al. Differential cancer predisposition in Lynch syndrome: insights from molecular analysis of brain and urinary tract tumors. *Carcinogenesis* **29**, 1351–1359 (2008).
31. Herrlinger, U. et al. Lomustine-temozolomide combination therapy versus standard temozolomide therapy in patients with newly diagnosed glioblastoma with methylated MGMT promoter (CeTeG/NOA-09): a randomised, open-label, phase 3 trial. *Lancet* **393**, 678–688 (2019).

**Publisher's note** Springer Nature remains neutral with regard to jurisdictional claims in published maps and institutional affiliations.

© The Author(s), under exclusive licence to Springer Nature Limited 2020

<sup>1</sup>Department of Oncologic Pathology, Dana-Farber Cancer Institute, Harvard Medical School, Boston, MA, USA. <sup>2</sup>Broad Institute of Harvard and MIT, Cambridge, MA, USA. <sup>3</sup>Sorbonne Université, Inserm, CNRS, UMR S 1127, Institut du Cerveau et de la Moelle épinière, ICM, AP-HP, Hôpitaux Universitaires La Pitié Salpêtrière - Charles Foix, Service de Neurologie 2-Mazarin, Paris, France. <sup>4</sup>Department of Medical Oncology, Dana-Farber Cancer Institute, Harvard Medical School, Boston, MA, USA. <sup>5</sup>Dana-Farber/Boston Children's Cancer and Blood Disorders Center, Boston, MA, USA. <sup>6</sup>Department of Pathology, Brigham & Women's Hospital, Boston, Harvard Medical School, MA, USA. <sup>7</sup>Department of Biomedical Informatics, Harvard Medical School, Boston, MA, USA. <sup>8</sup>Bioinformatics and Integrative Genomics PhD Program, Harvard Medical School, Boston, MA, USA. <sup>9</sup>European Molecular Biology Laboratory, European Bioinformatics Institute, Wellcome Genome Campus, Hinxton, UK. <sup>10</sup>Department of Neurology, Brigham and Women's Hospital, Harvard Medical School, Boston, MA, USA. <sup>11</sup>Foundation Medicine Inc., Cambridge, MA, USA. <sup>12</sup>Wake Forest Comprehensive Cancer Center and Department of Pathology, Wake Forest School of Medicine, Winston-Salem, NC, USA. <sup>13</sup>Center for Patient Derived Models, Dana-Farber Cancer Institute, Boston, MA, USA. <sup>14</sup>Drug Development Department (DITEP), INSERM U1015, Université Paris Saclay, Gustave Roussy, Villejuif, France. <sup>15</sup>Sorbonne Université, Inserm, CNRS, UMR S 1127, Institut du Cerveau et de la Moelle épinière, ICM, Paris, France. <sup>16</sup>Unité fonctionnelle d'Oncogénétique et Angiogénétique Moléculaire, Département de génétique, Hôpitaux Universitaires La Pitié Salpêtrière - Charles Foix, Paris, France. <sup>17</sup>Department of Diagnostic Radiology, Gustave Roussy, Villejuif, France. <sup>18</sup>IR4M (UMR8081), Université Paris-Sud, Centre National de la Recherche Scientifique, Orsay, France. <sup>19</sup>AP-HP, Université Paris Descartes, Hôpital Cochin, Service d'Anatomie et Cytologie Pathologiques, Paris, France. <sup>20</sup>Sorbonne Université, Inserm, CNRS, UMR S 1127, Institut du Cerveau et de la Moelle épinière, ICM, AP-HP, Hôpitaux Universitaires La Pitié Salpêtrière - Charles Foix, Service de Neuropathologie Laboratoire Escourrolle, Paris, France. <sup>21</sup>Sorbonne Université, Inserm, CNRS, UMR S 1127, Institut du Cerveau et de la Moelle épinière, ICM, AP-HP, Hôpitaux Universitaires La Pitié Salpêtrière - Charles Foix, Service de Neurochirurgie, Paris, France. <sup>22</sup>Department of Population and Quantitative Health Sciences, Case Western Reserve University School of Medicine, Cleveland, OH, USA. <sup>23</sup>Department of Radiation Oncology, Arthur G. James Hospital/Ohio State Comprehensive Cancer Center, Columbus, OH, USA. <sup>24</sup>Department of Neurosurgery, Brigham & Women's Hospital, Harvard Medical School, Boston, MA, USA. <sup>25</sup>Department of Neurosurgery, Boston Children's Hospital, Harvard Medical School, Boston, MA, USA. <sup>26</sup>Department of Pathology, Boston Children's Hospital, Harvard Medical School, Boston, MA, USA. <sup>27</sup>Department of Pediatrics, Harvard Medical School, Boston, MA, USA. <sup>28</sup>Department of Radiation Oncology, Brigham and Women's Hospital, Dana-Farber Cancer Institute, Boston Children's Hospital, Harvard Medical School, Boston, MA, USA. <sup>29</sup>Department of Radiology, Brigham and Women's Hospital, Dana-Farber Cancer Institute, Harvard Medical School, Boston, MA, USA. <sup>30</sup>Onconeurotek Tumor Bank, Institut du Cerveau et de la Moelle épinière, ICM, Paris, France. <sup>31</sup>Ludwig Center at Harvard Medical School, Harvard Medical School, Boston, MA, USA. <sup>32</sup>Laboratory of Systems Pharmacology, Harvard Medical School, Boston, MA, USA. <sup>33</sup>Sorbonne Université, Inserm, UMR 938, Centre de Recherche Saint Antoine, Equipe Instabilité des Microsatellites et Cancer, Equipe labellisée par la Ligue Nationale contre le Cancer, Paris, France. <sup>34</sup>These authors contributed equally: Mehdi Touat, Yvonne Y. Li. <sup>35</sup>These authors jointly supervised this work: Rameen Beroukhim, Prati Bandopadhyay, Franck Bielle, Keith L. Ligon. <sup>✉</sup>e-mail: mehdi.touat@gmail.com; rameen\_beroukhim@dfci.harvard.edu; pratiti\_bandopadhyay@dfci.harvard.edu; franck.bielle@aphp.fr; keith\_ligon@dfci.harvard.edu

## Article

### Methods

#### Datasets

For the DFCI-Profile dataset, clinical data and tumour variant calls identified through targeted next-generation sequencing (NGS) panels of 1,628 gliomas sequenced between June 2013 and November 2018 as part of a large institutional prospective profiling program (DFCI-Profile) were included<sup>46</sup> (Extended Data Fig. 1). The distinction between photon and proton radiotherapy was not systematically captured; the vast majority of patients underwent photon radiotherapy. For the MSKCC-IMPACT and FMI datasets, clinical data and tumour variant calls from a total of 545 and 8,121 samples, respectively, that could be assigned to a molecular subgroup (see below) were included<sup>15,17,32,33</sup>. For pan-cancer analyses in targeted panel sets, clinical data and tumour variant calls from the GENIE project (a repository of genomic data obtained during routine clinical care at international institutions) were downloaded from Synapse (public data, release v6.1)<sup>34</sup>. For pan-cancer analyses in whole-exome sequencing sets, clinical data and tumour variant calls from 17 hypermutated glioblastomas<sup>4</sup> and from the pan-cancer TCGA dataset were downloaded from the NCI Genomic Data Commons<sup>35</sup>. In addition, 247 gliomas collected at one site between 2009 and 2017 were analysed for protein expression of four MMR proteins (MSH2, MSH6, MLH1, and PMS2) using immunohistochemistry. Written informed consent or IRB waiver of consent was obtained from all participants. Patients of the FMI dataset were not consented for release of raw sequencing data. The study, including the consent procedure, was approved by the institutional ethics committees (10-417/11-104/17-000; Western Institutional Review Board (WIRB), Puyallup, WA).

#### Tumour genotyping and diagnosis

For the majority of samples, genomic testing was ordered by the pathologist or treating physician as part of routine clinical care to identify relevant genomic alterations that could potentially inform diagnosis and treatment decisions. Patients who underwent DFCI-Profile testing signed a clinical consent form, permitting the return of results from clinical sequencing. In total, 1,628 gliomas were sequenced as part of a cohort of 21,992 tumours prospectively profiled between June 2013 and November 2018. Research tumour diagnoses were reviewed and annotated according to histopathology, mutational status of *IDH1* and *IDH2* genes, and whole-arm co-deletion of chromosomes 1p and 19q (1p/19q co-deletion), according to WHO 2016 criteria<sup>12</sup>. All samples were assigned to one of four main molecular subgroups: *IDH1/2*-mutant and 1p/19q co-deleted oligodendrogliomas (high- and low-grade), *IDH1/2*-mutant astrocytomas (high- and low-grade), *IDH1/2* wild-type glioblastomas (high-grade only), and *IDH1/2* wild-type gliomas of other histologies (high- and low-grade), the latter including grade I pilocytic astrocytomas, glioneuronal tumours and other unclassifiable gliomas. For simplification, *IDH1/2* wild-type grade III anaplastic astrocytomas and grade IV diffuse intrinsic pontine gliomas were assigned to the group of *IDH1/2* wild-type glioblastomas in all analyses. Samples for which the clinical diagnosis of glioma could not be confirmed (other histology or possible non-tumour sample) and five samples with missing minimal clinical annotation were excluded from all analyses. For the MSKCC-IMPACT and FMI datasets, patients also signed a consent form, and samples were classified using the same procedure. *MGMT* promoter methylation status was determined as part of routine clinical care using chemical (bisulfite) modification of unmethylated, but not methylated, cytosines to uracil and subsequent PCR using primers specific for either methylated or the modified unmethylated DNA in the CpG island of the *MGMT* gene (GenBank accession number AL355531 nt46931-47011).

Targeted panel next-generation sequencing (DFCI-Profile) was performed using the previously validated OncoPanel assay at the Center for Cancer Genome Discovery (Dana-Farber Cancer Institute) for 277 (POPv1), 302 (POPv2), or 447 (POPv3) cancer-associated genes<sup>16,36</sup>.

In brief, between 50 and 200 ng tumour DNA was prepared as previously described<sup>16,37</sup>, hybridized to custom RNA bait sets (Agilent SureSelect TM, San Diego, CA) and sequenced using Illumina HiSeq 2500 with 2 × 100 paired-end reads. Sequence reads were aligned to reference sequence b37 edition from the Human Genome Reference Consortium using bwa, and further processed using Picard (version 1.90, <http://broadinstitute.github.io/picard/>) to remove duplicates and Genome Analysis Toolkit (GATK, version 1.6-5-g557da77) to perform localized realignment around indel sites<sup>38</sup>. Single-nucleotide variants were called using MuTect v1.1.4<sup>39</sup>, insertions and deletions were called using GATK Indelocator, and variants were annotated using Oncotator<sup>40</sup>. Copy number variants and structural variants were called using the internally developed algorithms RobustCNV<sup>41</sup> and BreaKmer<sup>42</sup> followed by manual review. To filter out potential germline variants, the standard pipeline removes SNPs present at >0.1% in Exome Variant Server, NHLBI GO Exome Sequencing Project (ESP), Seattle, WA (<http://evs.gs.washington.edu/EVS/>, accessed May 30, 2013), present in dbSNP, or present in an in-house panel of normal tissue, but rescues those also present in the COSMIC database<sup>43</sup>. For this study, variants were further filtered by removing variants present at >0.1% in the gnomAD v.2.1.1 database or annotated as benign or likely benign in the ClinVar database<sup>44,45</sup>. Arm-level copy number changes were generated using an in-house algorithm specific for panel copy number segment files followed by manual expert review. We set a copy number segment mean log<sub>2</sub> ratio threshold at which we could accurately call arm amplification and deletion based on the average observed noise in copy number segments. Chromosome arms were classified as amplified or deleted if more than 70% of the arm was altered. A sample was considered co-deleted if more than 70% of both 1p and 19q were deleted.

Sequencing data from MSKCC-IMPACT were generated at the Memorial Sloan Kettering Cancer Center using a custom targeted panel capture to examine the exons of 341 (IMPACT341) or 398 (IMPACT410) cancer-associated genes as previously described<sup>17</sup>. The FMI dataset comprised specimens sequenced as a part of clinical care using a targeted next-generation sequencing assay as previously described (FoundationOne or FoundationOne CDx, Cambridge, MA)<sup>15,33</sup>. Germline variants without clinical significance were further filtered by applying an algorithm to determine somatic or germline status<sup>46</sup>. Results were analysed for genomic alterations, TMB, MSI and mutational signatures. TMB was assessed by counting all mutations and then excluding germline and known driver mutations<sup>33,43,47</sup>. The remaining count was divided by the total covered exonic regions<sup>15,33</sup>. MSI status was determined as previously described<sup>48</sup>. A log<sub>2</sub>-ratio profile for each sample was obtained by normalizing the sequence coverage at all exons and ~3,500 genome-wide SNPs against a process-matched normal control. This profile was corrected for GC-bias, segmented and interpreted using allele frequencies of sequenced SNPs to estimate tumour purity and copy number at each segment. Loss of heterozygosity (LOH) was called if local copy number was 1, or if local copy number was 2 with an estimated tumour minor allele frequency of 0%. To assess 1p/19q co-deletion, we calculated the percentage of each chromosome arm that was monoallelic (under LOH)<sup>46</sup>. A sample was considered 1p/19q co-deleted if both 1p and 19q were >50% monoallelic.

For the DFCI-Profile and FMI datasets, the appropriate cutoffs for hypermutation (17.0 and 8.7 mut/Mb, respectively) were determined by examining the distribution of TMB in all samples and further confirmed using segmented linear regression analysis (Extended Data Fig. 2). For the MSKCC-IMPACT datasets, a threshold previously validated in this dataset was used<sup>17</sup>. In all analyses, the homopolymer indel burden was calculated by computing the number of single base insertions or deletions in homopolymer regions of at least 4 bases in length and dividing the count by the total exonic coverage as previously established<sup>49</sup>. Somatic variants were annotated as previously described<sup>15-17,36,37</sup>. In addition, for the DFCI-Profile and MSKCC-IMPACT datasets, variants in a selected list of glioma- and DNA-repair associated genes (*IDH1*, *IDH2*,

*TERT, ATRX, CIC, H3F3A, HIST1H3B, EGFR, PDGFRA, FGFR1, FGFR2, FGFR3, MET, KRAS, NRAS, HRAS, BRAF, NF1, PTPN11, PTEN, PIK3CA, PIK3C2B, PIK3R1, CDKN2A, CDKN2B, CDKN2C, CDK4, CDK6, CCND2, RB1, TP53, MDM2, MDM4, TP53BP1, PPM1D, CHEK1, CHEK2, RADS1, BRCA1, BRCA2, ATM, ATR, MLH1, MLH3, PMS1, PMS2, MSH2, MSH6, EPCAM, SETD2, POLE, POLD1, MUTYH, WRN*) were manually reviewed for oncogenicity using several clinical databases for variant annotation (OncoKB, ClinVar, COSMIC, ExAC, and ARUP).

### Mutational signature analyses

All variants detected by the sequencing pipeline covered by at least 30× read depth were stringently filtered for germline origin using the gnomAD (population allele frequency greater than 0.1%), and ClinVar (benign or likely benign annotation) databases<sup>44,45</sup>, as well as manual review of VAF distributions and variants with VAFs consistent with possible germline origin (45–55% or over 95%). The mutational spectrum of variants filtered during these steps was similar to a previously published germline mutation spectrum<sup>50</sup>. Signature analysis was performed for hypermutated samples in a two-step approach starting with the SomaticSignatures package in R for de novo signature extraction within each group<sup>51</sup>. To account for the inherent heuristic quality of the NMF approach, the NMF clustering step was repeated 100 times and chosen result was selected based on identifying signatures with the strongest Pearson's correlation coefficients when compared to the 30 well-established COSMIC signatures v2 ([https://cancer.sanger.ac.uk/cosmic/signatures\\_v2](https://cancer.sanger.ac.uk/cosmic/signatures_v2))<sup>14</sup> (Extended Data Fig. 5a–c). We then used the DeconstructSigs package in R to estimate the contribution of identified signatures using a regression model<sup>52</sup>. To account for the potential overfitting of a regression approach—owing to either lack of important signatures in the model, or inclusion of uninvolved signatures—we used only the signatures identified by the decomposition approach in step one, supplemented by any strong signature predictions identified through a first pass run of DeconstructSigs with the 30 COSMIC signatures to check for samples that may show strong correlation to an outlier signature. For the FMI dataset, mutational signatures were called as previously described<sup>17</sup>. All point mutations were included in the analysis except known oncogenic driver mutations and predicted germline mutations. A sample was deemed to have a dominant signature if a mutational signature had a score of 0.4 or greater.

To assess the ability of this method to detect hypermutation-associated signatures in targeted panel sequencing data, we compared the signature calls of exome-sequenced samples using all variants (previously published DeconstructSigs signature predictions<sup>52</sup>) versus using only variants that overlapped with the panel-targeted regions. Somatic variant calls for bladder cancer, colon adenocarcinoma, rectal adenocarcinoma, skin cutaneous melanoma, and lung adenocarcinoma (study abbreviations BLCA, COAD, READ, SKCM, LUAD) from the TCGA MC3 dataset were used<sup>53</sup> to assess the detection of COSMIC mutational signatures associated with APOBEC (signatures 2 and 13), mismatch repair (signature 6), ultraviolet light (signature 7), POLE (signature 10), and tobacco (signature 4). Variant calls for 17 hypermutated and 12 non-hypermutated glioma exome-sequenced samples were used for assessing temozolomide (signature 11) detection<sup>4</sup>. There were two COAD samples with known POLE exonuclease domain oncogenic mutations and a POLE signature predicted by DeconstructSigs; these were used for assessing POLE signature detection. For a given threshold number of variants ( $X^t$ ), we considered how many samples had at least  $X^t$  variants, and what percentage of these samples could correctly predict the exome-based signature using panel-restricted variants (with a predicted signature fraction greater than 0.1–0.2). This analysis showed that panel-based signature calls for the APOBEC, mismatch repair, tobacco, and ultraviolet light signatures reached 90% sensitivity with at least 20 somatic variants. Owing to the low number of samples with POLE-associated and temozolomide-associated hypermutation, we did not assess the sensitivity of signature detection at each variant count

threshold; we instead downsampled the number of variants in positive control samples to find the minimum number of variants necessary to reproducibly predict the known signature, which was also determined to be 20 somatic variants (Extended Data Fig. 4).

### Enrichment analysis

Mutation enrichment was statistically determined through a permutation test to control for confounders including variable mutability of different genes as well as sample mutation rates, which is of particular importance when assessing enrichment in hypermutated samples. First, we generated a list of every mutation in each of our samples. We calculated the difference in the mutation counts ( $\Delta$ ) between the group of interest and the reference group. We then randomly permuted the mutations 100,000 times, preserving sample and gene mutation counts, and computed the  $\Delta$  for each gene in each permutation. The  $P$  value for a given gene was determined by the fraction of permutations  $1-n$  (in our case,  $n = 100,000$ ) for which  $\Delta_n \geq \Delta$ . Storey  $q$  values were generated using the *qvalue* package in R to adjust for multiple comparisons. The analysis was first performed in the merged DFCI-Profile and MSKCC-IMPACT dataset, and further revalidated in the FMI dataset in an independent analysis.

### Single-cell whole-genome sequencing

Frozen glioma samples were mechanically dissociated into pools of single nuclei as previously described<sup>54</sup>, following which single nuclei were isolated by flow cytometry, using a DAPI-based stain. Nuclei were subjected to whole-genome multiple displacement (MDA) amplification (Qiagen, REPLI-g) followed by next-generation sequencing library construction for Illumina Sequencing (Qiagen QIAseq FX DNA library kit). Libraries were sequenced on the Illumina HiSeq platform in paired end mode. Single cells were sequenced to 0.1–1× coverage. Bulk pooled nuclei were sequenced to 60× coverage while matched germline DNA (extracted from blood) was sequenced to 30× coverage.

Reads were aligned to hg38 using *bwa mem*, and variants were jointly called across bulk normal tissue, primary tumour single cells, and recurrent tumour single cells using the GATK best practices pipeline<sup>38</sup> without variant quality score recalibration. Somatic mutations in single cells were called if they were monoallelic, had a homozygous reference genotype call but no alternate-allele support in bulk normal tissue, and had at least three supporting reads in a single cell. Germline heterozygous mutations (gHets) were called if they were monoallelic, were found in dbSNP (version 138, <http://www.ncbi.nlm.nih.gov/snp>), and had at least one supporting read and a heterozygous genotype call in bulk normal tissue. To assess sensitivity in each single cell, we computed the fraction of gHets detected with at least three supporting reads, analogous to our procedure for calling somatic mutations. To estimate the total number of somatic mutations present in each cell, we divided the total number of somatic mutations detected by sensitivity. To obtain 95% confidence intervals on the total mutational burden, we modelled the measurement of sensitivity using a beta distribution with Jeffrey's prior, in which the beta parameters ( $\alpha$ ,  $\beta$ ) are equal to the number of detected gHets + 0.5 and the number of undetected gHets + 0.5, respectively. We identified recurrent tumour single cells as hypermutated if their mutational burden was at least 1.5 times the highest mutational burden detected among primary tumour cells.

The method to detect microsatellite mutations was based on read-based phasing<sup>55,56</sup> and was previously validated using scWGS data from neurons (I.C.-C. et al., manuscript in preparation). First, the human genome was scanned to define a reference set of microsatellite repeats that can be captured using short reads (that is, between 6 and 60 bp) as previously described<sup>57</sup>. Heterozygous SNPs were then detected in the bulk normal sample using the variant caller GATK<sup>38</sup>. Next, the reads in a given cell mapping to each heterozygous SNP allele detected in the bulk sample and their mates were extracted. If any of the microsatellites in the reference set were covered by these reads, the distribution

## Article

of the allelic repeat lengths supported by the data was obtained by collecting the lengths of all intra-read microsatellite repeats mapped to the microsatellite locus under consideration. To discount truncated microsatellite repeats, we required 10-bp flanking sequences (both 5' and 3') of the intra-read microsatellite repeats to be identical to the reference genome. The same procedure was applied to the bulk sample. Finally, the distributions of microsatellite lengths from the single cell and the bulk sample were compared using the Kolmogorov–Smirnov test. The rates of microsatellite instability for each cell were computed as the number of sites mutated divided by the total number of microsatellites for which a call could be made. We applied FDR correction using 0.05 as a threshold for statistical significance, with a minimum of 8 single cell and 10 normal reads required to make a call. All the code is publicly available (<https://github.com/parklab/MSIprofiler>).

### Immunohistochemistry

For the revalidation of MMR defects in an independent set, all prospectively collected surgical samples representing consecutive relapses of diffuse glioma following treatment with alkylating agents in adult patients (surgery between 2009 and 2015) were included. An expert neuropathologist reviewed histological samples from the IHC Pitié Salpêtrière cohort (Supplementary Table 2) in order to assess the WHO 2016 integrated diagnosis and to select the tumour areas for immunohistochemistry and for DNA extraction when molecular testing from formalin-fixed paraffin-embedded (FFPE) tissue material was required. Diffuse gliomas harbouring unambiguous positive IDH1(R132H) immunostaining were classified as *IDH1/2*-mutant. *IDH1/2* status was tested by targeted sequencing in all diffuse gliomas harbouring negative or ambiguous IDH1(R132H) immunostaining. *IDH1/2*-mutant diffuse gliomas with loss of ATRX expression in tumour cells were classified as non 1p/19q co-deleted. 1p/19q co-deletion was tested in all *IDH1/2*-mutant diffuse gliomas with maintained ATRX expression. MGMT status was assessed in *IDH1/2* wild-type gliomas. FFPE sections (3 µm thick) were deparaffinized and immunolabelled with a Ventana Benchmark XT stainer (Roche, Basel, Switzerland). The secondary antibodies were coupled to peroxidase with diaminobenzidine as brown chromogen. For immunohistochemistry performed at Pitié-Salpêtrière (PSL) Hospital, the following antibodies were used: mouse monoclonal anti-ATRX (Bio SB, clone BSB-108, BSB3296, 1:100), mouse monoclonal anti-IDH1(R132H) (Dianova, clone H09, DIA-H09, 1:100), rabbit monoclonal anti-CD3 (Roche, clone 2GV6, 790-4341, prediluted), rabbit polyclonal anti-IBA1 (Wako, W1W019-19741, 1:500), mouse monoclonal anti-MLH1 (Roche, clone M1, 790-4535, prediluted), mouse monoclonal anti-MSH2 (Roche, clone G219-1129, 760-4265, prediluted), mouse monoclonal anti-MSH6 (Roche, clone 44, 760-4455, prediluted), rabbit monoclonal anti-PMS2 (Roche, clone EPR3947, 760-4531, prediluted). For immunohistochemistry performed at BWH, the following antibodies were used: mouse monoclonal anti-MLH1 (Leica, clone ES05, MLH1-L-CE, 1:75), mouse monoclonal anti-MSH2 (Merck Millipore, clone Ab-2-FE11, NA27, 1:200), mouse monoclonal anti-MSH6 (Leica, clone PU29, MSH6-L-CE, 1:50), mouse monoclonal anti-PMS2 (Cell Marque, MRQ-28, 288M-14-ASR, 1:100). An expert neuropathologist blinded to the molecular status of MMR deficiency analysed the immunostaining. If loss of expression of one or several MMR proteins was observed in tumour cells, this result was confirmed in an independent laboratory by a second expert pathologist with separate stainer and reagents: FFPE sections were immunolabelled with a BOND stainer (Leica, Wetzlar, Germany). Primary antibodies were as follows: mouse monoclonal anti-MLH1 (clone G168-728, BD Pharmingen), mouse monoclonal anti-MSH2 (clone 25D12, Diagnostic BioSystems), mouse monoclonal anti-MSH6 (clone 44, Diagnostic BioSystems), mouse monoclonal anti-PMS2 (clone A16-4, BD Pharmingen). The loss of expression of MMR proteins was defined as the total absence of nuclear labelling in tumour cells associated with a maintained expression in normal cells (as a positive internal control in the same tissue area). The density of

the immune infiltrate was studied after immunolabelling of T lymphocytes by CD3 and of macrophage/microglial cells by IBA1. The number of immunopositive cells was quantified by visual counting in the three areas (one square millimetre) of tumour tissue containing the highest density of immunopositive cells and a mean density was calculated.

### Patient-derived cell lines

All PDCLs with a name starting with BT were established from tumours resected at Brigham and Women's Hospital and Boston Children's Hospital (Boston, MA) and were maintained in neurosphere growth conditions using the NeuroCult NS-A Proliferation Kit (StemCell Technologies) supplemented with 0.0002% heparin (StemCell Technologies), EGF (20 ng/ml), and FGF (10 ng/ml; Miltenyi) in a humidified atmosphere of 5% CO<sub>2</sub> at 37 °C. The N16-1162 PDCL was established by the GlioTex team (Glioblastoma and Experimental Therapeutics) at the Institut du Cerveau et de la Moëlle épinière (ICM) laboratory and maintained as described above. SU-DIPG-XIII (DIPG13) cells were provided by Dr. Michelle Monje at Stanford University and were maintained in neurosphere growth conditions in a humidified atmosphere of 5% CO<sub>2</sub> at 37 °C in tumour stem medium (TSM) consisting of Dulbecco's modified Eagle's medium: nutrient mixture F12 (DMEM/F12), neurobasal-A medium, HEPES buffer solution 1 M, sodium pyruvate solution 100 nM, non-essential amino acids solution 10 mM, Glutamax-1 supplement and antibiotic-antimycotic solution (Thermo Fisher). The medium was supplemented with B-27 supplement minus vitamin A, (Thermo Fisher), 20 ng/ml human-EGF (Miltenyi), 20 ng/ml human-FGF-basic (Miltenyi), 20 ng/ml human-PDGF-AA, 20 ng/ml human-PDGF-BB (Shenandoah Biotech) and 2 µg/ml heparin solution (0.2%, Stem Cell Technologies). The identity of all cell lines established was confirmed by short tandem repeat assay or sequencing. All cell lines were tested for the absence of mycoplasma. Cell lines, xenografts, and model data available from the DFCI Center for Patient Derived Models.

### Viability assays

For short-term viability assays, cells were plated in 96-well plates and treated the following day with temozolomide (Selleckchem) or CCNU (Selleckchem) for 7–9 days incubation. Fresh medium was added after four days of incubation. Cell viability was assessed using the luminescent CellTiter-Glo reagent (Promega) according to the manufacturer's protocol. Luminescence was measured using the Modulus Microplate Reader (Promega). The surviving fraction (SF) for each [X] concentration was calculated as SF = mean viability in treated sample at concentration [X]/mean viability of untreated samples (vehicle). Dose–response curves and IC<sub>50</sub> were generated using Prism 8 (GraphPad Software, San Diego, USA) after log transformation of the concentrations. Curves were extrapolated using nonlinear regression with four-parameter logistic regression fitting on triplicates from survival fractions of three independent replicates, following the model:  $y = \text{Bottom} + (\text{Top} - \text{Bottom}) / (1 + 10^{([\log IC_{50} - x] \times \text{HillSlope})})$ .

### Generation of isogenic MMR-deficient cell lines

Oligos of the form 5'-CACCG[N20] (where [N20] is the 20-nucleotide target sequence; sgGFP, GAGCTGGACGGCAGCTAAA; sgMSH2, ATTCTGTTCTTATCCATGAG; sgMSH6, TTATTGGAGTCAGTGAAGT; sgMLH1, ACTACCAATGCCTCAACCG; sgPMS2, TCACTGCAGCAGCGATATG) and 5'-AAAC[rc20]C (where [rc20] is the reverse complement of [N20]) were purchased from Integrated DNA Technologies (IDT). For DIPG13 cells, oligos containing the sgRNA target sequence were annealed with their respective reverse complement and cloned into the lentiCRISPR all-in-one sgRNA/Cas9-delivery lentiviral expression vector (pXPR\_BRD001; now available as pXPR\_BRD023 lentiCRISPRv2) from the Broad Institute Genetics Perturbation Platform (GPP). For BT145 cells, oligos containing the sgRNA target sequence were annealed with their respective reverse complement and cloned into the pXPR\_BRD001

CRISPRko all-in-one sgRNA/Cas9-delivery lentiviral expression vector (available from the Broad Institute Genetics Perturbation Platform, GPP). Successful cloning of each sgRNA target sequence was confirmed via Sanger Sequencing. To generate lentivirus from these vectors, HEK293T cells were transfected with 10 µg of each expression plasmid with packaging plasmids encoding PSPAX2 and VSVG using lipofectamine. Lentivirus-containing supernatant was collected 48 and 72 h after transfection. DIPG13 and BT145 cells were seeded in a 12-well plate at  $1-3 \times 10^6$  cells/well in 3 ml medium and spin-infected (2,000 rpm for 2 h at 30 °C with no polybrene) with pLX311-Cas9 (DIPG13) or pXPR\_BRD051 (BT145) lentiviral vectors and selected with blasticidin (10 µg/ml, DIPG13) or hygromycin (300 µg/ml, BT145) to generate Cas9-expressing or knockout cells. DIPG13-Cas9 cells underwent a subsequent lentiviral spin-infection with the lentiCRISPR sgGFP, sgMSH2, or sgMSH6 vectors described above. Puromycin selection (0.4 µg/ml for DIPG13 cells) commenced 48 h post-infection.

#### Chronic treatment and sequencing of isogenic MMR-deficient cell lines

DIPG13-sgGFP, -sgMSH2, and -sgMSH6 cells were seeded at  $8 \times 10^5$  cells/well in 4 ml medium in a 6-well ULA plate. Each line was grown for 3 months under 3 conditions: no treatment, temozolomide (100 µM, Selleckchem), or DMSO vehicle. Cells were grown under these conditions in the absence of both blasticidin and puromycin. Cells were re-dosed with temozolomide or DMSO every 3–5 days, splitting over-confluent cells 1:2 or 1:4 as needed. After 3 months, genomic DNA was extracted using the QIAmp DNA Mini Kit. DNA was subjected to whole-exome Illumina sequencing. Reads were aligned to the Human Genome Reference Consortium build 38 (GRCh38). WES data were analysed using the Getz Lab CGA whole-exome sequencing characterization pipeline ([https://docs.google.com/document/d/1VO2kX\\_fgfUd0x3mBS9NjLUWGZu794WbTepBel3cBg08/edit#heading=h.yby87l2ztbcj](https://docs.google.com/document/d/1VO2kX_fgfUd0x3mBS9NjLUWGZu794WbTepBel3cBg08/edit#heading=h.yby87l2ztbcj)) developed at the Broad Institute which uses the following tools for quality control, calling, filtering and annotation of somatic mutations and copy number variation: PicardTools (<http://broadinstitute.github.io/picard/>) ContEst<sup>58</sup>, MuTect1<sup>39</sup>, Strelka<sup>39</sup>, Orientation Bias Filter<sup>60</sup>, DeTiN<sup>61</sup>, AllelicCapSeg<sup>62</sup>, MAFPoNFilter<sup>63</sup>, RealignmentFilter, ABSOLUTE<sup>64</sup>, GATK<sup>38</sup>, Variant Effect Predictor<sup>65</sup>, and Oncotator<sup>60</sup>.

#### Subcutaneous xenografts and drug treatment

BT145 cells ( $2 \times 10^6$ ) were resuspended in equal parts Hank's buffered salt solution (Life Technologies) and Matrigel (BD Biosciences) and then injected into both flanks of eight-week-old NU/NU male mice (Charles River). Tumour-bearing mice ( $n = 8$ ) were randomly assigned to the treatment or vehicle arm when tumours measured a volume of 100 mm<sup>3</sup>. Animals received 12 mg/kg/day temozolomide or vehicle (Ora-Plus oral suspension solution, Perrigo, Balcatta, Australia) by oral gavage for 5 consecutive days per 28-day cycle. An additional 4 weeks resting period without treatment was observed before the second cycle. Tumour volumes were calculated using the formula:  $0.5 \times \text{length} \times \text{width}^2$ . Body weights were monitored twice weekly. The investigators were not blinded to allocation during experiments and outcome assessment. Mice were euthanized when they showed signs of tumour-related illness or before reaching the maximum tumour burden. Tumours were subsequently removed, and a subset were submitted to OncoPanel sequencing for analyses of exonic mutations (POPv3, 447 genes) and mutational signature as defined above. To separate human and mouse sequenced reads in the DNA sequencing data generated for the PDX models, the 'raw' data were mapped to both the hg19 human and mm10 mouse reference genomes using BWA-MEM-0.7.17. The output of the alignment was name sorted by Samtools-1.7. We then used the software package Disambiguate (ngs\_disambiguate-1.0) to assign each read to the human or mouse genome and to produce final alignment files in BAM format. Final hg19 BAM files were coordinate sorted by Samtools-1.7. Duplicate reads were marked and removed from the

BAM files using Picard-2.0.1. GATK4.1.0.0 base recalibration was performed using BaseRecalibration and ApplyingRecalibration followed by CollectFIR2Counts and LearnReadOrientationModel to create a model for read orientation bias. Variant calling was performed using GATK-4.1.0.0/Mutect2 pipeline with the default parameters and filters except for the following modifications: (i) 'af-of-alleles-not-in-resource' was set to 0; (ii) 'MateOnSameContigOrNoMappedMateReadFilter' was disabled; (iii) the output of Step8 was used for fitting the read orientation model; and (iv) a germline resource from the gnomAD database was included ([https://console.cloud.google.com/storage/browser/\\_details/gatk-best-practices/somatic-b37/af-only-gnomad.raw.sites.vcf](https://console.cloud.google.com/storage/browser/_details/gatk-best-practices/somatic-b37/af-only-gnomad.raw.sites.vcf)). The capture targets intervals used for Mutect2 were POPv3. The generated variant calls were further filtered using the FilterMutectCalls module of GATK4.1.0.0 and the final output in VCF format was annotated with Ensemble Variant Effect Predictor (ensembl-vep-96.0) using vcf-2maf-1.6.16. The calls were additionally annotated with the OncoKB dataset using oncoKB-annotator and sorted as MAF files.

All in vivo studies were performed in accordance with Dana-Farber Cancer Institute animal facility regulations and policies under protocol number 09-016.

#### Immunoblotting

Proteins were extracted in lysis RIPA buffer (50 mM Tris, 150 mM NaCl, 5 mM EDTA, 0.5% sodium deoxycholic acid, 0.5% NP-40, 0.1% SDS) supplemented with protease inhibitor cocktail (Roche Molecular). Proteins were quantified using the PierceBCA Protein Assay Kit, according to the manufacturer's protocol. Samples were then prepared with 1× NuPAGE (Invitrogen) LDS sample buffer, and NuPAGE (Invitrogen) sample reducing agent followed by heating to 95 °C for 5 min. The samples were then loaded onto NuPAGE 4–12% Bis-Tris Gel (Invitrogen) with NuPAGE MOPS SDS (Invitrogen) buffer and run through electrophoresis. The transfer onto membrane was then done at 40 V overnight at 4 °C in NuPAGE transfer buffer (Invitrogen) with 10% methanol. Membranes were blocked with 5% skim milk in TBST for 1 h, then incubated with the following primary antibodies added to 5% BSA and incubated overnight at 4 °C on a shaker: mouse monoclonal anti-MGMT (Millipore, MT3.1, MAB16200, 1:500), mouse monoclonal anti-MSH2 (Calbiochem, FE11, NA27, 1:1,000), mouse monoclonal anti-MSH6 (Biosciences, 44, 610918, 1:500), mouse monoclonal anti-MLH1 (Cell Signaling, 4C9C7, 3515, 1:500), mouse monoclonal anti-PMS2 (BD Biosciences, A16-4, 556415, 1:1,000), mouse monoclonal anti-beta-actin (Sigma, AC-74, A2228, 1:10,000). After several cycles of washing and incubation with secondary goat anti-mouse antibody (Invitrogen 31430, 1:10,000), membranes were imaged by chemiluminescence using the Biorad ChemidocTM MP imaging system.

#### Microsatellite instability analysis

PCR amplification of the five mononucleotide markers (BAT25, BAT26, NR21, NR24, MONO27) was performed with the MSI Analysis System kit (Version 1.2, Promega). PCR products were analysed by an electrophoretic separation on the polymer POP7 50cm in an Applied Biosystems 3130XL sequencer and using Genemapper Software 5.

#### Outcome of patients treated with PD-1 blockade

For comparison of PFS and OS in patients treated with PD-1 pathway blockade according to TMB and MMR statuses, we retrospectively identified patients with glioma who had been treated with PD-1 blockade (alone or in combination with bevacizumab) for recurrent disease at our institutions. Patients for whom sequencing was not performed at the time of recurrence were excluded. Magnetic resonance imaging (MRI) tumour assessments were reviewed using the Response Assessment in Neuro-Oncology (RANO) criteria by three independent reviewers (M.J.L.-F., S.A., and R.Y.H.) who were blinded to the groups. PFS and OS duration were calculated from cycle 1 day 1 of PD-1 blockade therapy.

# Article

## Statistical analyses

Data were summarized as frequencies and proportions for categorical variables and as median and range for continuous variables. Continuous variables were compared using Mann–Whitney or Kruskal–Wallis tests; categorical variables were compared using Fisher’s exact or Chi-squared tests. Survival and PFS were estimated using the Kaplan–Meier method, and differences in survival or PFS between groups were evaluated by the log-rank test. Survival for subjects who were alive or lost to follow-up at the time of last contact on or before data cut-off was censored at the date of the last contact. Patient matching in a *k*-to-*k* fashion was conducted using coarsened exact matching according to diagnosis, primary versus recurrent status, and prior treatments. For evaluation of response to PD-1 blockade, patients with glioma from the DFCI-Profile cohort who were treated with anti-PD(L)-1 antibodies or other treatments (total *n* = 210) as part of their management were included in the analysis. For multivariable analysis, Cox proportional hazard regression was used to investigate the variables that affect survival. *P* values were considered statistically significant when  $<0.05$ . Statistical analyses were performed using STATA (v14.2, StataCorp LLC, College Station, USA), Prism 8 (GraphPad Software, San Diego, USA), and MedCalc Statistical Software, version 19.0.3 (MedCalc Software bvba, Ostend, Belgium). For enrichment analyses, mutated genes were considered significant when  $Q < 0.01$ . Where applicable, the means of population averages from multiple independent experiments ( $\pm$  s.d. or s.e.m.) are indicated. No statistical methods were used to pre-determine sample size.

## Reporting summary

Further information on research design is available in the Nature Research Reporting Summary linked to this paper.

## Data availability

Clinical and sequencing data from 1,495 samples from the DFCI-Profile and 545 samples from the MSKCC-IMPACT datasets are publicly available (GENIE v.6.1: <https://genie.cbioportal.org> or <https://www.synapse.org/>). All data for samples from the GENIE v.6.1 and TCGA pan-cancer datasets are publicly available. Data for samples from the FMI dataset are not publicly available, but de-identified, aggregated data can be accessed on request. dbGaP Study Accession: phs001967.v1.p1. All other data are available on request.

## Code Availability

The code for the detection of microsatellite mutations in single-cell DNA sequencing is publicly available (<https://github.com/parklab/MSIprofiler>).

32. Jonsson, P. et al. Genomic correlates of disease progression and treatment response in prospectively characterized gliomas. *Clin. Cancer Res.* **25**, 5537–5547 (2019).
33. Chalmers, Z. R. et al. Analysis of 100,000 human cancer genomes reveals the landscape of tumor mutational burden. *Genome Med.* **9**, 34 (2017).
34. Consortium, A. P. G.; AACR Project GENIE Consortium. AACR Project GENIE: powering precision medicine through an international consortium. *Cancer Discov.* **7**, 818–831 (2017).
35. Cancer Genome Atlas Research Network et al. The Cancer Genome Atlas Pan-Cancer analysis project. *Nat. Genet.* **45**, 1113–1120 (2013).
36. Garcia, E. P. et al. Validation of OncoPanel: a targeted next-generation sequencing assay for the detection of somatic variants in cancer. *Arch. Pathol. Lab. Med.* **141**, 751–758 (2017).
37. Ramkissoon, S. H. et al. Clinical targeted exome-based sequencing in combination with genome-wide copy number profiling: precision medicine analysis of 203 pediatric brain tumors. *Neuro-oncol.* **19**, 986–996 (2017).
38. McKenna, A. et al. The Genome Analysis Toolkit: a MapReduce framework for analyzing next-generation DNA sequencing data. *Genome Res.* **20**, 1297–1303 (2010).
39. Cibulskis, K. et al. Sensitive detection of somatic point mutations in impure and heterogeneous cancer samples. *Nat. Biotechnol.* **31**, 213–219 (2013).
40. Ramos, A. H. et al. Oncotator: cancer variant annotation tool. *Hum. Mutat.* **36**, E2423–E2429 (2015).
41. Bi, W. L. et al. Clinical identification of oncogenic drivers and copy-number alterations in pituitary tumors. *Endocrinology* **158**, 2284–2291 (2016).
42. Abo, R. P. et al. BreakMer: detection of structural variation in targeted massively parallel sequencing data using kmers. *Nucleic Acids Res.* **43**, e19 (2015).
43. Tate, J. G. et al. COSMIC: the catalogue of somatic mutations in cancer. *Nucleic Acids Res.* **47**, D941–D947 (2019).
44. Karczewski, K. J. et al. Variation across 141,456 human exomes and genomes reveals the spectrum of loss-of-function intolerance across human protein-coding genes. Preprint at <https://www.biorxiv.org/content/10.1101/531210v2> (2019).
45. Landrum, M. J. et al. ClinVar: improving access to variant interpretations and supporting evidence. *Nucleic Acids Res.* **46**, D1062–D1067 (2018).
46. Sun, J. X. et al. A computational approach to distinguish somatic vs. germline origin of genomic alterations from deep sequencing of cancer specimens without a matched normal. *PLOS Comput. Biol.* **14**, e1005965 (2018).
47. Garofalo, A. et al. The impact of tumor profiling approaches and genomic data strategies for cancer precision medicine. *Genome Med.* **8**, 79 (2016).
48. Trabucco, S. E. et al. A novel next-generation sequencing approach to detecting microsatellite instability and pan-tumor characterization of 1000 microsatellite instability-high cases in 67,000 patient samples. *J. Mol. Diagn.* **21**, 1053–1066 (2019).
49. Papke, D. J. Jr et al. Validation of a targeted next-generation sequencing approach to detect mismatch repair deficiency in colorectal adenocarcinoma. *Mod. Pathol.* **31**, 1882–1890 (2018).
50. Rahbari, R. et al. Timing, rates and spectra of human germline mutation. *Nat. Genet.* **48**, 126–133 (2016).
51. Gehring, J. S., Fischer, B., Lawrence, M. & Huber, W. SomaticSignatures: inferring mutational signatures from single-nucleotide variants. *Bioinformatics* **31**, 3673–3675 (2015).
52. Rosenthal, R., McGranahan, N., Herrero, J., Taylor, B. S. & Swanton, C. DeconstructSigs: delineating mutational processes in single tumors distinguishes DNA repair deficiencies and patterns of carcinoma evolution. *Genome Biol.* **17**, 31 (2016).
53. Ellrott, K. et al. Scalable open science approach for mutation calling of tumor exomes using multiple genomic pipelines. *Cell Syst.* **6**, 271–281.e277 (2018).
54. Francis, J. M. et al. EGFR variant heterogeneity in glioblastoma resolved through single-nucleus sequencing. *Cancer Discov.* **4**, 956–971 (2014).
55. Lodato, M. A. et al. Aging and neurodegeneration are associated with increased mutations in single human neurons. *Science* **359**, 555–559 (2018).
56. Bohrsen, C. L. et al. Linked-read analysis identifies mutations in single-cell DNA-sequencing data. *Nat. Genet.* **51**, 749–754 (2019).
57. Cortes-Ciriano, I., Lee, S., Park, W. Y., Kim, T. M. & Park, P. J. A molecular portrait of microsatellite instability across multiple cancers. *Nat. Commun.* **8**, 15180 (2017).
58. Cibulskis, K. et al. ContEst: estimating cross-contamination of human samples in next-generation sequencing data. *Bioinformatics* **27**, 2601–2602 (2011).
59. Saunders, C. T. et al. Strelka: accurate somatic small-variant calling from sequenced tumor-normal sample pairs. *Bioinformatics* **28**, 1811–1817 (2012).
60. Costello, M. et al. Discovery and characterization of artifactual mutations in deep coverage targeted capture sequencing data due to oxidative DNA damage during sample preparation. *Nucleic Acids Res.* **41**, e67 (2013).
61. Taylor-Weiner, A. et al. DeTIN: overcoming tumor-in-normal contamination. *Nat. Methods* **15**, 531–534 (2018).
62. Landau, D. A. et al. Evolution and impact of subclonal mutations in chronic lymphocytic leukemia. *Cell* **152**, 714–726 (2013).
63. Lawrence, M. S. et al. Discovery and saturation analysis of cancer genes across 21 tumour types. *Nature* **505**, 495–501 (2014).
64. Carter, S. L. et al. Absolute quantification of somatic DNA alterations in human cancer. *Nat. Biotechnol.* **30**, 413–421 (2012).
65. McLaren, W. et al. The Ensembl variant effect predictor. *Genome Biol.* **17**, 122 (2016).

**Acknowledgements** We thank the patients and families who took part in the study, as well as the staff, research coordinators and investigators at each participating institution. M.T. is supported by Fondation pour la Recherche Médicale (FDM 41635), Fondation Monahan, The Arthur Sachs Foundation and The Philippe Foundation. C.L.B. was funded by a Bioinformatics and Integrative Genomics training grant from NHGRI (T32HG002295). S.S. is supported by the Ludwig Center at Harvard. M.S. is supported by Institut National du Cancer (INCa), the Ligue Nationale contre le Cancer (Equipe Labellisée), and Investissements d’avenir. R.B. is supported by NIH R01 CA188228, R01 CA215489, and R01 CA219943, The Dana-Farber/Novartis Drug Discovery Program, The Gray Matters Brain Cancer Foundation, Ian’s Friends Foundation, The Bridge Project of MIT and Dana-Farber/Harvard Cancer Center, The Pediatric Brain Tumor Foundation, the Fund for Innovation in Cancer Informatics, and The Sontag Foundation. P.B. is supported by NIH K99 CA201592, R00CA201592-03, the Dana-Farber Cancer Institute and Novartis Institute of Biomedical Research Drug Discovery and Translational Research Program, the Pediatric Brain Tumor Foundation and the St Baldrick’s Foundation. F. Bielle is supported by Fondation ARC pour la recherche sur le cancer (PIA 20151203562), INCa, a grant Emergence (Sorbonne Université) and ARTC (Association pour la recherche sur les tumeurs cérébrales). K.L.L. is supported by R01CA188288, P01 CA163205, P50 CA165962, Pediatric Brain Tumor Foundation, and the Ivy Foundation. This work was in part supported by the SIRIC CURAMUS, which is funded by INCa, the French Ministry of Solidarity and Health and Inserm (INCA-DGOS-Inserm\_12560). We acknowledge K. Bryan, S. Valentin, B. Bonneau, A. Matos and I. Detrait for preparation and processing of samples; W. Pisano and S. Block for help in data collection; E. F. Cohen for mouse xenograft sequencing analyses; D. X. Jin and J. Moore for assistance with FMI dataset creation and curation; the members of the BWH Center for Advanced Molecular Diagnostics; Y. Marie, J. Gueguan and the ICM Genotyping and Sequencing Core Facility (IGENSEQ) for sharing expertise related to analysis of copy array and sequencing data; C. Perry and the DFCI Oncology Data Retrieval System (OncDRS) for the aggregation, management, and delivery of the operational research data used in this project; the American Association for Cancer Research and its financial and material support in the development of the AACR Project GENIE registry, and members of the consortium for their commitment to data sharing; the cBioPortal for Cancer Genomics (<https://www.cbioportal.org>) and the Memorial Sloan Kettering Cancer Center for data sharing of the MSKCC-IMPACT

dataset. We greatly appreciate feedback and support from M. L. Meyerson regarding bioinformatics and genomics analysis, I. K. Mellingshoff and T. J. Kaley for scientific advice, V. Rendo for scientific review of the manuscript, and M. Monje for providing the DIPG13 parental cell line. The content is solely the responsibility of the authors.

**Author contributions** M.T., R.B., P.B., F. Bielle and K.L.L. designed the study. M.T., Y.Y.L., R.B., P.B., F. Bielle and K.L.L. wrote the initial draft, with input from all authors. Y.Y.L. validated mutational signature analyses using TCGA data. M.T., Y.Y.L., L.F.S., R.S., D. Pavliak and L.A.A. performed TMB and mutational signature analyses of the DFCI-Profile, MSKCC-IMPACT and FMI datasets, and integrated TMB, signature and clinical data. L.F.S. developed the code for permutation tests. M.T., Y.Y.L., L.F.S. and R.S. performed and analysed the permutation tests. M.T., A.N.B., K.P., C. Bellamy, N.C., J.B., K.Q., P.H., S.M., L.T., R.B., P.B. and K.L.L. performed *in vitro* experiments in native and engineered models and analysed experimental data. M.T., K.P., J.B. and K.L.L. performed *in vivo* experiments in native models and analysed experimental data. M.T., F. Beuvon, K.M., S. Alexandrescu, D.M.M., S.S., F. Bielle, and K.L.L. reviewed histological and immunohistochemistry data on human samples. M.T. and J.B.I. performed survival analyses. M.T., Y.Y.L., C.L.B., I.C.-C., P.J.P., R.B., P.B. and K.L.L. performed single-cell sequencing experiments and analysed data. C.L.B., I.C.-C. and P.J.P. developed computational tools for the analysis of single-cell data. M.T., Y.Y.L., L.F.S., C.L.B., I.C.-C., S.H.R., F.D., A.S., R.S., D. Pavliak, L.A.A., E.G., G.M.F., F.C., A.D., A. Cherniack, P.J.P., R.B., P.B. and K.L.L. reviewed and analysed the bulk sequencing genomic data. M.T., J.B.I., C. Birzu, J.E.G., M.J.L.-F., R.J., N.Y., C. Baldini, E.G., S. Ammiri, F. Beuvon, K.M., A.A., C.D., C.H., F.L.-D., D. Psimaras, E.Q.L., L.N., J.R.M.-F., A. Carpentier, P.C., L.C., B.M., J.S.B.-S., A. Chakravarti, W.L.B., E. A. Chiocca, K.P.F., S. Alexandrescu, S.C., D.H.-K., T.T.B., B.M.A., R.Y.H., A.H.L., F.C., J.-Y.D., K.H.-X., D.M.M., S.S., M.S., P.Y.W., D.A.R., A.M., A.I., R.B., P.B., F. Bielle, and K.L.L. abstracted and reviewed clinical and treatment response data. Y.Y.L., L.F.S., C.L.B., I.C.-C., R.S., L.A.A., G.M.F., A. Cherniack, and R.B. created bioinformatics tools and systems to support data analysis. R.B., P.B., F. Bielle, and K.L.L. acquired funding and supervised the study. All authors participated in data analysis and approved the final manuscript.

**Competing interests** M.T. reports consulting or advisory role for Agios Pharmaceutical, Integragen, and Taiho Oncology, outside the submitted work; travel, accommodations, expenses from Merck Sharp & Dome, outside the submitted work. Y.Y.L. reports equity from g. Root Biomedical. S.H.R., R.S., D. Pavliak, L.A.A., G.M.F. and B.M.A. report employment with Foundation Medicine and stock interests from Roche. K.M. reports advisory board honoraria from Bristol-Myers Squibb, outside the submitted work. F.L.-D. reports fees from Pharmtrace, outside the submitted work. E.Q.L. reports consulting or advisory role for Eli Lilly; royalties from UpToDate; honoraria from Prime Oncology. L.N. reports consulting or advisory role for Bristol-Myers Squibb, outside the submitted work. T.T.B. reports honoraria from Champions Oncology, UpToDate, Imedex, NXDC, Merck, GenomiCare Biotechnology; consulting or advisory role for Merck, GenomiCare Biotechnology, NXDC, Amgen; travel, accommodations, expenses from Merck, Roche, Genentech, GenomiCare Biotechnology. A.H.L. reports leadership from Travera (I); stock and other ownership interests from Travera (I); consulting or advisory role for Travera (I). K.H.-X. reports advisory board honoraria from Bristol-Myers Squibb, outside the submitted work. S.S. reports personal fees from Rarecyte, outside the submitted work. P.Y.W. reports honoraria from Merck; consulting or advisory role for AbbVie, Agios Pharmaceuticals, AstraZeneca, Blue Earth Diagnostics, Eli Lilly, Genentech, Roche,

Immunomic Therapeutics, Kadmon Corporation, KIYATEC, Puma Biotechnology, Vascular Biogenics, Taiho Pharmaceutical, Deciphera Pharmaceuticals, VBI Vaccines; speakers' bureau from Merck, prime Oncology; research funding from Agios Pharmaceuticals (Inst), AstraZeneca (Inst), BeiGene (Inst), Eli Lilly (Inst), Roche (Inst), Genentech (Inst), Karyopharm Therapeutics (Inst), Kazia Therapeutics (Inst), MediciNova (Inst), Novartis (Inst), Oncocentrics (Inst), Sanofi (Inst), Aventis (Inst), VBI Vaccines (Inst); travel, accommodations, expenses from Merck. D.A.R. reports honoraria from AbbVie, Cavion, Genentech, Roche, Merck, Midatech Pharma, Momenta Pharmaceuticals, Novartis, Novocure, Regeneron Pharmaceuticals, Stemline Therapeutics, Celldex, OXIGENE, Monteris Medical, Bristol-Myers Squibb, Juno Therapeutics, Inovio Pharmaceuticals, Oncorus, Agenus, EMD Serono, Merck, Merck KGaA, Taiho Pharmaceutical, Advantagene; consulting or advisory role for Cavion, Genentech, Roche, Merck, Momenta Pharmaceuticals, Novartis, Novocure, Regeneron Pharmaceuticals, Stemline Therapeutics, Bristol-Myers Squibb, Inovio Pharmaceuticals, Juno Therapeutics, Celldex, OXIGENE, Monteris Medical, Midatech Pharma, Oncorus, AbbVie, Agenus, EMD Serono, Merck, Merck KGaA, Taiho Pharmaceutical; research funding from Celldex (Inst), Incyte (Inst), Midatech Pharma (Inst), Tragara Pharmaceuticals (Inst), Inovio Pharmaceuticals (Inst), Agenus (Inst), EMD Serono (Inst), Acerta Pharma (Inst), Omnixox. A.I. reports grants and other from Carthera (September 2019); research grants from Transgene; grants from Sanofi, and Air Liquide; and travel funding from Leo Pharma, outside the submitted work. R.B. reports consulting or advisory role for Novartis, Merck (I), Gilead Sciences (I), ViiV Healthcare (I); research funding from Novartis; patents, royalties, other intellectual property—Prognostic Marker for Endometrial Carcinoma (US patent application 13/911456, filed June 6, 2013), SF3B1 Suppression as a Therapy for Tumors Harboring SF3B1 Copy Loss (international application No. WO/2017/177191, PCT/US2017/026693, filed July 4, 2017), Compositions and Methods for Screening Pediatric Gliomas and Methods of Treatment Thereof (international application No. WO/2017/132574, PCT/US2017/015448, filed 1/27/2017). P.B. reports research grants from the Novartis Institute of Biomedical Research; patents, royalties, other intellectual property—Compositions and Methods for Screening Pediatric Gliomas and Methods of Treatment Thereof (international application No. WO/2017/132574, PCT/US2017/015448, filed 1/27/2017). F. Bielle reports employment from Celgene (I); stocks from Crossject (I); research grants from Sanofi and AbbVie; travel, accommodations, expenses from Bristol-Myers Squibb for travel expenses, outside the submitted work. K.L.L. reports grants and personal fees from BMS, grants from Amgen, personal fees and other from Travera LLC, personal fees from InteraGen, personal fees from Rarecyte, grants from Tragara, grants from Lilly, grants from Deciphera, grants from X4, all outside the submitted work; and has patent US20160032359A1 pending. Inst. denotes institutional funding; I denotes a competing interest involving a first degree relative of the author. The other authors report no competing interests.

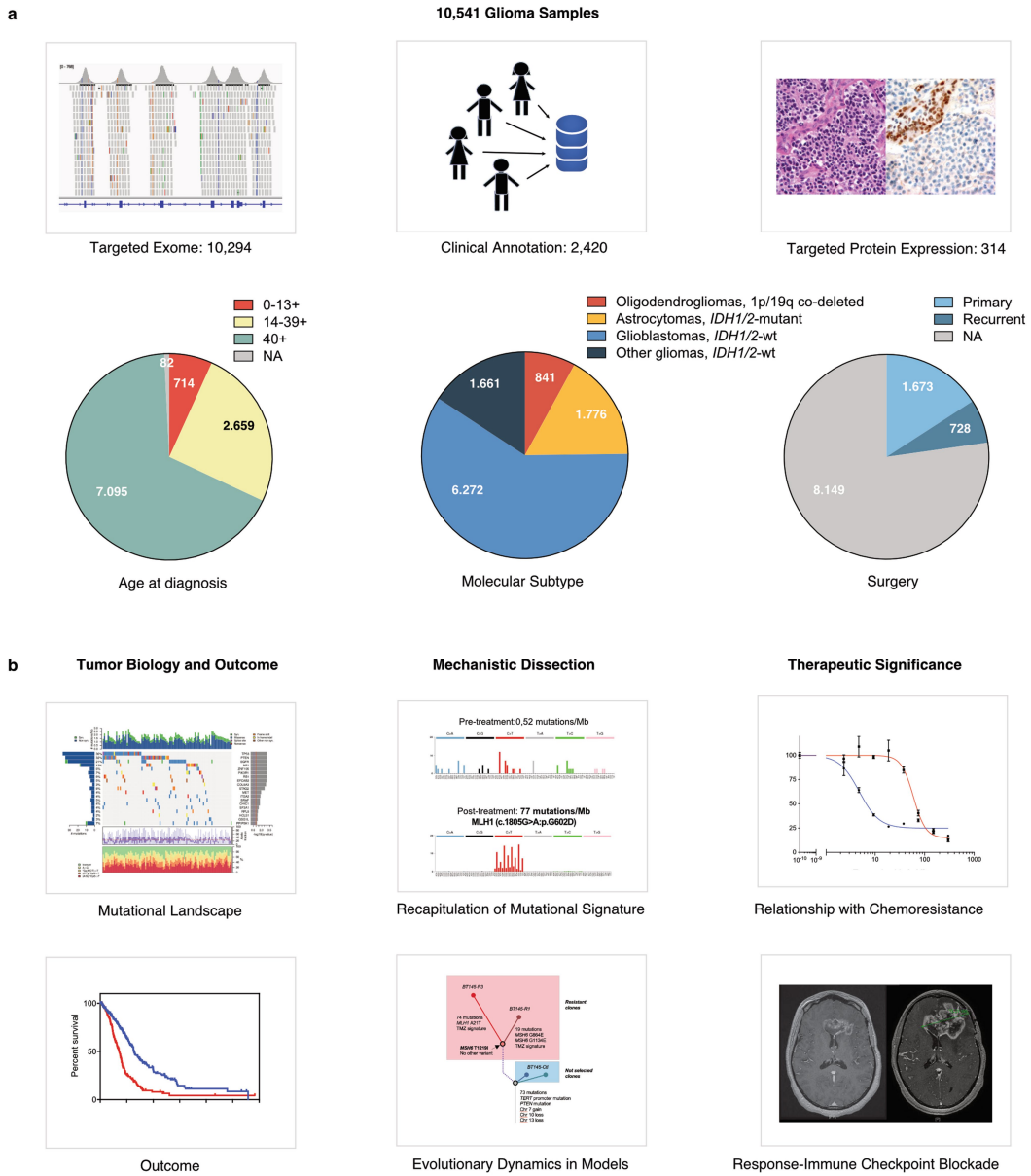
#### Additional information

**Supplementary information** is available for this paper at <https://doi.org/10.1038/s41586-020-2209-9>.

**Correspondence and requests for materials** should be addressed to M.T., R.B., P.B., F.B. or K.L.L.

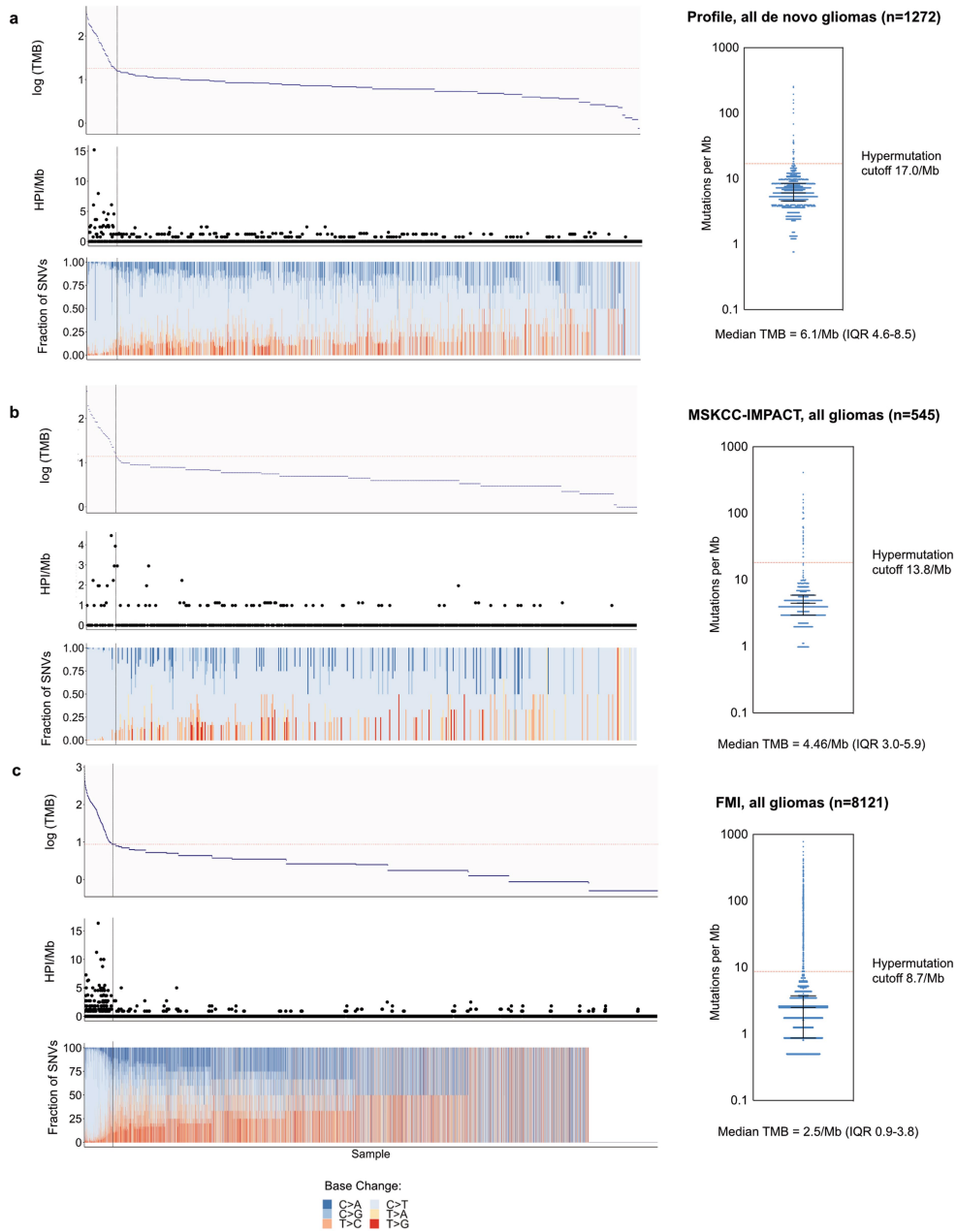
**Peer review information** Nature thanks Stefan Pfister and the other, anonymous, reviewer(s) for their contribution to the peer review of this work.

**Reprints and permissions information** is available at <http://www.nature.com/reprints>.



**Extended Data Fig. 1 | Overview of the clinical characteristics of the patients in the study and analyses performed.** **a.** Clinical datasets analysed and main demographics including age, histomolecular subtype and disease stage. 1,628 glioma samples from adult and paediatric patients were sequenced as part of a large institutional prospective sequencing program of consented patients (DFCI-Profile) and subsequently clinically annotated. We identified

545 and 8,121 gliomas with sequencing from the MSKCC-IMPACT and FMI datasets, respectively, and used them as a replication set (total set of 10,294 sequenced samples). In addition, 314 tumours—including 247 consecutive recurrent gliomas—were analysed for protein expression of four MMR proteins (MSH2, MSH6, MLH1, and PMS2) using immunohistochemistry. **b.** Analyses performed and key clinical questions that were addressed in the study.



**Extended Data Fig. 2 | Distributions of TMB, homopolymer indels, and SNV mutation spectra in the datasets used. a.** DFCI-Profile (de novo gliomas only); **b.** MSKCC-IMPACT; **c.** FMI (total  $n = 9,938$ ). After examining the distribution of TMB in each dataset for breakpoints, thresholds for hypermutation were further confirmed using segmented linear regression analysis (analysis restricted to de novo gliomas for DFCI-Profile). This method showed the presence of a breakpoint at 17.0 and 8.7 mutations per Mb for the DFCI-Profile and FMI datasets, respectively. For the MSKCC-IMPACT dataset, the cutoff used

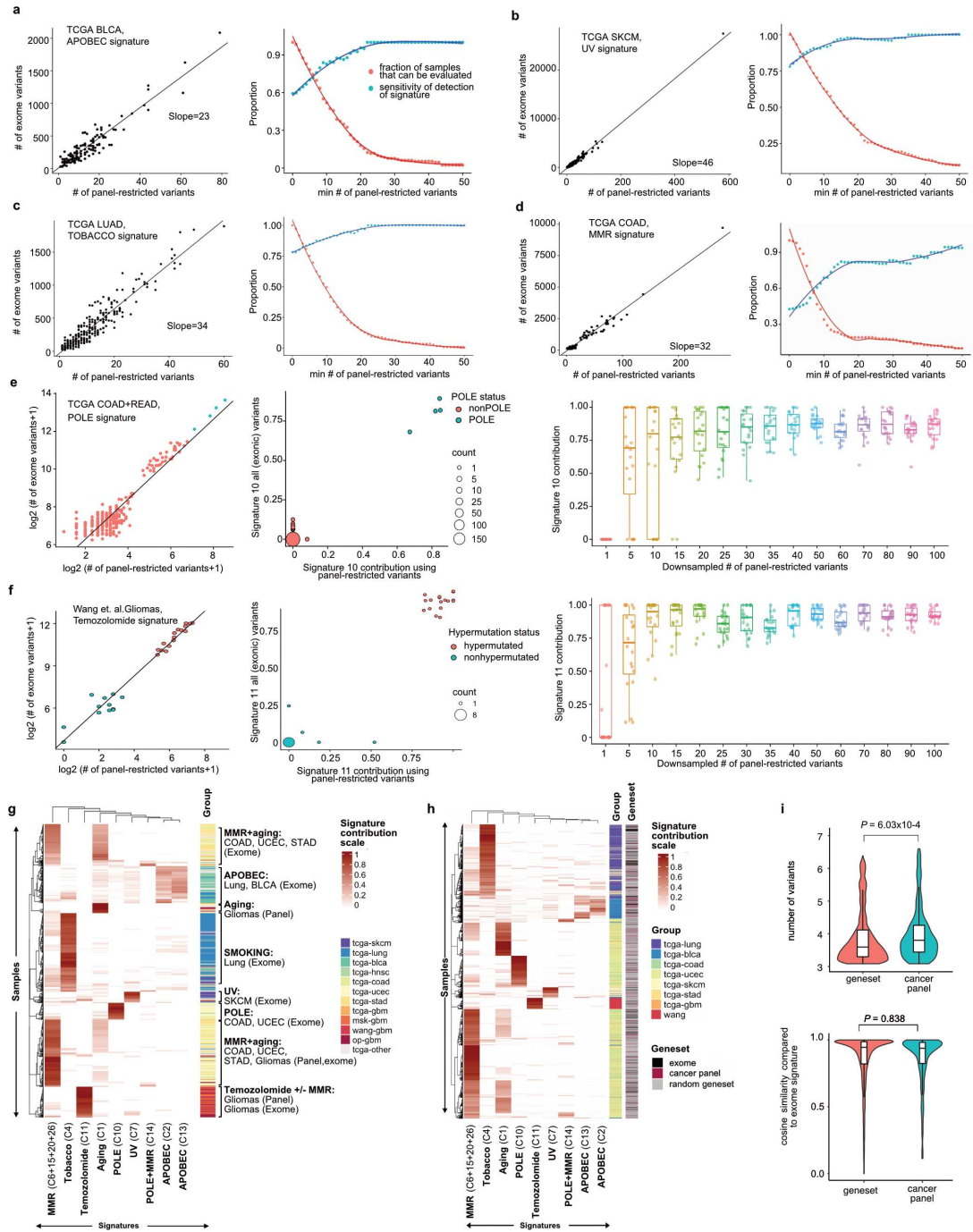
for hypermutation (13.8 mutations per Mb) was previously determined<sup>17</sup>. The frequency of hypermutation was similar in the three datasets (85 (5.2%) in DFCI-Profile; 29 (5.3%) in MSKCC-IMPACT; 444 (5.5%) in FMI). The median tumour mutation burden (TMB) in the combined datasets was 2.6 mutations per Mb (range, 0.0–781.3). Compared with non-hypermutated gliomas, hypermutated tumours showed atypical patterns of SNVs, consistent with abnormal mutational processes operating in these samples. Bars represent median and interquartile range for each dataset (right). HPI, homopolymer indels.



**Extended Data Fig. 3 | Integrated analysis of tumour mutation burden in hypermutated gliomas in the DFCI-Profile, MSKCC-IMPACT and FMI datasets.** **a**, Distribution of TMB, homopolymer indels, MMR mutations, and SNV mutational spectrum according to molecular status of *IDH1/2*, 1p/19q co-deletion (1p/19q), gain of chromosome 7 and/or deletion of chromosome 10 (7gain/10del), and *MGMT* promoter methylation, histological grade, age at initial diagnosis, and history of prior treatment with alkylating agents or radiation therapy (the distinction between photon and proton therapy was not systematically captured) in the DFCI-Profile dataset ( $n = 84$ , data not shown for the single sample from other gliomas, *IDH1/2*-wt subgroup). **b**, Top, distribution of histomolecular groups in non-hypermutated and hypermutated gliomas from the combined sequencing dataset ( $n = 2,173$ ). Bottom, distribution of molecular groups in de novo and post-treatment hypermutated gliomas from the DFCI-Profile dataset ( $n = 85$ ) (annotation not available for the MSKCC-IMPACT set). **c**, Prevalence of hypermutation according to *MGMT* promoter methylation and *IDH1/2* mutation status in post-temozolomide gliomas from the DFCI-Profile dataset ( $n = 150$ ). Two-sided Fisher's exact test. **d**, Number of temozolomide cycles according to *IDH1/2* mutation status in post-temozolomide diffuse gliomas from the DFCI-Profile dataset ( $n = 211$  gliomas). Patients who received combined chemoradiation but no adjuvant temozolomide were included. Two-sided Wilcoxon rank-sum test. **e**, Boxplots of TMB in post-treatment hypermutated gliomas according to the number of

temozolomide cycles received before surgery. Kruskal–Wallis test and Dunn's multiple comparison test. **f**, TMB in recurrent gliomas according to treatments received before surgery. Patients who received multiple treatment modalities were excluded. Kruskal–Wallis test and Dunn's multiple comparison test. Boxes, quartiles; centre lines, median ratio for each group; whiskers, absolute range (**d–f**). **g**, Integrated analysis of the FMI dataset ( $n = 8,121$  gliomas) depicting tumour mutation burden, the number of indels at homopolymer regions, and the SNV mutation spectrum detected in each tumour according to molecular status of *IDH1/2* and 1p/19q co-deletion (1p/19q), MSI status, and age at initial diagnosis. Dominant mutational signatures detected in hypermutated samples are depicted. The dotted line indicates the threshold for samples with a high mutation burden (8.7 mutations per Mb). **h**, Prevalence of hypermutation among molecularly defined subgroups in the FMI dataset ( $n = 8,121$  gliomas). Chi-squared test. **i**, Dominant mutational signatures detected in hypermutated samples in the FMI dataset ( $n = 8,121$  gliomas). Chi-squared test. **j**, Mutated genes and pathways enriched in hypermutated gliomas in the FMI dataset ( $n = 8,121$ ). Enrichment was assessed using a permutation test to control for random effects of hypermutability in tumours with high TMB. **k, l**, Proportion of TMB<sup>high</sup> versus TMB<sup>low</sup> samples with mutations in selected DNA repair genes and glioma drivers (**e**) and in the MMR pathway (*MSH2*, *MSH6*, *MLH1* and *PMS2*; **f**). Permutation test; \*\*\*\* $P < 0.0001$ , \*\*\* $P < 0.001$ , \*\* $P < 0.01$ ; ns, not significant.

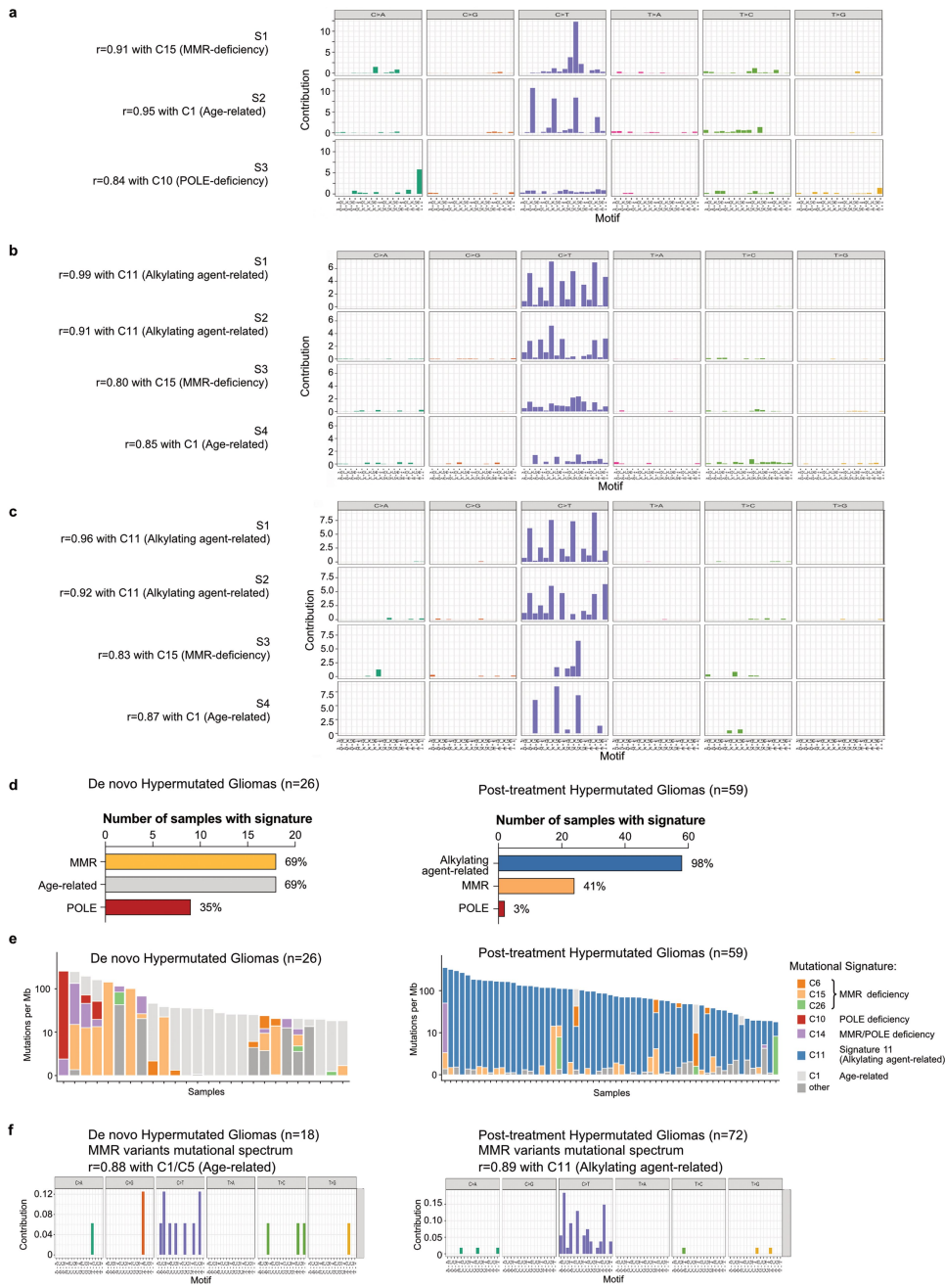
# Article



Extended Data Fig. 4 | See next page for caption.

**Extended Data Fig. 4 | Validation of known hypermutation-associated signatures using TCGA datasets.** Mutational signatures were predicted using exome-sequencing variants that overlapped with the panel-targeted regions, and then compared to previously published DeconstructSigs signature predictions based on all exome variants. The TCGA MC3 dataset was used to assess the detection of COSMIC mutational signatures associated with APOBEC (signatures 2 and 13), mismatch repair (signature 6), ultraviolet light (signature 7), POLE (signature 10), and tobacco (signature 4). Variant calls for 17 hypermutated and 12 non-hypermutated glioma exome-sequenced samples<sup>4</sup> were used to assess temozolomide (signature 11) detection. **a**, Detection of APOBEC-associated mutational signature in TCGA BLCA samples ( $n = 129$  out of 411 samples). **b**, Detection of ultraviolet-associated mutational signature in TCGA SKCM samples ( $n = 237$  out of 466 samples). **c**, Detection of tobacco smoking-associated mutational signature in TCGA LUAD samples ( $n = 250$  out of 513 samples). **d**, Detection of MMR-associated mutational signature in TCGA COAD ( $n = 188$  out of 380 samples). **e**, Detection of POLE-associated mutational signature in TCGA COAD and READ samples ( $n = 277$  out of 380 samples). **f**, Detection of temozolomide-associated mutational signature in ref.<sup>4</sup> ( $n = 29$ ). **g**, Unsupervised clustering of hypermutated samples. A total

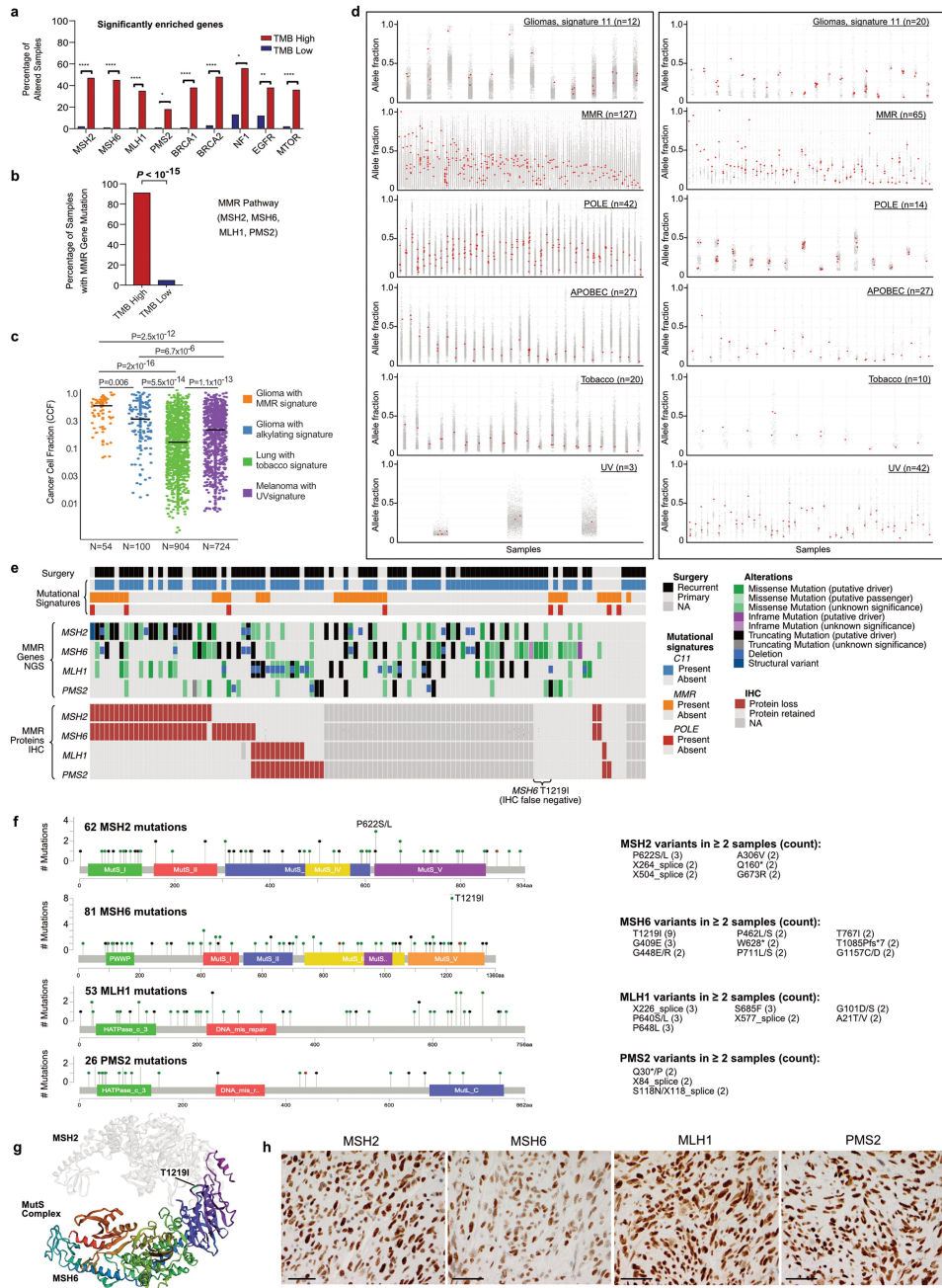
of 865 hypermutated tumour samples from exomes (pan-TCGA and Wang et al.<sup>4</sup>) and targeted panels (DFCI-Profile and MSK-IMPACT) were analysed for known hypermutation signatures (tobacco, UV, MMRD, POLE, TMZ, APOBEC). Samples and signatures underwent 2D hierarchical clustering based on Euclidean distance. **h**, Performance of cancer panel versus other genesets in mutational signature calling. We analysed 622 hypermutated tumour exomes (pan-TCGA and Wang et al.<sup>4</sup>, black) for their mutational signature contributions when restricted to variants from i) DFCI-Profile OncoPanel cancer panel genes (red), or ii) 9 randomly selected gene sets (grey) of similar total capture size to the cancer panel. For each sample, we assessed known hypermutation signatures for cancer panels and gene sets for which at least 20 single base substitutions were retained in the sample after restriction. Samples and signatures underwent 2D hierarchical clustering based on Euclidean distance. **i**, The violin plots represent the number of variants (top) and the cosine similarity of signature contributions (bottom) when using all exonic variants versus restriction to cancer panel or the 49 random gene sets. Boxes, quartiles; centre lines, median ratio for each group; whiskers, absolute range. Two-sided Welch's  $t$ -test.



Extended Data Fig. 5 | See next page for caption.

**Extended Data Fig. 5 | Mutational signature analysis of primary and secondary hypermutated cohort (n = 111).** **a**, Mutational signature analysis of newly diagnosed hypermutated gliomas in the DFCI-Profile dataset (n = 24). **b**, Mutational signature analysis of secondary hypermutated gliomas (samples in which hypermutation was detected in the recurrent tumour) in the DFCI-Profile dataset (n = 58). The novel COSMIC Signature 11-related signature (S2) was associated with 1p/19q co-deletion and lack of prior radiation therapy (66.7% of samples with high S2 versus 26.2% of samples with high S1 signature, Fisher  $P = 0.016$ ). **c**, Mutational signature analysis of hypermutated gliomas from the MSKCC-IMPACT dataset (n = 29). **d**, Mutational signature analysis in de novo (hypermutated at first diagnosis, n = 26, left) and post-treatment hypermutated gliomas (hypermutation in a recurrent tumour, n = 59, right). Percentage of samples exhibiting the most common mutational signatures and their hypothesized causes are displayed. MMR, C6, C14, C15, C26;

age-related, C1; POLE, C10, C14. Chi-squared test. **e**, Mutational signatures identified in individual de novo hypermutated gliomas (hypermutated at first diagnosis, n = 26, left) and post-treatment hypermutated gliomas (hypermutation in a recurrent tumour, n = 59, right). **f**, Mutational signature analysis of MMR variants in hypermutated gliomas from the DFCI-Profile and MSKCC-IMPACT datasets (n = 114). Ninety variants of the MMR genes *MSH2*, *MSH6*, *MLH1*, and *PMS2* were merged into two groups (de novo, n = 18; post-treatment, n = 72) according to the type of sample in which they were found and analysed for mutational signatures using a regression model (Rosenthal et al.<sup>52</sup>). In each sample, only the MMR variant with the highest VAF was included, to limit the inclusion of possible passenger variants. For signature discovery in both cohorts (**a**–**c**), variants were analysed using the non-negative matrix factorization (NMF) method and correlated with known COSMIC mutational signatures<sup>14</sup> using Pearson correlation.

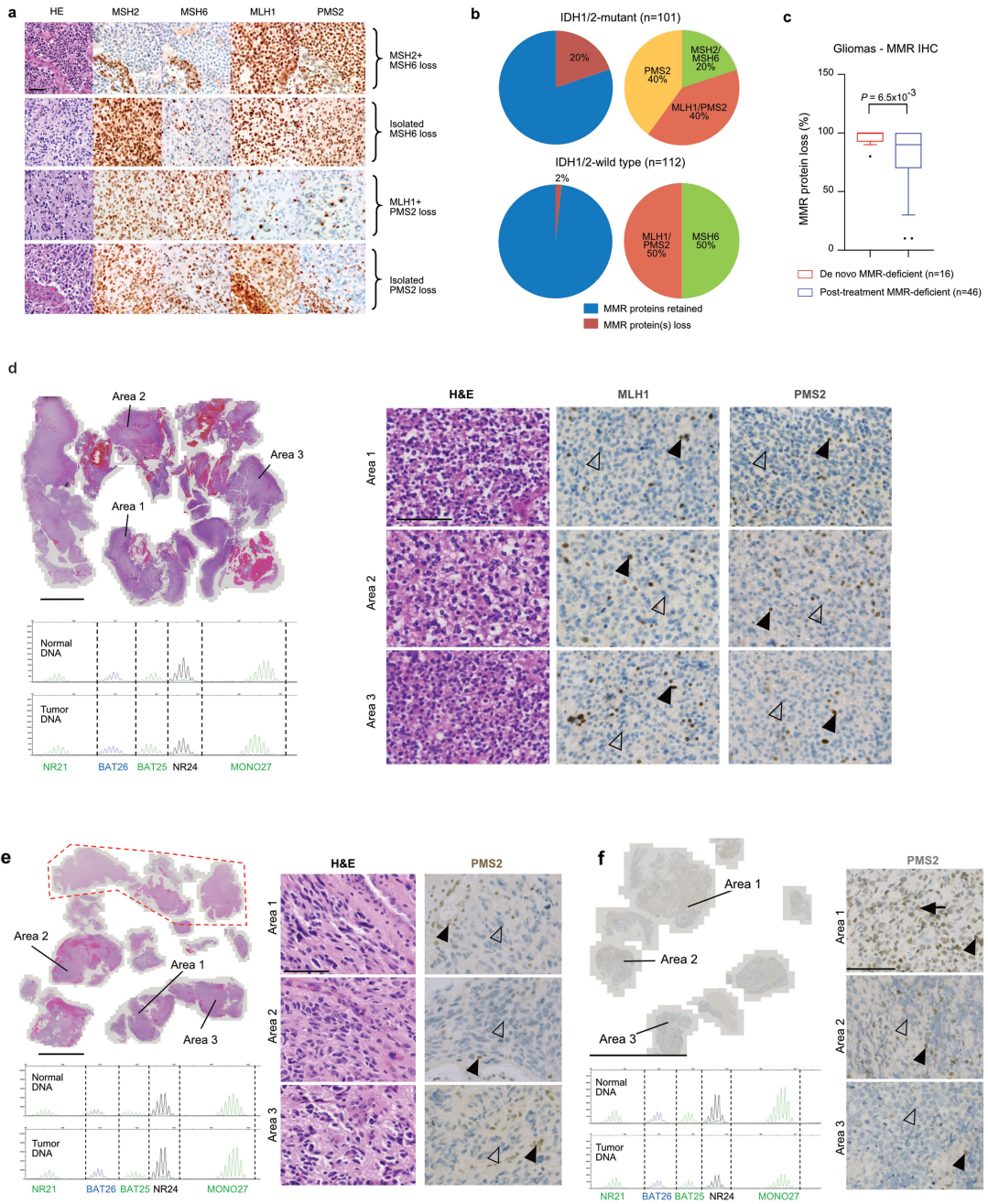


Extended Data Fig. 6 | See next page for caption.

**Extended Data Fig. 6 | Characteristics of MMR molecular variants in hypermutated gliomas.** **a, b**, Proportion of TMB<sup>high</sup> versus TMB<sup>low</sup> samples with mutations in selected DNA repair genes and glioma drivers (**a**) and in the MMR pathway (*MSH2*, *MSH6*, *MLH1* and *PMS2*) (**b**) in the merged DFCI-Profile/MSKCC-IMPACT dataset ( $n = 2,173$ ). Permutation test; \*\*\*\* $P < 10^{-5}$ , \*\* $P < 10^{-2}$ , \* $P < 0.05$ . **c**, CCFs of MMR gene mutations in post-treatment hypermutated gliomas versus other hypermutated cancers in the FMI dataset. Horizontal line, median. Two-sided Wilcoxon rank-sum test with Benjamini–Hochberg correction. **d**, VAF distribution of mutations in post-treatment hypermutated gliomas, non-glioma MMR-deficient cancers (diverse histologies) and other non-glioma hypermutated samples (diverse histologies) from the TCGA and MSKCC-IMPACT datasets. Each dot represents a mutation found in an individual sample (represented vertically). MMR mutations are depicted in red. Left,

hypermutated samples from the pan-TCGA dataset; right, hypermutated samples from the MSKCC-IMPACT dataset. **e**, Integrated view of mutational signatures and MMR gene mutations and protein expression in hypermutated gliomas ( $n = 114$ ). Tumours with the mutational hotspot MSH6(T1219I) (11.9% of post-treatment hypermutated gliomas) are highlighted. **f**, Mutation diagram of *MSH2*, *MSH6*, *MLH1*, and *PMS2* mutations found in hypermutated gliomas from the DFCI-Profile and MSKCC-IMPACT datasets ( $n = 114$ ). The hotspot MSH6 missense variant p.T1219I was found in nine samples. **g**, Hotspot MSH6 p.T1219I variant mapped to the bacterial MutS 3D structure (PDB 5YK4). **h**, Representative immunohistochemistry (IHC) images of the MMR proteins MSH2, MSH6, MLH1 and PMS2 in a hypermutated glioblastoma with MSH6(T1219I) mutation. Three independent samples were stained. Scale bar, 100  $\mu\text{m}$ .

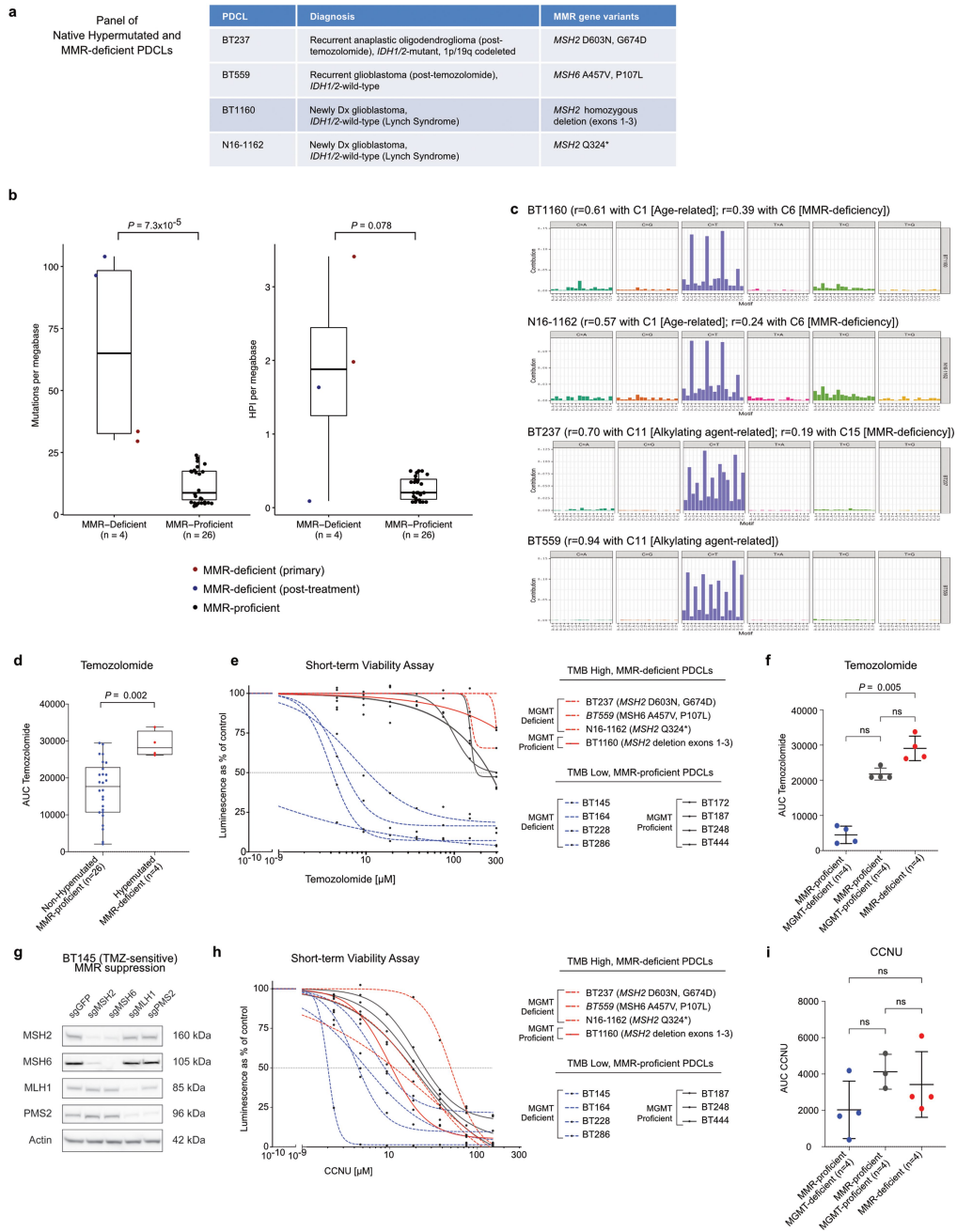
# Article



Extended Data Fig. 7 | See next page for caption.

**Extended Data Fig. 7 | Results of MMR IHC screening in 213 consecutive recurrent gliomas and patterns of MMR protein expression loss in three de novo or post-treatment MMR-deficient gliomas.** **a**, Recurrent patterns of MMR protein loss identified by IHC in gliomas. Scale bar, 50  $\mu$ m. **b**, Summary of MMR IHC screening results for 213 consecutive recurrent gliomas. All monocentric consecutive relapses of diffuse gliomas in adult patients following treatment with post-alkylating agents (surgery between 2009 and 2015) were included in the immunohistochemistry analysis. Further sequencing of samples in which MMR protein loss was identified showed hypermutation with MMR molecular defects in 18/19 (94.7%) samples. **c**, Percentage of tumour MMR protein loss in glioma samples with de novo ( $n=16$ ) or post-treatment ( $n=46$ ) MMR deficiency. Samples were scored by two pathologists in blinded fashion. Regional heterogeneity of MMR protein loss for the four MMR proteins MSH2, MSH6, MLH1, and PMS2 was scored as to the maximal percentage of protein loss among tumour cells for each sample (5% increments). Boxes, quartiles; centre lines, median ratio for each group; whiskers, absolute range, excluding outliers. Two-sided Wilcoxon rank-sum test. **d**, Clonal MMR deficiency in a de novo high-grade glioma. Top left, low magnification of haematoxylin and eosin (H&E) staining of the large surgical tumour pieces obtained from surgical resection. Right, high magnification in three tumour areas (H&E staining, MLH1 and PMS2 immunostaining) showing a highly cellular tumour with an oligodendroglial phenotype and a loss of expression of MLH1 and PMS2 in all tumour cells (open arrowheads). Normal cells have a maintained MLH1 and PMS2 expression (solid arrowheads). Bottom left, microsatellite testing via PCR amplification of five mononucleotide markers (BAT25, BAT26, NR21, NR24, and MONO27) showed the tumour to be MSS. Array CGH showed a homozygous deletion of the entire coding region of MLH1. Scale bars; top left, 5 mm; right, 100  $\mu$ m. **e**, Clonal MMR deficiency in a hypermutated post-treatment, *IDH1*-mutant glioblastoma. Top left,

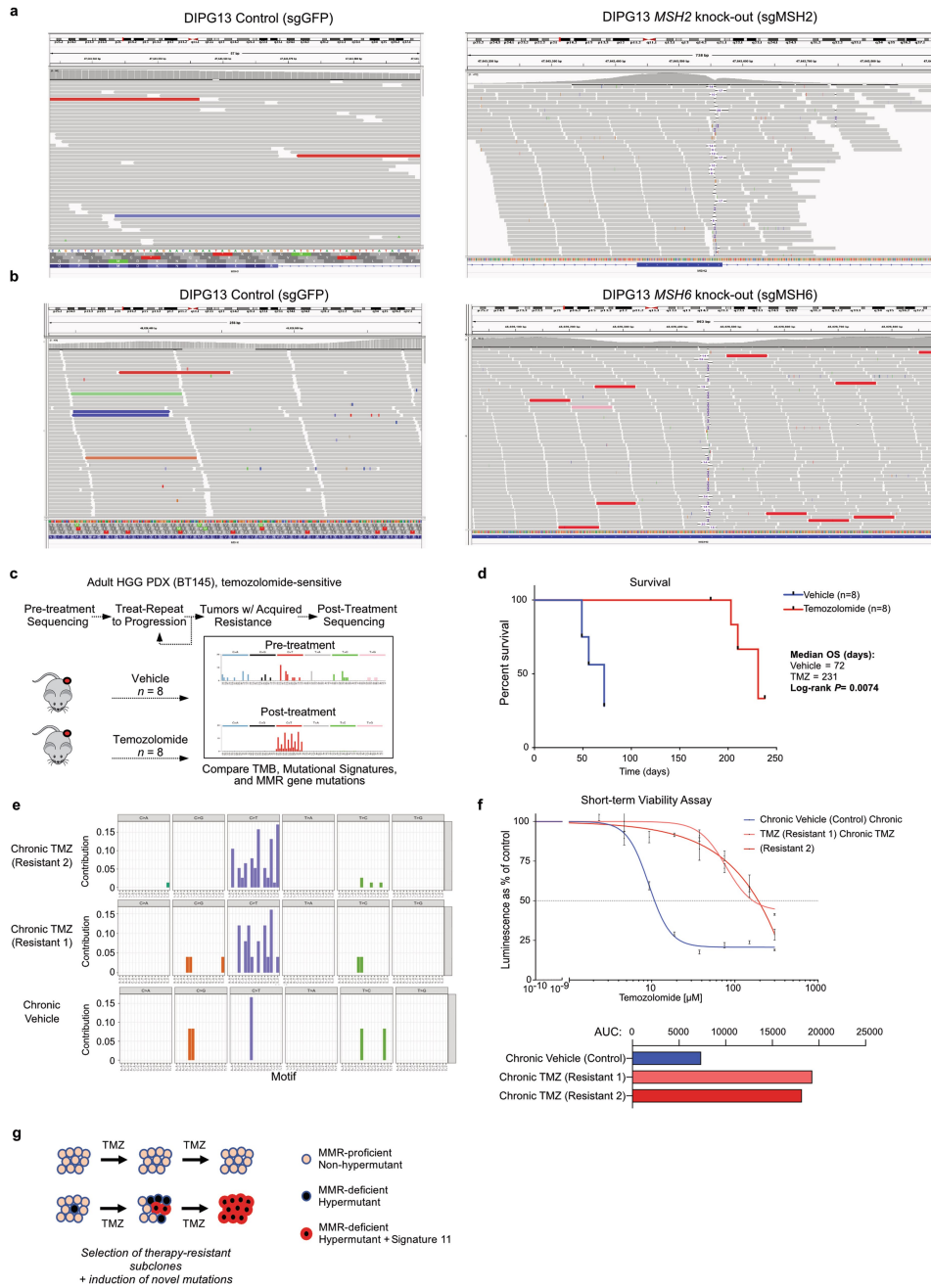
low-magnification image of H&E staining of tissue obtained from surgical resection, with three areas of tumour selected for images. Red dashed line delimits normal brain. Right, high-magnification images of H&E staining, showing highly cellular tumour and an astrocytic phenotype, and PMS2 IHC, showing loss of expression of PMS2 in all tumour cells (open arrowheads). Normal cells have maintained PMS2 expression (internal control, solid arrowheads). Bottom left, Microsatellite testing via PCR amplification of five mononucleotide markers (BAT25, BAT26, NR21, NR24, and MONO27) showed the tumour to be MSS. NGS showed a TMB of 120.1 per Mb and homopolymer indel burden of 3.8 per MB, with contributions from temozolomide (90%) and MMR-deficiency (10%) mutational signatures. A missense (p.P648L) hotspot MLH1 mutation known to be pathogenic from patients with Lynch syndrome with a VAF of 0.73 and loss of heterozygosity was present in this case. Scale bars, top left, 5 mm; right 100  $\mu$ m. **f**, Subclonal MMR deficiency in a hypermutated post-treatment *IDH1*-mutant glioblastoma. Top left, low-magnification image of PMS2 immunostaining of the tumour pieces obtained from surgical resection. Right, high magnification images of three areas of PMS2 immunostaining showing heterogeneous PMS2 expression across the sample consistent with a subclonal tumour. Area 1 shows that PMS2 is retained in atypical tumour cells (arrow); area 2 is heterogeneous with loss (open arrowhead) in some but not all tumour cells; area 3 is an example of diffuse loss of expression in tumour cells (open arrowhead). Normal cells have a maintained PMS2 expression (solid arrowheads in all images). Bottom left, microsatellite analysis via PCR amplification of five mononucleotide markers (BAT25, BAT26, NR21, NR24, and MONO27) showed the tumour to be MSS. NGS showed a TMB of 236.5 per Mb and homopolymer indel burden of 2.3 per MB, with 95% contribution of temozolomide mutational signature. Scale bars, top left 5 mm; right 100  $\mu$ m.



Extended Data Fig. 8 | See next page for caption.

**Extended Data Fig. 8 | Characterization of high-grade glioma PDCLs and their sensitivity to temozolomide and CCNU.** **a**, Clinico-molecular characteristics of four native newly diagnosed or recurrent glioma PDCL models harbouring hypermutation and MMR deficiency. **b**, Thirty glioma PDCLs, including four PDCLs derived from patients with de novo (BT1160, NI6-1162, both established from patients with Lynch syndrome) or post-treatment (BT237, BT559) MMR deficiency were molecularly characterized using whole-exome sequencing. The panels show the tumour mutational burden (left) and homopolymer indel burden (right) in each model. Boxes, quartiles; centre lines, median ratio for each group; whiskers, absolute range. Two-sided Wilcoxon rank-sum test. **c**, Mutational signature analysis was performed in the PDCL models of constitutional and post-treatment MMR deficiency using the R package DeconstructSigs to estimate the contributions of mutational signatures using a regression model (Rosenthal et al.<sup>52</sup>). For each PDCL, the contribution of the main COSMIC mutational signatures identified is

expressed as decimal. **d**, Boxplots of temozolomide AUC in non-hypermutated versus hypermutated PDCLs. Boxes, quartiles; centre lines, median ratio for each group; whiskers, absolute range. Two-sided Wilcoxon rank-sum test. **e, f**, A panel of 12 glioma PDCL models representing the different MGMT and MMR classes was selected and assessed for sensitivity to temozolomide in a short-term viability assay (**e**; dots represent means). The temozolomide AUC was compared between the three groups using a Kruskal–Wallis test and Dunn’s multiple comparison test (**f**; mean  $\pm$  s.d.). **g**, Western blot of the glioblastoma patient-derived cell line (BT145) in which the genes *MSH2*, *MSH6*, *MLH1* or *PMS2* have been knocked-out using the CRISPR–Cas9 system. **h, i**, A panel of 11 glioma PDCL models representing the different MGMT and MMR classes was selected and assessed for sensitivity to CCNU in a short-term viability assay (**h**; dots represent means). No CCNU data was available for the model BT172. The CCNU AUC was compared between the three groups using a Kruskal–Wallis test and Dunn’s multiple comparison test (**i**; mean  $\pm$  s.d.).



Extended Data Fig. 9 | See next page for caption.

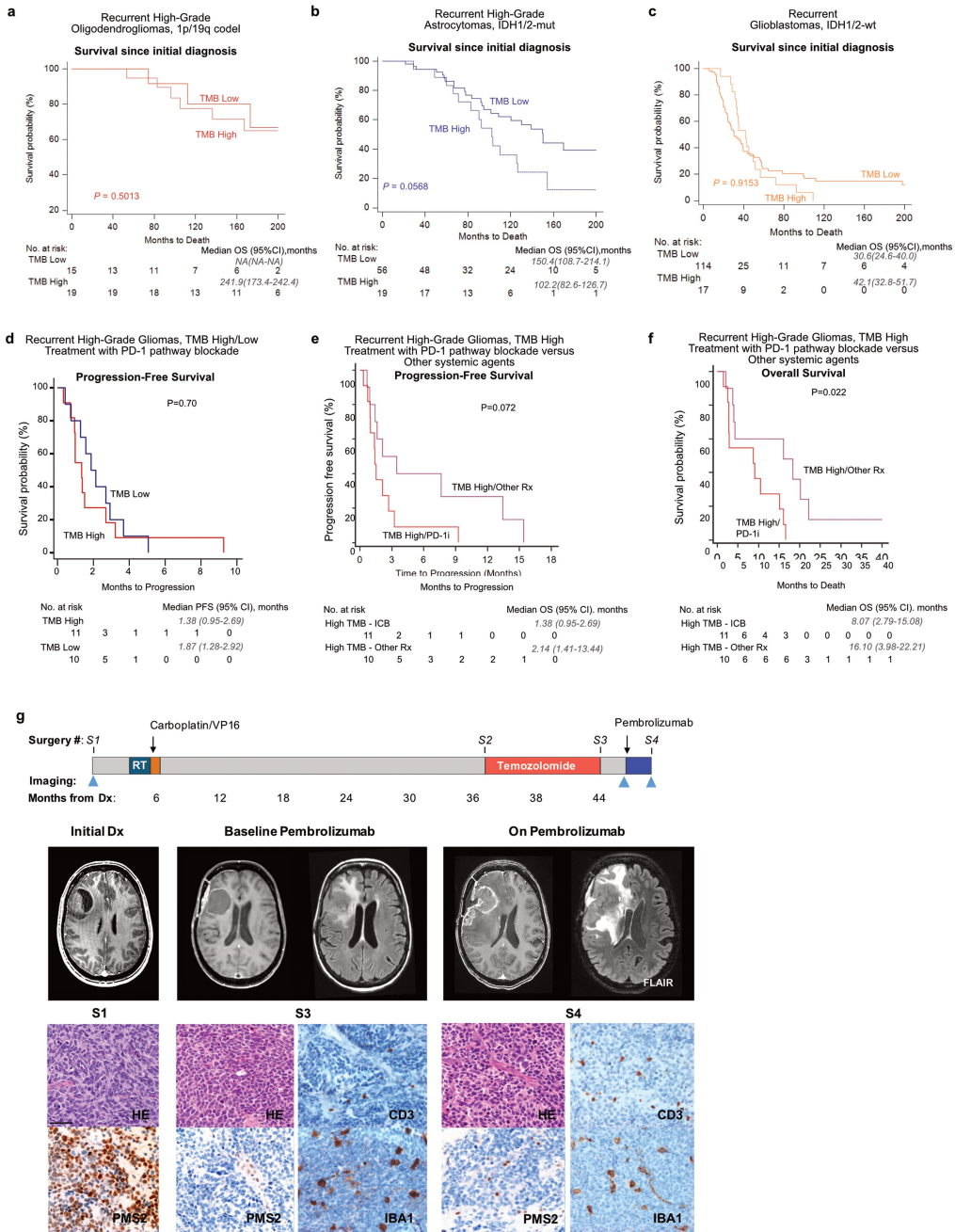
**Extended Data Fig. 9 | MMR-deficient models of glioma, continued.**

**a, b.** CRISPR-Cas9 *MSH2* and *MSH6* gene knockout in DIPG13 high-grade glioma cell line. **a.** Integrated genomics viewer (IGV) plots depicting *MSH2* reads in between the guide RNAs in the *MSH2* unedited line (sgGFP, left) and the *MSH2* CRISPR knockout line (right) confirming knockout in the *MSH2* edited line.

**b.** IGV plots depicting *MSH6* reads in between the guide RNAs in the *MSH6* unedited line (sgGFP, left) and the *MSH6* CRISPR knockout line (right) confirming knockout in the *MSH6* edited line. **c.** Overview of in vivo temozolomide resistance study. Treatment of subcutaneous BT145 PDX-bearing animals was initiated at a volume of 100 mm<sup>3</sup> and eight nude mice per group were randomized to 12 mg/kg/day temozolomide or vehicle for five consecutive days per 28-day cycle. Mice were treated until tumours reached a volume of 1,500 mm<sup>3</sup>, and tumours were sequenced to identify mutations and mutational signature. **d.** Survival of mice with BT145 xenografts (*n* = 8 mice per group) during treatment with vehicle (blue) or temozolomide (red). Two-sided log-rank test. **e.** Unique variants found in three sequenced BT145 tumours (two temozolomide-treated, and one vehicle-treated) were analysed for

correlation with known mutational signatures. COSMIC Signature 11 was found in the two temozolomide-treated tumours. Mutational signatures could not be called in the vehicle-treated tumour (too few variants). After filtering of truncal variants common to all tumours, the two temozolomide-treated tumours shared only four variants, including an *MSH6*(T1219I) mutation and three noncoding variants. **f.** BT145 xenografts chronically treated with vehicle (*n* = 1) or temozolomide (*n* = 2) were removed, dissociated and cultured in serum-free medium to establish cell lines. After three passages in culture, sensitivity to temozolomide was assessed. The results of the short-term viability assays (mean ± s.e.m.) and temozolomide AUC of each cell line are depicted. **g.** Model of acquired hypermutation with mutational signature 11 in gliomas. Top, MMR-proficient cells repair TMZ damage and do not develop signature 11. Resistance in these cells is mediated by non-MMR pathways (for example, MGMT expression). Bottom, TMZ induces and/or selects resistant subclonal MMR-deficient cells. Further TMZ exposure produces accumulation of mutations at specific trinucleotide contexts, detected as hypermutation with signature 11.

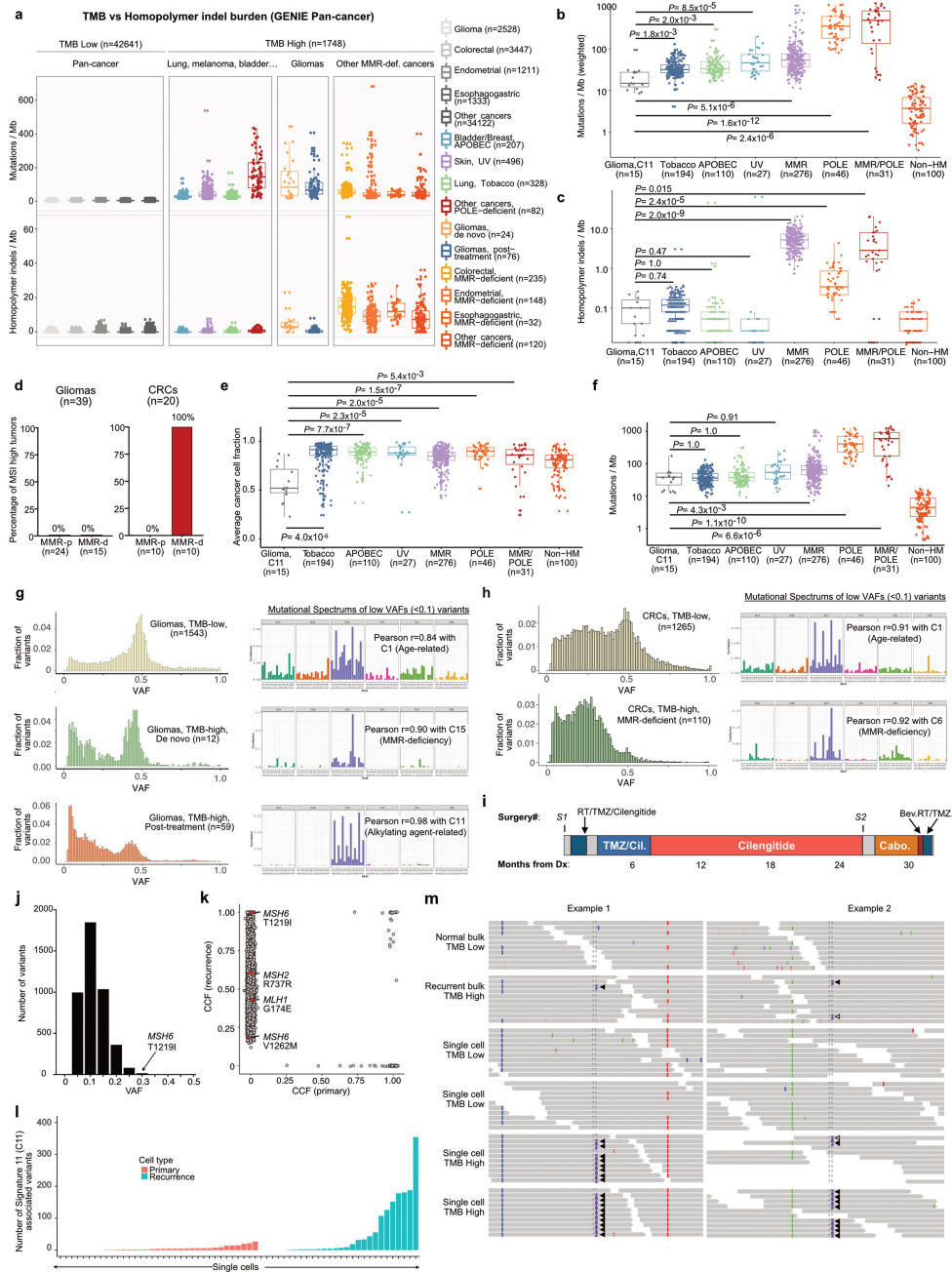
# Article



Extended Data Fig. 10 | See next page for caption.

**Extended Data Fig. 10 | Extended outcome data. a - c.** Survival of patients with recurrent high-grade glioma (WHO grade III or IV) from the time of initial diagnosis according to TMB status (solid curves, TMB<sup>low</sup>; dotted curves, TMB<sup>high</sup>). The curves include 240 recurrent samples from DFCI-Profile with available survival data from initial diagnosis. Two-sided log-rank test. **a.** Survival of patients with recurrent high-grade 1p/19q co-deleted oligodendroglioma from the time of initial diagnosis. **b.** Survival of patients with recurrent high-grade *IDH1/2*-mutant astrocytoma from the time of initial diagnosis. **c.** Survival of patients with recurrent *IDH1/2* wild-type glioblastoma from the time of initial diagnosis. **d.** PFS of 11 patients with hypermutated and MMR-deficient glioma who were treated with PD-1 blockade (single-agent or in combination with bevacizumab, red curve). A cohort of patients with non-hypermutated glioma who were treated with PD-1 blockade is depicted as control ( $n = 10$ , best matches according to diagnosis, primary versus recurrent status, and prior treatments, blue curve). A two-sided log-rank test is used.

**e, f.** PFS (**e**) and OS (**f**) of 11 patients with hypermutated and MMR-deficient glioma who were treated with PD-1 blockade (red curves). A cohort of hypermutated patients treated with other systemic agents is depicted as control (best matches according to diagnosis, primary vs recurrent status, and prior treatments were selected from the cohort of sequenced gliomas, purple curves). Two-sided log-rank test. Clinical and histomolecular characteristics of patients from both cohorts are provided in Supplementary Table 7. **g.** Lack of immune response following PD1 blockade (pembrolizumab) in a patient with post-treatment hypermutated MMR-deficient glioblastoma. Top, timeline; middle, MRI images; bottom, H&E images and IHC for PMS2 expression and tumour infiltration with CD3-positive T cells and IBA1-positive macrophages in the primary (S1), recurrent pre-pembrolizumab (S3) and recurrent post-pembrolizumab (S4) tumours. The tumour acquired a focal *PMS2* two-copy deletion, protein loss, and hypermutation in the post-temozolomide recurrent tumour (S3). Scale bar, 50  $\mu\text{m}$ .



Extended Data Fig. 11 | See next page for caption.

**Extended Data Fig. 11 | Molecular characteristics of hypermutated gliomas.**

**a.** Pan-cancer analysis of TMB and homopolymer indel burden in the GENIE dataset ( $n = 44,389$ ). Tumour samples from the GENIE dataset ( $v6.1$ ) were analysed for mutational and homopolymer indel burden. Statistical comparisons between groups are provided in Supplementary Table 6. **b.** TMB in hypermutated gliomas (post-treatment) versus MMR-deficient cancers and other hypermutated cancers from the TCGA and Wang et al.<sup>4</sup> exome datasets ( $n = 798$ ). Two-sided Wilcoxon rank-sum test with Bonferroni correction. **c.** Pan-cancer analysis of the homopolymer indel burden in hypermutated gliomas (post-treatment) versus MMR-deficient cancers and other hypermutated cancers from the TCGA and Wang et al.<sup>4</sup> exome datasets ( $n = 798$ ). Two-sided Wilcoxon rank-sum test with Bonferroni correction. **d.** Results of MSI analysis using the standard pentaplex assay in glioma ( $n = 39$ ) and CRC samples ( $n = 19$ ) according to MMR status (MMR-d, MMR deficient; MMR-p, MMR-proficient). **e.** Pan-cancer analysis of cancer cell fractions in hypermutated gliomas (post-treatment) versus MMR-deficient cancers and other hypermutated cancers from the TCGA and Wang et al.<sup>4</sup> exome datasets ( $n = 798$ ). Two-sided Wilcoxon rank-sum test with Bonferroni correction. **f.** Weighted TMB in hypermutated gliomas (post-treatment) versus MMR-deficient cancers and other hypermutated cancers from the TCGA and Wang et al.<sup>4</sup> exome datasets ( $n = 798$ ). The weighted TMB was calculated by weighing each individual mutation to its cancer cell fraction. Two-sided Wilcoxon rank-sum test with Bonferroni correction. **g.** Distribution of VAFs (left) and mutation spectrum analysis of low-allelic frequency variants ( $<0.1$ , right) in TMB<sup>low</sup> gliomas ( $n = 1,543$ , top), de novo hypermutated gliomas with MMR deficiency mutational signature ( $n = 12$ , middle), and post-treatment hypermutated gliomas ( $n = 59$ , bottom) from the DFCI-Profile dataset. **h.** Distribution of VAFs (left) and mutation signature analysis of low-allelic frequency variants ( $<0.1$ , right) in TMB<sup>low</sup> CRCs ( $n = 1,265$ , top) and TMB<sup>high</sup> CRCs with MMR deficiency mutational signature ( $n = 110$ , bottom) from the GENIE

dataset. **i.** Clinical timeline for the patient with hypermutated glioblastoma with an MSH6(T1219I) mutation in whom bulk and single-cell WGS was performed. **j.** Distribution of VAFs of mutations in the recurrent bulk sample. The median VAF in the recurrent sample was 0.11. The MSH6(T1219I) mutation had the 18<sup>th</sup>-highest VAF out of 4,350 coding mutations. **k.** Cancer cell fractions (CCFs) of mutations in the primary and recurrent tumour bulk samples. Each dot represents a coding mutation. The horizontal and vertical axes are estimated clonal frequency for each mutation in the primary and recurrent samples, respectively. Mutations of the four main MMR genes are depicted in red. **l.** Mutational spectra in 35 cells from the primary tumour (orange) and 28 from the recurrent tumour (green) submitted to scWGS sequencing (1 $\times$ ). Mutational signature analysis showed a strong contribution of mutational signature 11 in hypermutated cells from the recurrent tumour. **m.** Representative IGV plots ( $n = 2$  distinct genomic segment for each sample) of microsatellite insertions in the normal (TMB low) and recurrent (TMB high) bulk samples and recurrent TMB low ( $n = 2$ ) and TMB high ( $n = 2$ ) single cells. Solid arrowheads represent microsatellite insertions phased with a flanking heterozygous SNP allele. Open arrowheads represent microsatellite insertions for which the reads do not reach the flanking heterozygous SNP allele. Both hypermutated single cells showed multiple phased microsatellite insertions consistent with a true somatic microsatellite mutation. In general, a few reads with similar microsatellite insertions correctly phased with the same flanking heterozygous SNP allele were found in the recurrent bulk, but not in the normal bulk or non-hypermutated cells. For **a-c, e, f**, biological subgroups were identified on the basis of mutational burden, dominant signature and histology. For **b, c, e, f**, 100 non-hypermutated samples were randomly selected as controls. For all box plots: boxes, quartiles; centre lines, median ratio for each group; whiskers, absolute range, excluding outliers. RT, radiation therapy; Cil, cilengitide; Cabo, cabozantinib; Bev, bevacizumab.

## Reporting Summary

Nature Research wishes to improve the reproducibility of the work that we publish. This form provides structure for consistency and transparency in reporting. For further information on Nature Research policies, see [Authors & Referees](#) and the [Editorial Policy Checklist](#).

### Statistics

For all statistical analyses, confirm that the following items are present in the figure legend, table legend, main text, or Methods section.

- |                                     |  |
|-------------------------------------|--|
| n/a                                 | Confirmed  |
| <input type="checkbox"/>            | <input checked="" type="checkbox"/> The exact sample size ( $n$ ) for each experimental group/condition, given as a discrete number and unit of measurement  |
| <input type="checkbox"/>            | <input checked="" type="checkbox"/> A statement on whether measurements were taken from distinct samples or whether the same sample was measured repeatedly  |
| <input type="checkbox"/>            | <input checked="" type="checkbox"/> The statistical test(s) used AND whether they are one- or two-sided<br><i>Only common tests should be described solely by name; describe more complex techniques in the Methods section.</i>   |
| <input type="checkbox"/>            | <input checked="" type="checkbox"/> A description of all covariates tested   |
| <input type="checkbox"/>            | <input checked="" type="checkbox"/> A description of any assumptions or corrections, such as tests of normality and adjustment for multiple comparisons  |
| <input type="checkbox"/>            | <input checked="" type="checkbox"/> A full description of the statistical parameters including central tendency (e.g. means) or other basic estimates (e.g. regression coefficient) AND variation (e.g. standard deviation) or associated estimates of uncertainty (e.g. confidence intervals) |
| <input type="checkbox"/>            | <input checked="" type="checkbox"/> For null hypothesis testing, the test statistic (e.g. $F$ , $t$ , $r$ ) with confidence intervals, effect sizes, degrees of freedom and $P$ value noted<br><i>Give <math>P</math> values as exact values whenever suitable.</i>                            |
| <input checked="" type="checkbox"/> | <input type="checkbox"/> For Bayesian analysis, information on the choice of priors and Markov chain Monte Carlo settings  |
| <input checked="" type="checkbox"/> | <input type="checkbox"/> For hierarchical and complex designs, identification of the appropriate level for tests and full reporting of outcomes  |
| <input type="checkbox"/>            | <input checked="" type="checkbox"/> Estimates of effect sizes (e.g. Cohen's $d$ , Pearson's $r$ ), indicating how they were calculated   |

*Our web collection on [statistics for biologists](#) contains articles on many of the points above.*

### Software and code

Policy information about [availability of computer code](#)

Data collection

No software used for data collection

Data analysis

For WES analyses, we used the CGA WES Characterization pipeline developed at the Broad Institute to call, filter and annotate somatic mutations and copy number variation. The pipeline employs the following tools: MuTect[1], ContEst[2], Strelka[3], Orientation Bias Filter[4], DeTiN [5], AllelicCapSeg[6], MAFPoNFilter[7], RealignmentFilter, ABSOLUTE[8], GATK[9], PicardTools[10], Variant Effect Predictor [11], Oncotator [12].

1. MuTect1: Cibulskis, K, Lawrence, MS & Carter, SL. Sensitive detection of somatic point mutations in impure and heterogeneous cancer samples. *Nature* ... (2013). doi:10.1038/nbt.2514
2. ContEst: Cibulskis, K. et al. ContEst: estimating cross-contamination of human samples in next-generation sequencing data. *Bioinformatics* 27, 2601–2 (2011).
3. Strelka: Saunders, C. T. et al. Strelka: accurate somatic small-variant calling from sequenced tumor-normal sample pairs. *Bioinformatics* 28, 1811–7 (2012).
4. Orientation Bias Filter (oxoG, FFPE): Costello, M. et al. Discovery and characterization of artifactual mutations in deep coverage targeted capture sequencing data due to oxidative DNA damage during sample preparation. *Nucleic Acids Res.* 41, e67 (2013).
5. DeTiN: Taylor-Weiner, A. et al. DeTiN: overcoming tumor-in-normal contamination. *Nat Methods* 15, 531–534 (2018).
6. AllelicCapSeg: Landau, D. A. et al. Evolution and impact of subclonal mutations in chronic lymphocytic leukemia. *Cell* 152, 714–26 (2013).
7. MAFPoNFilter: Lawrence, M. et al. Discovery and saturation analysis of cancer genes across 21 tumour types. *Nature* 505, 495 (2014).
8. ABSOLUTE: Carter, S. L. et al. Absolute quantification of somatic DNA alterations in human cancer. *Nat. Biotechnol.* 30, 413–21 (2012). doi: 10.1038/nbt.2203.
9. GATK (Mutect2, somatic CNV): McKenna, A. et al. The Genome Analysis Toolkit: a MapReduce framework for analyzing next-generation DNA sequencing data. *Genome Res.* 20, 1297–303 (2010).
10. Picard Tools: [https://software.broadinstitute.org/gatk/documentation/tooldocs/4.0.1.0/picard\\_fingerprint\\_CrosscheckFingerprints.php](https://software.broadinstitute.org/gatk/documentation/tooldocs/4.0.1.0/picard_fingerprint_CrosscheckFingerprints.php)  
[https://software.broadinstitute.org/gatk/documentation/tooldocs/4.0.0.0/picard\\_analysis\\_CollectMultipleMetrics.php](https://software.broadinstitute.org/gatk/documentation/tooldocs/4.0.0.0/picard_analysis_CollectMultipleMetrics.php)

11. Variant Effect Predictor: McLaren, W. et al. The Ensembl Variant Effect Predictor. *Genome Biol.* 17, 122 (2016).
12. Oncotator: Ramos, A. H. et al. Oncotator: cancer variant annotation tool. *Hum. Mutat.* 36, E2423–9 (2015).

Additional tools used for PDX analyses, mutational signature analyses and statistical analyses included:

1. SAMtools (1.7): Li, H. et al A statistical framework for SNP calling, mutation discovery, association mapping and population genetical parameter estimation from sequencing data. *Bioinformatics* 2011;27:2987-93
2. BWA-MEM (0.7.17): <https://github.com/lh3/bwa>
3. Disambiguate (ngs\_disambiguate-1.0): <https://github.com/AstraZeneca-NGS/disambiguate>
4. Genemapper Software (5): <https://www.thermofisher.com/order/catalog/product/4475073#/4475073>
5. SomaticSignature (3.1): <https://bioconductor.org/packages/release/bioc/html/SomaticSignatures.html>
6. DeconstructSigs (1.8): <https://github.com/raerose01/deconstructSigs>
7. STATA (v14.2): <https://www.stata.com>
8. MedCalc (19.0.3): <https://www.medcalc.org>
9. Graphpad Prism (8): <https://www.graphpad.com/scientific-software/prism/>

For manuscripts utilizing custom algorithms or software that are central to the research but not yet described in published literature, software must be made available to editors/reviewers. We strongly encourage code deposition in a community repository (e.g. GitHub). See the Nature Research [guidelines for submitting code & software](#) for further information.

## Data

Policy information about [availability of data](#)

All manuscripts must include a [data availability statement](#). This statement should provide the following information, where applicable:

- Accession codes, unique identifiers, or web links for publicly available datasets
- A list of figures that have associated raw data
- A description of any restrictions on data availability

Clinical and sequencing data from 1495 samples from the DFCI-Profile and 545 samples from the MSKCC-IMPACT datasets are publicly available (GENIE v4.1: <https://www.synapse.org/>). All data for samples from the GENIE v6.1 and TCGA pan-cancer datasets are publicly available. Data for samples from the FMI dataset are not publicly available.

Detailed clinical annotation for the DFCI-Profile and MSKCC-IMPACT cohorts is provided in supplementary table 1.

## Field-specific reporting

Please select the one below that is the best fit for your research. If you are not sure, read the appropriate sections before making your selection.

- Life sciences       Behavioural & social sciences       Ecological, evolutionary & environmental sciences

For a reference copy of the document with all sections, see [nature.com/documents/nr-reporting-summary-flat.pdf](https://www.nature.com/documents/nr-reporting-summary-flat.pdf)

## Life sciences study design

All studies must disclose on these points even when the disclosure is negative.

Sample size	No statistical test was used to determine the sample size. We systematically collected data from 10,294 glioma samples from three large independent datasets. Based on prior literature (prevalence of hypermutation of 2-5% in gliomas), we hypothesized that this sample size would provide enough power (200-500 hypermutated samples) for clinical and molecular association studies.
Data exclusions	47 samples for which the clinical diagnosis of glioma could not be confirmed (other histology or possible non-tumor sample) and 5 samples with missing clinical annotation were excluded from all analyses. Exclusion criteria were pre-established.
Replication	In vivo experiments were performed using groups of 8 mice per group. All mice were included in the analysis. In vitro sensitivity assays were replicated in at least 3 independent experiments. All experiments that were technically valid were included in the analysis.
Randomization	For in vivo experiments, mice were randomized.
Blinding	No blinding was performed. Blinding was not relevant to our study.

## Reporting for specific materials, systems and methods

We require information from authors about some types of materials, experimental systems and methods used in many studies. Here, indicate whether each material, system or method listed is relevant to your study. If you are not sure if a list item applies to your research, read the appropriate section before selecting a response.

**Materials & experimental systems**

n/a	Included in the study
<input type="checkbox"/>	<input checked="" type="checkbox"/> Antibodies
<input type="checkbox"/>	<input checked="" type="checkbox"/> Eukaryotic cell lines
<input checked="" type="checkbox"/>	<input type="checkbox"/> Palaeontology
<input type="checkbox"/>	<input checked="" type="checkbox"/> Animals and other organisms
<input type="checkbox"/>	<input checked="" type="checkbox"/> Human research participants
<input checked="" type="checkbox"/>	<input type="checkbox"/> Clinical data

**Methods**

n/a	Included in the study
<input checked="" type="checkbox"/>	<input type="checkbox"/> ChIP-seq
<input checked="" type="checkbox"/>	<input type="checkbox"/> Flow cytometry
<input checked="" type="checkbox"/>	<input type="checkbox"/> MRI-based neuroimaging

**Antibodies**

Antibodies used	For immunohistochemistry, the following antibodies were used: mouse monoclonal anti-ATRX (Bio SB, clone BSB-108, BSB3296, 1:100), mouse monoclonal anti-IDH1 R132H (Dianova, clone H09, DIA-H09, 1:100), rabbit monoclonal anti-CD3 (Roche, clone 2GV6, 790-4341, prediluted), rabbit polyclonal anti-IBA1 (Wako, W1W019-19741, 1:500), mouse monoclonal anti-MLH1 (Roche, clone M1, 790-4535, prediluted), mouse monoclonal anti-MSH2 (Roche, clone G219-1129, 760-4265, prediluted), mouse monoclonal anti-MSH6 (Roche, clone 44, 760-4455, prediluted), rabbit monoclonal anti-PMS2 (Roche, clone EPR3947, 760-4531, prediluted). For immunohistochemistry performed at BWH, the following antibodies were used: mouse monoclonal anti-MLH1 (Leica, clone ES05, MLH1-L-CE, 1:75), mouse monoclonal anti-MSH2 (Merck Millipore, clone Ab-2-FE11, NA27, 1:200), mouse monoclonal anti-MSH6 (Leica, clone PU29, MSH6-L-CE, 1:50), mouse monoclonal anti-PMS2 (Cell Marque, MRQ-28, 288M-14-ASR, 1:100). For immunoblotting, the following antibodies were used: mouse monoclonal anti-MGMT (Millipore, MT3.1, MAB16200, 1:500), mouse monoclonal anti-MSH2 (Calbiochem, FE11, NA27, 1:1000), mouse monoclonal anti-MSH6 (Biosciences, 44, 610918, 1:500), mouse monoclonal anti-MLH1 (Cell Signaling, 4C9C7, 3515, 1:500), mouse monoclonal anti-PMS2 (BD Biosciences, A16-4, 556415, 1:1000), mouse monoclonal anti-beta-actin (Sigma, AC-74, A2228, 1:10000).
Validation	All antibodies used are commercially available and were validated by the manufacturer.

**Eukaryotic cell lines**Policy information about [cell lines](#)

Cell line source(s)	All patient-derived cell lines (PDCLs) and xenografts (PDXs) with a name starting with "BT" were established from tumors resected at Brigham and Women's Hospital and Boston Children's Hospital (Boston, MA). SU-DIPG-XIII (DIP13) cells were provided by Dr. Michelle Monje at Stanford University.
Authentication	The identity of all cell lines established were confirmed by short tandem repeat assay.
Mycoplasma contamination	All cell lines were tested for the absence of mycoplasma.
Commonly misidentified lines (See <a href="#">ICLAC</a> register)	No commonly misidentified cell lines were used.

**Animals and other organisms**Policy information about [studies involving animals](#); [ARRIVE guidelines](#) recommended for reporting animal research

Laboratory animals	Eight-week-old NU/NU male mice (Charles River).
Wild animals	The study did not involve wild animals.
Field-collected samples	The study did not involve samples collected from the field.
Ethics oversight	All in vivo studies were performed in accordance with Dana-Farber Cancer Institute animal facility regulations and policies under the protocol #09-016.

Note that full information on the approval of the study protocol must also be provided in the manuscript.

**Human research participants**Policy information about [studies involving human research participants](#)

Population characteristics	We systematically analyzed clinical data and somatic tumor variants identified through targeted next-generation sequencing (NGS) panels of 1,628 gliomas sequenced between June 2013 and November 2018 as part of a large institutional prospective profiling program (DFCI-Profile). All samples were assigned to a molecular subgroup based on histopathology, mutational status of IDH1 and IDH2 genes, and whole-arm co-deletion of chromosomes 1p and 19q (1p/19q co-deletion). A total of 545 independent samples from the GENIE project (a repository of genomic data obtained during routine clinical care at international institutions) were also identified and assigned to molecular subgroups. The combined sequencing set comprised 2,173 glioma samples, which included a broad spectrum of newly-diagnosed and recurrent glioma types including IDH1/2 wild-type
----------------------------	--

glioblastomas (1234 tumors, 56.8%), IDH1/2-mutant gliomas (640, 29.5%), and other rare subtypes of IDH1/2 wild-type gliomas (299, 13.8%). In addition, 247 gliomas collected at one site between 2009 and 2017 were analyzed for targeted protein expression using immunohistochemistry.

**Recruitment**

Genomic testing was ordered by the pathologist or treating physician as part of routine clinical care to identify relevant genomic alterations that could potentially inform diagnosis and treatment decisions. All patients undergoing genomic testing signed a clinical consent form, permitting to return results from clinical sequencing. No systematic bias likely to impact results were known at the time of data analysis.

**Ethics oversight**

The study, including the consent procedure, was approved by the institutional ethics committees (10-417/11-104/17-000; WIRB, Puyallup WA).

Note that full information on the approval of the study protocol must also be provided in the manuscript.

## DISCUSSION

Dans cette publication, nous caractérisons les mécanismes conduisant à l'hypermutation dans les gliomes malins. Une avancée importante a été l'identification de caractéristiques uniques dans les phénotype clinique et histomoléculaire des gliomes avec hypermutation secondaire à une déficience du système MMR (e.g. mauvais pronostic, absence de phénotype MSI, caractère sous-clonal et tardif de l'hypermutation). Ces différences avec les autres tumeurs MMR-déficientes pourraient en partie expliquer l'absence de réponse aux ICI que nous avons le plus fréquemment observé dans les gliomes. En particulier, la charge mutationnelle majoritairement sous-clonale des gliomes avec hypermutation post-traitement pourrait s'associer à l'absence de réponse immunitaire efficace contre certains néoantigènes tumoraux (Figure 20) <sup>119,122,132</sup>.

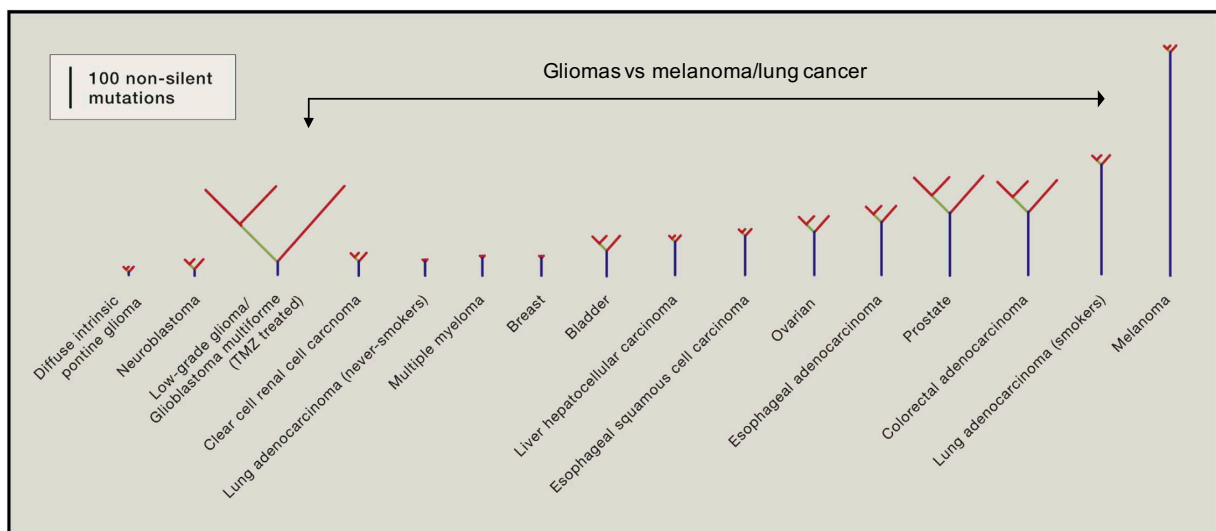


**Figure 20. Arbres phylogénétiques représentant la composition clonale des tumeurs du TCGA (d'après McGranahan et al. <sup>152</sup>).** Pour chaque type de cancer, le nombre moyen de mutations clonales et sous-clonales est représenté par des troncs (bleu) et des branches (vert et rouge) respectivement.

Par ailleurs, nos données montrant l'absence d'infiltrats lymphocytaires T significatifs et l'absence de réponse aux ICI même dans les gliomes avec déficience MMR lors du diagnostic initial (patients avec syndrome de Lynch notamment) suggèrent qu'au-delà du caractère clonal ou sous-clonal des néoantigènes tumoraux, des spécificités dans le microenvironnement immunosuppresseur des gliomes – notamment dans la population de cellules microgliales et macrophages (Figure 21)<sup>153</sup> – contribuent significativement à la résistance aux ICI. Des approches visant à augmenter à la fois l'antigénicité des cellules tumorales et l'infiltration tumorale par des lymphocytes cytotoxiques sont probablement toutes deux nécessaires afin d'améliorer la réponse à l'immunothérapie dans les gliomes. Depuis la publication de cette étude dans *Nature*, nous avons pu identifier plusieurs groupes d'intérêt permettant de mieux comprendre les mécanismes limitant le *trafficking* des cellules lymphocytaires dans les tumeurs gliales : d'une part des rares patients avec gliome hypermutant ayant répondu aux ICI, et d'autre part des sous-groupes uniques de gliomes présentant un important infiltrat inflammatoire T intratumoral. Une caractérisation systématique de ces tumeurs notamment par analyse du transcriptome et techniques multiplex sur lame (immunofluorescence multiplex) est en cours avec l'objectif d'obtenir une meilleure compréhension des mécanismes limitant la pénétration tumorale et l'activité des cellules T antitumorales. A plus long terme, ceci pourrait permettre le développement de nouvelles stratégies de combinaison visant à augmenter l'efficacité de l'immunothérapie dans les gliomes.

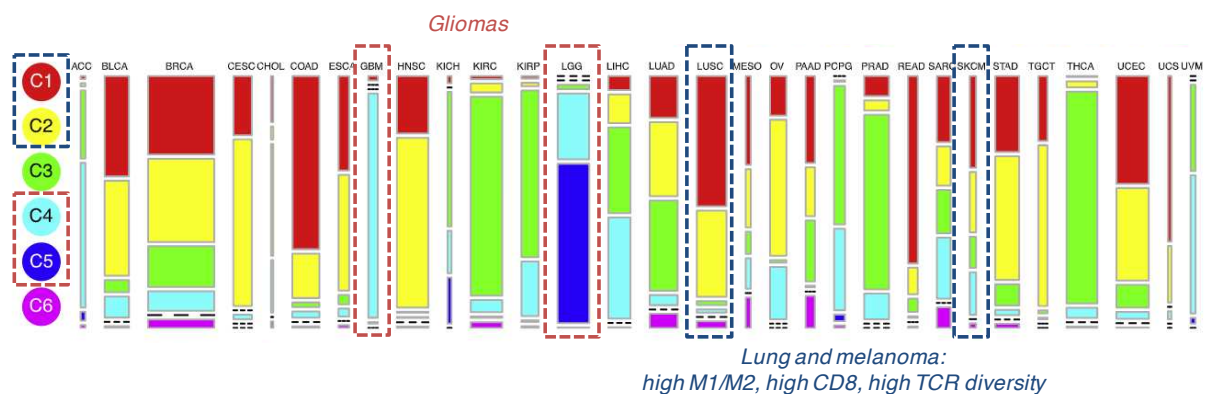


**Figure 21. Analyse pan-cancer des sous-types immunitaires dans les tumeurs TCGA (d'après Thorsson et al.<sup>153</sup>).** Les rectangles représentent la proportion d'échantillons appartenant à chaque sous-type immunitaire. Les gliomes sont enrichis en tumeurs des groupes C4 ("prominent macrophage and Th1 suppressed responses") et C5 ("highest macrophage response").

Une question légitime, fréquemment soulevée lors de la présentation de nos résultats, était de déterminer si la déficience MMR post-traitement était sélectionnée ou induite par le témozolomide. Bien qu'il soit difficile d'affirmer les origines du déficit en MMR post-traitement dans des échantillons

individuels, certaines de nos données suggèrent qu'au moins une part des déficits MMR sont induits par le traitement :

- La mutation MMR la plus fréquemment retrouvée dans les gliomes hypermutants post-traitement (environ 15%) est une mutation avec effet dominant négatif MSH6 T1219I retrouvée de façon exceptionnelle chez les patients avec syndrome de Lynch<sup>154-156</sup>, produit d'une transition C>T et également inductible dans des modèles in vitro chroniquement exposés au témozolomide (Table Supp. 4) ;

- Lorsque les mutations MMR des gliomes hypermutants post-traitement sont regroupées dans un échantillon virtuel, l'analyse des signatures mutationnelles de cet échantillon montre une forte contribution de signature 11, y compris après exclusion des mutations MMR les plus sous-clonales (Figure Supp. 5f).

Nous montrons ainsi qu'au moins une part des déficits MMR sont induits par le témozolomide. Cependant, étant donné que les déficits MMR secondaires se produisent dans les tumeurs les plus sensibles au témozolomide, il est peu probable que l'effet délétère de la déficience MMR secondaire (mauvais pronostic après la rechute), l'emporte sur les effets positifs démontrés avec le témozolomide dans les gliomes. Ces résultats ne remettent donc pas en question l'utilisation du témozolomide dans ces tumeurs. Pour aller plus loin, il faudrait pouvoir prédire plus rapidement l'émergence de clones hypermutants résistants – par exemple via le développement de biomarqueurs circulants, actuellement en cours au sein de l'équipe – et prévenir le développement de ce mécanisme de résistance dans les tumeurs les plus chimiosensibles comme les oligodendrogliomes, par exemple par l'utilisation de CCNU en association au témozolomide qui a récemment démontré des résultats positifs chez des patients atteints de glioblastome nouvellement diagnostiqué avec promoteur *MGMT* méthylé<sup>59</sup>. Nos données cliniques et expérimentales montrant que les cellules MMR déficientes conservent une sensibilité au CCNU soutiennent cette stratégie.

Enfin, nos travaux ouvrent des pistes de recherche concernant le diagnostic (détection du phénotype MSI sous-clonal notamment) et le traitement des gliomes hypermutants avec déficience MMR (stratégies de létalité synthétique notamment), ainsi que sur l'identification de mécanismes alternatifs de résistance non associés au développement d'une hypermutation (comme nous l'avons observé dans environ les deux tiers des échantillons avec promoteur *MGMT* méthylé). Ces nouveaux projets sont en cours dans notre équipe de recherche. Plus largement, ces travaux renforcent l'intérêt du développement de nouvelles méthodes bioinformatiques permettant de mieux caractériser les capacités de réparation et de remodelage de l'ADN dans les cellules tumorales et leur lien avec la sensibilité ou la réponse aux traitements anticancéreux.

## DISCUSSION

In this study, we characterized the mechanisms leading to hypermutation in malignant gliomas. An important breakthrough has been the identification of unique characteristics in the clinical and histomolecular phenotypes of gliomas with hypermutation secondary to MMR deficiency (e.g. poor prognosis, absence of MSI phenotype, late burst of subclonal mutations). These differences with other MMR-deficient tumors could at least in part explain the lack of response to ICIs that we have frequently observed in gliomas. Specifically, the predominantly subclonal mutational burden of gliomas with post-treatment hypermutation could be associated with the absence of an effective immune response against tumor neoantigens (Figure 20)<sup>119,122,132</sup>.

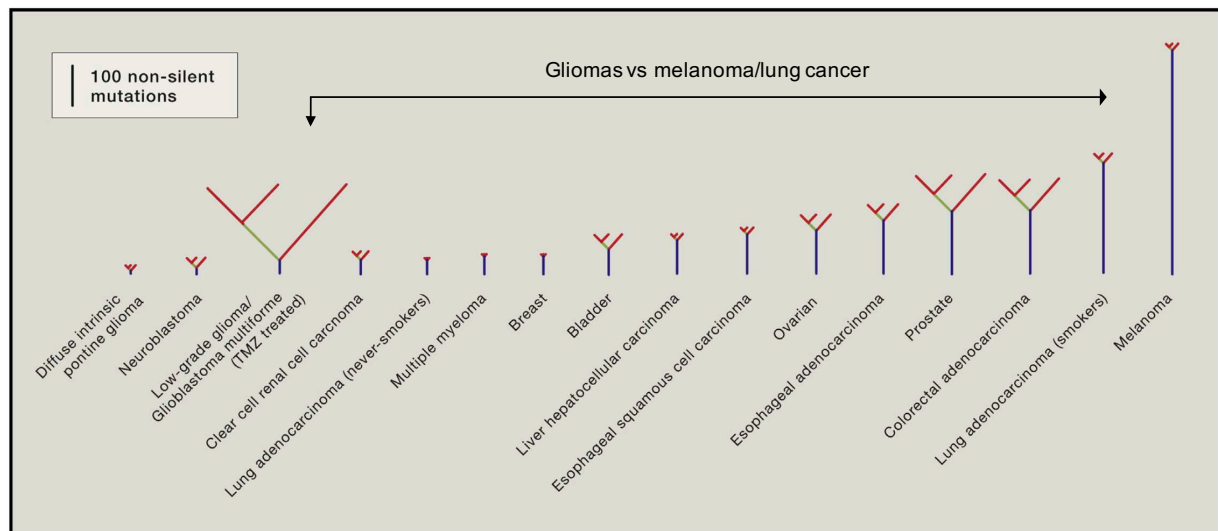


**Figure 20. Phylogenetic trees representing the clonal composition of TCGA tumors (from McGranahan et al.).** For each cancer type, the average number of clonal and subclonal mutations is represented by trunks (blue) and branches (green and red) respectively.

Furthermore, our data showing the absence of significant T lymphocyte infiltrates and the response to ICIs even in gliomas with MMR deficiency at initial diagnosis (patients with Lynch syndrome in particular) suggest that beyond clonal or subclonal nature of tumor neoantigens, specificities in the immunosuppressive microenvironment of gliomas - especially in the population

of microglial and macrophage cells (Figure 21) - contribute significantly to gliomas resistance to ICIs. Approaches aimed at increasing both antigenicity of tumor cells and tumor infiltration by cytotoxic lymphocytes are likely both necessary in order to improve the response to immunotherapy in gliomas. Since the publication of this study in Nature, we have been able to identify several groups which we expect will allow an improved understanding of the mechanisms limiting the trafficking of lymphocyte cells in glial tumors: rare patients with hypermutant glioma who responded to ICIs, and other unique subgroups of gliomas with significant intratumoral T cells infiltrate. Systematic characterization of these tumors, including transcriptome analysis and multiplex immunofluorescence is underway to obtain a better understanding of the mechanisms limiting tumor penetration and anti-tumor T cells activity. In the longer term, this could allow the development of new combination strategies aimed at increasing the efficacy of immunotherapy in gliomas.

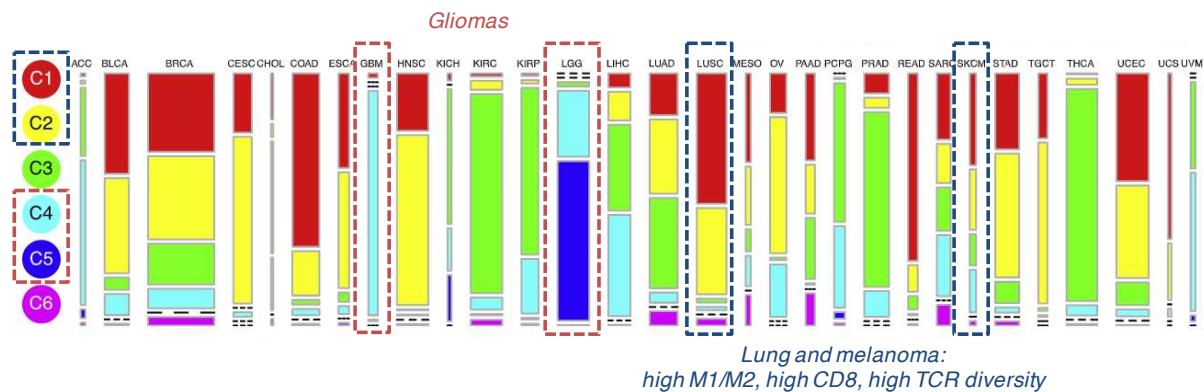


**Figure 21. Pan-cancer analysis of immune subtypes in TCGA tumors (from Thorsson et al. <sup>152</sup>).** The rectangles represent the proportion of samples belonging to each immune subtype. The gliomas are enriched with tumors of the C4 ("prominent macrophage and Th1 suppressed responses") and C5 ("highest macrophage response") groups.

A legitimate question, frequently raised when presenting our results, was whether post-treatment MMR deficiency was selected or induced by temozolomide. Although it is difficult to ascertain the origins of post-treatment MMR deficiency in individual samples, some of our data suggests that at least a part of MMR deficits are induced by treatment:

- The MMR mutation most frequently found in post-treatment hypermutated gliomas (~15%) is an MSH6 T1219I mutation with dominant negative effect found exceptionally in patients with Lynch syndrome <sup>153-155</sup>, product of a C transition > T and also inducible in in vitro models chronically exposed to temozolomide (Table Supp. 4);

- When the MMR mutations of post-treatment hypermutant gliomas are pooled together in a virtual sample, the analysis of the mutational signatures of this sample showed a strong contribution of signature 11, even after the exclusion of the most subclonal MMR mutations (Figure Supp . 5f).

We thereby show that at least a part of the MMR deficits are induced by temozolomide. However, since secondary MMR deficits occur in tumors most sensitive to temozolomide, the deleterious effect of secondary MMR deficiency (poor prognosis after relapse) is unlikely to outweigh its positive effects. These results therefore do not call into question the use of temozolomide in these tumors. To go further, it would be necessary to be able to more quickly predict the emergence of resistant hypermutant clones - for example via the development of circulating biomarkers, currently underway within our teams - and prevent the development of this resistance mechanism in the most chemosensitive such as oligodendrogliomas, for example by using CCNU in combination with temozolomide, which has recently shown positive results in patients with newly diagnosed glioblastoma with a methylated MGMT promoter <sup>59</sup>. Our clinical and experimental data show that MMR cells deficient maintain sensitivity to the CCNU support this strategy.

Finally, our work opens new avenues of research regarding the diagnosis (eg detection of the subclonal MSI phenotype) and the treatment of hypermutant gliomas with MMR deficiency (eg synthetic lethal strategies), as well as on the identification of alternative resistance mechanisms. not associated with the development of hypermutation, which we observed in approximately two-thirds of samples with methylated MGMT promoter. These new projects are underway in our research groups. More broadly, this work reinforces the interest in the development of new bioinformatics methods enabling to better characterize the DNA repair and remodeling capacities in tumor cells and their link with the sensitivity or response to anticancer treatments.

## **ANNEXE / ANNEX**

### **V. Autres contributions à des articles publiés sur la thématique pendant la Thèse de Sciences / Other contributions to articles published on the theme during the Thesis**

**Article sur la déficience MMR et la réponse à l'immunothérapie dans un autre sous-type de tumeur cérébrale primitive, les méningiomes / Article on MMR deficiency and response to immunotherapy in another subtype of primary brain tumor, meningiomas**

# Mismatch Repair Deficiency in High-Grade Meningioma: A Rare but Recurrent Event Associated With Dramatic Immune Activation and Clinical Response to PD-1 Blockade

Ian F. Dunn  
 Ziming Du  
 Mehdi Touat  
 Michael B. Sisti  
 Patrick Y. Wen  
 Renato Umeton  
 Adrian M. Dubuc  
 Matthew Ducar  
 Peter D. Canoll  
 Eric Severson  
 Julia A. Elvin  
 Shakti H. Ramkissoon  
 Jia-Ren Lin  
 Lais Cabrera  
 Brenda Acevedo  
 Peter K. Sorger  
 Keith L. Ligon  
 Sandro Santagata  
 David A. Reardon

Author affiliations and support information (if applicable) appear at the end of this article.

I.F.D. and Z.D. contributed equally to this work. S.S. and D.A.R. contributed equally to this work.

**Corresponding author:** David A. Reardon, MD, 450 Brookline Ave, Dana 2134, Boston, MA 02215-5450; e-mail: david\_reardon@dfci.harvard.edu.

## INTRODUCTION

Meningiomas are the most common primary tumor of the CNS; there are approximately 28,000 new diagnoses annually in the United States.<sup>1</sup> Currently, there are no approved systemic therapies for meningiomas that recur after local treatment: chemotherapy and hormonal agents have demonstrated minimal benefit in numerous clinical trials.<sup>2-4</sup>

Meningiomas comprise a heterogeneous group of neoplasms driven by mutations in a wide array of tumor suppressor genes and oncogenes.<sup>5-17</sup> Characterization of these mutations has revealed opportunities for rational therapy.<sup>18-20</sup> For example, a durable therapeutic response has been reported for a metastatic *AKT1* E17K-mutant meningioma treated with a pan-AKT inhibitor.<sup>21</sup>

Studies also suggest the potential for treating meningioma with immune checkpoint modulators<sup>22-24</sup>: programmed death ligand 1 (PD-L1) is expressed in a subset of meningiomas, and the tumor microenvironment is immunosuppressive.<sup>22-28</sup> Higher-grade meningiomas also harbor mutations predicted to generate neoantigens, which may foster susceptibility to immunotherapies.<sup>29</sup>

On the basis of these data, we initiated a phase II study of nivolumab, a humanized IgG4 programmed death 1 (PD-1)-blocking monoclonal antibody, in patients with higher-grade meningiomas that recurred after surgery and radiotherapy (ClinicalTrials.gov identifier: NCT02648997). We report here a patient with an atypical meningioma that was not controlled by repeated surgery and radiation but that was highly responsive to nivolumab.

## CASE REPORT

A 50-year-old woman with progressive headaches underwent a gross total resection (surgery 1) of a gadolinium-enhancing right frontal convexity atypical meningioma (WHO grade 2; Fig 1A). The tumor recurred 10 months later and was treated with stereotactic radiosurgery (SRS; SRS 1, 25 Gy/five fractions). Recurrent atypical meningioma was debulked 17 months (surgery 2) and 21 months (surgery 3) after the original diagnosis. The patient then underwent conventional radiotherapy (RT; conformal RT, 54 Gy/27 fractions). Three months later, she again underwent SRS (SRS 2, 14 Gy/one fraction) because of tumor spread to the sphenoid ridge and infratemporal fossa. Additional debulking surgeries for recurrent atypical meningioma were performed at 46 months (surgery 4) and 49 months (surgery 5). She then received bevacizumab for 11 months, mifepristone for 7 months, and temozolomide for 4 months. Each therapy was discontinued after disease progression occurred. A sixth debulking surgery (surgery 6) at 70 months confirmed recurrent atypical meningioma.

Five weeks later, the patient enrolled in our phase II nivolumab clinical trial. At that time, 75 months after the original diagnosis, painful subcutaneous masses overlaid the right convexity. The patient required oxycodone for scalp pain and dexamethasone (4 mg/day) for worsening headache. Pretreatment magnetic resonance imaging (MRI) showed an enlarging-enhancing right sphenoid wing mass, plaque-like dural enhancement over the right convexity, tumor erosion through the occipital skull, and an

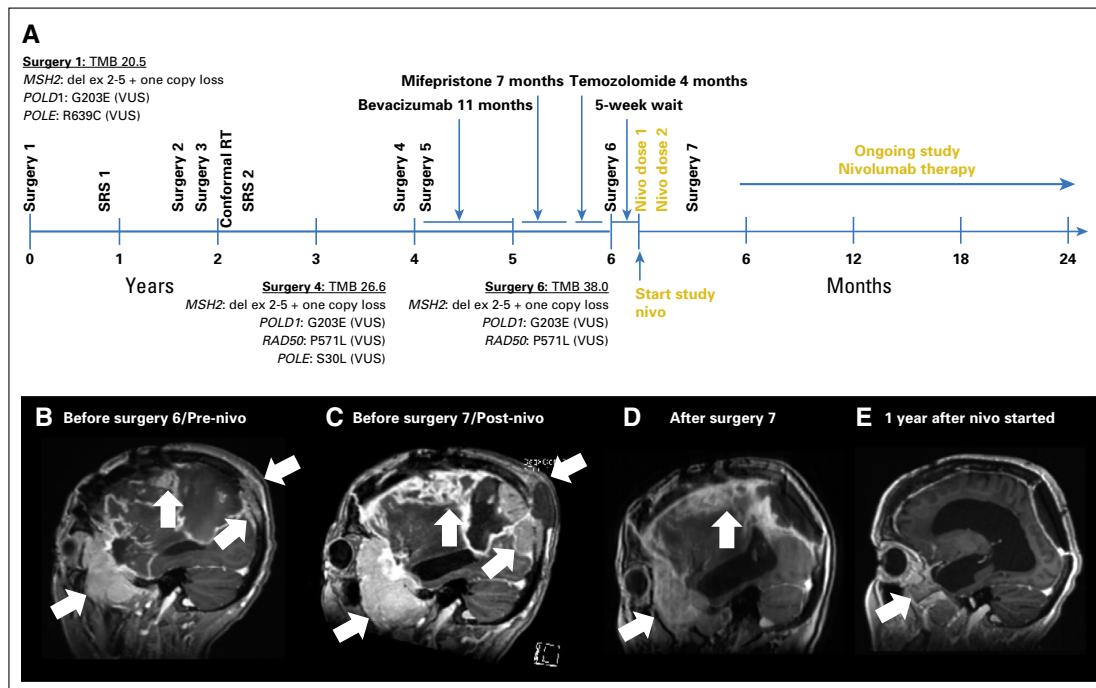


**Fig 1.** Patient treatment and radiographic assessment. (A) Timeline of patient therapy. Nivo, nivolumab; RT, radiation therapy; SRS, stereotactic radiosurgery; TMB, tumor mutational burden; VUS, variant of unknown significance. Sagittal T1 gadolinium-enhanced images (B) before initiation of study nivolumab therapy (before surgery 6), (C) after two doses of nivolumab therapy (before surgery 7), and (D) after subtotal resection (surgery 7) that demonstrate necrosis and no viable tumor; (E) ongoing response 1 year after initiation of nivolumab therapy. White arrows indicate bulky tumor burden, including occipital lesion growing into soft tissue external to skull. MSH2: del ex 2-5<sup>1</sup> indicates homozygous deletion of exons 2 to 5 of the DNA mismatch repair (MMR) gene MSH2.

increased fluid-attenuated inversion recovery (FLAIR) signal abnormality that involved the right hemisphere (Fig 1B).

The patient received nivolumab 3 mg/kg on days 1 (dose 1) and 15 (dose 2) of cycle 1 without incident, but her headaches and scalp pain worsened. The scalp masses were notably larger, erythematous, and more tender by day 28. Brain MRI showed significantly enlarged dural-based enhancing lesions, increased T2 and FLAIR signal abnormalities, and enlarged scalp masses (Fig 1C). Her physical examination and MRI appeared consistent with progressive disease, and we withheld additional nivolumab. She underwent palliative debulking surgery 3 weeks later (surgery 7). Immediately before surgery, her scalp masses were modestly smaller and less tender. Postoperative MRI showed a subtotal resection (Fig 1D).

## MATERIALS AND METHODS

### Patient Consent

Our patient provided informed consent for our institutional review board–approved study and consented to this publication. We obtained all

permissions required by law and by the Dana-Farber Cancer Institute (DFCI)/Harvard Cancer Center to allow the publication of images from the patient.

### Immunohistochemistry

We used immunohistochemistry (IHC) to evaluate protein expression using Envision Plus detection (Dako, Carpinteria, CA; Data Supplement) and published protocols.<sup>30,31</sup>

### Multiplexed Immunofluorescence

The protocol for tissue-based multiplexed cyclic immunofluorescence (t-CyCIF) of conventionally prepared formalin-fixed, paraffin-embedded specimens and image analysis are described elsewhere.<sup>32,33</sup> Antibodies are listed in the Data Supplement.

### Oncopanel Sequencing

We used targeted next-generation exome sequencing (Oncopanel version 3; DFCI/Brigham and Women's Hospital [BWH]) to detect mutations and copy number variations in 447 cancer genes.

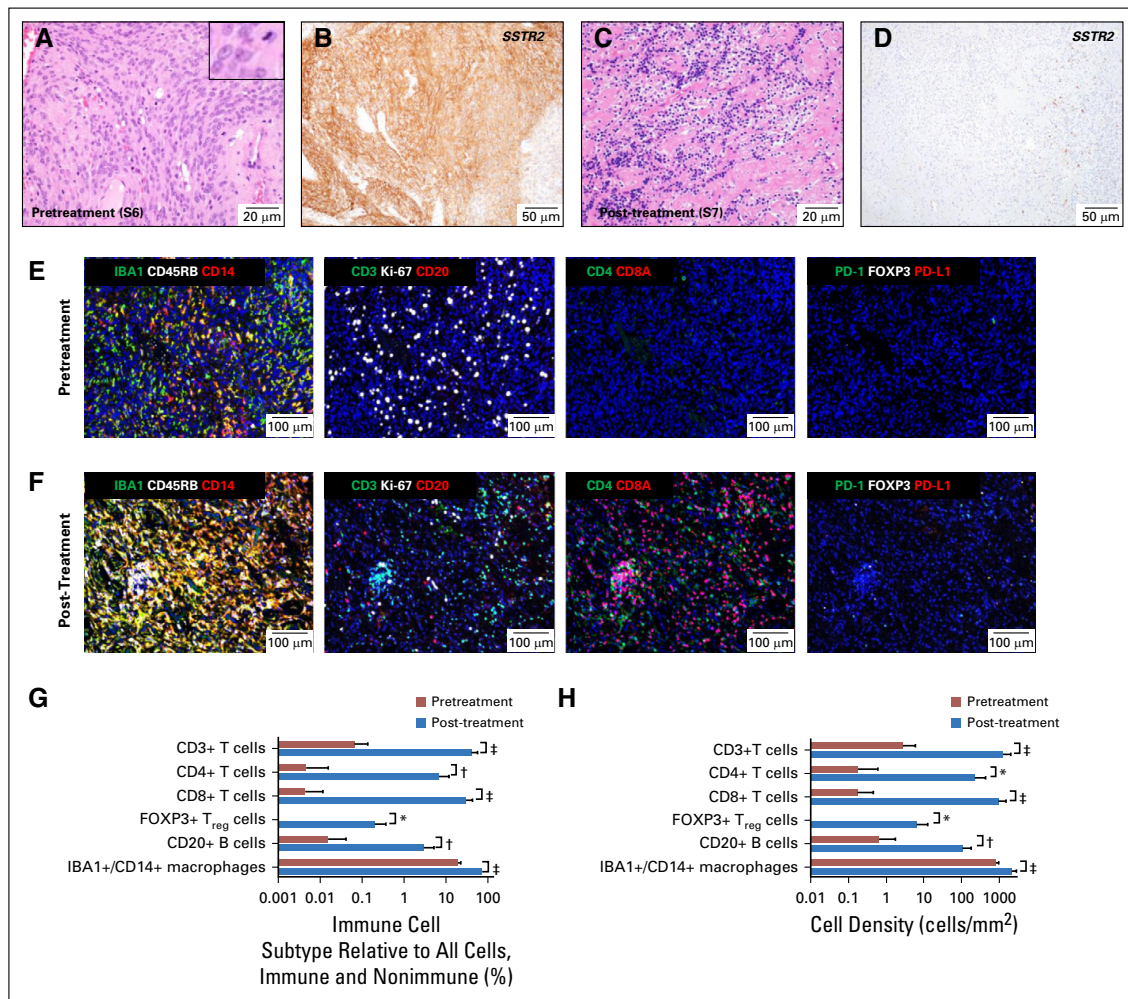


**Fig 2.** Histologic, immunohistochemical, and tissue-based multiplexed cyclic immunofluorescence (t-CyCIF) characterization of meningioma resection samples. Representative images of hematoxylin and eosin–stained section of meningioma resection (A) before treatment with nivolumab (surgery 6/sample 6; S6) and (C) after two doses of nivolumab (surgery 7/sample 7; S7). Representative images of immunohistochemistry for meningioma marker SSTR2a on resections (B) before treatment with nivolumab (surgery 6/sample 6; S6) and (D) after two nivolumab doses (surgery 7/sample 7; S7). The inset in (A) shows a mitotic figure and cells with prominent nucleoli; an elevated mitotic index of more than four mitoses per 10 high-powered fields was used for grading. (E) A representative field of view of t-CyCIF imaging data of 11 biomarkers (ionized calcium-binding adapter molecule 1 [IBA], CD45RB, CD14, CD3, marker of proliferation Ki-67 [Ki-67], CD20, CD4, CD8A, programmed cell death 1 [PD-1], forkhead box P3 [FOXP3], programmed death ligand 1 [PD-L1]) generated from a single section of pretreatment meningioma (surgery 6/sample 6) and (F) from a single section of the post-treatment meningioma (surgery 7/sample 7). Comparison of the images in (E) and (F) showed a marked increase in macrophages; T lymphocytes (CD3+), including CD4+ T cells and CD8A+ T cells; and B lymphocytes (CD20+) after nivolumab treatment. The majority of T cells after treatment were CD8A+. The antibodies used for this characterization and a detailed analysis of the absolute number, relative number and density of various immune subtypes are provided in Table 1 and the Data Supplement. (G) Bar graph of the percentage of immune cell subtypes relative to all cells (immune and nonimmune) before (red bars) and after (blue bars) nivolumab treatment. (H) Bar graph of cell density before (red bars) and after (blue bars) nivolumab treatment. The analysis was performed on 10 representative views (tiles) from the t-CyCIF data collected from samples 6 and 7. *t* test statistical analysis was performed. \*,  $P < .01$ , †,  $P < .001$ , ‡,  $P < .0001$ . The bar graphs represent the most pertinent data derived from the immune profile of the pre-nivolumab (sample 6) and post-nivolumab (sample 7)–treated meningioma samples using t-CyCIF. Detailed data are listed in Table 1 and the Data Supplement.

We processed and annotated data as previously described.<sup>9,34,35</sup> We calculated tumor mutational burden (TMB) by determining the number of nonsynonymous mutations per megabase (Mb) of exonic sequence data across sequenced genes.<sup>35,36</sup>

## RESULTS

Histopathologic examination of the tissue resected 5 weeks before nivolumab treatment (sample 6) revealed a highly proliferative atypical meningioma (Fig 2A). In contrast, tissue resected 3 weeks after nivolumab dose 2 (sample 7) had dense fibrosis with extensive immune cell infiltration and necrosis (Fig 2C). Tumor cells were absent in the hematoxylin and eosin-stained slides, but IHC with a marker of meningioma, SSTR2a<sup>30</sup> (Figs 2B and 2D), revealed one small cluster (approximately 1,000 cells/ $\mu\text{m}^2$ ) of possible residual tumor cells (which represented < 0.0001% of resected tissue; image and data not shown).

To characterize the effects of nivolumab, we profiled the tumor and its microenvironment using t-CyCIF, a method for highly multiplexed immunofluorescence imaging of formalin-fixed, paraffin-embedded specimens.<sup>32</sup> We imaged 11 markers (Data Supplement) on pre- and post-treatment samples to measure changes in immune cell types and the relative density of the immune infiltrate (Table 1; Figs 2E-2H; Appendix Fig A1; Data Supplement). We have previously shown that PD-L1 is overexpressed in tumor cells of some higher-grade meningiomas,<sup>22</sup> but, in this pretreatment specimen (sample 6), we found PD-L1 restricted to immune cells. Post-treatment (in sample 7), we observed a marked increase in IBA1+/CD14+ macrophages, CD4+ and CD8+ T cells, CD20+ B cells, and FOXP3+ regulatory T cells ( $T_{\text{reg}}$  cells; Table 1; Figs 2E-2H; Appendix Fig A1). The fraction of CD8+ T cells increased from 7% to 73% (Table 1) and CD8+ T-cell density increased from 0.5 to 304 cells/ $\text{mm}^2$ ; the CD8+ T cell-to- $T_{\text{reg}}$  ratio increased 20-fold (from 5.8 to 115; Figs 2G-2H; Data Supplement). These data are consistent with a highly active antitumor immune response after treatment.

We used targeted-exome sequencing to characterize genomic aberrations in specimens from the original resection (sample 1); the resection before treatment with bevacizumab, mifepristone, and

temozolomide (sample 4); and the resection before treatment with nivolumab (sample 6; Fig 1A; Data Supplement). This analysis revealed a significantly elevated TMB of 20.5, 26.6, and 38.0 mutations/Mb in the samples, respectively (Data Supplement).<sup>37</sup> These levels were greater than those of 228 other meningiomas sequenced as part of the BWH/DFCI profile initiative.<sup>35</sup> Copy number variation in the three samples was characteristic of higher-grade aggressive meningioma<sup>38-41</sup> (Fig 3A; Data Supplement). Notably, homozygous deletion of exons 2 to 5 of the DNA mismatch repair (MMR) gene *MSH2* was present in all three samples (Figs 3A-3B) but was absent in a peripheral-blood specimen.

IHC showed that tumor cells were negative for the *MSH2* protein and its heterodimeric partner, *MSH6*, but that expression of *MLH1* and *PMS2* protein was retained (Figs 3C-3F). Loss of *MSH2/MSH6* in sample 1 demonstrated that *MSH2* had been inactivated before any therapy and independent of temozolomide exposure, a known driver of acquired MMR deficiency in gliomas.<sup>42,43</sup> Thus, the tumor was MMR deficient at the original diagnosis, and there was a progressive increase in TMB (Data Supplement).

The patient resumed nivolumab after surgery 7 and continued biweekly therapy for more than 2 years. MRI scans have shown gradual and continued regression of enhancing lesions and associated T2/FLAIR signal abnormalities (Fig 1E). Scalp lesions have disappeared, and narcotics and dexamethasone are no longer required for pain control and cerebral edema.

Given the dramatic response of this *MSH2*-deficient tumor to nivolumab, we investigated the prevalence of elevated TMB and MMR deficiency in meningioma (Fig 3G; Data Supplement). We used sequencing data from the BWH/DFCI profile initiative ( $n = 228$  patient cases)<sup>35</sup> or BWH/DFCI patient cases screened only by MMR-protein IHC ( $n = 237$  patient cases)<sup>22,44</sup> to study specimens from 465 patients ( $n = 288$  with grade 1,  $n = 132$  with grade 2, and  $n = 45$  with grade 3 disease). Among the 228 sequenced specimens, the cohort mean TMB was 4.2 mutations/Mb (grade 1, 4.0; grade 2, 4.4; grade 3, 6.5; Data Supplement). Seven of the 228 specimens had TMBs of 10 or more mutations/Mb, a commonly used threshold for hypermutation<sup>36</sup>; one of these meningiomas (TMB, 18 mutations/Mb) had a truncating mutation in the DNA MMR

**Table 1.** Immune Profile of the Pre-Nivolumab (Sample 6) and Post-Nivolumab (Sample 7)-Treated Meningioma Samples Using t-CyCIF

Ratio	Pretreatment Total Cell No. (% of total cells)	Post-Treatment Total Cell No. (% of total cells)	Fold Change
All cells	160,967 (100)	128,307 (100)	
CD45RB+ (lymphocytes)	1,743 (1.08)	65,896 (51.36)	47.56
IBA1+/CD14+ (macrophages)	29,614 (18.4)	69,378(54.07)	2.94
CD45RB+ or IBA1+ or CD14+ (immune cells)	62,970 (39.12)	106,483 (82.99)	2.12
CD45RB-/IBA1-/CD14- (tumor cells, fibroblast)	97,997 (60.88)	21,823 (17.01)	0.28
CD45RB+/CD3+ (T cells)	513 (0.32)	42,273 (32.95)	102.97
CD45RB+/CD20+ (B cells)	43 (0.027)	3,307 (2.58)	95.56
CD45RB+/CD3+/CD4+ (CD4+ T cells)	27 (0.017)	8,457 (6.59)	387.65
CD45RB+/CD3+/CD8A+ (CD8A+ T cells)	35 (0.022)	30,906 (24.09)	1,095.00
CD45RB+/CD3+/CD4-/CD8A-	452 (0.28)	6,665 (5.19)	18.54
CD45RB+/CD3+/PD-1+	13 (0.0081)	79 (0.062)	7.65
CD45RB+/PD-L1+	2 (0.0012)	100 (0.078)	65.00
IBA1+/CD14+/PD-L1+	5 (0.0031)	59 (0.046)	14.84
CD45RB+/PD-1+/PD-L1+	0 (0)	25 (0.019)	
CD45RB+/CD3+/CD4+/FOXP3 (T <sub>reg</sub> cells)	6 (0.0037)	270 (0.21)	56.76
Ratio of CD8A+ T cells v T <sub>reg</sub> cells	5.83	114.47	19.63
Ki67+	22,239 (13.82)	7,317 (5.7)	0.41
CD45RB+/Ki67+	443 (0.28)	4,824 (3.76)	13.43
CD45RB+/CD3+/Ki67+	217 (0.13)	3,635 (2.83)	21.77
CD45RB+/CD3+/CD8A+/Ki67+	8 (0.005)	3,116 (2.43)	486
CD45RB+/CD3+/CD4+/Ki67+	9 (0.0056)	634 (0.49)	87.5
CD45RB+/CD3+/CD4-/CD8A-/Ki67+	200 (0.12)	328 (0.26)	2.17
IBA1+/CD14+/Ki67+	4,872 (3.03)	4,153 (3.24)	1.07
CD45RB-/IBA1-/CD14-/Ki67+	12,968 (8.06)	1,035 (0.81)	0.10

Abbreviations: PD-1, programmed cell death 1; PD-L1, programmed cell death 1 ligand; t-CyCIF, tissue-based multiplexed cyclic immunofluorescence; T<sub>reg</sub>, regulatory T cells.

regulator *SETD2* as well as a splice site mutation in *MSH2* of unclear functional significance. We discovered one occurrence with MMR protein loss discovered by IHC (one of 237 occurrences), and sequencing confirmed biallelic inactivation of *MSH6* and a TMB of 10 mutations/Mb (Table 2; Fig 3G; Data Supplement). Among the sequenced meningiomas, elevated TMB was significantly positively associated with anaplastic histology, Ki-67 proliferative index, and chromosomal instability<sup>38</sup> but not with prior radiotherapy, radiation induced meningioma, or recurrent tumor (Data Supplement).

In a second cohort of 615 sequenced meningiomas (Foundation Medicine cohort), 14 tumors had a TMB of more than 10 mutations/Mb. Among these 14 specimens, two grade 3 meningiomas had inactivating mutations in *MSH2* and *MSH6*; one grade 2 meningioma had a

substitution in the DNA polymerase domain of the *POLE* subunit of DNA polymerase epsilon, and another grade 3 meningioma had a truncating mutation in *SETD2* (Table 2; Fig 3G; Data Supplement). Thus, across two cohorts of sequenced meningioma samples (n = 843), 21 (2.5%) had high TMBs.<sup>36</sup> Three of 1,080 meningiomas screened by sequencing or IHC (0.3%) had detectable inactivating mutations in *MSH2* or *MSH6*. The number of notable tumors increased to six (0.6%) when MMR-related genes (eg, *SETD2*, *POLE*) were considered.

## DISCUSSION

In our patient with an *MSH2*-deficient meningioma, nivolumab treatment generated a robust anticancer immune response, as evidenced by dramatically increased infiltrating CD8+ T cells and a durable therapeutic response. Notably,

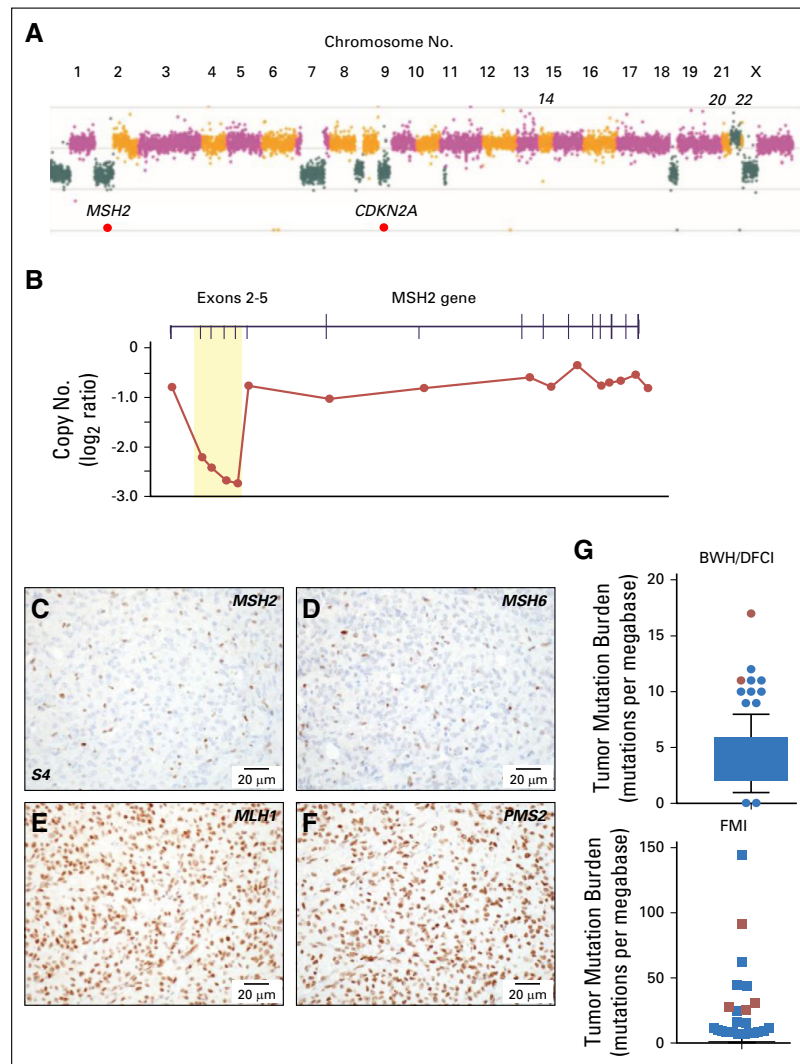


**Fig 3.** Genomic and immunohistochemical characterization of meningioma samples. (A) Copy number analysis from targeted next-generation sequencing data from sample 6 identified a genome-wide profile characteristic of a high-grade meningioma, including loss of 1p, 9p and monosomy of chromosomes 18 and 22. Focal homozygous deletion of *CDKN2A/CDKN2B* and intragenic deletion of *MSH2* were present. (B) Gene-level view of *MSH2* showed a homozygous intragenic deletion of exons 2 through 5 of *MSH2* (NM\_000251; log<sub>2</sub> ratio from -2.21 to -2.73) in the setting of 2p arm-level single copy loss. Copy number is depicted as a log<sub>2</sub> ratio value. Immunohistochemistry on pretreatment meningioma resection (surgery 4/sample 4; S4) for (C) *MSH2*, (D) *MSH6*, (E) *MLH1*, and (F) *PMS2*. *MSH2* and *MSH6* staining was present only in nontumor cells. (G) Box and whiskers plot (5th to 95th percentiles) of tumor mutational burden (TMB; mutations per megabase) for Brigham and Women's Hospital (BWH)/Dana-Farber Cancer Institute (DFCI) profile initiative cohort (n = 228 sequenced cases; Data Supplement) plus sequencing data for the mismatch repair (MMR)-deficient case BWH/DFCI 2 and for the Foundation Medicine cohort (FMI; n = 615 sequenced cases; Data Supplement). Patient cases with loss of function changes in MMR and MMR-related genes (from Table 2) are highlighted in red (dots and squares). For the BWH/DFCI profile initiative cohort, the mean TMB was 4.25 mutations/megabase (standard deviation, 2.55; standard error of the mean, 0.17; lower 95% CI of mean, 3.91; upper 95% CI of mean, 4.58). For the Foundation Medicine cohort, the mean TMB was 2.77 mutations/megabase (standard deviation, 8.08; standard error of the mean, 0.33; lower 95% CI of mean, 2.14; upper 95% CI of mean, 3.41).

**Table 2.** Additional Meningiomas With Mutations in MMR Genes and MMR-Related Genes From the BWH/DFCI Profile Initiative Cohort and the Foundation Medicine Cohort

Patient	WHO Grade	TMB (mutations/ megabase)	Gene	Amino Acid Alteration	MMR IHC in Tumor Cells
BWH/DFCI-1	3	18	<i>MSH2</i> <i>SETD2</i>	1510+8delT Splice site (VUS) E1595Sfs*15	<i>MSH2/MSH6</i> retained
BWH/DFCI-2	2	10	<i>MSH6</i>	F1088Sfs*2	<i>MSH2/MSH6</i> negative
FMI-4	3	30	<i>MSH2</i>	Homozygous deletion	NA
FMI-6	3	28	<i>MSH6</i>	C559fs*3	NA
FMI-7	3	91	<i>SETD2</i>	N34fs*77	NA
FMI-10	2	25	<i>POLE</i>	R762W	NA

Abbreviations: BWH, Brigham and Women's Hospital; DFCI, Dana-Farber Cancer Institute; fs, frameshift; IHC, immunohistochemistry; MMR, mismatch repair; NA, tissue sections not available for analysis; TMB, tumor mutational burden; VUS, variant of unknown significance.

the enlargement of lesions and increased signal abnormalities seen on the MRI after nivolumab reflected pseudoprogression, not tumor growth. In addition to inactivation of *MSH2*, sequencing of the patient's tumors revealed missense mutations in *POLD1* (R639C), *RAD50* (P571L), and *POLE* (G203E, S30L), but these changes are of unclear significance and are predicted to be nonpathogenic.<sup>45</sup> An increase in TMB from 26.6 mutations/MB in sample 4 (before experimental therapies) to 38.0 in sample 6 raises the possibility that temozolomide can augment TMB in meningioma. However, this neoplasm was MMR deficient at the time of original diagnosis; thus, temozolomide did not drive acquired MMR deficiency.

This work also shows that approximately 2.5% of meningiomas have a high mutation burden, a phenotype that has been linked with neoantigen

expression in other tumor types.<sup>46,47</sup> In a subset of mutation-rich meningiomas, loss of function alterations in MMR and MMR-related genes can be detected. It is possible that other, as yet unknown or undetected, mutations contribute to high TMB in the remaining tumors. In all, this first report, to our knowledge, of a dramatic response of an MMR-deficient meningioma to immunotherapy and our characterization of meningioma cohorts from two different institutions indicate that screening meningiomas is warranted to identify a molecularly defined subtype that is likely responsive to immunotherapy.

DOI: <https://doi.org/10.1200/PO.18.00190>  
Published online on [ascopubs.org/journal/po](https://ascopubs.org/journal/po) on  
November 27, 2018.

#### AUTHOR CONTRIBUTIONS:

**Conception and design:** Ian F. Dunn, Mehdi Touat, Peter K. Sorger, Keith L. Ligon, Sandro Santagata, David A. Reardon

**Provision of study material or patients:** Ian F. Dunn, Michael B. Sisti, Peter D. Canoll, Keith L. Ligon, Sandro Santagata, David A. Reardon

**Administrative support:** Eric Severson, Brenda Acevedo

**Financial support:** Peter K. Sorger, Sandro Santagata

**Data analysis and interpretation:** Mehdi Touat, Patrick Y. Wen, Renato Umeton, Adrian M. Dubuc, Matthew Ducar, Peter D. Canoll, Eric Severson, Shakti H. Ramkissoon, Jia-Ren Lin, Peter K. Sorger, Keith L. Ligon, Sandro Santagata, David A. Reardon

**Collection and assembly of data:** Ziming Du, Mehdi Touat, Michael B. Sisti, Julia A. Elvin, Shakti H.

Ramkissoon, Lais Cabrera, Brenda Acevedo, Keith L. Ligon, Sandro Santagata, David A. Reardon

**Manuscript writing:** All authors

**Final approval of manuscript:** All authors

#### AUTHORS' DISCLOSURES OF POTENTIAL CONFLICTS OF INTEREST

The following represents disclosure information provided by authors of this manuscript. All relationships are considered compensated. Relationships are self-held unless noted. I = Immediate Family Member, Inst = My Institution. Relationships may not relate to the subject matter of this manuscript. For more information about ASCO's conflict of interest policy, please refer to [www.asco.org/rwc](http://www.asco.org/rwc) or [ascopubs.org/po/author-center](http://ascopubs.org/po/author-center).

**Ian F. Dunn**

No relationship to disclose

[ascopubs.org/journal/po](https://ascopubs.org/journal/po) JCO™ Precision Oncology 7

Downloaded from [ascopubs.org](https://ascopubs.org) by ASCO on November 29, 2018 from 066.102.234.242  
Copyright © 2018 American Society of Clinical Oncology. All rights reserved.

**Ziming Du**

No relationship to disclose

**Mehdi Touat****Consulting or Advisory Role:** Agios, Taiho Pharmaceutical  
**Travel, Accommodations, Expenses:** Merck Sharp & Dohme**Michael B. Sisti**

No relationship to disclose

**Patrick Y. Wen****Consulting or Advisory Role:** AbbVie, Genentech, Roche, Agios, AstraZeneca, Karyopharm Therapeutics, Vivus, Monteris Medical, Aurora Biopharma, Vascular Biogenics, Kadmon, Ziopharm Oncology, GW Pharmaceuticals, Lilly, Immunomic Therapeutics**Speakers' Bureau:** Merck**Research Funding:** Agios (Inst), Abbvie (Inst), Angiochem (Inst), Genentech (Inst), Roche (Inst), GlaxoSmithKline (Inst), AstraZeneca (Inst), ImmunoCellular Therapeutics (Inst), Karyopharm Therapeutics (Inst), Merck (Inst), Novartis (Inst), Oncoceutics (Inst), Sanofi (Inst), ARIAD (Inst), Vascular Biogenics (Inst), Lilly**Research Funding:** Karyopharm Therapeutics**Renato Umeton**

No relationship to disclose

**Adrian M. Dubuc**

No relationship to disclose

**Matthew Ducar**

No relationship to disclose

**Peter D. Canoll**

No relationship to disclose

**Eric Severson****Employment:** Foundation Medicine, Partners Healthcare**Julia A. Elvin****Employment:** Foundation Medicine**Stock and Other Ownership Interests:** Foundation Medicine**Shakti H. Ramkissoon****Employment:** Foundation Medicine**Stock and Other Ownership Interests:** Foundation Medicine**Affiliations****Ian F. Dunn, Ziming Du, Patrick Y. Wen, Adrian M. Dubuc, Keith L. Ligon, and Sandro Santagata**, Brigham and Women's Hospital; **Ziming Du, Jia-Ren Lin, Peter K. Sorger, and Sandro Santagata**, Harvard Medical School; **Mehdi Touat, Patrick Y. Wen, Renato Umeton, Matthew Ducar, Lais Cabrera, Brenda Acevedo, Keith L. Ligon, Sandro Santagata, and David A. Reardon**, Dana-Farber Cancer Institute, Boston; **Julia A. Elvin**, Foundation Medicine, Cambridge, MA; **Michael B. Sisti and Peter D. Canoll**, Columbia University Medical Center, New York City, NY; **Eric Severson and Shakti H. Ramkissoon**, Foundation Medicine, Morrisville; and **Shakti H. Ramkissoon**, Wake Forest School of Medicine, Winston-Salem, NC.**Support**

Supported by the Ludwig Center at Harvard Medical School (P.K.S. and S.S.) and by National Cancer Institute Grant No. U54-CA225088 (to P.K.S. and S.S.).

**Jia-Ren Lin**

No relationship to disclose

**Lais Cabrera**

No relationship to disclose

**Brenda Acevedo**

No relationship to disclose

**Peter K. Sorger****Leadership:** RareCyte, Merrimack, Applied BioMath**Stock and Other Ownership Interests:** RareCyte, Merrimack, Applied BioMath, Glencoe Software**Honoraria:** Novartis**Research Funding:** Merck (Inst)**Keith L. Ligon****Stock and Other Ownership Interests:** Travera**Consulting or Advisory Role:** Midatech**Research Funding:** Plexikon (Inst), Amgen (Inst), X4 Pharma (Inst), Tragara (Inst), Bristol-Myers Squibb (Inst)**Patents, Royalties, Other Intellectual Property:**

Molecular Diagnostics Assay patent

**Sandro Santagata****Consulting or Advisory Role:** RareCyte**David A. Reardon****Honoraria:** AbbVie, Cavion, Genentech, Roche, Merck, Midatech, Momenta Pharmaceuticals, Novartis, Novocure, Regeneron, Stemline Therapeutics, Celldex, Oxigene, Monteris Medical, Bristol-Myers Squibb, Juno Therapeutics, Inovio Pharmaceuticals, Oncorus**Consulting or Advisory Role:** Cavion, Genentech, Roche, Merck, Momenta Pharmaceuticals, Novartis, Novocure, Regeneron, Stemline Therapeutics, Bristol-Myers Squibb, Inovio Pharmaceuticals, Juno Therapeutics, Celldex, Oxigene, Monteris Medical, Midatech, Oncorus**Research Funding:** Celldex (Inst), Incyte (Inst), Midatech (Inst), Tragara (Inst), Inovio Pharmaceuticals (Inst), Agenus (Inst), EMD Serono (Inst), Acerta Pharma (Inst)**ACKNOWLEDGMENT**

We thank George Zanazzi, MD, for assistance with sample procurement, the staff at the Brigham and Women's Hospital Center for Advanced Molecular Diagnostics for sequencing, Terri Woo for assistance with immunohistochemistry, and members of the Lab for Systems Pharmacology for helpful comments on the manuscript.

## REFERENCES

1. Zhang AS, Ostrom QT, Kruchko C, et al: Complete prevalence of malignant primary brain tumors registry data in the United States compared with other common cancers, 2010. *Neuro-oncol* 19:726-735, 2017
2. Kaley T, Barani I, Chamberlain M, et al: Historical benchmarks for medical therapy trials in surgery- and radiation-refractory meningioma: A RANO review. *Neuro-oncol* 16:829-840, 2014
3. Goldbrunner R, Minniti G, Preusser M, et al: EANO guidelines for the diagnosis and treatment of meningiomas. *Lancet Oncol* 17:e383-e391, 2016
4. Furtner J, Schöpf V, Seystahl K, et al: Kinetics of tumor size and peritumoral brain edema before, during, and after systemic therapy in recurrent WHO grade II or III meningioma. *Neuro-oncol* 18:401-407, 2016
5. Brastianos PK, Horowitz PM, Santagata S, et al: Genomic sequencing of meningiomas identifies oncogenic SMO and AKT1 mutations. *Nat Genet* 45:285-289, 2013
6. Clark VE, Erson-Omay EZ, Serin A, et al: Genomic analysis of non-NF2 meningiomas reveals mutations in TRAF7, KLF4, AKT1, and SMO. *Science* 339:1077-1080, 2013
7. Reuss DE, Piro RM, Jones DTW, et al: Secretory meningiomas are defined by combined KLF4 K409Q and TRAF7 mutations. *Acta Neuropathol* 125:351-358, 2013
8. Clark VE, Harmanci AS, Bai H, et al: Recurrent somatic mutations in POLR2A define a distinct subset of meningiomas. *Nat Genet* 48:1253-1259, 2016
9. Abedalthagafi MS, Merrill PH, Bi WL, et al: Angiomatous meningiomas have a distinct genetic profile with multiple chromosomal polysomies including polysomy of chromosome 5. *Oncotarget* 5:10596-10606, 2014
10. Abedalthagafi MS, Bi WL, Merrill PH, et al: ARID1A and TERT promoter mutations in dedifferentiated meningioma. *Cancer Genet* 208:345-350, 2015
11. Abedalthagafi M, Bi WL, Aizer AA, et al: Oncogenic PI3K mutations are as common as AKT1 and SMO mutations in meningioma. *Neuro-oncol* 18:649-655, 2016
12. Sahn F, Schrimpf D, Olar A, et al: TERT promoter mutations and risk of recurrence in meningioma. *J Natl Cancer Inst* 108:108, 2015
13. Peyre M, Gaillard S, de Marcellus C, et al: Progesterin-associated shift of meningioma mutational landscape. *Ann Oncol* 29:681-686, 2017
14. Shankar GM, Abedalthagafi M, Vaubel RA, et al: Germline and somatic BAP1 mutations in high-grade rhabdoid meningiomas. *Neuro-oncol* 19:535-545, 2017
15. Peyre M, Gauchotte G, Giry M, et al: De novo and secondary anaplastic meningiomas: A study of clinical and histomolecular prognostic factors. *Neuro-oncol* 20:1113-1121, 2018
16. Guerrini-Rousseau L, Dufour C, Varlet P, et al: Germline SUFU mutation carriers and medulloblastoma: Clinical characteristics, cancer risk and prognosis. *Neuro-oncol* 20:1122-1132, 2017
17. Juratli TA, McCabe D, Nayyar N, et al: DMD genomic deletions characterize a subset of progressive/higher-grade meningiomas with poor outcome. *Acta Neuropathol* 136:779-792, 2018
18. Nowosielski M, Galldiks N, Iglseder S, et al: Diagnostic challenges in meningioma. *Neuro-oncol* 19:1588-1598, 2017
19. Yesilöz Ü, Kirches E, Hartmann C, et al: Frequent AKT1 E17K mutations in skull base meningiomas are associated with mTOR and ERK1/2 activation and reduced time to tumor recurrence. *Neuro-oncol* 19:1088-1096, 2017
20. Boetto J, Bielle F, Sanson M, et al: SMO mutation status defines a distinct and frequent molecular subgroup in olfactory groove meningiomas. *Neuro-oncol* 19:345-351, 2017

21. Weller M, Roth P, Sahm F, et al: Durable control of metastatic AKT1-mutant WHO grade 1 meningothelial meningioma by the AKT inhibitor, AZD5363. *J Natl Cancer Inst* 109:1-4, 2017
22. Du Z, Abedalthagafi M, Aizer AA, et al: Increased expression of the immune modulatory molecule PD-L1 (CD274) in anaplastic meningioma. *Oncotarget* 6:4704-4716, 2015
23. Han SJ, Reis G, Kohanbash G, et al: Expression and prognostic impact of immune modulatory molecule PD-L1 in meningioma. *J Neurooncol* 130:543-552, 2016
24. Wang S, Liechty B, Patel S, et al: Programmed death ligand 1 expression and tumor infiltrating lymphocytes in neurofibromatosis type 1 and 2 associated tumors. *J Neurooncol* 138:183-190, 2018
25. Fang L, Lowther DE, Meizlish ML, et al: The immune cell infiltrate populating meningiomas is composed of mature, antigen-experienced T and B cells. *Neuro-oncol* 15:1479-1490, 2013
26. Domingues PH, Teodósio C, Otero Á, et al: Association between inflammatory infiltrates and isolated monosomy 22/del(22q) in meningiomas. *PLoS One* 8:e74798, 2013
27. Domingues PH, Teodósio C, Ortiz J, et al: Immunophenotypic identification and characterization of tumor cells and infiltrating cell populations in meningiomas. *Am J Pathol* 181:1749-1761, 2012
28. Talari NK, Panigrahi M, Madigubba S, et al: Altered tryptophan metabolism in human meningioma. *J Neurooncol* 130:69-77, 2016
29. Bi WL, Greenwald NF, Abedalthagafi M, et al: Genomic landscape of high-grade meningiomas. *NPJ Genom Med* 2:pii:15, 2017
30. Menke JR, Raleigh DR, Gown AM, et al: Somatostatin receptor 2a is a more sensitive diagnostic marker of meningioma than epithelial membrane antigen. *Acta Neuropathol* 130:441-443, 2015
31. Watkins JC, Yang EJ, Muto MG, et al: Universal screening for mismatch-repair deficiency in endometrial cancers to identify patients with Lynch syndrome and Lynch-like syndrome. *Int J Gynecol Pathol* 36:115-127, 2017
32. Lin J-R, Izar B, Wang S, et al: Highly multiplexed immunofluorescence imaging of human tissues and tumors using t-CyCIF and conventional optical microscopes. *eLife* 7:7, 2018
33. Coy S, Rashid R, Lin J-R, et al: Multiplexed immunofluorescence reveals potential PD-1/PD-L1 pathway vulnerabilities in craniopharyngioma. *Neuro-oncol* 20:1101-1112, 2018
34. Ramkissoon SH, Bandopadhyay P, Hwang J, et al: Clinical targeted exome-based sequencing in combination with genome-wide copy number profiling: precision medicine analysis of 203 pediatric brain tumors. *Neuro-oncol* 19:986-996, 2017
35. Sholl LM, Do K, Shivdasani P, et al: Institutional implementation of clinical tumor profiling on an unselected cancer population. *JCI Insight* 1:e87062, 2016
36. Campbell BB, Light N, Fabrizio D, et al: Comprehensive analysis of hypermutation in human cancer. *Cell* 171:1042-1056.e10, 2017
37. Nowak JA, Yurgelun MB, Bruce JL, et al: Detection of mismatch repair deficiency and microsatellite instability in colorectal adenocarcinoma by targeted next-generation sequencing. *J Mol Diagn* 19:84-91, 2017
38. Aizer AA, Abedalthagafi M, Bi WL, et al: A prognostic cytogenetic scoring system to guide the adjuvant management of patients with atypical meningioma. *Neuro-oncol* 18:269-274, 2016
39. Sahm F, Schrimpf D, Stichel D, et al: DNA methylation-based classification and grading system for meningioma: A multicentre, retrospective analysis. *Lancet Oncol* 18:682-694, 2017
40. Olar A, Wani KM, Wilson CD, et al: Global epigenetic profiling identifies methylation subgroups associated with recurrence-free survival in meningioma. *Acta Neuropathol* 133:431-444, 2017
41. Louis DN, Perry A, Reifenberger G, et al: The 2016 World Health Organization classification of tumors of the central nervous system: A summary. *Acta Neuropathol* 131:803-820, 2016

42. Cahill DP, Levine KK, Betensky RA, et al: Loss of the mismatch repair protein MSH6 in human glioblastomas is associated with tumor progression during temozolomide treatment. *Clin Cancer Res* 13:2038-2045, 2007
43. Hunter C, Smith R, Cahill DP, et al: A hypermutation phenotype and somatic MSH6 mutations in recurrent human malignant gliomas after alkylator chemotherapy. *Cancer Res* 66:3987-3991, 2006
44. Du Z, Brewster R, Merrill PH, et al: Meningioma transcription factors link cell lineage with systemic metabolic cues. *Neuro-oncol* 20:1331-1343, 2018
45. Shihab HA, Gough J, Cooper DN, et al: Predicting the functional, molecular, and phenotypic consequences of amino acid substitutions using hidden Markov models. *Hum Mutat* 34:57-65, 2013
46. Germano G, Lamba S, Rospo G, et al: Inactivation of DNA repair triggers neoantigen generation and impairs tumour growth. *Nature* 552:116-120, 2017
47. Rizvi NA, Hellmann MD, Snyder A, et al: Cancer immunology: Mutational landscape determines sensitivity to PD-1 blockade in non-small-cell lung cancer. *Science* 348:124-128, 2015

## Appendix

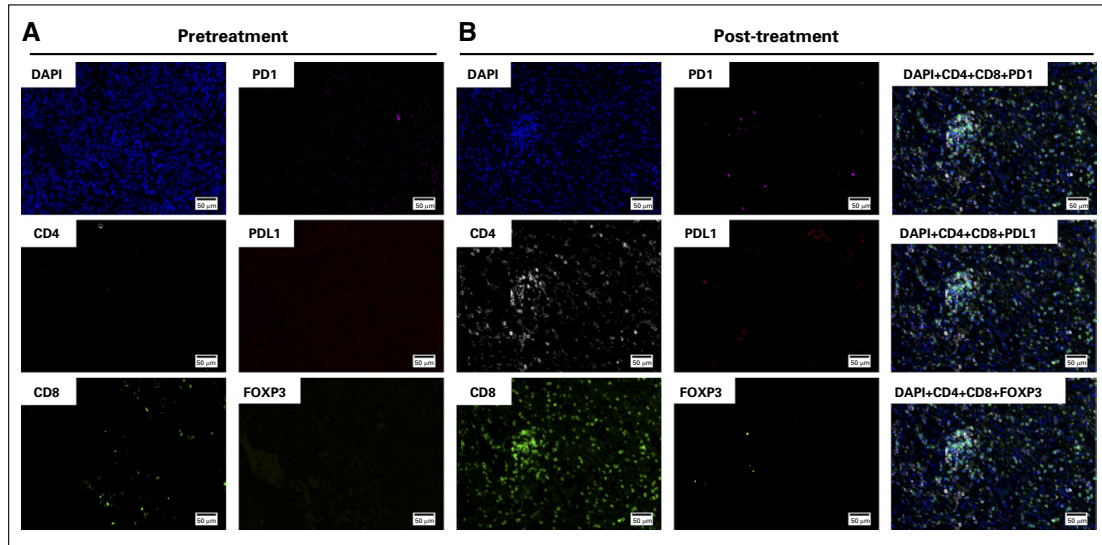


**Fig A1.** Tissue-based multiplexed cyclic immunofluorescence (t-CyCIF) characterization of resection tissues before and after nivolumab treatment. (A) A representative field of view of t-CyCIF imaging data of selected biomarkers generated from a single section of pretreatment meningioma (surgery 6/sample 6). (B) A representative field of view of t-CyCIF imaging data of selected biomarkers generated from a single section of the post-treatment meningioma (surgery 7/sample 7). FOXP3, forkhead box P3; PD-1, programmed death 1; PD-L1, programmed death ligand 1.

**VI. Autres articles publiés pendant la Thèse de Sciences /  
Other articles published during the Science Thesis**

**A. Revue sur le développement de thérapies ciblées dans les gliomes  
malins / Review on the development of targeted therapies in gliomas**

REVIEW

# Glioblastoma targeted therapy: updated approaches from recent biological insights

M. Touat<sup>1,2</sup>, A. Idbaih<sup>1,3</sup>, M. Sanson<sup>1,3</sup> & K. L. Ligon<sup>4\*</sup>

<sup>1</sup>Inserm U 1127, CNRS UMR 7225, Sorbonne Universités, UPMC Univ Paris 06 UMR S 1127, Institut du Cerveau et de la Moelle épinière, ICM, Paris; <sup>2</sup>Gustave Roussy, Université Paris-Saclay, Département d'Innovation Thérapeutique et d'Essais Précoces (DITEP), Villejuif; <sup>3</sup>AP-HP, Hôpitaux Universitaires La Pitié Salpêtrière - Charles Foix, Service de Neurologie 2-Mazarin, Paris, France; <sup>4</sup>Department of Oncologic Pathology, Dana-Farber/Brigham and Women's Cancer Center, Boston, USA

\*Correspondence to: Dr Keith L. Ligon, Dana-Farber Cancer Institute, 450 Brookline Avenue, JF215B Boston, MA 02215, USA. Tel: +1-617-632-2357; E-mail: keith\_ligon@dfci.harvard.edu

Glioblastoma (WHO grade IV astrocytoma) is the most frequent primary brain tumor in adults, representing a highly heterogeneous group of neoplasms that are among the most aggressive and challenging cancers to treat. An improved understanding of the molecular pathways that drive malignancy in glioblastoma has led to the development of various biomarkers and the evaluation of several agents specifically targeting tumor cells and the tumor microenvironment. A number of rational approaches are being investigated, including therapies targeting tumor growth factor receptors and downstream pathways, cell cycle and epigenetic regulation, angiogenesis and antitumor immune response. Moreover, recent identification and validation of prognostic and predictive biomarkers have allowed implementation of modern trial designs based on matching molecular features of tumors to targeted therapeutics. However, while occasional targeted therapy responses have been documented in patients, to date no targeted therapy has been formally validated as effective in clinical trials. The lack of knowledge about relevant molecular drivers *in vivo* combined with a lack of highly bioactive and brain penetrant-targeted therapies remain significant challenges. In this article, we review the most promising biological insights that have opened the way for the development of targeted therapies in glioblastoma, and examine recent data from clinical trials evaluating targeted therapies and immunotherapies. We discuss challenges and opportunities for the development of these agents in glioblastoma.

**Key words:** glioma, cancer genomics, targeted therapies, precision medicine, personalized medicine, biomarkers

## Introduction

Glioblastoma is the most frequent and aggressive primary malignant brain tumor in adults [1], with a median overall survival (OS) between 10 and 20 months [2–4]. Standard of care is maximal safe surgery followed by concomitant radio-chemotherapy and adjuvant chemotherapy with temozolomide, which can be combined with intermediate-frequency alternating electric fields [2, 4, 5]. Once recurrence occurs, therapeutic options are limited, including bevacizumab and nitrosoureas, although bevacizumab is not approved in Europe. Unlike in most other cancers, this lack of progress has been sustained despite growing insight into the biology of the disease [6–11]. Fortunately, these significant advances have continued to stimulate the development and re-purposing of numerous targeted therapies in clinical trials.

## Genomic landscape of glioblastoma

Glioblastomas constitute a highly heterogeneous group of invasive malignant brain tumors [12]. It was the first tumor to undergo comprehensive molecular characterization [6–10, 13–15]. Briefly, these studies showed that most tumors harbor recurrent molecular alterations disrupting core pathways involved in regulation of growth (receptor tyrosine kinase [RTK], mitogen-activated protein kinase [MAPK] and phosphoinositide 3-kinase [PI3K] signaling pathways), cell cycle, DNA repair and apoptosis (Retinoblastoma/E2F and p53 tumor suppressor pathways) as well as control of chromatin state and telomere length (Table 1). Frequently, these alterations derive from copy number aberrations (CNAs). The most common amplification events involve chromosomes 7 (*EGFR/MET/CDK6*), 12 (*CDK4* and *MDM2*) and 4 (*PDGFRA*), while recurrent

homozygous deletions are found in chromosomes 9 (*CDKN2A/B*) and 10 (*PTEN*). In addition, genome-wide sequencing highlighted single nucleotide variants (SNVs) and short insertions and deletions, resulting in recurrent mutations in the *TERT* promoter, *PTEN*, *TP53*, *EGFR*, *PIK3CA*, *PIK3R1*, *NF1* and *RBI* [10].

Most of these recurrent and biologically relevant genomic variants continue to be attractive targets for drug development [16–23] (Table 1). However, none of the recurrent genomic variants in glioblastoma has been strongly associated with clear prognostic and predictive value so far. This challenges the assumption that these variants are necessarily obligate cancer drivers in glioblastoma and suggests that strong cancer cell plasticity and redundancy among alterations that drive tumor growth may contribute to therapy failure more than previously assumed (Figure 1). Increasingly, it is being recognized that glioblastomas are characterized by significant inter- and intra-tumor genomic heterogeneity, which can exist as temporal or spatial [10, 24–33]. This represents challenges for appropriate driver identification due to glioblastoma being inherently limited in the amount and locations that one can sample, as well as the limited opportunities for reoperation [34–36]. The evidence that such heterogeneity might be relevant comes from multisector genome-wide sequencing of primary and post-treatment tumors, which revealed substantial divergence in the landscape of driver alterations between primary and recurrent tumors [30, 32, 33, 37, 38]. Moreover, heterogeneity at the single cell level can exist as multiple genomic alterations within redundant pathways (e.g. mosaic amplifications of *EGFR*, *MET* and *PDGFRA*) [10, 24, 29, 39, 40], or multiple unique variants of a single gene (e.g. multiple *EGFR* oncogenic variants in a single cell) [29, 30, 40], which overall results in heterogeneity in drug sensitivity within individual tumor cells [41] (Figure 1).

## Targeting growth factor receptors and their downstream signaling pathways

Drugs directed against alterations that lead to constitutive activation of growth factor RTKs are the most common type of targeted therapy in all types of cancer with successful responses seen in many cancers. These drugs have also been of great interest in glioblastoma because direct alterations in RTKs and/or downstream MAPK/PI3K signaling pathways represent a hallmark of this tumor (Table 1) [10].

### EGFR-targeted therapies

*EGFR* amplification, rearrangement or point mutations are found in approximately half of glioblastomas and multiple alterations in *EGFR* often co-exist within an individual tumor [10, 30, 42–44]. Nearly 20% of glioblastomas harbor deletion of exons 2–7 of *EGFR*, resulting in EGFRvIII, a constitutively active oncogenic variant frequently associated with *EGFR* amplification. Preclinical studies have demonstrated that EGFRvIII-driven tumors are only weakly sensitive to first generation EGFR tyrosine kinase inhibitors (TKI) erlotinib and gefitinib [45, 46]. Indeed, EGFRvIII—as most other *EGFR* SNVs found in glioblastoma—alters the extracellular domain of EGFR in glioblastoma, while in contrast lung adenocarcinomas typically harbor direct activating mutations in the kinase domain [45].

Rindopepimut is an EGFRvIII peptide vaccine that demonstrated signs of activity in preclinical models of glioblastoma and early phase trials [16, 47, 48]. The recently completed randomized phase II study ReACT evaluated the association of rindopepimut plus bevacizumab in EGFRvIII-positive recurrent glioblastoma.

**Table 1. Genomic alterations and example targeted therapies in glioblastoma**

Gene	Alteration or target	Target frequency in glioblastoma <sup>a</sup> (%)	Candidate therapy (drug example)
<b>Growth factor receptors</b>			
<i>EGFR</i>	Deletion (EGFRvIII), mutation, translocation and/or amplification	55	EGFR vaccine or antibody-drug conjugate (rindopepimut, ABT-414)
<i>KIT</i>	Amplification, mutation	10	KIT inhibitor (imatinib)
<i>PDGFRA</i>	Amplification	15	PDGFR inhibitor (dasatinib)
<i>FGFR1, FGFR3</i>	Translocation (e.g. FGFR3-TACC3)	3	FGFR1/3 inhibitor (JNJ-42756493)
<i>MET</i>	Amplification, translocation	3	MET inhibitor (cabozantinib)
<b>MAPK and PI3K/mTOR signaling pathways</b>			
<i>PTEN</i>	Deletion, mutation	40	AKT inhibitor, mTOR inhibitor (voxtalisib)
<i>PIK3CA</i>	Amplification, mutation	10	mTOR inhibitor, PI3K inhibitor (buparlisib)
<i>NF1</i>	Deletion, mutation	14	MEK inhibitor (trametinib)
<i>BRAF</i>	Mutation (BRAF V600E)	2	BRAF inhibitor (vemurafenib), MEK inhibitor (trametinib)
<b>Cell cycle pathways</b>			
<i>MDM2</i>	Amplification	10	MDM2 inhibitor (AMG232)
<i>TP53</i>	Wild-type (no mutations)	60	MDM2 inhibitor (AMG232)
<i>CDK4/6</i>	Amplification	20	CDK4/6 inhibitor (ribociclib)
<i>RBI</i>	Wild-type (no mutations)	90	CDK4/6 inhibitor (ribociclib)
<b>Others</b>			
<i>IDH1</i>	Mutation	6	IDH1 inhibitor (AG120)
<i>MYC, MYCN</i>	Amplification	5	Bromodomain inhibitor (OTX-015)

<sup>a</sup>Source: cbiportal.org (glioblastoma TCGA dataset, n = 281 tumor samples with sequencing and CNA data) [10].

Advantage to rindopepimut therapy was reported across multiple endpoints including 2-year OS rate and progression-free survival (PFS), although the trial failed to meet its primary endpoint [49] (Table 2). Preliminary analyses from the phase III randomized study of rindopepimut in newly diagnosed EGFRvIII-positive glioblastoma indicated that its benefit on OS will not reach statistical significance (23 months from diagnosis in both arms), resulting in the closure of the trial [50]. Subgroup analyses suggested that rindopepimut might have failed due to reduced amount of EGFRvIII antigen burden in patients that underwent gross total resection (2-year survival rate of 30% in patients with non-minimal residual disease versus 19% in patients with minimal residual disease), although these results will need confirmation after longer follow-up. Further development of rindopepimut is uncertain.

Other EGFRvIII-targeted therapies are being evaluated. ABT-114 is an antibody drug conjugate (ADC) consisting of an anti-

EGFR MAb, conjugated to the tubulin inhibitor monomethylauristatin F. ABT-114 demonstrated cytotoxicity against glioblastoma patient-derived xenograft models expressing either wild-type EGFR or EGFRvIII [51]. Preliminary data from a phase I trial of ABT-114 monotherapy in EGFR-amplified recurrent glioblastoma showed a 6 months PFS rate of 28.3% [52] (Table 2). OS from trial entry was 9 months, which was considered encouraging, as 56% of patients had already undergone two to three prior therapies. No dose-limiting toxicity was reported, although specific ocular toxicities were frequently observed (mostly reversible blurred vision, with some patients presenting with keratitis or corneal epithelial microcysts). The clinical development of ABT-114 is ongoing with randomized phase II/III trials (Table 3).

In addition, several trials have evaluated more broadly effective EGFR-targeted therapies (Table 2). A variety of first and second

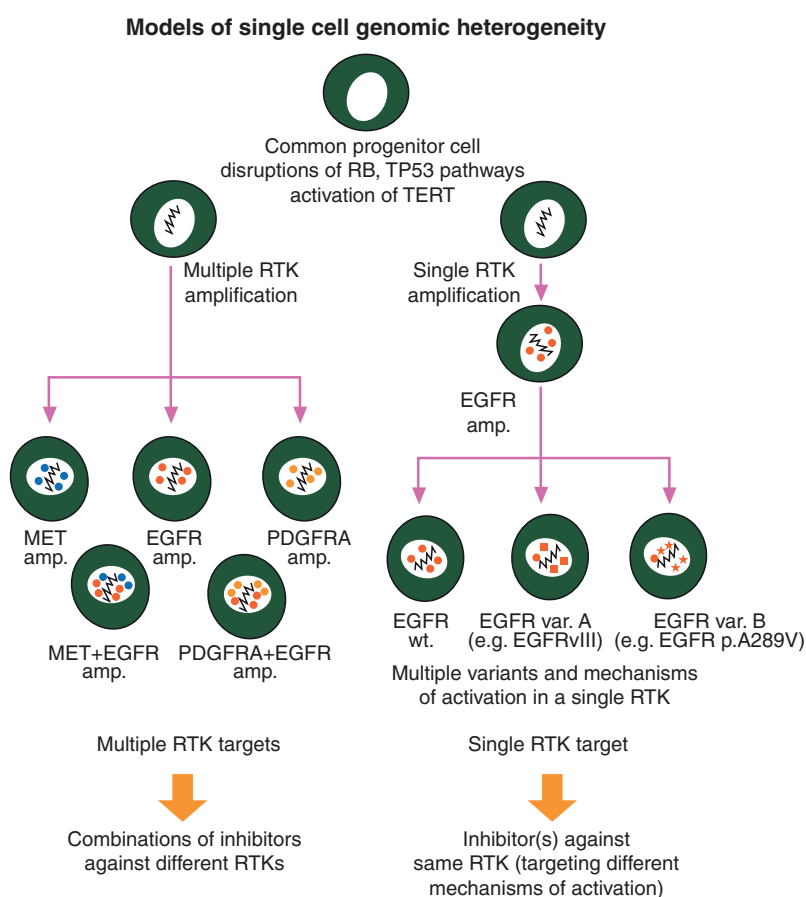


**Figure 1.** Cellular heterogeneity of RTK aberrations in glioblastoma: implications for appropriate drug targeting (adapted from Francis et al. [30]). Dynamics of the glioblastoma genome may generate or select for subclonal populations of tumor cells that are highly resistant to treatment, overall suggesting that comprehensive characterization of tumor heterogeneity is a prerequisite for the success of pharmacological inhibition of RTK alterations. Left, multiple amplifications of distinct RTK genes can be observed in non-overlapping subclonal populations from individual tumors, or within individual tumor cells. In other cases (right), tumor heterogeneity may exist as multiple alterations within a single RTK gene.

Table 2. Recently reported trials of targeted therapies in recurrent glioblastoma

Design	Drug regimen	Target(s)	Population, number of patients (n)	Median OS (months)	Median PFS (months)	PFS-6	Reference
<b>Growth factor receptors, MAPK/PI3K signaling pathways</b>							
Phase II, randomized	Onartuzumab + bevacizumab (ona/beva) or bevacizumab + placebo (beva/p)	MET (onartuzumab), VEGF (bevacizumab)	First recurrence, n = 64 (ona/beva), n = 65 (beva/p)	8.8 (ona/beva), 12.6 (beva/p)	3.9 (ona/beva), 2.9 (beva/p)	33.9% (ona/beva), 29% (beva/p)	[97]
Phase II, double-blind, randomized	Bevacizumab + rindopepimut (beva/rindo) or bevacizumab + placebo (beva/p)	VEGF (bevacizumab), EGFRvIII (rindopepimut)	First or second recurrence, bevacizumab-naïve, EGFRvIII-positive, n = 73	11.6 (beva/rindo), 9.3 (beva/p)	NA	28% (beva/rindo), 16% (beva/p)	[49]
Phase II, randomized	Temozolomide (TMZ) or afatinib (afa) or afatinib + temozolomide (afa/TMZ)	EGFR (Afatinib)	First recurrence, n = 39 (TMZ), n = 41 (afa), n = 39 (afa/TMZ)	10.6 (TMZ), 9.8 (afa), 8 (afa/TMZ)	1.9 (TMZ), 1 (afa), 1.5 (afa/TMZ)	23% (TMZ), 3% (afa), 10% (afa/TMZ)	[62]
Phase I, single-agent	ABT-414	EGFR, EGFRvIII	Any recurrence, n = 60	9.0	NA	28.3%	[52]
Phase II, single-agent	PX-866	PI3K	First recurrence, n = 33	NA	NA	17%	[101]
Phase II, single-arm	Buparlisib + bevacizumab	PI3K (buparlisib), VEGF (bevacizumab)	First recurrence, n = 68	10.8	5.3	NA	[102]
Phase II, single-arm	Erlotinib + sorafenib	EGFR (erlotinib), VEGFR, PDGFR, Raf kinases (sorafenib)	NA, n = 56	5.7	2.5	14%	[71]
<b>DNA repair and other epigenetic modifiers</b>							
Phase II, randomized	Bevacizumab (beva) + vorinostat (beva/vor) or bevacizumab (beva)	Histone deacetylases (vorinostat), VEGF (bevacizumab)	First recurrence, n = 49 (beva/vor), n = 41 (beva)	8.3 (beva/vor), 7.0 (beva)	4.2 (beva/vor), 3.6 (beva)	NA	[154]
Phase II, randomized	Sequential temozolomide + veliparib	PARP (veliparib)	NA, n = 141	10.3 (beva-naïve), 4.7 (beva-resistant)	2.0 (beva-naïve), 2.0 (beva-resistant)	17.0% (beva-naïve), 4.4% (beva-resistant)	[129]
Phase II, single-arm	Panobinostat + bevacizumab	Histone deacetylases (panobinostat), VEGF (bevacizumab)	First or second recurrence, n = 24	9.0	5.0	30.4%	[143]
<b>Antiangiogenics</b>							
Phase III, double-blind, randomized	Lomustine + bevacizumab (lom/beva) vs. lomustine (lom)	VEGF (beva)	First recurrence, n = 288 (lom/beva), n = 149 (lom)	9.1 (lom/beva), 8.6 (lom)	4.2 (lom/beva), 1.5 (lom)	NA	[169]
Phase III, double-blind, randomized	CCNU + placebo (CCNU) or cediranib (ced) or cediranib + CCNU (CCNU/ced)	VEGFR1-3 and PDGFR (ced)	First recurrence, n = 65 (CCNU), n = 131 (ced), n = 129 (CCNU/ced)	9.8 (CCNU), 8.0 (ced), 9.4 (CCNU/ced)	2.7 (CCNU), 3.1 (ced), 4.2 (CCNU/ced)	24.5% (CCNU), 16% (ced), 34.5% (CCNU/ced)	[155]
Phase II, randomized	Axitinib (axi) or physician's choice (lomustine or bevacizumab)		First recurrence, n = 22 (axi), n = 22 (control)	6.3 (axi), 3.7 (control)		34% (axi), 28% (control)	[165]

Continued

**Table 2. Continued**

Design	Drug regimen	Target(s)	Population, number of patients (n)	Median OS (months)	Median PFS (months)	PFS-6	Reference
Phase II, randomized	Bevacizumab + placebo (beva/p) vs. bevacizumab + dasatinib (beva/dasa)	SRC, c-KIT, EPHA2, PDGFR (dasa), VEGF (beva)	First or second recurrence, n = 38 (beva/p), n = 83 (beva/dasa)	7.9 (beva/p), 7.2 (beva/dasa)	NA	18.4% (beva/p), 27.2% (beva/dasa)	[164]
Phase II, single-agent	Dasatinib	SRC, c-KIT, EPHA2, PDGFR	First recurrence, overexpression of at least 2 putative dasatinib targets, n = 50	7.9	1.7	6%	[84]
Phase II, single-arm	Pazopanib + lapatinib	VEGFR1-3, c-Kit, PDGFR (pazopanib), EGFR (lapatinib)	NA, n = 41	NA	1.9	7.5%	[65]
Phase II, single-agent	Sunitinib	VEGFR1-2, c-Kit, PDGFR, FLT3, CSF-1R, RET	NA, n = 63	9.4 (beva-naïve), 4.4 (beva-resistant)	1 (beva-naïve), 1 (beva-resistant)	10.4% (beva-naïve), 0% (beva-resistant)	[152]
Phase II, single-agent	Nintedanib	VEGFR1-3, FGFR1-3, PDGFR	First or second recurrence, n = 25	6	1	NA	[157]
<b>Immune checkpoint inhibitors</b>							
Phase II/III, randomized	Nivolumab (3 mg/kg, nivo1) or nivolumab (1 mg/kg) + ipilimumab (3 mg/kg, nivo1/ipi3) or nivolumab (3 mg/kg) + ipilimumab (1 mg/kg, nivo3/ipi1)	PD1 (nivolumab), CTLA-4 (ipilimumab)	First recurrence, n = 10 (nivo3), n = 10 (nivo1/ipi3), n = 20 (nivo3/ipi1)	10.5 (nivo3), 9.3 (nivo1/ipi3), 7.3 (nivo3/ipi1)	1.9 (nivo3), 2.1 (nivo1/ipi3), 2.4 (nivo3/ipi1)	NA	[183]
Phase II, single-agent	Durvalumab	PD-L1	First or second recurrence, bevacizumab-naïve, n = 30	6.7	3.2	20%	[185]
Phase Ib, single-agent	Pembrolizumab	PD1	Any recurrence, n = 26	14.0	3.0	44%	[184]

Abbreviations: NA, data not available.

Table 3. Ongoing randomized phase 3 trials evaluating investigational agents in glioblastoma

ClinicalTrials.gov Identifier	Population	Treatment arms	Primary endpoint	Status <sup>a</sup>	Sponsor
<b>Newly diagnosed glioblastoma</b>					
NCT00045968	Sufficient tumor lysate after surgery	Experimental: RT/TMZ followed by TMZ + DCVax-L (dendritic cells vaccine) Comparator: RT/TMZ followed by TMZ + placebo	PFS	Accrual suspended	Northwest Biotherapeutics
NCT02617589	Unmethylated MGMT promoter	Experimental: RT + nivolumab (anti-PD1 MAb) Comparator: RT/TMZ followed by TMZ	OS	Recruiting	Bristol-Myers Squibb
NCT02546102	HLA-A2 positive patients	Experimental: RT/TMZ followed by TMZ + ICT-107 (dendritic cells vaccine) Comparator: RT/TMZ followed by TMZ + placebo	OS	Recruiting	ImmunoCellular Therapeutics
NCT02573324	EGFR-amplified	Experimental: RT/TMZ/ABT-414 followed by TMZ + ABT-414 (anti-EGFR ADC) Comparator: RT/TMZ/placebo followed by TMZ + placebo	OS	Recruiting	AbbVie
NCT02152982	Unmethylated MGMT promoter	Experimental: RT/TMZ + followed by TMZ + veliparib (PARP inhibitor) Comparator: RT/TMZ followed by TMZ + placebo	OS	Not yet recruiting	National Cancer Institute
<b>Recurrent glioblastoma</b>					
NCT0201771	First progression	Experimental: nivolumab (anti-PD1 MAb) Comparator: bevacizumab	OS	Accrual completed	Bristol-Myers Squibb
NCT02511405	First or second progression	Experimental: bevacizumab + VB-111 (viral toxin) Comparator: bevacizumab	OS	Recruiting	Vascular Biogenics
NCT02414165	First or second progression, candidate for resection	Experimental: TOCA-511 (viral gene therapy injected in tumor resection cavity) + TOCA-FC (5-fluorocytosine) Comparator: Investigator's choice (single agent lomustine or temozolomide or bevacizumab)	OS	Recruiting	Tocagen

<sup>a</sup>Source: clinicaltrials.gov (November 2016).

generation EGFR/HER2 TKI or anti-EGFR monoclonal antibodies (Mab) have been evaluated as monotherapy [53–62] or in association with various agents or radiation therapy [63–79]. The results of these trials have been comprehensively reviewed elsewhere [18, 80]. Overall, disappointing results were reported despite some anecdotal response observed, suggesting the lack of efficacy of the currently available agents. Further studies evaluating novel agents or combinations are warranted to re-evaluate the value of EGFR inhibition in molecularly selected populations.

### Targeting other receptor tyrosine kinases

Oncogenic *FGFR-TACC* fusions are found in nearly 3% of glioblastomas, with promising evidence of actionability provided by preclinical studies [21, 81]. Encouraging evidence of activity was recently reported in a phase I study evaluating JNJ-42756493—a highly selective pan-FGFR TKI—in three patients harboring *FGFR3-TACC3*-positive glioblastomas [21, 82]. Phase II clinical trials evaluating other selective FGFR inhibitors (e.g. BGJ398 and AZD4547) are currently ongoing [83].

*PDGFRA* amplification is found in nearly 15% of glioblastomas [10]. This receptor is highly active in all glioma types and represents one of the more underexplored targets for therapy. A recently reported phase II trial evaluated the efficacy of dasatinib, a multikinase

inhibitor targeting PDGFR, c-KIT, SRC and EPHA2 [84] (Table 2). Despite the fact that patients were selected on the basis of overexpression of at least 2 putative dasatinib targets, no response was reported. Additional trials evaluated other multikinase inhibitors without showing any consistent clinical activity in glioblastoma [85–89].

Finally, preclinical evidences indicated an oncogenic role for c-MET signaling pathway activation in glioblastoma, notably by promoting tumor growth and invasiveness as well as drug resistance [90–94]. Rare responses have been documented in patients receiving crizotinib, a c-MET/ALK inhibitor and represent some of the first evidence of targeted therapy success [95, 96]. *MET* amplification or mutation as well as overexpression of c-MET or its ligand, the hepatocyte growth factor (HGF), have been proposed as predictive biomarkers, although efficacy and its molecular determinants remain unclear to date. A recently reported randomized phase II trial investigated the safety and efficacy of bevacizumab plus onartuzumab—a Mab against MET—versus bevacizumab plus placebo in recurrent glioblastoma (Table 2) [97]. Overall, there was no evidence of clinical benefit with bevacizumab plus onartuzumab compared with bevacizumab plus placebo, although exploratory biomarker analyses suggested benefit in patients with unmethylated O6-methylguanine–DNA methyltransferase (MGMT) or high HGF expression in tumor tissue. Further understanding of the role of these RTKs in the

progression of glioblastoma, as well as evaluation of highly brain penetrant and potent inhibitors is warranted.

### Targeting PI3K/AKT/mTOR and MAPK signaling pathways

In light of the disappointing activity observed with existing RTK inhibitors, agents designed to interfere with downstream molecules remain attractive. The PI3K/AKT/mTOR signaling pathway is dysregulated in the vast majority of glioblastomas through various molecular alterations (Table 1). mTOR inhibitors such as temsirolimus and everolimus have been FDA-approved to treat various solid cancers including subependymal giant cell astrocytoma, a low grade brain tumor arising in patients with tuberous sclerosis complex, with good response in this special type of astrocytoma. However, when evaluated in glioblastoma as monotherapy, or in combination with either EGFR TKIs, bevacizumab or temozolomide and radiation therapy, these agents have not demonstrated significant clinical activity [66–70, 98–100].

Nonetheless, it has been hypothesized that a subset of patients may benefit from PI3K/AKT/mTOR signaling inhibition, and novel agents with a broader range of activity are currently being evaluated. PX-866 is an oral PI3K inhibitor recently tested in a phase II trial [101]. While the study was negative, durable stabilization was observed in 21% of patients. No association between outcome and PTEN, PIK3CA or PIK3R1 status was observed. The dual PI3K/mTOR inhibitor voxalisib and the pan-class I PI3K inhibitor buparlisib have been evaluated in other trials. Preliminary results from phase II trials evaluating buparlisib indicated activity in association with bevacizumab [102], while limited efficacy was observed in patients receiving buparlisib as monotherapy, even in the presence of PIK3CA, PIK3R1 or PTEN molecular alterations (Table 2).

Targeting of MAPK pathway signaling, activated in all glioblastoma, is also a rational approach. A small subset of patients (3%), especially those with giant cell or epithelioid morphology (11%), harbors the BRAF V600E mutation [103], a well-known targetable oncogene. The BRAF inhibitor vemurafenib has shown promising efficacy in individual patients with BRAF-mutant (V600E) high-grade gliomas of non-glioblastoma types [104, 105]. The RAF multikinase inhibitor sorafenib has been evaluated in several small phase I/II studies as monotherapy or in combination with bevacizumab, temozolomide, temsirolimus [106–110] or radiation therapy and temozolomide [111]. Unfortunately, limited efficacy was observed and has not supported further development of sorafenib in glioblastoma (Table 2). Future preclinical studies and trials should focus on combined inhibition of MAPK and other pathways, as well as identifying predictive biomarkers. The presence of responses in other glioma types with BRAF alterations suggests these agents may be some of the most promising for future success in targeted therapies.

### Targeting DNA repair and cell cycle control pathways

Disruption of p53 and Retinoblastoma/E2F tumor suppressor pathways is found in more than 80% of glioblastomas [10]. TP53 encodes the tumor suppressor protein p53 that causes cell-cycle arrest and promotes apoptosis upon DNA damage [112]. TP53

mutation/deletion results in growth advantage and clonal expansion of glioma cells, as well as impairment of DNA repair, promoting overall genetic instability and transformation [113, 114]. Besides direct gene mutation or deletion, p53 inactivation may be caused by MDM2 or MDM4 amplification (20% of patient overall) [10, 115]. The first therapeutic strategies targeting p53 were centered on attempting reactivation of the pathway using gene therapy or pharmacological approaches, although these have failed to demonstrate clinical efficacy [116]. A key disadvantage of the original nutlin-based drugs was the low potency and poor blood–brain barrier (BBB) penetration. However, MDM2 inhibition has recently re-emerged as an attractive strategy to restore p53 function with advances in the chemical properties of nutlin-based agents (RG7112, RG7388), as well as other classes of agents recently developed (HDM201, AMG232). Preclinical studies have demonstrated striking antitumor efficacy in MDM2-amplified glioblastoma models [117, 118]. Most importantly, TP53-wild-type models also showed marked response to these agents and blood–tumor and blood–brain penetration of the more novel agents has been in a range as feasible for clinical trials. Given that about 50% of glioblastoma patients have TP53-wild-type tumors this represents an attractive strategy for the majority of patients.

Cell cycle progression is frequently deregulated through various recurrent molecular alterations including inactivation of CDKN2A/CDKN2B and RB1 as well as amplification of CDK4 and CDK6 (Table 1) [10, 119]. Novel agents designed to inhibit CDK4 and CDK6 have demonstrated strong antitumor efficacy in RB1-wild-type glioblastoma models [120–123], and have been subsequently evaluated in phase II. Results from this study as well as other trials evaluating newer compounds (NCT02345824) should shed light on the value of CDK inhibitors in glioblastoma, and the biomarker profile of the patients that may respond.

Finally, synthetic lethal approaches have been developed as novel strategies to target tumors harboring alterations disrupting DNA repair and tumor suppressor pathways. WEE1—a nuclear serine/threonine kinase—acts as a gatekeeper against mitotic catastrophe in glioblastoma. Recent preclinical works demonstrated that small-molecule inhibition of WEE1 sensitized glioblastoma to DNA damaging agents including radiation therapy [124–126]. Combination of the WEE1 inhibitor AZD1775 with radiation therapy and temozolomide is currently being evaluated (NCT01849146). Other promising strategies exploiting synthetic lethal interactions include association of DNA repair inhibitors (e.g. the PARP inhibitors veliparib and olaparib) with radiation therapy and/or temozolomide, which have demonstrated antitumor efficacy in animal models [127–128], and are currently evaluated in randomized trials (Table 3) [129].

### Targeting epigenetic deregulation and tumor metabolism

#### Targeting isocitrate dehydrogenase

IDH1 mutations are found in 6% of primary glioblastomas [7, 130–132]. These mutations confer a gain-of-function, resulting in the production of D-2-hydroxyglutarate (D2HG), which interferes with cellular metabolism and epigenetic regulation [132,

133]. Small-molecule inhibitors of mutant IDH enzymes have demonstrated activity in preclinical models [17], and are being evaluated in phase I/II trials (NCT02073994, NCT02481154). Preliminary reports indicated favorable safety profile and signs of activity, mainly in patients with lower grade tumors [134]. IDH1 peptide vaccines represent an alternative approach that has demonstrated activity in preclinical models [135, 136], and are being evaluated in clinical trials (NCT02454634, NCT02193347).

### Targeting histone deacetylase and other epigenetic modifiers

Histone deacetylase (HDAC) inhibitors represent an emerging class of therapeutics that has shown activity in hematologic malignancies. Despite encouraging efficacy in preclinical models including histone H3-mutant pediatric glioblastoma [137–139], only modest activity has been observed in clinical trials evaluating HDAC inhibitors as a single agent, or in combination with temozolomide, bortezomib or bevacizumab [140–143] (Table 2). Beyond HDAC inhibitors, other epigenetic modifiers have recently gained interest for the treatment of glial tumors. These include BET bromodomain proteins inhibitors and EZH2 inhibitors, which have recently entered in clinical trials (NCT01897571, NCT02711137), and have both demonstrated antitumor activity in preclinical models [144–147].

### Targeting tumor angiogenesis

A multitude of anti-angiogenic targeted therapies have been evaluated in clinical trials of glioblastoma as monotherapy or in combinations with various agents, all with no significant survival benefit to patients [63, 84, 106, 148–168] (Table 2). In 2009, bevacizumab received provisional FDA-approval for the treatment of recurrent glioblastoma on the basis of radiographic response rates ranging from 28% to 59% reported in two single-arm trials [148, 149]. However, subsequent trials failed to demonstrate superiority of bevacizumab alone or combined with lomustine in terms of OS [161, 169]. In newly diagnosed glioblastoma, two recently reported placebo-controlled randomized trials evaluating the benefit from the addition of bevacizumab to standard of care showed no difference in OS, while significant improvement in PFS was demonstrated in both trials (extension of median PFS of 3.4 and 4.6 months) [162, 163].

Given the encouraging preclinical data, what went wrong? The lack of the target being expressed in tumor cells is something that became clearer with time. The level of dependency of the tumor ecosystem on the vasculature now appears to be low. Despite the lack of clear survival benefit of antiangiogenic agents in glioblastoma, prolonged PFS with long-lasting tumor response or stabilization has been proposed to be present in a subset of patients receiving bevacizumab. The identification of biomarkers to predict response of antiangiogenics agents may therefore be warranted. One possibility for this comes from post-hoc analysis from the AVAglio randomized phase III trial [170], which reported significant OS advantage of adding bevacizumab to standard of care in patients with proneural *IDH1* wild-type tumors, albeit this needs to be validated further in an independent trial.

### Immunotherapies

Immunotherapy for glioblastoma has gained considerable interest over the past years. The concept of the central nervous system (CNS) as an ‘immune privileged site’ has been recently challenged by the discovery of the CNS lymphatic system, which is connected to the deep cervical lymph nodes [171–174]. Therapeutic targeting of immune checkpoint programmed cell death 1 (PD1)/programmed death-ligand 1 (PD-L1) and cytotoxic T-lymphocyte-associated molecule-4 (CTLA-4) using MAbs has been associated with significant clinical benefit in several human malignancies [175, 176]. These treatments aim at enhancing antitumor immune responses, by blocking negative regulatory pathways in T-cell activation. In glioblastoma, PD-L1 is expressed in some patients [177, 178], and preclinical studies have provided rationale for the evaluation of immune checkpoint blockers (ICBs) [179–182].

Several clinical trials evaluating ICBs are ongoing (Tables 2 and 3), including randomized phase III trials of the anti-PD1 nivolumab. Preliminary data on efficacy and safety of ICBs as monotherapy or in combination were recently reported [183–186] (Table 2). Overall, the response rates observed with these agents in recurrent disease were low; however, the observation of a relative increase in 6-month PFS and OS suggested a possible benefit in a subset of patients. Recent studies in non-CNS cancers have indicated that patients whose tumors bear high neoantigen and/or mutation load may derive enhanced clinical benefit from immune checkpoint inhibitors [187–190]. Partial responses to nivolumab were recently reported in two pediatric patients that developed hypermutant glioblastoma in the context of biallelic mismatch repair deficiency [191], suggesting that this subset of patients may be responsive to this strategy.

Beyond targeting of immune checkpoints, other approaches taking advantage of the immune system and the tumor micro-environment are being explored. Dendritic cell and peptide vaccines have entered clinical trials, with promising signs of activity reported in preclinical studies and early phase trials [16, 47, 48, 135, 136, 192–197]. These encouraging results need further confirmation in the ongoing larger randomized trials. Other immune-cells based approaches include engineered chimeric antigen receptor (CAR T)/NK cells re-directed to specific tumor antigens (e.g. EGFRvIII), which have demonstrated promising antitumor efficacy in animal models [198, 199], and are currently evaluated in several phase I/II trials (NCT01109095, NCT02442297, NCT02664363, NCT01454596). However, these novel approaches will require further standardization and optimization efforts, and costs and technical issues associated with cell-based therapy will likely limit its widespread application.

### Development of targeted therapies in glioblastoma: current state of the art and future directions

#### Lessons learned from the clinical development of targeted therapies

Unlike the experience in some other human malignancies harboring activating oncogenic alterations (e.g. *EGFR* or *ALK* in lung adenocarcinoma), efforts in the field of precision medicine have not yet

demonstrated consistent clinical activity in glioblastoma. Several factors may explain such disappointing results. A central element of precision medicine is the matching of a selective drug and its mechanism of action using a robust biomarker (e.g. a molecular assay defining a specific biologic subgroup) to select patients that are expected to benefit from the drug ('selecting the right drug for the right patient'). Before evaluation in large trials, scientists and investigators should provide: (i) strong evidence of antitumor activity in disease-relevant models [200] and (ii) proof-of-concept (i.e. demonstration of the feasibility) as well as evidence of effective target modulation in early phase trials. In glioblastoma, few if any trials that evaluated targeted therapies have met these preliminary requirements.

As far as target relevance and selection are concerned, most of the trials had not implemented molecular enrichment for patient selection. It is likely that most patients have received investigational agents in the absence of the relevant target in their tumor. Defining relevant targets is often challenging. Although early studies suggested that *EGFR* and *PTEN* status could predict response to EGFR-targeted therapies [201, 202], outcome was not correlated with the presence of *EGFR* amplification, *EGFR*III, *PTEN* loss or other molecular alterations in subsequent studies, and molecular predictors for the efficacy of EGFR targeted therapies remain undetermined. Future precision medicine studies should more largely implement systematic molecular characterization, including assessment of non-invasive biomarkers [203, 204], which will theoretically enable physicians to identify the most relevant targets for each patient, and allow further correlation of molecular profile with outcome (Figure 2).

In trials that have failed despite molecular enrichment [50], other potential sources of failures have to be considered. As previously mentioned, the marked heterogeneity and plasticity of glioblastoma cells are likely major factors mediating the currently observed resistance to targeted therapies [31, 40, 205]. As an illustration, in a phase II trial, analyses of tissues from glioblastoma

patients treated with gefitinib before debulking surgery revealed significant intratumoral accumulation of gefitinib associated with dephosphorylation of EGFR, while downstream canonical pathways were not significantly dephosphorylated when compared with untreated controls [31, 40, 206]. This indicated concomitant activation of redundant cell signaling pathways, a resistance mechanism observed in EGFR-driven glioma models [205]. This clearly implies that exploring combinations of targeted therapies to avoid emergence of resistant subclones is needed (Figure 1). Moreover, future studies should explore approaches that have the potential to more broadly inhibit tumor cell growth and survival [207, 208]. Agents that more broadly target pathways rather than single mutation variants have the potential to improve outcome in a much wider population of patients, even in the absence of actionable mutation targets identified by genomic profiling. As an illustration, novel MDM2 inhibitors have been reported to inhibit the growth of *TP53*-wild-type glioblastoma PDCLs, regardless of the tumor *MDM2* amplification status [117, 118]. However, such approaches are expected to go along with more side effects. Other examples include synthetic lethal approaches and immunotherapy, which are investigated in large trials (Table 3).

Regarding drug relevance, most of the tested agents were neither primarily designed to inhibit alterations that are specific to glioblastoma, nor developed for targeting tumors located in the brain. Most currently available agents display inadequate pharmacokinetic properties due to poor crossing of the BBB [209–211]. The BBB is universally disrupted in glioblastomas but not necessarily within more infiltrative non-enhancing areas of the tumor. Given this mixed BBB setting, novel agents should be optimized for brain penetration. Other approaches include the use of tailored regimens (e.g. higher doses in pulsed schedules) and other strategies to actively break down the BBB (e.g. transient opening of the BBB by pulsed ultrasound) [212, 213], which may improve drug delivery and target inhibition using agents that are unlikely to adequately penetrate the tumor. In this

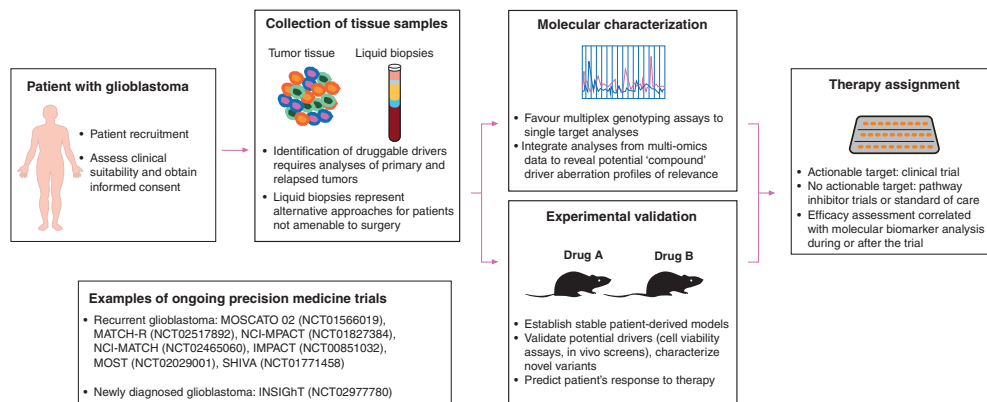


**Figure 2.** Current implementation of precision medicine in glioblastoma. Practical implications of implementing precision medicine approaches in glioblastoma are depicted in this figure. Appropriate molecular profiling requires analysis of tumor tissue from the relapsed tumor. Further steps include target identification and selection, and treatment selection. Main limitations include difficulties in obtaining tumor tissue from relapse, target prioritization, and availability of optimal drugs in the context of CNS disease and related molecular alterations. This figure features pictures from 'Servier medical art' by Servier, used under Creative Commons Attribution 3.0 France.

context, having a molecular assay that confirms effective modulation of the target in the tumor is essential; otherwise conclusions on relevance of the target will remain elusive. Novel trial designs should more often incorporate tissue biomarkers collection during treatment, enabling evaluation of pharmacodynamics markers.

### Novel biomarker-driven trial designs

Overall, considering the lack of clear demonstration of the benefit of targeted therapies in glioblastoma, proof-of concept in well molecularly characterized populations should be established in early phase and small-randomized phase II trials before further evaluation in registration trials. Academic groups and industry should collaborate in order to identify: (i) the best targets, drugs/combinations to be tested in clinical trials; (ii) the best population and (iii) the best biomarkers. Within the context of more precise and systematic molecular characterization of glioblastoma and increasing availability of novel targeted therapies, novel trial designs will be essential to more rapidly test agents. Practical implications for such precision medicine studies are represented in Figure 2.

A popular design is the ‘basket trial’ that involves screening of patients with cancer independent of tumor histology, for recruitment of a specific and often rare molecularly-defined population. A recently reported basket phase II trial evaluating vemurafenib in several *BRAF*<sup>V600</sup>-mutant non-melanoma tumors reported responses in high-grade glioma patients [105]. Similarly, crizotinib is currently investigated in *MET*-amplified glioblastomas (NCT02034981) as part of a larger trial with 23 molecularly defined cohorts. However, basket trials require robust preclinical studies to identify relevant biomarkers that will predict treatment response with high confidence, and well-established diagnostic assays available in real-time for patient selection [32, 214–220] (listed in supplementary Table S1, available at *Annals of Oncology* online). Moreover, such trial designs can present a major challenge when the molecular alterations in question are rare, requiring such trials to screen and reject a high number of patients who are then disappointed.

Other new approaches are multi-arm ‘master protocol’ and ‘umbrella’ trials, which most commonly involve screening for multiple targets [221], arms and agents, and yield added benefit that a higher proportion of patients may enter into the trial once screened. Such trials may include randomization between ‘standard’ and ‘molecularly tailored’ treatment arms, allowing assessing the utility of precision medicine approaches. These designs have been aided by translation of modern methods of high-throughput multiplex diagnostic assays, allowing to simultaneously measuring a host of targets using platforms such as targeted exomes or CGH/SNP arrays [208, 222]. These are now commonplace in an increasing number of centers and aid designing novel trials based on systematic molecular screening programs for treatment stratification (Figure 2). As an illustration, personalized medicine trials such as MOSCATO 02 (NCT01566019) and INSIGHT (NCT02977780) studies are currently evaluating the feasibility and the utility of genomic profiling to inform treatment decisions in patients with glioblastoma.

### Conclusion

An improved understanding of the molecular pathways that drive malignancy in glioblastoma has led to the development of various biomarkers and several agents targeting specific molecular pathways in malignant cells. The concept of precision medicine driven by molecular stratification for the treatment of glioblastoma is appealing and scientifically sound; however, no evidence has yet demonstrated an improved patient outcome within the context of this disease, likely as a result of both scientific and logistical challenges that have hampered the success of clinical trials. The identification of relevant driver molecular events and highly bioactive and specific drugs remain the biggest challenges. With the recent incorporation in clinical practice of modern methods allowing molecular characterization and appropriate stratification of patients, there is hope that novel trials evaluating targeted therapies may be more effective. Identification of relevant targets, compounds and biomarkers for appropriate patient selection during early phase trials are essential for successful development of novel therapies.

### Funding

MT receives research grants from Fondation pour la Recherche Médicale (FDM 41635). KLL receives funding from NIH (R01CA188288, R01 CA170592, P50 CA165962), The Ivy Foundation, The PLGA Foundation, and ABC2 Foundation.

### Disclosure

MT and MS have declared no conflicts of interest. AI reports grants from Fondation ARC pour la recherche sur le Cancer, other from IntselChimos, personal fees from Novartis (janv 2014), other from Hoffmann-La Roche, other from Beta-Innov (Juillet 2014), personal fees from Lettre du Cancérologue, other from CARthera, personal fees from BMS (nov 2015), personal fees from Roche (dec 2015), personal fees from Cipla (dec 2015) (certified continuing education), outside the submitted work. DFCI receives funding for KLL's research with the following entities: Amgen, Tragara and X4. DFCI and KLL have patents related to molecular diagnostics of cancer.

### References

- Ostrom QT, Gittleman H, Liao P et al. CBRUS statistical report: primary brain and central nervous system tumors diagnosed in the United States in 2007–2011. *Neuro Oncol* 2014; 16(Suppl 4): iv1–iv63.
- Stupp R, Mason WP, van den Bent MJ et al. Radiotherapy plus concomitant and adjuvant temozolomide for glioblastoma. *N Engl J Med* 2005; 352: 987–996.
- Ronning PA, Helseth E, Meling TR, Johannesen TB. A population-based study on the effect of temozolomide in the treatment of glioblastoma multiforme. *Neuro Oncol* 2012; 14: 1178–1184.
- Stupp R, Taillibert S, Kanner AA et al. Maintenance therapy with tumor-treating fields plus temozolomide vs temozolomide alone for glioblastoma: a randomized clinical trial. *JAMA* 2015; 314: 2535–2543.
- Weller M, van den Bent M, Hopkins K et al. EANO guideline for the diagnosis and treatment of anaplastic gliomas and glioblastoma. *Lancet Oncol* 2014; 15: e395–e403.
- Phillips HS, Kharbanda S, Chen R et al. Molecular subclasses of high-grade glioma predict prognosis, delineate a pattern of disease progression, and resemble stages in neurogenesis. *Cancer Cell* 2006; 9: 157–173.

7. Parsons DW, Jones S, Zhang X et al. An integrated genomic analysis of human glioblastoma multiforme. *Science* 2008; 321: 1807–1812.
8. Network CGAR. Comprehensive genomic characterization defines human glioblastoma genes and core pathways. *Nature* 2008; 455: 1061–1068.
9. Noushmehr H, Weisenberger DJ, Diefes K et al. Identification of a CpG island methylator phenotype that defines a distinct subgroup of glioma. *Cancer Cell* 2010; 17: 510–522.
10. Brennan CW, Verhaak RG, McKenna A et al. The somatic genomic landscape of glioblastoma. *Cell* 2013; 155: 462–477.
11. Frattini V, Trifonov V, Chan JM et al. The integrated landscape of driver genomic alterations in glioblastoma. *Nat Genet* 2013; 45: 1141–1149.
12. Louis DN, Perry A, Reifenberger G et al. The 2016 World Health Organization classification of tumors of the central nervous system: a summary. *Acta Neuropathol* 2016; 131: 803–820.
13. Verhaak RG, Hoadley KA, Purdom E et al. Integrated genomic analysis identifies clinically relevant subtypes of glioblastoma characterized by abnormalities in PDGFRA, IDH1, EGFR, and NF1. *Cancer Cell* 2010; 17: 98–110.
14. Yoshihara K, Wang Q, Torres-Garcia W et al. The landscape and therapeutic relevance of cancer-associated transcript fusions. *Oncogene* 2015; 34: 4845–4854.
15. Ceccarelli M, Barthel FP, Malta TM et al. Molecular profiling reveals biologically discrete subsets and pathways of progression in diffuse glioma. *Cell* 2016; 164: 550–563.
16. Babu R, Adamson DC. Rindopepimut: an evidence-based review of its therapeutic potential in the treatment of EGFRvIII-positive glioblastoma. *Core Evid* 2012; 7: 93–103.
17. Rohle D, Popovici-Muller J, Palaskas N et al. An inhibitor of mutant IDH1 delays growth and promotes differentiation of glioma cells. *Science* 2013; 340: 626–630.
18. Reardon DA, Wen PY, Mellingshoff IK. Targeted molecular therapies against epidermal growth factor receptor: past experiences and challenges. *Neuro Oncol* 2014; 16(Suppl 8): vii7–vii13.
19. Thomas AA, Brennan CW, DeAngelis LM, Omuro AM. Emerging therapies for glioblastoma. *JAMA Neurol* 2014; 71: 1437–1444.
20. Gallego O, Cuatrecasas M, Benavides M et al. Efficacy of erlotinib in patients with relapsed glioblastoma multiforme who expressed EGFRvIII and PTEN determined by immunohistochemistry. *J Neurooncol* 2014; 116: 413–419.
21. Di Stefano AL, Fucci A, Frattini V et al. Detection, characterization and inhibition of FGFR-TACC fusions in IDH wild type glioma. *Clin Cancer Res* 2015; 21: 3307–3317.
22. Meyer M, Reimand J, Lan X et al. Single cell-derived clonal analysis of human glioblastoma links functional and genomic heterogeneity. *Proc Natl Acad Sci USA* 2015; 112: 851–856.
23. Prados MD, Byron SA, Tran NL et al. Toward precision medicine in glioblastoma: the promise and the challenges. *Neuro Oncol* 2015; 17: 1051–1063.
24. Snuderl M, Fazlollahi L, Le LP et al. Mosaic amplification of multiple receptor tyrosine kinase genes in glioblastoma. *Cancer Cell* 2011; 20: 810–817.
25. Lass U, Nümann A, von Eckardstein K et al. Clonal analysis in recurrent astrocytic, oligoastrocytic and oligodendroglial tumors implicates IDH1- mutation as common tumor initiating event. *PLoS One* 2012; 7: e41298.
26. Little SE, Popov S, Jury A et al. Receptor tyrosine kinase genes amplified in glioblastoma exhibit a mutual exclusivity in variable proportions reflective of individual tumor heterogeneity. *Cancer Res* 2012; 72: 1614–1620.
27. Sottoriva A, Spiteri I, Piccirillo SG et al. Intratumor heterogeneity in human glioblastoma reflects cancer evolutionary dynamics. *Proc Natl Acad Sci USA* 2013; 110: 4009–4014.
28. Johnson BE, Mazar T, Hong C et al. Mutational analysis reveals the origin and therapy-driven evolution of recurrent glioma. *Science* 2014; 343: 189–193.
29. Patel AP, Tirosh I, Trombetta JJ et al. Single-cell RNA-seq highlights intratumoral heterogeneity in primary glioblastoma. *Science* 2014; 344: 1396–1401.
30. Francis JM, Zhang CZ, Maire CL et al. EGFR variant heterogeneity in glioblastoma resolved through single-nucleus sequencing. *Cancer Discov* 2014; 4: 956–971.
31. Nathanson DA, Gini B, Mottahedeh J et al. Targeted therapy resistance mediated by dynamic regulation of extrachromosomal mutant EGFR DNA. *Science* 2014; 343: 72–76.
32. Kim H, Zheng S, Amiri SS et al. Whole-genome and multisector exome sequencing of primary and post-treatment glioblastoma reveals patterns of tumor evolution. *Genome Res* 2015; 25: 316–327.
33. Kim J, Lee IH, Cho HJ et al. Spatiotemporal evolution of the primary glioblastoma genome. *Cancer Cell* 2015; 28: 318–328.
34. Yap TA, Gerlinger M, Futreal PA et al. Intratumor heterogeneity: seeing the wood for the trees. *Sci Transl Med* 2012; 4: 127ps110.
35. Burrell RA, McGranahan N, Bartek J, Swanton C. The causes and consequences of genetic heterogeneity in cancer evolution. *Nature* 2013; 501: 338–345.
36. McGranahan N, Favero F, de Bruin EC et al. Clonal status of actionable driver events and the timing of mutational processes in cancer evolution. *Sci Transl Med* 2015; 7: 283ra254.
37. Touat M, Dhermain F, André F, Sanson M. Adapting the drivers to the road: a new strategy for cancer evolution? *Ann Oncol* 2015; 26: 827–829.
38. Wang J, Cazzato E, Ladewig E et al. Clonal evolution of glioblastoma under therapy. *Nat Genet* 2016; 48: 768–776.
39. Stommel JM, Kimmelman AC, Ying H et al. Coactivation of receptor tyrosine kinases affects the response of tumor cells to targeted therapies. *Science* 2007; 318: 287–290.
40. Szerlip NJ, Pedraza A, Chakravarty D et al. Intratumoral heterogeneity of receptor tyrosine kinases EGFR and PDGFRA amplification in glioblastoma defines subpopulations with distinct growth factor response. *Proc Natl Acad Sci USA* 2012; 109: 3041–3046.
41. Stevens MM, Maire CL, Chou N et al. Drug sensitivity of single cancer cells is predicted by changes in mass accumulation rate. *Nat Biotechnol* 2016; 34: 1161–1167.
42. Nishikawa R, Ji XD, Harmon RC et al. A mutant epidermal growth factor receptor common in human glioma confers enhanced tumorigenicity. *Proc Natl Acad Sci USA* 1994; 91: 7727–7731.
43. Frederick L, Wang XY, Eley G, James CD. Diversity and frequency of epidermal growth factor receptor mutations in human glioblastomas. *Cancer Res* 2000; 60: 1383–1387.
44. Maire CL, Ligon KL. Molecular pathologic diagnosis of epidermal growth factor receptor. *Neuro Oncol* 2014; 16(Suppl 8): viii1–viii6.
45. Vivanco I, Robins HI, Rohle D et al. Differential sensitivity of glioma-versus lung cancer-specific EGFR mutations to EGFR kinase inhibitors. *Cancer Discov* 2012; 2: 458–471.
46. Schulte A, Liffers K, Kathagen A et al. Erlotinib resistance in EGFR-amplified glioblastoma cells is associated with upregulation of EGFRvIII and PI3Kp110δ. *Neuro Oncol* 2013; 15: 1289–1301.
47. Sampson JH, Heimberger AB, Archer GE et al. Immunologic escape after prolonged progression-free survival with epidermal growth factor receptor variant III peptide vaccination in patients with newly diagnosed glioblastoma. *J Clin Oncol* 2010; 28: 4722–4729.
48. Schuster J, Lai RK, Recht LD et al. A phase II, multicenter trial of rindopepimut (CDX-110) in newly diagnosed glioblastoma: the ACT III study. *Neuro Oncol* 2015; 17: 854–861.
49. Reardon DA, Desjardins A, Schuster J et al. IMCT-08ReACT: long-term survival from a randomized phase II study of rindopepimut (CDX-110) plus bevacizumab in relapsed glioblastoma. *Neuro Oncol* 2015; 17(Suppl 5): v109.
50. Weller M, Butowski N, Tran D et al. ATIM-03. ACT IV: an international, double-blind, phase 3 trial of rindopepimut in newly diagnosed, EGFRvIII-expressing glioblastoma. *Neuro-Oncology* 2016; 18(Suppl 6): vi17–vi18.

51. Phillips AC, Boghaert ER, Vaidya KS et al. ABT-414, an antibody-drug conjugate targeting a tumor-selective EGFR epitope. *Mol Cancer Ther* 2016; 15: 661–669.
52. van den Bent M, Gan H, Lassman A et al. ACTR-07. Efficacy of a novel antibody-drug conjugate (ADC), ABT-414, as monotherapy in epidermal growth factor receptor (EGFR) amplified (EGFRamp), recurrent glioblastoma (rGBM). *Neuro-Oncology* 2016; 18(Suppl 6): vi2.
53. Rich JN, Reardon DA, Peery T et al. Phase II trial of gefitinib in recurrent glioblastoma. *J Clin Oncol* 2004; 22(1): 133–142.
54. Franceschi E, Cavallo G, Lonardi S et al. Gefitinib in patients with progressive high-grade gliomas: a multicentre phase II study by Gruppo Italiano Cooperativo di Neuro-Oncologia (GICNO). *Br J Cancer* 2007; 96(7): 1047–1051.
55. van den Bent MJ, Brandes AA, Rampling R et al. Randomized phase II trial of erlotinib versus temozolomide or carmustine in recurrent glioblastoma: EORTC brain tumor group study 26034. *J Clin Oncol* 2009; 27: 1268–1274.
56. Neyns B, Sadones J, Joossens E et al. Stratified phase II trial of cetuximab in patients with recurrent high-grade glioma. *Ann Oncol* 2009; 20: 1596–1603.
57. Thiessen B, Stewart C, Tsao M et al. A phase I/II trial of GW572016 (lapatinib) in recurrent glioblastoma multiforme: clinical outcomes, pharmacokinetics and molecular correlation. *Cancer Chemother Pharmacol* 2010; 65: 353–361.
58. Raizer JJ, Abrey LE, Lassman AB et al. A phase II trial of erlotinib in patients with recurrent malignant gliomas and nonprogressive glioblastoma multiforme postirradiation therapy. *Neuro Oncol* 2010; 12: 95–103.
59. Yung WK, Vredenburgh JJ, Cloughesy TF et al. Safety and efficacy of erlotinib in first-relapse glioblastoma: a phase II open-label study. *Neuro Oncol* 2010; 12: 1061–1070.
60. Uhm JH, Ballman KV, Wu W et al. Phase II evaluation of gefitinib in patients with newly diagnosed Grade 4 astrocytoma: Mayo/North Central Cancer Treatment Group Study N0074. *Int J Radiat Oncol Biol Phys* 2011; 80: 347–353.
61. Lv S, Teugels E, Sadones J et al. Correlation of EGFR, IDH1 and PTEN status with the outcome of patients with recurrent glioblastoma treated in a phase II clinical trial with the EGFR-blocking monoclonal antibody cetuximab. *Int J Oncol* 2012; 41: 1029–1035.
62. Reardon DA, Nabors LB, Mason WP et al. Phase I/randomized phase II study of afatinib, an irreversible ErbB family blocker, with or without protracted temozolomide in adults with recurrent glioblastoma. *Neuro Oncol* 2015; 17: 430–439.
63. Sathornsumetee S, Desjardins A, Vredenburgh JJ et al. Phase II trial of bevacizumab and erlotinib in patients with recurrent malignant glioma. *Neuro Oncol* 2010; 12: 1300–1310.
64. Hasselbalch B, Lassen U, Hansen S et al. Cetuximab, bevacizumab, and irinotecan for patients with primary glioblastoma and progression after radiation therapy and temozolomide: a phase II trial. *Neuro Oncol* 2010; 12: 508–516.
65. Reardon DA, Groves MD, Wen PY et al. A phase I/II trial of pazopanib in combination with lapatinib in adult patients with relapsed malignant glioma. *Clin Cancer Res* 2013; 19: 900–908.
66. Reardon DA, Quinn JA, Vredenburgh JJ et al. Phase I trial of gefitinib plus sirolimus in adults with recurrent malignant glioma. *Clin Cancer Res* 2006; 12: 860–868.
67. Doherty L, Gigas DC, Kesari S et al. Pilot study of the combination of EGFR and mTOR inhibitors in recurrent malignant gliomas. *Neurology* 2006; 67: 156–158.
68. Reardon DA, Desjardins A, Vredenburgh JJ et al. Phase 2 trial of erlotinib plus sirolimus in adults with recurrent glioblastoma. *J Neurooncol* 2010; 96: 219–230.
69. Wen PY, Chang SM, Lamborn KR et al. Phase I/II study of erlotinib and temsirolimus for patients with recurrent malignant gliomas: North American Brain Tumor Consortium trial 04-02. *Neuro Oncol* 2014; 16: 567–578.
70. Kreisl TN, Lassman AB, Mischel PS et al. A pilot study of everolimus and gefitinib in the treatment of recurrent glioblastoma (GBM). *J Neurooncol* 2009; 92: 99–105.
71. Peereboom DM, Ahluwalia MS, Ye X et al. NABTT 0502: a phase II and pharmacokinetic study of erlotinib and sorafenib for patients with progressive or recurrent glioblastoma multiforme. *Neuro Oncol* 2013; 15: 490–496.
72. Prados MD, Lamborn KR, Chang S et al. Phase 1 study of erlotinib HCl alone and combined with temozolomide in patients with stable or recurrent malignant glioma. *Neuro Oncol* 2006; 8: 67–78.
73. Prados MD, Yung WK, Wen PY et al. Phase-1 trial of gefitinib and temozolomide in patients with malignant glioma: a North American brain tumor consortium study. *Cancer Chemother Pharmacol* 2008; 61: 1059–1067.
74. Brown PD, Krishnan S, Sarkaria JN et al. Phase I/II trial of erlotinib and temozolomide with radiation therapy in the treatment of newly diagnosed glioblastoma multiforme: North Central Cancer Treatment Group Study N0177. *J Clin Oncol* 2008; 26: 5603–5609.
75. Krishnan S, Brown PD, Ballman KV et al. Phase I trial of erlotinib with radiation therapy in patients with glioblastoma multiforme: results of North Central Cancer Treatment Group protocol N0177. *Int J Radiat Oncol Biol Phys* 2006; 65: 1192–1199.
76. Prados MD, Chang SM, Butowski N et al. Phase II study of erlotinib plus temozolomide during and after radiation therapy in patients with newly diagnosed glioblastoma multiforme or gliosarcoma. *J Clin Oncol* 2009; 27: 579–584.
77. Peereboom DM, Shepard DR, Ahluwalia MS et al. Phase II trial of erlotinib with temozolomide and radiation in patients with newly diagnosed glioblastoma multiforme. *J Neurooncol* 2010; 98: 93–99.
78. Chakravarti A, Wang M, Robins HI et al. RTOG 0211: a phase 1/2 study of radiation therapy with concurrent gefitinib for newly diagnosed glioblastoma patients. *Int J Radiat Oncol Biol Phys* 2013; 85: 1206–1211.
79. Clarke JL, Molinaro AM, Phillips JJ et al. A single-institution phase II trial of radiation, temozolomide, erlotinib, and bevacizumab for initial treatment of glioblastoma. *Neuro Oncol* 2014; 16: 984–990.
80. Seystahl K, Wick W, Weller M. Therapeutic options in recurrent glioblastoma—an update. *Crit Rev Oncol Hematol* 2016; 99: 389–408.
81. Singh D, Chan JM, Zoppoli P et al. Transforming fusions of FGFR and TACC genes in human glioblastoma. *Science* 2012; 337: 1231–1235.
82. Taberner J, Bahleda R, Dienstmann R et al. Phase I dose-escalation study of JNJ-42756493, an oral pan-fibroblast growth factor receptor inhibitor, in patients with advanced solid tumors. *J Clin Oncol* 2015; 33: 3401–3408.
83. Touat M, Ileana E, Postel-Vinay S et al. Targeting FGFR Signaling in Cancer. *Clin Cancer Res* 2015; 21: 2684–2694.
84. Lassman AB, Pugh SL, Gilbert MR et al. Phase 2 trial of dasatinib in target-selected patients with recurrent glioblastoma (RTOG 0627). *Neuro Oncol* 2015; 17: 992–998.
85. Wen PY, Yung WK, Lamborn KR et al. Phase I/II study of imatinib mesylate for recurrent malignant gliomas: North American Brain Tumor Consortium Study 99-08. *Clin Cancer Res* 2006; 12: 4899–4907.
86. Reardon DA, Dresemann G, Taillibert S et al. Multicentre phase II studies evaluating imatinib plus hydroxyurea in patients with progressive glioblastoma. *Br J Cancer* 2009; 101: 1995–2004.
87. Razis E, Selviaridis P, Labropoulos S et al. Phase II study of neoadjuvant imatinib in glioblastoma: evaluation of clinical and molecular effects of the treatment. *Clin Cancer Res* 2009; 15: 6258–6266.
88. Dresemann G, Weller M, Rosenthal MA et al. Imatinib in combination with hydroxyurea versus hydroxyurea alone as oral therapy in patients with progressive pretreated glioblastoma resistant to standard dose temozolomide. *J Neurooncol* 2010; 96: 393–402.
89. Holdhoff M, Supko JG, Gallia GL et al. Intratumoral concentrations of imatinib after oral administration in patients with glioblastoma multiforme. *J Neurooncol* 2010; 97: 241–245.
90. Li Y, Li A, Glas M et al. c-Met signaling induces a reprogramming network and supports the glioblastoma stem-like phenotype. *Proc Natl Acad Sci USA* 2011; 108: 9951–9956.
91. Jahangiri A, De Lay M, Miller LM et al. Gene expression profile identifies tyrosine kinase c-Met as a targetable mediator of antiangiogenic therapy resistance. *Clin Cancer Res* 2013; 19: 1773–1783.

92. Petterson SA, Dahlrot RH, Hermansen SK et al. High levels of c-Met is associated with poor prognosis in glioblastoma. *J Neurooncol* 2015; 122: 517–527.
93. Johnson J, Ascierio ML, Mittal S et al. Genomic profiling of a Hepatocyte growth factor-dependent signature for MET-targeted therapy in glioblastoma. *J Transl Med* 2015; 13: 306.
94. Wen PY, Schiff D, Cloughesy TF et al. A phase II study evaluating the efficacy and safety of AMG 102 (rilutumumab) in patients with recurrent glioblastoma. *Neuro Oncol* 2011; 13: 437–446.
95. Chi AS, Batchelor TT, Kwak EL et al. Rapid radiographic and clinical improvement after treatment of a MET-amplified recurrent glioblastoma with a mesenchymal-epithelial transition inhibitor. *J Clin Oncol* 2012; 30: e30–e33.
96. Le Rhun E, Chamberlain MC, Zairi F et al. Patterns of response to crizotinib in recurrent glioblastoma according to ALK and MET molecular profile in two patients. *CNS Oncol* 2015; 4: 381–386.
97. Cloughesy T, Finocchiaro G, Belda-Iniesta C et al. Randomized, double-blind, placebo-controlled, multicenter phase II study of onartuzumab plus bevacizumab versus placebo plus bevacizumab in patients with recurrent glioblastoma: efficacy, safety, and hepatocyte growth factor and O(6)-methylguanine-DNA methyltransferase biomarker analyses. *J Clin Oncol* 2016; 35: 343–351.
98. Galanis E, Buckner JC, Maurer MJ et al. Phase II trial of temsirolimus (CCI-779) in recurrent glioblastoma multiforme: a North Central Cancer Treatment Group Study. *J Clin Oncol* 2005; 23: 5294–5304.
99. Lassen U, Sorensen M, Gaziel TB et al. Phase II study of bevacizumab and temsirolimus combination therapy for recurrent glioblastoma multiforme. *Anticancer Res* 2013; 33: 1657–1660.
100. Ma DJ, Galanis E, Anderson SK et al. A phase II trial of everolimus, temozolomide, and radiotherapy in patients with newly diagnosed glioblastoma: NCCCTG N057K. *Neuro Oncol* 2015; 17: 1261–1269.
101. Pitz MW, Eisenhauer EA, MacNeil MV et al. Phase II study of PX-866 in recurrent glioblastoma. *Neuro Oncol* 2015; 17: 1270–1274.
102. Massacesi C, Di Tomaso E, Urban P et al. PI3K inhibitors as new cancer therapeutics: implications for clinical trial design. *Onc Targets* 2016; 9: 203–210.
103. Dias-Santagata D, Lam Q, Vernovsky K et al. BRAF V600E mutations are common in pleomorphic xanthoastrocytoma: diagnostic and therapeutic implications. *PLoS One* 2011; 6: e17948.
104. Chamberlain MC. Salvage therapy with BRAF inhibitors for recurrent pleomorphic xanthoastrocytoma: a retrospective case series. *J Neurooncol* 2013; 114: 237–240.
105. Hyman DM, Puzanov I, Subbiah V et al. Vemurafenib in multiple non-melanoma cancers with BRAF V600 mutations. *N Engl J Med* 2015; 373: 726–736.
106. Hainsworth JD, Ervin T, Friedman E et al. Concurrent radiotherapy and temozolomide followed by temozolomide and sorafenib in the first-line treatment of patients with glioblastoma multiforme. *Cancer* 2010; 116: 3663–3669.
107. Galanis E, Anderson SK, Lafky JM et al. Phase II study of bevacizumab in combination with sorafenib in recurrent glioblastoma (N0776): a north central cancer treatment group trial. *Clin Cancer Res* 2013; 19: 4816–4823.
108. Reardon DA, Vredenburgh JJ, Desjardins A et al. Effect of CYP3A-inducing anti-epileptics on sorafenib exposure: results of a phase II study of sorafenib plus daily temozolomide in adults with recurrent glioblastoma. *J Neurooncol* 2011; 101: 57–66.
109. Zustovitch F, Landi L, Lombardi G et al. Sorafenib plus daily low-dose temozolomide for relapsed glioblastoma: a phase II study. *Anticancer Res* 2013; 33: 3487–3494.
110. Lee EQ, Kuhn J, Lamborn KR et al. Phase I/II study of sorafenib in combination with temsirolimus for recurrent glioblastoma or gliosarcoma: North American Brain Tumor Consortium study 05-02. *Neuro Oncol* 2012; 14: 1511–1518.
111. Hottinger AF, Aissa AB, Espeli V et al. Phase I study of sorafenib combined with radiation therapy and temozolomide as first-line treatment of high-grade glioma. *Br J Cancer* 2014; 110: 2655–2661.
112. Vousden KH, Lane DP. p53 in health and disease. *Nat Rev Mol Cell Biol* 2007; 8: 275–283.
113. Sidransky D, Mikkelsen T, Schwchheimer K et al. Clonal expansion of p53 mutant cells is associated with brain tumour progression. *Nature* 1992; 355: 846–847.
114. Böglér O, Huang HJ, Cavenee WK. Loss of wild-type p53 bestows a growth advantage on primary cortical astrocytes and facilitates their *in vitro* transformation. *Cancer Res* 1995; 55: 2746–2751.
115. Reifemberger G, Liu L, Ichimura K et al. Amplification and overexpression of the MDM2 gene in a subset of human malignant gliomas without p53 mutations. *Cancer Res* 1993; 53: 2736–2739.
116. Duffy MJ, Synnott NC, McGowan PM et al. p53 as a target for the treatment of cancer. *Cancer Treat Rev* 2014; 40: 1153–1160.
117. Costa B, Bendinelli S, Gabelloni P et al. Human glioblastoma multiforme: p53 reactivation by a novel MDM2 inhibitor. *PLoS One* 2013; 8: e72281.
118. Verreault M, Schmitt C, Goldwirt L et al. Preclinical efficacy of the MDM2 inhibitor RG7112 in MDM2-amplified and TP53 wild-type glioblastomas. *Clin Cancer Res* 2016; 22: 1185–1196.
119. Ohgaki H, Kleihues P. Genetic alterations and signaling pathways in the evolution of gliomas. *Cancer Sci* 2009; 100: 2235–2241.
120. Michaud K, Solomon DA, Oermann E et al. Pharmacologic inhibition of cyclin-dependent kinases 4 and 6 arrests the growth of glioblastoma multiforme intracranial xenografts. *Cancer Res* 2010; 70: 3228–3238.
121. Wiedemeyer WR, Dunn IF, Quayle SN et al. Pattern of retinoblastoma pathway inactivation dictates response to CDK4/6 inhibition in GBM. *Proc Natl Acad Sci USA* 2010; 107: 11501–11506.
122. Cen L, Carlson BL, Schroeder MA et al. p16-Cdk4-Rb axis controls sensitivity to a cyclin-dependent kinase inhibitor PD0332991 in glioblastoma xenograft cells. *Neuro Oncol* 2012; 14: 870–881.
123. Barton KL, Misuraca K, Cordero F et al. PD-0332991, a CDK4/6 inhibitor, significantly prolongs survival in a genetically engineered mouse model of brainstem glioma. *PLoS One* 2013; 8: e77639.
124. Mir SE, De Witt Hamer PC, Krawczyk PM et al. In silico analysis of kinase expression identifies WEE1 as a gatekeeper against mitotic catastrophe in glioblastoma. *Cancer Cell* 2010; 18: 244–257.
125. De Witt Hamer PC, Mir SE, Noske D et al. WEE1 kinase targeting combined with DNA-damaging cancer therapy catalyzes mitotic catastrophe. *Clin Cancer Res* 2011; 17: 4200–4207.
126. Toledo CM, Ding Y, Hoellerbauer P et al. Genome-wide CRISPR-Cas9 Screens Reveal Loss of Redundancy between PKMYT1 and WEE1 in Glioblastoma Stem-like Cells. *Cell Rep* 2015; 13: 2425–2439.
127. Gupta SK, Mladek AC, Carlson BL et al. Discordant *in vitro* and *in vivo* chemopotentiating effects of the PARP inhibitor veliparib in temozolomide-sensitive versus -resistant glioblastoma multiforme xenografts. *Clin Cancer Res* 2014; 20: 3730–3741.
128. Venere M, Hamerlik P, Wu Q et al. Therapeutic targeting of constitutive PARP activation compromises stem cell phenotype and survival of glioblastoma-initiating cells. *Cell Death Differ* 2014; 21: 258–269.
129. Robins HI, Zhang P, Gilbert M et al. ATCT-27NRG Oncology/RTOG 0929: a randomized phase I/II study of ABT-888IN combination with temozolomide in recurrent temozolomide resistant glioblastoma. *Neuro Oncol* 2015; 17(Suppl 5): v7.
130. Yan H, Parsons DW, Jin G et al. IDH1 and IDH2 mutations in gliomas. *N Engl J Med* 2009; 360: 765–773.
131. Hartmann C, Meyer J, Balss J et al. Type and frequency of IDH1 and IDH2 mutations are related to astrocytic and oligodendroglial differentiation and age: a study of 1,010 diffuse gliomas. *Acta Neuropathol* 2009; 118: 469–474.
132. Mondesir J, Willekens C, Touat M et al. IDH1 and IDH2 mutations as novel therapeutic targets: current perspectives. *J Blood Med* 2016; 7: 171–180.
133. Turcan S, Rohle D, Goenka A et al. IDH1 mutation is sufficient to establish the glioma hypermethylator phenotype. *Nature* 2012; 483: 479–483.
134. Mellinghoff IK, Touat M, Maher E et al. ACTR-46. AG120, a first-in-class mutant IDH1 inhibitor in patients with recurrent or progressive

- IDH1 mutant glioma: results from the phase 1 glioma expansion cohorts. *Neuro-Oncology* 2016; 18(suppl 6): vi12.
135. Schumacher T, Bunse L, Pusch S et al. A vaccine targeting mutant IDH1 induces antitumour immunity. *Nature* 2014; 512: 324–327.
  136. Pellegatta S, Valletta L, Corbetta C et al. Effective immuno-targeting of the IDH1 mutation R132H in a murine model of intracranial glioma. *Acta Neuropathol Commun* 2015; 3: 4.
  137. Xu J, Sampath D, Lang FF et al. Vorinostat modulates cell cycle regulatory proteins in glioma cells and human glioma slice cultures. *J Neurooncol* 2011; 105: 241–251.
  138. Cornago M, Garcia-Alberich C, Blasco-Angulo N et al. Histone deacetylase inhibitors promote glioma cell death by G2 checkpoint abrogation leading to mitotic catastrophe. *Cell Death Dis* 2014; 5: e1435.
  139. Grasso CS, Tang Y, Truffaux N et al. Functionally defined therapeutic targets in diffuse intrinsic pontine glioma. *Nat Med* 2015; 21: 555–559.
  140. Galanis E, Jaeckle KA, Maurer MJ et al. Phase II trial of vorinostat in recurrent glioblastoma multiforme: a north central cancer treatment group study. *J Clin Oncol* 2009; 27: 2052–2058.
  141. Lee EQ, Puduvalli VK, Reid JM et al. Phase I study of vorinostat in combination with temozolomide in patients with high-grade gliomas: North American Brain Tumor Consortium Study 04-03. *Clin Cancer Res* 2012; 18: 6032–6039.
  142. Puduvalli VK, Wu J, Yuan Y, Armstrong TS et al. Brain Tumor Trials Collaborative Bayesian Adaptive Randomized Phase II trial of bevacizumab plus vorinostat versus bevacizumab alone in adults with recurrent glioblastoma (BTTC-1102). 2015 ASCO Annual Meeting. *J Clin Oncol* 2015; 33(suppl; abstr 2012).
  143. Lee EQ, Reardon DA, Schiff D et al. Phase II study of panobinostat in combination with bevacizumab for recurrent glioblastoma and anaplastic glioma. *Neuro Oncol* 2015; 17: 862–867.
  144. Cheng Z, Gong Y, Ma Y et al. Inhibition of BET bromodomain targets genetically diverse glioblastoma. *Clin Cancer Res* 2013; 19: 1748–1759.
  145. de Vries NA, Hulsman D, Akhtar W et al. Prolonged Ezh2 depletion in glioblastoma causes a robust switch in cell fate resulting in tumor progression. *Cell Rep* 2015; 14: S2211–S1247.
  146. Pastori C, Kapranov P, Penas C et al. The Bromodomain protein BRD4 controls HOTAIR, a long noncoding RNA essential for glioblastoma proliferation. *Proc Natl Acad Sci USA* 2015; 112: 8326–8331.
  147. Bai H, Harmanci AS, Erson-Omay EZ et al. Integrated genomic characterization of IDH1-mutant glioma malignant progression. *Nat Genet* 2016; 48: 59–66.
  148. Friedman HS, Prados MD, Wen PY et al. Bevacizumab alone and in combination with irinotecan in recurrent glioblastoma. *J Clin Oncol* 2009; 27: 4733–4740.
  149. Kreisl TN, Kim L, Moore K et al. Phase II trial of single-agent bevacizumab followed by bevacizumab plus irinotecan at tumor progression in recurrent glioblastoma. *J Clin Oncol* 2009; 27: 740–745.
  150. de Groot JF, Lamborn KR, Chang SM et al. Phase II study of aflibercept in recurrent malignant glioma: a North American Brain Tumor Consortium study. *J Clin Oncol* 2011; 29: 2689–2695.
  151. Neyns B, Sadones J, Chaskis C et al. Phase II study of sunitinib malate in patients with recurrent high-grade glioma. *J Neurooncol* 2011; 103: 491–501.
  152. Kreisl TN, Smith P, Sul J et al. Continuous daily sunitinib for recurrent glioblastoma. *J Neurooncol* 2013; 111: 41–48.
  153. Hutterer M, Nowosielski M, Haybaeck J et al. A single-arm phase II Austrian/German multicenter trial on continuous daily sunitinib in primary glioblastoma at first recurrence (SURGE 01-07). *Neuro Oncol* 2014; 16: 92–102.
  154. Batchelor TT, Duda DG, di Tomaso E et al. Phase II study of cediranib, an oral pan-vascular endothelial growth factor receptor tyrosine kinase inhibitor, in patients with recurrent glioblastoma. *J Clin Oncol* 2010; 28: 2817–2823.
  155. Batchelor TT, Mulholland P, Neyns B et al. Phase III randomized trial comparing the efficacy of cediranib as monotherapy, and in combination with lomustine, versus lomustine alone in patients with recurrent glioblastoma. *J Clin Oncol* 2013; 31: 3212–3218.
  156. Lee EQ, Kaley TJ, Duda DG et al. A multicenter, phase II, randomized, noncomparative clinical trial of radiation and temozolomide with or without vandetanib in newly diagnosed glioblastoma patients. *Clin Cancer Res* 2015; 21: 3610–3618.
  157. Muhic A, Poulsen HS, Sorensen M et al. Phase II open-label study of nintedanib in patients with recurrent glioblastoma multiforme. *J Neurooncol* 2013; 111: 205–212.
  158. Stupp R, Hegi ME, Gorlia T et al. Cilengitide combined with standard treatment for patients with newly diagnosed glioblastoma with methylated MGMT promoter (CENTRIC EORTC 26071-22072 study): a multicentre, randomised, open-label, phase 3 trial. *Lancet Oncol* 2014; 15: 1100–1108.
  159. Nabors LB, Fink KL, Mikkelsen T et al. Two cilengitide regimens in combination with standard treatment for patients with newly diagnosed glioblastoma and unmethylated MGMT gene promoter: results of the open-label, controlled, randomized phase II CORE study. *Neuro Oncol* 2015; 17: 708–717.
  160. Wick W, Puduvalli VK, Chamberlain MC et al. Phase III study of enzastaurin compared with lomustine in the treatment of recurrent intracranial glioblastoma. *J Clin Oncol* 2010; 28: 1168–1174.
  161. Taal W, Oosterkamp HM, Walenkamp AM et al. Single-agent bevacizumab or lomustine versus a combination of bevacizumab plus lomustine in patients with recurrent glioblastoma (BELOB trial): a randomised controlled phase 2 trial. *Lancet Oncol* 2014; 15: 943–953.
  162. Chinot OL, Wick W, Mason W et al. Bevacizumab plus radiotherapy-temozolomide for newly diagnosed glioblastoma. *N Engl J Med* 2014; 370: 709–722.
  163. Gilbert MR, Dignam JJ, Armstrong TS et al. A randomized trial of bevacizumab for newly diagnosed glioblastoma. *N Engl J Med* 2014; 370: 699–708.
  164. Galanis E, Anderson SK, Anastasiadis P et al. NCCTG N0872 (Alliance): a randomized placebo-controlled phase II trial of bevacizumab plus dasatinib in patients with recurrent glioblastoma (GBM). 2015 ASCO Annual Meeting. *J Clin Oncol* 2015; 33(suppl; abstr 2004).
  165. Duerinckx J, Du Four S, Vandervorst F et al. Randomized phase II study of axitinib versus physicians best alternative choice of therapy in patients with recurrent glioblastoma. *J Neurooncol* 2016; 128: 147–155.
  166. Tanaka S, Louis DN, Curry WT et al. Diagnostic and therapeutic avenues for glioblastoma: no longer a dead end? *Nat Rev Clin Oncol* 2013; 10: 14–26.
  167. Batchelor TT, Reardon DA, de Groot JF et al. Antiangiogenic therapy for glioblastoma: current status and future prospects. *Clin Cancer Res* 2014; 20: 5612–5619.
  168. Wick W, Platten M, Wick A et al. Current status and future directions of anti-angiogenic therapy for gliomas. *Neuro Oncol* 2016; 18: 315–328.
  169. Wick W, Brandes A, Gorlia T et al. LB-05phase III trial exploring the combination of bevacizumab and lomustine in patients with first recurrence of a glioblastoma: the EORTC 26101 trial. *Neuro Oncol* 2015; 17(Suppl 5): v1.
  170. Sandmann T, Bourgon R, Garcia J et al. Patients with proneural glioblastoma may derive overall survival benefit from the addition of bevacizumab to first-line radiotherapy and temozolomide: retrospective analysis of the AVAglio trial. *J Clin Oncol* 2015; 33: 2735–2744.
  171. Hatterer E, Davoust N, Didier-Bazes M et al. How to drain without lymphatics? Dendritic cells migrate from the cerebrospinal fluid to the B-cell follicles of cervical lymph nodes. *Blood* 2006; 107: 806–812.
  172. Iff JJ, Wang M, Liao Y et al. A paravascular pathway facilitates CSF flow through the brain parenchyma and the clearance of interstitial solutes, including amyloid  $\beta$ . *Sci Transl Med* 2012; 4: 147ra111.
  173. Louveau A, Smirnov I, Keyes TJ et al. Structural and functional features of central nervous system lymphatic vessels. *Nature* 2015; 523: 337–341.
  174. Aspelund A, Antila S, Proulx ST et al. A dural lymphatic vascular system that drains brain interstitial fluid and macromolecules. *J Exp Med* 2015; 212: 991–999.
  175. Garon EB, Rizvi NA, Hui R et al. Pembrolizumab for the treatment of non-small-cell lung cancer. *N Engl J Med* 2015; 372: 2018–2028.

176. Robert C, Schachter J, Long GV et al. Pembrolizumab versus Ipilimumab in Advanced Melanoma. *N Engl J Med* 2015; 372: 2521–2532.
177. Berghoff AS, Kiesel B, Widhalm G et al. Programmed death ligand 1 expression and tumor-infiltrating lymphocytes in glioblastoma. *Neuro Oncol* 2015; 17: 1064–1075.
178. Nduom EK, Wei J, Yaghi NK et al. PD-L1 expression and prognostic impact in glioblastoma. *Neuro Oncol* 2016; 18: 195–205.
179. Fecci PE, Ochiai H, Mitchell DA et al. Systemic CTLA-4 blockade ameliorates glioma-induced changes to the CD4+ T cell compartment without affecting regulatory T-cell function. *Clin Cancer Res* 2007; 13: 2158–2167.
180. Agarwalla P, Barnard Z, Fecci P et al. Sequential immunotherapy by vaccination with GM-CSF-expressing glioma cells and CTLA-4 blockade effectively treats established murine intracranial tumors. *J Immunother* 2012; 35: 385–389.
181. Preusser M, Lim M, Hafner DA et al. Prospects of immune checkpoint modulators in the treatment of glioblastoma. *Nat Rev Neurol* 2015; 11: 504–514.
182. Reardon DA, Gokhale PC, Klein SR et al. Glioblastoma eradication following immune checkpoint blockade in an orthotopic, immunocompetent model. *Cancer Immunol Res* 2016; 4: 124–135.
183. Reardon DA, Sampson JH, Sahebjam S et al. Safety and activity of nivolumab (nivo) monotherapy and nivo in combination with ipilimumab (ipi) in recurrent glioblastoma (GBM): updated results from checkmate-143. 2016 ASCO Annual Meeting. *J Clin Oncol* 2016; 34(Suppl): abstr 2014.
184. Reardon DA, Kim T-M, Frenel J-S et al. ATIM-35. Results of the phase IB KEYNOTE-028 multi-cohort trial of pembrolizumab monotherapy in patients with recurrent PD-L1-positive glioblastoma multiforme (GBM). *Neuro-Oncology* 2016; 18(Suppl 6): vi25–vi26.
185. Reardon D, Kaley T, Dietrich J et al. ATIM-04. Phase 2 study to evaluate the clinical efficacy and safety of MEDI4736 (durvalumab [DUR]) in patients with glioblastoma (GBM): results for cohort B (DUR monotherapy), bevacizumab (BEV) naïve patients with recurrent GBM. *Neuro-Oncology* 2016; 18(Suppl 6): vi18.
186. Omuro A, Vlahovic G, Baehring J et al. ATIM-16. Nivolumab combined with radiotherapy with or without temozolomide in patients with newly diagnosed glioblastoma: results from phase 1 safety cohorts in checkmate 143. *Neuro-Oncology* 2016; 18(suppl 6): vi21.
187. Snyder A, Makarov V, Merghoub T et al. Genetic basis for clinical response to CTLA-4 blockade in melanoma. *N Engl J Med* 2014; 371: 2189–2199.
188. Van Allen EM, Miao D, Schilling B et al. Genomic correlates of response to CTLA-4 blockade in metastatic melanoma. *Science* 2015; 350: 207–211.
189. Rizvi NA, Hellmann MD, Snyder A et al. Cancer immunology. Mutational landscape determines sensitivity to PD-1 blockade in non-small cell lung cancer. *Science* 2015; 348: 124–128.
190. Le DT, Uram JN, Wang H et al. PD-1 blockade in tumors with mismatch-repair deficiency. *N Engl J Med* 2015; 372: 2509–2520.
191. Bouffet E, Larouche V, Campbell BB et al. Immune checkpoint inhibition for hypermutant glioblastoma multiforme resulting from germline biallelic mismatch repair deficiency. *J Clin Oncol* 2016; 34: 2206–2211.
192. Ardon H, Van Gool SW, Verschuere T et al. Integration of autologous dendritic cell-based immunotherapy in the standard of care treatment for patients with newly diagnosed glioblastoma: results of the HGG-2006 phase I/II trial. *Cancer Immunol Immunother* 2012; 61: 2033–2044.
193. Phuphanich S, Wheeler CJ, Rudnick JD et al. Phase I trial of a multi-epitope-pulsed dendritic cell vaccine for patients with newly diagnosed glioblastoma. *Cancer Immunol Immunother* 2013; 62: 125–135.
194. Bloch O, Crane CA, Fuks Y et al. Heat-shock protein peptide complex-96 vaccination for recurrent glioblastoma: a phase II, single-arm trial. *Neuro Oncol* 2014; 16: 274–279.
195. Hdeib A, Sloan AE. Dendritic cell immunotherapy for solid tumors: evaluation of the DCVax® platform in the treatment of glioblastoma multiforme. *CNS Oncol* 2015; 4: 63–69.
196. Phuphanich S, Wheeler C, Rudnick J et al. ATIM-25. Ten-year follow up with long term remission in patients with newly diagnosed glioblastoma (GBM) treated with ICT-107 vaccine (phase I). *Neuro-Oncology* 2016; 18(Suppl 6): vi23.
197. Reardon D, Peereboom D, Nabors B et al. ATIM-11. Phase 2 trial of SL-701, a novel immunotherapy comprised of synthetic short peptides against GBM targets IL-13R $\alpha$ 2, EphA2, and survivin, in adults with second-line recurrent GBM: interim results. *Neuro-Oncology* 2016; 18(Suppl 6): vi20.
198. Johnson LA, Scholler J, Ohkuri T et al. Rational development and characterization of humanized anti-EGFR variant III chimeric antigen receptor T cells for glioblastoma. *Sci Transl Med* 2015; 7: 275ra222.
199. O'Rourke D, Desai A, Morrisette J et al. IMCT-15PILOT study of T cells redirected to EGFRvIII with a chimeric antigen receptor in patients with EGFRvIII+ glioblastoma. *Neuro-Oncology* 2015; 17(Suppl 5): v110–v111.
200. Rosenberg S, Verreault M, Schmitt C et al. Multi-omics analysis of primary glioblastoma cell lines shows recapitulation of pivotal molecular features of parental tumors. *Neuro Oncol* 2016 [epub ahead of print]; now160.
201. Mellinger IK, Wang MY, Vivanco I et al. Molecular determinants of the response of glioblastomas to EGFR kinase inhibitors. *N Engl J Med* 2005; 353: 2012–2024.
202. Haas-Kogan DA, Prados MD, Tihan T et al. Epidermal growth factor receptor, protein kinase B/Akt, and glioma response to erlotinib. *J Natl Cancer Inst* 2005; 97: 880–887.
203. Touat M, Duran-Peña A, Alentorn A et al. Emerging circulating biomarkers in glioblastoma: promises and challenges. *Expert Rev Mol Diagn* 2015; 15: 1311–1323.
204. Pentsova EI, Shah RH, Tang J et al. Evaluating cancer of the central nervous system through next-generation sequencing of cerebrospinal fluid. *J Clin Oncol* 2016; 34: 2404–2415.
205. Klingler S, Guo B, Yao J et al. Development of resistance to EGFR-targeted therapy in malignant glioma can occur through EGFR-dependent and -independent mechanisms. *Cancer Res* 2015; 75: 2109–2119.
206. Hegi ME, Diserens AC, Bady P et al. Pathway analysis of glioblastoma tissue after preoperative treatment with the EGFR tyrosine kinase inhibitor gefitinib—a phase II trial. *Mol Cancer Ther* 2011; 10: 1102–1112.
207. Yu C, Mannan AM, Yvone GM et al. High-throughput identification of genotype-specific cancer vulnerabilities in mixtures of barcoded tumor cell lines. *Nat Biotechnol* 2016; 34: 419–423.
208. Xiu J, Piccioni D, Juarez T et al. Multi-platform molecular profiling of a large cohort of glioblastomas reveals potential therapeutic strategies. *Oncotarget* 2016; 7: 21556–21569.
209. Oberoi RK, Parrish KE, Sio TT et al. Strategies to improve delivery of anticancer drugs across the blood–brain barrier to treat glioblastoma. *Neuro Oncol* 2016; 18: 27–36.
210. Lassman AB, Rossi MR, Raizer JJ et al. Molecular study of malignant gliomas treated with epidermal growth factor receptor inhibitors: tissue analysis from North American Brain Tumor Consortium Trials 01-03 and 00-01. *Clin Cancer Res* 2005; 11: 7841–7850.
211. de Vries NA, Buckle T, Zhao J et al. Restricted brain penetration of the tyrosine kinase inhibitor erlotinib due to the drug transporters P-gp and BCRP. *Invest New Drugs* 2012; 30: 443–449.
212. Dréan A, Goldwirt L, Verreault M et al. Blood–brain barrier, cytotoxic chemotherapies and glioblastoma. *Expert Rev Neurother* 2016; 16: 1285–1300.
213. Carpentier A, Canney M, Vignot A et al. Clinical trial of blood–brain barrier disruption by pulsed ultrasound. *Sci Transl Med* 2016; 8: 343re342.
214. Andre F, Mardis E, Salm M et al. Prioritizing targets for precision cancer medicine. *Ann Oncol* 2014; 25: 2295–2303.
215. Aldape KD, Ballman K, Furth A et al. Immunohistochemical detection of EGFRvIII in high malignancy grade astrocytomas and evaluation of prognostic significance. *J Neuropathol Exp Neurol* 2004; 63: 700–707.
216. Capper D, Zentgraf H, Bals J et al. Monoclonal antibody specific for IDH1 R132H mutation. *Acta Neuropathol* 2009; 118: 599–601.

217. Capper D, Weissert S, Bals J et al. Characterization of R132H mutation-specific IDH1 antibody binding in brain tumors. *Brain Pathol* 2010; 20: 245–254.
218. Capper D, Preusser M, Habel A et al. Assessment of BRAF V600E mutation status by immunohistochemistry with a mutation-specific monoclonal antibody. *Acta Neuropathol* 2011; 122: 11–19.
219. Fischer I, de la Cruz C, Rivera AL, Aldape K. Utility of chromogenic in situ hybridization (CISH) for detection of EGFR amplification in glioblastoma: comparison with fluorescence in situ hybridization (FISH). *Diagn Mol Pathol* 2008; 17: 227–230.
220. Nikiforova MN, Wald AI, Melan MA et al. Targeted next-generation sequencing panel (GliOSeq) provides comprehensive genetic profiling of central nervous system tumors. *Neuro Oncol* 2016; 18: 379–387.
221. Herbst RS, Gandara DR, Hirsch FR et al. Lung master protocol (Lung-MAP)-a biomarker-driven protocol for accelerating development of therapies for squamous cell lung cancer: SWOG S1400. *Clin Cancer Res* 2015; 21: 1514–1524.
222. Ramkissoon SH, Bi WL, Schumacher SE et al. Clinical implementation of integrated whole-genome copy number and mutation profiling for glioblastoma. *Neuro Oncol* 2015; 17: 1344–1355.

**B. Article sur le ciblage des mutation BRAF par vemurafenib dans les gliomes malins / Article on the targeting of BRAF mutations with vemurafenib**



## BRAF Inhibition in $BRAF^{V600}$ -Mutant Gliomas: Results From the VE-BASKET Study

Thomas Kaley, Mehdi Touat, Vivek Subbiah, Antoine Hollebecque, Jordi Rodon, A. Craig Lockhart, Vicki Keedy, Franck Bielle, Ralf-Dieter Hofheinz, Florence Joly, Jean-Yves Blay, Ian Chau, Igor Puzanov, Noopur S. Raje, Jurgen Wolf, Lisa M. DeAngelis, Martina Makrutski, Todd Riehl, Bethany Pitcher, Jose Baselga, and David M. Hyman

Author affiliations and support information (if applicable) appear at the end of this article.

Published at [jco.org](http://jco.org) on October 23, 2018.

T.K., M.T., and V.S. contributed equally to this work.

Clinical trial information: NCT01524978.

Corresponding author: David M. Hyman, MD, Memorial Sloan Kettering Cancer Center, 1275 York Ave, New York, NY 10065; e-mail: [hymand@mskcc.org](mailto:hymand@mskcc.org).

© 2018 by American Society of Clinical Oncology. Creative Commons Attribution Non-Commercial No Derivatives 4.0 License.



0732-183X/18/3635w-3477w/\$20.00

### A B S T R A C T

#### Purpose

$BRAF^{V600}$  mutations are frequently found in several glioma subtypes, including pleomorphic xanthoastrocytoma (PXA) and ganglioglioma and much less commonly in glioblastoma. We sought to determine the activity of vemurafenib, a selective inhibitor of  $BRAF^{V600}$ , in patients with gliomas that harbor this mutation.

#### Patients and Methods

The VE-BASKET study was an open-label, nonrandomized, multicohort study for  $BRAF^{V600}$ -mutant nonmelanoma cancers. Patients with  $BRAF^{V600}$ -mutant glioma received vemurafenib 960 mg twice per day continuously until disease progression, withdrawal, or intolerable adverse effects. Key end points included confirmed objective response rate by RECIST version 1.1, progression-free survival, overall survival, and safety.

#### Results

Twenty-four patients (median age, 32 years; 18 female and six male patients) with glioma, including malignant diffuse glioma ( $n = 11$ ; six glioblastoma and five anaplastic astrocytoma), PXA ( $n = 7$ ), anaplastic ganglioglioma ( $n = 3$ ), pilocytic astrocytoma ( $n = 2$ ), and high-grade glioma, not otherwise specified ( $n = 1$ ), were treated. Confirmed objective response rate was 25% (95% CI, 10% to 47%) and median progression-free survival was 5.5 months (95% CI, 3.7 to 9.6 months). In malignant diffuse glioma, best response included one partial response and five patients with stable disease, two of whom had disease stabilization that lasted more than 1 year. In PXA, best response included one complete response, two partial responses, and three patients with stable disease. Additional partial responses were observed in patients with pilocytic astrocytoma and anaplastic ganglioglioma (one each). The safety profile of vemurafenib was generally consistent with that of previously published studies.

#### Conclusion

Vemurafenib demonstrated evidence of durable antitumor activity in some patients with  $BRAF^{V600}$ -mutant gliomas, although efficacy seemed to vary qualitatively by histologic subtype. Additional study is needed to determine the optimal use of vemurafenib in patients with primary brain tumors and to identify the mechanisms driving differential responses across histologic subsets.

*J Clin Oncol* 36:3477-3484. © 2018 by American Society of Clinical Oncology. Creative Commons Attribution Non-Commercial No Derivatives 4.0 License: <https://creativecommons.org/licenses/by-nc-nd/4.0/>

### INTRODUCTION

Gliomas represent a heterogeneous group of tumors with a range of behaviors.<sup>1</sup> Aggressive malignant diffuse gliomas include WHO grade IV glioblastoma (GBM) and WHO grade III isocitrate dehydrogenase (*IDH*) 1/2 wild-type anaplastic gliomas.<sup>1</sup> For decades, standard of care for GBM, including surgery, chemoradiation with temozolomide, and bevacizumab at recurrence has not significantly improved median overall

survival (OS) of 14 to 18 months.<sup>2-4</sup> Recurrent GBM is highly resistant, with a historical median progression-free survival (PFS) of 9 weeks and a 6-month PFS of 5% to 15% for nonbevacizumab therapies.<sup>5,6</sup> Patients with recurrent grade III malignant diffuse gliomas fare only slightly better, with a median PFS of 13 weeks and 31% 6-month PFS in patients with recurrent anaplastic astrocytoma.<sup>5</sup>

Patients with *IDH1/2*-mutant grade II astrocytomas and oligodendrogliomas have better prognoses, although these tumors eventually

DOI: <https://doi.org/10.1200/JCO.2018.78.9990>

© 2018 by American Society of Clinical Oncology 3477

Downloaded from [ascopubs.org](http://ascopubs.org) by 31.34.66.224 on October 18, 2020 from 031.034.066.224  
Copyright © 2020 American Society of Clinical Oncology. All rights reserved.

progress and transform into malignant diffuse gliomas.<sup>1</sup> Low-grade gliomas also encompass rarer *IDH1/2* wild-type histologies, including pilocytic astrocytoma (PA), pleomorphic xanthoastrocytoma (PXA), and ganglioglioma. These are more indolent, usually occur in younger patients, and can sometimes be cured with surgery and radiation<sup>1</sup>; however, a subset of tumors exhibit higher-grade histologic features or aggressive biology at initial presentation or relapse. There is no standard effective treatment for these patients.

Irrespective of glioma subtype, radiographic volumetric response to conventional chemotherapies is rare, occurring in 6% of patients with GBM and in 14% with patients with anaplastic gliomas.<sup>5,6</sup> Bevacizumab seems to delay disease progression and ameliorate neurologic symptoms in patients with GBM but provides no survival advantage.<sup>4,7,8</sup> Radiographic response rates with bevacizumab may be up to 40%,<sup>9,10</sup> but these are often pseudoresponses that result from blood–brain barrier reconstitution and decreased enhancement on magnetic resonance imaging, rather than an indication of true antitumor effects.<sup>11</sup>

Selective targeting of oncogenic mutations has revolutionized the treatment of genomically defined subtypes of non–small-cell lung cancer (NSCLC), breast, gastric, and ovarian cancers, melanoma, and other solid and hematologic cancers.<sup>12</sup> Targeted approaches include selective inhibition of the *BRAF*<sup>V600</sup> oncogene, which is the standard treatment of melanoma, NSCLC, anaplastic thyroid cancer, and Erdheim–Chester disease.<sup>13–18</sup> *BRAF*<sup>V600</sup> inhibition has shown promise in *BRAF*<sup>V600</sup>-mutant papillary thyroid cancer,<sup>19</sup> colorectal cancer,<sup>20</sup> and hairy cell leukemia.<sup>21</sup> Of importance, *BRAF*<sup>V600</sup> mutations have been identified in several glioma subtypes, specifically in select rare *IDH1/2* wild-type gliomas, including PXAs (38% to 100%), gangliogliomas (18% to 57%), anaplastic gangliogliomas (AGGs; 50%), PAs (9%), and less commonly (< 3%) in high-grade gliomas, including GBM.<sup>22–26</sup> Despite the *BRAF*<sup>V600</sup> mutation being a recurrent genomic event across multiple glioma subtypes, to our knowledge no prospective therapeutic study has investigated targeted therapy in this setting, although retrospective case series provide some evidence for the activity of RAF inhibitors with or without MEK inhibitors.<sup>27–32</sup>

Vemurafenib is a selective oral inhibitor of the oncogenic *BRAF*<sup>V600</sup> kinase approved globally for the treatment of patients with *BRAF*<sup>V600</sup>-mutant metastatic or unresectable melanoma and in the United States for patients with Erdheim–Chester disease. The VE-BASKET study was a nonrandomized, open-label, histology-agnostic, basket study for patients with nonmelanoma solid tumors and myeloma that harbors *BRAF*<sup>V600</sup> mutations.<sup>33</sup> VE-BASKET enrolled 24 patients with glioma. We now report the final efficacy and safety of vemurafenib in this cohort.

## PATIENTS AND METHODS

### Study Design and Population

The phase II, histology-independent VE-BASKET study was conducted at 23 centers worldwide in patients with a range of *BRAF*<sup>V600</sup> mutation–positive tumor types. Nine centers enrolled one or more patients with glioma. The study design has been described in full elsewhere.<sup>33</sup> In brief, the study included six cohorts of patients with prespecified cancers—NSCLC, ovarian, colorectal, and breast cancers, cholangiocarcinoma, and multiple myeloma—as well as a seventh cohort

of patients with other *BRAF*<sup>V600</sup> mutation–positive cancers. The other cohort permitted enrollment of patients with cancer types not otherwise specified, including gliomas. As this cohort was anticipated to enroll a heterogeneous patient group, no maximum cohort size was specified. Rather, the cohort remained open until the last disease prespecified cohort closed. Written informed consent was obtained from all participants. The study was performed in accordance with provisions of the Declaration of Helsinki and Good Clinical Practice guidelines. The protocol was approved by institutional review boards or human research ethics committees at each participating center. Eligibility was confirmed by the sponsor on all patients.

Patients with brain tumors were required to have histologically confirmed glioma (any grade) and confirmation of *BRAF*<sup>V600</sup> mutation in tumor material obtained at any point in treatment. Testing for *BRAF*<sup>V600</sup> mutation was performed according to local testing procedures in a Clinical Laboratories Improvement Amendment–accredited laboratory or equivalent for sites outside the United States. Central pathologic confirmation of locally reported glioma subtypes and *BRAF* mutation was not performed. As the clinical trial database did not capture glioma-specific biomarkers (methylguanine–DNA–methyltransferase [*MGMT*] promoter methylation, *IDH1* mutation, or *CDKN2A/B* deletion), these data, when available, were extracted directly from pathology reports without source verification by the study sponsor. All patients had recurrent disease after standard therapy; there was no limit on the number of prior therapies, and prior bevacizumab was permitted. Patients had measurable disease (Response Evaluation Criteria in Solid Tumors [RECIST] version 1.1<sup>34</sup>), were age  $\geq$  16 years, with Eastern Cooperative Oncology Group performance status of 0 to 2 and acceptable laboratory parameters. Patients were excluded if they had prior treatment with a *BRAF* or MEK inhibitor, were unable to swallow pills, had intractable vomiting, a corrected QT interval of 450 milliseconds or more, or known leptomeningeal metastases.

### Treatment

Patients received vemurafenib 960 mg twice per day continuously in 28-day cycles until they experienced disease progression, unacceptable toxicity, or withdrew. The vemurafenib dose could be reduced on the basis of toxicity in decrements of 240 mg at each dose administration to a minimum permitted dose of 480 mg twice per day. Patients who were unable to tolerate this minimum dose were removed from the study. Patients were assessed for response by magnetic resonance imaging and clinical examination every two cycles. As VE-BASKET was not specifically designed for the treatment of primary brain tumors, responses were determined using RECIST.<sup>34</sup> Treatment toxicities were evaluated using National Cancer Institute Common Terminology Criteria, version 4.0.<sup>35</sup> Patients were required to have dermatologic assessments at baseline, after cycle 1, then every 12 weeks to evaluate for cutaneous squamous cell carcinoma (SCC), keratoacanthoma, basal cell carcinoma, and any other malignancy. Head and neck examinations were performed at baseline and every 12 weeks thereafter to evaluate for noncutaneous SCC. All patients were required to undergo chest computed tomography at baseline and at least every 6 months thereafter to evaluate for noncutaneous SCC.

### Statistical Analysis

The primary end point of the study was unconfirmed objective radiographic response rate at week 8 or first assessment, as assessed by individual investigators using RECIST version 1.1. Secondary end points included confirmed objective response rate (ORR), clinical benefit rate (defined as confirmed complete response [CR] or partial response [PR] of any duration or stable disease [SD] lasting  $\geq$  6 months), PFS, OS, and toxicity. PFS and OS were estimated using the Kaplan–Meier method and 95% CIs (Clopper–Pearson method). The protocol used an adaptive Simon two-stage design<sup>36</sup> for all tumor-specific cohorts to minimize the number of patients treated if vemurafenib was deemed to be ineffective for a specific tumor type. A response rate of 15% at week 8 was considered low, a response rate of 45% was considered high, and a response rate of 35% was

**Table 1.** Baseline Characteristics

Characteristic	PXA (n = 7)	Malignant Diffuse Glioma* (n = 11)	Other† (n = 6)	All Patients (n = 24)
Sex, No. (%)				
Male	1 (14)	3 (27)	2 (33)	6 (25)
Female	6 (86)	8 (73)	4 (67)	18 (75)
Median age, years (range)	29 (18-57)	42 (23-57)	25.5 (21-81)	32 (18-81)
ECOG performance status, No. (%)				
0	5 (71)	5 (45)	2 (33)	12 (50)
1	1 (14)	4 (36)	1 (17)	6 (25)
2	0	2 (18)	2 (33)	4 (17)
Missing	1 (14)	0	1 (17)	2 (8)
Prior radiotherapy, No. (%)	6 (86)	11 (100)	6 (100)	23 (96)
No. of prior systemic therapies, No. (%)				
0	3 (43)	1 (9)	2 (33)	6 (25)
1	3 (43)	5 (45)	2 (33)	10 (42)
2	0	2 (18)	1 (17)	3 (13)
≥ 3	1 (14)	3 (27)	1 (17)	5 (21)
Median time from first diagnosis to enrollment, months (range)	18.0 (4.0-76.8)	13.4 (3.7-110.0)	30.9 (5.6-141.0)	15.7 (3.7-141.0)
BRAF assay, No. (%)				
Sanger	2 (29)	3 (27)	3	8 (33)
Sequenom	3 (43)	3 (27)	0	6 (25)
PCR	2 (29)	1 (9)	1 (17)	4 (17)
NGS	0	1 (9)	1 (17)	2 (8)
SNaPshot	0	1 (9)	1 (17)	2 (8)
IHC	0	1 (9)	0	1 (4)
Unknown	0	1 (9)	0	1 (4)

Abbreviations: ECOG, Eastern Cooperative Oncology Group; IHC, immunohistochemistry; NGS, next-generation sequencing; PCR, polymerase chain reaction; PXA, pleomorphic xanthoastrocytoma.  
 \*Anaplastic astrocytoma, n = 5; glioblastoma, n = 6.  
 †Pilocytic astrocytoma, n = 2; anaplastic ganglioglioma, n = 3; high-grade glioma, not otherwise specified, n = 1.

considered low but still desirable and indicative of efficacy. Assuming response rates as specified in the hypothesis testing, a power of 80% for a high response rate and 70% for the low but still desirable response rate, and a two-sided  $\alpha$  level of .1, seven, 13, or 19 patients were required in each cohort, depending on results obtained. However, this analysis only applied to prespecified tumor cohorts 1 to 6. As patients with glioma enrolled in cohort 7 (other solid tumors) were considered an exploratory group, response and survival end points were analyzed and reported descriptively. The study was permanently closed and the final data lock performed on January 12, 2017.

## RESULTS

Twenty-four patients with gliomas (median age, 32 years; 18 female patients) were enrolled, including 11 with malignant diffuse glioma (six with GBM and five with anaplastic astrocytoma), seven with PXA, two with PA, three with AGG, and one with a high-grade glioma, not otherwise specified (Table 1). Of the 11 patients with malignant diffuse glioma, four had *MGMT* testing and all were unmethylated. Across the entire cohort, 18 patients had *IDH1* testing (all wild type) and 10 *CDKN2A/B* testing (nine deleted and one wild type). Of the six patients with GBM, all had received prior temozolomide and two had received bevacizumab. Four of five patients with anaplastic astrocytoma had received prior temozolomide. Among the 13 remaining patients with lower-grade glioma, eight had received prior temozolomide and one had received bevacizumab.

Aggregate clinical efficacy data are summarized in Table 2. One CR was observed in a patient with PXA, and five patients

achieved PR—two with PXA and one each with anaplastic astrocytoma, AGG, and PA—for a confirmed ORR in the overall group of 25% (95% CI, 10% to 47%; Table 2). CR lasted 25.9 months or more (censored at last assessment), and PRs lasted 13.1, 9.9, 7.5, 3.4, and 2.4 months. An additional three patients achieved SD that lasted 6 months or more (12.9, 14.9, and 24.8 [censored at last assessment] months), one each with anaplastic astrocytoma, GBM, and PXA, for an overall confirmed clinical benefit rate of 38% (95% CI, 19% to 59%).

Efficacy data at the individual patient level are shown in Figure 1. In patients with PXA (n = 7), best response included one patient with CR, two with PR, three with SD (one that lasted  $\geq$  6 months), and one with progressive disease, which yielded a confirmed clinical benefit rate of 57% (95% CI, 18% to 90%). Best response in patients with malignant diffuse glioma (n = 11) included one patient with PR, five with SD (two of whom had SD that lasted  $\geq$  6 months, thus meeting the definition for clinical benefit), three with progressive disease, and response data unavailable for two as a result of early withdrawal. This yielded a clinical benefit rate of 27% (95% CI, 6% to 61%). In the six patients with GBM, best response was SD in three patients, with two experiencing progression at 3.6 months (censored at the last assessment) and 3.7 months, and one with prolonged SD until 12.9 months. One of five patients with anaplastic astrocytoma achieved PR and two had SD that progressed after 14.9 and 5.6 months. Responses among patients with other tumor types included PR in one patient with PA who was treated for 15.3 months and PR in one patient with AGG who was treated for 13.8 months for a confirmed clinical benefit rate of 33% (95% CI, 4.3% to 77.7%).

Outcome	PXA (n = 7)	Malignant Diffuse Glioma* (n = 11)	Other† (n = 6)	All Patients (n = 24)
Confirmed objective response rate, % (95% CI)	42.9 (9.9 to 81.6)	9.1 (0.2 to 41.3)	33.3 (4.3 to 77.7)	25.0 (9.8 to 46.7)
Best overall response, No. (%)				
Complete response	1 (14.3)	0	0	1 (4.2)
Partial response	2 (28.6)	1 (9.1)	2 (33.3)	5 (20.8)
Stable disease	3 (42.9)	5 (45.5)	2 (33.3)	10 (41.7)
Progressive disease	1 (14.3)	3 (27.3)	1 (16.7)	5 (20.8)
Missing/not evaluable	0	2 (18.2)	1 (16.7)	3 (12.5)
Confirmed clinical benefit‡, % (95% CI)	57.1 (18.4 to 90.1)	27.3 (6.0 to 61.0)	33.3 (4.3 to 77.7)	37.5 (18.8 to 59.4)
Unconfirmed response rate (ORR8§), No. (%)	3 (42.86)	1 (9.09)	1 (16.67)	5 (20.83)

Abbreviations: ORR8, overall response rate at week 8; PXA, pleomorphic xanthoastrocytoma.  
 \*Glioblastoma, n = 6; anaplastic astrocytoma, n = 5.  
 †Pilocytic astrocytoma, n = 2; anaplastic ganglioglioma, n = 3; high-grade glioma, not otherwise specified, n = 1.  
 ‡Clinical benefit includes patients whose best response was confirmed complete response, partial response, or stable disease that lasted ≥ 6 months.  
 §Unconfirmed response rate at week 8 or at first available response assessment.

Overall median PFS for all patients was 5.5 months (95% CI, 3.7 to 9.6 months; Fig 2). Median PFS durations for the PXA, malignant diffuse gliomas, and other cohorts were 5.7 months (95% CI, 3.0 months to not reached [NR]), 5.3 months (95% CI, 1.8 to 12.9 months), and 3.7 months (95% CI, 2.0 to 13.6 months), respectively. Median OS for all patients was 28.2 months (95% CI, 9.6 to 40.1 months). Median OS durations for PXA, malignant

diffuse glioma, and other cohorts were NR (95% CI, 5.0 months to NR), 11.9 months (95% CI, 8.3 to 40.1 months), and 28.2 months (95% CI, 12.8 to 31.6 months), respectively. The longest treatment duration was 39.1 months in a patient with PXA, which was ongoing at study closure (Fig 3)—this was the only patient who had received no radiotherapy or temozolomide before protocol initiation. All patients discontinued the study. Three patients with

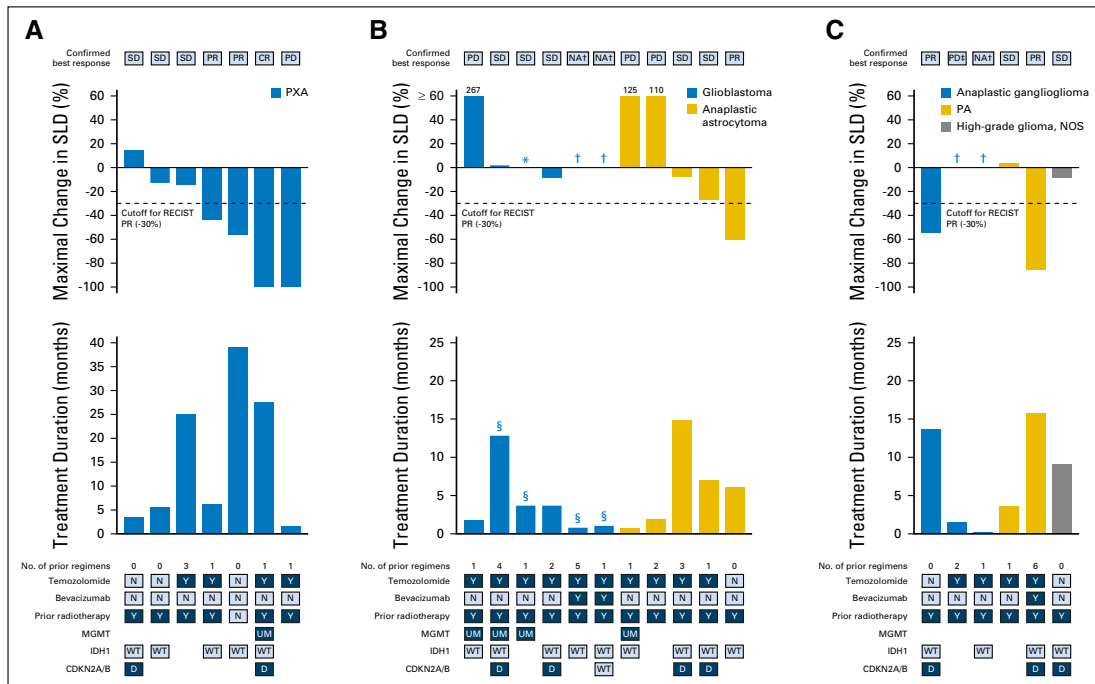


**Fig 1.** Integrated efficacy and treatment duration by patient. Maximal decrease in sum of the longest diameters (SLD), confirmed best response, treatment duration, and prior regimens in patients with (A) PXA, (B) malignant diffuse glioma, and (C) other tumor types. Numbers that appear above individual waterfall bars indicate the percent maximal increase in SLD from baseline. (\*) Unchanged from baseline. (†) Patient had no postbaseline assessments. (‡) Patients with secondary malignant diffuse glioma. CR, complete response; D, deleted; *MGMT*, methylguanine-DNA-methyltransferase gene promoter methylation; *IDH1*, isocitrate dehydrogenase 1 gene; N, no; NA, not available; NOS, not otherwise specified; PA, pilocytic astrocytoma; PD, progressive disease; PR, partial response; PXA, pleomorphic xanthoastrocytoma; SD, stable disease; UM, unmethylated; WT, wild type; Y, yes.

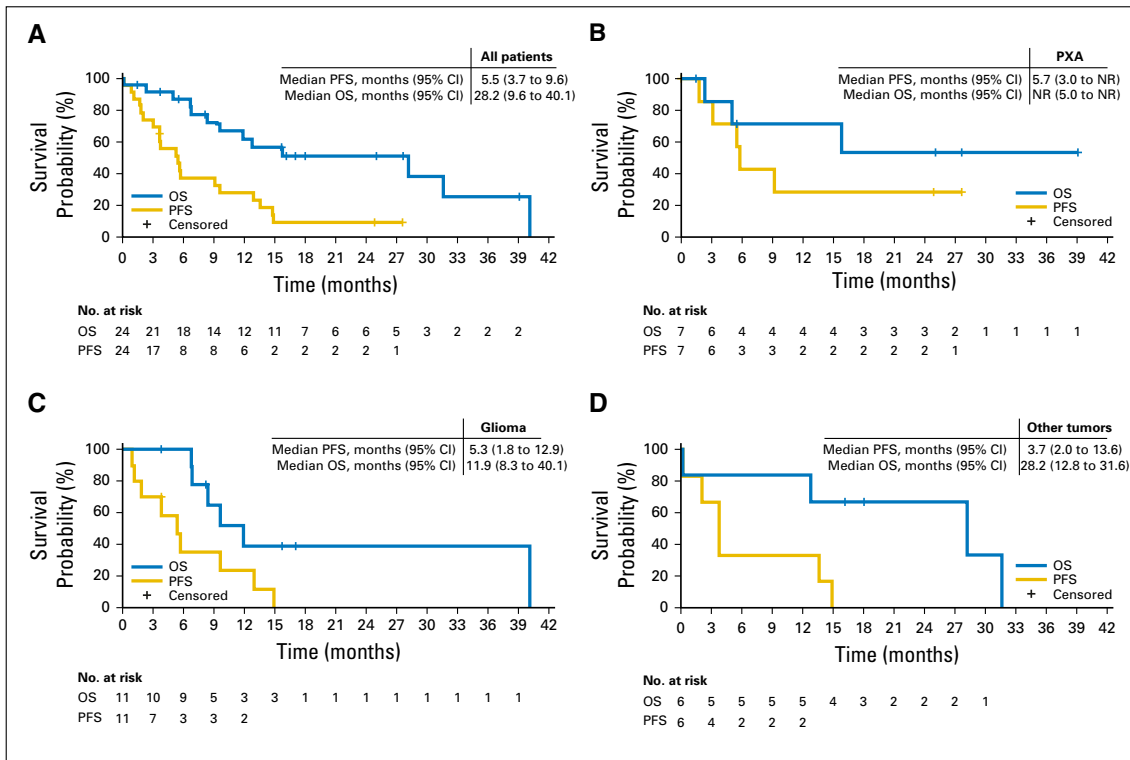


Fig 2. Progression-free survival (PFS) and overall survival (OS) curves in the (A) cohort overall, as well as in patients with (B) pleomorphic xanthoastrocytoma (PXA), (C) malignant diffuse glioma, and (D) other tumor types. NR, not reached.

PXA were enrolled in an extension trial to continue vemurafenib because of ongoing response or SD at the closure of the VE-BASKET study.

Adverse events, occurring in 20% or more of patients, regardless of cause, are listed in Table 3. Arthralgia (16 of 24 patients;

67%), melanocytic nevus (nine of 24 patients; 38%), palmar-plantar erythrodysesthesia (nine of 24 patients; 38%), and photosensitivity reaction (nine of 24 patients; 38%) were the most common adverse events. Maculopapular rash was the most common grade 3 and 4 event (three of 24 patients; 13%). No grade

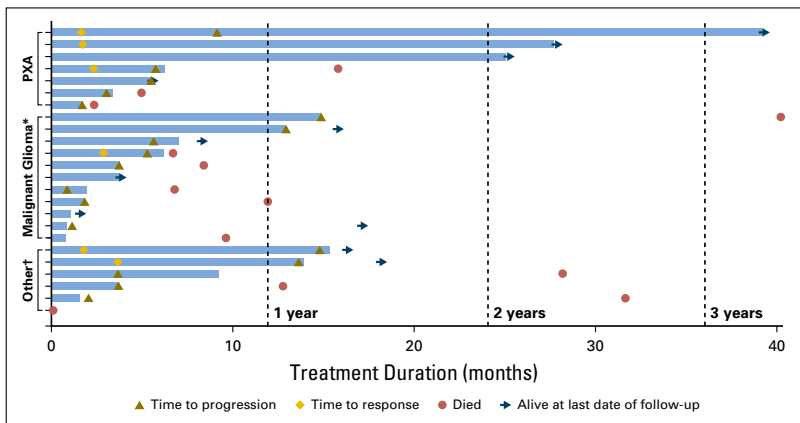


Fig 3. Time to events in individual patients. (\*) Anaplastic astrocytoma, n = 5; glioblastoma, n = 6. (†) Anaplastic ganglioglioma, n = 3; pilocytic astrocytoma, n = 2; high-grade glioma, not otherwise specified, n = 1. The first patient with pleomorphic xanthoastrocytoma (PXA; top swimmer lane) experienced his or her first progression at 9 months but continued on treatment beyond progression.

**Table 3.** Treatment-Emergent Adverse Events With an Incidence of  $\geq 20\%$ , Irrespective of Causality (n = 24)

Adverse Event	All Grades	Grade 3 and 4
Arthralgia	16 (67)	0
Melanocytic nevus	9 (38)	0
Palmar-plantar erythrodysesthesia	9 (38)	0
Photosensitivity reaction	9 (38)	0
Alopecia	8 (33)	0
Fatigue	7 (29)	1 (4)
Pruritus	7 (29)	0
Rash	7 (29)	0
Rash maculopapular	7 (29)	3 (13)
Skin papilloma	7 (29)	0
Asthenia	6 (25)	0
Folliculitis	6 (25)	0
Headache	6 (25)	0
Hyperkeratosis	6 (25)	0
Keratosis pilaris	6 (25)	0
Constipation	5 (21)	0
Diarrhea	5 (21)	0
Nausea	5 (21)	0
Decreased appetite	5 (21)	0

NOTE. Data are given as No. (%).

5 treatment-related events occurred, and no new vemurafenib safety signals were identified. Ten patients required one or more vemurafenib dose reduction and one discontinued as a result of intolerable adverse effects.

## DISCUSSION

Our data suggest that vemurafenib may have clinically meaningful activity in patients with  $BRAF^{V600}$ -mutant gliomas but that this activity varies by histologic subtype. The highest response rate was observed in patients with low-grade tumors, particularly PXA, a histology in which  $BRAF^{V600}$  mutations seem to be a common and early genomic event. In the overall population, including tumors of all grades and histologic subtypes, confirmed ORR was 25% and the clinical benefit rate was 38%—rates numerically higher than those historically observed with other agents used in unselected patients with refractory glioma.<sup>37</sup> Although encouraging, these results should be interpreted with caution given the limited number of patients and the descriptive nature of the analysis. These data, however, justify the continued pursuit of this therapeutic strategy through additional dedicated glioma studies.

Although the efficacy reported here is encouraging, the greatest degree of activity was observed in patients with  $IDH1/2$  wild-type low-grade gliomas, specifically PXAs. Historically, PXAs are associated with a better prognosis than GBMs and have been managed with curative intent by surgery, sometimes followed by radiotherapy. For a subset of patients with higher-grade histology or refractory disease, including those enrolled in this study, there is no established standard of care or effective chemotherapy regimen. In our patients, vemurafenib achieved a radiographic response or prolonged stabilization in more than 50% of patients with PXA, which suggests that this strategy may be associated with clinically meaningful benefit. Although one durable response was observed

in a patient with PA, only two such patients were enrolled, which precludes the interpretation of efficacy within in this histology.

The 11 patients with high-grade gliomas experienced a more variable response, with PR in one and SD of 6 months or more in two other patients. Although the overall clinical benefit rate was lower than in patients with PXA, AGG, or PA, patients with high-grade glioma were more heavily pretreated, which makes the observed responses even more notable. In addition, patients with PXA, AGG, and PA were younger than those in the high-grade glioma group. The incidence of  $BRAF^{V600}$  mutations is age dependent in patients with gangliogliomas,<sup>1</sup> although the etiology that underlies this association is unclear.

The lack of a detailed genomic characterization of the tumors of patients enrolled in this study is a limitation. An important consideration when targeting any oncogene in glioma is whether the previously detected oncogenic alteration is present at the time of treatment and whether, if present, the mutation occurs as the dominant clone. As  $BRAF^{V600}$  mutation status was not confirmed by biopsy immediately before enrollment in the VE-BASKET study, it is unclear whether the mutation was present in the tumors of all patients at the start of vemurafenib treatment. Moreover, GBMs demonstrate substantial temporal and spatial intratumoral heterogeneity,<sup>38</sup> and it is possible that in some primary GBMs,  $BRAF^{V600}$  mutations are subclonal or among multiple mutations present and driving tumor growth. These factors, at least in part, may account for the variable efficacy of vemurafenib monotherapy in this subgroup. Of interest, the one patient with GBM who achieved prolonged SD that lasted 12.9 months had a secondary GBM that evolved from a prior low-grade lesion, in keeping with our observation that lower-grade  $BRAF^{V600}$ -mutant gliomas seem to be more sensitive to vemurafenib. Another consideration is that the  $BRAF$  mutation may not be present in all components of the tumor. This latter mechanism has been potentially implicated in gangliogliomas in which a subset of  $BRAF^{V600}$ -mutant gangliogliomas had expression in both neuronal and glial tumor components.<sup>39</sup>

Of note, as a multihistology basket trial, several characteristics of the VE-BASKET study were suboptimal for the evaluation and treatment of patients with gliomas. The clinical trial was not designed to collect glioma biomarkers, such as *MGMT* promoter methylation, *IDH* mutation, or *CDKN2A/B* deletion status, although we were ultimately able to gather available data on most patients. It is possible that complete biomarker status may have helped provide additional context to the differential activity observed.<sup>40-42</sup> *MGMT* promoter methylation testing is only routine in malignant diffuse gliomas, where it is important for prognostication and in the evaluation of pseudoprogression after chemoradiation. There are no data to suggest that *MGMT* promoter methylation status would influence radiographic response or PFS with BRAF inhibitors. *IDH* mutation testing is not currently recommended for PXA, AGG, or PA. Moreover, prior studies have demonstrated mutual exclusivity between *IDH* and  $BRAF^{V600}$  mutations in gliomas,<sup>23,43,44</sup> which indicates that this biomarker might not be relevant in our cohort. Accordingly, *IDH1* mutation status was available for 18 (75%) of 24 patients in this study, all of whom all had wild-type *IDH1* tumors.

The current study used RECIST, which is designed primarily for the assessment of solid tumors, instead of dedicated brain

tumor response criteria, such as the Macdonald or Response Assessment in Neuro-Oncology criteria.<sup>11</sup> However, prior studies showed similarity in response assessments between one-dimensional and two-dimensional measurement methods in patients with high-grade gliomas.<sup>45,46</sup> Moreover, given the lack of a substantial antiangiogenic effect of vemurafenib, it is unlikely that pseudoresponses might have occurred in our patients. Another limitation is the lack of central review of investigator-reported response assessments. In summary, although the inclusion of patients with primary brain tumors in this study provided the opportunity to evaluate genomically targeted therapy in this relatively large, prospectively accrued group of patients with *BRAF*<sup>V600</sup>-mutant gliomas, future histology-agnostic studies should be designed to address brain tumor-specific considerations to optimize the interpretation of the findings.

Despite its shortcomings, the current study serves as an initial proof of concept that *BRAF*<sup>V600</sup> is a targetable oncogene in at least a subset of patients with primary brain tumors. Responses were observed across all glioma subsets, with the strongest signal observed in patients with lower-grade gliomas, particularly the PXA subgroup. Additional evaluation is needed to clarify the precise use of RAF and MEK inhibitors—alone or in combination—in patients with primary brain tumors. Several such studies that permit the enrollment of pediatric or adult patients with glioma are currently ongoing (ClinicalTrials.gov identifiers: NCT01748149, NCT01677741, NCT02124772, NCT02684058, NCT02285439, and NCT03429803). These studies may also help elucidate the

underlying mechanisms that drive the differential responses across histologic subsets.

#### AUTHORS' DISCLOSURES OF POTENTIAL CONFLICTS OF INTEREST

Disclosures provided by the authors are available with this article at [jco.org](http://jco.org).

#### AUTHOR CONTRIBUTIONS

**Conception and design:** Mehdi Touat, Martina Makrutzki, Jose Baselga, David M. Hyman

**Administrative support:** Martina Makrutzki, Bethany Pitcher, Jose Baselga, David M. Hyman

**Provision of study materials or patients:** Thomas Kaley, Mehdi Touat, Vivek Subbiah, Franck Bielle, Jean-Yves Blay, David M. Hyman

**Collection and assembly of data:** Thomas Kaley, Mehdi Touat, Vivek Subbiah, Franck Bielle, Martina Makrutzki, Bethany Pitcher, David M. Hyman

**Data analysis and interpretation:** Thomas Kaley, Mehdi Touat, Vivek Subbiah, Antoine Hollebecque, Jordi Rodon, A. Craig Lockhart, Vicki Keedy, Ralf-Dieter Hofheinz, Florence Joly, Jean-Yves Blay, Ian Chau, Igor Puzanov, Noopur S. Raju, Jurgen Wolf, Lisa M. DeAngelis, Martina Makrutzki, Todd Riehl, Bethany Pitcher, Jose Baselga, David M. Hyman

**Manuscript writing:** All authors

**Final approval of manuscript:** All authors

**Accountable for all aspects of the work:** All authors

#### REFERENCES

- Louis DN, Ohgaki H, Wiestler OD, et al: World Health Organization Histological Classification of Tumours of the Central Nervous System (ed 2). Lyon, France, International Agency for Research on Cancer, 2016
- Stupp R, Hegi ME, Mason WP, et al: Effects of radiotherapy with concomitant and adjuvant temozolomide versus radiotherapy alone on survival in glioblastoma in a randomised phase III study: 5-year analysis of the EORTC-NCIC trial. *Lancet Oncol* 10: 459-466, 2009
- Stupp R, Taillibert S, Kanner AA, et al: Maintenance therapy with tumor-treating fields plus temozolomide vs temozolomide alone for glioblastoma: A randomized clinical trial. *JAMA* 314: 2535-2543, 2015
- Wick W, Gorlia T, Bendszus M, et al: Lomustine and bevacizumab in progressive glioblastoma. *N Engl J Med* 377:1954-1963, 2017
- Wong ET, Hess KR, Gleason MJ, et al: Outcomes and prognostic factors in recurrent glioma patients enrolled onto phase II clinical trials. *J Clin Oncol* 17:2572-2578, 1999
- Lamborn KR, Chang SM, Prados MD: Prognostic factors for survival of patients with glioblastoma: Recursive partitioning analysis. *Neuro-oncol* 6: 227-235, 2004
- Gilbert MR, Dignam JJ, Armstrong TS, et al: A randomized trial of bevacizumab for newly diagnosed glioblastoma. *N Engl J Med* 370:699-708, 2014
- Chinot OL, Wick W, Mason W, et al: Bevacizumab plus radiotherapy-temozolomide for newly

diagnosed glioblastoma. *N Engl J Med* 370:709-722, 2014

9. Kreisl TN, Kim L, Moore K, et al: Phase II trial of single-agent bevacizumab followed by bevacizumab plus irinotecan at tumor progression in recurrent glioblastoma. *J Clin Oncol* 27:740-745, 2009

10. Friedman HS, Prados MD, Wen PY, et al: Bevacizumab alone and in combination with irinotecan in recurrent glioblastoma. *J Clin Oncol* 27: 4733-4740, 2009

11. Wen PY, Macdonald DR, Reardon DA, et al: Updated response assessment criteria for high-grade gliomas: Response assessment in neuro-oncology working group. *J Clin Oncol* 28:1963-1972, 2010

12. Hyman DM, Taylor BS, Baselga J: Implementing genome-driven oncology. *Cell* 168:584-599, 2017

13. Ascierto PA, McArthur GA, Dréno B, et al: Cobimetinib combined with vemurafenib in advanced *BRAF*<sup>V600</sup>-mutant melanoma (coBRIM): Updated efficacy results from a randomised, double-blind, phase 3 trial. *Lancet Oncol* 17: 1248-1260, 2016

14. Robert C, Karaszewska B, Schachter J, et al: Improved overall survival in melanoma with combined dabrafenib and trametinib. *N Engl J Med* 372: 30-39, 2015

15. Planchard D, Besse B, Groen HJM, et al: Dabrafenib plus trametinib in patients with previously treated *BRAF*<sup>V600E</sup>-mutant metastatic non-small-cell lung cancer: An open-label, multicentre phase 2 trial. *Lancet Oncol* 17:984-993, 2016

16. Planchard D, Smit EF, Groen HJM, et al: Dabrafenib plus trametinib in patients with previously untreated *BRAF*<sup>V600E</sup>-mutant metastatic non-small-cell lung cancer: An open-label, phase 2 trial. *Lancet Oncol* 18:1307-1316, 2017

17. Diamond EL, Subbiah V, Lockhart AC, et al: Vemurafenib for *BRAF*<sup>V600</sup>-mutant Erdheim-Chester disease and Langerhans cell histiocytosis: Analysis of data from the histology-independent phase 2 open-label VE-BASKET study. *JAMA Oncol* 4:384-388, 2018

18. Subbiah V, Kreitman RJ, Wainberg ZA, et al: Dabrafenib and trametinib treatment in patients with locally advanced or metastatic *BRAF*<sup>V600</sup>-mutant anaplastic thyroid cancer. *J Clin Oncol* 36:7-13, 2018

19. Brose MS, Cabanillas ME, Cohen EE, et al: Vemurafenib in patients with *BRAF*<sup>V600E</sup>-positive metastatic or unresectable papillary thyroid cancer refractory to radioactive iodine: A non-randomised, multicentre, open-label, phase 2 trial. *Lancet Oncol* 17:1272-1282, 2016

20. Corcoran RB, Atreya CE, Falchook GS, et al: Combined BRAF and MEK inhibition with dabrafenib and trametinib in *BRAF*<sup>V600</sup>-mutant colorectal cancer. *J Clin Oncol* 33:4023-4031, 2015

21. Tiacchi E, Park JH, De Carolis L, et al: Targeting mutant *BRAF* in relapsed or refractory hairy-cell leukemia. *N Engl J Med* 373:1733-1747, 2015

22. Chi AS, Batchelor TT, Yang D, et al: *BRAF*<sup>V600E</sup> mutation identifies a subset of low-grade diffusely infiltrating gliomas in adults. *J Clin Oncol* 31: e233-e236, 2013

23. Brennan CW, Verhaak RG, McKenna A, et al: The somatic genomic landscape of glioblastoma. *Cell* 155:462-477, 2013 [Erratum: *Cell* 157:753, 2014]

24. Dougherty MJ, Santi M, Brose MS, et al: Activating mutations in *BRAF* characterize a spectrum of pediatric low-grade gliomas. *Neuro-oncol* 12: 621-630, 2010

25. Schindler G, Capper D, Meyer J, et al: Analysis of *BRAF*<sup>V600E</sup> mutation in 1,320 nervous system tumors reveals high mutation frequencies in pleomorphic xanthoastrocytoma, ganglioglioma and extra-cerebellar

- pliocytic astrocytoma. *Acta Neuropathol* 121:397-405, 2011
26. Dias-Santagata D, Lam O, Vernovsky K, et al: *BRAF*<sup>V600E</sup> mutations are common in pleomorphic xanthoastrocytoma: Diagnostic and therapeutic implications. *PLoS One* 6:e17948, 2011
27. Chamberlain MC: Salvage therapy with BRAF inhibitors for recurrent pleomorphic xanthoastrocytoma: A retrospective case series. *J Neurooncol* 114:237-240, 2013
28. Bautista F, Paci A, Minard-Colin V, et al: Vemurafenib in pediatric patients with *BRAF*<sup>V600E</sup> mutated high-grade gliomas. *Pediatr Blood Cancer* 61:1101-1103, 2014
29. Burger MC, Ronellenfitch MW, Lorenz NI, et al: Dabrafenib in patients with recurrent, *BRAF*<sup>V600E</sup> mutated malignant glioma and leptomeningeal disease. *Oncol Rep* 38:3291-3296, 2017
30. Johanns TM, Ferguson CJ, Grierson PM, et al: Rapid clinical and radiographic response with combined dabrafenib and trametinib in adults with *BRAF*-mutated high-grade glioma. *J Natl Compr Canc Netw* 16:4-10, 2018
31. Brown NF, Carter T, Kitchen N, et al: Dabrafenib and trametinib in *BRAF*<sup>V600E</sup> mutated glioma. *CNS Oncol* 6:291-296, 2017
32. Migliorini D, Aguiar D, Vargas MI, et al: *BRAF/MEK* double blockade in refractory anaplastic pleomorphic xanthoastrocytoma. *Neurology* 88:1291-1293, 2017
33. Hyman DM, Puzanov I, Subbiah V, et al: Vemurafenib in multiple nonmelanoma cancers with *BRAF*<sup>V600</sup> mutations. *N Engl J Med* 373:726-736, 2015
34. Eisenhauer EA, Therasse P, Bogaerts J, et al: New response evaluation criteria in solid tumours: Revised RECIST guideline (version 1.1). *Eur J Cancer* 45:228-247, 2009
35. US National Institutes of Health: Common Terminology Criteria for Adverse Events (CTCAE), version 4.0. [https://evs.nci.nih.gov/ftp1/CTCAE/CTCAE\\_4.03\\_2010-06-14\\_QuickReference\\_5x7.pdf](https://evs.nci.nih.gov/ftp1/CTCAE/CTCAE_4.03_2010-06-14_QuickReference_5x7.pdf)
36. Lin Y, Shih WJ: Adaptive two-stage designs for single-arm phase IIa cancer clinical trials. *Biometrics* 60:482-490, 2004
37. Touat M, Idbaih A, Sanson M, et al: Glioblastoma targeted therapy: Updated approaches from recent biological insights. *Ann Oncol* 28:1457-1472, 2017
38. Qazi MA, Vora P, Venugopal C, et al: Intratumoral heterogeneity: Pathways to treatment resistance and relapse in human glioblastoma. *Ann Oncol* 28:1448-1456, 2017
39. Koelsche C, Wöhrer A, Jeibmann A, et al: Mutant *BRAF* V600E protein in ganglioglioma is predominantly expressed by neuronal tumor cells. *Acta Neuropathol* 125:891-900, 2013
40. Mistry M, Zhukova N, Merico D, et al: *BRAF* mutation and *CDKN2A* deletion define a clinically distinct subgroup of childhood secondary high-grade glioma. *J Clin Oncol* 33:1015-1022, 2015
41. Huillard E, Hashizume R, Phillips JJ, et al: Cooperative interactions of *BRAF*<sup>V600E</sup> kinase and *CDKN2A* locus deficiency in pediatric malignant astrocytoma as a basis for rational therapy. *Proc Natl Acad Sci USA* 109:8710-8715, 2012
42. Lassaletta A, Zapotocky M, Mistry M, et al: Therapeutic and prognostic implications of *BRAF*<sup>V600E</sup> in pediatric low-grade gliomas. *J Clin Oncol* 35:2934-2941, 2017
43. Cancer Genome Atlas Research Network, Brat DJ, Verhaak RG, et al: Comprehensive, integrative genomic analysis of diffuse lower-grade gliomas. *N Engl J Med* 372:2481-2498, 2015
44. Zehir A, Benayed R, Shah RH, et al: Mutational landscape of metastatic cancer revealed from prospective clinical sequencing of 10,000 patients. *Nat Med* 23:703-713, 2017
45. Galanis E, Buckner JC, Maurer MJ, et al: Validation of neuroradiologic response assessment in gliomas: Measurement by RECIST, two-dimensional, computer-assisted tumor area, and computer-assisted tumor volume methods. *Neuro Oncol* 8:156-165, 2006
46. Shah GD, Kesari S, Xu R, et al: Comparison of linear and volumetric criteria in assessing tumor response in adult high-grade gliomas. *Neuro Oncol* 8:38-46, 2006

### Affiliations

Thomas Kaley, Lisa M. DeAngelis, Jose Baselga, and David M. Hyman, Memorial Sloan Kettering Cancer Center; Thomas Kaley, Lisa M. DeAngelis, Jose Baselga, and David M. Hyman, Weill Cornell Medical College, New York; Igor Puzanov, Roswell Park Cancer Institute, Buffalo, NY; Mehdi Touat and Antoine Hollebecque, Institut Gustave Roussy, Villejuif; Franck Bielle, Assistance Publique-Hôpitaux de Paris, Hôpitaux Universitaires Pitié Salpêtrière-Charles Foix, Paris; Florence Joly, Centre François Baclesse, Caen; Jean-Yves Blay, Centre Léon Bérard, Lyon, France; Vivek Subbiah, MD Anderson Cancer Center, Houston, TX; Jordi Rodon, Vall d'Hebron University Hospital, Barcelona, Spain; A. Craig Lockhart, Sylvester Comprehensive Cancer Center, University of Miami, Miami, FL; Vicki Keedy, Vanderbilt University Medical Center, Nashville, TN; Ralf-Dieter Hofheinz, Universitätsmedizin Mannheim, Mannheim; Jurgen Wolf, Universitätsklinikum Köln, Cologne, Germany; Ian Chau, The Royal Marsden National Health Service Foundation Trust, London, United Kingdom; Noopur S. Raje, Massachusetts General Hospital, Boston, MA; Martina Makrutzki, F Hoffmann-La Roche, Basel, Switzerland; Todd Riehl, Genentech, South San Francisco, CA; and Bethany Pitcher, F Hoffmann-La Roche, Mississauga, Ontario, Canada.

### Support

Funded by F Hoffmann-La Roche and supported by Grants No. P30-CA008748 and 1R01-CA201247-01A1 from the National Institutes of Health.

### Prior Presentation

Presented in part at the Annual Meeting of the American Society of Clinical Oncology, Chicago, IL, June 1, 2017.

**AUTHORS' DISCLOSURES OF POTENTIAL CONFLICTS OF INTEREST**

**BRAF Inhibition in *BRAF*<sup>V600</sup>-Mutant Gliomas: Results From the VE-BASKET Study**

The following represents disclosure information provided by authors of this manuscript. All relationships are considered compensated. Relationships are self-held unless noted. I = Immediate Family Member, Inst = My Institution. Relationships may not relate to the subject matter of this manuscript. For more information about ASCO's conflict of interest policy, please refer to [www.asco.org/rwc](http://www.asco.org/rwc) or [ascopubs.org/jco/site/iffc](http://ascopubs.org/jco/site/iffc).

**Thomas Kaley**

**Research Funding:** Eli Lilly, Ludwig Institute for Cancer Research

**Mehdi Touat**

**Consulting or Advisory Role:** Agios Pharmaceuticals, Taiho Oncology  
**Travel, Accommodations, Expenses:** Merck Sharp & Dohme

**Vivek Subbiah**

**Consulting or Advisory Role:** MedImmune

**Research Funding:** Novartis (Inst), GlaxoSmithKline (Inst), NanoCarrier (Inst), Northwest Biotherapeutics (Inst), Genentech (Inst), Berg Pharma (Inst), Bayer (Inst), Incyte (Inst), Fujifilm (Inst), PharmaMar (Inst), D3 Oncology Solutions (Inst), Pfizer (Inst), Amgen (Inst), AbbVie (Inst), Multivir (Inst), Blueprint Medicines (Inst), Loxo (Inst), Vegenics (Inst), Takeda (Inst), Alfasigma (Inst), Agensys (Inst), Idera (Inst), Boston Biomedical (Inst)

**Travel, Accommodations, Expenses:** PharmaMar, Bayer

**Antoine Hollebécque**

**Honoraria:** Merck Serono, Amgen

**Consulting or Advisory Role:** Amgen, Gritstone Oncology

**Travel, Accommodations, Expenses:** Amgen, Servier

**Jordi Rodon**

**Research Funding:** Roche

**A. Craig Lockhart**

No relationship to disclose

**Vicki Keedy**

**Consulting or Advisory Role:** Karyopharm Therapeutics

**Research Funding:** Pfizer (Inst), CytRx Corporation (Inst), Medpacto (Inst), Plexxikon (Inst), Roche (Inst), Eli Lilly (Inst), BioMed Valley Discoveries (Inst), Immune Design (Inst), GlaxoSmithKline (Inst), Tracora Pharma (Inst), Advenchen Laboratories (Inst), Daiichi Sankyo (Inst)

**Franck Bielle**

**Employment:** Celgene (I)

**Stock or Other Ownership:** Crossject

**Research Funding:** Sanofi

**Ralf-Dieter Hofheinz**

**Honoraria:** Amgen, Boehringer Ingelheim, Bristol-Myers Squibb, Merck, Roche, Medac, Servier, Sanofi

**Consulting or Advisory Role:** Merck, Roche, Sanofi, Amgen, Bristol-Myers Squibb

**Research Funding:** Sanofi (Inst), Merck (Inst), Amgen (Inst)

**Florence Joly**

**Consulting or Advisory Role:** Roche

**Travel, Accommodations, Expenses:** Roche

**Jean-Yves Blay**

**Honoraria:** Roche

**Consulting or Advisory Role:** Roche, Novartis, GlaxoSmithKline, Bayer, PharmaMar, Merck

**Research Funding:** Roche (Inst)

**Ian Chau**

**Honoraria:** Eli Lilly

**Consulting or Advisory Role:** Sanofi, Eli Lilly, Bristol-Myers Squibb, MSD Oncology, Bayer, Genentech, Five Prime Therapeutics, Merck Serono, AstraZeneca, MedImmune

**Research Funding:** Janssen-Cilag (Inst), Sanofi (Inst), Merck Serono (Inst), Eli Lilly (Inst)

**Travel, Accommodations, Expenses:** Eli Lilly, Bristol-Myers Squibb

**Igor Puzanov**

**Consulting or Advisory Role:** Amgen, Genentech, Bristol-Myers Squibb

**Travel, Accommodations, Expenses:** Amgen, Merck

**Noopur S. Raje**

**Consulting or Advisory Role:** Amgen, Celgene, Takeda, Novartis, Bristol-Myers Squibb, Merck

**Research Funding:** AstraZeneca (Inst)

**Jurgen Wolf**

**Honoraria:** AbbVie, AstraZeneca, Bristol-Myers Squibb, Boehringer Ingelheim, MSD Oncology, Novartis, Roche

**Consulting or Advisory Role:** AbbVie, AstraZeneca, Bristol-Myers Squibb, Boehringer Ingelheim, Chugai Pharma, Ignyta, Eli Lilly, MSD Oncology, Novartis, Pfizer, Roche

**Research Funding:** Bristol-Myers Squibb, Novartis, Pfizer

**Lisa M. DeAngelis**

**Consulting or Advisory Role:** Genentech, Tocagen, Sapience, BTG

**Martina Makrutzki**

**Employment:** F Hoffmann-La Roche

**Todd Riehl**

**Employment:** Genentech

**Stock or Other Ownership:** Genentech

**Bethany Pitcher**

**Employment:** F Hoffmann-La Roche

**Jose Baselga**

**Leadership:** Infinity Pharmaceuticals, Varian Medical Systems, Bristol-Myers Squibb, Foghorn Therapeutics, Aura Biosciences, Grail

**Stock or Other Ownership:** PMV Pharma, Juno Therapeutics, Infinity Pharmaceuticals, Grail, Varian Medical Systems, Tango Therapeutics, ApoGen Biosciences, Venthera, Foghorn Therapeutics, Aura Biosciences

**Honoraria:** Genentech, Novartis, Eli Lilly

**Consulting or Advisory Role:** Grail, Eli Lilly, Novartis, Genentech, PMV Pharma, ApoGen, Juno Therapeutics

**Patents, Royalties, Other Intellectual Property:** Patents related to PI3K, PDK1 inhibitors; HER2 receptor, and LIF antibodies, and methods for diagnosis

**Travel, Accommodations, Expenses:** Genentech, Novartis, Eli Lilly

**David M. Hyman**

**Consulting or Advisory Role:** Atara Biotherapeutics, Chugai Pharma, CytomX Therapeutics, Boehringer Ingelheim, AstraZeneca, Pfizer, Bayer, Debiopharm Group, ArQule, Genentech

**Research Funding:** AstraZeneca, Puma Biotechnology, Loxo

Kaley et al

***Acknowledgment***

The investigators thank the patients who participated in this study and their families. Editorial support was provided by Miller Medical Communications. Funding for editorial support was provided by F Hoffmann-La Roche.

**C. Article sur le ciblage de fusion ATG7-RAF1 par cobimetinib dans un gliome malin / Article on the targeting of an ATG7-RAF1 fusion with cobimetinib**

# Successful Targeting of an ATG7-RAF1 Gene Fusion in Anaplastic Pleomorphic Xanthoastrocytoma With Leptomeningeal Dissemination

Mehdi Touat, MD<sup>1</sup>; Nadia Younan, MD<sup>1</sup>; Philipp Euskirchen, MD<sup>1,2,3,4,5</sup>; Maxime Fontanilles, MD<sup>1</sup>; Karima Mokhtari, MD<sup>1</sup>; Caroline Dehais, MD<sup>1</sup>; Patrick Tilleul, PharmD<sup>6</sup>; Amithys Rahimian-Aghda, MSc<sup>1</sup>; Adam Resnick, PhD<sup>7</sup>; Anne-Paule Gimenez-Roqueplo, MD, PhD<sup>8,9,10</sup>; Hélène Blons, PharmD, PhD<sup>8,9,11</sup>; Khê Hoang-Xuan, MD, PhD<sup>1</sup>; Jean-Yves Delattre, MD, PhD<sup>1</sup>; Ahmed Idbaih, MD, PhD<sup>1</sup>; Pierre Laurent-Puig, MD, PhD<sup>8,9,11</sup>; and Marc Sanson, MD, PhD<sup>1</sup>

## INTRODUCTION

Pleomorphic xanthoastrocytoma (PXA) is an uncommon primary brain tumor occurring primarily in children and young adults.<sup>1</sup> Although PXA is typically considered a relatively indolent entity, some tumors are accompanied by anaplastic features associated with high rates of recurrence after local treatment and unfavorable outcome.<sup>2</sup> Accordingly, anaplastic PXA (WHO grade 3) has been added to the 2016 WHO classification of CNS tumors as a distinct entity.<sup>1</sup> There is no standard management for patients with anaplastic PXA that recurs after surgery; neither chemotherapy nor radiotherapy have demonstrated clinical benefit in this disease.<sup>2,3</sup>

In recent years, the identification of activating *BRAF*<sup>V600E</sup> mutations in ~50% of patients with PXA has refined our understanding of these disorders as malignancies driven by aberrant activation of the mitogen-activated protein kinase (MAPK) signaling pathway.<sup>1,3-5</sup> This was further supported by the observation of both preclinical and clinical activity of vemurafenib, a selective *BRAF*<sup>V600E</sup> inhibitor, in *BRAF*<sup>V600E</sup>-mutant gliomas.<sup>6,7</sup> However, patients with *BRAF* wild-type PXA are not candidates for treatment with selective *BRAF*<sup>V600E</sup> inhibitors, and little is known about the spectrum of molecular alterations occurring in this population. Recent studies showed that a subset of *BRAF* wild-type PXA might harbor rare *BRAF* or *RAF1* fusions,<sup>8,9</sup> which have been associated with exquisite sensitivity to MAPK signaling inhibition in preclinical models.<sup>10</sup> It remains unknown whether patients who have glioma with *BRAF* or *RAF1* gene fusions might respond to therapies targeting MAPK signaling. We hypothesized that alternative non-*BRAF*<sup>V600E</sup> mutations might promote dependency on MAPK signaling in patients with *BRAF* wild-type anaplastic PXA. In support of this, we report that treatment with the MEK inhibitor cobimetinib resulted in major clinical response in a patient with refractory *BRAF* wild-type

anaplastic PXA harboring an in-frame *ATG7-RAF1* fusion.

## CASE REPORT

A 20-year-old woman initially presented in 2014 with seizures that revealed a right occipital mass on brain magnetic resonance imaging (MRI; Fig 1). She underwent complete surgical resection of the right occipital lesion in December 2014. Histopathologic analysis showed a tumor composed of pleomorphic glial cells with the presence of mitoses, necrosis, and microvascular proliferation, consistent with WHO grade 3 anaplastic PXA (Fig 2). Although rhabdoid morphology was observed in some sectors, both epithelial membrane antigen and p53 immunostainings were negative, and we did not observe loss of INI1, features that were previously associated with rhabdoid glioblastomas and CNS atypical teratoid/rhabdoid tumors, respectively. Furthermore, targeted sequencing of the tumor did not find mutations in *BRAF* (exons 11 and 15), *IDH1*, *IDH2*, *H3F3A*, *HIST1H3B*, or *SMARCB1*. Array comparative genomic hybridization revealed a 9p deletion involving *CDKN2A* and *CDKN2B*, which have been previously associated with poor outcome in *BRAF*<sup>V600E</sup>-mutant gliomas.<sup>3,11,12</sup> Given the unfavorable prognosis, she was first treated with adjuvant chemoradiotherapy (60 Gy in 30 fractions over 6 weeks along with once-per-day temozolomide 75 mg/m<sup>2</sup>) followed by temozolomide (200 mg/m<sup>2</sup>) for 6 cycles until November 2015 (Fig 1A).

In February 2016, routine surveillance MRI scans showed increased contrast enhancement in the right occipital lobe. She underwent a second gross total resection, with pathologic and sequencing analyses confirming recurrent WHO grade 3 anaplastic PXA with wild-type *BRAF*. A regimen of combined bevacizumab (10 mg/kg) and lomustine (90 mg/m<sup>2</sup>) was started in March 2016. In June 2016, she was admitted for rapid clinical deterioration. Brain MRI scans

Author affiliations and support information (if applicable) appear at the end of this article.

Accepted on September 20, 2018 and published at [ascopubs.org/journal/po](https://ascopubs.org/journal/po) on March 21, 2019; DOI <https://doi.org/10.1200/P0.18.00298>

ASCO

JCO® Precision Oncology

1

Downloaded from [ascopubs.org](https://ascopubs.org) by 185.250.44.61 on April 29, 2020 from 185.250.44.061  
Copyright © 2020 American Society of Clinical Oncology. All rights reserved.

**CONTEXT****Key Objective**

To report the successful treatment of a patient with refractory *BRAF*-wild-type anaplastic PXAs harboring an in-frame *ATG7-RAF1* fusion with the MEK inhibitor cobimetinib.

**Knowledge Generated**

We report for the first time, to our knowledge, that *RAF1* gene fusions are actionable molecular events in high-grade gliomas. This report highlights the oncogenic role of MAPK-activating alterations including *RAF1* rearrangements and *BRAF*<sup>V600E</sup> mutations in a subset of pediatric and adult gliomas.

**Relevance**

Cobimetinib can achieve therapeutic exposure within the CNS, including the cerebrospinal fluid in patients with *RAF1*-translocated high-grade gliomas.

showed leptomeningeal enhancement in the posterior cerebral fossa (Fig 1B). Neoplastic meningitis was confirmed by lumbar puncture showing 42 white blood cells per  $\mu\text{L}$  (84% lymphocytes), hyperproteinorachia (0.55 g/L), and the presence of tumor cells in the cerebrospinal fluid (CSF; Fig 1B). Intravenous thiotepa (45 mg/m<sup>2</sup>) was begun, but the treatment was discontinued after one infusion because of grade 4 thrombopenia and febrile neutropenia with infectious pneumonia, which required intravenous antibiotics.

The patient was enrolled in the precision medicine program EXORARE for tumor molecular characterization using RNA sequencing and matched tumor or normal whole-exome sequencing. The patient signed an informed consent for a pangenomic analysis of the primary tumor (first surgery in 2014). RNA sequencing revealed a fusion between exon 18 of *ATG7* and exon 8 of *RAF1* (*ATG7-RAF1*; Fig 3A). Reverse transcriptase-polymerase chain reaction and Sanger sequencing confirmed the expression of an in-frame *ATG7-RAF1* fusion transcript in the recurrent tumor (second surgery, 2016; Fig 3B). Interestingly, no additional molecular alteration was found by whole-exome among 475 genes previously associated with cancer, which suggested that the *ATG7-RAF1* fusion was the main oncogenic driver. Moreover, previous reports showed that fusions involving exon 8 of *RAF1* are recurrent events in cancer including PXA<sup>8,9,13</sup> and can result in constitutive activation of the tyrosine kinase domain and downstream MAPK signaling through the loss of the N-terminal autoinhibitory domain of *RAF1*.<sup>14</sup> Treatment with sorafenib (200 mg twice per day) was then started in October 2016 through off-label use after informed consent. Unfortunately, her clinical condition rapidly deteriorated with partial seizures, confusion, cerebellar ataxia, diplopia, hypoacusia, headaches, and diffuse pain in the lower limbs, for which treatment with intravenous morphine, steroids, and midazolam was begun.

On the basis of preclinical data suggesting that MEK inhibition in astrocytomas harboring *RAF1* fusions has

superior efficacy,<sup>10</sup> sorafenib was discontinued and treatment with off-label cobimetinib (60 mg per day, 3 weeks on and 1 week off) was started in November 2016, after family members provided informed consent (Fig 1A). The patient dramatically improved after a few days of treatment, with complete regression of the confusion and headaches and partial regression of the cerebellar ataxia and pain in the lower limbs. In December 2016, she presented with sudden visual loss with severe bilateral papilledema as a result of chronic intracranial hypertension (> 70 cm of water at the lumbar puncture), for which she was treated with a ventriculoperitoneal shunt.

Treatment with full-dose cobimetinib was continued because she gradually improved with complete regression of the neoplastic meningitis symptoms and recovery of gait. Treatments with intravenous morphine, steroids, and midazolam were progressively discontinued. Subsequent lumbar puncture showed complete cytologic response in the CSF (Fig 1B) with regression of both pleocytosis (1 white blood cell per  $\mu\text{L}$ ) and hyperproteinorachia (0.15 g/L; Fig 1B). Serial restaging brain MRI scans showed stabilization of the leptomeningeal disease (Fig 1B). Cobimetinib was well tolerated, with only grade 1 rash, nausea, and increase in creatinine kinase level. In June 2017, after seven cycles of cobimetinib, the patient died at home after repeated generalized seizures complicated with cardiac arrest. Her symptoms suggested disease progression, but no autopsy was performed.

**DISCUSSION**

Molecular alterations that involve the MAPK pathway, including *BRAF*<sup>V600E</sup> mutations and *BRAF* and *RAF1* fusions, have been identified in a wide range of pediatric and adult gliomas,<sup>2-5,8,9,15-18</sup> in which they result in constitutive activation of the pathway and drive tumor growth.<sup>6,10,11,19</sup> Although most efforts to develop targeted therapies for the treatment of gliomas have been unsuccessful to date,<sup>20</sup> vemurafenib has yielded promising signals of activity in *BRAF*<sup>V600E</sup>-mutant gliomas.<sup>7</sup> Here we report for the first time, to our knowledge, that *RAF1* gene fusions are

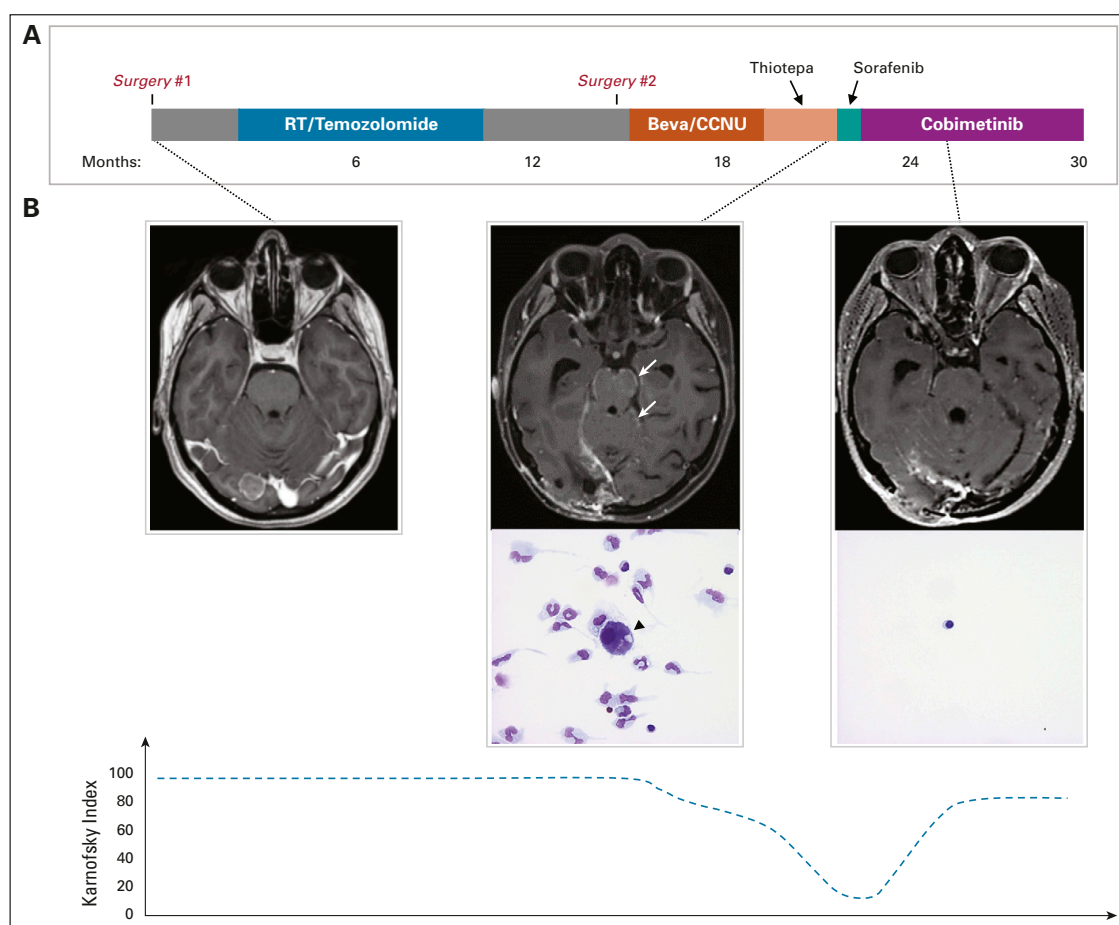


**FIG 1.** Sustained response to cobimetinib in a 20-year-old patient with refractory ATG7-*RAF1*-translocated anaplastic pleomorphic xanthoastrocytoma. (A) Timeline of treatment from initial presentation. (B) Top: serial contrast-enhanced T1-weighted images of brain magnetic resonance imaging (MRI) and cerebrospinal fluid (CSF; May-Grünwald-Giemsa stain) cytology at (left) initial presentation, (middle) pretreatment, and (right) during treatment with cobimetinib showing the right occipital lesion, the leptomeningeal enhancement on the brain MRI (white arrows), and the presence of neoplastic cells in the CSF (black arrowheads) before treatment with cobimetinib was started. A complete cytologic response to cobimetinib was observed after 3 months of treatment with cobimetinib. Bottom: evolution of performance status as evaluated by the Karnofsky index. The dotted curve was drawn on the basis of data points collected during follow-up. Beva, bevacizumab; CCNU, chloroethyl-cyclohexyl-nitrosourea; RT, radiation therapy.

actionable molecular events in high-grade gliomas. These data support the oncogenic role of MAPK signaling in a subset of gliomas characterized by high rates of molecular alterations activating this pathway. The observation of clinical activity with both *BRAF* and *MEK* inhibitors suggest that *BRAF*- and *RAF1*-driven gliomas, even in patients who have been heavily pretreated, display a high level of MAPK pathway dependency and possibly less molecular heterogeneity than the majority of gliomas driven by other alterations such as *EGFR* variants.<sup>20-22</sup>

Despite previous reports indicating activity of sorafenib in treating patients with cancer who harbor mutations of

*BRAF* or *ARAF* (both paralogs of *RAF1*),<sup>23,24</sup> our patient did not respond to treatment with sorafenib. It is not clear whether the rapid clinical deterioration we observed with sorafenib was caused by true primary resistance to *RAF* inhibition or by suboptimal drug exposure because of the inability of sorafenib to adequately penetrate the CSF.<sup>25</sup> Although cobimetinib showed modest brain penetration in mouse models,<sup>26</sup> the dramatic clinical response seen in a patient with leptomeningeal dissemination indicates that cobimetinib can achieve therapeutic exposure within the CNS, as suggested by previous reports.<sup>27</sup> A trial of cobimetinib in patients with glioma who harbor MAPK pathway

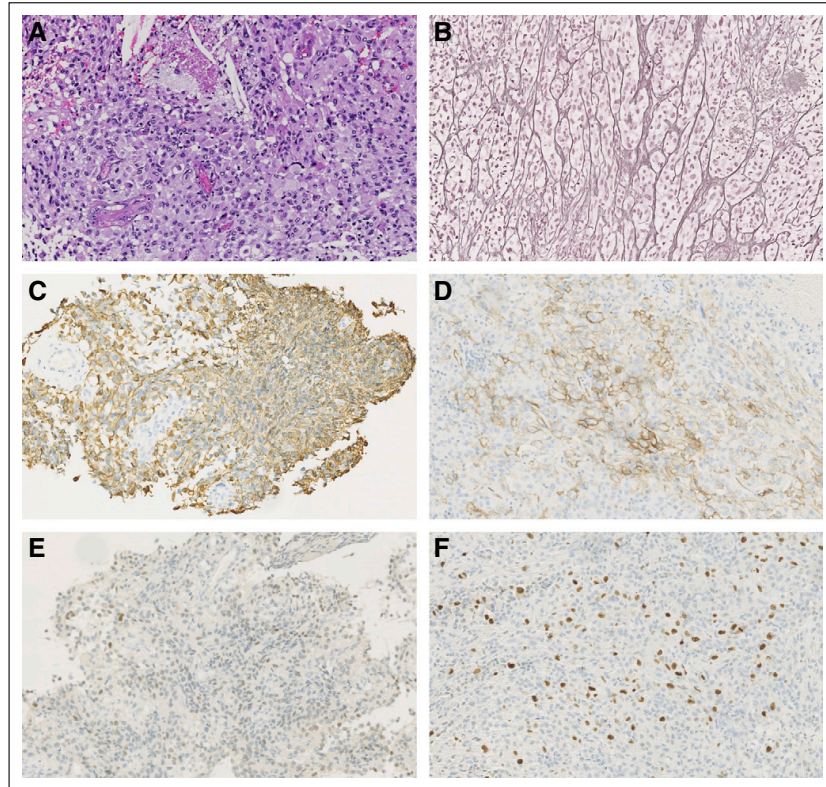


**FIG 2.** Histopathologic analysis of the primary tumor. (A) Hematoxylin-eosin and (B) reticulin colorations showing a pleomorphic tumor proliferation, with the presence of xanthomatous cells with nuclear atypia, reticulin fibers, microvascular proliferation, and necrosis. (C-F) Immunohistochemical stains showing tumor cell immunoreactivity for (C) glial fibrillary acidic protein, (D) CD34, and (E) oligodendrocyte transcription factor 2. (F) High mitotic activity was noted on MIB-1 staining.

alterations is currently ongoing (NCT02639546; Safety and Pharmacokinetics of Cobimetinib in Pediatric and Young Adult Participants With Previously Treated Solid Tumors [iMATRIXcobi]), although adult patients are not yet eligible for this study. Additional studies are warranted to determine the efficacy of cobimetinib in adult patients with glioma who have *BRAF* or *RAF1* gene fusions. Furthermore, novel MEK inhibitors optimized for achieving higher brain exposure might have a role in these diseases.<sup>28</sup>

In conclusion, our report provides evidence for the oncogenic role of MAPK alterations, including *RAF1* rearrangements, in pediatric and adult brain tumors and

suggests that *RAF1* fusions may represent potential therapeutic targets in a subset of patients with *BRAF* wild-type high-grade gliomas. In addition, this finding has potential relevance to other tumor types driven by *RAF1* fusions. A recent report of a patient with melanoma with an *ANO10-RAF1* fusion reported long-lasting clinical improvement after treatment with the MEK inhibitor trametinib,<sup>29</sup> suggesting that patients with *RAF1* fusion-driven tumors might respond to MEK inhibition regardless of histology. Our report also highlights the usefulness of comprehensive molecular profiling, including fusion detection, for identifying potentially targetable alterations in patients with advanced rare cancers.

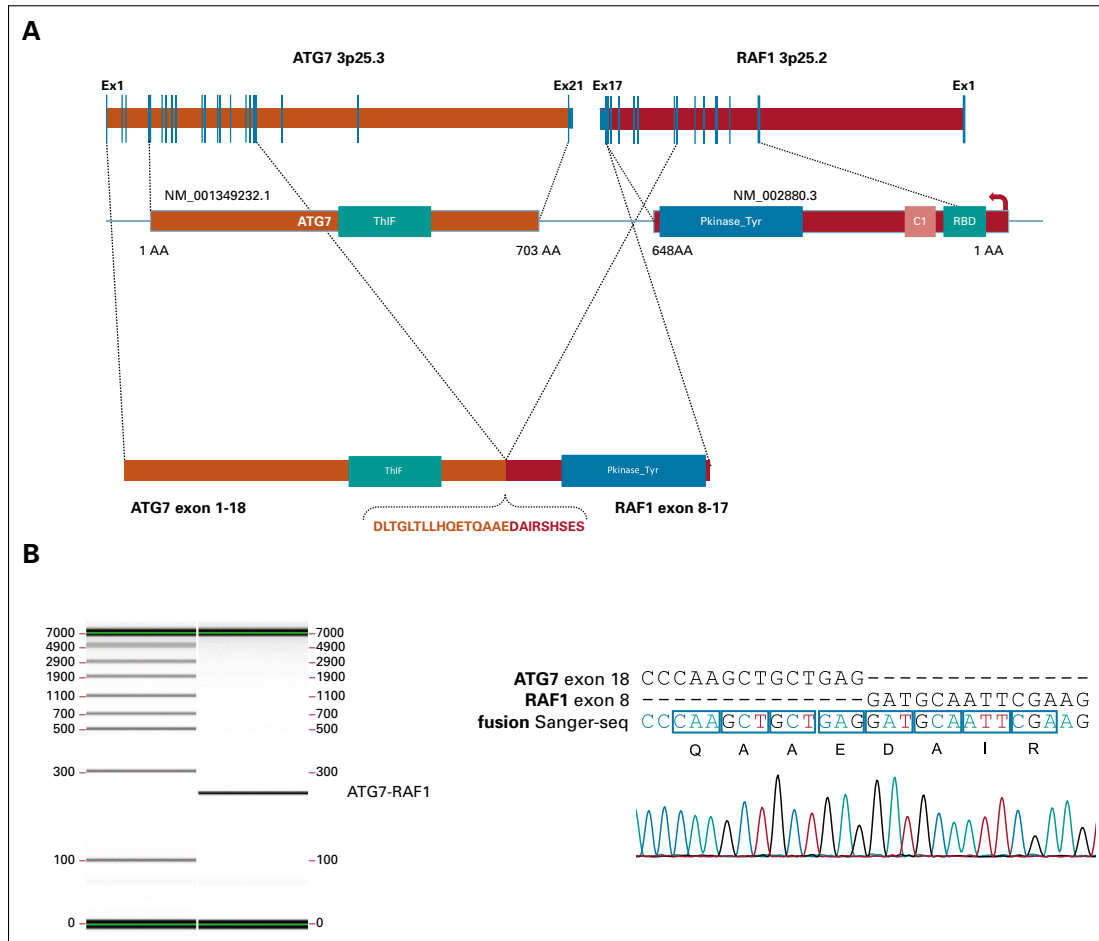


**FIG 3.** *ATG7-RAF1* gene fusion identified by RNA sequencing in the primary and recurrent tumors. (A) Schematic representation of the *ATG7-RAF1* gene fusion protein identified by using RNA sequencing of the primary tumor sample. The predicted fusion protein (bottom) includes the tyrosine kinase domain of *RAF1* and the THIF domain of *ATG7*. The predicted translation at the breakpoint is shown. (B) Confirmation of the *ATG7-RAF1* fusion in the recurrent tumor by reverse transcriptase polymerase chain reaction (RT-PCR) and Sanger sequencing (seq.). Left: primers spanning the fused exons yielded a fusion-specific amplicon with an expected size of 241 bp. Right: Sanger sequencing chromatogram of the PCR product confirming a fusion event between *ATG7* and *RAF1* and showing the reading frame and putative translation at the breakpoint. C1, protein kinase C-like phorbol ester/diacylglycerol binding domain; *RAF1*, Raf-1 proto-oncogene serine/threonine kinase; *ATG7*, autophagy related 7; RBD, *RAF*-like RAS-binding domain; ThIF, THIF-type NAD/FAD binding fold; Tyr, tyrosine-protein kinase catalytic domain.

**AFFILIATIONS**

- <sup>1</sup>Inserm, CNRS, UMR S 1127, Institut du Cerveau et de la Moelle épinière (ICM), Assistance Publique-Hôpitaux de Paris (AP-HP), Hôpitaux Universitaires La Pitié Salpêtrière-Charles Foix, Paris, France
- <sup>2</sup>Universitätsmedizin Berlin, Berlin, Germany
- <sup>3</sup>Berlin Institute of Health, Berlin, Germany
- <sup>4</sup>German Cancer Consortium, Partner Site Berlin, Berlin, Germany
- <sup>5</sup>German Cancer Research Center, Heidelberg, Germany
- <sup>6</sup>AP-HP, Hôpitaux Universitaires La Pitié Salpêtrière - Charles Foix, Paris, France
- <sup>7</sup>Children's Hospital of Philadelphia, Philadelphia, PA

- <sup>8</sup>AP-HP, Hôpital Européen Georges-Pompidou, Paris, France
- <sup>9</sup>Université Paris Descartes, Sorbonne Paris Cité, Paris, France
- <sup>10</sup>INSERM, UMR 970, Paris-Cardiovascular Research Center, Paris, France
- <sup>11</sup>INSERM, UMR S 1147, Paris, France

**CORRESPONDING AUTHOR**

Mehdi Touat, MD, Service de Neurologie 2 Mazarin, Groupe Hospitalier Pitié Salpêtrière, 47-83 Boulevard de l'Hôpital, Paris, France; e-mail: mehdi.touat@gmail.com.

## SUPPORT

Supported by Grant EXORARE from the Cancéropôle Ile de France/INCa, and by Grant No. INCa-DGOS-Inserm\_12560 from the SiRIC CURAMUS. M.T. received Grant No. FDM 41635 from the Fondation pour la Recherche Médicale. P.E. is a participant of the BIH-Charité Clinician Scientist Program funded by the Charité-Universitätsmedizin Berlin and the Berlin Institute of Health.

### AUTHOR CONTRIBUTIONS

**Conception and design:** Mehdi Touat, Patrick Tilleul, Adam Resnick, Anne-Paule Gimenez-Roqueplo, Pierre Laurent-Puig, Marc Sanson

**Financial support:** Anne-Paule Gimenez-Roqueplo, Jean-Yves Delattre, Marc Sanson

**Provision of study materials or patients:** Karima Mokhtari, Caroline Dehais, Adam Resnick, Jean-Yves Delattre

**Collection and assembly of data:** Mehdi Touat, Nadia Younan, Philipp Euskirchen, Maxime Fontanilles, Karima Mokhtari, Caroline Dehais, Amithys Rahimian-Aghda, Hélène Blons, Pierre Laurent-Puig, Marc Sanson

**Data analysis and interpretation:** Mehdi Touat, Philipp Euskirchen, Khê Hoang-Xuan, Jean-Yves Delattre, Ahmed Idbaih, Hélène Blons, Pierre Laurent-Puig, Marc Sanson

**Manuscript writing:** All authors

**Final approval of manuscript:** All authors

**Accountable for all aspects of the work:** All authors

### AUTHORS' DISCLOSURES OF POTENTIAL CONFLICTS OF INTEREST AND DATA AVAILABILITY STATEMENT

The following represents disclosure information provided by authors of this manuscript. All relationships are considered compensated. Relationships are self-held unless noted. I = Immediate Family Member, Inst = My Institution. Relationships may not relate to the subject matter of this manuscript. For more information about ASCO's conflict of interest policy, please refer to [www.asco.org/rwc](http://www.asco.org/rwc) or [ascopubs.org/po/author-center](http://ascopubs.org/po/author-center).

### Mehdi Touat

**Consulting or Advisory Role:** Agios Pharmaceutical, Taiho Oncology  
**Travel, Accommodations, Expenses:** Merck Sharp & Dohme

### Maxime Fontanilles

**Travel, Accommodations, Expenses:** Roche

### Patrick Tilleul

**Honoraria:** Takeda, Astellas Pharma, Roche, Biogen, Evidera, Baxter, Grünenthal Group, Chiesi, Bristol-Myers Squibb, MSD, Sandoz-Novartis, Pfizer, AstraZeneca

### Hélène Blons

**Honoraria:** AstraZeneca, Bristol-Myers Squibb, MSD Oncology

### Khê Hoang-Xuan

**Travel, Accommodations, Expenses:** AbbVie

### Ahmed Idbaih

**Travel, Accommodations, Expenses:** CarThera

### Pierre Laurent-Puig

**Honoraria:** Amgen, AstraZeneca, Boehringer Ingelheim, Merck Serono, Merck, Roche, Sanofi

**Consulting or Advisory Role:** Merck, Bristol-Myers Squibb, Boehringer Ingelheim

**Patents, Royalties, Other Intellectual Property:** Inventor of mir31-3p (license to IntegraGen)

**Travel, Accommodations, Expenses:** Roche, Merck

### Marc Sanson

**Consulting or Advisory Role:** AbbVie, Genenta

**Travel, Accommodations, Expenses:** Abbvie

No other potential conflicts of interest were reported.

### ACKNOWLEDGMENT

The authors thank Ines Detrait and Delphine Le Corre for tissue preparation and acid nucleic extractions, and Dr Yvan Bieche and IntegraGen for the genomic analyses performed in this patient.

## REFERENCES

- Louis DN, Ohgaki H, Wiestler OD, et al: World Health Organization Histological Classification of Tumours of the Central Nervous System, 4th Edition Revised. Lyon, France, International Agency for Research on Cancer, 2016
- Ida CM, Rodriguez FJ, Burger PC, et al: Pleomorphic xanthoastrocytoma: Natural history and long-term follow-up. *Brain Pathol* 25:575-586, 2015
- Lassaletta A, Zapotocky M, Mistry M, et al: Therapeutic and prognostic implications of BRAF V600E in pediatric low-grade gliomas. *J Clin Oncol* 35:2934-2941, 2017
- Dias-Santagata D, Lam Q, Vernovsky K, et al: BRAF V600E mutations are common in pleomorphic xanthoastrocytoma: Diagnostic and therapeutic implications. *PLoS One* 6:e17948, 2011
- Schindler G, Capper D, Meyer J, et al: Analysis of BRAF V600E mutation in 1,320 nervous system tumors reveals high mutation frequencies in pleomorphic xanthoastrocytoma, ganglioglioma and extra-cerebellar pilocytic astrocytoma. *Acta Neuropathol* 121:397-405, 2011
- Nicolaidis TP, Li H, Solomon DA, et al: Targeted therapy for BRAFV600E malignant astrocytoma. *Clin Cancer Res* 17:7595-7604, 2011
- Kaley T, Touat M, Subbiah V, et al: BRAF inhibition in BRAFV600-mutant gliomas: Results from the VE-BASKET Study. *J Clin Oncol* [epub ahead of print on October 23, 2018]
- Phillips JJ, Gong H, Chen K, et al: Activating NRF1-BRAF and ATG7-RAF1 fusions in anaplastic pleomorphic xanthoastrocytoma without BRAF p.V600E mutation. *Acta Neuropathol* 132:757-760, 2016
- Phillips JJ, Gong H, Chen K, et al: The genetic landscape of anaplastic pleomorphic xanthoastrocytoma. *Brain Pathol* 29:85-96, 2018
- Jain P, Fierst TM, Han HJ, et al: CRAF gene fusions in pediatric low-grade gliomas define a distinct drug response based on dimerization profiles. *Oncogene* 36:6348-6358, 2017
- Huillard E, Hashizume R, Phillips JJ, et al: Cooperative interactions of BRAFV600E kinase and CDKN2A locus deficiency in pediatric malignant astrocytoma as a basis for rational therapy. *Proc Natl Acad Sci USA* 109:8710-8715, 2012
- Mistry M, Zhukova N, Merico D, et al: BRAF mutation and CDKN2A deletion define a clinically distinct subgroup of childhood secondary high-grade glioma. *J Clin Oncol* 33:1015-1022, 2015
- Hartmaier RJ, Albacker LA, Chmielecki J, et al: High-throughput genomic profiling of adult solid tumors reveals novel insights into cancer pathogenesis. *Cancer Res* 77:2464-2475, 2017
- Karoulia Z, Gavathiotis E, Poulikakos PI: New perspectives for targeting RAF kinase in human cancer. *Nat Rev Cancer* 17:676-691, 2017

15. Jones DT, Hutter B, Jäger N, et al: Recurrent somatic alterations of *FGFR1* and *NTRK2* in pilocytic astrocytoma. *Nat Genet* 45:927-932, 2013
16. Johnson A, Severson E, Gay L, et al: Comprehensive genomic profiling of 282 pediatric low- and high-grade gliomas reveals genomic drivers, tumor mutational burden, and hypermutation signatures. *Oncologist* 22:1478-1490, 2017
17. Reinhardt A, Stichel D, Schrimpf D, et al: Anaplastic astrocytoma with piloid features, a novel molecular class of IDH wildtype glioma with recurrent *MAPK* pathway, *CDKN2A/B* and *ATRX* alterations. *Acta Neuropathol* 136:273-291, 2018
18. Deng MY, Sill M, Chiang J, et al: Molecularly defined diffuse leptomeningeal glioneuronal tumor (DLGNT) comprises two subgroups with distinct clinical and genetic features. *Acta Neuropathol* 136:239-253, 2018
19. Sievert AJ, Lang SS, Boucher KL, et al: Paradoxical activation and *RAF* inhibitor resistance of *BRAF* protein kinase fusions characterizing pediatric astrocytomas. *PNAS* 110:5957-5962, 2013
20. Touat M, Idhahbi A, Sanson M, et al: Glioblastoma targeted therapy: Updated approaches from recent biological insights. *Ann Oncol* 28:1457-1472, 2017
21. Szerlip NJ, Pedraza A, Chakravarty D, et al: Intratumoral heterogeneity of receptor tyrosine kinases *EGFR* and *PDGFRA* amplification in glioblastoma defines subpopulations with distinct growth factor response. *Proc Natl Acad Sci USA* 109:3041-3046, 2012
22. Francis JM, Zhang CZ, Maire CL, et al: *EGFR* variant heterogeneity in glioblastoma resolved through single-nucleus sequencing. *Cancer Discov* 4:956-971, 2014
23. Imielinski M, Greulich H, Kaplan B, et al: Oncogenic and sorafenib-sensitive *ARAF* mutations in lung adenocarcinoma. *J Clin Invest* 124:1582-1586, 2014
24. Casadei Gardini A, Chiadini E, Faloppi L, et al: Efficacy of sorafenib in *BRAF*-mutated non-small-cell lung cancer (NSCLC) and no response in synchronous *BRAF* wild type-hepatocellular carcinoma: A case report. *BMC Cancer* 16:429, 2016
25. Kim A, McCully C, Cruz R, et al: The plasma and cerebrospinal fluid pharmacokinetics of sorafenib after intravenous administration in non-human primates. *Invest New Drugs* 30:524-528, 2012
26. Choo EF, Ly J, Chan J, et al: Role of P-glycoprotein on the brain penetration and brain pharmacodynamic activity of the MEK inhibitor cobimetinib. *Mol Pharm* 11:4199-4207, 2014
27. Touat M, Gratioux J, Condette Auliac S, et al: Vemurafenib and cobimetinib overcome resistance to vemurafenib in *BRAF*-mutant ganglioglioma. *Neurology* 91:523-525, 2018
28. Gampa G, Kim M, Cook-Rostie N, et al: Brain distribution of a novel MEK inhibitor E6201: Implications in the treatment of melanoma brain metastases. *Drug Metab Dispos* 46:658-666, 2018
29. Kim KB, Semrad T, Schrock AB, et al: Significant clinical response to a MEK inhibitor therapy in a patient with metastatic melanoma harboring an *RAF1* fusion. *JCO Precis Oncol* doi:10.1200/PO.17.00138



**D. Article sur le ciblage d'altérations moléculaires de la voie PI3K par buparlisib dans les gliomes malins / Article on the targeting of PI3K aberrations with buparlisib**



original report

# Buparlisib in Patients With Recurrent Glioblastoma Harboring Phosphatidylinositol 3-Kinase Pathway Activation: An Open-Label, Multicenter, Multi-Arm, Phase II Trial

Patrick Y. Wen, MD<sup>1,2</sup>; Mehdi Touat, MD<sup>1,2</sup>; Brian M. Alexander, MD, MPH<sup>1,2</sup>; Ingo K. Mellinghoff, MD<sup>3</sup>; Shakti Ramkissoon, MD, PhD<sup>1</sup>; Christine S. McCluskey<sup>1</sup>; Kristine Pelton<sup>1</sup>; Sam Haidar, MS<sup>1</sup>; Sankha S. Basu, MD, PhD<sup>1,2</sup>; Sarah C. Gaffey<sup>1</sup>; Loreal E. Brown, MSN<sup>1</sup>; Juan Emmanuel Martinez-Ledesma, PhD<sup>4</sup>; Shaofang Wu, PhD<sup>4</sup>; Jungwoo Kim, PhD<sup>5</sup>; Wei Wei, PhD<sup>6,10</sup>; Mi-Ae Park, PhD<sup>1</sup>; Jason T. Huse, MD, PhD<sup>4</sup>; John G. Kuhn, PharmD<sup>7</sup>; Mikael L. Rinne, MD, PhD<sup>1,2</sup>; Howard Colman, MD, PhD<sup>8</sup>; Nathalie Y.R. Agar, PhD<sup>1,2</sup>; Antonio M. Omuro, MD<sup>3</sup>; Lisa M. DeAngelis, MD<sup>3</sup>; Mark R. Gilbert, MD<sup>4</sup>; John F. de Groot, MD<sup>4</sup>; Timothy F. Cloughesy, MD<sup>6</sup>; Andrew S. Chi, MD, PhD<sup>9</sup>; Thomas M. Roberts, PhD<sup>1</sup>; Jean J. Zhao, PhD<sup>1</sup>; Eudocia Q. Lee, MD, MPH<sup>1,2</sup>; Lakshmi Nayak, MD<sup>1,2</sup>; James R. Heath, PhD<sup>10</sup>; Laura L. Horky, MD, PhD<sup>1</sup>; Tracy T. Batchelor, MD, MPH<sup>1</sup>; Rameen Beroukhi, MD, PhD<sup>1,2</sup>; Susan M. Chang, MD<sup>12</sup>; Azra H. Ligon, PhD<sup>2</sup>; Ian F. Dunn, MD<sup>2</sup>; Dimpay Koul, PhD<sup>4</sup>; Geoffrey S. Young, MD<sup>2</sup>; Michael D. Prados, MD<sup>1,2</sup>; David A. Reardon, MD<sup>1,2</sup>; W.K. Alfred Yung, MD<sup>4</sup>; and Keith L. Ligon, MD, PhD<sup>1,2</sup>

abstract

**PURPOSE** Phosphatidylinositol 3-kinase (PI3K) signaling is highly active in glioblastomas. We assessed pharmacokinetics, pharmacodynamics, and efficacy of the pan-PI3K inhibitor buparlisib in patients with recurrent glioblastoma with PI3K pathway activation.

**METHODS** This study was a multicenter, open-label, multi-arm, phase II trial in patients with PI3K pathway-activated glioblastoma at first or second recurrence. In cohort 1, patients scheduled for re-operation after progression received buparlisib for 7 to 13 days before surgery to evaluate brain penetration and modulation of the PI3K pathway in resected tumor tissue. In cohort 2, patients not eligible for re-operation received buparlisib until progression or unacceptable toxicity. Once daily oral buparlisib 100 mg was administered on a continuous 28-day schedule. Primary end points were PI3K pathway inhibition in tumor tissue and buparlisib pharmacokinetics in cohort 1 and 6-month progression-free survival (PFS6) in cohort 2.

**RESULTS** Sixty-five patients were treated (cohort 1, n = 15; cohort 2, n = 50). In cohort 1, reduction of phosphorylated AKT<sup>S473</sup> immunohistochemistry score was achieved in six (42.8%) of 14 patients, but effects on phosphoribosomal protein S6<sup>S235/236</sup> and proliferation were not significant. Tumor-to-plasma drug level was 1.0. In cohort 2, four (8%) of 50 patients reached 6-month PFS6, and the median PFS was 1.7 months (95% CI, 1.4 to 1.8 months). The most common grade 3 or greater adverse events related to treatment were lipase elevation (n = 7 [10.8%]), fatigue (n = 4 [6.2%]), hyperglycemia (n = 3 [4.6%]), and elevated ALT (n = 3 [4.6%]).

**CONCLUSION** Buparlisib had minimal single-agent efficacy in patients with PI3K-activated recurrent glioblastoma. Although buparlisib achieved significant brain penetration, the lack of clinical efficacy was explained by incomplete blockade of the PI3K pathway in tumor tissue. Integrative results suggest that additional study of PI3K inhibitors that achieve more-complete pathway inhibition may still be warranted.

J Clin Oncol 37:741-750. © 2019 by American Society of Clinical Oncology

## INTRODUCTION

Glioblastoma is the most common malignant primary brain tumor.<sup>1</sup> Despite treatment with surgery, radiation therapy (RT), and chemotherapy, outcomes have not substantially improved over the past two decades, with median overall survival (OS) of only 14 to 18 months.<sup>2-4</sup> Limited drug delivery as a result of the blood-brain barrier (BBB) represents one of the most significant challenges and partly explains why many agents that target oncogenic pathways of glioblastoma but whose chemical properties do not allow significant

BBB penetration have minimal efficacy.<sup>5</sup> However, few studies directly examined tumor tissue during treatment,<sup>6,7</sup> which prevents reliable conclusions about drug effectiveness with regard to level of target inhibition and effects on cell death and proliferation. Studies designed to confirm drug penetration and target engagement therefore may be critical to understanding trial results and improving outcomes in glioblastoma.

The PI3K pathway is activated in most glioblastomas.<sup>8</sup> *PTEN* loss and *PIK3CA* or *PIK3R1* mutations represent

## ASSOCIATED CONTENT

### Appendix

Author affiliations and support information (if applicable) appear at the end of this article.

Accepted on December 13, 2018 and published at [jco.org](https://doi.org/10.1200/JCO.18.01207) on February 4, 2019; DOI <https://doi.org/10.1200/JCO.18.01207>

Clinical trial information: NCT01339052.

ASCO

Journal of Clinical Oncology®

Volume 37, Issue 9 741

Downloaded from [ascopubs.org](https://ascopubs.org) by 31.34.66.224 on October 18, 2020 from 031.034.066.224  
Copyright © 2020 American Society of Clinical Oncology. All rights reserved.

Université Paris-Saclay

Espace Technologique / Immeuble Discovery

Route de l'Orme aux Merisiers RD 128 / 91190 Saint-Aubin, France

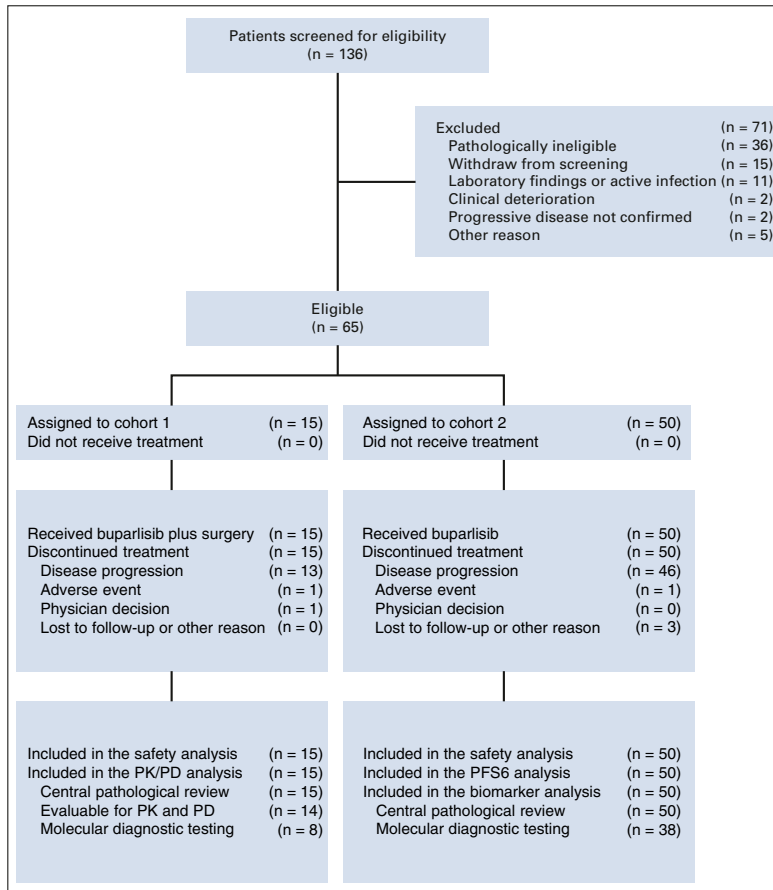


**FIG 1.** Study flow. PD, pharmacodynamics; PFS6, 6-month progression free survival; PK, pharmacokinetics.

potential therapeutic targets that are found in approximately 45% of glioblastomas.<sup>8,9</sup> Previous trials of mechanistic target of rapamycin (mTOR) complex 1 inhibitors did not show significant efficacy.<sup>6,10,11</sup> More recently, PI3K inhibitors have been evaluated. In a trial of the pan-PI3K inhibitor PX-866 in 32 molecularly unselected patients with recurrent glioblastoma, one patient achieved a partial response (PR), and the 6-month progression-free survival (PFS6) rate was 17%.<sup>12</sup> However, this study did not evaluate whether adequate brain penetration and target engagement was achieved.

Buparlisib (NVP-BKM120) is an oral pan-PI3K inhibitor that targets all four isoforms of class 1 PI3K ( $\alpha$ ,  $\beta$ ,  $\gamma$ , and  $\delta$ ).<sup>13</sup> Buparlisib has high penetration across the BBB. In pre-clinical studies, buparlisib enters the brain at therapeutic concentrations demonstrated to inhibit the PI3K pathway in normal brain and glioma models *in vitro* and *in vivo*.<sup>14-16</sup> The Ivy Foundation Early Phase Clinical Trials Consortium conducted a phase II trial of buparlisib in patients with recurrent glioblastoma with evidence of PI3K pathway

activation to assess the pharmacokinetics, pharmacodynamics, and efficacy of buparlisib in this population.

## METHODS

### Study Design and Participants

This study was a multicenter, open-label, and multi-arm phase II trial in patients with recurrent glioblastoma at first or second relapse. Written informed consent was obtained from all participants. The study was approved by the local institutional review board of each participating institution and consisted of two cohorts: a surgery plus treatment arm (cohort 1) and a treatment-only arm (cohort 2; Appendix Fig A1, online only). Eligible participants were age 18 years or older with a centrally confirmed diagnosis of glioblastoma. Patients must have not responded to prior RT, with an interval of at least 12 weeks from RT completion to study entry. Tumor progression was confirmed by magnetic resonance imaging or computed tomography scan. Prior treatment with bevacizumab or vascular endothelial growth

**TABLE 1.** Baseline Patient Demographics and Clinical Characteristics

Characteristic	Cohort, No. (%)	
	1	2
No. of patients	15	50
Median age, years (range)	55 (39-68)	56 (29-80)
Sex		
Male	11 (73.3)	37 (74.0)
Female	4 (26.7)	13 (26.0)
KPS		
100	2 (13.3)	9 (18.0)
90	10 (66.7)	23 (46.0)
80	2 (13.3)	15 (30.0)
70	1 (6.7)	3 (6.0)
Corticosteroids at baseline		
Yes	7 (46.67)	24 (48.0)
No	8 (53.33)	26 (52.0)
Histology*		
GBM, <i>IDH1/2</i> wild type	13 (86.7)	37 (74.0)
GBM, <i>IDH1/2</i> mutant	1 (6.7)	11 (22.0)
GBM, NOS	1 (6.7)	2 (4.0)
Median No. of prior systemic therapies (range)	1 (1-2)	1 (1-2)
Prior bevacizumab	0 (0)	0 (0)

Abbreviations: GBM, glioblastoma; KPS, Karnofsky performance status; NOS, not otherwise specified.

\*Diagnosis according to WHO 2016 diagnostic criteria.

factor receptor<sup>44</sup> inhibitors, PI3K, AKT, or mTOR inhibitors was not permitted. Patients had a Karnofsky performance status greater than or equal to 60, adequate organ and bone marrow function, fasting plasma glucose less than 120 mg/dL, hemoglobin A1C less than or equal to 8%, baseline left ventricular ejection fraction greater than or equal to 50%, and QTc less than 480 ms. Patients on enzyme-inducing anticonvulsants, warfarin, more than 4 mg/d dexamethasone, strong CYP3A inhibitors or inducers, or QT-prolonging medications were excluded, as were patients with a history of clinically significant cardiovascular events, intratumoral hemorrhage, or psychiatric disorders. Histomolecular criteria for eligibility included *PIK3CA* or *PIK3R1* mutation, loss of PTEN activity through *PTEN* mutation, homozygous deletion or negative PTEN expression (< 10% of tumor cells that stained positive), or positive phosphorylated AKT<sup>S473</sup> (pAKT<sup>S473</sup>) by central immunohistochemistry (IHC) review. Cohort 1 surgical patients were required to have positive expression of pAKT<sup>S473</sup> within the archival tumor.

#### Procedure

Buparlisib was supplied by Novartis (East Hanover, NJ). The dose of buparlisib was 100 mg administered orally daily.<sup>17,18</sup>

In cohort 1, participants received a pre-operative course of buparlisib for 7 to 13 days. The last dose of buparlisib was on the day of surgery. Whenever possible, tissue from both enhancing and nonenhancing tumor was collected. After recovery from surgery, participants resumed buparlisib in a manner consistent with cohort 2. In cohort 2, participants received buparlisib 100 mg daily for each 28-day cycle until disease progression or unacceptable toxicity.

Tumor assessments were performed with magnetic resonance imaging scans every 8 weeks using the Response Assessment in Neuro-Oncology criteria (Appendix Table A1, online only).<sup>19</sup> PFS6 was defined as the proportion of participants alive and progression free at 6-months from cycle 1, day 1, of buparlisib. Only participants who had measurable disease at baseline and received at least one dose of therapy were evaluable for response, which was centrally reviewed for participants who achieved response or PFS6. Adverse events were evaluated using the National Cancer Institute Common Terminology Criteria for Adverse Events (version 4.0). Additional analyses, including pharmacokinetics and IHC studies, tumor genomic profiling, reverse-phase protein array (RPPA), and matrix-assisted laser desorption/ionization-mass spectrometry imaging are described in the Appendix (online only).

#### Outcomes

The primary objectives in cohort 1 were to evaluate PI3K pathway modulation as a result of buparlisib in tumor tissue and to evaluate buparlisib concentration in enhancing and nonenhancing tumor tissue and plasma. Secondary end points included pharmacokinetics and safety of buparlisib in this population. Exploratory end points included correlation of <sup>18</sup>F-fluorodeoxyglucose (FDG) positron emission tomography with response.

In cohort 2, the primary objective was to investigate the treatment efficacy of buparlisib in participants with recurrent glioblastoma as assessed by PFS6. Secondary end points were response rates and the median PFS, OS, and safety profile of buparlisib. Exploratory end points included correlation of outcomes with tumor genomics.

#### Sample Size Justification

The cohort 1 primary end point was the modulation of the PI3K pathway as assessed by IHC for pAKT<sup>S473</sup> and phosphorylated S6 S235/236 (pS6<sup>S235/236</sup>). On the basis of historical data or mTOR complex 1 inhibitors in recurrent glioblastoma,<sup>6</sup> a pharmacodynamic response rate less than 40% was considered to be low, a response rate of greater than or equal to 75% was considered to be high, and this portion of the trial was considered a success if nine (60%) of 15 participants showed a pathologic response. With a sample size of 15 patients, there was a 94% chance of this occurring if the true response rate was 75% and a 10% chance of this occurring if the true response rate was 40%.

The cohort 2 primary end point was PFS6. Historical comparison data suggested that ineffective therapies in

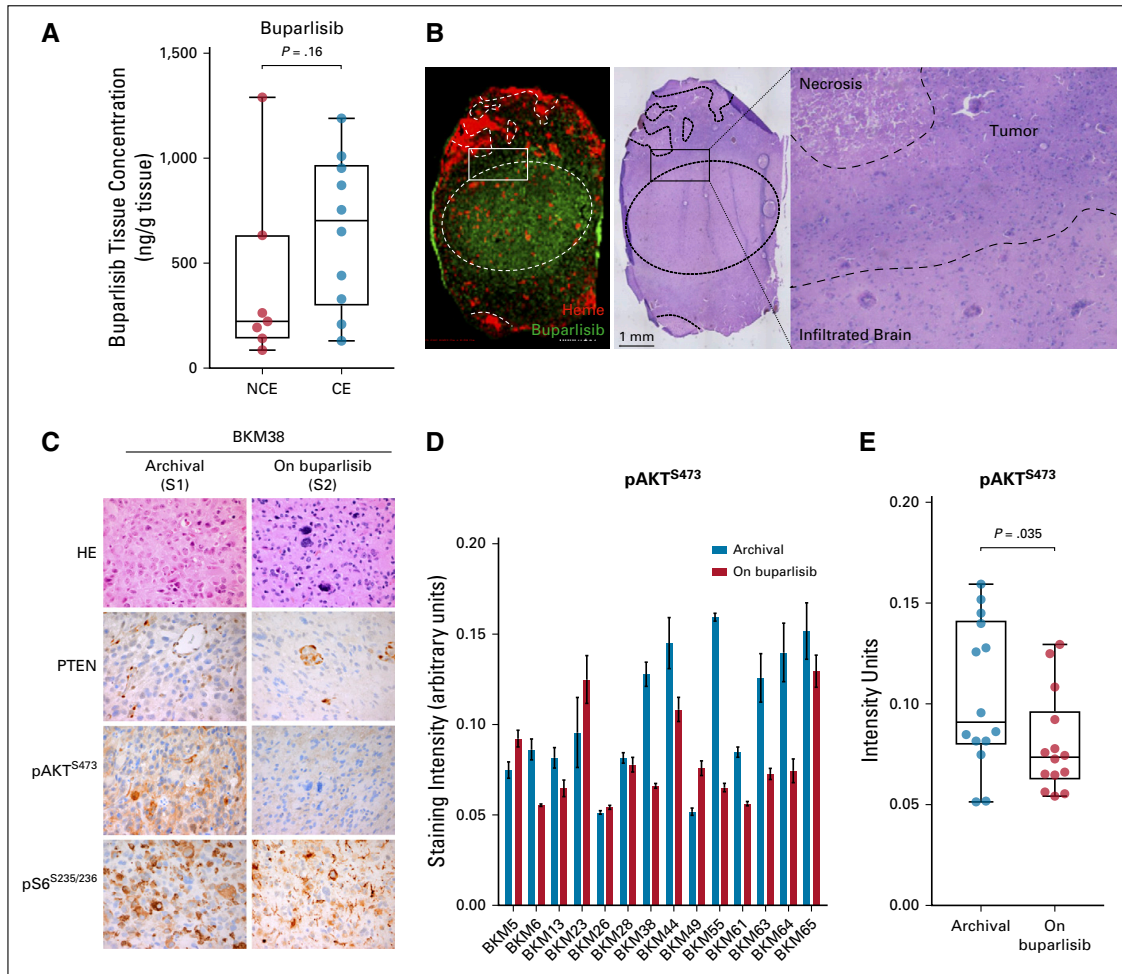


**FIG 2.** Buparlisib pharmacokinetics and phosphatidylinositol 3-kinase pathway modulation as a result of buparlisib in tumor tissue in cohort 1. (A) Box plots of buparlisib concentration in non-contrast-enhancing (NCE) and contrast-enhancing (CE) tumor tissue assessed by liquid chromatography-tandem mass spectrometry. Difference between groups was calculated using the Mann-Whitney  $U$  test. (B) Histopathologic and matrix-assisted laser desorption/ionization-mass spectrometry imaging drug analysis on stereotactically registered specimens collected from a patient in cohort 1 treated with buparlisib. Image on the left demonstrates location of buparlisib (green) and vessels as measured by heme (red). Hematoxylin and eosin (HE) staining of the corresponding tissue. Outlined area delineates tumor and adjacent infiltrated brain parenchyma. (C) Representative microscopy images of the HE staining and PTEN, phosphorylated AKT (pAKT), and phosphorylated S6 (pS6) in tumor samples collected at baseline and on buparlisib treatment from a patient in cohort 1. (D) Quantification of pAKT immunohistochemistry (IHC) staining intensity in the surgical cohort. Data are mean  $\pm$  SEM ( $n = 5$  to 7 replicates for each sample). (E) Box plots of mean pAKT IHC staining intensity in the archival and resected tissues from the surgical cohort ( $n = 14$ ). Difference between groups was calculated using the Wilcoxon test (See Appendix).

recurrent glioblastoma have a PFS6 rate of approximately 9% to 16%.<sup>5,20,21</sup> The trial was sized to differentiate between a 15% and a 32% PFS6. With a total sample size of 50 participants, this design yielded at least 90% power with a one-sided  $\alpha$  less than .1 to detect a true PFS6 rate of at least 32%. If the number of successes was 12 or more, the therapy was to be considered worthy of additional study. More statistical analysis details are provided in the Appendix.

## RESULTS

### Patient Characteristics

Between May 9, 2011, and February 26, 2014, 136 patients were screened for eligibility from seven centers in the United States. Of these patients, 71 were excluded (Fig 1). Sixty-five patients were eligible and assigned to receive buparlisib (cohort 1,  $n = 15$ ; cohort 2,  $n = 50$ ; Fig 1).

**TABLE 2.** Response to Treatment

Response	Response to Treatment	
	Cohort 1 (n = 15)	Cohort 2 (n = 50)
Best response†, No (%)		
CR	0 (0)	0 (0)
PR	0 (0)	0 (0)
SD	6 (40)	21 (42)
PD	9 (60)	27 (54)
Not evaluable	0 (0)	2 (4)
Disease control rate (CR, PR, or SD), % (95% CI)†	40 (20 to 64)	43.8 (31 to 58)
PFS6 rate, % (95% CI)*	26.7 (11 to 52)	8 (3 to 19)
Median PFS, months (95% CI)‡	1.8 (1.1 to 5.6)	1.7 (1.4 to 1.8)
Median OS, months (95% CI)§	17.9 (9.3 to 29.2)	9.8 (8.4 to 12.1)

Abbreviations: CR, complete response; OS, overall survival; PD, progressive disease; PR, partial response; PFS, progression-free survival; PFS6, 6-month progression-free survival; SD, stable disease.

\*Censored patients (two patients in cohort 2) were included in the calculations of PFS6 proportions as patients not reaching PFS6.

†Assessed per Response Assessment in Neuro-Oncology.

‡Kaplan-Meier estimates; three patients from cohort 2 were censored without having progressed.

§Kaplan-Meier estimate; two patients from cohort 1 were lost to follow-up, three patients from cohort 2 were lost to follow-up, and two patients from cohort 2 were still alive at data cutoff.

Baseline characteristics of patients are listed in Table 1. Sixty-four patients (98.5%) had received RT and temozolomide, and 31 (41.7%) and eight (12.3%) had received surgery or systemic therapy, respectively, for progressive disease. Demonstration of PI3K pathway activation in archival tumor tissue was based on IHC of PTEN and pAKT<sup>S473</sup> status in 62 patients (95.4%) and genomic testing in three (4.6%). Overall, 31 enrolled patients (47.7%) had combined negative PTEN and positive pAKT<sup>S473</sup> IHC; 24 (36.9%) had positive pAKT<sup>S473</sup> IHC; seven (10.8%) had negative PTEN IHC; and three (4.6%) had genomic testing showing *PTEN* inactivation or *PIK3CA* mutation.

#### Pharmacokinetics and Pharmacodynamics of Buparlisib

Buparlisib was absorbed rapidly, achieving a maximum plasma concentration of  $471 \pm 147$  ng/mL and  $820 \pm 192$  ng/mL within a median of 1.5 hours postdose on days 1 and 8, respectively (Appendix Table A2, online only). Both maximum plasma concentration and exposure (0- to 5-hour area under the curve) increased between days 1 and 8, with an accumulation ratio of  $1.88 \pm 0.503$  and  $2.42 \pm 0.726$ , respectively (Appendix Table A2). The accumulation of buparlisib was consistent with the reported half-life of approximately 40 hours reaching steady state by day 8.<sup>17,18</sup>

Resected tumor tissue was evaluable for pharmacokinetics and pharmacodynamics analyses in 14 patients. The average time between the last dose of buparlisib and the time

of tumor sampling was  $5 \pm 1.61$  hours. The average plasma concentration at the time of the tumor sampling was  $585 \pm 192$  ng/mL. The geometric mean concentration of buparlisib in the tumor tissue was 612 ng/g (range, 86 to 6,947 ng/g), with a resulting tumor-to-plasma geometric mean ratio of 1.0 (range, 0.18 to 8.44). There was no significant difference between the non-contrast-enhancing (CE) and CE tumor tissue concentrations of buparlisib (mean,  $404 \pm 429$  v  $654 \pm 363$ , respectively;  $P = 0.16$ ; Fig 2A). Brain penetration of buparlisib also was confirmed by matrix-assisted laser desorption/ionization-mass spectrometry imaging performed on tumor specimens that showed the presence of drug in the tumor as well as in the infiltrated brain parenchyma (Fig 2B).

A decrease in pAKT<sup>S473</sup> IHC score was achieved in six patients (42.9%) and was statistically significant in the overall cohort (Figs 2C to 2E), whereas the analysis of an independent set of pre- and post-treatment (RT + temozolomide) glioblastoma pairs did not show significant change in pAKT<sup>S473</sup> or pS6<sup>S235/236</sup> IHC (Appendix Fig A2, online only). A reduction in pAKT<sup>T308</sup> only in post-buparlisib treatment tumor also was observed in RPPA analysis of 299 antibodies (Appendix Table A4, online only). Nevertheless, in seven patients (50%), no change in pAKT<sup>S473</sup> IHC score was noted, and one patient (7.1%) had an increase in pAKT<sup>S473</sup> IHC score, which suggested an incomplete blockade of PI3K signaling in approximately one half of patients. This finding was consistent with the absence of modulation of pS6<sup>S235/236</sup> by IHC and lack of consistent changes in pS6<sup>S235/236</sup>, pS6<sup>S240/244</sup>, and p70 S6<sup>T389</sup> kinases in the RPPA analysis (Appendix Fig A3, online only; Appendix Table A4). Moreover, RPPA analysis did not show a consistent change in members of the mitogen-activated protein kinase (MAPK) pathway when comparing buparlisib-treated versus control glioblastoma pairs (Appendix Table A4). Finally, there was no significant change in tumor cell proliferation between baseline and post-buparlisib treatment samples as assessed by the IHC proliferation marker Ki-67 (Appendix Fig A2).

#### Outcome

At final analysis (April 30, 2018), none of the 65 patients remained on treatment. The most frequent reason for treatment discontinuation in both groups was disease progression (59 [90.8%]; Fig 1). The median follow-up was 15.6 months (range, 3.6 to 36.6 months) in cohort 1 versus 9.8 months (range, 1.0 to 71.2 months) in cohort 2.

The study did not meet its primary end point for PFS6 with buparlisib in cohort 2 (n = 50); four patients (8%; 95% CI, 3% to 19%) reached PFS6, and the median PFS was 1.7 months (95% CI, 1.4 to 1.8 months; Table 2; Appendix Fig A4, online only). OS data were mature, with 58 deaths in the total population at the cutoff date (cohort 1, n = 13; cohort 2, n = 45). Two patients were still alive, and five were lost to follow-up. The median OS was 17.9 months (95% CI,



**FIG 3.** Relationship between mutations in phosphatidylinositol 3-kinase (PI3K) pathway members and response to buparlisib. Patient outcomes, including best overall response (BOR), median progression-free survival (PFS), and median overall survival (OS), are shown in the top rows; tumor genotyping and immunohistochemistry (IHC) results are shown in the middle rows; and integrative biomarker analysis for *PI3K/PTEN* signaling is shown in the bottom rows. Missense mutations are displayed in green, amplifications in orange, and deletions in blue. All mutations were reviewed by a molecular diagnostician to confirm that they were deemed pathogenic/hotspot mutations and were not commonly identified in normal databases as germline single nucleotide polymorphisms.

9.3 to 29.2 months) in cohort 1 and 9.8 months (95% CI, 8.4 to 12.1 months) in cohort 2 (Table 2; Appendix Fig A4).

Best overall response was evaluable in 63 patients (96.9%). No patients achieved a radiographic response (Table 2). Six patients (40%; 95% CI, 20% to 64%) in cohort 1 and 21 (43.8%; 95% CI, 31% to 58%) in cohort 2 had disease stabilization as best response. In addition, 12 patients in cohort 1 had an FDG-positron emission tomography scan performed before and after treatment with buparlisib (mean delay, 11.4 days; range, 7 to 25 days). Six of the 12 patients had a modest decrease in tumor-to-background ratio in FDG uptake (−2.35% to −18.7%), but there was no correlation with outcome.

#### Correlation of Outcomes With Genotyping

Correlation between outcome and tumor genotyping was assessed in 46 patients (71.9%; eight [53.3%] in cohort 1 and 38 [76%] in cohort 2) for whom copy number array and/or tumor-targeted sequencing was available (Fig 3).

Overall, pathogenic variants of *PTEN*, *PIK3CA*, or *PIK3R1* were identified in 27 patients (56.3%; Fig 3).

Candidate biomarkers, including *PTEN*, *PIK3CA*, *PIK3R1*, *EGFR*, *PDGFRA*, *IDH1/2*, and *TP53* molecular alterations and IHC evidence for PTEN inactivation, pAKT<sup>S473</sup>, and pS6<sup>S235/236</sup> activation, were evaluated for their association with outcome. Although no statistically significant association was found between PFS6 or OS and any of the candidate biomarkers, there was a shorter PFS in patients with *IDH1/2*-mutant versus *IDH1/2* wild-type glioblastoma (median PFS, 0.9 months [interquartile range (IQR), 0.9-1.8 months] v 1.8 months [IQR, 1.1-3.6 months], respectively; log-rank  $P = .002$ ; Appendix Fig A5, online only). No statistically significant association was found between PFS and *PIK3CA/PIK3R1*-mutant glioblastoma (median PFS, 2.2 months [IQR, 1.8-2.8 months] v 1.8 months [IQR, 0.9-2.8 months] in *PIK3CA/PIK3R1* mutant v *PIK3CA/PIK3R1* wild type, respectively; log-rank  $P = .67$ ) or *PTEN* molecular alterations (median PFS, 1.8 months [IQR,

**TABLE 3.** Summary of Grade 3 to 4 Treatment-Related Adverse Events

Adverse Event (CTCAE grade)	No. (%)
Increased lipase (4)	1 (1.5)
Increased lipase (3)	6 (9.2)
Fatigue (3)	4 (6.2)
Increased ALT (3)	3 (4.6)
Hyperglycemia (3)	3 (4.6)
Hypophosphatemia (3)	2 (3.1)
Rash acneiform (3)	2 (3.1)
Rash maculopapular (3)	2 (3.1)
Diarrhea (3)	1 (1.5)
Increased AST (3)	1 (1.5)
Increased serum amylase (3)	1 (1.5)
Decreased lymphocyte count (3)	1 (1.5)
Decreased platelet count (3)	1 (1.5)
Anxiety (3)	1 (1.5)
Depression (3)	1 (1.5)
Photosensitivity (3)	1 (1.5)
Pruritus (3)	1 (1.5)
Confluent erythema (3)	1 (1.5)

Abbreviation: CTCAE, Common Terminology Criteria for Adverse Events (version 4.0).

1.3-3.6 months] v 1.8 months [IQR, 0.9-2.8 months] in *PTEN* mutant v *PTEN* wild type, respectively; log-rank  $P = .57$ ; Appendix Fig A5).

#### Toxicity

Table 3 lists the most common grade 3 and 4 adverse events. Overall, grade 3 to 4 treatment-related adverse events were reported in 40.0% (95% CI, 19.8% to 64.3%) of patients in cohort 1 and 32.0% (95% CI, 20.8% to 45.8%) of patients in cohort 2. Only one patient (1.5%) experienced a grade 4 toxicity that was at least possibly related to treatment, and consisted of an asymptomatic lipase increase. No suicidality was reported. No on-treatment deaths occurred. Buparlisib treatment was discontinued in two patients (3.1%) as a result of adverse events, one in each arm. The most common adverse events that led to dose reduction or discontinuation were increased lipase in six patients (9.2%) and increased ALT and hyperglycemia in five (7.7%).

#### DISCUSSION

This study shows that the brain-penetrant PI3K inhibitor buparlisib has minimal single-agent efficacy in patients with recurrent glioblastoma.<sup>5,20,21</sup> Buparlisib did not meet the primary pharmacodynamic and efficacy end points of this study. These findings are consistent with previous results wherein PI3K/mTOR inhibitors alone or in combination with cytotoxic or targeted therapies in patients with glioblastoma unselected for PI3K pathway activation showed no clinical

benefit.<sup>6,9-11,12,22-27</sup> Although PI3K pathway activation was confirmed in all patients, post hoc analyses did not show a correlation between the mutation status of *PTEN*, *PIK3CA*, and *PIK3R1* and outcome. Of note, a shorter PFS was observed in patients with *IDH1/2*-mutant tumors. However, because this was a post hoc analysis in a relatively small number of patients with *IDH1/2*-mutant tumors, definitive conclusions will require increased numbers.

To our knowledge, this study provides the first evidence that buparlisib can achieve adequate brain penetration in patients with glioblastoma. Buparlisib accumulation was seen in both CE and non-CE areas of tumor, with a trend to higher accumulation in CE areas. These findings are consistent with preclinical and early-phase studies of buparlisib<sup>14,16,28,29</sup> as well as with the phase III trial BELLE-2 in human epidermal growth factor receptor 2–negative metastatic breast cancer.<sup>30</sup> In this study, a higher rate of psychiatric adverse effects, including depression and anxiety, was observed with buparlisib, which were not reported with other PI3K inhibitors<sup>31-35</sup> and were attributed to the high BBB penetration of buparlisib.

Our multidimensional analysis, including IHC, study of cell proliferation and signaling markers, RPPA, and tumor genomic profiling provide important insights for understanding mechanisms of resistance to single-agent PI3K inhibitors in glioblastoma. Although our analyses document inhibition of pAKT<sup>S473</sup> in a subset of patients, blockade of the PI3K pathway activity was incomplete, as evidenced by the limited effects on downstream pS6<sup>S235/236</sup>. This was associated with minimal effects on tumor cell proliferation and outcome. The morphometric IHC and RPPA analyses suggest that persistent downstream signaling occurred through incomplete blockade of PI3K pathway together with activity of complementary pathways, including MAPK signaling. Previous studies showed that buparlisib concentrations required to fully inhibit PI3K activity generate toxic off-target effects on cytoskeleton dynamics,<sup>36</sup> which suggests that the therapeutic window of buparlisib might be too narrow in glioblastoma. The robust activity of PI3K signaling in glioblastoma may require more potent and selective inhibitors that would achieve greater pathway inhibition without causing dose-limiting adverse events.

Besides incomplete PI3K pathway inhibition, the persistent activity of p70 S6 kinases and the MAPK pathway observed in the RPPA analysis suggests activation of alternate pro-survival pathways that also may contribute to buparlisib resistance. This phenomenon might be overcome by a combination of buparlisib or other PI3K inhibitor with inhibiting complementary signaling or feedback molecules, such as sonic hedgehog, ribosomal S6 kinase, or insulin.<sup>37-40</sup>

A limitation of our study was the use of historical data as reference because of a lack of a control arm in the study design. Nevertheless, the absence of radiologic response

observed in this study suggests that buparlisib has minimal single-agent efficacy in this population and is unlikely to demonstrate benefit against controls in future trials. Another limitation was that biomarker analyses for study entry were performed on archival tissues instead of use of an immediate pretreatment biopsy sample because the feasibility of performing sequential biopsies was limited by ethical considerations. However, recent studies that addressed clonal evolution of glioblastoma under therapy using whole-exome sequencing of pre- and post-treatment-paired tumors showed that molecular alterations of *PTEN*, *PIK3CA*, or *PI3R1* are rarely lost in recurrent samples.<sup>41-43</sup> This suggests that although a certain degree of clonal evolution occurs after treatment with DNA-damaging agents, alterations in the PI3K pathway are likely retained as targets in recurrent tumors in a majority of patients.

In conclusion, this study shows that buparlisib does not provide clinically meaningful benefit in patients with PI3K-

activated recurrent glioblastoma. Our finding that pathway inhibition was incomplete suggests that additional studies are warranted to assess whether more potent and selective PI3K inhibitors may achieve greater pathway inhibition and clinical benefit. Careful assessment of tissue pharmacokinetics and pharmacodynamics through the surgical arm of the study was important to our understanding that poor pathway inhibition was likely the basis for the modest response seen in patients. This suggests that in glioblastoma, more routine use of studies specifically designed to confirm drug penetration and target engagement may be beneficial to perform before considering advancing a drug for more testing. In addition, investigation of how PI3K inhibitors can be combined with complementary therapeutics to provide clinical benefit in glioblastoma are still warranted and should include studies designed to understand the dependency and associations between biomarkers and response to PI3K inhibitors, including *PTEN*, *PIK3CA*, *PI3R1*, and *IDH1/2* mutations.

#### AFFILIATIONS

- <sup>1</sup>Dana-Farber Cancer Institute, Boston, MA  
<sup>2</sup>Brigham and Women's Hospital, Boston, MA  
<sup>3</sup>Memorial Sloan Kettering Cancer Center, New York, NY  
<sup>4</sup>The University of Texas M.D. Anderson Cancer Center, Houston, TX  
<sup>5</sup>California Institute of Technology, Pasadena, CA  
<sup>6</sup>David Geffen School of Medicine at University of California, Los Angeles, Los Angeles, CA  
<sup>7</sup>The University of Texas, San Antonio, San Antonio, TX  
<sup>8</sup>Huntsman Cancer Institute and University of Utah, Salt Lake City, UT  
<sup>9</sup>New York University School of Medicine, New York, NY  
<sup>10</sup>Institute for Systems Biology, Seattle, WA  
<sup>11</sup>Massachusetts General Hospital, Boston, MA  
<sup>12</sup>University of California, San Francisco, San Francisco, CA

#### CORRESPONDING AUTHOR

Patrick Y. Wen, MD, Center for Neuro-Oncology, Dana Farber Cancer Institute, 450 Brookline Ave, Dana 2-2202, Boston, MA 02215; Twitter: @PatrickWen3; e-mail: pwen@partners.org

#### PRIOR PRESENTATION

Presented at the American Society of Clinical Oncology 2014 Annual Meeting, Chicago, IL, May 30-June 3, 2014.

#### SUPPORT

Supported by the Ivy Foundation Early Phase Clinical Trials Consortium, DFHCC/MIT Bridge Project (R01CA188288, P50 CA165962), and by Novartis, which provided the drug and funding.

#### AUTHORS' DISCLOSURES OF POTENTIAL CONFLICTS OF INTEREST AND DATA AVAILABILITY STATEMENT

Disclosures provided by the authors and data availability statement (if applicable) are available with this article at DOI <https://doi.org/10.1200/JCO.18.01207>.

#### AUTHOR CONTRIBUTIONS

**Conception and design:** Patrick Y. Wen, Mehdi Touat, Shakti Ramkissoon, Howard Colman, Eudocia Q. Lee, Susan M. Chang, Michael D. Prados, W.K. Alfred Yung, Keith L. Ligon

**Financial support:** Keith L. Ligon

**Administrative support:** Christine S. McCluskey, Loreal E. Brown, W.K. Alfred Yung

**Provision of study material or patients:** Patrick Y. Wen, Ingo K. Mellingshoff, Howard Colman, Antonio M. Omuro, Lisa M. DeAngelis, Mark R. Gilbert, John F. de Groot, Timothy F. Cloughesy, Eudocia Q. Lee, Lakshmi Nayak, Tracy T. Batchelor, Susan M. Chang, Ian F. Dunn, Geoffrey S. Young, Michael D. Prados, W.K. Alfred Yung, Keith L. Ligon

**Collection and assembly of data:** Patrick Y. Wen, Mehdi Touat, Ingo K. Mellingshoff, Shakti Ramkissoon, Christine S. McCluskey, Kristine Pelton, Sankha S. Basu, Sarah C. Gaffey, Loreal E. Brown, Jungwoo Kim, Wei Wei, Mi-Ae Park, Jason T. Huse, Mikael L. Rinne, Howard Colman, Nathalie Y.R. Agar, Antonio M. Omuro, Lisa M. DeAngelis, Mark R. Gilbert, John F. de Groot, Andrew S. Chi, Eudocia Q. Lee, James R. Heath, Laura L. Horky, Tracy T. Batchelor, Rameen Beroukhi, Susan M. Chang, Ian F. Dunn, Dimpy Koul, Geoffrey S. Young, Michael D. Prados, David A. Reardon, Keith L. Ligon

**Data analysis and interpretation:** Patrick Y. Wen, Mehdi Touat, Brian M. Alexander, Ingo K. Mellingshoff, Shakti Ramkissoon, Kristine Pelton, Sam Haidar, Sankha S. Basu, Juan Emmanuel Martinez-Ledesma, Shaofang Wu, Wei Wei, Mi-Ae Park, John G. Kuhn, Nathalie Y.R. Agar, Antonio M. Omuro, Lisa M. DeAngelis, Mark R. Gilbert, John F. de Groot, Timothy F. Cloughesy, Thomas M. Roberts, Jean J. Zhao, Lakshmi Nayak, James R. Heath, Laura L. Horky, Susan M. Chang, Azra H. Ligon, Dimpy Koul, Michael D. Prados, Keith L. Ligon

**Manuscript writing:** All authors

**Final approval of manuscript:** All authors

**Accountable for all aspects of the work:** All authors

#### ACKNOWLEDGMENT

We thank the patients who took part in the study and their families as well as the staff, research coordinators, and investigators at each participating institution. We acknowledge the support of the Ben and Catherine Ivy Foundation and Lisa Doherty, APRN, OCN; Debra Conrad LaFrankie, RN, OCN; Sandra French Ruland, RN, BSN, OCN; Jennifer Stefanik, NP, and Jann N. Sarkaria, MD, for sharing unpublished results. Finally, we acknowledge the Center for Cancer Genome Discovery; Paul Van Hummelen and Aaron Thorner; and the members of the Brigham and Women's Hospital Center for Advanced Molecular Diagnostics, Clinical Cytogenetics Division.

## REFERENCES

- Ostrom QT, Gittleman H, Liao P, et al: CBTRUS statistical report: Primary brain and other central nervous system tumors diagnosed in the United States in 2010-2014. *Neuro-oncol* 19:v1-v88, 2017
- Wen PY, Kesari S: Malignant gliomas in adults. *N Engl J Med* 359:492-507, 2008
- Stupp R, Hegi ME, Mason WP, et al: Effects of radiotherapy with concomitant and adjuvant temozolomide versus radiotherapy alone on survival in glioblastoma in a randomised phase III study: 5-year analysis of the EORTC-NCIC trial. *Lancet Oncol* 10:459-466, 2009
- Stupp R, Taillibert S, Kanner AA, et al: Maintenance therapy with tumor-treating fields plus temozolomide vs temozolomide alone for glioblastoma: A randomized clinical trial. *JAMA* 314:2535-2543, 2015
- Toutat M, Idbaih A, Sanson M, et al: Glioblastoma targeted therapy: Updated approaches from recent biological insights. *Ann Oncol* 28:1457-1472, 2017
- Cloughesy TF, Yoshimoto K, Nghiemphu P, et al: Antitumor activity of rapamycin in a phase I trial for patients with recurrent PTEN-deficient glioblastoma. *PLoS Med* 5:e8, 2008
- Hegi ME, Diserens AC, Bady P, et al: Pathway analysis of glioblastoma tissue after preoperative treatment with the EGFR tyrosine kinase inhibitor gefitinib—a phase II trial. *Mol Cancer Ther* 10:1102-1112, 2011
- Brennan CW, Verhaak RG, McKenna A, et al: The somatic genomic landscape of glioblastoma. *Cell* 155:462-477, 2013 [Erratum: *Cell* 157:753, 2014]
- Wen PY, Lee EQ, Reardon DA, et al: Current clinical development of PI3K pathway inhibitors in glioblastoma. *Neuro-oncol* 14:819-829, 2012
- Chang SM, Wen P, Cloughesy T, et al: Phase II study of CCI-779 in patients with recurrent glioblastoma multiforme. *Invest New Drugs* 23:357-361, 2005
- Ma DJ, Galanis E, Anderson SK, et al: A phase II trial of everolimus, temozolomide, and radiotherapy in patients with newly diagnosed glioblastoma: NCCTG N057K. *Neuro-oncol* 17:1261-1269, 2015
- Pitz MW, Eisenhauer EA, MacNeil MV, et al: Phase II study of PX-866 in recurrent glioblastoma. *Neuro-oncol* 17:1270-1274, 2015
- Burger MT, Pecchi S, Wagman A, et al: Identification of NVP-BKM120 as a potent, selective, orally bioavailable class I PI3 kinase inhibitor for treating cancer. *ACS Med Chem Lett* 2:774-779, 2011
- Koul D, Fu J, Shen R, et al: Antitumor activity of NVP-BKM120—a selective pan class I PI3 kinase inhibitor showed differential forms of cell death based on p53 status of glioma cells. *Clin Cancer Res* 18:184-195, 2012
- Maire CL, Ramkissoon S, Hayashi M, et al: Pten loss in Olig2 expressing neural progenitor cells and oligodendrocytes leads to interneuron dysplasia and leukodystrophy. *Stem Cells* 32:313-326, 2014
- Netland IA, Forde HE, Sleire L, et al: Treatment with the PI3K inhibitor buparlisib (NVP-BKM120) suppresses the growth of established patient-derived GBM xenografts and prolongs survival in nude rats. *J Neurooncol* 129:57-66, 2016
- Bendell JC, Rodon J, Burris HA, et al: Phase I, dose-escalation study of BKM120, an oral pan-class I PI3K inhibitor, in patients with advanced solid tumors. *J Clin Oncol* 30:282-290, 2012
- Rodon J, Braña I, Siu LL, et al: Phase I dose-escalation and -expansion study of buparlisib (BKM120), an oral pan-class I PI3K inhibitor, in patients with advanced solid tumors. *Invest New Drugs* 32:670-681, 2014
- Wen PY, Macdonald DR, Reardon DA, et al: Updated response assessment criteria for high-grade gliomas: Response assessment in Neuro-Oncology Working Group. *J Clin Oncol* 28:1963-1972, 2010
- Wong ET, Hess KR, Gleason MJ, et al: Outcomes and prognostic factors in recurrent glioma patients enrolled onto phase II clinical trials. *J Clin Oncol* 17:2572-2578, 1999
- Lamborn KR, Yung WK, Chang SM, et al: Progression-free survival: An important end point in evaluating therapy for recurrent high-grade gliomas. *Neuro-oncol* 10:162-170, 2008
- Wen PY, Chang SM, Lamborn KR, et al: Phase I/II study of erlotinib and temsirolimus for patients with recurrent malignant gliomas: North American Brain Tumor Consortium trial 04-02. *Neuro-oncol* 16:567-578, 2014
- Reardon DA, Quinn JA, Vredenburgh JJ, et al: Phase I trial of gefitinib plus sirolimus in adults with recurrent malignant glioma. *Clin Cancer Res* 12:860-868, 2006
- Doherty L, Gigas DC, Kesari S, et al: Pilot study of the combination of EGFR and mTOR inhibitors in recurrent malignant gliomas. *Neurology* 67:156-158, 2006
- Kreisl TN, Lassman AB, Mischel PS, et al: A pilot study of everolimus and gefitinib in the treatment of recurrent glioblastoma (GBM). *J Neurooncol* 92:99-105, 2009
- Reardon DA, Desjardins A, Vredenburgh JJ, et al: Phase 2 trial of erlotinib plus sirolimus in adults with recurrent glioblastoma. *J Neurooncol* 96:219-230, 2010
- Lassen U, Sorensen M, Gaziel TB, et al: Phase II study of bevacizumab and temsirolimus combination therapy for recurrent glioblastoma multiforme. *Anticancer Res* 33:1657-1660, 2013
- Nanni P, Nicoletti G, Palladini A, et al: Multiorgan metastasis of human HER-2+ breast cancer in Rag2-/-;Il2rg-/- mice and treatment with PI3K inhibitor. *PLoS One* 7:e39626, 2012
- Maira M, Schnell C, Lollini P, et al: Preclinical and preliminary clinical activity of NVP-BKM120, an oral pan-class I PI3K inhibitor, in the brain. *Ann Oncol* 23, 2012 (suppl 9; abstr 1675P)
- Baselga J, Im SA, Iwata H, et al: Buparlisib plus fulvestrant versus placebo plus fulvestrant in postmenopausal, hormone receptor-positive, HER2-negative, advanced breast cancer (BELLE-2): A randomised, double-blind, placebo-controlled, phase 3 trial. *Lancet Oncol* 18:904-916, 2017
- Gopal AK, Kahl BS, de Vos S, et al: PI3K $\delta$  inhibition by idelalisib in patients with relapsed indolent lymphoma. *N Engl J Med* 370:1008-1018, 2014
- Saura C, Sachdev J, Patel MR, et al: Ph1b study of the PI3K inhibitor taselisib (GDC-0032) in combination with letrozole in patients with hormone receptor-positive advanced breast cancer. *Cancer Res* 75, 2015 (suppl 9; abstr PD5-2)
- Sarker D, Ang JE, Baird R, et al: First-in-human phase I study of pictilisib (GDC-0941), a potent pan-class I phosphatidylinositol-3-kinase (PI3K) inhibitor, in patients with advanced solid tumors. *Clin Cancer Res* 21:77-86, 2015
- Mayer IA, Abramson VG, Formisano L, et al: A phase Ib study of alpelisib (BYL719), a PI3K $\alpha$ -specific inhibitor, with letrozole in ER+/HER2- metastatic breast cancer. *Clin Cancer Res* 23:26-34, 2017
- Dreyling M, Santoro A, Mollica L, et al: Copanlisib in patients with relapsed or refractory indolent B-cell lymphoma (Chronos-1). *Hematol Oncol* 35:119-120, 2017
- Brachmann SM, Kleylein-Sohn J, Gaulis S, et al: Characterization of the mechanism of action of the pan class I PI3K inhibitor NVP-BKM120 across a broad range of concentrations. *Mol Cancer Ther* 11:1747-1757, 2012
- Filbin MG, Dabral SK, Pazyna-Murphy MF, et al: Coordinate activation of Shh and PI3K signaling in PTEN-deficient glioblastoma: New therapeutic opportunities. *Nat Med* 19:1518-1523, 2013
- Serra V, Eichhorn PJ, García-García C, et al: RSK3/4 mediate resistance to PI3K pathway inhibitors in breast cancer. *J Clin Invest* 123:2551-2563, 2013

39. Hopkins B, Pauli C, Du X, et al: Suppression of insulin feedback enhances the efficacy of PI3k inhibitors. *Nature* 560:499-503, 2018 [Erratum: *Nature* 563:E24, 2018]
40. Ni J, Ramkissoon SH, Xie S, et al: Combination inhibition of PI3K and mTORC1 yields durable remissions in mice bearing orthotopic patient-derived xenografts of HER2-positive breast cancer brain metastases. *Nat Med* 22:723-726, 2016
41. Kim J, Lee IH, Cho HJ, et al: Spatiotemporal evolution of the primary glioblastoma genome. *Cancer Cell* 28:318-328, 2015
42. Kim H, Zheng S, Amini SS, et al: Whole-genome and multiseq exome sequencing of primary and post-treatment glioblastoma reveals patterns of tumor evolution. *Genome Res* 25:316-327, 2015
43. Wang J, Cazzato E, Ladewig E, et al: Clonal evolution of glioblastoma under therapy. *Nat Genet* 48:768-776, 2016
44. Louis DN, Ohgaki H, Wiestler OD, et al: World Health Organization Histological Classification of Tumours of the Central Nervous System (ed 2). Lyon, France, International Agency for Research on Cancer, 2016
45. Akbani R, Ng KS, Werner HMJ, et al: A pan-cancer proteomic perspective on the Cancer Genome Atlas *Nature Comms*: 5:3887, 2014

---

### CancerLinQ<sup>®</sup> – Shaping the Future of Cancer Care

ASCO's CancerLinQ<sup>®</sup> is a groundbreaking health information technology platform that aims to rapidly improve the quality of cancer care. It assembles vast amounts of usable, searchable, real-world cancer information into a powerful database. This in turn provides immediate feedback to doctors to help them improve and personalize care for people with cancer. CancerLinQ<sup>®</sup> is the only major cancer data initiative being driven by a nonprofit physician group.

For more information, visit [CancerLinQ.org](https://www.cancerlinq.org)

**CancerLinQ<sup>®</sup>**

**AUTHORS' DISCLOSURES OF POTENTIAL CONFLICTS OF INTEREST****Buparlisib in Patients With Recurrent Glioblastoma Harboring Phosphatidylinositol 3-Kinase Pathway Activation: An Open-Label, Multicenter, Multi-Arm, Phase II Trial**

The following represents disclosure information provided by authors of this manuscript. All relationships are considered compensated. Relationships are self-held unless noted. I = Immediate Family Member, Inst = My Institution. Relationships may not relate to the subject matter of this manuscript. For more information about ASCO's conflict of interest policy, please refer to [www.asco.org/rwc](http://www.asco.org/rwc) or [ascopubs.org/jco/site/ife](http://ascopubs.org/jco/site/ife).

**Patrick Y. Wen****Honoraria:** Merck**Consulting or Advisory Role:** AbbVie, Agios Pharmaceuticals, AstraZeneca, Blue Earth Diagnostics, Eli Lilly, Genentech, Roche, Immunomic Therapeutics, Kadmon Corporation, KIYATEC, Puma Biotechnology, Vascular Biogenics, Taiho Pharmaceutical, Deciphera Pharmaceuticals, VBI Vaccines**Speakers' Bureau:** Merck, prime Oncology**Research Funding:** Agios Pharmaceuticals (Inst), AstraZeneca (Inst), BeiGene (Inst), Eli Lilly (Inst), Roche (Inst), Genentech (Inst), Karyopharm Therapeutics (Inst), Kazia Therapeutics (Inst), MediciNova (Inst), Novartis (Inst), Oncoceutics (Inst), Sanofi (Inst), Aventis (Inst), VBI Vaccines (Inst)**Travel, Accommodations, Expenses:** Merck**Mehdi Touat****Consulting or Advisory Role:** Agios Pharmaceuticals, Taiho Pharmaceutical**Travel, Accommodations, Expenses:** Merck Sharp & Dohme**Brian M. Alexander****Employment:** Foundation Medicine**Ingo K. Mellinghoff****Honoraria:** Roche**Consulting or Advisory Role:** Agios Pharmaceuticals, Puma Biotechnology, Debiopharm Group**Research Funding:** General Electric, Amgen, Eli Lilly**Shakti Ramkissoon****Employment:** Foundation Medicine**Stock and Other Ownership Interests:** Foundation Medicine**Sam Haidar****Employment:** Philips Healthcare**Stock and Other Ownership Interests:** Johnson & Johnson**Wei Wei****Patents, Royalties, Other Intellectual Property:** US patent application pending from a technology related to health or medicine (application No. 15/045241)**Jason T. Huse****Employment:** Champions Oncology**Research Funding:** Taiho Pharmaceutical (Inst)**John G. Kuhn****Consulting or Advisory Role:** TG Therapeutics**Research Funding:** Methodist Health System**Mikael L. Rinne****Employment:** Novartis Institutes for BioMedical Research**Consulting or Advisory Role:** N-of-One**Howard Colman****Honoraria:** Merck Sharp & Dohme**Consulting or Advisory Role:** Novocure, AbbVie, Foundation Medicine, Innocrin Pharmaceuticals, Tactical Therapeutics, Deciphera Pharmaceuticals, NewLink Genetics, Best Doctors, Merck**Research Funding:** NewLink Genetics, Plexikon, Kadmon Corporation, Orbus Therapeutics, Merck, DNatrix, AbbVie, BeiGene, FORMA Therapeutics (Inst)**Nathalie Y.R. Agar****Consulting or Advisory Role:** Bayesian Dx**Patents, Royalties, Other Intellectual Property:** IP portfolio at Partners Healthcare for surgical margin delineation and intraoperative diagnosis largely based on mass spectrometry**Travel, Accommodations, Expenses:** Bruker**Antonio M. Omuro****Consulting or Advisory Role:** Stemline Therapeutics, Bristol-Myers Squibb, Alexion Pharmaceuticals, Novocure, Inovio Pharmaceuticals**Lisa M. DeAngelis****Consulting or Advisory Role:** Roche, CarThera, BMJ Publishing Group, BTG, Tocagen, Sapience Therapeutics**John F. de Groot****Employment:** Helsinn Therapeutics (I), Ziopharm Oncology (I)**Leadership:** Ziopharm Oncology (I)**Stock and Other Ownership Interests:** Gilead Sciences, Ziopharm Oncology (I)  
**Consulting or Advisory Role:** Celldex, Deciphera Pharmaceuticals, Vascular Biogenics, Foundation Medicine, Genentech, Roche, OmnioX, OXiGENE, AbbVie, Novogen, Kadmon Corporation, Merck, Five Prime Therapeutics, Insys Therapeutics, AstraZeneca, Boston Biomedical, GW Pharmaceuticals, CarThera  
**Research Funding:** Deciphera Pharmaceuticals, Novartis, Eli Lilly, Sanofi, EMD Serono, Mundipharma Aventis, AstraZeneca**Timothy F. Cloughesy****Stock and Other Ownership Interests:** Notable Labs**Consulting or Advisory Role:** Roche, Genentech, Celgene, Tocagen, VBL Therapeutics, NewGen Therapeutics, Novartis, Agios Pharmaceuticals, Cortice Biosciences, Novocure, AbbVie, OXiGENE, Wellcome Trust, Pfizer, Notable Labs, Bristol-Myers Squibb, Merck, Insys Therapeutics, Human Longevity, Sunovion, Boston Biomedical, Novogen, Alexion Pharmaceuticals, GW Pharmaceuticals, Eli Lilly, Genocoea Biosciences, Puma Biotechnology  
**Other Relationship:** Global Coalition for Adaptive Research**Thomas M. Roberts****Leadership:** iKang Healthcare Group, Geode Therapeutics, Crimson Pharmaceutical**Stock and Other Ownership Interests:** iKang Healthcare Group, Crimson Pharmaceutical, Geode Therapeutics**Consulting or Advisory Role:** Novartis Institutes for BioMedical Research**Patents, Royalties, Other Intellectual Property:** Applied for patents combining PI3K inhibitors with immunotherapies**Jean J. Zhao****Leadership:** Crimson Pharmaceutical, Geode Therapeutics**Stock and Other Ownership Interests:** Crimson Pharmaceutical, Geode Therapeutics**Speakers' Bureau:** Ruijin Hospital**Research Funding:** Eli Lilly, Puma Biotechnology**Patents, Royalties, Other Intellectual Property:** Several intellectual properties at Dana-Faber Cancer Institute as a co-inventor**Travel, Accommodations, Expenses:** Ruijin Hospital, Princess Margaret Cancer Centre**Eudocia Q. Lee****Honoraria:** MedLink, UpToDate**Consulting or Advisory Role:** Eli Lilly**Lakshmi Nayak****Honoraria:** Bristol-Myers Squibb**Travel, Accommodations, Expenses:** Bristol-Myers Squibb**James R. Heath****Leadership:** Indi Molecular, PACT pharma, Sofie Biosciences, IsoPlexis, Nirmidas Biotech, Arivale**Stock and Other Ownership Interests:** Indi Molecular, IsoPlexis, PACT pharma**Tracy T. Batchelor****Honoraria:** Champions Oncology, UpToDate, Imedex, NXDC, Merck, GenomiCare Biotechnology**Consulting or Advisory Role:** Merck, GenomiCare Biotechnology, NXDC, Amgen**Travel, Accommodations, Expenses:** Merck, Roche, Genentech, GenomiCare Biotechnology

**Rameen Beroukhim**

**Consulting or Advisory Role:** Novartis, Merck (I), Gilead Sciences (I), ViiV Healthcare (I)

**Research Funding:** Novartis

**Patents, Royalties, Other Intellectual Property:** Prognostic Marker for Endometrial Carcinoma (US patent application 13/911456, filed June 6, 2013), SF3B1 Suppression as a Therapy for Tumors Harboring SF3B1 Copy Loss (international application No. WO/2017/177191, PCT/US2017/026693, filed July 4, 2017), Compositions and Methods for Screening Pediatric Gliomas and Methods of Treatment Thereof (international application No. WO/2017/132574, PCT/US2017/015448, filed 1/27/2017)

**Susan M. Chang**

**Consulting or Advisory Role:** Tocagen

**Research Funding:** Novartis (Inst), Agios Pharmaceuticals (Inst)

**Azra H. Ligon**

**Leadership:** Travera (I)

**Stock and Other Ownership Interests:** Travera (I)

**Consulting or Advisory Role:** Travera (I)

**Geoffrey S. Young**

**Research Funding:** Siemens Healthineers

**Michael D. Prados**

**Stock and Other Ownership Interests:** Quadriga BioSciences

**Consulting or Advisory Role:** Nativis, Tocagen

**Research Funding:** Genentech (Inst), Roche (Inst), Novartis (Inst), Nativis (Inst)

**David A. Reardon**

**Honoraria:** AbbVie, Cavion, Genentech, Roche, Merck, Midatech Pharma, Momenta Pharmaceuticals, Novartis, Novocure, Regeneron Pharmaceuticals, Stemline Therapeutics, Celldex, OXiGENE, Monteris Medical, Bristol-Myers Squibb, Juno Therapeutics, Inovio Pharmaceuticals, Oncorus, Agenus, EMD Serono, Merck, Merck KGaA, Taiho Pharmaceutical, Advantagene

**Consulting or Advisory Role:** Cavion, Genentech, Roche, Merck, Momenta Pharmaceuticals, Novartis, Novocure, Regeneron Pharmaceuticals, Stemline Therapeutics, Bristol-Myers Squibb, Inovio Pharmaceuticals, Juno Therapeutics, Celldex, OXiGENE, Monteris Medical, Midatech Pharma, Oncorus, AbbVie, Agenus, EMD Serono, Merck, Merck KGaA, Taiho Pharmaceutical

**Research Funding:** Celldex (Inst), Incyte (Inst), Midatech Pharma (Inst), Tragara Pharmaceuticals (Inst), Inovio Pharmaceuticals (Inst), Agenus (Inst), EMD Serono (Inst), Acerta Pharma (Inst), Omnixox

**W.K. Alfred Yung**

**Stock and Other Ownership Interests:** DNATrix

**Honoraria:** DNATrix, Amgen

**Consulting or Advisory Role:** DNATrix, Boehringer Ingelheim

**Patents, Royalties, Other Intellectual Property:** DNATrix

**Keith L. Ligon**

**Stock and Other Ownership Interests:** Travera

**Consulting or Advisory Role:** Midatech Pharma, Bristol-Myers Squibb

**Research Funding:** Plexikon (Inst), Amgen (Inst), X4 Pharmaceuticals (Inst), Tragara Pharmaceuticals (Inst), Bristol-Myers Squibb (Inst), Eli Lilly (Inst)

**Patents, Royalties, Other Intellectual Property:** Molecular diagnostics assay patent

No other potential conflicts of interest were reported.

## APPENDIX

## Pharmacokinetic Evaluation

The analytic method for the quantitative determination of buparlisib in human plasma and tumor was developed and validated by Novartis (Basel, Switzerland). The method consists of a solid phase extraction using a 96-well plate with Oasis HLB cartridge (10 mg, 30  $\mu$ m; Waters, Milford, MA) and analysis by liquid chromatography-tandem mass spectrometry in multiple-reaction monitoring mode using electrospray ionization in the positive ion mode. The method is suitable for the determination of buparlisib in human plasma (EDTA) over the range of 1.00 ng/mL (lower limit of quantification) to 1,000 ng/mL (upper limit of quantification). No matrix effect was observed; mean recovery ranged from 59% to 61%. Buparlisib was stable in stock and diluted solutions, in matrix, and after multiple freeze-thaw cycles. The assay method exhibited sufficient specificity and selectivity, accuracy, precision, and sensitivity for the purposes and conclusions of the individual studies. For pharmacokinetic studies, blood samples were collected at the following time points on days 1 and 8 ( $\pm$  1 day) before surgery: predose and at 0.5, 1.5, 3, and 5 hours postdose. Non-contrast-enhancing and contrast-enhancing brain tumor tissue and a concomitant blood sample were obtained at the time of surgery. Standard pharmacokinetic parameters were determined using noncompartmental methods. The tumor-to-plasma ratio was calculated by dividing the tumor geometric mean concentration by the plasma geometric mean concentration at the time of surgery.

## Immunohistochemical Studies

Immunohistochemical (IHC) stainings for *PTEN* (#9559, 1:50 dilution, heated citrate retrieval; Cell Signaling Technologies, Danvers, MA), positive phosphorylated AKT (pAKT) S473 (#4060, 1:75 dilution, EDTA retrieval; Cell Signaling Technologies), and phosphorylated S6 (pS6) S235/236 (#4858, 1:75 dilution, EDTA retrieval; Cell Signaling Technologies) were performed on 5- $\mu$ m formalin-fixed paraffin-embedded (FFPE) tissue sections.

In the surgical component of the trial, modulation of the phosphatidylinositol 3-kinase pathway response in tumor tissue was determined by pathologist-performed semiquantitative IHC scoring of pAKT and pS6 on the basis of previously established methods in preclinical models and clinical trials of glioblastoma.<sup>6,22</sup> Sample staining was scored for intensity in tumor cells on a 0 to 2+ scale (0, no staining; 1+, weak positive staining; 2+, strong positive staining, with 1+ and 2+ being the average intensity of all positive cells in the cohort). Staining within nontumor elements (eg, macrophages, vessels) was not included in the scoring. Change in pAKT and pS6 IHC scores was the difference in score from baseline to surgery in each participant. Participants were classified into three groups; a reduction of staining score of one or more degrees qualified for response, whereas no change or an increase in score qualified for no response.

## Matrix-Assisted Laser Desorption/Ionization-Mass Spectrometry Imaging Drug Analysis on Surgical Specimens

Surgical sections were flash frozen after surgery, stored at  $-80^{\circ}\text{C}$ , and placed at  $-25^{\circ}\text{C}$  1 hour before use. Twelve-micrometer coronal tissue sections were prepared using a Microm HM550 cryostat (Thermo Fisher Scientific, Waltham, MA) and thaw mounted onto indium tin oxide-coated microscopic slides (Bruker, Billerica, MA) for matrix-assisted laser desorption/ionization-mass spectrometry imaging and onto optical slides for hematoxylin and eosin staining. Samples were dried for 15 minutes in a desiccator. 2,5-Dihydroxybenzoic acid (40 mg/mL solution in methanol OH/0.2% trifluoroacetic acid 70:30 volume-to-volume ratio) was deposited using the TM-Sprayer system (HTX Technologies, Chapel Hill, NC) as previously described (Sun Y et al: *Neuro-oncol* 19:774-785, 2017). Mass spectra were acquired

using a 9.4-T solarix XR Fourier transform ion cyclotron resonance mass spectrometer (Bruker).

## Tumor Genotyping

Targeted exome next-generation sequencing (OncoPanel) was performed at the Dana-Farber Cancer Institute Center for Cancer Genome Discovery on an approximately 50-mm thickness of FFPE tumor tissue using the OncoPanel version 2.0 custom targeted exome capture panel to examine the exons of 275 cancer-causing genes and their respective single nucleotide variants and indels. Data were annotated as previously described (Sholl LM, et al: *JCI Insight* 1:e87062, 2016; Ramkissoon SH, et al: *Neuro-oncol* 19:986-996, 2017). Array comparative genomic hybridization copy number testing was performed using SurePrint G3 1M feature stock arrays (Agilent Technologies, Santa Clara, CA) from approximately 1  $\mu$ g of total DNA extracted from FFPE tissue (approximately 200- $\mu$ m thickness of tissue) using fragmentation simulation methodology (Craig JM, et al: *PLoS One* 7:e38881, 2012). Amplification was calculated as greater than 2.0 log-ratio, and single-copy losses generally were calculated as less than  $-0.3$  log-ratio change compared with a pooled DNA normal. Results were analyzed using CytoGenomics and Genomic Workbench software (Agilent Technologies).

## Reverse-Phase Protein Analysis

For comparison of signaling changes in buparlisib-treated patients, 11 paired untreated versus standard-of care-treated glioblastoma tumor sets obtained from The University of Texas M.D. Anderson Cancer Center were used as controls. Frozen tumor tissue approximately the size of a grain of rice was placed in 2-mL tubes with ceramic beads using a Precellys homogenizer (Bertin Instruments, Montigny-le Bretonneux, France). Tissue was lysed using ice-cold lysis solution. Lysates from flash-frozen tissues were prepared and analyzed by reverse-phase protein analysis using 299 antibodies as described previously.<sup>45</sup> Reverse phase protein microarrays were printed on nitrocellulose-coated glass FAST Slides (Schleicher & Schuell BioScience, Keene, NH) by a GeneTAC G3 arrayer (Genomic Solutions, Ann Arbor, MI). Antibody staining of each reverse phase protein microarray was done using an autostainer (BioGenex, Fremont, CA). The slide images were quantified using MicroVigene 4.0 (VigeneTech, Carlisle, MA). The spot-level raw data were processed using the R package SuperCurve ([https://r-forge.r-project.org/R/?group\\_id=1899](https://r-forge.r-project.org/R/?group_id=1899)), which returns the estimated protein concentrations (raw concentration) and a quality control score for each slide. Raw concentration data were normalized by median centering of each sample across all proteins to correct loading bias.

## Statistical Analyses

Data were summarized as frequencies and proportions for categorical variables and as medians and ranges for continuous variables. Intrapatient mean differences were evaluated with the paired Wilcoxon test. Intercohort mean differences were evaluated with the Mann-Whitney *U* test. Survival analyses (ie, progression-free survival [PFS], overall survival) were performed using the Kaplan-Meier method, and differences between groups were evaluated by the log-rank test. Survival for participants who were alive or lost to follow-up at the time of last contact on or before data cutoff was censored at the date of the last contact alive. Patients who were censored for PFS before 6-month PFS (PFS6) determination were included in the calculation of the PFS6 proportion as patients who did not reach PFS6. For biomarker evaluation, categorical groups were explored while considering variable distribution to evaluate the possible association with outcome using the Fisher's exact test (PFS6) or the log-rank test (PFS, overall survival). Differentially expressed proteins in pre- and post-treatment samples were determined using Limma (Ritchie ME, et al: *Nucleic Acids Res* 43:e47, 2015), a software package used to perform differential expression analysis, and the R language (<http://www.R-project.org>). *P* = .05 was set for statistical significance for all evaluations.

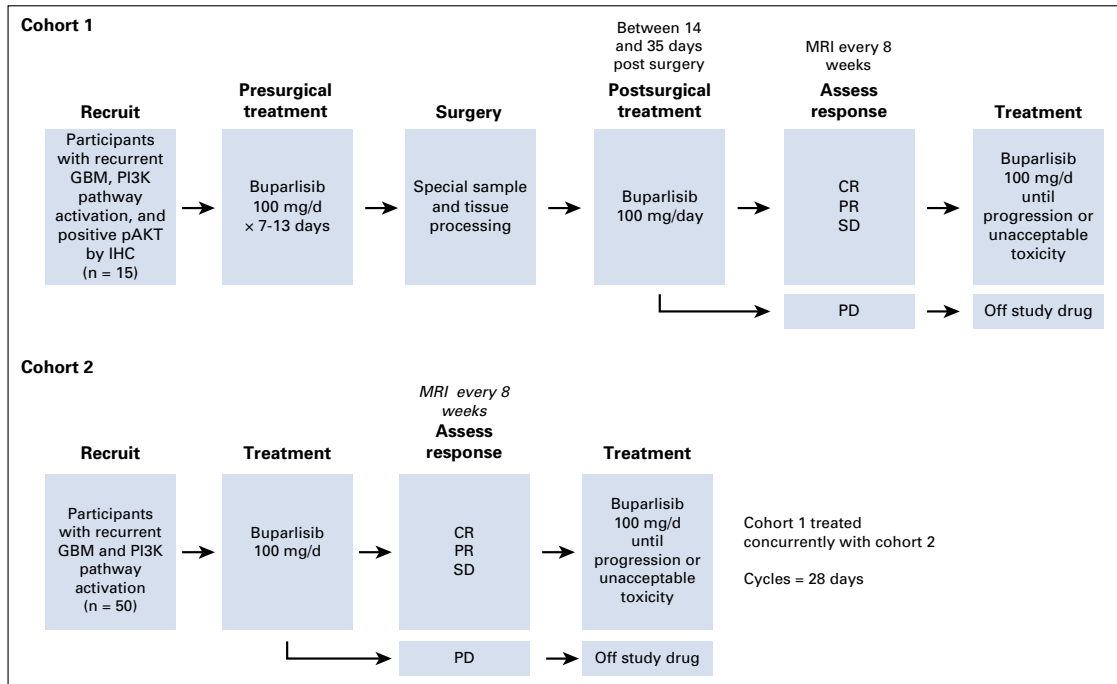


**FIG A1.** Treatment schema. CR, complete response; GBM, glioblastoma; IHC, immunohistochemistry; MRI, magnetic resonance imaging; pAKT, phosphorylated AKT; PD, progressive disease; PI3K, phosphatidylinositol 3-kinase; PR, partial response; SD, stable disease.

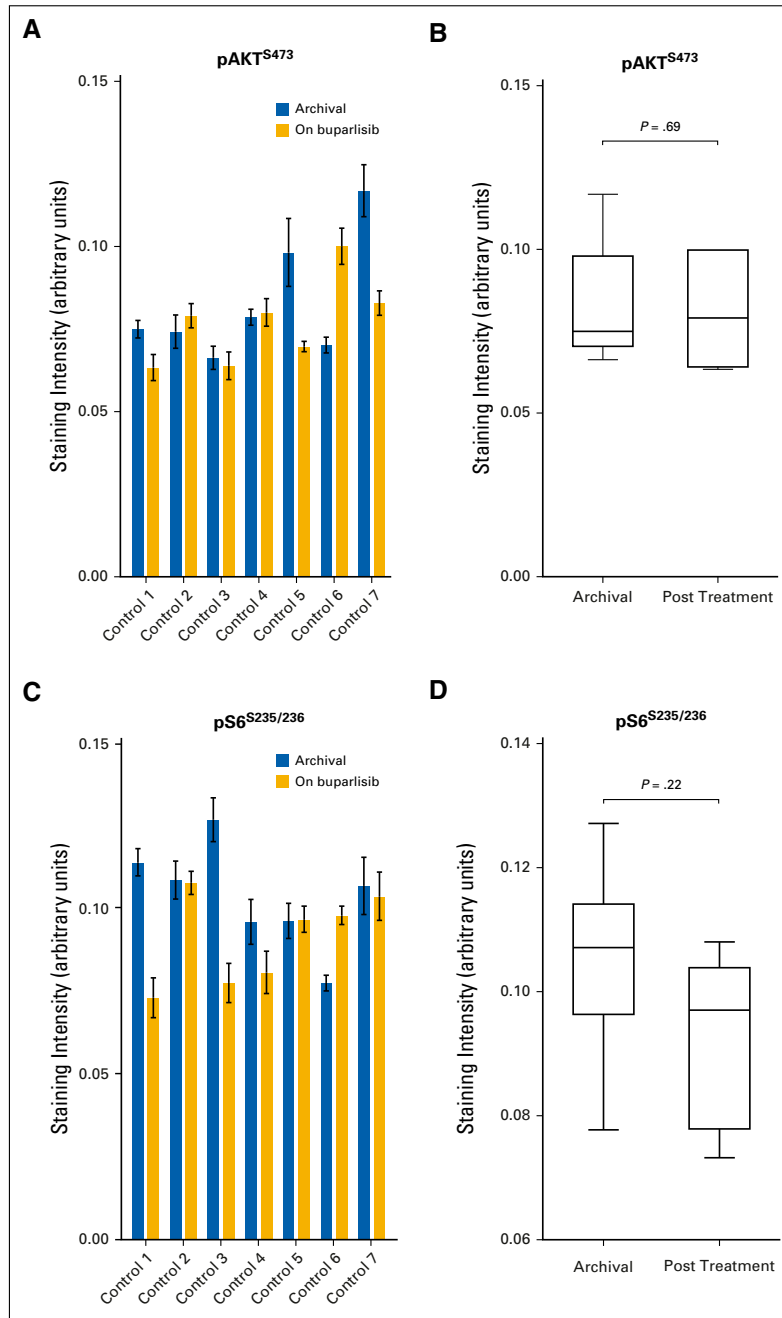


**FIG A2.** Phosphatidylinositol 3-kinase pathway modulation as a result of buparlisib in tumor tissue in the control cohort. Quantification of (A and B) phosphorylated AKT<sup>S473</sup> (pAKT<sup>S473</sup>) and (C and D) phosphorylated S6 S235/236 (pS6<sup>S235/236</sup>) immunohistochemistry staining in the surgical cohort. The control cohort consisted of seven patients treated with standard of care for whom surgical resection of tumor tissue was performed at initial diagnosis and recurrence. (B and D) Differences between groups were calculated using the paired Wilcoxon test.

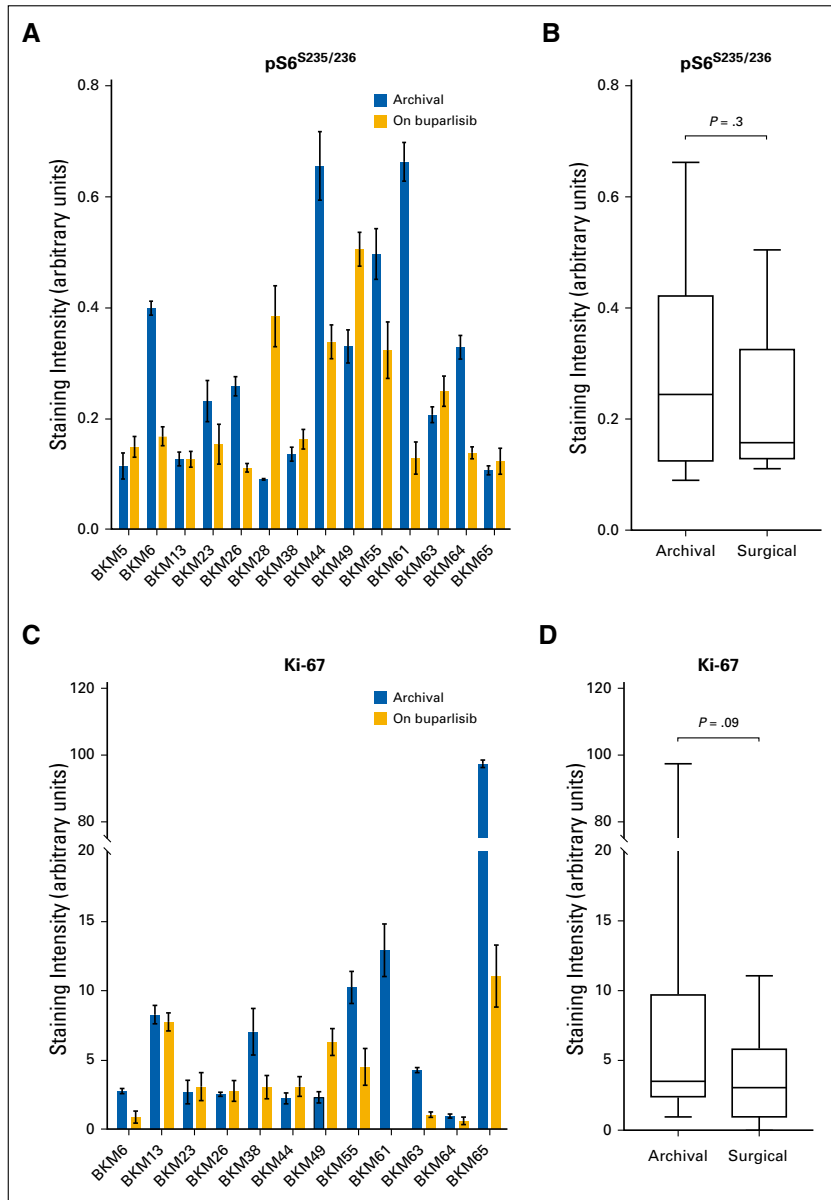


**FIG A3.** Phosphatidylinositol 3-kinase pathway modulation and changes in tumor cell proliferation as a result of buparlisib in tumor tissue in cohort 1. (A and B) Quantification of phosphorylated S6 S235/236 (pS6<sub>S235/236</sub>) immunohistochemistry staining and (C and D) tumor cell proliferation as assessed by the IHC proliferation marker Ki-67 in the surgical cohort. (B and D) Differences between groups were calculated using the paired Wilcoxon test.

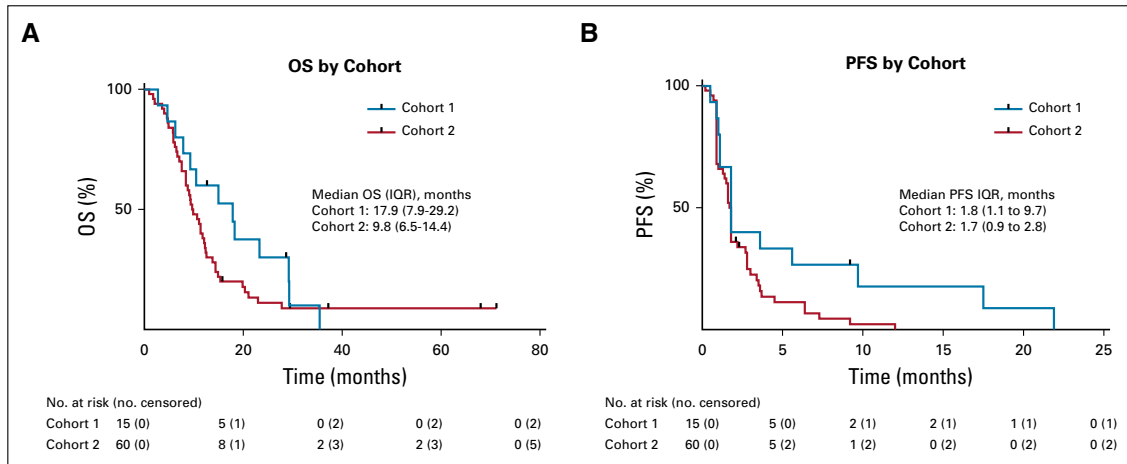
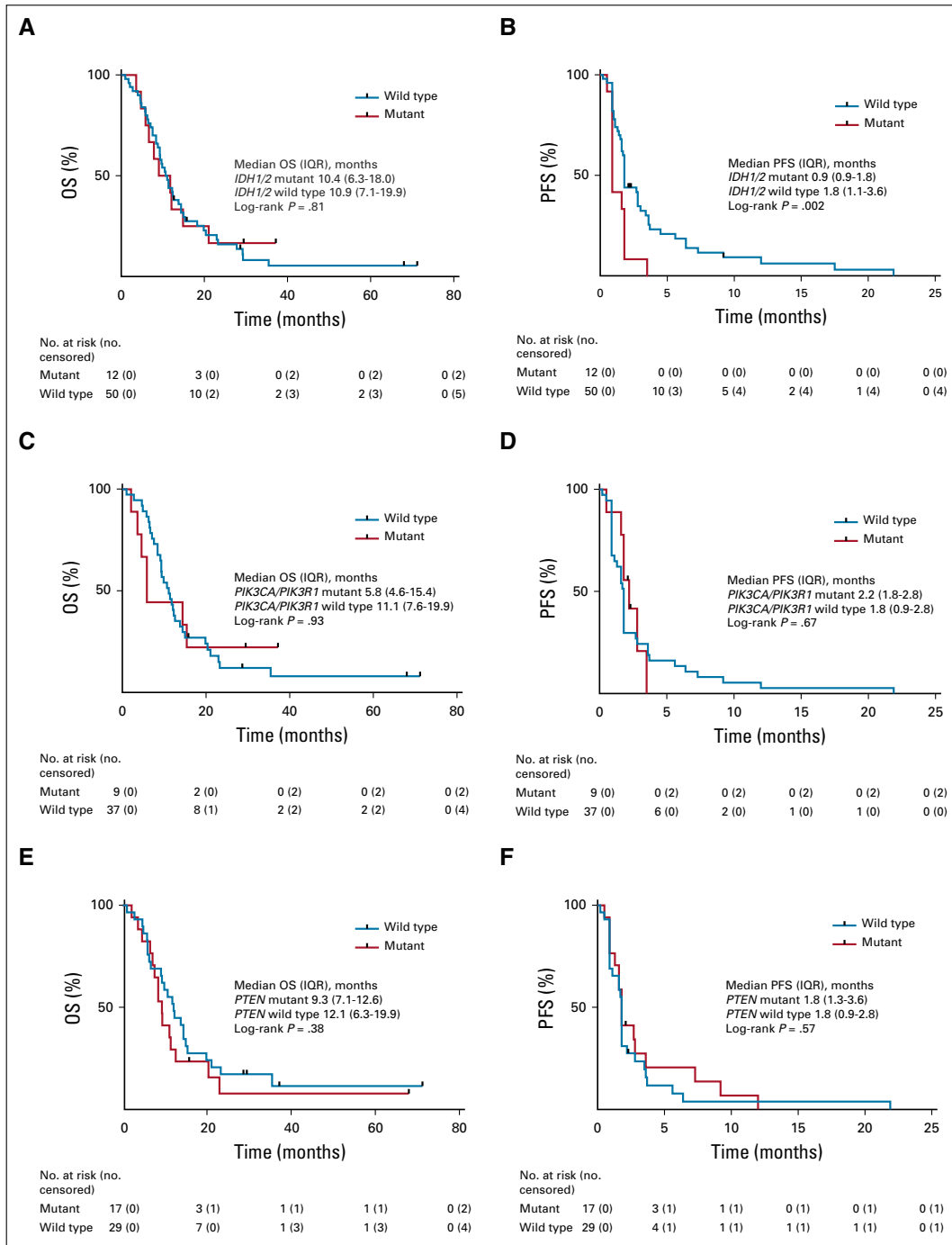


FIG A4. Kaplan-Meier curves of (A) overall survival (OS) and (B) progression-free survival (PFS) in cohorts 1 and 2. IQR, interquartile range.



**FIG A5.** Kaplan-Meier curves of overall survival (OS) and progression-free survival (PFS) by (A and B) *IDH1/2* status, (C and D) *PIK3CA/PIK3R1* status, and (E and F) PFS by *PTEN* status. Differences between groups were evaluated using the log-rank test. IQR, interquartile range.

**TABLE A1.** Summary of the Response Assessment in Neuro-Oncology Response Criteria

Assessment	CR	PR	SD	PD
T1 Gd+	None	≥ 50% decrease	< 50% decrease to < 25% increase	≥ 25% increase*
T2/FLAIR	Stable or decrease	Stable or decrease	Stable or decrease	Increase*
New lesion	None	None	None	Present*
Corticosteroids	None	Stable or decrease	Stable or decrease	NA
Clinical status	Stable or increase	Stable or increase	Stable or increase	Decrease*
Requirement for response	All	All	All	Any*

Abbreviations: CR, complete response; NA, not applicable (increase in corticosteroids alone will not be taken into account in determining progression in the absence of persistent clinical deterioration); PD, progressive disease; PR, partial response; SD, stable disease; T1 Gd+, gadolinium-enhancing lesion on T1 magnetic resonance imaging; T2/FLAIR, fluid-attenuated inversion recovery on T2 magnetic resonance imaging.

\*Progression occurs when criterion is present.

**TABLE A2.** Buparlisib Pharmacokinetic Parameters

Day	Cmax (ng/mL), Mean ± SEM	Tmax (h), Median (range)	AUC <sub>0-5 h</sub> (µg · h/mL), Mean ± SEM
1	471 ± 147	1.5 (1.5-5)	1.42 ± 0.5
8	820 ± 192	1.5 (0.5-9)	3.27 ± 1.43

Abbreviations: AUC<sub>0-5 h</sub>, 0- to 5-hour area under the curve; Cmax, maximum plasma concentration; Tmax, maximum time.

**TABLE A3.** Buparlisib Pharmacokinetic Parameters in Cohort 1

Time (hours)	Cohort 1 (n = 15)	
	Presurgery Concentration (ng/mL)*	Range
Predose	426 ± 160	203-746
0.5	507 ± 218	252-948
1.5	705 ± 301	281-1,300
3	676 ± 218	408-1,290
5	623 ± 244	397-1,030

\*Patients in the surgical cohort had presurgery sampling performed after 5 to 9 days of treatment with buparlisib.

**TABLE A4.** Reverse-Phase Protein Array Analysis of Buparlisib-Treated Contrast-Enhancing Tumors Versus Unrelated SOC-Treated Control Tumors

Protein	Symbol	Buparlisib Treated	SOC Treated	P
<b>Cyclin-E1-M-V</b>	<b>CCNE1</b>	<b>0.1172</b>	<b>-0.0771</b>	<b>.0029</b>
<b>Mcl-1-R-V</b>	<b>MCL1</b>	<b>0.2553</b>	<b>-0.2491</b>	<b>.0069</b>
<b>Cyclin-B1-R-V</b>	<b>CCNB1</b>	<b>0.3047</b>	<b>-0.2241</b>	<b>.0168</b>
<b>RPA32-T-C</b>	<b>RPA2</b>	<b>0.0824</b>	<b>-0.1633</b>	<b>.0194</b>
<b>D-a-Tubulin-R-V</b>	<b>TUBA1A</b>	<b>-0.5775</b>	<b>0.0379</b>	<b>.0208</b>
<b>Akt_pT308-R-V</b>	<b>AKT1</b>	<b>-0.2614</b>	<b>0.0723</b>	<b>.0219</b>
<b>Connexin-43-R-C</b>	<b>CNST43</b>	<b>-1.1597</b>	<b>0.3410</b>	<b>.0244</b>
<b>eIF4G-R-C</b>	<b>EIF4G1</b>	<b>0.3188</b>	<b>-0.3195</b>	<b>.0340</b>
<b>HSP27_pS82-R-V</b>	<b>HSBP1</b>	<b>0.2195</b>	<b>-0.2570</b>	<b>.0371</b>
<b>Rb_pS807_S811-R-V</b>	<b>RB1</b>	<b>-0.5456</b>	<b>0.1168</b>	<b>.0401</b>
<b>Annexin-I-M-V</b>	<b>ANXA1</b>	<b>0.6267</b>	<b>-0.1652</b>	<b>.0403</b>
<b>Hif-1-alpha-M-C</b>	<b>HIF1A</b>	<b>-0.0044</b>	<b>0.1676</b>	<b>.0444</b>
JNK2-R-C	MAPK9	-0.0820	0.0755	.0619
p38-MAPK-R-V	MAPK14	0.2682	-0.2081	.0622
p38_pT180_Y182-R-V	MAPK14	-0.3590	-0.0877	.2718
MAPK_pT202_Y204-R-V	MAPK3	-0.1771	0.1634	.0850
p44-42-MAPK-R-V	MAPK3	-0.2158	-0.1204	.6713
JNK_pT183_Y185-R-V	MAPK8	0.1351	0.0227	.3315
MEK1-R-V	MAP2K1	-0.3323	-0.1404	.4235
MEK1_pS217_S221-R-V	MAP2K1	-0.0759	-0.0575	.7944
RSK-R-C	RPS6KA1	-0.2927	-0.0392	.1175
p70-S6K_pT389-R-V	RPS6KB1	-0.0628	-0.1197	.8281
S6_pS235_S236-R-V	RPS6	0.1864	-0.2722	.1689
S6_pS240_S244-R-V	RPS6	0.0869	-0.2706	.2182
S6-M-V	RPS6	0.1897	-0.1757	.3136
p90RSK_pT573-R-C	RPS6K	-0.0128	-0.0574	.8178
Akt_pS473-R-V	AKT1	-0.3848	0.0711	.2000

NOTE. Differences in pre- and post-treatment protein expression in each group were evaluated using Limma (Ritchie ME, et al: *Nucleic Acids Res* 43:e47, 2015). Selected proteins and proteins that showed statistically significant changes between buparlisib-treated (contrast-enhancing regions) and unrelated control tumors that underwent SOC (radiation therapy and temozolomide) are shown.

Abbreviation: SOC, standard of care.

**E. Article sur le ciblage de mutations IDH1 par ivosidenib dans les gliomes malins / Article on the targeting of IDH1 mutations with ivosidenib**



# Ivosidenib in Isocitrate Dehydrogenase 1–Mutated Advanced Glioma

Ingo K. Mellinghoff, MD<sup>1</sup>; Benjamin M. Ellingson, PhD<sup>2</sup>; Mehdi Touat, MD<sup>3</sup>; Elizabeth Maher, MD, PhD<sup>4</sup>; Macarena I. De La Fuente, MD<sup>5</sup>; Matthias Holdhoff, MD, PhD<sup>6</sup>; Gregory M. Cote, MD, PhD<sup>7</sup>; Howard Burris, MD<sup>8</sup>; Filip Janku, MD, PhD<sup>9</sup>; Robert J. Young, MD<sup>10</sup>; Raymond Huang, MD, PhD<sup>11</sup>; Liewen Jiang, PhD<sup>12</sup>; Sung Choe, PhD<sup>13</sup>; Bin Fan, PhD<sup>14</sup>; Katharine Yen, PhD<sup>15</sup>; Min Lu, PhD<sup>15</sup>; Chris Bowden, MD<sup>16</sup>; Lori Steelman, MS<sup>16</sup>; Shuchi S. Pandya, MD<sup>16</sup>; Timothy F. Cloughesy, MD<sup>17</sup>; and Patrick Y. Wen, MD<sup>18</sup>

**PURPOSE** Diffuse gliomas are malignant brain tumors that include lower-grade gliomas (LGGs) and glioblastomas. Transformation of low-grade glioma into a higher tumor grade is typically associated with contrast enhancement on magnetic resonance imaging. Mutations in the isocitrate dehydrogenase 1 (*IDH1*) gene occur in most LGGs (> 70%). Ivosidenib is an inhibitor of mutant IDH1 (mIDH1) under evaluation in patients with solid tumors.

**METHODS** We conducted a multicenter, open-label, phase I, dose escalation and expansion study of ivosidenib in patients with *mIDH1* solid tumors. Ivosidenib was administered orally daily in 28-day cycles.

**RESULTS** In 66 patients with advanced gliomas, ivosidenib was well tolerated, with no dose-limiting toxicities reported. The maximum tolerated dose was not reached; 500 mg once per day was selected for the expansion cohort. The grade  $\geq 3$  adverse event rate was 19.7%; 3% (n = 2) were considered treatment related. In patients with nonenhancing glioma (n = 35), the objective response rate was 2.9%, with 1 partial response. Thirty of 35 patients (85.7%) with nonenhancing glioma achieved stable disease compared with 14 of 31 (45.2%) with enhancing glioma. Median progression-free survival was 13.6 months (95% CI, 9.2 to 33.2 months) and 1.4 months (95% CI, 1.0 to 1.9 months) for the nonenhancing and enhancing glioma cohorts, respectively. In an exploratory analysis, ivosidenib reduced the volume and growth rates of nonenhancing tumors.

**CONCLUSION** In patients with *mIDH1* advanced glioma, ivosidenib 500 mg once per day was associated with a favorable safety profile, prolonged disease control, and reduced growth of nonenhancing tumors.

J Clin Oncol 38:3398-3406. © 2020 by American Society of Clinical Oncology

Creative Commons Attribution Non-Commercial No Derivatives 4.0 License

## INTRODUCTION

Diffuse gliomas represent the most common malignant primary brain tumor in adults and include glioblastoma (GBM) and WHO grade 2 and WHO grade 3 tumors. The latter are referred to as lower-grade gliomas (LGGs). LGGs grow at a slower rate, but eventually “transform” into a higher tumor grade.<sup>1</sup> Patients with LGGs with long-term disease control suffer from treatment-related symptoms, including radiation-induced cognitive changes.<sup>2-5</sup> Brain magnetic resonance imaging (MRI) plays a central role in disease monitoring.<sup>6,7</sup> Malignant transformation of LGGs is often associated with the appearance of contrast enhancement.

Mutations in the isocitrate dehydrogenase 1 (*IDH1*) gene, and less commonly in the *IDH2* gene, are found in more than 70% of LGGs.<sup>8</sup> *IDH* mutant (*mIDH*) gliomas have emerged as a separate glioma entity with a distinct molecular pathogenesis. *IDH* mutations in glioma occur early during tumor development, cluster in key arginine residues within the enzyme’s active site, are associated with a distinctive pattern of DNA

hypermethylation, persist throughout the disease, and are associated with a better prognosis compared with *IDH* wildtype gliomas of the same tumor grade.<sup>8-15</sup> Cancer-associated *IDH1/2* mutations lead to the abnormal production of the oncometabolite D(-)-2-hydroxyglutarate (2-HG),<sup>16,17</sup> which inhibits  $\alpha$ -ketoglutarate-dependent enzymes, resulting in tumorigenesis.<sup>18-20</sup>

The contribution of mIDH enzymes to the growth of established cancers remains incompletely understood. Inhibition of the mIDH enzyme reduced tumor cell proliferation in experimental models of *mIDH* leukemia and *mIDH* glioma.<sup>21,22</sup> In clinical trials for patients with advanced acute myeloid leukemia, another human cancer harboring *IDH* mutations,<sup>23,24</sup> the first-in-class, Food and Drug Administration–approved inhibitors of mIDH2 (enasidenib) and mIDH1 (ivosidenib) induced clinical and molecular remissions.<sup>25,26</sup>

We designed a multicenter, open-label, phase I dose escalation and expansion study of ivosidenib in patients with *mIDH1* advanced solid tumors. Data from

## ASSOCIATED CONTENT

### Data Supplement Protocol

Author affiliations and support information (if applicable) appear at the end of this article.

Accepted on April 10, 2020 and published at [ascopubs.org/journal/jco](https://ascopubs.org/journal/jco) on June 12, 2020; DOI <https://doi.org/10.1200/JCO.19.03327>

ASCO

3398 Volume 38, Issue 29

Journal of Clinical Oncology®

Downloaded from [ascopubs.org](https://ascopubs.org) by 31.34.66.224 on October 18, 2020 from 031.034.066.224  
Copyright © 2020 American Society of Clinical Oncology. All rights reserved.

**CONTEXT****Key Objectives**

To determine safety and tolerability of oral ivosidenib as a single agent in patients with glioma and to determine the recommended phase II dose.

**Knowledge Generated**

Ivosidenib was well tolerated, with no dose-limiting toxicities. 500 mg once per day was selected for the expansion cohort. In exploratory analyses, ivosidenib reduced the growth of nonenhancing tumors.

**Relevance**

Our findings point toward an important contribution of the mutant IDH1 enzyme to the growth of *mIDH1* LGGs. Further evaluation of mIDH inhibitors for the treatment of *mIDH* LGGs appears warranted.

cholangiocarcinoma and chondrosarcoma cohorts have been reported.<sup>27,28</sup> Here we report results for the advanced glioma cohort in the phase I study, including LGG and GBM.

**METHODS****Study Design**

This phase I, multicenter, open-label study comprised a dose escalation and a dose expansion phase (Data Supplement, online only). The primary objectives were to assess the safety and tolerability of oral ivosidenib as a single agent and to determine the maximum tolerated dose or recommended phase II dose of ivosidenib in patients with solid tumors. Secondary objectives included evaluation of dose-limiting toxicities (DLTs) during cycle 1 of dose escalation, pharmacokinetic and pharmacodynamic findings (reported elsewhere<sup>29</sup>), and characterization of preliminary clinical response. DLTs were defined as any grade  $\geq 3$  event reported to be at least possibly related to ivosidenib. The data reported here are from patients with glioma who were enrolled in both phases.

Patients underwent baseline screening evaluations within 28 days before study day 1. Dose escalation was performed using a 3+3 design, with patients enrolled into sequential 3-patient cohorts of increasing doses from 100 mg twice per day (200 mg/d) to 1,200 mg once per day. Treatment with ivosidenib was continuous; 1 cycle was defined as 28 days.

**Patients**

Eligible patients included men and women  $\geq 18$  years of age with an Eastern Cooperative Oncology Group performance status of 0 to 1 and an expected survival of  $\geq 3$  months. All patients had an established diagnosis of *mIDH1* glioma that had recurred after, or not responded to, initial surgery, radiation, or chemotherapy. *IDH1* mutation status was based on local laboratory testing with retrospective central confirmation. Because this study was initiated before the most recent revision of the WHO Classification of Tumors of the Central Nervous System,<sup>30</sup> we used the 2007 classification.<sup>31</sup>

Transformation of LGGs to a higher tumor grade is frequently associated with the appearance of tumor contrast enhancement on T1-weighted brain MRI. For the dose expansion phase, patients were therefore separated into 2 cohorts on the basis of the presence or absence of tumor contrast enhancement at the time of enrollment according to the investigator. The “nonenhancing” glioma cohort comprised patients with *mIDH1* glioma that had progressed within 12 months before enrollment and did not enhance on T1-weighted postgadolinium MRI. Patients in this cohort required at least 3 full sets of “historical” MRI examinations (not including screening), each separated by at least 2 months, and were ineligible if they had had surgery or radiation therapy within 6 months of enrollment. The second cohort comprised patients with progressive *mIDH1* gliomas who did not meet these criteria.

**Study Oversight**

The study was designed by the sponsor in collaboration with the lead investigators. Clinical data were generated by investigators and research staff at each participating site. Safety data were reviewed at regular intervals by study investigators and the sponsor. All authors vouch for the accuracy and completeness of the data and analyses and for the adherence of the study to the protocol. The study was conducted in accordance with the principles of the Declaration of Helsinki and Good Clinical Practice guidelines. The protocol was approved by relevant institutional review boards or ethics committees at each site. Written informed consent was provided by all the patients before screening and enrollment.

**Study Assessments**

Toxicity was evaluated by the collection of adverse events (AEs), serious AEs, and AEs leading to discontinuation, graded according to the National Cancer Institute Common Terminology Criteria for Adverse Events v4.03. Treatment efficacy was assessed by investigators using MRI every 2 cycles ( $56 \pm 3$  days) according to Response Assessment in Neuro-Oncology (RANO) criteria for high-grade gliomas.<sup>32</sup>

for all patients in the dose escalation phase and for those with enhancing glioma in the expansion phase. For patients with nonenhancing glioma in the expansion cohort, response was assessed using the RANO criteria for LGG (RANO LGG).<sup>33</sup> End points included best overall response and objective response rate (defined as complete response plus partial response plus minor response). Progression-free survival (PFS) was defined as the interval from first dose to disease progression or death.

### Exploratory Assessments

Tumor growth rate was assessed by volume in the non-enhancing glioma expansion cohort. Tumor volume measurements were performed at the same visits as the RANO assessments using either 2-dimensional T2-weighted images, 3-dimensional T2-weighted images, or fluid-attenuated inversion recovery (FLAIR) images in compliance with the international standardized brain tumor imaging protocol.<sup>34</sup> All patients needed at least 3 “historical” pretreatment

**TABLE 1.** Baseline Characteristics of All Patients With Glioma

Characteristic	Treated Patients With Glioma, Total (n = 66)
Median age, years (range)	41.0 (21-71)
Female sex	25 (37.9)
ECOG performance status at baseline	
0	30 (45.5)
1	36 (54.5)
Tumor type at screening	
Oligodendroglioma	23 (34.8)
Astrocytoma	19 (28.8)
Oligoastrocytoma	12 (18.2)
Glioblastoma	12 (18.2)
Tumor grade (WHO) at screening	
2	32 (48.5)
3	18 (27.3)
4	12 (18.2)
Unknown	4 (6.1)
1p/19q codeleted, No. of total No. (% of those tested)	18 of 54 (33.3)
Mutated ATRX protein, No. of total No. (% of those tested)	23 of 25 (92.0)
Patients with prior radiotherapies	49 (74.2)
Patients with prior systemic therapy	50 (75.8)
Median No. of prior systemic therapies, range	2.0 (1-6)
Temozolomide	48 (72.7)
Procarbazine plus lomustine plus vincristine	8 (12.1)
Bevacizumab	10 (15.2)
Median time since last systemic therapy, months (range)	3.7 (0.7-139.5)
Median duration of last systemic therapy, months (range)	7.0 (0.0-36.0)
Receiving anticonvulsant therapy	53 (80.3)
<i>IDH1</i> genotype	
R132H	57 (86.4)
R132C	1 (1.5)
R132G	1 (1.5)
R132S	1 (1.5)
R132 (unknown)	5 (7.6)
Other	1 (1.5)

NOTE. Data are presented as No. (%) unless indicated otherwise.

Abbreviations: ATRX, alpha-thalassemia mental retardation syndrome X-linked; ECOG, Eastern Cooperative Oncology Group; *IDH1*, isocitrate dehydrogenase 1.

MRIs, each separated by  $\geq 2$  months, acquired with  $\leq 5$ -mm slice thickness and up to 1-mm interslice gap. Tumor volumes were segmented using a semiautomated approach by an imaging contract research organization (MedQIA, Los Angeles, CA). A centralized review of coregistered MRIs was also performed. In a post hoc exploratory analysis, the tumor growth rate after treatment versus before treatment was determined using a linear mixed-effects model.<sup>35</sup> Using this model, the percentage change in tumor volume per 6 months was derived from the slope estimates from the mixed-effects model, adjusted for 6 months.

Exploratory assessments also included confirmation of baseline *mIDH1* status and identification of co-occurring mutations. Archival formalin-fixed paraffin-embedded samples were collected for analysis by next-generation sequencing using the FoundationOne panel (Foundation Medicine, Cambridge, MA),<sup>36</sup> which includes 361 genes. Foundation Medicine provides a “known/likely oncogenic” call to identify known or likely oncogenic variants on the basis of current literature and likely somatic status of the variant.

### Statistical Analysis

The safety analysis set comprised all patients with glioma who received at least 1 dose of study treatment. Patients who had received at least 1 dose of ivosidenib were included in the efficacy analysis. Efficacy results are reported separately for contrast-enhancing and nonenhancing tumors, and they combine the dose escalation and dose expansion cohorts. Descriptive statistics are reported for safety outcomes and other clinical parameters. PFS was estimated using Kaplan-Meier methods, and medians with

associated 95% CIs were calculated. Statistical analyses were carried out (by L.J.) using SAS software version 9.3 or higher. Association of baseline gene or pathway mutation status and PFS was assessed using the log-rank test.

## RESULTS

### Patients

This study was initiated in March 2014 across 12 study sites in the United States and one in France, and 168 patients with *mIDH1* solid tumors were enrolled, including 66 with glioma. At the data cutoff date (January 16, 2019), enrollment was complete, and the study was ongoing. Twelve of 66 patients (18.2%) had GBM; the remainder had LGGs. The median number of prior systemic therapies was 2 (range, 1 to 6) and included temozolomide (48 of 66 patients); combination procarbazine, lomustine, and vincristine (eight of 66 patients); and bevacizumab (10 of 66 patients). Forty-nine of 66 patients had received prior radiotherapy (Table 1).

Twenty patients were treated in the dose escalation phase, and 46 were treated in the dose expansion phase (24 with nonenhancing disease). In the dose escalation phase, patients received ivosidenib doses of 100 mg twice per day ( $n = 1$ ), 300 mg once per day ( $n = 6$ ), 500 mg once per day ( $n = 4$ ), 600 mg once per day ( $n = 5$ ), and 900 mg once per day ( $n = 4$ ). Fifty patients received 500 mg once per day (4 in dose escalation and all 46 patients in dose expansion). At the data cutoff date, 15 patients (22.7%) were still receiving treatment and 51 (77.3%) had discontinued; all but one discontinued for disease progression (Data Supplement).

### Safety

No DLTs were reported, and the maximum tolerated dose was not reached. A dose of 500 mg once per day was selected for expansion on the basis of the pharmacokinetic/pharmacodynamic data from all solid tumor cohorts, including less-than-dose-proportional increases in exposure and maximum suppression of plasma 2-HG at 500 mg in patients with nonglioma solid tumors, as well as the safety profile and preliminary clinical activity observed in the dose escalation phase. Plasma 2-HG was not elevated above normal levels in patients with glioma.<sup>29</sup>

Most patients (63 of 66 [95.5%]) experienced at least 1 AE of any grade or causality. The most common AEs ( $\geq 10\%$ ) were headache (39.4%), nausea (22.7%), fatigue (22.7%), vomiting (19.7%), seizure (18.2%), diarrhea (16.7%), hyperglycemia (15.2%), aphasia (15.2%), neutrophil count decreased (12.1%), depression (10.6%), hypophosphatemia (10.6%), and paresthesia (10.6%; Table 2; Data Supplement). Grade  $\geq 3$  AEs were observed in 13 of 66 patients (19.7%). These included headache (4.5%), hypophosphatemia (3.0%), and seizure (3.0%; Table 2; Data Supplement). Treatment-related AEs were observed in 39 of 66 patients (59.1%); most were grade 1 or grade 2. The most common treatment-related AEs of any grade were

**TABLE 2.** Adverse Events Occurring in  $\geq 10\%$  of Patients With Glioma

Event	Ivosidenib 500 mg Once per Day (n = 50)		All Treated Patients (N = 66)	
	Any Grade	Grade $\geq 3$	Any Grade	Grade $\geq 3$
Any adverse event	48 (96.0)	7 (14.0)	63 (95.5)	13 (19.7)
Headache	19 (38.0)	1 (2.0)	26 (39.4)	3 (4.5)
Fatigue	14 (28.0)	0	15 (22.7)	0
Nausea	10 (20.0)	0	15 (22.7)	0
Vomiting	8 (16.0)	0	13 (19.7)	0
Seizure	8 (16.0)	2 (4.0)	12 (18.2)	2 (3.0)
Diarrhea	10 (20.0)	0	11 (16.7)	0
Aphasia	5 (10.0)	0	10 (15.2)	0
Hyperglycemia	7 (14.0)	1 (2.0)	10 (15.2)	1 (1.5)
Neutrophil count decreased	5 (10.0)	0	8 (12.1)	1 (1.5)
Depression	5 (10.0)	0	7 (10.6)	0
Hypophosphatemia	6 (12.0)	2 (4.0)	7 (10.6)	2 (3.0)
Paresthesia	5 (10.0)	0	7 (10.6)	0

NOTE. Data are presented as No. (%). Adverse events occurring in  $\geq 10\%$  of all 66 patients are shown; percentages indicated for 500 mg once per day and all treated are based on the respective No. for each category.

fatigue (13.6%), decreased neutrophil count (12.1%), and diarrhea (10.6%; Data Supplement). Grade  $\geq 3$  treatment-related AEs were reported in 2 patients (neutropenia, decreased weight, hyponatremia, and arthralgia). Serious AEs were reported for 11 patients (16.7%), but none were considered related to treatment. No patients discontinued study treatment owing to an AE. Eight patients (12.1%) had a dose interruption because of an AE; no patients required dose reduction for AEs. Two patients (3.0%) died within 30 days of the last dose (unrelated to AEs; both had enhancing glioma and both had received ivosidenib 500 mg once per day). There were no clinically meaningful changes in hematology parameters, coagulation parameters, vital signs, physical examination assessments, left ventricular ejection fraction, or Eastern Cooperative Oncology Group performance status.

**Investigator-Reported Response**

All 66 patients in the dose escalation and dose expansion phases were evaluable for efficacy. According to the investigator's assessment of response, 1 patient had a partial response, 44 patients (66.7%) had a best response of stable disease, and 21 patients (31.8%) had a best response of progressive disease.

As of the data cutoff, patients with nonenhancing tumors had a median treatment duration of 18.4 months (range, 1.4-47.2 months) compared with a treatment duration of 1.9 months (range, 0.4-39.9 months) for patients with enhancing tumors. Fifteen (22.7%) remained on treatment (Figs 1A and 1B). In patients with measurable disease at baseline, tumor measurements decreased from baseline in 22 of 33 nonenhancing tumors (66.7%) and in 9 of 27

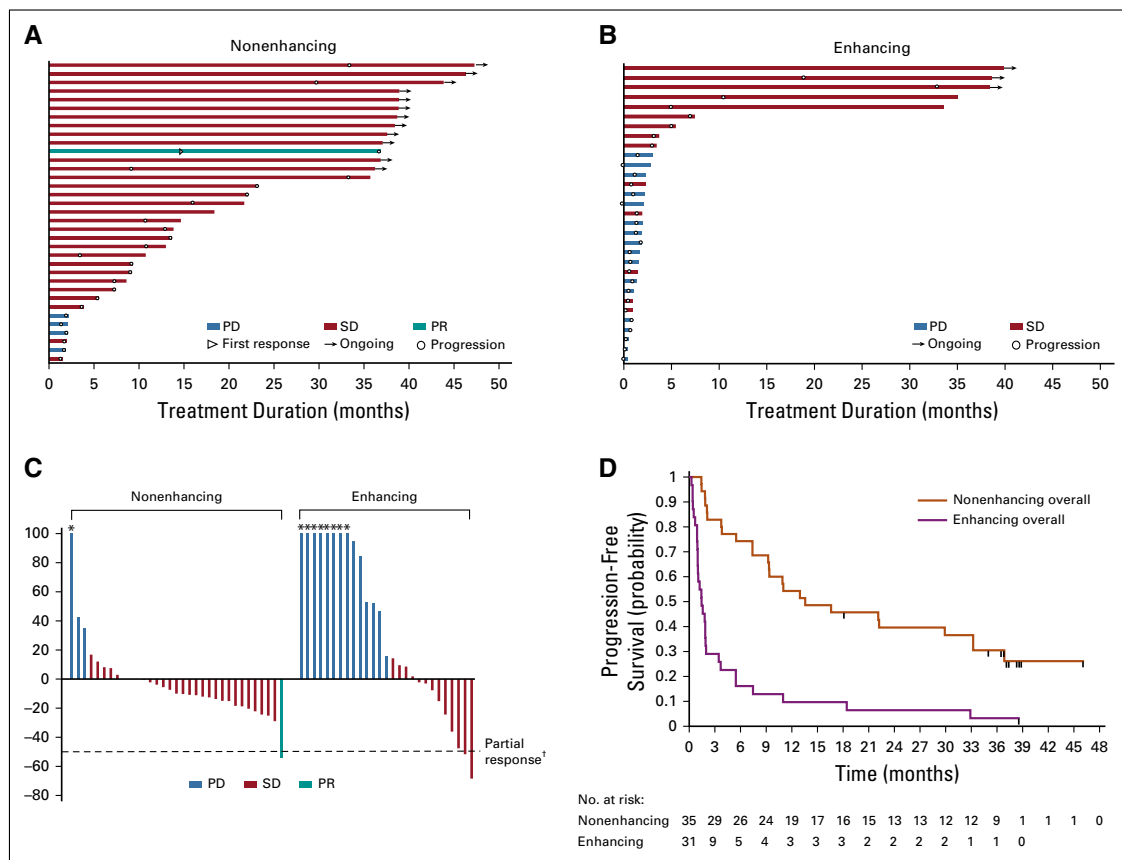


**FIG 1.** Clinical activity and efficacy of ivosidenib in patients with glioma. (A) Time receiving ivosidenib for the 35 patients with nonenhancing glioma. Twelve patients remain on treatment as of the data cutoff. (B) Time receiving ivosidenib for the 31 patients with enhancing glioma. Three patients remain on treatment as of the data cutoff. (C) Best response in evaluable patients with measurable disease (27 enhancing and 33 nonenhancing), expressed as the percent change in sum of products of the diameters from the target lesions at start of treatment. (D) Investigator-assessed progression-free survival according to glioma type for all evaluable patients with glioma (n = 66). Tick marks indicate censored data. PD, progressive disease; PR, partial response; SD, stable disease. (\*) Lesion growth > 100%. (†) Two patients with enhancing disease had decreases of > 50% that were not confirmed and are indicated as SD.

**TABLE 3.** Investigator-Reported Best Overall Response in Efficacy-Evaluable Patients

Response	RANO Criteria		RANO LGG Criteria
	Enhancing (n = 31)	Nonenhancing Escalation (n = 11)	Nonenhancing Expansion (n = 24)
Best overall response, No. (%)			
Complete response	0	0	0
Partial response	0	0	1 (4.2)
Minor response	0	0	0
Stable disease	14 (45.2)	9 (81.8)	21 (87.5)
Progressive disease	17 (54.8)	2 (18.2)	2 (8.3)
Objective response rate, <sup>a</sup> No. (%) [95% CI] <sup>b</sup>	0	0	1 (4.2) [0.1 to 21.1]

NOTE. Includes patients who had baseline and postbaseline response assessments or discontinued prematurely.

Abbreviations: LGG, lower-grade gliomas; RANO, Response Assessment in Neuro-Oncology.

<sup>a</sup>Complete response, partial response, or minor response.

<sup>b</sup>95% 2-sided exact binomial CI.

enhancing tumors (33.3%; Fig 1C). The patient with a partial response had a nonenhancing tumor and received ivosidenib 500 mg once per day. The majority of patients had disease control, with a best response of stable disease observed in 30 of 35 patients with nonenhancing tumors (85.7%) and 14 of 31 patients with enhancing tumors (45.2%; Table 3). The median PFS times were 13.6 months (95% CI, 9.2 to 33.2 months) and 1.4 months (95% CI, 1.0 to 1.9 months) for the nonenhancing and enhancing glioma cohorts, respectively, across all doses (Fig 1D). PFS curves for patients receiving 500 mg were similar (Data Supplement).

#### Exploratory Evaluation of Tumor Genetics

We examined tumor genetic profiles by targeted sequencing for 15 patients with enhancing glioma and for 16 with nonenhancing glioma. In the nonenhancing glioma group, the presence of genetic alterations in cell cycle pathway genes was associated with shorter PFS ( $P < .001$ ; Data Supplement).

#### Exploratory Evaluation of Tumor Volume Growth Rates

We supplemented the investigator-based assessment of tumor response with a quantitative evaluation of tumor volumes before and during treatment with ivosidenib for all 24 patients in the nonenhancing expansion cohort. As defined by the study protocol, this analysis included at least 3 brain MRIs before enrollment, each separated by at least 2 months. No patient had received surgery or radiation within 6 months before enrollment. In total, this analysis included 239 MRI scans from 24 patients, including 63 historical MRIs. The estimated tumor growth rate per 6 months was 26% (95% CI, 9% to 46%) in the pretreatment period and 9% (95% CI, 1% to 20%) with ivosidenib (Data Supplement). The percentage change of tumor growth rate after treatment versus before treatment estimated from the model was -14% (95% CI, -25% to -0.4%).

We also performed a centralized review of MRIs after image coregistration to minimize scan-to-scan variability related to

head tilt.<sup>37</sup> Figure 2 and Data Supplement show brain MRIs and manually segmented tumor volume growth curves for selected patients with nonenhancing glioma. Patient 1 had an anaplastic oligodendroglioma that was initially treated with surgery, radiation, and temozolomide. Following this initial tumor therapy, the patient was off therapy for 3 years and developed a slowly progressive T2/FLAIR signal abnormality. Visual inspection of coregistered images and volume growth curves showed tumor shrinkage after the initiation of ivosidenib (Fig 2A). Despite a best response of stable disease according to the investigator, this patient subsequently achieved partial response by RANO LGG. Patient 2 had an astrocytoma and had undergone tumor resection 6 years before enrollment and had received no additional therapy in the interim. MRIs demonstrated an increase in tumor volume before enrollment. Visual inspection of coregistered images and volume growth curves showed tumor shrinkage after initiation of ivosidenib (Fig 2B). Best response by investigator for this patient was stable disease. Patient 3 had an oligodendroglioma diagnosed 4 years before enrollment and was observed without additional therapy since the initial surgery. Treatment with ivosidenib resulted in reduction of tumor volumes (Fig 2C). Best response by investigator for this patient was stable disease. Patient 4 had an oligodendroglioma diagnosed by biopsy 8 years before enrollment, was initially treated with surgery and 1 year of temozolomide, and then was observed for 7 years without additional therapy. The gradual increase in tumor volume before enrollment stabilized after initiation of ivosidenib (Fig 2D). Best response by investigator for this patient was stable disease. All of these patients were receiving ivosidenib at the time of analysis.

#### DISCUSSION

The majority of human LGGs harbor *IDH* mutations.<sup>30</sup> Standard treatment of LGG consists of radiation and chemotherapy. There are no approved molecularly targeted

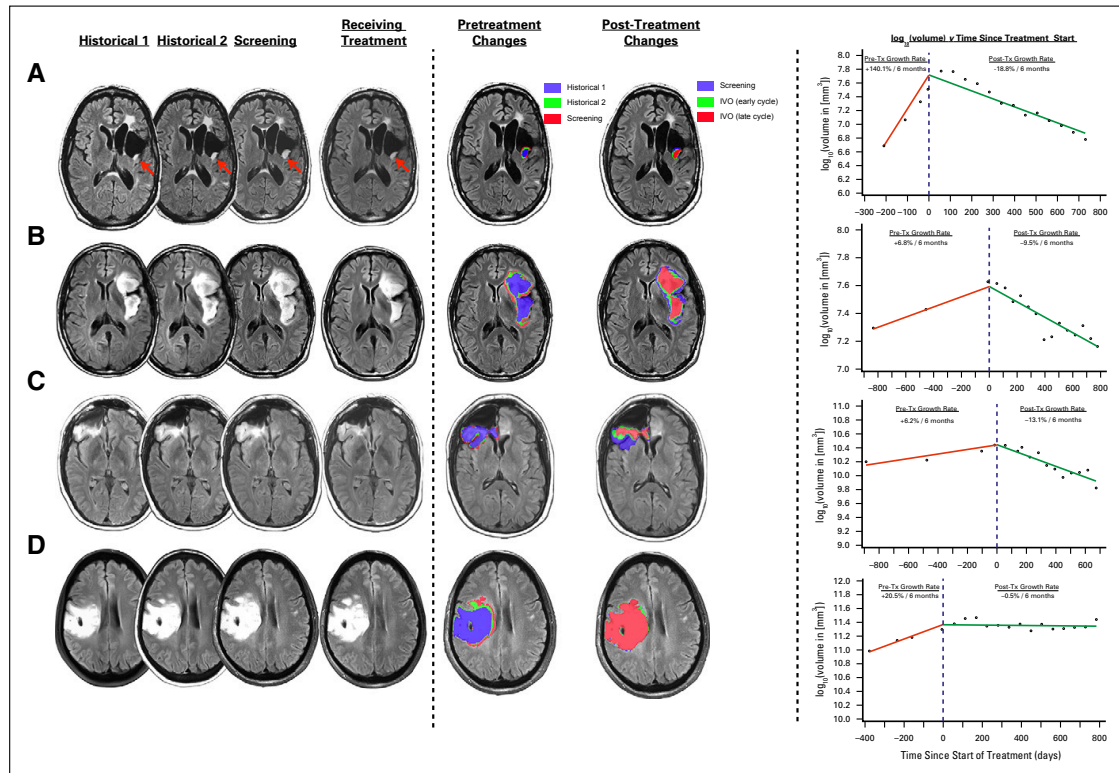


**FIG 2.** (A-D) Examples of brain magnetic resonance images and manually segmented tumor volume growth curves in 4 patients with nonenhancing glioma treated with ivosidenib. IVO, ivosidenib; Tx, treatment with ivosidenib.

therapies for LGG, and *IDH* mutations represent a novel opportunity for early therapeutic intervention. Our study shows that continuous daily oral therapy with ivosidenib was well tolerated and was not associated with DLTs in patients with advanced *mIDH1* glioma. An ivosidenib dose of 500 mg once per day was selected for the expansion phase.

The median PFS for patients with nonenhancing gliomas in our study compares favorably to that reported for temozolomide in advanced *mIDH1* LGG (approximately 7 months).<sup>38</sup> However, comparisons with earlier LGG studies, and in particular retrospective single-center studies, should be made with caution because these studies often included patients with both *IDH* wildtype and *mIDH* LGGs and used variable definitions of disease progression (ie, treatment-naïve progressive disease v progression after standard therapy).<sup>39</sup> More direct evidence for the antitumor activity of ivosidenib in *mIDH* LGG stems from our exploratory analysis of tumor volumes, which documented shrinkage in several patients. Compared with conventional 2-dimensional measurements, tumor volume measurements that incorporate changes in tumor growth rates may

represent the diffuse intracranial growth of LGG with greater confidence and accuracy,<sup>7,40</sup> but broader implementation of this approach for LGG will require harmonization of image acquisition and analysis,<sup>34,41</sup> as well as regulatory guidance.

Despite the heterogeneous patient population in our trial, the nonrandomized design, and the lack of central pathology review, the data from our trial suggest that ivosidenib has greater activity against nonenhancing gliomas than against enhancing gliomas. This finding may seem surprising because the absence of contrast enhancement is typically associated with impaired drug delivery. In a perioperative clinical trial (ClinicalTrials.gov identifier: NCT03343197), we recently observed that ivosidenib (at 500 mg once per day orally) reduces intratumoral 2-HG levels in nonenhancing gliomas by > 90%<sup>42</sup> and is associated with objective responses. We hypothesize that ivosidenib may be more effective in nonenhancing gliomas because these tumors represent an earlier disease stage with fewer genetic alterations, reminiscent of the greater antitumor activity of the BCR-ABL inhibitor imatinib in earlier stages of chronic myeloid leukemia.<sup>43,44</sup> In support

of this hypothesis, we found that the presence of genetic alterations in cell cycle genes (lesions that are associated with LGG progression)<sup>5,45</sup> was associated with shorter PFS

within the subgroup of nonenhancing gliomas. On the basis of these data, additional clinical development of mIDH inhibitors for *mIDH* low-grade gliomas is warranted.

## AFFILIATIONS

<sup>1</sup>Department of Neurology, Memorial Sloan Kettering Cancer Center, New York, NY

<sup>2</sup>UCLA Brain Tumor Imaging Laboratory, Department of Radiological Sciences, David Geffen School of Medicine, University of California, Los Angeles, Los Angeles, CA

<sup>3</sup>Drug Development Department, Gustave Roussy Cancer Center, Villejuif, France

<sup>4</sup>Department of Neurology and Neurotherapeutics, University of Texas Southwestern Medical Center, Dallas, TX

<sup>5</sup>Department of Neurology and Sylvester Comprehensive Cancer Center, University of Miami, Miami, FL

<sup>6</sup>The Sidney Kimmel Comprehensive Cancer Center at Johns Hopkins, Baltimore, MD

<sup>7</sup>Henri and Belinda Termeer Center for Targeted Therapies, Massachusetts General Hospital Cancer Center, Boston, MA

<sup>8</sup>Sarah Cannon Research Institute, Nashville, TN

<sup>9</sup>Department of Investigational Cancer Therapeutics, Division of Cancer Medicine, The University of Texas MD Anderson Cancer Center, Houston, TX

<sup>10</sup>Radiology, Neuroradiology Service, Memorial Sloan Kettering Cancer Center, New York, NY

<sup>11</sup>Department of Radiology, Brigham and Women's Hospital, Dana-Farber Cancer Institute, Boston, MA

<sup>12</sup>Biostatistics, Agios Pharmaceuticals, Cambridge, MA

<sup>13</sup>Bioinformatics, Agios Pharmaceuticals, Cambridge, MA

<sup>14</sup>Pharmacology, Agios Pharmaceuticals, Cambridge, MA

<sup>15</sup>Clinical Sciences, Agios Pharmaceuticals, Cambridge, MA

<sup>16</sup>Medical, Agios Pharmaceuticals, Cambridge, MA

<sup>17</sup>Department of Neurology, Ronald Reagan UCLA Medical Center, University of California, Los Angeles, Los Angeles, CA

<sup>18</sup>Center for Neuro-Oncology, Dana-Farber Cancer Institute, Boston, MA, USA

## CORRESPONDING AUTHOR

Ingo K. Mellinghoff, MD, Department of Neurology and Human Oncology & Pathogenesis Program, Memorial Sloan Kettering Cancer Center, 1275 York Ave, New York, NY 10065; e-mail: mellingi@mskcc.org.

## EQUAL CONTRIBUTION

I.K.M., B.M.E., and T.F.C. contributed equally to this work.

## REFERENCES

- Mandonnet E, Delattre JY, Tanguy ML, et al: Continuous growth of mean tumor diameter in a subset of grade II gliomas. *Ann Neurol* 53:524-528, 2003
- van den Bent MJ, Smits M, Kros JM, et al: Diffuse infiltrating oligodendroglioma and astrocytoma. *J Clin Oncol* 35:2394-2401, 2017
- Weller M, van den Bent M, Tonn JC, et al: European Association for Neuro-Oncology (EANO) guideline on the diagnosis and treatment of adult astrocytic and oligodendroglial gliomas. *Lancet Oncol* 18:e315-e329, 2017
- Buckner JC, Shaw EG, Pugh SL, et al: Radiation plus procarbazine, CCNU, and vincristine in low-grade glioma. *N Engl J Med* 374:1344-1355, 2016
- Jonsson P, Lin AL, Young RJ, et al: Genomic correlates of disease progression and treatment response in prospectively characterized gliomas. *Clin Cancer Res* 25:5537-5547, 2019
- Cairncross JG, Pexman JH, Rathbone MP, et al: Postoperative contrast enhancement in patients with brain tumor. *Ann Neurol* 17:570-572, 1985
- Pallud J, Taillandier L, Capelle L, et al: Quantitative morphological magnetic resonance imaging follow-up of low-grade glioma: A plea for systematic measurement of growth rates. *Neurosurgery* 71:729-739, discussion 739-740, 2012
- Yan H, Parsons DW, Jin G, et al: *IDH1* and *IDH2* mutations in gliomas. *N Engl J Med* 360:765-773, 2009
- Parsons DW, Jones S, Zhang X, et al: An integrated genomic analysis of human glioblastoma multiforme. *Science* 321:1807-1812, 2008

## CLINICAL TRIAL INFORMATION

NCT02073994

## SUPPORT

Supported by Agios Pharmaceuticals. Translational research studies were supported by National Institutes of Health Grant Nos. 1 R35 NS105109 01 and P30CA008748 (I.K.M.) and the National Brain Tumor Society Defeat GBM Initiative (I.K.M. and T.F.C.).

## AUTHORS' DISCLOSURES OF POTENTIAL CONFLICTS OF INTEREST AND DATA AVAILABILITY STATEMENT

Disclosures provided by the authors and data availability statement (if applicable) are available with this article at DOI <https://doi.org/10.1200/JCO.19.03327>.

## AUTHOR CONTRIBUTIONS

**Conception and design:** Ingo K. Mellinghoff, Benjamin M. Ellingson, Mehdi Touat, Gregory M. Cote, Howard Burris, Robert J. Young, Raymond Huang, Chris Bowden, Shuchi S. Pandya, Timothy F. Cloughesy, Patrick Y. Wen

**Provision of study material or patients:** Mehdi Touat, Howard Burris, Filip Janku, Timothy F. Cloughesy, Patrick Y. Wen

**Collection and assembly of data:** Ingo K. Mellinghoff, Benjamin M. Ellingson, Mehdi Touat, Elizabeth Maher, Macarena I. De La Fuente, Matthias Holdhoff, Howard Burris, Filip Janku, Robert J. Young, Raymond Huang, Lori Steelman, Shuchi S. Pandya, Timothy F. Cloughesy, Patrick Y. Wen

**Data analysis and interpretation:** Ingo K. Mellinghoff, Mehdi Touat, Gregory M. Cote, Howard Burris, Raymond Huang, Liewen Jiang, Sung Choe, Bin Fan, Katharine Yen, Min Lu, Chris Bowden, Lori Steelman, Shuchi S. Pandya, Timothy F. Cloughesy, Patrick Y. Wen

**Manuscript writing:** All authors

**Final approval of manuscript:** All authors

**Accountable for all aspects of the work:** All authors

## ACKNOWLEDGMENT

We thank the participating patients and their families, and the nurses, research coordinators, and study management team. Tara Nimkar of Agios Pharmaceuticals provided operational support for this study. MedQIA (Los Angeles, CA) assisted with image analysis. Medical writing support was provided by Mark Poirier of Excel Scientific Solutions, Fairfield, CT.

10. Watanabe T, Nobusawa S, Kleihues P, et al: *IDH1* mutations are early events in the development of astrocytomas and oligodendrogliomas. *Am J Pathol* 174:1149-1153, 2009
11. van den Bent MJ, Dubbink HJ, Marie Y, et al: *IDH1* and *IDH2* mutations are prognostic but not predictive for outcome in anaplastic oligodendroglial tumors: A report of the European Organization for Research and Treatment of Cancer Brain Tumor Group. *Clin Cancer Res* 16:1597-1604, 2010
12. Turcan S, Rohle D, Goenka A, et al: *IDH1* mutation is sufficient to establish the glioma hypermethylator phenotype. *Nature* 483:479-483, 2012
13. Sanson M, Marie Y, Paris S, et al: Isocitrate dehydrogenase 1 codon 132 mutation is an important prognostic biomarker in gliomas. *J Clin Oncol* 27:4150-4154, 2009
14. Nouchmeh H, Weisenberger DJ, Diefes K, et al: Identification of a CpG island methylator phenotype that defines a distinct subgroup of glioma. *Cancer Cell* 17:510-522, 2010
15. Brat DJ, Verhaak RG, Aldape KD, et al: Comprehensive, integrative genomic analysis of diffuse lower grade gliomas. *N Engl J Med* 372:2481-2498, 2015
16. Dang L, White DW, Gross S, et al: Cancer-associated *IDH1* mutations produce 2-hydroxyglutarate. *Nature* 462:739-744, 2009
17. Ward PS, Patel J, Wise DR, et al: The common feature of leukemia-associated *IDH1* and *IDH2* mutations is a neomorphic enzyme activity converting alpha-ketoglutarate to 2-hydroxyglutarate. *Cancer Cell* 17:225-234, 2010
18. Chowdhury R, Yeoh KK, Tian YM, et al: The oncometabolite 2-hydroxyglutarate inhibits histone lysine demethylases. *EMBO Rep* 12:463-469, 2011
19. Xu W, Yang H, Liu Y, et al: Oncometabolite 2-hydroxyglutarate is a competitive inhibitor of  $\alpha$ -ketoglutarate-dependent dioxygenases. *Cancer Cell* 19:17-30, 2011
20. Losman JA, Cooper RE, Koivunen P, et al: (R)-2-hydroxyglutarate is sufficient to promote leukemogenesis and its effects are reversible. *Science* 339:1621-1625, 2013
21. Wang F, Travins J, DeLaBarre B, et al: Targeted inhibition of mutant *IDH2* in leukemia cells induces cellular differentiation. *Science* 340:622-626, 2013
22. Rohle D, Popovici-Muller J, Palaskas N, et al: An inhibitor of mutant *IDH1* delays growth and promotes differentiation of glioma cells. *Science* 340:626-630, 2013
23. Kosmider O, Gelsi-Boyer V, Slama L, et al: Mutations of *IDH1* and *IDH2* genes in early and accelerated phases of myelodysplastic syndromes and MDS/myeloproliferative neoplasms. *Leukemia* 24:1094-1096, 2010
24. Mardis ER, Ding L, Dooling DJ, et al: Recurring mutations found by sequencing an acute myeloid leukemia genome. *N Engl J Med* 361:1058-1066, 2009
25. Stein EM, DiNardo CD, Pollyea DA, et al: Enasidenib in mutant *IDH2* relapsed or refractory acute myeloid leukemia. *Blood* 130:722-731, 2017
26. DiNardo CD, Stein EM, de Botton S, et al: Durable remissions with ivosidenib in *IDH1*-mutated relapsed or refractory AML. *N Engl J Med* 378:2386-2398, 2018
27. Lowery MA, Burris HA III, Janku F, et al: Safety and activity of ivosidenib in patients with *IDH1*-mutant advanced cholangiocarcinoma: A phase 1 study. *Lancet Gastroenterol Hepatol* 4:711-720, 2019
28. Tap WD, Villalobos VM, Cote GM, et al: Phase 1 study of the mutant *IDH1* inhibitor ivosidenib: Safety and clinical activity in patients with advanced chondrosarcoma. *J Clin Oncol* 38:1693-1701, 2020
29. Fan B, Mellinghoff IK, Wen PY, et al: Clinical pharmacokinetics and pharmacodynamics of ivosidenib, an oral, targeted inhibitor of mutant *IDH1*, in patients with advanced solid tumors. *Invest New Drugs* 38:433-444, 2020
30. Louis DN, Perry A, Reifenberger G, et al: The 2016 World Health Organization classification of Tumors of the Central Nervous System: A summary. *Acta Neuropathol* 131:803-820, 2016
31. Louis DN, Ohgaki H, Wiestler OD, et al: The 2007 WHO classification of tumours of the central nervous system. *Acta Neuropathol* 114:97-109, 2007
32. Wen PY, Macdonald DR, Reardon DA, et al: Updated response assessment criteria for high-grade gliomas: Response assessment in neuro-oncology working group. *J Clin Oncol* 28:1963-1972, 2010
33. van den Bent MJ, Wefel JS, Schiff D, et al: Response assessment in neuro-oncology (a report of the RANO group): Assessment of outcome in trials of diffuse low-grade gliomas. *Lancet Oncol* 12:583-593, 2011
34. Ellingson BM, Bendszus M, Boxerman J, et al: Consensus recommendations for a standardized brain tumor imaging protocol in clinical trials. *Neuro-oncol* 17:1188-1198, 2015
35. Fitzmaurice GM, Laird NM, Ware JH: *Applied longitudinal analysis* (ed 2). Hoboken, NJ, John Wiley & Sons, 2011
36. Frampton GM, Fichtenholtz A, Otto GA, et al: Development and validation of a clinical cancer genomic profiling test based on massively parallel DNA sequencing. *Nat Biotechnol* 31:1023-1031, 2013
37. Reuter M, Gerstner ER, Rapalino O, et al: Impact of MRI head placement on glioma response assessment. *J Neurooncol* 118:123-129, 2014
38. Dubbink HJ, Taal W, van Marion R, et al: *IDH1* mutations in low-grade astrocytomas predict survival but not response to temozolomide. *Neurology* 73:1792-1795, 2009
39. Nahed BV, Redjal N, Brat DJ, et al: Management of patients with recurrence of diffuse low grade glioma: A systematic review and evidence-based clinical practice guideline. *J Neurooncol* 125:609-630, 2015
40. Rees J, Watt H, Jäger HR, et al: Volumes and growth rates of untreated adult low-grade gliomas indicate risk of early malignant transformation. *Eur J Radiol* 72:54-64, 2009
41. Freyschlag CF, Krieg SM, Kerschbaumer J, et al: Imaging practice in low-grade gliomas among European specialized centers and proposal for a minimum core of imaging. *J Neurooncol* 139:699-711, 2018
42. Mellinghoff IK, Cloughesy TF, Wen PY, et al: A phase 1, open-label, perioperative study of AG-120 and AG-881 in recurrent *IDH1* mutant, low-grade glioma: Results from cohort 1. *J Clin Oncol* 37(15\_suppl abstr):2003, 2019
43. Druker BJ, Talpaz M, Resta DJ, et al: Efficacy and safety of a specific inhibitor of the BCR-ABL tyrosine kinase in chronic myeloid leukemia. *N Engl J Med* 344:1031-1037, 2001
44. Druker BJ, Sawyers CL, Kantarjian H, et al: Activity of a specific inhibitor of the BCR-ABL tyrosine kinase in the blast crisis of chronic myeloid leukemia and acute lymphoblastic leukemia with the Philadelphia chromosome. *N Engl J Med* 344:1038-1042, 2001
45. Shirahata M, Ono T, Stichel D, et al: Novel, improved grading system(s) for *IDH*-mutant astrocytic gliomas. *Acta Neuropathol* 136:153-166, 2018

**AUTHORS' DISCLOSURES OF POTENTIAL CONFLICTS OF INTEREST****Ivosidenib in Isocitrate Dehydrogenase 1–Mutated Advanced Glioma**

The following represents disclosure information provided by authors of this manuscript. All relationships are considered compensated unless otherwise noted. Relationships are self-held unless noted. I = Immediate Family Member, Inst = My Institution. Relationships may not relate to the subject matter of this manuscript. For more information about ASCO's conflict of interest policy, please refer to [www.asco.org/rwc](http://www.asco.org/rwc) or [ascopubs.org/jco/authors/author-center](http://ascopubs.org/jco/authors/author-center).

Open Payments is a public database containing information reported by companies about payments made to US-licensed physicians ([Open Payments](#)).

**Ingo K. Mellingerhoff**

**Honoraria:** Roche

**Consulting or Advisory Role:** Agios, Puma Biotechnology, Debiopharm Group, Black Diamond Therapeutics, Voyager Therapeutics

**Research Funding:** General Electric, Amgen, Lilly

**Travel, Accommodations, Expenses:** Voyager Therapeutics, AstraZeneca, Roche, Puma Biotechnology, Agios

**Benjamin M. Ellingson**

**Consulting or Advisory Role:** Siemens, Roche/Genentech, Bristol-Myers Squibb, Northwest Biotherapeutics, Nativis, Omnix, Agios, Medicenna, MedQIA, Novogen, Tocagen, Imaging Endpoints

**Research Funding:** Siemens, Roche/Genentech, Agios

**Travel, Accommodations, Expenses:** Siemens

**Mehdi Touat**

**Consulting or Advisory Role:** Agios, Taiho Pharmaceutical, Integragen

**Travel, Accommodations, Expenses:** Merck Sharp & Dohme

**Elizabeth Maher**

**Consulting or Advisory Role:** Agios, Curadev, Curadev (I), FORMA Therapeutics

**Research Funding:** Curadev, Curadev (I)

**Travel, Accommodations, Expenses:** Agios, FORMA Therapeutics

**Macarena I. De La Fuente**

**Consulting or Advisory Role:** Agios, Puma Biotechnology, Foundation Medicine, FORMA Therapeutics

**Other Relationship:** Targeted Oncology (I), OncLive (I), OncInfo (I)

**Matthias Holdhoff**

**Consulting or Advisory Role:** Celgene, AbbVie, BTG, Newlink Genetics, DPClinical

**Travel, Accommodations, Expenses:** Arbor Pharmaceuticals

**Gregory M. Cole**

**Consulting or Advisory Role:** Agios, PharmaMar, Epizyme

**Research Funding:** MacroGenics (Inst), Boston Biomedical (Inst), PharmaMar (Inst), Epizyme (Inst), Agios (Inst), Eisai (Inst), Merck (Inst), Plexikon (Inst), CBA (Inst), Bavarian Nordic

**Research Funding:** Bayer (Inst), Springworks Therapeutics (Inst)

**Travel, Accommodations, Expenses:** PharmaMar

**Howard Burris**

**Employment:** HCA Healthcare/Sarah Cannon

**Leadership:** HCA Healthcare/Sarah Cannon

**Stock and Other Ownership Interests:** HCA Healthcare/Sarah Cannon

**Consulting or Advisory Role:** AstraZeneca (Inst), FORMA Therapeutics (Inst), Celgene (Inst), Incyte (Inst)

**Research Funding:** Roche/Genentech (Inst), Bristol-Myers Squibb (Inst), Incyte (Inst), AstraZeneca (Inst), MedImmune (Inst), MacroGenics (Inst), Novartis (Inst), Boehringer Ingelheim (Inst), Lilly (Inst), Seattle Genetics (Inst), Merck (Inst), Agios (Inst), Jounce Therapeutics (Inst), Moderna Therapeutics (Inst), CytomX Therapeutics (Inst), GlaxoSmithKline (Inst), Verastem (Inst), Tesaro (Inst), Millennium (Inst), BioMed Valley Discoveries (Inst), TG Therapeutics (Inst), Vertex (Inst), eFFECTOR Therapeutics (Inst), Janssen (Inst), Gilead Sciences (Inst), BioAtla (Inst), CicloMed (Inst), Harpoon therapeutics (Inst), Arch (Inst), Arvinas (Inst), Revolution Medicines (Inst), Array BioPharma (Inst), Bayer (Inst), BIND Therapeutics (Inst), Kymab (Inst), miRNA Therapeutics (Inst), Pfizer (Inst)

**Expert Testimony:** Novartis (Inst)

**Uncompensated Relationships:** Daiichi Sankyo (Inst), Pfizer (Inst)

**Open Payments Link:** <https://openpaymentsdata.cms.gov/physician/201030/summary>

**Filip Janku**

**Stock and Other Ownership Interests:** Trovogene

**Consulting or Advisory Role:** Deciphera, Trovogene, Novartis, Sequenom, Foundation Medicine, Guardant Health, Synlogic, Valeant/Dendreon, IFM Therapeutics, Sotio, PureTech, Jazz Pharmaceuticals, Immunomet, IDEAYA Biosciences

**Research Funding:** Novartis (Inst), BioMed Valley Discoveries (Inst), Roche (Inst), Agios (Inst), Astellas Pharma (Inst), Deciphera (Inst), Plexikon (Inst), Piquor (Inst), Fujifilm (Inst), Symphogen (Inst), Bristol-Myers Squibb (Inst), Asana

Biosciences (Inst), Astex Pharmaceuticals (Inst), Genentech (Inst), Bristol-Myers Squibb (Inst), Proximagen (Inst)

**Other Relationship:** Bio-Rad

**Robert J. Young**

**Stock and Other Ownership Interests:** Alexion, Agios, Biogen, Celgene, Gilead Sciences, Karyopharm Therapeutics, Spark Therapeutics, Regeneron, Stemline Therapeutics, Vertex, Merck, Amgen

**Consulting or Advisory Role:** Agios, Puma Biotechnology, NordicNeuroLab, ICON Clinical Research

**Research Funding:** Agios (Inst)

**Raymond Huang**

**Consulting or Advisory Role:** Agios

**Research Funding:** Agios

**Liewen Jiang**

**Employment:** Agios

**Stock and Other Ownership Interests:** Agios

**Sung Choe**

**Employment:** Agios

**Stock and Other Ownership Interests:** Agios

**Patents, Royalties, Other Intellectual Property:** Patents derived from my work at Agios

**Travel, Accommodations, Expenses:** Agios

**Bin Fan**

**Employment:** Agios

**Stock and Other Ownership Interests:** Agios

**Travel, Accommodations, Expenses:** Agios

**Katherine Yen**

**Employment:** Agios Pharmaceuticals

**Leadership:** Auron Therapeutics

**Stock and Other Ownership Interests:** Agios Therapeutics, Auron Therapeutics

**Consulting or Advisory Role:** Agios Therapeutics

**Research Funding:** Auron Therapeutics, Auron Therapeutics

**Patents, Royalties, Other Intellectual Property:** Patents around IDH mutant inhibitors and methods of treatment

**Travel, Accommodations, Expenses:** Agios Therapeutics, Auron Therapeutics

**Min Lu**

**Employment:** Agios

**Stock and Other Ownership Interests:** Agios

**Chris Bowden**

**Employment:** Agios

**Leadership:** Agios, Miragen, Ziopharm

**Stock and Other Ownership Interests:** Agios

**Lori Steelman**

**Employment:** Agios

**Stock and Other Ownership Interests:** Infinity Pharmaceuticals

**Shuchi S. Pandya**

**Employment:** Agios Pharmaceuticals

**Stock and Other Ownership Interests:** Agios

**Research Funding:** Agios

**Travel, Accommodations, Expenses:** Agios

**Timothy F. Cloughesy**

**Stock and Other Ownership Interests:** Notable Labs, Katmai Pharmaceuticals

**Consulting or Advisory Role:** Roche/Genentech, Celgene, Tocagen, VBL Therapeutics, NewGen Therapeutics, Novartis, Agios, Cortice, Novocure, AbbVie, Oxigene, Wellcome Trust, Pfizer, Notable Labs, Bristol-Myers Squibb, Merck, Insys Therapeutics, Human Longevity, Sunovion, Boston Biomedical, Novogen, Alexion Pharmaceuticals, GW Pharmaceuticals, Lilly, Genocera Biosciences, Puma Biotechnology, Deciphera, Boehringer Ingelheim, Kiyatec, VBI Vaccines, Bayer, DellMar Pharmaceuticals, QED, Amgen, Pascal Bio, Karyopharm Therapeutics

**Patents, Royalties, Other Intellectual Property:** U.S. Provisional application No. 62/819,322: Compositions and methods for treating cancer; Filing date: March

15, 2019; Inventor(s): David A. Nathanson et al. FH Reference No. UCH-17760 (32246-17760) Your Reference No. [UCLA 2019-630-1] US

**Other Relationship:** Global Coalition for Adaptive Research 501(c)(3)

**Patrick Y. Wen**

**Consulting or Advisory Role:** Agios, AstraZeneca, Vascular Biogenics, Immunomic Therapeutics, Kayatec, Puma Biotechnology, Taiho Pharmaceutical, Deciphera, VBI Vaccines, Tocagen, Bayer, Blue Earth

Diagnostics, Karyopharm, Deciphera, Voyager, Taiho Pharmaceutical, QED, Imvax, Elevate Bio, Integral Health

**Speakers' Bureau:** Merck, Prime Oncology

**Research Funding:** Agios (Inst), AbbVie (Inst), AstraZeneca (Inst), Merck (Inst), Novartis (Inst), Oncoceutics (Inst), Lilly (Inst), AstraZeneca (Inst), Beigene (Inst), Kazia (Inst), MediciNova (Inst), Vacular Biogenics (Inst), VBI Vaccines (Inst), Puma (Inst), Celgene (Inst), Bayer (Inst)

No other potential conflicts of interest were reported.

## CONCLUSIONS

En conclusion, nos travaux rapportés dans l'*Article 1*<sup>19</sup> permettent une meilleure caractérisation clinique et biologique des deux voies principales conduisant à l'hypermutation dans les gliomes (*i.e.* voie *de novo* associée à des anomalies constitutionnelles du système MMR ou des gènes des polymérases ; voie post-traitement, plus fréquente, retrouvée dans les gliomes les plus chimiosensibles en récurrence après témozolomide). Nous montrons que l'hypermutation post-traitement résulte de dommages à l'ADN induits par le témozolomide dans des cellules MMR-déficientes et que celle-ci représente un nouveau biomarqueur de résistance acquise au témozolomide. En comparaison à d'autres cancers MMR-déficients, nous montrons que les gliomes hypermutés MMR-déficients présentent des caractéristiques uniques (*e.g.* mauvais pronostic, absence de phénotype MSI, caractère sous-clonal et tardif de l'hypermutation) s'associant à l'absence fréquente de réponse aux traitements par ICI. A l'inverse, nous rapportons dans l'*Article 2*<sup>20</sup> un cas de réponse spectaculaire aux traitements par ICI chez un patient avec méningiome agressif hypermuté et MMR-déficient. Ceci indique l'existence de différences importantes dans les mécanismes déterminant la réponse aux ICI entre différentes tumeurs du SNC, selon leur localisation, cellules d'origine et voies d'oncogénèse, et leurs interactions avec le microenvironnement immunitaire. Ces différences font l'objet de travaux actuellement en cours au sein de l'équipe, avec comme objectifs d'identifier : i) de meilleurs biomarqueurs permettant de sélectionner les patients les plus susceptibles de bénéficier des ICI, et ii) de nouvelles stratégies de combinaison visant à contourner les mécanismes de résistance à l'immunothérapie mis en jeu dans les gliomes.

Le développement des thérapies ciblées dans les gliomes malins a été grevé par les échecs de très nombreux essais cliniques, ce malgré la présence de candidats moléculaires récurrents et potentiellement ciblables (voir *Article 3*<sup>21</sup> pour une revue de la littérature et discussion sur les facteurs expliquant potentiellement ces échecs). Ceci a conduit à remettre en question le concept de médecine de précision dans les gliomes malins. Les résultats que nous rapportons dans les *Articles 4, 5 et 7*<sup>22-25</sup> apportent la preuve que certains sous-types rares de gliomes malins peuvent bénéficier de tels traitements (*i.e.* gliomes avec mutations activatrices *BRAF*, gliomes avec mutations *IDH1/2*, gliomes avec gène de fusion *ATG7-RAF1*). Nous illustrons par ailleurs dans l'*Article 6*<sup>24</sup> l'intérêt majeur de

nouvelles méthodologies d'essais cliniques incluant des bras chirurgicaux au cours du développement précoce de nouvelles thérapies visant à documenter de façon systématique : i) la pénétration cérébrale intraparenchymateuse des agents expérimentaux, et ii) leurs effets pharmacodynamiques sur les cellules tumorales. De tels essais sont en effet de nature à apporter des informations clés sur le caractère ciblable ou non des principales anomalies moléculaires retrouvées dans les gliomes (*e.g.* amplification de l'*EGFR*), et sur les mécanismes de résistance potentiels. Nos observations supportent leur mise en place de façon plus systématique avant la progression vers des essais randomisés de plus grande envergure. A terme, nous anticipons que ces nouveaux essais permettront d'identifier les stratégies de combinaisons qui permettront de contourner les multiples mécanismes de résistance mis en jeu dans les gliomes malins, barrière principale au progrès thérapeutique dans ces pathologies.

Collectivement, nos travaux supportent un changement dans la pratique clinique visant à élargir les applications du séquençage tumoral, non seulement pour le diagnostic histomoléculaire, mais également pour l'identification de modifications génétiques associées à une résistance ou une réponse aux chimiothérapies et aux thérapies ciblées. Compte tenu de l'adaptation rapide des cellules de gliomes aux traitements les plus efficaces, cette pratique implique le développement de nouveaux biomarqueurs, peu invasifs, qui pourront être utilisés de façon longitudinale pour monitorer la réponse au traitement et anticiper la récurrence.

## CONCLUSIONS

In conclusion, our findings reported in *Article 1*<sup>19</sup> advance the clinical and biological characterization of the two main pathways leading to hypermutation in gliomas (ie de novo pathway associated with constitutional defects in the MMR pathway or polymerase genes; post-treatment pathway, more common, found in the most chemosensitive gliomas recurring after temozolomide). We show that post-treatment hypermutation results from DNA damage induced by temozolomide in MMR-deficient cells and that post-treatment hypermutation represents a new biomarker of acquired resistance to temozolomide. We show that MMR-deficient hypermutated gliomas present unique characteristics when compared to other MMR-deficient cancers (eg poor prognosis, lack of classic MSI phenotype, subclonal and late burst of hypermutation) associated with the frequent lack of response to ICI treatments. By contrast, we report in *Article 2*<sup>20</sup> a case of a spectacular response to ICI in a patient with aggressive hypermutated and MMR-deficient meningioma. This suggests the existence of important differences in the determinants of the response to ICI between different CNS tumors, depending on their location, cells of origin and pathways of oncogenesis, and their interactions with the immune microenvironment. These differences are the subject of works currently underway within the team, with the aim of identifying: i) new biomarkers improving the selection of the patients most likely to benefit from ICKs, and ii) new combination strategies aimed at bypassing the mechanisms of resistance to immunotherapy involved in gliomas.

The development of targeted therapies in malignant gliomas has been hampered by the failures of a large number of clinical trials, despite the presence of recurrent and potentially targetable molecular candidates (review of the literature and discussion of the factors potentially explaining these failures in *Article 3*<sup>21</sup>). This has led to questioning the concept of precision medicine in malignant gliomas. The results reported in *Articles 4, 5 and 7*<sup>22-25</sup> provide the proof of principle that certain rare subtypes of malignant gliomas may benefit from such treatment (ie gliomas with *BRAF* activating mutations, gliomas with *IDH1/2* mutations, gliomas with *ATG7-RAF1* fusion gene). We also illustrate in *Article 6*<sup>24</sup> the key potential of new early clinical trial designs that include surgical arms aimed at systematically documenting: i) the intraparenchymal cerebral penetration of experimental agents, and ii) their pharmacodynamic effects on tumor cells. Such trials are likely to

provide key information on whether the main molecular abnormalities found in gliomas (e.g. *EGFR* amplification) are targetable, as well as providing insights on potential resistance mechanisms. Our observations support their implementation in a more systematic way before the progression to larger randomized trials. Ultimately, we anticipate that these new trials enable the identification of novel combination strategies that will bypass the multiple resistance mechanisms involved in malignant gliomas, the main barrier to therapeutic progress in these cancers.

Collectively, our work supports a shift in clinical practice aimed at expanding the applications of tumor sequencing, not only for histomolecular diagnosis, but also for the identification of genetic changes associated with resistance or response to chemotherapy and targeted therapy. Given the rapid adaptation of glioma cells to the most effective treatments, this practice will require the development of new, minimally invasive biomarkers that can be used longitudinally to monitor the response to treatment and anticipate recurrence.

## REFERENCES

- 1 Louis, D. N. *et al.* The 2016 World Health Organization Classification of Tumors of the Central Nervous System: a summary. *Acta Neuropathol* **131**, 803-820, doi:10.1007/s00401-016-1545-1 (2016).
- 2 Ostrom, Q. T. *et al.* CBTRUS Statistical Report: Primary brain and other central nervous system tumors diagnosed in the United States in 2012-2016. *Neuro Oncol* **21**, v1-v100, doi: 10.1093/neuonc/noz150 (2019).
- 3 Phillips, H. S. *et al.* Molecular subclasses of high-grade glioma predict prognosis, delineate a pattern of disease progression, and resemble stages in neurogenesis. *Cancer Cell* **9**, 157-173, doi:10.1016/j.ccr.2006.02.019 (2006).
- 4 Network, C. G. A. R. Comprehensive genomic characterization defines human glioblastoma genes and core pathways. *Nature* **455**, 1061-1068, doi:10.1038/nature07385 (2008).
- 5 Verhaak, R. G. *et al.* Integrated genomic analysis identifies clinically relevant subtypes of glioblastoma characterized by abnormalities in PDGFRA, IDH1, EGFR, and NF1. *Cancer Cell* **17**, 98-110, doi:10.1016/j.ccr.2009.12.020 (2010).
- 6 Brennan, C. W. *et al.* The somatic genomic landscape of glioblastoma. *Cell* **155**, 462-477, doi:10.1016/j.cell.2013.09.034 (2013).
- 7 Brat, D. J. *et al.* Comprehensive, Integrative Genomic Analysis of Diffuse Lower-Grade Gliomas. *N Engl J Med* **372**, 2481-2498, doi:10.1056/NEJMoa1402121 (2015).
- 8 Ceccarelli, M. *et al.* Molecular Profiling Reveals Biologically Discrete Subsets and Pathways of Progression in Diffuse Glioma. *Cell* **164**, 550-563, doi:10.1016/j.cell.2015.12.028 (2016).
- 9 Parsons, D. W. *et al.* An integrated genomic analysis of human glioblastoma multiforme. *Science* **321**, 1807-1812, doi:10.1126/science.1164382 (2008).
- 10 Noushmehr, H. *et al.* Identification of a CpG island methylator phenotype that defines a distinct subgroup of glioma. *Cancer Cell* **17**, 510-522, doi:10.1016/j.ccr.2010.03.017 (2010).
- 11 Zhang, J. *et al.* Whole-genome sequencing identifies genetic alterations in pediatric low-grade gliomas. *Nat Genet* **45**, 602-612, doi:10.1038/ng.2611 (2013).
- 12 Jones, D. T. *et al.* Recurrent somatic alterations of FGFR1 and NTRK2 in pilocytic astrocytoma. *Nat Genet* **45**, 927-932, doi:10.1038/ng.2682 (2013).
- 13 Wu, G. *et al.* The genomic landscape of diffuse intrinsic pontine glioma and pediatric non-brainstem high-grade glioma. *Nat Genet* **46**, 444-450, doi:10.1038/ng.2938 (2014).
- 14 Taylor, K. R. *et al.* Recurrent activating ACVR1 mutations in diffuse intrinsic pontine glioma. *Nat Genet* **46**, 457-461, doi:10.1038/ng.2925 (2014).
- 15 Mack, S. C. *et al.* Epigenomic alterations define lethal CIMP-positive ependymomas of infancy. *Nature* **506**, 445-450, doi:10.1038/nature13108 (2014).
- 16 Parker, M. *et al.* C11orf95-RELA fusions drive oncogenic NF- $\kappa$ B signalling in ependymoma. *Nature* **506**, 451-455, doi:10.1038/nature13109 (2014).

- 17 Castel, D. *et al.* Histone H3F3A and HIST1H3B K27M mutations define two subgroups of diffuse intrinsic pontine gliomas with different prognosis and phenotypes. *Acta Neuropathol* **130**, 815-827, doi:10.1007/s00401-015-1478-0 (2015).
- 18 Sturm, D. *et al.* New Brain Tumor Entities Emerge from Molecular Classification of CNS-PNETs. *Cell* **164**, 1060-1072, doi:10.1016/j.cell.2016.01.015 (2016).
- 19 Touat, M. *et al.* Mechanisms and therapeutic implications of hypermutation in gliomas. *Nature* **580**, 517-523, doi:10.1038/s41586-020-2209-9 (2020).
- 20 Dunn, I. F. *et al.* Mismatch repair deficiency in high-grade meningioma: a rare but recurrent event associated with dramatic immune activation and clinical response to PD-1 blockade. *JCO Precis Oncol* **2018**, doi:10.1200/PO.18.00190 (2018).
- 21 Touat, M., Idhah, A., Sanson, M. & Ligon, K. L. Glioblastoma targeted therapy: updated approaches from recent biological insights. *Ann Oncol* **28**, 1457-1472, doi:10.1093/annonc/mdx106 (2017).
- 22 Kaley, T. *et al.* BRAF Inhibition in BRAF(V600)-Mutant Gliomas: Results From the VE-BASKET Study. *J Clin Oncol* **36**, 3477-3484, doi:10.1200/JCO.2018.78.9990 (2018).
- 23 Touat, M. *et al.* Successful Targeting of an ATG7-RAF1 Gene Fusion in Anaplastic Pleomorphic Xanthoastrocytoma With Leptomeningeal Dissemination. *JCO Precision Oncology*, 1-7, doi:10.1200/po.18.00298 (2019).
- 24 Wen, P. Y. *et al.* Buparlisib in Patients With Recurrent Glioblastoma Harboring Phosphatidylinositol 3-Kinase Pathway Activation: An Open-Label, Multicenter, Multi-Arm, Phase II Trial. *J Clin Oncol* **37**, 741-750, doi:10.1200/JCO.18.01207 (2019).
- 25 Mellinghoff, I. K. *et al.* Ivosidenib in Isocitrate Dehydrogenase 1-Mutated Advanced Glioma. *J Clin Oncol* **38**, 3398-3406, doi:10.1200/JCO.19.03327 (2020).
- 26 Melin, B. S. *et al.* Genome-wide association study of glioma subtypes identifies specific differences in genetic susceptibility to glioblastoma and non-glioblastoma tumors. *Nat Genet* **49**, 789-794, doi:10.1038/ng.3823 (2017).
- 27 Labreche, K. *et al.* Diffuse gliomas classified by 1p/19q co-deletion, TERT promoter and IDH mutation status are associated with specific genetic risk loci. *Acta Neuropathol* **135**, 743-755, doi:10.1007/s00401-018-1825-z (2018).
- 28 Wen, P. Y. & Kesari, S. Malignant gliomas in adults. *N Engl J Med* **359**, 492-507, doi:10.1056/NEJMra0708126 (2008).
- 29 Weller, M. *et al.* EANO guideline for the diagnosis and treatment of anaplastic gliomas and glioblastoma. *Lancet Oncol* **15**, e395-403, doi:10.1016/S1470-2045(14)70011-7 (2014).
- 30 Lapointe, S., Perry, A. & Butowski, N. A. Primary brain tumours in adults. *Lancet* **392**, 432-446, doi:10.1016/S0140-6736(18)30990-5 (2018).
- 31 Capper, D. *et al.* Characterization of R132H mutation-specific IDH1 antibody binding in brain tumors. *Brain Pathol* **20**, 245-254, doi:10.1111/j.1750-3639.2009.00352.x (2010).
- 32 Yan, H. *et al.* IDH1 and IDH2 mutations in gliomas. *N Engl J Med* **360**, 765-773, doi:10.1056/NEJMoa0808710 (2009).
- 33 Picca, A. *et al.* FGFR1 actionable mutations, molecular specificities, and outcome of adult midline gliomas. *Neurology* **90**, e2086-e2094, doi:10.1212/WNL.0000000000005658 (2018).
- 34 Frampton, G. M. *et al.* Development and validation of a clinical cancer genomic profiling test based on massively parallel DNA sequencing. *Nat Biotechnol* **31**, 1023-1031, doi:10.1038/nbt.2696 (2013).

- 35 Sholl, L. M. *et al.* Institutional implementation of clinical tumor profiling on an unselected cancer population. *JCI Insight* **1**, e87062, doi:10.1172/jci.insight.87062 (2016).
- 36 Garcia, E. P. *et al.* Validation of OncoPanel: A Targeted Next-Generation Sequencing Assay for the Detection of Somatic Variants in Cancer. *Arch Pathol Lab Med* **141**, 751-758, doi:10.5858/arpa.2016-0527-OA (2017).
- 37 Ramkissoon, S. H. *et al.* Clinical targeted exome-based sequencing in combination with genome-wide copy number profiling: precision medicine analysis of 203 pediatric brain tumors. *Neuro Oncol* **19**, 986-996, doi:10.1093/neuonc/nov294 (2017).
- 38 Zehir, A. *et al.* Mutational landscape of metastatic cancer revealed from prospective clinical sequencing of 10,000 patients. *Nat Med* **23**, 703-713, doi:10.1038/nm.4333 (2017).
- 39 Capper, D. *et al.* DNA methylation-based classification of central nervous system tumours. *Nature* **555**, 469-474, doi:10.1038/nature26000 (2018).
- 40 Pfaff, E. *et al.* Feasibility of real-time molecular profiling for patients with newly diagnosed glioblastoma without MGMT promoter hypermethylation-the NCT Neuro Master Match (N2M2) pilot study. *Neuro Oncol* **20**, 826-837, doi:10.1093/neuonc/nox216 (2018).
- 41 Massard, C. *et al.* High-Throughput Genomics and Clinical Outcome in Hard-to-Treat Advanced Cancers: Results of the MOSCATO 01 Trial. *Cancer Discov* **7**, 586-595, doi:10.1158/2159-8290.CD-16-1396 (2017).
- 42 van den Bent, M. J. *et al.* Adjuvant procarbazine, lomustine, and vincristine chemotherapy in newly diagnosed anaplastic oligodendroglioma: long-term follow-up of EORTC brain tumor group study 26951. *J Clin Oncol* **31**, 344-350, doi:10.1200/JCO.2012.43.2229 (2013).
- 43 Cairncross, G. *et al.* Phase III trial of chemoradiotherapy for anaplastic oligodendroglioma: long-term results of RTOG 9402. *J Clin Oncol* **31**, 337-343, doi:10.1200/JCO.2012.43.2674 (2013).
- 44 Cairncross, J. G. *et al.* Benefit from procarbazine, lomustine, and vincristine in oligodendroglial tumors is associated with mutation of IDH. *J Clin Oncol* **32**, 783-790, doi:10.1200/JCO.2013.49.3726 (2014).
- 45 Buckner, J. C. *et al.* Radiation plus Procarbazine, CCNU, and Vincristine in Low-Grade Glioma. *N Engl J Med* **374**, 1344-1355, doi:10.1056/NEJMoa1500925 (2016).
- 46 Hegi, M. E. *et al.* MGMT gene silencing and benefit from temozolomide in glioblastoma. *N Engl J Med* **352**, 997-1003, doi:10.1056/NEJMoa043331 (2005).
- 47 Sanai, N. & Berger, M. S. Glioma extent of resection and its impact on patient outcome. *Neurosurgery* **62**, 753-764; discussion 264-756, doi:10.1227/01.neu.0000318159.21731.cf (2008).
- 48 Sanai, N., Polley, M. Y., McDermott, M. W., Parsa, A. T. & Berger, M. S. An extent of resection threshold for newly diagnosed glioblastomas. *J Neurosurg* **115**, 3-8, doi:10.3171/2011.2.JNS10998 (2011).
- 49 Capelle, L. *et al.* Spontaneous and therapeutic prognostic factors in adult hemispheric World Health Organization Grade II gliomas: a series of 1097 cases: clinical article. *J Neurosurg* **118**, 1157-1168, doi:10.3171/2013.1.JNS121 (2013).
- 50 Shaw, E. G. *et al.* Recurrence following neurosurgeon-determined gross-total resection of adult supratentorial low-grade glioma: results of a prospective clinical trial. *J Neurosurg* **109**, 835-841, doi:10.3171/JNS/2008/109/11/0835 (2008).

- 51 van den Bent, M. J. *et al.* Long-term efficacy of early versus delayed radiotherapy for low-grade astrocytoma and oligodendroglioma in adults: the EORTC 22845 randomised trial. *Lancet* **366**, 985-990, doi:10.1016/S0140-6736(05)67070-5 (2005).
- 52 KRUMBHAAR, E. B. RÔLE OF THE BLOOD AND THE BONE MARROW IN CERTAIN FORMS OF GAS POISONING: I. PERIPHERAL BLOOD CHANGES AND THEIR SIGNIFICANCE. *Journal of the American Medical Association* **72**, 39-41, doi:10.1001/jama.1919.26110010018009f (1919).
- 53 Fu, D., Calvo, J. A. & Samson, L. D. Balancing repair and tolerance of DNA damage caused by alkylating agents. *Nat Rev Cancer* **12**, 104-120, doi:10.1038/nrc3185 (2012).
- 54 Stupp, R. *et al.* Radiotherapy plus concomitant and adjuvant temozolomide for glioblastoma. *N Engl J Med* **352**, 987-996, doi:10.1056/NEJMoa043330 (2005).
- 55 Stupp, R. *et al.* Effects of radiotherapy with concomitant and adjuvant temozolomide versus radiotherapy alone on survival in glioblastoma in a randomised phase III study: 5-year analysis of the EORTC-NCIC trial. *Lancet Oncol* **10**, 459-466, doi:10.1016/S1470-2045(09)70025-7 (2009).
- 56 Wick, W. *et al.* Temozolomide chemotherapy alone versus radiotherapy alone for malignant astrocytoma in the elderly: the NOA-08 randomised, phase 3 trial. *Lancet Oncol* **13**, 707-715, doi:10.1016/S1470-2045(12)70164-X (2012).
- 57 Wick, W. *et al.* Lomustine and Bevacizumab in Progressive Glioblastoma. *N Engl J Med* **377**, 1954-1963, doi:10.1056/NEJMoa1707358 (2017).
- 58 Perry, J. R. *et al.* Short-Course Radiation plus Temozolomide in Elderly Patients with Glioblastoma. *N Engl J Med* **376**, 1027-1037, doi:10.1056/NEJMoa1611977 (2017).
- 59 Herrlinger, U. *et al.* Lomustine-temozolomide combination therapy versus standard temozolomide therapy in patients with newly diagnosed glioblastoma with methylated MGMT promoter (CeTeG/NOA-09): a randomised, open-label, phase 3 trial. *Lancet* **393**, 678-688, doi:10.1016/S0140-6736(18)31791-4 (2019).
- 60 Stevens, M. F. *et al.* Antitumor activity and pharmacokinetics in mice of 8-carbamoyl-3-methyl-imidazo[5,1-d]-1,2,3,5-tetrazin-4(3H)-one (CCRG 81045; M & B 39831), a novel drug with potential as an alternative to dacarbazine. *Cancer Res* **47**, 5846-5852 (1987).
- 61 Carter, S. K. & Newman, J. W. Nitrosoureas: 1,3-bis(2-chloroethyl)-1-nitrosourea (NSC-409962; BCNU) and 1-(2-chloroethyl)-3-cyclohexyl-1-nitrosourea (NSC-79037; CCNU)--clinical brochure. *Cancer Chemother Rep* **3** **1**, 115-151 (1968).
- 62 Preston, B. D., Albertson, T. M. & Herr, A. J. DNA replication fidelity and cancer. *Semin Cancer Biol* **20**, 281-293, doi:10.1016/j.semcancer.2010.10.009 (2010).
- 63 Persidis, A. Cancer multidrug resistance. *Nat Biotechnol* **17**, 94-95, doi:10.1038/5289 (1999).
- 64 Munoz, J. L. *et al.* Temozolomide induces the production of epidermal growth factor to regulate MDR1 expression in glioblastoma cells. *Mol Cancer Ther* **13**, 2399-2411, doi:10.1158/1535-7163.MCT-14-0011 (2014).
- 65 Rocha, C. R. *et al.* Glutathione depletion sensitizes cisplatin- and temozolomide-resistant glioma cells in vitro and in vivo. *Cell Death Dis* **5**, e1505, doi:10.1038/cddis.2014.465 (2014).
- 66 Rocha, C. R., Kajitani, G. S., Quinet, A., Fortunato, R. S. & Menck, C. F. NRF2 and glutathione are key resistance mediators to temozolomide in glioma and melanoma cells. *Oncotarget* **7**, 48081-48092, doi:10.18632/oncotarget.10129 (2016).
- 67 Kohsaka, S. *et al.* Inhibition of GSH synthesis potentiates temozolomide-induced bystander effect in glioblastoma. *Cancer Lett* **331**, 68-75, doi:10.1016/j.canlet.2012.12.005 (2013).

- 68 Erasmus, H., Gobin, M., Niclou, S. & Van Dyck, E. DNA repair mechanisms and their clinical impact in glioblastoma. *Mutat Res Rev Mutat Res* **769**, 19-35, doi:10.1016/j.mrrev.2016.05.005 (2016).
- 69 Hegi, M. E. *et al.* Correlation of O6-methylguanine methyltransferase (MGMT) promoter methylation with clinical outcomes in glioblastoma and clinical strategies to modulate MGMT activity. *J Clin Oncol* **26**, 4189-4199, doi:10.1200/JCO.2007.11.5964 (2008).
- 70 Kitange, G. J. *et al.* Induction of MGMT expression is associated with temozolomide resistance in glioblastoma xenografts. *Neuro Oncol* **11**, 281-291, doi:10.1215/15228517-2008-090 (2009).
- 71 Nikolova, T., Roos, W. P., Kramer, O. H., Strik, H. M. & Kaina, B. Chloroethylating nitrosoureas in cancer therapy: DNA damage, repair and cell death signaling. *Biochim Biophys Acta Rev Cancer* **1868**, 29-39, doi:10.1016/j.bbcan.2017.01.004 (2017).
- 72 Esteller, M. *et al.* Inactivation of the DNA-repair gene MGMT and the clinical response of gliomas to alkylating agents. *N Engl J Med* **343**, 1350-1354, doi:10.1056/NEJM200011093431901 (2000).
- 73 Branch, P., Aquilina, G., Bignami, M. & Karran, P. Defective mismatch binding and a mutator phenotype in cells tolerant to DNA damage. *Nature* **362**, 652-654, doi:10.1038/362652a0 (1993).
- 74 Kat, A. *et al.* An alkylation-tolerant, mutator human cell line is deficient in strand-specific mismatch repair. *Proc Natl Acad Sci U S A* **90**, 6424-6428, doi:10.1073/pnas.90.14.6424 (1993).
- 75 Karran, P. & Bignami, M. DNA damage tolerance, mismatch repair and genome instability. *Bioessays* **16**, 833-839, doi:10.1002/bies.950161110 (1994).
- 76 Aquilina, G. *et al.* A mismatch recognition defect in colon carcinoma confers DNA microsatellite instability and a mutator phenotype. *Proc Natl Acad Sci U S A* **91**, 8905-8909, doi:10.1073/pnas.91.19.8905 (1994).
- 77 Branch, P., Hampson, R. & Karran, P. DNA mismatch binding defects, DNA damage tolerance, and mutator phenotypes in human colorectal carcinoma cell lines. *Cancer Res* **55**, 2304-2309 (1995).
- 78 de Wind, N., Dekker, M., Berns, A., Radman, M. & te Riele, H. Inactivation of the mouse Msh2 gene results in mismatch repair deficiency, methylation tolerance, hyperrecombination, and predisposition to cancer. *Cell* **82**, 321-330, doi:10.1016/0092-8674(95)90319-4 (1995).
- 79 Gratas, C., Sery, Q., Rabe, M., Oliver, L. & Vallette, F. M. Bak and Mcl-1 are essential for Temozolomide induced cell death in human glioma. *Oncotarget* **5**, 2428-2435, doi:10.18632/oncotarget.1642 (2014).
- 80 Roos, W. P. *et al.* Apoptosis in malignant glioma cells triggered by the temozolomide-induced DNA lesion O6-methylguanine. *Oncogene* **26**, 186-197, doi:10.1038/sj.onc.1209785 (2007).
- 81 Jiricny, J. The multifaceted mismatch-repair system. *Nat Rev Mol Cell Biol* **7**, 335-346, doi:10.1038/nrm1907 (2006).
- 82 Li, G. M. Mechanisms and functions of DNA mismatch repair. *Cell Res* **18**, 85-98, doi:10.1038/cr.2007.115 (2008).
- 83 Liu, L. & Gerson, S. L. Targeted modulation of MGMT: clinical implications. *Clin Cancer Res* **12**, 328-331, doi:10.1158/1078-0432.CCR-05-2543 (2006).
- 84 Cejka, P. *et al.* Methylation-induced G(2)/M arrest requires a full complement of the mismatch repair protein hMLH1. *EMBO J* **22**, 2245-2254, doi:10.1093/emboj/cdg216 (2003).

- 85 D'Atri, S. *et al.* Involvement of the mismatch repair system in temozolomide-induced apoptosis. *Mol Pharmacol* **54**, 334-341, doi:10.1124/mol.54.2.334 (1998).
- 86 Wick, W. *et al.* MGMT testing--the challenges for biomarker-based glioma treatment. *Nat Rev Neurol* **10**, 372-385, doi:10.1038/nrneuro.2014.100 (2014).
- 87 Hunter, C. *et al.* A hypermutation phenotype and somatic MSH6 mutations in recurrent human malignant gliomas after alkylator chemotherapy. *Cancer Res* **66**, 3987-3991, doi:10.1158/0008-5472.CAN-06-0127 (2006).
- 88 Cahill, D. P. *et al.* Loss of the mismatch repair protein MSH6 in human glioblastomas is associated with tumor progression during temozolomide treatment. *Clin Cancer Res* **13**, 2038-2045, doi:10.1158/1078-0432.CCR-06-2149 (2007).
- 89 Yip, S. *et al.* MSH6 mutations arise in glioblastomas during temozolomide therapy and mediate temozolomide resistance. *Clin Cancer Res* **15**, 4622-4629, doi:10.1158/1078-0432.CCR-08-3012 (2009).
- 90 Johnson, B. E. *et al.* Mutational analysis reveals the origin and therapy-driven evolution of recurrent glioma. *Science* **343**, 189-193, doi:10.1126/science.1239947 (2014).
- 91 van Thuijl, H. F. *et al.* Evolution of DNA repair defects during malignant progression of low-grade gliomas after temozolomide treatment. *Acta Neuropathol* **129**, 597-607, doi:10.1007/s00401-015-1403-6 (2015).
- 92 Kim, H. *et al.* Whole-genome and multisector exome sequencing of primary and post-treatment glioblastoma reveals patterns of tumor evolution. *Genome Res* **25**, 316-327, doi:10.1101/gr.180612.114 (2015).
- 93 Kim, J. *et al.* Spatiotemporal Evolution of the Primary Glioblastoma Genome. *Cancer Cell* **28**, 318-328, doi:10.1016/j.ccell.2015.07.013 (2015).
- 94 Wang, J. *et al.* Clonal evolution of glioblastoma under therapy. *Nat Genet* **48**, 768-776, doi:10.1038/ng.3590 (2016).
- 95 Barthel, F. P. *et al.* Longitudinal molecular trajectories of diffuse glioma in adults. *Nature* **576**, 112-120, doi:10.1038/s41586-019-1775-1 (2019).
- 96 Wang, Q. *et al.* Tumor Evolution of Glioma-Intrinsic Gene Expression Subtypes Associates with Immunological Changes in the Microenvironment. *Cancer Cell* **32**, 42-56.e46, doi:10.1016/j.ccell.2017.06.003 (2017).
- 97 Happold, C. *et al.* Distinct molecular mechanisms of acquired resistance to temozolomide in glioblastoma cells. *J Neurochem* **122**, 444-455, doi:10.1111/j.1471-4159.2012.07781.x (2012).
- 98 McFaline-Figueroa, J. L. *et al.* Minor Changes in Expression of the Mismatch Repair Protein MSH2 Exert a Major Impact on Glioblastoma Response to Temozolomide. *Cancer Res* **75**, 3127-3138, doi:10.1158/0008-5472.CAN-14-3616 (2015).
- 99 Nagel, Z. D. *et al.* DNA Repair Capacity in Multiple Pathways Predicts Chemoresistance in Glioblastoma Multiforme. *Cancer Res* **77**, 198-206, doi:10.1158/0008-5472.CAN-16-1151 (2017).
- 100 Pepponi, R. *et al.* The effect of O6-alkylguanine-DNA alkyltransferase and mismatch repair activities on the sensitivity of human melanoma cells to temozolomide, 1,3-bis(2-chloroethyl)1-nitrosourea, and cisplatin. *J Pharmacol Exp Ther* **304**, 661-668, doi:10.1124/jpet.102.043950 (2003).
- 101 Friedman, H. S. *et al.* Methylator resistance mediated by mismatch repair deficiency in a glioblastoma multiforme xenograft. *Cancer Res* **57**, 2933-2936 (1997).

- 102 Allan, J. M. & Travis, L. B. Mechanisms of therapy-related carcinogenesis. *Nat Rev Cancer* **5**, 943-955, doi:10.1038/nrc1749 (2005).
- 103 Alexandrov, L. B. *et al.* Signatures of mutational processes in human cancer. *Nature* **500**, 415-421, doi:10.1038/nature12477 (2013).
- 104 Stratton, M. R., Campbell, P. J. & Futreal, P. A. The cancer genome. *Nature* **458**, 719-724, doi:10.1038/nature07943 (2009).
- 105 Alexandrov, L. B. *et al.* The repertoire of mutational signatures in human cancer. *Nature* **578**, 94-101, doi:10.1038/s41586-020-1943-3 (2020).
- 106 Vogelstein, B. *et al.* Cancer genome landscapes. *Science* **339**, 1546-1558, doi:10.1126/science.1235122 (2013).
- 107 Tomasetti, C., Li, L. & Vogelstein, B. Stem cell divisions, somatic mutations, cancer etiology, and cancer prevention. *Science* **355**, 1330-1334, doi:10.1126/science.aaf9011 (2017).
- 108 Vogelstein, B. & Kinzler, K. W. The multistep nature of cancer. *Trends Genet* **9**, 138-141 (1993).
- 109 Cancer Genome Atlas Research, N. *et al.* The Cancer Genome Atlas Pan-Cancer analysis project. *Nat Genet* **45**, 1113-1120, doi:10.1038/ng.2764 (2013).
- 110 Nik-Zainal, S. *et al.* Landscape of somatic mutations in 560 breast cancer whole-genome sequences. *Nature* **534**, 47-54, doi:10.1038/nature17676 (2016).
- 111 Morganella, S. *et al.* The topography of mutational processes in breast cancer genomes. *Nat Commun* **7**, 11383, doi:10.1038/ncomms11383 (2016).
- 112 Rosenthal, R., McGranahan, N., Herrero, J., Taylor, B. S. & Swanton, C. DeconstructSigs: delineating mutational processes in single tumors distinguishes DNA repair deficiencies and patterns of carcinoma evolution. *Genome Biol* **17**, 31, doi:10.1186/s13059-016-0893-4 (2016).
- 113 Campbell, B. B. *et al.* Comprehensive Analysis of Hypermutation in Human Cancer. *Cell* **171**, 1042-1056.e1010, doi:10.1016/j.cell.2017.09.048 (2017).
- 114 Chalmers, Z. R. *et al.* Analysis of 100,000 human cancer genomes reveals the landscape of tumor mutational burden. *Genome Med* **9**, 34, doi:10.1186/s13073-017-0424-2 (2017).
- 115 Larkin, J. *et al.* Five-Year Survival with Combined Nivolumab and Ipilimumab in Advanced Melanoma. *N Engl J Med* **381**, 1535-1546, doi:10.1056/NEJMoa1910836 (2019).
- 116 Reardon, D. A. *et al.* Effect of Nivolumab vs Bevacizumab in Patients With Recurrent Glioblastoma: The CheckMate 143 Phase 3 Randomized Clinical Trial. *JAMA Oncol* **6**, 1003-1010, doi:10.1001/jamaoncol.2020.1024 (2020).
- 117 Bouffet, E. *et al.* Immune Checkpoint Inhibition for Hypermutant Glioblastoma Multiforme Resulting From Germline Biallelic Mismatch Repair Deficiency. *J Clin Oncol*, doi:10.1200/JCO.2016.66.6552 (2016).
- 118 Rizvi, N. A. *et al.* Cancer immunology. Mutational landscape determines sensitivity to PD-1 blockade in non-small cell lung cancer. *Science* **348**, 124-128, doi:10.1126/science.aaa1348 (2015).
- 119 McGranahan, N. *et al.* Clonal neoantigens elicit T cell immunoreactivity and sensitivity to immune checkpoint blockade. *Science* **351**, 1463-1469, doi:10.1126/science.aaf1490 (2016).
- 120 Samstein, R. M. *et al.* Tumor mutational load predicts survival after immunotherapy across multiple cancer types. *Nat Genet* **51**, 202-206, doi:10.1038/s41588-018-0312-8 (2019).

- 121 McGranahan, N. *et al.* Clonal status of actionable driver events and the timing of mutational processes in cancer evolution. *Sci Transl Med* **7**, 283ra254, doi:10.1126/scitranslmed.aaa1408 (2015).
- 122 Rosenthal, R. *et al.* Neoantigen-directed immune escape in lung cancer evolution. *Nature* **567**, 479-485, doi:10.1038/s41586-019-1032-7 (2019).
- 123 Le, D. T. *et al.* PD-1 Blockade in Tumors with Mismatch-Repair Deficiency. *N Engl J Med* **372**, 2509-2520, doi:10.1056/NEJMoa1500596 (2015).
- 124 Le, D. T. *et al.* Mismatch repair deficiency predicts response of solid tumors to PD-1 blockade. *Science* **357**, 409-413, doi:10.1126/science.aan6733 (2017).
- 125 Yarchoan, M., Hopkins, A. & Jaffee, E. M. Tumor Mutational Burden and Response Rate to PD-1 Inhibition. *N Engl J Med* **377**, 2500-2501, doi:10.1056/NEJMc1713444 (2017).
- 126 Johanns, T. M. *et al.* Immunogenomics of Hypermutated Glioblastoma: A Patient with Germline POLE Deficiency Treated with Checkpoint Blockade Immunotherapy. *Cancer Discov* **6**, 1230-1236, doi:10.1158/2159-8290.CD-16-0575 (2016).
- 127 Lukas, R. V. *et al.* Clinical activity and safety of atezolizumab in patients with recurrent glioblastoma. *J Neurooncol* **140**, 317-328, doi:10.1007/s11060-018-2955-9 (2018).
- 128 Van Allen, E. M. *et al.* Genomic correlates of response to CTLA-4 blockade in metastatic melanoma. *Science* **350**, 207-211, doi:10.1126/science.aad0095 (2015).
- 129 Keenan, T. E., Burke, K. P. & Van Allen, E. M. Genomic correlates of response to immune checkpoint blockade. *Nat Med* **25**, 389-402, doi:10.1038/s41591-019-0382-x (2019).
- 130 Marabelle, A. *et al.* Efficacy of Pembrolizumab in Patients With Noncolorectal High Microsatellite Instability/Mismatch Repair-Deficient Cancer: Results From the Phase II KEYNOTE-158 Study. *J Clin Oncol*, JCO1902105, doi:10.1200/JCO.19.02105 (2019).
- 131 Overman, M. J. *et al.* Nivolumab in patients with metastatic DNA mismatch repair-deficient or microsatellite instability-high colorectal cancer (CheckMate 142): an open-label, multicentre, phase 2 study. *Lancet Oncol* **18**, 1182-1191, doi:10.1016/S1470-2045(17)30422-9 (2017).
- 132 Gejman, R. S. *et al.* Rejection of immunogenic tumor clones is limited by clonal fraction. *Elife* **7**, doi:10.7554/eLife.41090 (2018).
- 133 Gylling, A. H. *et al.* Differential cancer predisposition in Lynch syndrome: insights from molecular analysis of brain and urinary tract tumors. *Carcinogenesis* **29**, 1351-1359, doi:10.1093/carcin/bgn133 (2008).
- 134 Bakry, D. *et al.* Genetic and clinical determinants of constitutional mismatch repair deficiency syndrome: report from the constitutional mismatch repair deficiency consortium. *Eur J Cancer* **50**, 987-996, doi:10.1016/j.ejca.2013.12.005 (2014).
- 135 Shlien, A. *et al.* Combined hereditary and somatic mutations of replication error repair genes result in rapid onset of ultra-hypermutated cancers. *Nat Genet* **47**, 257-262, doi:10.1038/ng.3202 (2015).
- 136 Wimmer, K. *et al.* Diagnostic criteria for constitutional mismatch repair deficiency syndrome: suggestions of the European consortium 'care for CMMRD' (C4CMMRD). *J Med Genet* **51**, 355-365, doi:10.1136/jmedgenet-2014-102284 (2014).
- 137 Vasen, H. F. *et al.* Guidelines for surveillance of individuals with constitutional mismatch repair-deficiency proposed by the European Consortium "Care for CMMR-D" (C4CMMR-D). *J Med Genet* **51**, 283-293, doi:10.1136/jmedgenet-2013-102238 (2014).

- 138 Guerrini-Rousseau, L. *et al.* Constitutional mismatch repair deficiency-associated brain tumors: report from the European C4CMMRD consortium. *Neurooncol Adv* **1**, vdz033, doi:10.1093/noajnl/vdz033 (2019).
- 139 Sa, J. K. *et al.* Hypermutagenesis in untreated adult gliomas due to inherited mismatch mutations. *Int J Cancer* **144**, 3023-3030, doi:10.1002/ijc.32054 (2019).
- 140 Tomita-Mitchell, A. *et al.* Mismatch repair deficient human cells: spontaneous and MNNG-induced mutational spectra in the HPRT gene. *Mutat Res* **450**, 125-138, doi:10.1016/s0027-5107(00)00020-8 (2000).
- 141 Gylling, A. H. *et al.* Differential cancer predisposition in Lynch syndrome: insights from molecular analysis of brain and urinary tract tumors. *Carcinogenesis* **29**, 1351-1359, doi:10.1093/carcin/bgn133 (2008).
- 142 Lavoine, N. *et al.* Constitutional mismatch repair deficiency syndrome: clinical description in a French cohort. *J Med Genet* **52**, 770-778, doi:10.1136/jmedgenet-2015-103299 (2015).
- 143 Vande Perre, P. *et al.* Germline mutation p.N363K in POLE is associated with an increased risk of colorectal cancer and giant cell glioblastoma. *Fam Cancer* **18**, 173-178, doi:10.1007/s10689-018-0102-6 (2019).
- 144 Erson-Omay, E. Z. *et al.* Somatic POLE mutations cause an ultramutated giant cell high-grade glioma subtype with better prognosis. *Neuro Oncol* **17**, 1356-1364, doi:10.1093/neuonc/nov027 (2015).
- 145 Silva, F. C., Valentin, M. D., Ferreira Fde, O., Carraro, D. M. & Rossi, B. M. Mismatch repair genes in Lynch syndrome: a review. *Sao Paulo Med J* **127**, 46-51, doi:10.1590/s1516-31802009000100010 (2009).
- 146 Perez-Cabornero, L. *et al.* Genotype-phenotype correlation in MMR mutation-positive families with Lynch syndrome. *Int J Colorectal Dis* **28**, 1195-1201, doi:10.1007/s00384-013-1685-x (2013).
- 147 Hampel, H. *et al.* Screening for the Lynch syndrome (hereditary nonpolyposis colorectal cancer). *N Engl J Med* **352**, 1851-1860, doi:10.1056/NEJMoa043146 (2005).
- 148 Latham, A. *et al.* Microsatellite Instability Is Associated With the Presence of Lynch Syndrome Pan-Cancer. *J Clin Oncol* **37**, 286-295, doi:10.1200/JCO.18.00283 (2019).
- 149 Bai, H. *et al.* Integrated genomic characterization of IDH1-mutant glioma malignant progression. *Nat Genet* **48**, 59-66, doi:10.1038/ng.3457 (2016).
- 150 Maxwell, J. A. *et al.* Mismatch repair deficiency does not mediate clinical resistance to temozolomide in malignant glioma. *Clin Cancer Res* **14**, 4859-4868, doi:10.1158/1078-0432.CCR-07-4807 (2008).
- 151 Körber, V. *et al.* Evolutionary Trajectories of IDH. *Cancer Cell* **35**, 692-704.e612, doi:10.1016/j.ccell.2019.02.007 (2019).
- 152 McGranahan, N. *et al.* Clonal Heterogeneity and Tumor Evolution: Past, Present, and the Future. *Cell* **188**, 613-628, doi: 10.1016/j.cell.2017.01.018 (2017).
- 153 Thorsson, V. *et al.* The Immune Landscape of Cancer. *Immunity* **48**, 812-830 e814, doi:10.1016/j.immuni.2018.03.023 (2018).
- 154 Berends, M. J. *et al.* Molecular and clinical characteristics of MSH6 variants: an analysis of 25 index carriers of a germline variant. *Am J Hum Genet* **70**, 26-37, doi:10.1086/337944 (2002).
- 155 Yang, G. *et al.* Dominant effects of an Msh6 missense mutation on DNA repair and cancer susceptibility. *Cancer Cell* **6**, 139-150, doi:10.1016/j.ccr.2004.06.024 (2004).

156 Geng, H. *et al.* Biochemical analysis of the human mismatch repair proteins hMutSa MSH2(G674A)-MSH6 and MSH2-MSH6(T1219D). *J Biol Chem* **287**, 9777-9791, doi:10.1074/jbc.M111.316919 (2012).

**Titre :** Mécanismes et implications thérapeutiques de l'hypermutation dans les gliomes

**Mots clés :** gliomes, hypermutation, résistance, chimiothérapie, immunothérapie, mismatch repair

**Résumé :** Une élévation majeure de la charge mutationnelle (hypermutation) est observée dans certains gliomes. Néanmoins, les mécanismes de ce phénomène et ses implications thérapeutiques notamment concernant la réponse à la chimiothérapie ou à l'immunothérapie sont encore mal connus. Sur le plan du mécanisme, une association entre hypermutation et mutations des gènes de la voie de réparation des mésappariements de l'ADN (MMR) a été rapportée dans les gliomes, cependant la plupart des mutations MMR observées dans ce contexte n'étaient pas fonctionnellement caractérisées, et leur rôle dans le développement d'hypermutation restait de ce fait incertain. De plus, l'impact de l'hypermutation sur l'immunogénicité des cellules gliales et sur leur sensibilité au blocage des points de contrôles immunitaires (par exemple par traitement anti-PD-1) n'est pas connu. Dans cette étude, nous analysons de manière exhaustive les déterminants cliniques et moléculaires de la charge et des signatures mutationnelles dans 10 294 gliomes, dont 558 (5,4%) tumeurs hypermutées. Nous identifions deux principales voies responsables d'hypermutation dans les gliomes : une voie "de novo" associée à des déficits constitutionnels du système MMR et de la polymérase epsilon (POLE), ainsi qu'une voie "post-traitement", plus fréquente, associée à l'acquisition de déficits MMR et de résistance secondaire dans les gliomes récidivant après chimiothérapie par témozolomide. Expérimentalement, la signature mutationnelle des gliomes hypermutés post-traitement

(signature COSMIC 11) était reproduite par les dommages induits par le témozolomide dans les cellules MMR déficientes. Alors que le déficit MMR s'associe à l'acquisition de résistance au témozolomide, des données cliniques et expérimentales suggèrent que les cellules MMR déficientes conservent une sensibilité à la nitrosouree lomustine. De façon inattendue, les gliomes MMR déficients présentaient des caractéristiques uniques, notamment l'absence d'infiltrats lymphocytaires T marqués, une hétérogénéité intratumorale importante, une survie diminuée ainsi qu'un faible taux de réponse aux traitements anti-PD-1. De plus, alors que l'instabilité des microsatellites n'était pas détectée par des analyses en bulk dans les gliomes MMR déficients, le séquençage du génome entier à l'échelle de la cellule unique de gliome hypermuté post-traitement permettait de démontrer la présence de mutations des microsatellites. Collectivement, ces résultats supportent un modèle dans lequel des spécificités dans le profil mutationnel des gliomes hypermutés pourraient expliquer l'absence de reconnaissance par le système immunitaire ainsi que l'absence de réponse aux traitements par anti-PD-1 dans les gliomes MMR déficients. Nos données suggèrent un changement de pratique selon lequel la recherche d'hypermutation par séquençage tumoral lors de la récidive après traitement pourrait informer le pronostic et guider la prise en charge thérapeutique des patients.

**Title :** Mechanisms and therapeutic implications of hypermutation in gliomas

**Keywords :** gliomas, hypermutation, resistance, chemotherapy, immunotherapy, mismatch repair

**Abstract :** High tumor mutational burden (hypermutation) is observed in some gliomas; however, the mechanisms by which hypermutation develops and whether it predicts chemotherapy or immunotherapy response are poorly understood. Mechanistically, an association between hypermutation and mutations in the DNA mismatch-repair (MMR) genes has been reported in gliomas, but most MMR mutations observed in this context were not functionally characterized, and their role in causing hypermutation remains unclear. Furthermore, whether hypermutation enhances tumor immunogenicity and renders gliomas responsive to immune checkpoint blockade (e.g. PD-1 blockade) is not known. Here, we comprehensively analyze the clinical and molecular determinants of mutational burden and signatures in 10,294 gliomas, including 558 (5.4%) hypermutated tumors. We delineate two main pathways to hypermutation: a de novo pathway associated with constitutional defects in DNA polymerase and MMR genes, and a more common, post-treatment pathway, associated with acquired resistance driven by MMR defects in chemotherapy-sensitive gliomas recurring after temozolomide. Experimentally, the mutational signature of post-treatment hypermutated gliomas

(COSMIC signature 11) was recapitulated by temozolomide-induced damage in MMR-deficient cells. While MMR deficiency was associated with acquired temozolomide resistance in glioma models, clinical and experimental evidence suggest that MMR-deficient cells retain sensitivity to the chloroethylating nitrosourea lomustine. MMR-deficient gliomas exhibited unique features including the lack of prominent T-cell infiltrates, extensive intratumoral heterogeneity, poor survival and low response rate to PD-1 blockade. Moreover, while microsatellite instability in MMR-deficient gliomas was not detected by bulk analyses, single-cell whole-genome sequencing of post-treatment hypermutated glioma cells demonstrated microsatellite mutations. Collectively, these results support a model where differences in the mutation landscape and antigen clonality of MMR-deficient gliomas relative to other MMR-deficient cancers may explain the lack of both immune recognition and response to PD-1 blockade in gliomas. Our data suggest a change in practice whereby tumor re-sequencing at relapse to identify progression and hypermutation could inform prognosis and guide therapeutic management.